

# **New insights into the bacterial catabolism of chitin and the peptidoglycan-teichoic acid complex**

## **Dissertation**

der Mathematisch-Naturwissenschaftlichen Fakultät  
der Eberhard Karls Universität Tübingen  
zur Erlangung des Grades eines  
Doktors der Naturwissenschaften  
(Dr. rer. nat.)

vorgelegt von  
Axel Walter  
aus Freiburg im Breisgau

Tübingen  
2021

Gedruckt mit Genehmigung der Mathematisch-Naturwissenschaftlichen Fakultät der Eberhard Karls Universität Tübingen.

Tag der mündlichen Qualifikation:

06.09.2021

Dekan:

Prof. Dr. Thilo Stehle

1. Berichterstatter:

Prof. Dr. apl. Christoph Mayer

2. Berichterstatter:

Prof. Dr. Hannes Link

3. Berichterstatter:

Prof. Dr. Fabian Commichau

# Contents

<b>Abbreviations</b>	<b>i</b>
<b>Abstract</b>	<b>ii</b>
<b>Zusammenfassung</b>	<b>iii</b>
<b>List of publications</b>	<b>iv</b>
<b>Declaration of personal contribution</b>	<b>v</b>
<b>1 Introduction</b>	<b>1</b>
1.1 Amino sugars of the bacteria cell envelope . . . . .	1
1.2 Peptidoglycan and chitin catabolism . . . . .	2
1.3 Degradation of teichoic acids in Gram-positive bacteria . . . . .	7
1.4 Research objective . . . . .	10
<b>2 Results</b>	<b>11</b>
2.1 Characterization of the chitinase ChiA of <i>E. coli</i> and chitin oligomer analysis .	11
2.2 New functions of the <i>chb</i> operon of <i>E. coli</i> in chitin and peptidoglycan catabolism	17
2.3 Recycling of the peptidoglycan-wallteichoic acid complex and differential diges- tion of teichoic acids . . . . .	20
<b>3 Discussion</b>	<b>25</b>
3.1 ChiA is a pure chitinase devoid of lysozyme-like activity . . . . .	25
3.2 The <i>chb</i> operon revisited: new functions in chitin and peptidoglycan catabolism	27
3.3 Wall- and lipoteichoic acids are enantiomeric polymers . . . . .	31
3.4 Conclusion . . . . .	34
<b>4 References</b>	<b>36</b>
<b>Appendix</b>	<b>48</b>
Publication 1 . . . . .	48
Publication 2 . . . . .	74
Publication 3 . . . . .	138
Publication 4 . . . . .	149
Publication 5 . . . . .	170
Publication 6 . . . . .	191
<b>Acknowledgement</b>	<b>202</b>

## Abbreviations

$\alpha$	alpha
$\beta$	beta
BPC	base peak chromatogram
$^{\circ}\text{C}$	degree celsius
CAA	casamino acids
chitobiose	GlcN-GlcN
CMP	cytidine monophosphate
$\Delta$	genetic deletion
DNA	deoxyribonucleic acid
diacetyl-chitobiose	N,N'-diacetyl-chitobiose (GlcNAc-GlcNAc)
DA	degree of acetylation
DP	degree of polymerization
EIC	extracted ion chromatogram
ELSD	evaporative light scattering detector
FACE	fluorophore assisted carbohydrate electrophoresis
Glc	glucose
GlcN	glucosamine
GlcNAc	N-acetylglucosamine
GroP	glycerol-phosphate
HPLC	high-performance liquid chromatography
IPTG	isopropyl -D-1-thiogalactopyranoside
kDa	kilodalton
LC-MS	liquid chromatographymass spectrometry
LTA	lipoteichoic acid
min	minutes
ml	millilitres
mM	millimolar
MurNAc	N-acetylmuramicacid
OD	optical density
%	percent
PG	phosphatidylglycerol
PGN	peptidoglycan
PTS	phosphotransferase system
TA	teichoic acid
WTA	wallteichoic acid

## Abstract

In search for the elusive peptidoglycan (PGN) recycling pathway in *Escherichia coli*, as suggested by Plumbridge, we became aware of the bifunctional periplasmic enzyme ChiA. It was described as chitinase/lysozyme based on tests with artificial substrates. However, assays using colloidal chitin and PGN clearly revealed ChiA as a sole chitinase, since ChiA digested neither intact PGN nor PGN from which peptides were removed (PGN-derived glycans) by the amidase CwIC. These experiments also revealed a strict requirement for intact peptidation by the widely used lysozyme mutanolysin. Even though ChiA expression and secretion is inhibited under laboratory conditions, ChiA-dependent growth on chitin oligomers was demonstrated by artificial expression.

*E. coli* utilizes the ChiA products N,N'-diacetyl-chitobiose and N,N',N''-triacetylchitotriose via the *chb* operon. The 6-phospho- $\beta$ -glycosidase ChbF cleaves exclusively after prior deacetylation of the substrates by ChbG. An unusual NAD<sup>+</sup>-dependent mechanism of ChbF and molecular modelling strongly suggest a necessity for deacetylation at the non-reducing end of the disaccharide. Contrary to previous suggestions by Verma et al.,  $\Delta$ *chbF* accumulation products were deacetylated at the non-reducing end, proven by enzymatic assays and mass spectrometry. Besides that, the coactivator of the transcriptional regulator ChbR could be identified as the products of ChbG activity, which explains absence of *chb* induction in  $\Delta$ *chbG* cells. Further on, a possible connection of *chb* with PGN recycling was recognized.

Although the PGN recycling is generally well understood, the accompanying turnover of wall teichoic acids (WTA) has been neglected so far. In *Bacillus subtilis* 168, both WTA and lipoteichoic acids (LTA) are glycerol-phosphate (GroP) polymers and because cells without at least one type of teichoic acids (TA) are not viable, their degradation needs to be tightly regulated. Differential digestion by the *sn*-3-glycerol-phosphate (Gro3P) stereospecific phosphodiesterase GlpQ revealed a stereoisomery of these polymers. GlpQ cleaved exclusively non-glycosylated WTA and cleaved LTA only after alkaline pretreatment, opening the *sn*-1-glycerol-phosphate (Gro1P) polymer and thus giving GlpQ access to now free Gro3P ends.

WTA and LTA stereoisomery emphasises their different roles and allows a regulation of degradation by stereospecific enzymes. This approach was possible due to the recent elucidation of LTA glycosylation mechanisms by Rismondo et al. and thus access to non-glycosylated LTA. In addition to its stereospecificity, GlpQ also acts specifically on non-glycosylated substrate, suggesting possible protection against undesired degradation by glycosylation.

Furthermore, this work deals with the purification of the WTA linker disaccharide as well as oligomeric sized peptidoglycan and chitin chains and addresses the question why this has not been accomplished so far in a larger scale even though the need for well-defined oligomers in research and medicine is growing.

## Zusammenfassung

Auf der Suche nach dem schwer fassbaren Peptidoglykan (PGN) Recyclingweg in *Escherichia coli*, wie von Plumbridge vorgeschlagen, wurden wir auf das bifunktionelle periplasmatische Enzym ChiA aufmerksam. Es wurde als Chitinase/Lysozym beschrieben, basierend auf Tests mit künstlichen Substraten. Assays an kolloidalem Chitin und PGN wiesen ChiA jedoch als Chitinase aus, da ChiA weder intaktes PGN noch das Zuckerrückgrat verdaut, von dem Peptidvernetzungen durch die Amidase CwlC entfernt werden. Diese Experimente zeigten auch den Bedarf für eine intakte Peptidierung durch das Lysozym Mutanolysin. Obwohl die ChiA Expression und Sekretion unter Laborbedingungen gehemmt ist, konnte ChiA-abhängiges Wachstum auf Chitin Oligomeren durch künstliche Expression nachgewiesen werden.

*E. coli* verwertet Chitinase Produkte, hauptsächlich N,N'-Diacetyl-Chitobiose, über das *chb*-Operon. Die 6-Phospho- $\beta$ -Glucosidase ChbF spaltet nach vorheriger Deacetylierung des Substrats durch ChbG. Ein ungewöhnlicher NAD<sup>+</sup> abhängiger Mechanismus von ChbF und die molekulare Modellierung deuten stark auf eine notwendige Deacetylierung am nicht-reduzierenden Ende hin. Im Gegensatz zu früheren Vermutungen von Verma et al. waren die  $\Delta$ *chbF*-Akkumulationsprodukte am nicht-reduzierenden Ende deacetyliert, was durch enzymatische Assays und Massenspektrometrie nachgewiesen wurde. Außerdem konnte der Coaktivator des Transkriptionsregulators ChbR als ChbG Produkt identifiziert werden, was die fehlende *chb*-Induktion in  $\Delta$ *chbG*-Zellen erklärt. Weiterhin wurde ein möglicher Zusammenhang von *chb* mit PGN-Recycling erkannt.

Obwohl das PGN Recycling gut verstanden ist, wurde der begleitende Abbau von Wandteichoinsäuren (WTA) bisher vernachlässigt. In *Bacillus subtilis* 168 bestehen sowohl WTA als auch Lipoteichoinsäuren (LTA) aus Glycerol-Phosphat (GroP), und da Zellen ohne mindestens eine der beiden Teichoinsäuren (TA) nicht lebensfähig sind, muss ihr Abbau streng reguliert werden. Der differentielle Verdau durch die stereospezifische Gro3P Phosphodiesterase GlpQ zeigte eine Stereoisomerie dieser Polymere. GlpQ spaltete ausschließlich nicht glykosylierte WTA und spaltete LTA nur nach alkalischer Vorbehandlung, wobei das Gro1P Polymer geöffnet wurde und damit GlpQ Zugang zu den nun freien Gro3P Enden bekam.

WTA und LTA Stereoisomerie heben ihre unterschiedlichen Rollen hervor und ergeben eine elegante Möglichkeit, den Abbau durch stereospezifische Enzyme zu regulieren. Dieser Ansatz wurde durch die Aufklärung der LTA Glykosylierung durch Rismondo et al. und damit den Zugang zu nicht glykosylierter LTA möglich. Zusätzlich zu seiner Stereospezifität wirkt GlpQ auch spezifisch auf nicht glykosyliertes Substrat, was auf Glykosylierung als einen möglichen Schutz vor unerwünschtem Abbau hindeutet.

Darüber hinaus befasst sich diese Arbeit mit der Aufreinigung des WTA Linker Disaccharids sowie oligomerer Peptidoglykan- und Chitinketten und geht der Frage nach, warum dies bisher nicht in größerem Maßstab gelungen ist, obwohl der Bedarf an wohldefinierten Oligomeren in Forschung und Medizin wächst.

# List of publications

## Accepted publications

### Publication 1

**Walter, A.**, Friz, S., Mayer, C. (2021). Chitin and diacetylchitobiose metabolism of *Escherichia coli* revisited: adjustment of the roles of ChiA, ChbR, ChbF and ChbG. *Microbial Physiology*.

### Publication 2

**Walter, A.**, & Mayer, C. (2019). Peptidoglycan Structure, Biosynthesis, and Dynamics During Bacterial Growth. In *Extracellular Sugar-Based Biopolymers Matrices* (pp. 237-299). Springer, Cham.

### Publication 3

Mayer, C., Kluj, R. M., Mühleck, M., **Walter, A.**, Unsleber, S., Hottmann, I., & Borisova, M. (2019). Bacteria's different ways to recycle their own cell wall. *International Journal of Medical Microbiology*, 309(7), 151326.

### Publication 4

**Walter, A.**, Unsleber, S., Rismondo, J., Jorge, A. M., Peschel, A., Gründling, A., & Mayer, C. (2020). Phosphoglycerol-type wall and lipoteichoic acids are enantiomeric polymers differentiated by the stereospecific glycerophosphodiesterase GlpQ. *Journal of Biological Chemistry*, 295(12), 4024-4034.

### Publication 5

Du, X., Larsen, J., Li, M., **Walter, A.**, Slavetinsky, C., Both, A., Sanchez Carballo, P. M., Stegger, M., Lehmann, E., Liu, Y., Liu, J., Slavetinsky, J., Duda, K. A., Krismer, B., Heilbronner, S., Weidenmaier, C., Mayer, C., Rohde, H., Winstel, V., & Peschel, A. (2021). Emerging *Staphylococcus epidermidis* clones express *Staphylococcus aureus*-type wall teichoic acid to shift from a commensal to pathogen lifestyle. Accepted in *Nature Microbiology*.

### Publication 6

Vollmer, B., Steblau, N., Ladwig, N., Mayer, C., Macek, B., Mitousis, L., Sigle, S., **Walter, A.**, Wohlleben, W., & Muth, G. (2019). Role of the *Streptomyces* spore wall synthesizing complex SSSC in differentiation of *Streptomyces coelicolor* A3 (2). *International Journal of Medical Microbiology*, 309(6), 151327.

# **Declaration of personal contribution**

## **Publication 1**

All experiments were done by me, except for the MS/MS Fragmentation, construction of pET28a-CwlC, pET16b-NagZ, pET28a-Atl(Glc) and pQE32-ChbBCA and purification of Atl (Glc) and NagZ. The script was written by Prof. Christoph Mayer and me.

## **Publication 2**

The book chapter was written by Prof. Christoph Mayer and me.

## **Publication 3**

I contributed the section about degradation of wall teichoic acids and the role of the teichoicase GlpQ.

## **Publication 4**

All experiments were done by me, except for the purification of LTA and purification and biochemical characterization of GlpQ. The script was written by Prof. Christoph Mayer and me.

## **Publication 5 and 6**

I provided experimental advice for the digesting of WTA and performed HPLC-MS measurements.



# 1 Introduction

## 1.1 Amino sugars of the bacteria cell envelope

Bacteria have evolved a specialized cell envelope that defines cell shape, provides stability against the internal turgor pressure and serves as an interface to the extracellular environment. A recurring building block in cell envelope structures is the amino sugar N-acetylglucosamine (GlcNAc), which occurs in the glycan (saccharide) backbone of peptidoglycan (PGN) and other glycopolymers such as lipopolysaccharides and teichoic acids.

The biosynthesis of UDP-GlcNAc, which is used as the general precursor of cell envelope structures, starts with fructose6P, derived from the central metabolism. The reaction involves the bifunctional isomerase/amidotransferase GlmS, the phosphoglucosamine mutase GlmM and the bifunctional N-acetyl and uridyl transferase GlmU (Fig. 6.15, publication 2) (Walter and Mayer 2019).

A major component of the cell envelope is PGN, responsible for the rigidity of the cell wall. PGN is a heteropolymer of glycan strands cross-linked by peptides, forming a huge and solid sacculus with a mesh-like structure that surrounds the whole cell (Weidel et al. 1960; Weidel and Pelzer 1964; Rogers 1974; Höltje 1998; Seltmann and Holst 2002; Walter and Mayer 2019). The sugar chains consist of  $\beta$ -1,4-linked GlcNAc and N-acetylmuramic acid (MurNAc), which is a GlcNAc substituted by an ether-linked D-lactate at the C3 hydroxyl group. A pentapeptide is attached to the carboxylate of the D-lactyl group of MurNAc via an amide bond. Cross-linking occurs via *meso*-2,6-diaminopimelic acid (m-DAP) at position three and D-alanine (D-Ala) at position four (Fig. 6.9, publication 2) in exchange of a D-Ala at position five in a transpeptidation reaction (Fig. 6.16 B, publication 2). PGN is composed in this manner in most Gram-negative bacteria (e.g. *Escherichia coli*) and some Gram-positive bacteria (e.g. *Bacillus subtilis*) with considerable variations in other bacteria (Schleifer and Kandler 1972). Based on the composition of the cell envelope, bacteria can be classified as Gram-negative and Gram-positive. The distinction is based on the thickness of the PGN layer and the presence or not of anionic co-polymers. Gram-positive bacteria are visualized by staining with crystal violet, a dye readily retained by a thick PGN (Gram 1884) interwoven with anionic polymers such as wallteichoic acids (WTA) covalently attached to MurNAc-C6 via a linker disaccharide, and membrane-bound lipoteichoic acids (LTA) (Silhavy et al. 2010; Walter and Mayer 2019). The WTA linker disaccharide in *B. subtilis* is ManNAc-GlcNAc built from UDP-GlcNAc and UDP-ManNAc, the latter provided by the UDP-N-acetylglucosamine 2-epimerase MnaA (Soldo et al. 2002; Swoboda et al. 2010). Recently, the mechanism of LTA glycosylation in *B. subtilis* has been elucidated. Intracellularly, the glycosyltransferase CsbB attaches GlcNAc from UDP-GlcNAc to undecaprenylphosphate, which is flipped across the membrane by GtcA and subsequently YfhO transfers GlcNAc to the chain polymers *sn*-1-glycerol-phosphate (Gro1P) C2 (Rismondo et al. 2018; Rismondo et al. 2019).

In contrast, Gram-negative bacteria possess a thin PGN layer between the cytoplasmic and

outer membrane, establishing the periplasmic space (Matias et al. 2003; Vollmer and Höltje 2004). The outer membrane contains lipopolysaccharides (Walter and Mayer 2019), porins such as the chitoporin ChiP (Soyas and Suginta 2016), and specialized secretion systems such as a type II secretion system (cryptic *gsp* secretome) capable of secreting the endo-chitinase ChiA if activated (Francetic et al. 2000b). Chitin, a polymer of  $\beta$ -1,4-linked GlcNAc, is usually found in cell walls of fungi and exoskeletons of arthropods but not in bacteria, yet some species, many of them plant pathogens, have acquired chitin synthase genes (Gonçalves et al. 2016). Amino sugar polysaccharides are important constituents of exopolysaccharides of biofilm matrices and are crucial for pathogenic bacteria like *Staphylococcus epidermidis*, which protects itself against components of the human innate immune system with extracellular polymers of  $\beta$ -1,6-linked GlcNAc, known as polysaccharide intercellular adhesin (Mack et al. 1996; Vuong et al. 2004).

## 1.2 Peptidoglycan and chitin catabolism

Due to cell growth PGN is subject to constant build-up and degradation, known as PGN turnover (Boothby et al. 1973; Doyle et al. 1988; Park and Uehara 2008; Reith and Mayer 2011; Walter and Mayer 2019) which accounts for about 50 % of cell wall material per generation (Park and Uehara 2008; Reith and Mayer 2011; Borisova et al. 2016; Walter and Mayer 2019). The majority of cell wall material is taken up into the cell and efficiently recycled (Park and Uehara 2008; Gisin et al. 2013; Kluj et al. 2018).

A variety of enzymes act on PGN, such as the bacteriolytic agents lysozyme (Fleming and Allison 1922) and mutanolysin from *Streptomyces griseus* (Yokogawa et al. 1974). Enzymes with lysozyme activity cleave the MurNAc-GlcNAc glycosidic bond, yielding muropeptides that can reveal PGN composition (Glauner 1988). Other PGN-active enzymes include autolysins, involved in cell wall recycling and turnover (Smith et al. 2000). During growth, the rigid cell wall must be reorganized constantly, hence specialized pathways have evolved for cell wall recycling, conserving energy and resources (Walter and Mayer 2019; Mayer et al. 2019). Relevant autolysins for this study are the bifunctional N-acetylmuramyl-L-alanine amidase/endo-N-acetylglucosaminidase Atl from *Staphylococcus aureus* (Oshida et al. 1995), the N-acetylmuramoyl-L-alanine amidase CwlC from *B. subtilis* (Shida et al. 2000) and the exo-N-acetylglucosaminidase NagZ from *B. subtilis* (Litzinger et al. 2010a; Litzinger et al. 2010b). Amidases can be utilized to generate denuded, peptide free glycan strands (Harz et al. 1990). Exo-lytic N-acetylglucosaminidases cleave GlcNAc entities from the non-reducing end (NagZ), whereas endo-N-acetylglucosaminidases cleave GlcNAc-MurNAc linkages within the glycan backbone of PGN (Atl glucosaminidase domain) (Walter and Mayer 2019).

In *E. coli*, lytic transcosylases (LTs), such as Slt70 cleave the PGN glycan backbone into smaller fragments that can be taken up into the cell. Unlike lysozymes and chitinases, LTs are not hydrolases. They cleave the MurNAc-GlcNAc  $\beta$ -1,4-glycosidic bond with a concomi-

tant formation of 1,6-anhydroMurNAc (anhMurNAc) (Romeis et al. 1993; Scheurwater et al. 2008). Endopeptidases cleave the peptide cross-links yielding anhydromuropeptides (GlcNAc-anhMurNAc-peptides), from which the peptid stems are removed by amidases (Park and Uehara 2008). Subsequently (Fig. 6.23, publication 2), the anhydromuropeptide permease AmpG transports GlcNAc-anhMurNAc and anhydromuropeptides into the cytoplasm in a proton motive force dependent manner (Jacobs et al. 1994; Cheng and Park 2002). The disaccharide is cleaved by NagZ yielding GlcNAc and anhMurNAc (Cheng et al. 2000), which are phosphorylated at C6 by NagK (Uehara and Park 2004) and AnmK (Uehara et al. 2005), respectively. The etherase MurQ is a unique ether hydrolase that cleaves between the D-lactic acid and GlcNAc moiety of MurNAc6P, yielding GlcNAc6P (Uehara et al. 2005; Jaeger et al. 2005; Uehara et al. 2006; Mayer et al. 2019). GlcNAc6P efficiently derepresses the *nag* repressor NagC (Plumbridge 1991).

Alternatively, intracellular GlcNAc6P levels increase upon cell wall turnover involving the GlcNAc specific PTS transporter NagE. How GlcNAc is supplied within the periplasm is not clear (Plumbridge 2009) and the question of this missing alternative cell wall recycling pathway is part of this work.

NagA decetylates GlcNAc6P providing GlcN6P (White and Pasternak 1967; Peri et al. 1990; Souza et al. 1997), funneled into PGN biosynthesis (Walter and Mayer 2019) or glycolysis (Montero-Morán et al. 2001). Of further interest for this work is the ribonucleotide monophosphatase NagD, catalyzing the dephosphorylation of a broad range of substrates (Kuznetsova et al. 2006; Tremblay et al. 2006).

In *B. subtilis*, contrary to *E. coli*, muropeptides are processed outside the cell. *B. subtilis* NagZ, an orthologue to *E. coli* NagZ, and AmiE release the single sugars GlcNAc and MurNAc (Litzinger et al. 2010a; Walter and Mayer 2019). They are transported into the cell by the PTS transporters NagP and MurP (Reizer et al. 1988) (Fig. 6.23, publication 2). *B. subtilis* possesses an etherase, orthologous to *E. coli* MurQ, that converts MurNAc6P to GlcNAc6P (Reith and Mayer 2011).

Chitin is the most abundant nitrogen containing polysaccharide on earth with an annual turnover rate of  $10^{11}$  tons mainly derived from the exoskeletons of crustaceans and insects and the cell walls of fungi (Tharanathan and Kittur 2003). Basically, chitin is composed of  $\beta$ -1,4-linked GlcNAc subunits (Fig. 1). If the majority of GlcNAc residues ( $> 75\%$ ) are deacetylated to GlcN, it is referred to as chitosan. Thus the assignment to chitin or chitosan depends on the degree of acetylation (DA) (No and Meyers 1995; Rinaudo 2006; Schmitz et al. 2019). DA can be modified by deacetylation with alkaline hydrolysis (Mima et al. 1983) or acetylation with acetic anhydride (Hirano et al. 1976; Kubota et al. 2000; Lu et al. 2004). However, due to the large amounts of chemical waste, enzymatic methods are gaining popularity (Shirvan et al. 2019).

Due to functional requirements of, for example, crustacean shells, chitin forms a hard and re-

calcitrant material in nature by formation of hydrogen bonds between chains as well as protein and mineral intercalations. Acid treatment breaks chitin down into individual sugar strands forming a colloid (Shimahara and Takiguchi 1988), giving access to enzymes.

Chitin and chitosan oligosaccharides, especially with defined degree of polymerization (DP), are of great interest for applications in research and medicine (Rinaudo 2006; Schmitz et al. 2019). Therefore this work investigates methods to separate mixtures of chitin oligomers to purify oligomers with defined DP.

Due to abundance, chitin plays a key role in the global nitrogen and carbon cycle and bacteria have evolved sophisticated metabolic pathways to utilize this substrate. Through the secretion of chitinases, chitinolytic bacteria such as soil-dwelling *Bacillus* or *Streptomyces* (Hamid et al. 2013) and marine *Vibrio* (Blokesch 2012; Adams et al. 2019) strains that live in close proximity to chitin producers can cleave chitin into smaller components, mostly N,N'-diacetylchitobiose (GlcNAc-GlcNAc, diacetyl-chitobiose), taken up and metabolized within cell (Hamid et al. 2013). Besides chitinases, some bacteria are also equipped with chitosanases. In combination, these enzymes can cleave chitin and chitosan with varying DA (Thadathil and Velappan 2014). In nature, chitosan is found in Zygomycete fungi and some green algae (Davis and Eveleigh 1984). This study utilizes the Csn chitosanase from *B. subtilis* as a positive control in enzyme assays (Rivas et al. 2000).

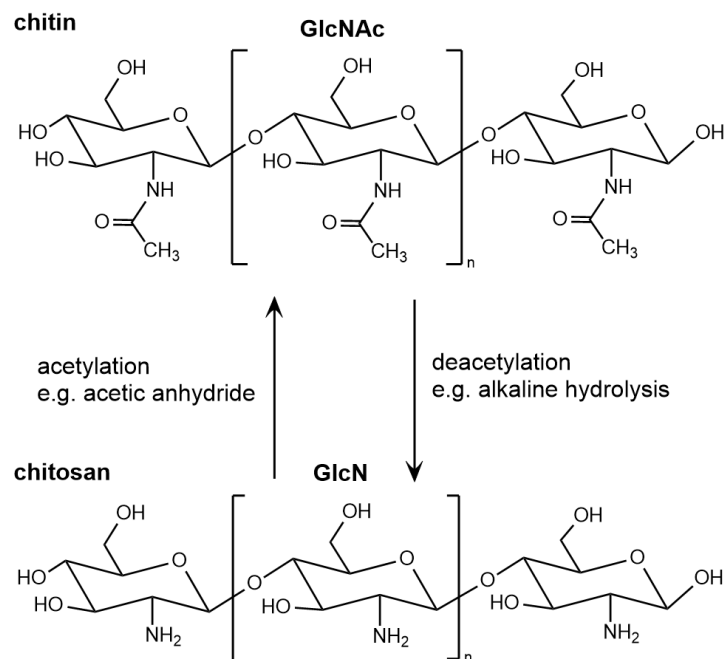


**Fig. 1. Chitin and chitosan composition.** Chitin is a polysaccharide of β-1,4-linked GlcNAc residues. Deacetylation, e.g. by alkaline hydrolysis, converts chitin into chitosan, a polysaccharide of β-1,4-linked GlcN residues which is defined by a low DA of < 75%. Conversely chitosan can be acetylated with acetic anhydride yielding chitin.

This work takes a closer look at the chitin metabolism in *E. coli*. ChiA (YheB), a putative bifunctional enzyme with lysozyme and chitinase activity (Francetic et al. 2000a; Francetic et al. 2000b) could provide the substrate for the enzymes of the *chb* operon for chitobiose utilization. Furthermore, *E. coli* possesses the chitoporin ChiP for the uptake of chitooligomers into the periplasm. (Soysa and Suginta 2016).

ChiA has been described as a bifunctional enzyme with chitinase and lysozyme activ-

ity (Francetic et al. 2000a). It cleaves ethylene glycol chitin (EGC), a soluble chitin derivative commonly used as a test substrate for lysozyme activity (Wang and Chang 1997), while a chitinase from *Serratia marcescens*, used as control, does not (Francetic et al. 2000a). Based on cleavage of 4-MU-GlcNAc<sub>3</sub> but not 4-MU-GlcNAc an endo-acting chitinase mechanism was proposed (Francetic et al. 2000a). ChiA could be, like some chitinases from *Pseudomonas aeruginosa* (Wang and Chang 1997) or *Vibrio cholerae* (Connell et al. 1998), a bifunctional enzyme (Francetic et al. 2000a). This work aims to clarify the substrate specificity of ChiA for the natural substrates colloidal chitin, chitosan and PGN.

Previous work by Plumbridge has shown that GlcNAc6P levels in *E. coli*  $\Delta$ *nagA*, deficient in the GlcNAc6P deacetylase NagA, drop only to about 50% if other known PGN recycling enzymes such as AmpG, NagZ, AnmK, MurQ, and NagK are knocked out as well (Plumbridge 2009). Intriguingly, additional knockout of NagE reduces GlcNAc6P levels further to 0%. Consequently, there must be an alternative recycling pathway providing GlcNAc in the periplasm, and ChiA may be responsible.

ChiA's native signal sequence allows export to the periplasm via the Sec system and a cryptic type 2 secretion system (*gsp* secretome) can secrete ChiA into the medium (Francetic et al. 2000b). However, both ChiA and *gsp* secretome expression is silenced under standard laboratory growth conditions by the nucleoid-structuring protein H-NS (Pon et al. 1988). Thus their genes are cryptic and expressed only in a  $\Delta$ *hns* background (Francetic et al. 2000a; Francetic et al. 2000b).

ChiA can be assigned to family 18 of the glycosyl hydrolases (GH18) based on its catalytic domain. This family contains many chitinases and lysozymes with a conserved mechanism dependent on a proton donor amino acid in the protein and a catalytic/nucleophilic base in the substrate, which is the carbonyl oxygen of the GlcNAc C2 N-acetyl group. Cleavage occurs via a nucleophilic attack on the C1 carbon (Tews et al. 1997). Some human and insect chitinases are inhibited by completely deacetylated chitosan, as the binding of GlcN is energetically more advantageous compared to GlcNAc, but cleavage can no longer occur due to the missing N-acetyl group (Chen et al. 2014). Furthermore, ChiA contains five chitin binding domains (CBD) from which the N-terminal CBD was characterized to bind specifically to chitin (Brun et al. 1997; Simpson and Barras 1999; Francetic et al. 2000a).

The *chbBCARFG* operon in *E. coli* was first described as the cryptic *cel* operon because a mutation enabled the utilization of various  $\beta$ -glycosides such as cellobiose (Glc-Glc), arbutin, and salicin (Parker and Hall 1990). The inducer turned out to actually be diacetyl-chitobiose, which is utilized without prior mutation. Consequently, the operon was renamed *chb* (Keyhani and Roseman 1997). A phosphotransferase system (PTS) transporter consisting of ChbB (EIIB), ChbC (EIIC), and ChbA (EIIA) imports diacetyl-chitobiose and phosphorylates at the C6 of the non-reducing end yielding intracellular diacetyl-chitobiose-phosphate (diacetyl-chitobiose-P) (Keyhani et al. 2000a; Keyhani et al. 2000b; Keyhani et al. 2000c).

Unusually, diacetyl-chitobiose-P is not cleaved directly, instead, the monodeacetylase ChbG removes an acetyl group. Accordingly, ChbG is dispensible for growth on chitobiose (GlcN-GlcN) and cellobiose (Verma and Mahadevan 2012). Subsequently, the disaccharide is cleaved by the 6-phospho- $\beta$ -glucosidase ChbF. It belongs to the glycosyl transferase family 4 (GH4), whose mechanism suggests the decisive reactions occur at the non-reducing end (Yip et al. 2007). In contrast, Verma et al. suggests deacetylation at the reducing since the product GlcNAc6P efficiently derepresses NagC, a repressor of the *chb* operon (Verma and Mahadevan 2012; Plumbridge and Pellegrini 2004). Furthermore, the expression of *chb* is regulated by the transcriptional repressor/activator ChbR and is subject to carbon catabolite repression, thus activated by cAMP-CAP (Plumbridge and Pellegrini 2004). ChbR binds to the *chb* promoter by default repressing transcription, however, upon binding of a coactivator ChbR functions as activator (Plumbridge and Pellegrini 2004). This work aims to elucidate the identity of the coactivator and to determine the site of deacetylation by ChbG. Moreover, the induction of *chb* affects the import of chitin oligomers. By default, the chitoporin ChiP is constitutive expressed but silenced by the sRNA ChiX pairing with *chiP* mRNA. However, the *chb* mRNA pairs with ChiX leading to it's degradation by a ribonuclease. Consequently, high induction and expression of *chb* leads to derepression of ChiP expression (Figueroa-Bossi et al. 2009; Rasmussen et al. 2009).

The 6-phospho- $\beta$ -glucosidase ChbF, investigated in this work, belongs to the glycoside hydrolase family 4 (GH4) (Thompson et al. 1999; CAZypedia 2018), requiring  $\text{NAD}^+$  and a divalent cation for catalytic activity (Thompson et al. 1998; Raasch et al. 2000). GH4 is represented by  $\alpha$  and  $\beta$  glycosidases with distinct substrate specificity and in some cases a phosphorylated substrate is required (Henrissat and Bairoch 1996; Henrissat and Davies 1997). Well studied are the *B. subtilis* 6-phospho- $\alpha$ -glucosidase GlvA (Yip et al. 2007) and the *Thermotoga maritima* 6-phospho- $\beta$ glucosidase BglT (Yip and Withers 2006). Accordingly, they are retaining glycosidases but without the classical double-displacement mechanism (Koshland Jr 1953). Redox and elimination steps at the non-reducing end sugar are involved instead (see Fig. 2).  $\text{NAD}^+$  oxidizes the C3 hydroxyl group and thereby increases C2 proton acidity. A catalytic base residue, potentially a tyrosine conserved in all GH4 enzymes, deprotonates C2 in an E1cb elimination reaction resulting in a C2 carbanion and the unsaturated intermediate undergoes addition of water at the anomeric center releasing the reducing end sugar (Yip et al. 2004; Varrot et al. 2005). This mechanism indicates a heavy focus on the C2, thus the effect of an amino or N-acetyl functional group on ChbF activity is discussed in this work.

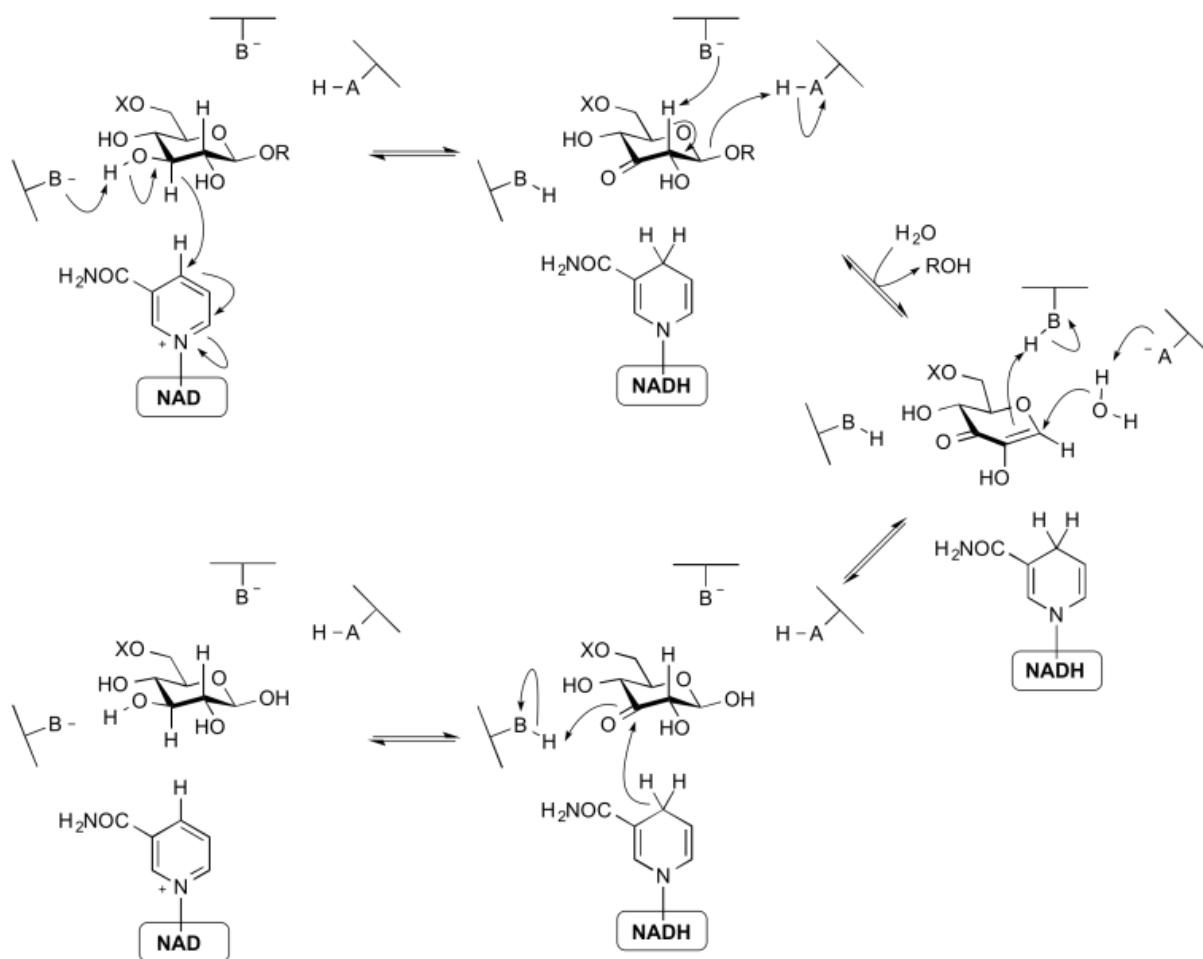


**Fig. 2. GH4 mechanism depending on NAD in a redox and elimination reaction.** NAD<sup>+</sup> oxidizes the C3 hydroxyl group thereby increasing C2 proton acidity. A catalytic base, potentially a tyrosine which is conserved in all GH4 enzymes, deprotonates C2 in an E1cb elimination reaction resulting in a C2 carbanion and the unsaturated intermediate undergoes addition of water at the anomeric center releasing the reducing end sugar (Yip et al. 2004; Varrot et al. 2005). This figure was obtained from CAZypedia (CAZypedia 2017).

### 1.3 Degradation of teichoic acids in Gram-positive bacteria

In most Gram-positive bacteria teichoic acids (TAs) are a major component of the cell envelope. TAs are anionic glycopolymers of glycerol-phosphate (GroP), ribitol-phosphate or sugar-phosphate units connected via phosphodiester bonds and modified with sugars or D-Ala residues. In *B. subtilis* 168 they are comprised of GroP modified with D-Ala and glucose (WTA) or GlcNAc (LTA) (Brown et al. 2013). While glycosylation greatly increases stability to alkaline hydrolysis, D-alanylation adds a positive charge, reducing the net anionic charge and thus decreasing cation binding (Neuhaus and Baddiley 2003; Brown et al. 2013; Percy and Gründling 2014).

The functions of TAs are diverse (Swoboda et al. 2010) and include pathogenicity (Morath et al. 2001; Weidenmaier et al. 2004), antibiotic resistance (Kovács et al. 2006; Brown et al. 2012), cation homeostasis (Archibald et al. 1961), phosphate reservoir (Grant 1979), cell di-

vision (LTA) and elongation (WTA) (Schirner et al. 2009). While cells lacking LTA or WTA suffer from growth defects but are viable, cells with neither do not grow at all. Accordingly, WTA and LTA may have vital and overlapping functions (Schirner et al. 2009). Although the structure and biosynthesis of TAs is well understood, knowledge about the degradation and potential recycling of TAs is still insufficient. Considering the necessity of either LTA or WTA for cell survival, differential degradation pathways are crucial. Therefore, previously unknown differences on which possible LTA and WTA hydrolases can recognize their respective substrate must exist and their biosynthesis suggests a difference in stereochemistry (Fig. 2, publication 4).

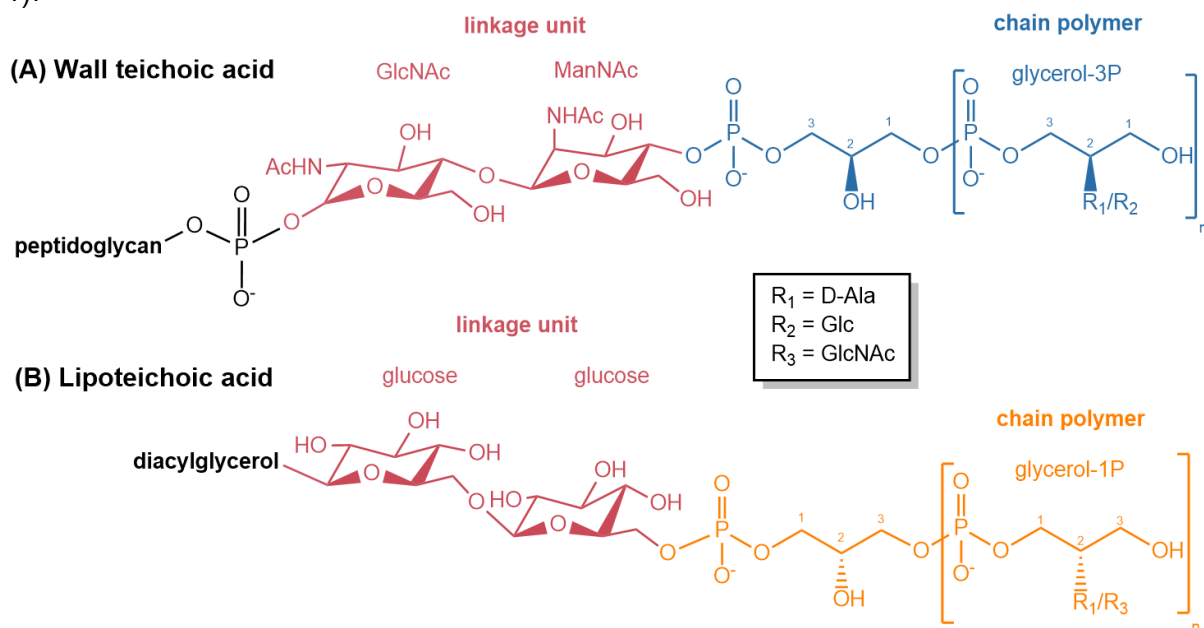


**Fig. 3. Teichoic acid composition in *Bacillus subtilis* 168.** **A**, WTA chain polymers (blue) of  $n = 40-60$  Gro3P (modified with D-Ala or Glc residues) attach to PGN via a linkage unit consisting of the linker disaccharide ManNAc- $\beta$ -1,4-GlcNAc (red) and one unmodified Gro3P. **B**, LTA chain polymers (orange) of Gro1P (modified with D-Ala or GlcNAc) anchor in the cytoplasmic membrane via a glycolipid comprised of the Glc- $\beta$ -1,6-Glc (red) linkage unit bound to diacylglycerol.

WTA (Fig. 3 A) are highly abundant in Gram-positive bacteria constituting up to 60 % of the cell wall total mass. In *B. subtilis* 168 they are comprised of 40-60 GroP repeats attached to every ninth PGN MurNAc residue via the linker disaccharide N-acetylmannosamine- $\beta$ -1,4-GlcNAc (ManNAc- $\beta$ -1,4-GlcNAc) and modified with D-Ala or Glc (Brown et al. 2013). As noted, WTA biosynthesis (Fig. 1 A, publication 4) provides evidence for *sn*-3 configuration of the GroP polymer subunits. Chain elongation occurs in the cytoplasm catalyzed by the *sn*-3-glycerol-phosphate (Gro3P) cytidyltransferase TagD and the teichoic acid poly(GroP) polymerase TagF. TagD provides CPD-glycerol (Park et al. 1993; Brown et al. 2013) for TagF, which transfers Gro3P directly to the growing chain polymer (Pooley et al. 1992; Schertzer and Brown 2003; Brown et al. 2013). Subsequently, the poly(Gro)  $\alpha$ -glucosyltransferase TagE adds glucose to the C2 hydroxyl group of Gro3P (Allison et al. 2011; Brown et al. 2013).



WTA function as a phosphate storage allowing further growth under phosphate starvation accompanied by the switch of WTA with phosphate-free teichuronic acids (Grant 1979; Ellwood and Tempest 1969), regulated by the PhoPR two-component system (Botella et al. 2011; Fritz and Mascher 2014). It has been shown that phosphate starvation induces the exo-acting GlpQ und endo-acting PhoD phosphodiesterases (Myers et al. 2016). Additionally, WTA turnover likely occurs concomitant with PGN turnover during normal cell growth (Mayer et al. 2019). The linker disaccharide is of particular interest for this work, since nothing is known about its degradation so far. In order to test possible enzymes for this substrate, purification of the linker disaccharide is investigated in this work.

*B. subtilis* 168 type I LTA (Fig. 3 B) is a GroP polymer membrane-anchored via Glc- $\beta$ -1,6-Glc-diacylglycerol (Percy and Gründling 2014). The precursor for biosynthesis (Fig. 1 B, publication 4) is phosphatidylglycerol (PG) (Fig. 2, publication 4), which contains *sn*-1-glycerol-phosphate (Gro1P) even though Gro3P is the initial substrate. The LTA precursor is generated by a series of reactions within the cytoplasm. CdsA transfers CMP to phosphatidic acid (phosphorylated diacylglycerol) and PgsA exchanges CMP with Gro3P forming PG-phosphate (Percy and Gründling 2014). Intriguingly, PG is formed by the release of the *sn*-3-phosphoryl group (the original phosphate group from Gro3P) while a Gro1P entity is retained with the phosphate group originating from phosphatidic acid. After translocation across the cytoplasmic membrane LtaS attaches Gro1P to the growing chain polymer (Reichmann and Gründling 2011). Alanylation of LTA is catalyzed by the Dlt system. DltA transfers D-Ala to DltC-Ppant, and DltB together with DltD adds D-Ala to Gro1P C2 (Percy and Gründling 2014).

The *B. subtilis* stereospecific exo-acting *sn*-Gro3P phosphodiesterase GlpQ (Myers et al. 2016) is of crucial importance for this work because of its stereospecificity. Previous studies on orthologues from *E. coli* and *Staphylococcus aureus* suggest a broad substrate spectrum for glycerophosphodiesterases (e.g. phosphatidylcholine, glycerophosphocholine, glycerophosphoethanolamine, glycerophosphoglycerol, bis(glycerophospho)-glycerol) (Larson et al. 1983; Jorge et al. 2017). All of these substrates contain Gro3P. Accordingly, GlpQ cannot cleave phosphatidylglycerol or lysophosphatidylglycerol, both of which possess a free Gro1P end (Larson and Loo-Bhattacharya 1988). The co-crystal structure of GlpQ in complex with Gro3P indicates that binding of Gro3P is highly favoured compared to Gro1P, as discussed in this work. GlpQ is not able to cleave LTA from *S. aureus*, which may be due to hindrance by modifications such as glycosylation or alanylation (Jorge et al. 2017). In this work GlpQ is used as a tool to elucidate the stereochemistry of TAs in *B. subtilis* 168 by differential digestion (Fig. 8, publication 4) and possible preferences of GlpQ regarding substrate modifications will be clarified.

## 1.4 Research objective

This work studies different aspects of bacterial amino sugar polymer catabolism. ChiA and its role in PGN degradation was explored, motivated by the work of Plumbridge, which indicates the existence of an alternative PGN recycling pathway in *E. coli* (Plumbridge 2009). Therefore, ChiA, described as a bifunctional enzyme with lysozyme and chitinase activity (Francetic et al. 2000a), was investigated in more detail and tested on natural substrates.

These experiments led to more open questions concerning the *chb* operon. The 6-phospho- $\beta$ -glucosidase ChbF with its unusual mechanism is of particular interest. Prior to cleavage by ChbF, diacetyl-chitobiose is deacetylated by ChbG. Contrary to the suggestion by Verma et al. (Verma and Mahadevan 2012), the mechanism of ChbF indicates that decisive reactions occur at the non-reducing end sugar requiring deacetylation at the non-reducing end. A thorough characterization of the ChbG product could clarify this question and possibly reveal other potential substrates such as the PGN disaccharide GlcNAc-MurNAc.

The importance of oligomeric sized chitin and PGN chains in medicine and research is becoming increasingly apparent, yet obtaining defined oligomers is not trivial. Therefore, this work also deals with their preparation, separation and detection.

A neglected aspect of PGN turnover and recycling in Gram-positive bacteria is the presence of WTAs covalently attached to PGN, which should undergo a turnover like PGN. This raises the question how WTA and LTA degradation is regulated, since in *B. subtilis* 168 both consist of GroP polymers and cells missing both are not viable. The recent discovery and characterization of the stereospecific phosphodiesterase GlpQ (Myers et al. 2016; Jorge et al. 2017) provides a convenient tool for the elucidation of TA stereochemistry. Accordingly, stereoisomery of LTA and WTA would allow differential degradation by stereospecific enzymes.

## 2 Results

### 2.1 Characterization of the chitinase ChiA of *E. coli* and chitin oligomer analysis

ChiA was described as a bifunctional enzyme with chitinase and lysozyme activity solely based on its ability to cleave the fluorogenic chitinase substrate 4-MU-(GlcNAc)<sub>3</sub> and to utilize the artificial chitinase/lysozyme substrate ethylene glycol chitin (EGC) (Francetic et al. 2000a). To reexamine ChiA function and specificity, the enzyme was purified and tested on the natural substrates colloidal chitin, chitosan and PGN. Colloidal chitin was prepared by acetylation of low molecular weight chitosan (2 - 3 kDa) with acetic anhydride. The used chitosan contained very small water-soluble fragments up to chitobiose (Fig. 8 A, publication 1). However, the smaller oligomers were removed by washing steps, thus the colloidal chitin contained no potential chitinase products (Fig. 7 A, publication 1). ChiA released diacetyl-chitobiose and triacetyl-chitobiose in approximately equal amounts (Fig. 7 B, publication 1), while a commercially available chitinase from *Streptomyces griseus* released exclusively diacetyl-chitobiose (Fig. 7 C, publication 1). As mentioned, chitosan contained minor oligomers such as chitobiose, chitotriose and chitotetraose (Fig. 8 A, publication 1). ChiA did not increase the amounts of these when incubated with chitosan and did not cleave chitotetraose. However, diacetyl-chitotriose was identified as minor product of chitosan digestion by ChiA (Fig. 8 B, publication 1). This trisaccharide was identified as GlcN-GlcNAc-GlcNAc, because further digestion with NagZ did not give rise to GlcNAc. In contrast, the *B. subtilis* chitosanase Csn completely digested chitotetraose and released chitobiose and chitotriose from chitosan as well as a mass corresponding to monoacetyl-chitotriose, presumably GlcN-GlcN-GlcNAc (Fig. 8 C, publication 1).

To test PGN as a substrate of ChiA, this was purified from *E. coli* and *B. subtilis* 168 cells harvested in exponential phase at OD<sub>600</sub> = 1 and WTA were removed from *B. subtilis* PGN by incubation with HCl. Compared to the controls (Fig. 9 A and Fig. 10 A, publication 1), ChiA did not release any products (Fig. 9 B, Fig 10 B, publication 1). *S. aureus* Atl glucosaminidase domain released large amounts of muropeptides and smaller amounts of MurNAc-GlcNAc (Fig. 9 C, Fig. 10 C, publication 1). In contrast, mutanolysin yielded exclusively muropeptides from *B. subtilis* PGN (Fig. 10 D, publication 1). To investigate if the peptides in the PGN interfere with cleavage, peptide-free (GlcNAc-MurNAc)<sub>n</sub> glycan chains were generated by incubation of PGN with the amidase CwIC, which readily removed peptides (Fig. 9 D, Fig. 10 E, publication 1). However, ChiA did not release products from these denuded glycan chains (Fig. 9 E, Fig. 10 F, publication 1), whereas Atl (Glc) released exclusively MurNAc-GlcNAc in significant amounts (Fig. 9 F, Fig. 10 G, publication 1). Surprisingly, mutanolysin did not release GlcNAc-MurNAc from *B. subtilis* PGN, yet peaks occurred at retention times from 28

- 38 min, the masses of which could not be associated with known PGN fragments (Fig. 10 H, publication 1).

Once ChiA was confirmed as a sole chitinase, growth experiments in minimal medium were performed to investigate *E. coli*'s dependence on ChiA for chitin utilization. In minimal medium supplemented with 0.1 % Glc and 0.2 % pentaacetyl-chitopentaose, wt and  $\Delta chiA$  grew exponentially, reaching stationary phase after 7 h (Fig. 11 C, publication 1) similar to growth on Glc as the sole carbon source (Fig. 11 A, publication 1) indicating that pentaacetyl-chitopentaose does not serve as a nutrient source for *E. coli* independent on the presence or not of ChiA. In contrast, wt and  $\Delta chiA$  both utilized diacetyl-chitobiose, growing in a biphasic pattern in the presence of 0.1 % Glc and 0.2 % diacetyl-chitobiose (Fig. 11 B, publication 1). Artificial expression of ChiA from plasmid pET22b-ChiA restored pentaacetyl-chitopentaose utilization. In minimal medium containing 0.1 % casamino acids (CAA) (to prevent carbon catabolite repression), 0.2 % pentaacetyl-chitopentaose and 0.5 M IPTG (for artificial expression of ChiA), growth of *E. coli* K12 wt and *E. coli* BL21 (DE3) pET22b-ChiA was compared. While the wt did not utilize pentaacetyl-chitobiose, the periplasmic expression of ChiA provided a significant growth advantage (Fig. 11 D, publication 1). *E. coli* BL21 (DE3) wt, like K12 wt, did not utilize pentaacetyl-chitopentaose. These results indicated that ChiA is usually not expressed in *E. coli* and hence does not support growth on chitin and chitin oligomers.

In order to establish analytic systems for chitin and chitosan we evaluated several HPLC columns for the purification of chitin and chitosan oligomers with defined chain lengths. Chitin oligomers were purified by acetone precipitation after hydrolysis of chitin flakes derived from crab shells in concentrated hydrochloric acid (Kazami et al. 2015). Of all columns tested, separation was best on a Shodex Asahipak NH2P column, giving good resolution with cleanly separated single peaks. Deacetylated oligomers were detected on either side of peaks containing completely acetylated oligomers (Fig. 5 C). The Luna Omega SUGAR column (2.1 x 150 mm) separated chitin oligomers as well, however, no partially deacetylated oligomers were detected and the peaks partially overlapped (Fig. 5 B). A Superdex 30 Increase 3.2/300 size exclusion column (designed for biomolecules from 100 to 7000 Da) separated the oligomers sequentially from high to low degree of polymerization (DP), yet with unsatisfactory resolution (Fig. 5 D). On the C18 Gemini column, the oligomers appeared as double peaks with broad and overlapping retention times (Fig. 5 A).

The separation of chitosan oligomers proved to be considerably more difficult. While maltodextrins from DP1 to DP15 separated very well on the Shodex Asahipak NH2P column (Fig. 4 A), chitosan oligomers < 1.5 kDa eluted in a distinct peak followed by rudimentary, densely packed peaks at 50 % ACN (Fig. 4 B). Further testing revealed precipitation of chitosan at ACN levels greater than 60 %. However, even in isocratic conditions with 50 % ACN and different flow rates (0.35, 0.5, and 1 ml/min), no improved separation was observed on a

Shodex Asahipak NH2P column. In a solvent-free approach on a Superdex 30 size exclusion column with 100 % LC-MS buffer (pH 3.5, which increased the solubility of chitosan), only chitobiose and chitotriose were detected in broad, overlapping peaks (Fig. 4 C).

In addition to HPLC, fluorophore assisted carbohydrate electrophoresis (FACE) (Jackson 1990) was performed. Labeling the sugars at the reducing end with ANTS (8-aminonaphthalene-1,3,6-trisulfonic acid) allowed electrophoretic separation in slightly alkaline medium (pH 8.5), where ANTS is negatively charged, in 32 % gel followed by detection under UV light. Maltodextrins (Fig. 6 A) and chitin oligomers (Fig. 6 B) were separated very well and the size of individual bands was determined by standards. Based on intensity, it appeared that mainly smaller chitin oligomers DP1 to DP5 were present in decreasing concentration with weaker bands in between. While smaller chitosan oligomers (< 1.5 kDa) were well separated, higher molecular weight chitosan (2 - 3 kDa) precipitated in the slightly alkaline environment of the gel loading pocket (Fig. 6 C). Chitosan oligomers appeared as double bands, which was observed with the chitopentaose standard as well. Further LC-MS analysis confirmed the standard to be pure chitopentaose.

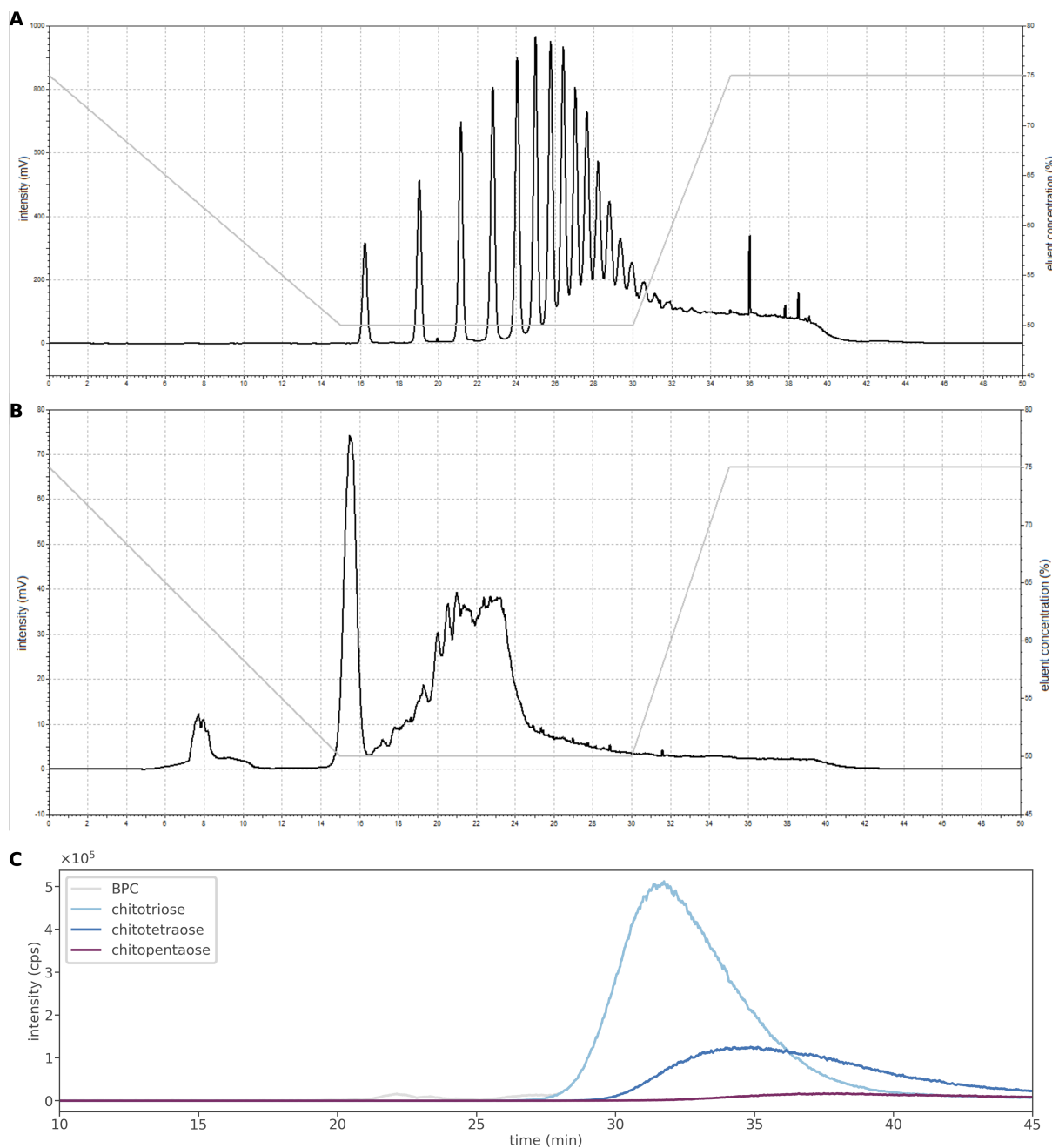


**Fig. 4. Maltodextrins were easily separated by HPLC compared to chitosan oligomers.** Maltodextrin and chitosan oligomer (< 1.5 kDa) separation by HPLC. On a Shodex Asahipak NH2P column distilled H<sub>2</sub>O and ACN as eluent was used with a flow rate of 0.35 ml/min. Shown are the evaporative light scattering detector (ELSD) chromatograms (black) and eluent concentrations (gray). **A**, maltodextrins separated at 50 % ACN with distinct peaks. **B**, chitosan oligomers eluted at 50 % ACN, after a dominant single peak at 15.5 min several poorly separated peaks were visible between 17 and 25 min. **C**, LC-MS analysis of chitosan oligomers (< 1.5 kDa) on a Superdex 30 size exclusion column in 100 % LC-MS buffer with a flow rate of 0.075 ml/min. Chitotriose eluted from 26 to 40 min and chitotetraose from 30 to 46 min. Chitopentaose intensities are very low and other masses were not detected. Shown is BPC mass range  $(M+H)^+$   $m/z = 100 - 2000$  (gray) and EICs of chitotriose  $(M+H)^+$   $m/z = 502.2243 \pm 0.05$  (light blue), chitotetraose  $(M+H)^+$   $m/z = 663.2931 \pm 0.05$  (blue) and chitopentaose  $(M+H)^+$   $m/z = 824.3619 \pm 0.05$  (purple).

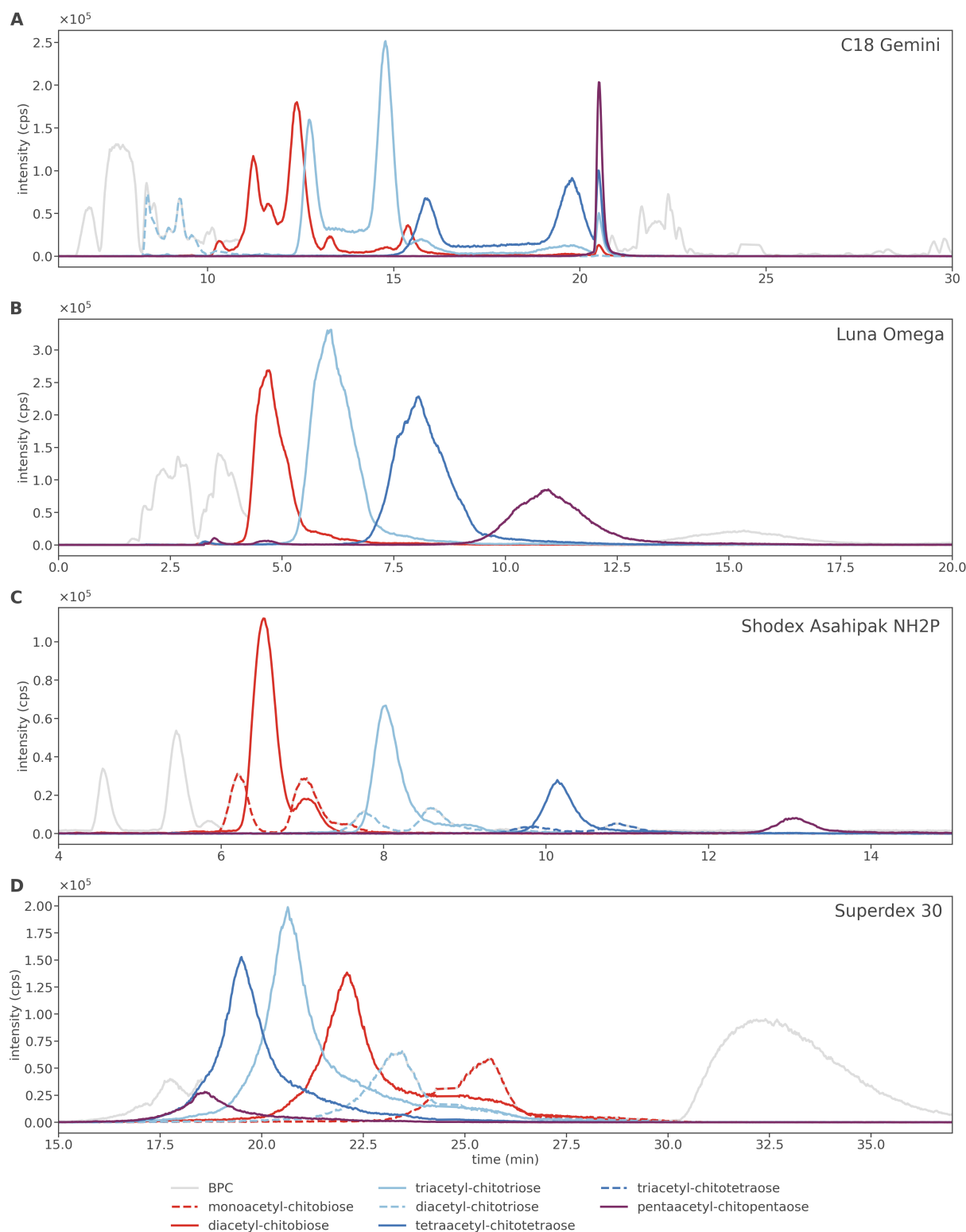


**Fig. 5. Shodex Asahipak NH2P separated chitin oligomers most efficiently.** Comparison of chitin oligomer separation on different columns in LC-MS. **A**, On a C18 Gemini column chitin oligomers from DP2 to DP4 appeared successively from 10 to 20 min as double peaks and DP5 at 20.6 min as a single peak. Monoacetyl-chitobiose was detected from 8.4 to 9.4 min. **B**, Exclusively fully acetylated oligomers were detected on a Luna Omega with a flow rate of 0.2 ml/min in 70 % ACN and 30 % LC-MS buffer. DP2 to DP5 eluted successively from 4 to 30 min as single peaks.

**Fig. 5. C,** The Shodex Asahipak NH2P column with a flow rate of 1 ml/min in 70 % ACN and 30 % LC-MS buffer separated chitin oligomers of DP2 to DP5 with distinct single peaks and partially deacetylated variants appeared as shoulder peaks before and after the fully acetylated oligomer. **D,** The Superdex 30 size exclusion column with a 0.075 ml/min flow rate in 100 % LC-MS buffer separated the oligomers from largest to smallest from 17.5 to 27 min detected in overlaying peaks. Shown are BPC mass range **A,C**  $(M+H)^+$   $m/z = 200 - 2000$  (gray), **B,D**  $(M+H)^+$   $m/z = 100 - 2000$  (gray) and the EICs for **A,B,D** of monoacetyl-chitobiose  $(M+H)^+$   $m/z = 383.166 \pm 0.05$  (red, dashed), diacetyl-chitobiose  $(M+H)^+$   $m/z = 425.1766 \pm 0.05$  (red, solid), diacetyl-chitotriose  $(M+H)^+$   $m/z = 586.2454 \pm 0.05$  (light blue, dashed), triacetyl-chitotriose  $(M+H)^+$   $m/z = 628.256 \pm 0.05$  (light blue, solid), tetraacetyl-chitotetraose  $(M+H)^+$   $m/z = 831.3353 \pm 0.02$  (blue, solid), pentaacetyl-chitopentaose  $(M+H)^+$   $m/z = 1034.4147 \pm 0.05$  (purple, solid) and for **C** monoacetyl-chitobiose  $(M+Na)^+$   $m/z = 405.148 \pm 0.02$  (red, dashed), diacetyl-chitobiose  $(M+Na)^+$   $m/z = 447.1585 \pm 0.02$  (red, solid), diacetyl-chitotriose  $(M+Na)^+$   $m/z = 608.2273 \pm 0.02$  (light blue, dashed), triacetyl-chitotriose  $(M+Na)^+$   $m/z = 650.2379 \pm 0.02$  (light blue, solid), triacetyl-chitotetraose  $(M+Na)^+$   $m/z = 811.3067 \pm 0.02$  (blue, dashed), tetraacetyl-chitotetraose  $(M+Na)^+$   $m/z = 853.3173 \pm 0.02$  (blue, solid), pentaacetyl-chitopentaose  $(M+Na)^+$   $m/z = 1056.3967 \pm 0.02$  (purple, solid).

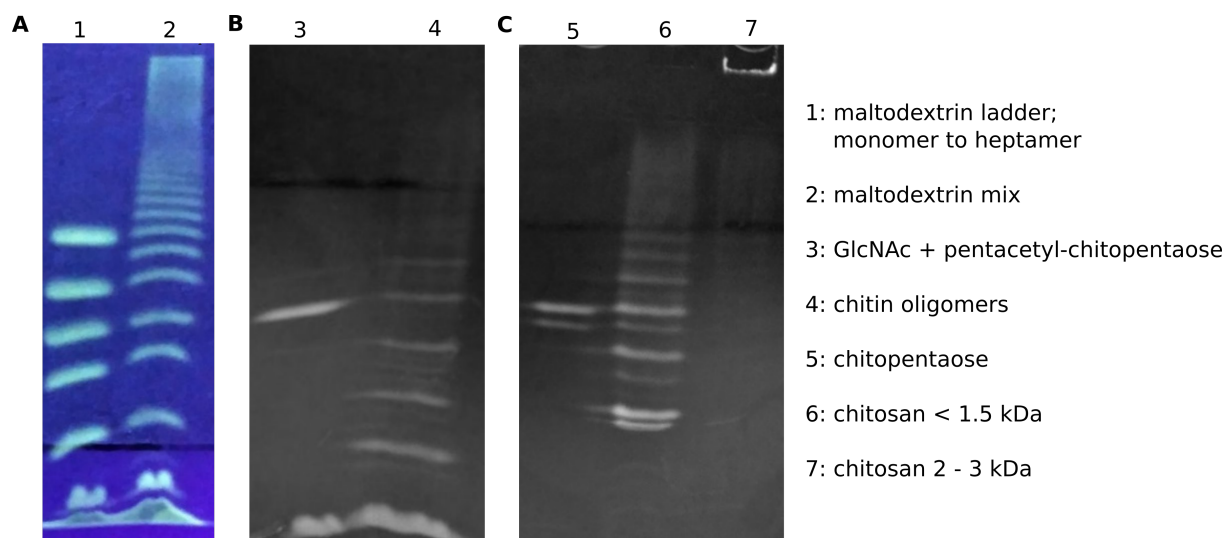


**Fig. 6. Chitin oligomer separation by FACE.** Sugar oligomer mixtures and standards were applied to FACE and visualized under UV light. **A,** maltodextrins (2) and a defined ladder from DP1 to DP7 (without DP6) (1) showed distinct bands. **B,** chitin oligomers (5) from DP1 to DP6 were visible alongside GlcNAc and pentaacetyl-chitopentaose as standards (4). Concentrations reduced significantly above DP6. **C,** chitopentaose (5) as well as chitosan oligomers < 1.5 kDa (6) appeared as double bands. Chitosan 2 - 3 kDa (7) was visible only in the loading pocket.



## 2.2 New functions of the *chb* operon of *E. coli* in chitin and peptidoglycan catabolism

Growth experiments were performed with ChbG and ChbF mutants to gain a better understanding of chitinase product metabolic pathways in *E. coli*. Accumulation products were characterized by LC-MS and enzymatic assays.

*E. coli* grew only on diacetyl-chitobiose and not on chitobiose as the sole substrate in M9 minimal medium depending on ChbG and ChbF. In contrast to the wt, which grew biphasic in M9 minimal medium supplemented with 0.1 % Glc and 0.2 % diacetyl-chitobiose, only Glc was utilized in  $\Delta chbG::kan$  and  $\Delta chbF::kan$  knockouts (Fig. 11 B, publication 1).

Both mutants were analyzed by LC-MS for possible accumulation products after growth in M9 casmino acid (CAA) minimal medium supplemented with 2 mM diacetyl-chitobiose or triacetyl-chitotriose. In the  $\Delta chbG::kan$  cytosolic fraction, no accumulation product was detected. Conversely, single deacetylated and partially dephosphorylated variants of the substrates were found in  $\Delta chbF::kan$  cytosolic fractions (Fig. 1 A, Fig. 2 A, publication 1).

A comparisons between cells harvested in exponential ( $OD_{600} = 1$ ) and stationary (overnight) growth phase revealed growth phase independent dephosphorylation and the addition of EDTA during cell disruption, to inhibit possible ion-dependent periplasmic phosphatases, did not abolish dephosphorylation. While diacetyl-chitobiose-phosphate (diacetyl-chitobiose-P) and diacetyl-chitobiose are present in approximately equal amounts during growth with diacetyl-chitobiose (Fig. 1 A, publication 1), more than ten times as much dephosphorylated product was detected after growth with triacetyl-chitotriose (Fig. 2 A, publication 1).

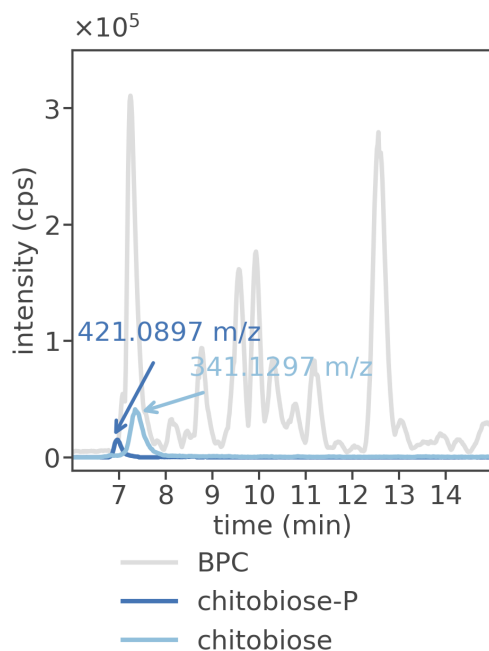


**Fig. 7. Accumulation of chitobiose and chitobiose-P in  $\Delta chbF::kan$  cells.** The cytosolic fraction of *E. coli*  $\Delta chbF::kan$  cells, grown in M9 CAA minimal medium supplemented with 2 mM chitobiose, was extracted and analyzed by LC-MS. Accumulation products with masses corresponding to chitobiose-P (blue) and chitobiose (light blue) were detected. Shown are BPC mass range  $(M+H)^+ m/z = 120 - 800$  (gray) and EICs of chitobiose-P  $(M+H)^+ m/z = 421.1218 \pm 0.05$  (blue) and chitobiose  $(M+H)^+ m/z = 341.1555 \pm 0.05$  (light blue).

Cells grown in the presence of chitobiose accumulated products with masses corresponding to chitobiose-P and chitobiose. Although the medium was supplemented with 2 mM chitobiose,

according to the experiment with diacetyl-chitobiose, the intensities of detected accumulation products were significantly lower in total and in relation to the background of the BPC (Fig. 7). Double mutants, deficient in the complete *nag* operon and *chbG* or *chbF*, were generated by P1 phage transduction of  $\Delta nag::tet$  into  $\Delta chbG::kan$  and  $\Delta chbF::kan$ . However, despite the absence of NagC repressor no accumulation product was detectable in  $\Delta chbG::kan \Delta nag::tet$  cells grown with diacetyl-chitobiose. Unexpectedly, almost complete dephosphorylation of the accumulation product was observed in  $\Delta nag::tet \Delta chbF::kan$  cells grown with chitobiose (Fig. 8 A) and diacetyl-chitobiose (Fig. 8 B) despite the absence of the phosphatase NagD.

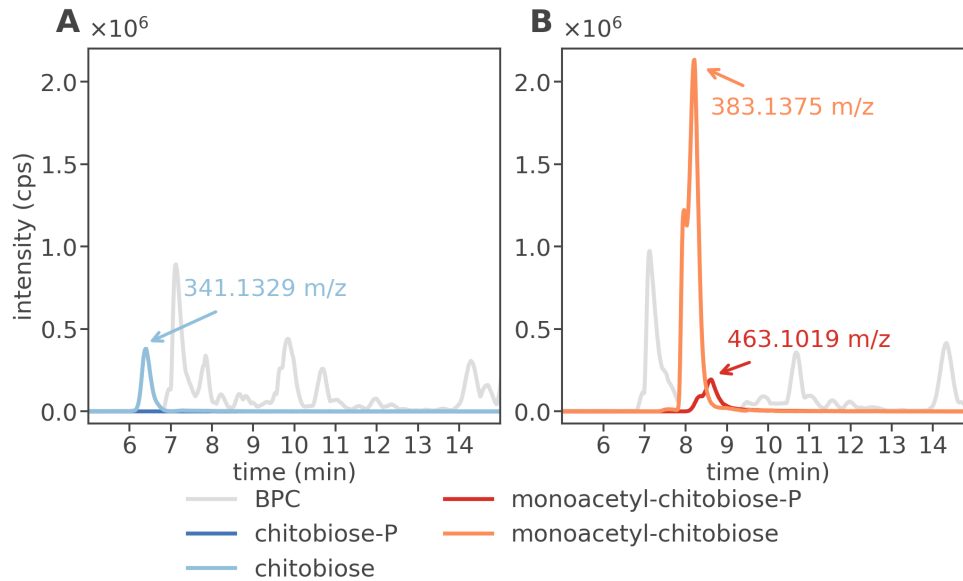


**Fig. 8. Almost complete dephosphorylation of accumulation products detected in  $\Delta nag::tet \Delta chbF::kan$  cells.** The cytosolic fraction of *E. coli nag::tet \Delta chbF::kan* cells, grown in M9 CAA minimal medium supplemented with 2 mM chitobiose or 2 mM diacetyl-chitobiose, was extracted and analyzed by LC-MS. **A**, after growth with chitobiose the dephosphorylated accumulation product chitobiose (light blue) was detected exclusively. **B**, after growth with diacetyl-chitobiose monoacetyl-chitobiose (orange) accumulated almost exclusively compared to monoacetyl-chitobiose-P (red). Shown are BPC mass range (M+H)<sup>+</sup> m/z = 120 - 800 (gray) and EICs of chitobiose (M+H)<sup>+</sup> m/z = 341.1555 +/- 0.05 (light blue), monoacetyl-chitobiose-P (M+H)<sup>+</sup> m/z = 463.1324 +/- 0.05 (red) and monoacetyl-chitobiose (M+H)<sup>+</sup> m/z = 383.166 +/- 0.05 (orange)

Cytosolic fractions containing  $\Delta chbF::kan$  accumulation products were treated with ChbF. It appeared that ChbF acted specifically on the phosphorylated accumulation products. Thus, the monoacetyl-chitobiose-P peak disappeared completely and masses corresponding to GlcN-phosphate (GlcN-P) and GlcNAc were detected (Fig. 1 B, publication 1). Accordingly, the intensity of diacetyl-chitotriose-P decreased significantly and masses corresponding to GlcN-P and diacetyl-chitobiose were detected (Fig. 2 B, publication 1). The measured intensity of GlcN-P was significantly lower compared to GlcNAc and diacetyl-chitobiose, respectively. The cytosolic fraction containing monoacetyl-chitobiose was additionally tested for digestion by NagZ. While NagZ readily released GlcNAc from diacetyl-chitobiose, monoacetyl-chitobiose

was not accepted as a substrate (Fig. 1 C, publication 1).

To test ChbF on diacetyl-chitobiose-P, i.e. substrate acetylated at the non-reducing end, expression of the ChbBCA PTS transporter on pQE32-ChbBCA was induced by IPTG in a  $\Delta chbG::kan$  background. After growth in M9 CAS minimal medium supplemented with 2 mM diacetyl-chitobiose, diacetyl-chitobiose and diacetyl-chitobiose-P were detected, however, neither were cleaved by ChbF (Fig. 6, publication 1).

The position of deacetylation in the ChbG product or ChbF substrate was determined also by reduction with sodium borohydride followed by digestion with ChbF and fragmentation by MS/MS. Reduction was complete and individual peaks with masses corresponding to the reduced products appeared (Fig. 3 A, publication 1). The dephosphorylated variant was detected at a much lower intensity compared to prior reduction. Reduced GlcNAc was released after incubation with ChbF, but GlcN-P was not detected and the substrate peak of reduced monoacetyl-chitobiose-P did not vanish completely (Fig. 3 B, publication 1).

Fragmentation of reduced monoacetyl-chitobiose-P by MS/MS yielded the mass of reduced GlcNAc and, at very low intensity, the mass of GlcN-P -H<sub>2</sub>O. The difference between reduced monoacetyl-chitobiose-P and reduced GlcNAc corresponded to the mass of GlcN-P -H<sub>2</sub>O.

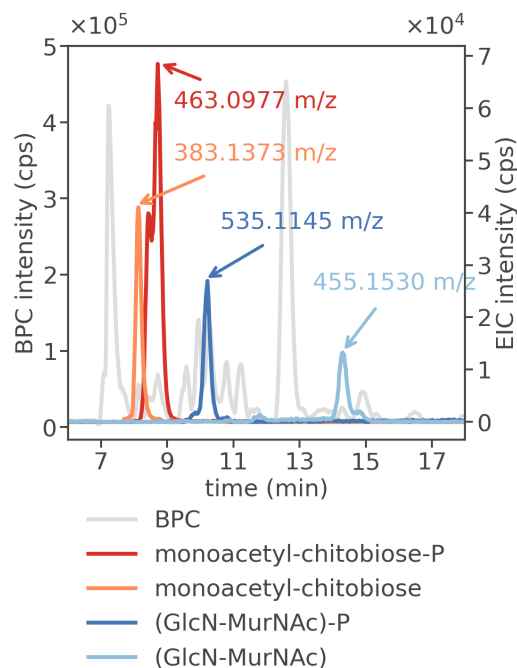


**Fig. 9. Removal of lactyl residue from GlcN-MurNAc/(GlcN-MurNAc)-P accumulation products.** The cytosolic fraction of *E. coli*  $\Delta chbF::kan$  cells, grown in M9 CAA minimal medium supplemented with 2 mM GlcNAc-MurNAc was extracted and analyzed by LC-MS. Masses corresponding to GlcN-MurNAc (light blue) and (GlcN-MurNAc)-P (blue) as well as compounds with the mass difference of a lactyl residue, monoacetyl-chitobiose (orange) and monoacetyl-chitobiose-P (red) were detected. Shown are BPC mass range (M+H)<sup>+</sup> m/z = 120 - 800 (gray) and EICs of (GlcN-MurNAc)-P (M+H)<sup>+</sup> m/z = 535.1535 +/- 0.05 (blue), GlcN-MurNAc (M+H)<sup>+</sup> m/z = 455.1872 +/- 0.05 (light blue), monoacetyl-chitobiose-P (M+H)<sup>+</sup> m/z = 463.1324 +/- 0.05 (red) and monoacetyl-chitobiose (M+H)<sup>+</sup> m/z = 383.166 +/- 0.05 (orange)

In order to investigate a possible involvement of the *chb* operon in PGN recycling  $\Delta chbF::kan$  cells were grown in M9 CAA minimal medium supplemented with 2 mM GlcNAc-MurNAc and checked for accumulation products. Within the cytosolic fraction (GlcN-MurNAc)-P and GlcN-MurNAc was detected with low intensities and monoacetyl-chitobiose-P and monoacetyl-chitobiose with significantly higher intensity (Fig. 9). The GlcNAc-MurNAc substrate was examined for diacetyl-chitobiose impurities, which could not be detected. ChbF was able to cleave (GlcN-MurNAc)-P yielding MurNAc whereas a mass corresponding to GlcN-P could not be observed (Fig. 10).

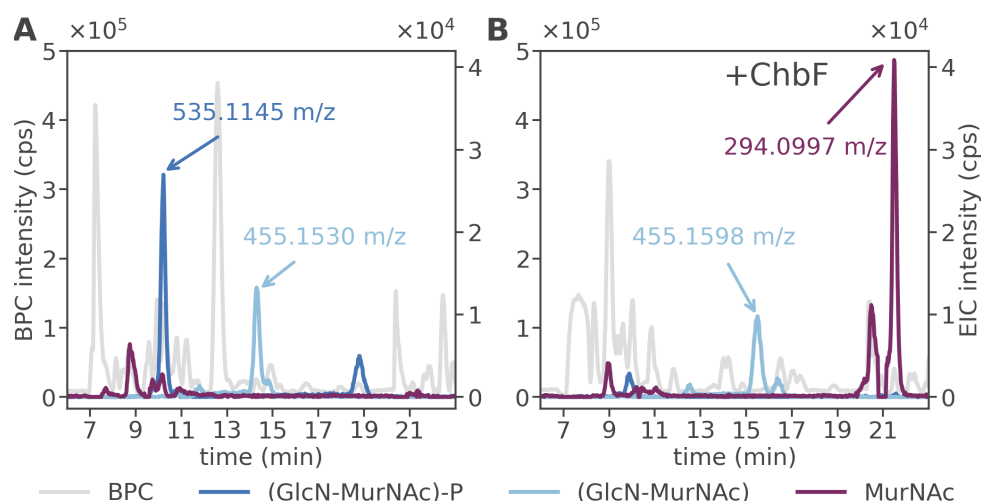
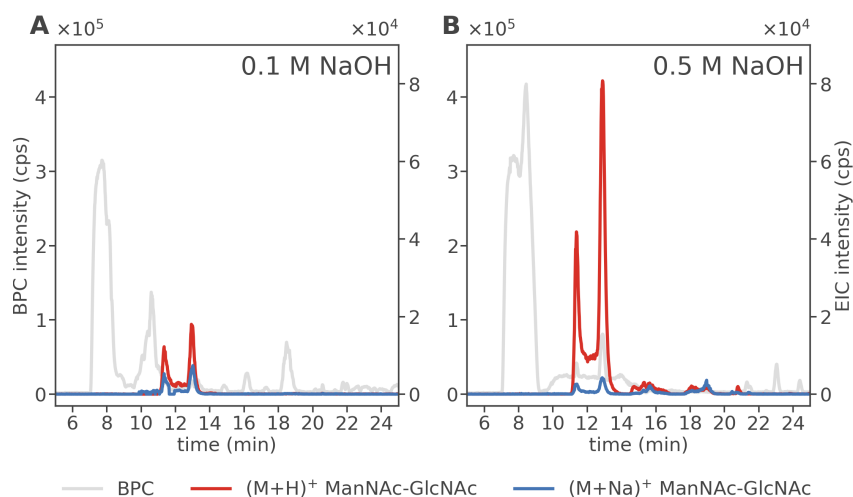


**Fig. 10. ChbF cleaves (GlcN-MurNAc)-P yielding MurNAc.** The cytosolic fraction of *E. coli*  $\Delta chbF::kan$  cells, grown in M9 CAA minimal medium supplemented with 2 mM GlcNAc-MurNAc was extracted, incubated with ChbF and analyzed by LC-MS. **A**, masses corresponding to GlcN-MurNAc (light blue) and (GlcN-MurNAc)-P (blue) occurred in the control. **B**, by the action of ChbF (GlcN-MurNAc)-P disappeared and a distinct double peak with the mass of MurNAc (purple) appeared. Shown are BPC mass range  $(M+H)^+$   $m/z = 120 - 800$  (gray) and EICs of (GlcN-MurNAc)-P  $(M+H)^+$   $m/z = 535.1535 \pm 0.05$  (blue), GlcN-MurNAc  $(M+H)^+$   $m/z = 455.1872 \pm 0.05$  (light blue) and MurNAc  $(M+H)^+$   $m/z = 294.1183 \pm 0.02$  (purple)

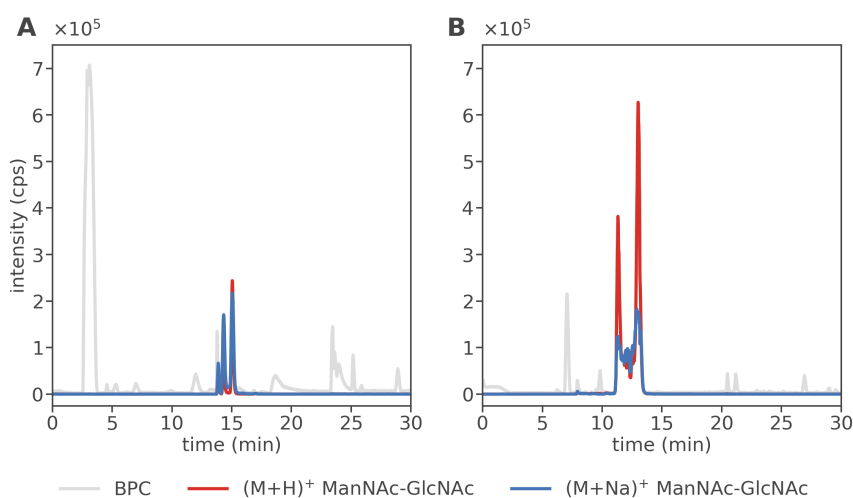
### 2.3 Recycling of the peptidoglycan-wallteichoic acid complex and differential digestion of teichoic acids

The WTA linker disaccharide ManNAc-GlcNAc was obtained by chemical hydrolysis of purified PGN-WTA complex. The GroP chain polymers were removed by alkaline hydrolysis with NaOH (2h, 60 °C) and the resulting PGN with ManNAc-GlcNAc still attached was neutralized by washing with bidistilled H<sub>2</sub>O. A significantly greater amount of ManNAc-GlcNAc was released if 0.5 M NaOH was applied compared to 0.1 M NaOH (Fig. 11). In comparison to the BPC, ManNAc-GlcNAc was the dominant peak when the higher concentration of NaOH was applied. The acid-labile phosphodiester bond between MurNAc and the linker disaccharide was cleaved by 5 % TCA (2h, 60 °C) and the sample was neutralized with NaOH (Hancock and Poxton 1988).

Different HPLC columns were tested for purification and programs were optimized especially for the separation of salts from ManNAc-GlcNAc. In a three-step gradient (water with 0 %, 8 %, and 40 % acetonitrile (ACN) as eluent for 10 min each, flow rate 0.5 ml/min) on a Hypercarb column (100 x 4.6 mm), ManNAc-GlcNAc eluted at 8 % ACN, clearly separated from the salt peak, which was detected after 3 min (Fig. 12 A). After several runs and collected fractions, no salt peak was detected and ManNAc-GlcNAc was almost pure, with few other masses present in the BPC at low intensity (Fig. 12 B).



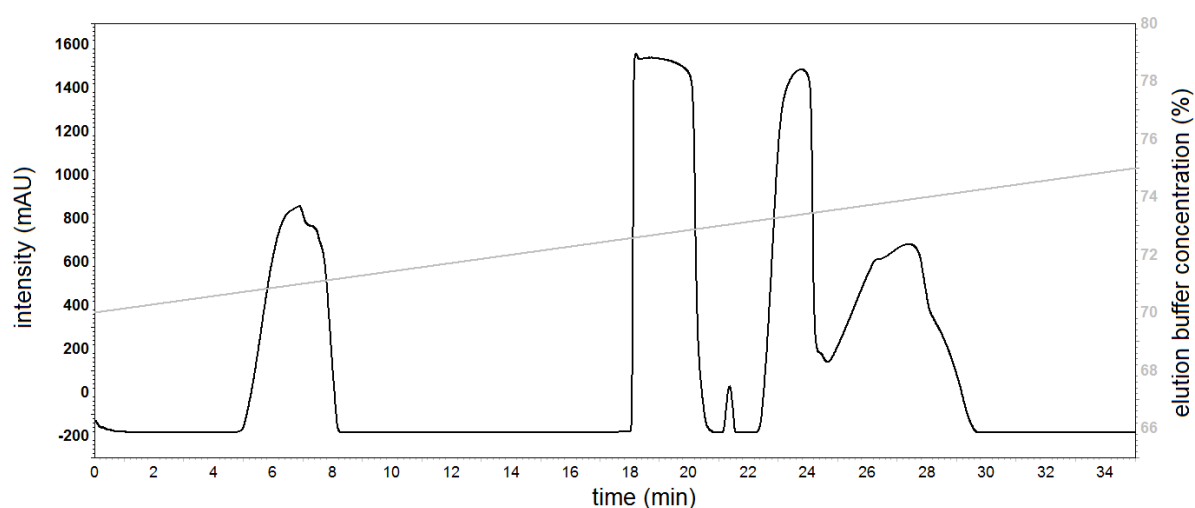
**Fig. 11. Application of 0.5 M NaOH during ManNAc-GlcNAc preparation yields significantly more product than 0.1 M NaOH.** Two NaOH concentrations were used during ManNAc-GlcNAc preparation and the amount of product was compared in LC-MS. **A**, 0.1 M NaOH yields only small amounts of ManNAc-GlcNAc compared to **B**, 0.5 M NaOH, where significant amounts with 4-fold higher intensities were detected. Shown are BPC mass range  $(M+H)^+$   $m/z = 120 - 800$  (gray) and EICs of ManNAc-GlcNAc  $(M+H)^+$   $m/z = 425.1766 \pm 0.05$  (red) and  $(M+Na)^+$   $m/z = 447.1585 \pm 0.05$  (blue).



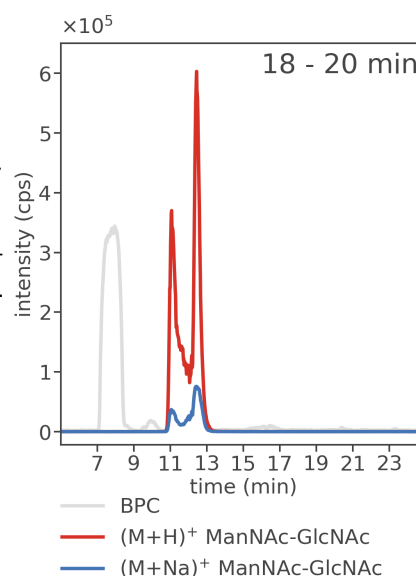
**Fig. 12. HyperCarb column effectively applied in small scale ManNAc-GlcNAc purification.** **A**, On an analytical HyperCarb column a three-step gradient in distilled  $H_2O$  with ACN as an eluent (0 %, 8 % and 40 % for 10 min each) and a flow rate of 0.5 ml/min was applied. LC-MS detects ManNAc-GlcNAc at 15 min and 8 % ACN, clearly separated from the salt peak at 4 min. **B**, ManNAc-GlcNAc containing fractions were collected. They contained ManNAc-GlcNAc with some minor other peaks, the salt peak was removed completely. Shown are BPC mass range  $(M+H)^+$   $m/z = 120 - 800$  (gray) and EICs of ManNAc-GlcNAc  $(M+H)^+$   $m/z = 425.1766 \pm 0.05$  (red) and  $(M+Na)^+$   $m/z = 447.1585 \pm 0.05$  (blue).

A linear gradient (70 % to 75 % ACN in water, 35 min, flow rate 0.8 ml/min) was applied to a Shodex Asahipak NH2P-50 4E column (250 x 4.6 mm) specifically designed for the separation of sugars. ManNAc-GlcNAc was detected from 18 to 20 min, however, the collected fraction still contained significant amounts of salt (peak at 7 min in LC-MS) (Fig. 13).

On a semi-preparative C18 Gemini column, ManNAc-GlcNAc was purified using a linear gradient (0 % to 40 % ACN in LC-MS buffer (0.1 % formic acid, 0.05 % ammonium formate in bidistilled H<sub>2</sub>O), 50 min, flow rate 0.95 ml/min). The collected fractions revealed ManNAc-GlcNAc with salts from 15.5 to 16.5 min and very pure ManNAc-GlcNAc without other compounds from 16.5 to 17.5 min. However, the concentrated samples were acidic at pH 3.5 (from LC-MS buffer) and ManNAc-GlcNAc was not detected in NMR.



**Fig. 13. Shodex Asahipak NH2P amino sugar column did not separate ManNAc-GlcNAc and salts.** On an Shodex Asahipak NH2P column a linear gradient from 70 to 75 % ACN in distilled H<sub>2</sub>O was applied with a flow rate of 0.8 ml/min (top). ManNAc-GlcNAc was detected by LC-MS (right) in the peak from 18 to 20 min together with a significant amount of salts, indicated by the BPC peak at 7 min. Shown are the absorption at 205 nm (black) and the eluent concentration (gray) in the HPLC chromatogram (top) and the LC-MS (bottom) BPC mass range (M+H)<sup>+</sup> m/z = 200 - 2000 (gray) and EICs of ManNAc-GlcNAc (M+H)<sup>+</sup> m/z = 425.1766 +/- 0.05 (red) and (M+Na)<sup>+</sup> m/z = 447.1585 +/- 0.05 (blue).



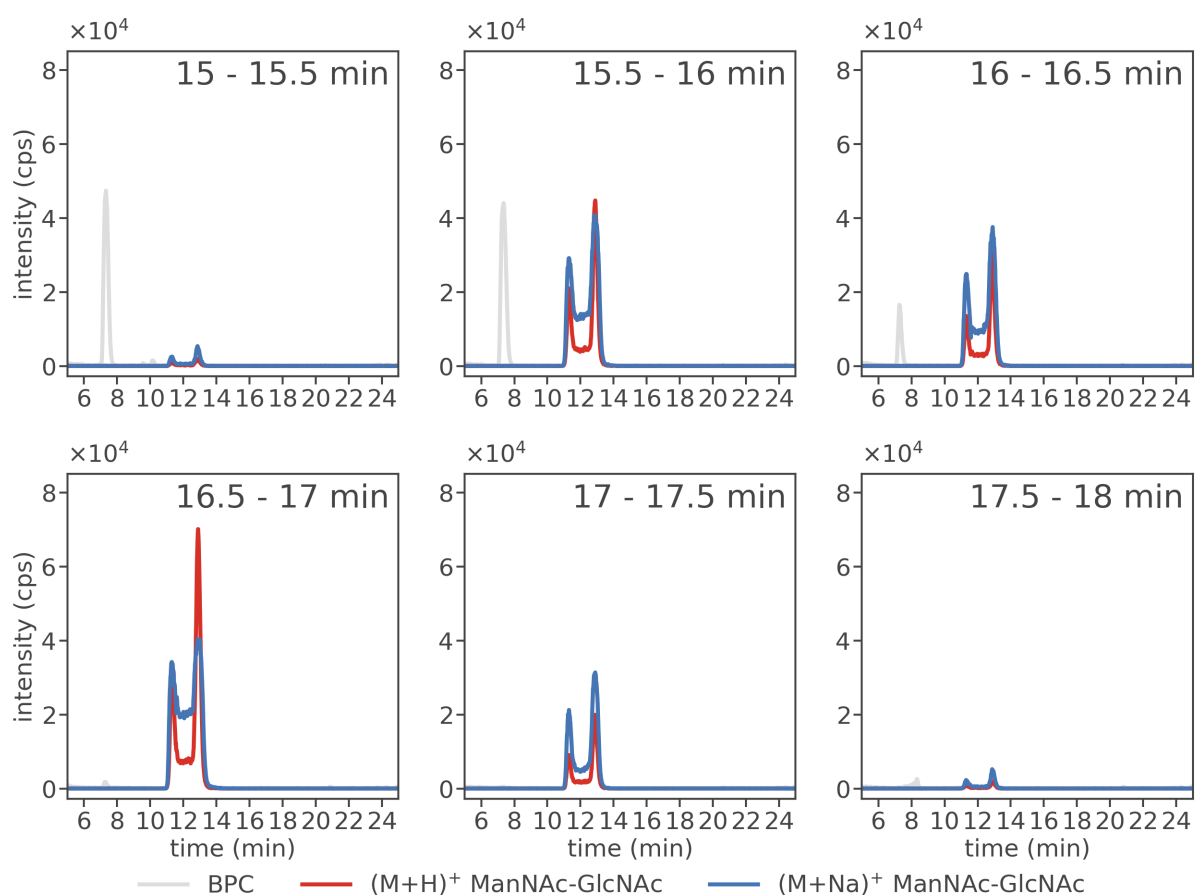
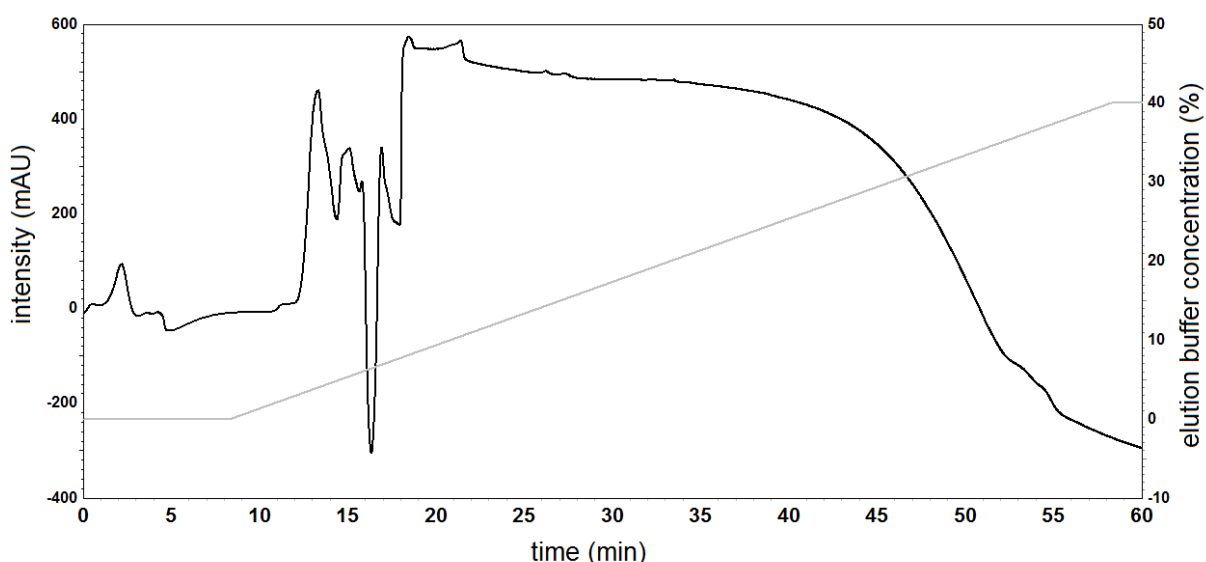


**Fig. 14. Pure ManNAc-GlcNAc obtained and effective removal of salts by purification with C18 Gemini column.** ManNAc-GlcNAc purification by HPLC on a semi-preparative C18 Gemini column in LC-MS buffer with a linear gradient from 0 to 40 % ACN over 50 min and a flow rate of 0.95 ml/min. Fractions were collected every 0.5 min and checked for purity and salt content by LC-MS. ManNAc-GlcNAc eluted from 15.5 to 17.5 min together with a salt peak until 16.5 min. From 16.5 to 17.5 min no other peaks appear in the BPC. Shown are the absorption at 205 nm (black) and the eluent concentration (gray) in the HPLC chromatogram (top) and the LC-MS (bottom) BPC mass range  $(M+H)^+$   $m/z = 200 - 2000$  (gray) and the EICs of ManNAc-GlcNAc  $(M+H)^+$   $m/z = 425.1766 \pm 0.05$  (red) and  $(M+Na)^+$   $m/z = 447.1585 \pm 0.05$  (blue).

*B. subtilis* 168 TAs and *Listeria monocytogenes* LTA were digested by the stereospecific glycerophosphodiesterase GlpQ to elucidate their stereochemistry (Fig. 8, publication 4). Non-glycosylated TAs were used as well to gain a deeper understanding of GlpQ substrate specificity. *B. subtilis* GlpQ was heterologously expressed in *E. coli* and its activity on glycerophosphocholine was confirmed. A temperature optimum of 55 °C and half-maximal activity at 30 °C was revealed and a narrow pH optimum was determined at pH 8.0 (Fig. S1 B, publication 4). Whereas GlpQ released significant amounts of GroP from isolated cell walls (PGN-WTA) derived from  $\Delta tagE::erm$  cells without WTA glycosylation (Fig. 4 D, publication 4), 22-fold less was released from wt PGN-WTA (Fig. 4 C, publication 4). In both cases, unmodified GroP was detected exclusively. GlpQ completely digested non-glycosylated WTA up to the linker disaccharide ManNAc-GlcNAc. The same amount of ManNAc-GlcNAc was detected in wt and  $\Delta tagE::erm$  PGN-WTA samples after digestion with NaOH, cleaving the GroP polymer, and TCA, releasing the linker disaccharide (Fig. 5 A, B, publication 4). TCA digestion alone released only very small amounts (Fig. 5 C, D, publication 4), however, after subsequent GlpQ and TCA digestion, the ManNAc-GlcNAc amount differed significantly in wt and  $\Delta tagE::erm$  with 3.6 % and 59 % of total ManNAc-GlcNAc (determined by NaOH and TCA digestion) (Fig. 5 E, F, publication 4).

In contrast to WTA, GlpQ did not cleave LTA isolated from wt and LTA glycosyltransferase deficient  $\Delta csbB::erm$  cells. Only very small amounts of GroP were detected (Fig. 6 C, D, publication 4). NMR analysis confirmed the removal of alanylation by preincubation at pH 8 (Fig. S5, publication 4). GlpQ released significantly more GroP after pretreatment of LTA in alkaline conditions (0.1 M NaOH, 60 °C, 30 min). The intensity of the pretreatment, determined by NaOH concentration, temperature and incubation time, was chosen in such a way that the chain polymers were precleaved but no single GroP residues were detected (Fig. 6 E, F, publication 4). GlpQ released 4.6 fold more GroP from non-glycosylated  $\Delta csbB::erm$  LTA (Fig. 6 H, publication 4) compared to wt LTA (Fig. 6 G, publication 4). These results have been confirmed with LTA obtained from *L. monocytogenes*.



## 3 Discussion

### 3.1 ChiA is a pure chitinase devoid of lysozyme-like activity

Previous characterization of ChiA substrate specificity and thus assignment as a bifunctional enzyme with chitinase and lysozyme activity is based solely on activity on artificial substrates (Francetic et al. 2000a). It was described as an endo-chitinase based on cleavage of the fluorogenic substrate 4-MU-(GlcNAc)<sub>3</sub>, but not of 4-MU-GlcNAc (Francetic et al. 2000a). As expected, the chitinase activity of ChiA was confirmed on colloidal chitin. The release of diacetyl-chitobiose and triacetyl-chitotriose in approximately equal amounts could be attributed to ChiA's five chitin binding domains, with cleavage occurring in between. Possibly ChiA requires binding to at least four substrate subunits, hence triacetyl-chitotriose is not cleaved further. Accordingly, ChiA binds anywhere in the substrate and acts as an endo-chitinase as described (Francetic et al. 2000a).

The release of GlcN-GlcNAc-GlcNAc from chitosan demonstrates the importance of acetylation for ChiA activity. The fact that no GlcN-GlcN-GlcNAc could be detected suggests that at least a large proportion of the sugars needs to be acetylated and cleavage might only be possible between two GlcNAc residues. Thus, ChiA is not a chitosanase but a chitinase that also cleaves partially deacetylated substrate.

Francetic et al. used ethylene glycol chitin (EGC) as lysozyme test substrate (Francetic et al. 2000a), which is basically modified chitin where ethylene glycol (C<sub>2</sub>H<sub>6</sub>O<sub>2</sub>) is attached to C6 of the GlcNAc residue (Li et al. 2013). However, the decisive difference between chitin and PGN glycan chains is the lactyl residue on MurNAc C3 and therefore EGC is sub-optimal as lysozyme test substrate. Even though some chitinases from *P. aeruginosa* (Wang and Chang 1997) and *V. cholerae* (Connell et al. 1998) were described as bifunctional enzymes with lysozyme activity utilizing EGC and a monofunctional chitinase from *S. marcescens* could not cleave EGC (Francetic et al. 2000a), demonstration of activity on the natural substrate PGN is more appropriate for an exact classification.

The catalytic domain of ChiA is classified as glycosyl hydrolase family 18, which includes both chitinases and lysozymes (CAZypedia 2018). However, ChiA showed no activity on whole PGN and on denuded glycan chains, where the peptides have been removed by CwIC. Complete removal of peptide cross-linking by CwIC (Shida et al. 2000) can be assumed because Atl (Glc) (Oshida et al. 1995) subsequently released exclusively MurNAc-GlcNAc. In contrast to a previous characterization of Atl (Glc) on *S. aureus* PGN revealing a strict specificity for glycan strands without peptides (Nega et al. 2020), Atl (Glc) readily released muropeptides from *B. subtilis* PGN. No preference for *E. coli* or *B. subtilis* glycan chains can be detected either, the former representing unmodified (GlcNAc-MurNAc)<sub>n</sub> polymers and the latter being partially O-acetylated and deacetylated (MurNAc 33% by PdaA and GlcNAc 19% by PdaB) (Fukushima et al. 2004; Fukushima et al. 2005; Walter and Mayer 2019).

Unexpectedly, mutanolysin did not release GlcNAc-MurNAc from denuded *B. subtilis* glycan

chains, thus peptidation seems to be required. Yet some peaks appeared that could not be assigned to known compounds. Possibly CwlC does not release peptides from O-acetylated or deacetylated MurNAc, a potential target for mutanolysin, however, the masses do not match any of these compounds.

The results disprove lysozyme activity of ChiA. It is therefore not a bifunctional enzyme but a strict chitinase that can cleave partially deacetylated chitin and thus not involved in the enigmatic alternative PGN recycling pathways suggested by Plumbridge.

*E. coli* possesses a type II secretion system (*gsp* secretome) for ChiA secretion (Francetic et al. 2000b) and the chitoporin ChiP for chitin oligomer uptake into the periplasm (Soyas and Suginta 2016). Periplasmic populations of ChiA could cleave those oligomers providing chitobiose and chitotriose for utilization by *chb* (Keyhani and Roseman 1997). Yet, *E. coli* K12 did not grow on pentaacetyl-chitopentaose. This is consistent with the silencing of both ChiA and the *gsp* secretome expression by the nucleoid structuring protein H-NS (Francetic et al. 2000a; Francetic et al. 2000b). Artificial expression of ChiA clearly enabled chitin oligomer utilization in a ChiA-dependent manner. Therefore ChiA does not need to be secreted and export to the periplasm, due to the ChiA signal sequence recognized by the Sec system (Crane and Randall 2017), is sufficient. The resulting chitinase products, degraded by enzymes of the *chb* operon, indirectly ensure the expression of ChiP and thus increased import of chitin oligomers. By default, ChiP expression is repressed by the sRNA ChiX, but binding of the *chb* transcript to ChiX leads to its degradation (Figueroa-Bossi et al. 2009; Rasmussen et al. 2009). Evolutionary pressure, for example, chitin-containing foods such as fungi, insects, or crustaceans in the intestines of animals and competition for these resources with other members of the microbiome, might select against the repression of ChiA expression and secretion by H-NS in some *E. coli* strains. On the other hand, repression might have emerged only in laboratory strains due to the absence of chitin or chitin oligomers. H-NS binds to genes acquired by lateral gene transfer, and functions as a gene silencer that increases bacterial fitness by silencing xenotic genes. H-NS does not co-localize with RNA polymerase and does not bind to actively transcribed genes, therefore gene expression is silenced by preventing RNA polymerase binding to DNA (Lucchini et al. 2006). In *Salmonella* the loss of H-NS resulted in severe growth defects (Ali et al. 2014) and the un-controlled expression of several pathogenicity islands (Lucchini et al. 2006). Also in *Salmonella* a mechanism to counter H-NS silencing has been identified, where a counter-silencer protein binds local DNA and disrupts the structure of the silencing complex allowing transcription (Will et al. 2014). It is possible that such a mechanism is also possible in *E. coli*, allowing expression of ChiA and *gsp* secretome under appropriate selection pressure.

Chitin and chitosan oligomers of defined chain length are of increasing interest in research and medicine (Rinaudo 2006; Schmitz et al. 2019). However, obtaining defined and pure

substrates is difficult because it is impossible to reliably stop the cleavage of polymers at the desired final chain length by chemical or enzymatic means. One possibility would be to mask sections of defined length in the sugar chains of chitin, chitosan or PGN sugar backbone by binding proteins such as the chitin binding domains of ChiA or the widely used binding module LysM, recognizing GlcNAc-containing polysaccharides (Mesnage et al. 2014). However, prerequisite is the clean separation of oligomers similar to PGN glycan separation done previously (Harz et al. 1990). For short chitin oligomers, separation via a Shodex Asahipak NH2P turned out to be particularly efficient. The spacing of the peaks increased with increasing chain length, allowing a clean collection of fractions. However, intensities, also in fluorophore-assisted carbohydrate electrophoresis (FACE), showed negative correlation of concentration and chain length for chitin oligomers obtained by acetone precipitation. Therefore, hardly any statements can be made about the behavior of higher molecular weight chitins. The biggest issue with chitosan oligomers was solubility in buffers with a high content of organic solvents such as ACN, which is indispensable for separation on reversed phase HPLC columns. Thus, chitosan oligomers cannot be separated on the Shodex Asahipak NH2P, even if a concentration of 50 % ACN was used at which the oligomers were still soluble. Additionally, higher molecular weight chitosan (2 - 3 kDA) is insoluble in the slightly alkaline milieu required for FACE. This complicates separation by electrophoresis because, for separation by size, this method must ensure a uniform charge on the molecule. However, at low pH, which increases the solubility of chitin and chitosan molecules, GlcN or GlcNAc residues are positively charged. Size exclusion chromatography, applicable without organic solvents, has the drawback of low resolution. Here, the Superdex 30 Increase 3.2/300 was selected as a column designed for the separation of small biomolecules (100 - 7000 Da). To increase the resolution, a series connection of several size exclusion columns would be advisable as has been done before, where a series of three Superdex 30 26/600 columns with a total length of 1.8 m was used to separate chitosan oligomers (Hamer et al. 2015).

### **3.2 The *chb* operon revisited: new functions in chitin and peptidoglycan catabolism**

With the confirmation of ChiA as a sole chitinase, the degradation of chitin end products in *E. coli* was studied in more detail. Of particular interest was the unusual mechanism of ChbF, a member of the glycosyl hydrolase family 4 (CAZypedia 2018). Other enzymes of this family, such as *B. subtilis* GlvA, suggest the decisive steps of hydrolysis take place at the non-reducing end of the disaccharide (Yip et al. 2007). ChbF cleaves a number of disaccharides such as cellobiose, salicin, and arbutin (Parker and Hall 1990). In these, the reducing end residues differ considerably, whereas the non-reducing end always consists of Glc. Unique in the *chb* pathway is a hydrolysis preceding deacetylation by ChbG. Verma et al. proposed deacetylation at the reducing end, thus GlcNAc6P-GlcN cleavage by ChbF yields GlcNAc6P and GlcN. The reason

for this assumption is efficient repression of the *chb* repressor NagC by GlcNAc6P (Verma and Mahadevan 2012). However, this conclusion cannot be reconciled with the previously known substrates of ChbF and the mechanism of GH4 enzymes, according to which the reducing end sugar is variable. In contrast, non-reducing end sugar acetylation could even be detrimental. Also GlcNAc6P would be generated by NagK (Uehara and Park 2004) from GlcNAc if ChbF would cleave GlcN6P-GlcNAc.

As expected, upon growth on diacetyl-chitobiose, monoacetyl-chitobiose-P was found in  $\Delta chbF::kan$  cytosolic fraction, taken up and phosphorylated by the PTS transporter Chb-BCA (Keyhani et al. 2000a; Keyhani et al. 2000b; Keyhani et al. 2000c) and deacetylated by ChbG (Verma and Mahadevan 2012). The presence of monoacetyl-chitobiose in approximately equal amounts suggests incomplete activity of a phosphatase. Cleavage of monoacetyl-chitobiose-P by ChbF into GlcN-P and GlcNAc indirectly locates the deacetylation at the non-reducing end, since phosphorylation at the non-reducing end sugar C6 was previously described (Keyhani et al. 2000c). The exo-N-acetyl-glucosaminidase NagZ cleaves GlcNAc from the non-reducing end (Litzinger et al. 2010a; Litzinger et al. 2010b) and hence should yield GlcNAc and GlcN from non-phosphorylated monoacetyl-chitobiose if GlcNAc was at the non-reducing end. NagZ readily cleaved diacetyl-chitobiose, yet the absence of products from monoacetyl-chitobiose identifies the disaccharide as GlcN-GlcNAc.

Accumulation of diacetyl-chitotriose-P and, to a lesser extent, chitobiose-P during the growth of  $\Delta chbF$  on triacetyl-chitotriose and chitobiose hints at the wide substrate range of ChbF. Cleavage of diacetyl-chitotriose-P into GlcN-P and diacetylchitobiose by ChbF not only demonstrates the importance of deacetylation at the non-reducing end but also suggest flexibility in regards to the reducing end residues.

The evidence for the position of deacetylation so far was indirect by a missing NagZ product from monoacetyl-chitobiose and GlcN-P as ChbF product together with the prior information of phosphorylation at non-reducing end by ChbBCA (Keyhani et al. 2000c). Reduction with sodium borohydride was performed for direct, unequivocal evidence.

The reduction of the hemiacetal at the reducing end sugar to a sugar alcohol can be detected in MS by a mass shift equivalent to the addition of H<sub>2</sub>. Thus, the release of reduced GlcNAc by ChbF clearly proved that acetylation is maintained at the reducing end. Lower activity of ChbF compared to the non-reduced sample can be explained by the increased salt content, since reduction takes place in 0.5 M borate buffer (Schaub and Dillard 2017; Kluj et al. 2018). Elevated salt levels explain also the absence of a GlcN-P product. The retention time of GlcN-P is with 8 min very close to the salt peak at 7 min. While salt is low in the unreduced sample, greatly increased salt concentration broadens the salt peak and quenches the detection of GlcN-P. Fragmentation of reduced monoacetyl-chitobiose-P by MS/MS and the concomitant formation of reduced GlcNAc clearly demonstrated the composition of the disaccharide. The mass difference between reduced monoacetyl-chitobiose and reduced GlcNAc

equals the mass of anhydrous GlcN-P. Since MS fragmentation is not hydrolysis the anhydrous mass is expected. The hardly present peak for GlcN-P itself as well as the generally higher intensity of GlcNAc in the HPLC-MS measurements can be explained by different tendencies to protonation in positive ion mode.

The existence of the monodeacetylase ChbG with its specificity for the non-reducing end sugar together with the non-utilization of diacetyl-chitobiose-P by ChbF must be explained by the unusual mechanism of ChbF. Oxidation of the C3 hydroxyl group by the NAD<sup>+</sup> cofactor increases acidity of the C2 proton and a E1cb elimination can take place with the aid of a catalytic base. The proton is released first and the C2 becomes a carbanion (Yip et al. 2004; Varrot et al. 2005; CAZypedia 2017). This reaction is supported by an electron-withdrawing electronegative functional group that increases the C2 positive dipole. When comparing the C2 dipoles of known ChbF substrates such as cellobiose-P (Glc6P-Glc) and GlcN6P-GlcNAc with GlcNAc6P-GlcN the difference becomes apparent. In all cases the non-reducing end sugar C2 is  $\delta^+$ , however, it is stronger with hydroxyl and amino groups compared to an N-acetyl group. An acetyl group is more electronegative than the hydrogens of -NH<sub>2</sub>, hence nitrogen  $\delta^-$  is less pronounced in an N-acetyl functional group and accordingly C2  $\delta^+$  is lower as well. Another possible reason for the necessity of deacetylation could be the spatial arrangement of the substrate in the binding pocket. An amino acid sequence alignment with ChbF and other GH4 members revealed high sequence similarity, particularly at the substrate binding site, a conserved cysteine residue located in close proximity to the C2 functional group and a divalent cation is involved in substrate binding. Therefore, an electronegative functional group would enhance binding. Based on a crystal structure of the *B. subtilis*  $\alpha$ -phospho-glucosidase GlvA with bound Glc6P (pdb identifier 1U8X), the steric effects of amino or N-acetyl group were modeled with PyMOL. GlvA Met173 was exchanged with ChbF Ile174 and the Glc6P C2 hydroxyl group was replaced with amino and N-acetyl group (Fig. 5, publication 1). While there is no problem finding room for the amino group, there is not enough space for an N-acetyl group. The acetyl group's oxygen interferes spatially with isoleucine and the methyl group with sulfur of the cysteine residue.

According to Verma et al., expression of the PTS transporter and ChbF alone from a heterologous promoter did not support growth on diacetyl-chitobiose and triacetyl-chitotriose (Verma and Mahadevan 2012). Indeed, ChbF did not cleave diacetyl-chitobiose-P, which underlines the critical importance of deacetylation at the non-reducing end by ChbG.

The *chb* operon is activated in glucose deficiency by CAP-cAMP and repressed by NagC in the absence of GlcNAc6P (Plumbridge and Pellegrini 2004). While these mechanisms have already been adequately studied, the identity of the coactivator of the dual function repressor/activator ChbR remains elusive. Verma et al. observed ChbG-dependent activation of ChbR and thus proposed deacetylated phosphorylated sugars such as monoacetyl-chitobiose-P

and chitobiose-P as ChbR coactivators (Verma and Mahadevan 2012).

Accordingly, no diacetyl-chitobiose-P accumulation product was found in *E. coli*  $\Delta chbG::kan$ . The reason could be either no induction of the *chb* operon or degradation of the accumulation product via alternative pathways. In the latter case, degradation of the dephosphorylated accumulation product by NagZ is a possibility. Utilization of diacetyl-chitobiose would give a significant growth advantage. However, alternative degradation can be ruled out because  $\Delta chbG::kan$  exhibited the same growth behavior as  $\Delta chbF::kan$  on Glc and diacetyl-chitobiose. Hence, lack of induction can be assumed.

The first step in the pathway where induction occurs is in  $\Delta chbF::kan$ . Thus, the coactivator of ChbR must be the ChbG product. Higher concentration of accumulation products in growth on diacetyl-chitobiose compared to chitobiose suggest monoacetyl-chitobiose-P as the main inducer. Repression by NagC can be excluded as a factor here, due to derepression by GlcNAc6P generated during PGN recycling constantly (Plumbridge 2009; Walter and Mayer 2019). Low accumulation product concentration in  $\Delta chbF::kan$  cells grown with chitobiose and the generally poorer growth on chitobiose compared with diacetyl-chitobiose suggest inefficient coactivation of ChbR by completely decetylated products such as chitobiose-P.

In all  $\Delta chbF::kan$  cytosolic fractions dephosphorylated variants of the expected accumulation products have been detected. Growth phase independent accumulation suggests it cannot be a stationary phase enzyme, such as the acid phosphatase (Dassa et al. 1982; Brøndsted and Atlung 1996). The addition of EDTA during cell disruption also excluded the Zn<sup>2+</sup>- and Mg<sup>2+</sup>-dependent periplasmic alkaline phosphatase PhoA (O'Brie and Herschlag 2001), as dephosphorylation was still observed. Consequently, an intracellular phosphatase of exponential growth was assumed. This would explain the low amount of accumulation product in  $\Delta chbG::kan$  cells grown on diacetyl-chitobiose with simultaneous expression of the ChbBCA PTS transporter. NagZ can cleave the phosphatase product diacetyl-chitobiose intracellularly (Litzinger et al. 2010a; Litzinger et al. 2010b). Thus the phosphatase would dephosphorylate almost all diacetyl-chitobiose-P unhindered by accumulating product, whereas in  $\Delta chbF::kan$  cells the accumulation product cannot be withdrawn by NagZ resulting in a reaction equilibrium between monacetyl-chitobiose and monoacetyl-chitobiose-P.

The ribonucleotide monophosphatase NagD with broad substrate range (Tremblay et al. 2006) can be excluded as well, since no reduction in dephosphorylation was detected in a  $\Delta nag::tet \Delta chbF::kan$  double mutant. The unexpected and almost complete dephosphorylation of chitobiose-P and monoacetyl-chitobiose-P allows the conclusion that it could be a phosphatase repressed by NagC and is increasingly expressed in its absence. Other possible candidates include the pyridoxal phosphate phosphatase YigL, dephosphorylating Glc6P, as well as YbiV and HxpB, described as sugar phosphatases with a wide substrate range (Kuznetsova et al. 2006).

A possible alternative PGN recycling pathway explaining intracellular elevated GlcNAc6P levels (Plumbridge 2009) might be related to the utilization of PGN sugars via the *chb* operon. The cytosolic fraction of  $\Delta chbF::kan$  cells grown with GlcNAc-MurNAc accumulates a compound with the mass of deacetylated (GlcNAc-MurNAc)-phosphate. Based on previous results of this work and the known phosphorylation at the non-reducing end sugar C6 (Keyhani et al. 2000c), the accumulation product can be confidently assumed to be GlcN6P-MurNAc. Unexpectedly, GlcN6P-GlcNAc accumulation was detected as well. Since impurities of the GlcNAc-MurNAc substrate were excluded, the MurNAc lactyl group might be removed by an etherase, possibly the N-acetylmuramic acid 6-phosphate etherase MurQ (Jaeger et al. 2005; Uehara et al. 2006). The lyase-type mechanism in which MurNAc C2 is deprotonated by a catalytic base and the lactyl group gets transferred to an enzymatic acid/base (Jaeger et al. 2005) might also occur with GlcN6P-MurNAc. Thus, the *chb* pathway might be involved in PGN recycling, possibly with the assistance of MurQ or a yet to be identified etherase.

### 3.3 Wall- and lipoteichoic acids are enantiomeric polymers

The motivation for the purification of the WTA linker disaccharide ManNAc-GlcNAc was to explore enzymes possibly involved in its recycling, acting together with phosphodiesterases such as GlpQ and PhoD (Myers et al. 2016) in cell wall turnover or during phosphate starvation. It seems consequential to assume that besides PGN and WTA chains also the linker may be recycled during cell wall turnover. Up to now, however, the fate of the linker disaccharide is unknown. Since phosphodiester bonds are susceptible to chemical hydrolysis, GroP polymers can be effectively cleaved in alkaline conditions and ManNAc-GlcNAc can be released from PGN under acidic conditions (Hancock and Poxton 1988). The reaction conditions should be chosen appropriately harsh, as an increase from 0.1 to 0.5 M NaOH provided a significant increase in yield. Removing TCA and NaOH salts is crucial to obtain a pure product, attempted here by HPLC. ManNAc-GlcNAc was difficult to separate from salts on a C18 Gemini semi-preparative column. Therefore, approximately half of the fractions needed to be discarded. Yield was low and not detectable in NMR. The biggest drawback of the C18 Gemini purification method were components of the buffer, formic acid and ammonium formate. They concentrated in the collected fractions and, although volatile in theory, were not completely removed by lyophilization. Attempts on the C18 Gemini to better separate the salt from ManNAc-GlcNAc and thus to be able to use all fractions remained unsuccessful. However, the C18 Gemini can also be used with water and ACN, eliminating the problems with salt in the collected fractions. The Shodex Asahipak NH2P column is designed for high pH stability and features amino functional groups. Even if a distinct peak containing ManNAc-GlcNAc was present, salts were not satisfactorily removed. Desalting improved on a Hypercarb column, based on porous graphitic carbon and compared to carbon modified silica phases the retention of polar compounds should be improved. In fact, ManNAc-GlcNAc was clearly separated from salts. Yet, purity was not

as good as with the C18 Gemini column.

Due to the complex isolation of PGN-WTA, an efficient method for cleaning is particularly important. The separation by Hypercarb column works sufficiently well, but there are no commercially available preparative columns. Therefore, it would be useful to test the loading capacities of the existing Hypercarb column with readily available substrate such as diacetylchitobiose, which at least on the C18 Gemini column has the same retention times and peak shapes as ManNAc-GlcNAc. One possibility to reduce the amount of salt in the samples could be a modified strategy for chemical digestion of PGN-WTA. To dissolve PGN-(ManNAc-GlcNAc) in TCA large volumes are needed because of the large PGN molecule. Prior isolation of WTAs, neutralization by dialysis and digestion with lower NaOH concentrations in increased temperature could drastically reduce the salt concentration and overall volume. Thus fewer HPLC runs in smaller columns, such as the Hypercarb column, would be sufficient for the final purification. However, this approach would require clean separation of GroP and ManNAc-GlcNAc. An alternative to chemical degradation of teichoic acids is the enzymatic cleavage using GlpQ (and/or PhoD) phosphodiesterases/teichoicases using a  $\Delta tagE$  strain with non-glycosylated WTA.

In *B. subtilis*, WTA and LTA both consist of GroP polymers and are spatially co-located in the cell wall compartment. It is known that WTA are degraded under phosphate depletion and replaced by teichuronic acids (Grant 1979; Ellwood and Tempest 1969). Furthermore, cells that do not produce either WTA or LTA are not viable (Schirner et al. 2009). This raises the question of how it is regulated that only one type of teichuronic acid is degraded at a time. Stereoisomery of the chain polymer building blocks could prevent simultaneous degradation by utilizing stereospecific enzymes. That WTA and LTA GroP subunits could be enantiomers has been supposed, but never clearly shown.

Therefore, WTA and LTA were differentially digested with GlpQ. GlpQ was recently described as an exo-acting stereospecific phosphodiesterase that preferentially cleaves non-glycosylated WTA, demonstrated indirectly based on the release of  $P_i$  upon digestion of WTA with GlpQ (Myers et al. 2016). Similarly, homologous enzymes from *E. coli* and *S. aureus* show a preference for Gro3P (Larson et al. 1983; Larson and Loo-Bhattacharya 1988; Jorge et al. 2017).

Crystal structure of GlpQ with Gro3P bound in the active site (pdb identifier 5T9B), together with data from other characterized phosphodiesterases, reveals a central divalent cation required for substrate coordination (Ohshima et al. 2008; Shi et al. 2008; Myers et al. 2016). Indeed, GlpQ was inhibited by EDTA. Closer examination of the active site strongly suggests *sn*-3 stereospecificity. Thus, the substrate binding pocket is divided into a hydrophilic side (His43, His85, Glu70, Glu152, Asp72) harbouring  $Ca^{2+}$  and a hydrophobic side (Phe190, Tyr259, Phe279) (Fig. 3, publication 4). The phosphate group of the substrate is oriented towards His43, Arg44 and His85 while the C1 and C2 hydroxyl groups face  $Ca^{2+}$  and binding is reinforced by the opposite hydrophobic side pushing away the hydrophilic regions of the sub-



strate. Consequently the binding of Gro1P becomes highly unlikely, because its C2 hydroxyl group would have to face the hydrophobic side, resulting in unstable binding. The confident assumption of GlpQ as a Gro3P specific phosphodiesterase based on the crystal structure and previous descriptions (Myers et al. 2016) is the foundation for experiments and conclusions in this work.

The release of GroP but not GroP-Glc from WTA directly proves GlpQ's specificity for unglycosylated WTA. Because D-Ala is removed at slightly alkaline conditions (Morath et al. 2001) no definite statement can be made about a possible hindrance of GlpQ due to alanylation. Even if alanylation was still partially preserved at the time of GlpQ digestion, the unstable product would likely have decayed into GroP and D-Ala at the time of measurement. In contrast, glycosylation is pH-stable and consequently an absent GroP-Glc product is clear evidence for the specificity of GlpQ for unglycosylated WTA. Accordingly, exolytic digestion of wt WTA can be assumed to happen only to the first occurrence of glycosylation, whereas unglycosylated WTA obtained from glycosyltransferase TagE (Allison et al. 2011) deficient cells gets completely degraded by GlpQ leaving solely the linker disaccharide ManNAc-GlcNAc attached to PGN. The fact that not all linker disaccharides are exposed after GlpQ digestion (compared to after chemical removal of chain polymers with NaOH) could be due to residual alanylation. As shown by NMR, LTA incubated for 24 h in pH 8 had a residual amount of about 30 % alanylation.

In agreement with studies on *S. aureus* GlpQ, which cannot cleave LTA (Jorge et al. 2017), only very small amounts of GroP were released from LTA preparations by *B. subtilis* GlpQ. These may be artefacts due to co-purified lipid-bound WTA precursors, readily digested by GlpQ (Myers et al. 2016). However, after alkaline pretreatment, GlpQ preferentially degraded non-glycosylated LTA releasing significant amounts of GroP. The reaction conditions during pretreatment were strong enough to randomly cleave the phosphodiester bonds within the chain polymer and mild enough not to generate individual GroP products. Thereby free Gro3P ends were accessible to GlpQ (Fig. 8, publication 4).

These experiments directly demonstrate the stereoisomery of WTA and LTA, with Gro3P WTA and Gro1P LTA. The origin of this lies in biosynthesis, where Gro3P is used as starting material in both polymers. In WTA, the chains are assembled in the cytoplasm by TagF, attaching Gro3P to the chain from CDP-glycerol (Fig. 1 A, publication 4) (Formstone et al. 2008; Swoboda et al. 2010). In LTA, however, Gro3P is transferred to phosphatidylglycerol-CMP by PgsA releasing CMP. The terminal phosphate of phosphatidylglycerol-phosphate derives from Gro3P and is cleaved off during translocation across the membrane or during polymerization of the growing LTA chain, possibly to energize these processes. Hence, a Gro1P residue remains and gets attached to the chain by LtaS (Fig. 1 B, publication 4) (Percy and Gründling 2014). This enzymatic evidence was only possible due to the recent elucidation of LTA glycosylation in *B. subtilis* and *L. monocytogenes* (Rismondo et al. 2018; Rismondo et al. 2019). By utilizing stereospecific enzymes, cells can avoid simultaneous degradation of WTA and LTA

and thereby ensure cell viability (Schirner et al. 2009). Also, glycosylation provides additional protection against accidental degradation by GlpQ and a potential mechanism for fine tuning degradation.

### 3.4 Conclusion

The bacterial amino sugar metabolism is a very complex process, because it involves not only the enzymatic processes of degradation of nutrient sources such as chitin, chitosan and their oligomers for energy production, but also the build-up and degradation (turnover) of various cell wall structures, e.g. the PGN-WTA complex of Gram-positive bacteria.

In search of the alternative PGN recycling pathway in *E. coli* suggested by Plumbridge et al. (Plumbridge 2009), the periplasmic ChiA, classified as a bifunctional enzyme with lysozyme and chitinase activity (Francetic et al. 2000a), was studied in more detail. Tests on the natural substrates chitin, chitosan and PGN glycan chains freed from peptides revealed that ChiA as a sole chitinase. Under laboratory conditions, the expression of ChiA is inhibited by H-NS, but growth on the chitin oligomer pentaacetyl-chitopentaose was facilitated by artificial expression of ChiA. Chitinase products can be metabolized via the *chb* operon. It was shown that the 6-phospho- $\beta$ -glucosidase ChbF, due to an unusual mechanism, requires substrates with a deacetylated non-reducing end residue. This step is accomplished by ChbG and is also crucial for the induction of the operon, thus the ChbG product is the coactivator of the transcriptional regulator ChbR. Little was previously known about the recycling of the PGN-WTA complex in Gram-positive bacteria. In addition to experiments on the purification of the WTA linker disaccharide ManNAc-GlcNAc, new insights into the structure of TAs in *B. subtilis* 168 were gained using the stereospecific phosphodiesterase GlpQ (Myers et al. 2016), involved in WTA turnover during phosphate starvation. Differential digestion revealed the building blocks of the two glycopolymers to be enantiomers. This allows targeted degradation of only one polymer at a time by stereospecific enzymes.

Collaborative projects have contributed to the structural elucidation of WTA by HPLC-MS. Hence it was shown that some *Staphylococcus epidermidis* strains can switch from a commensal to a pathogenic lifestyle by forming *Staphylococcus aureus*-type WTA, which increases host mortality and enables exchange of DNA with *S. aureus* through bacteriophages. Furthermore, HPLC-MS experiments helped to elucidate the composition of cell wall glycopolymers in *Streptomyces* sp. mycelia and spores.

In addition, new topics could be initiated that are of particular interest for future research. The alternative PGN recycling pathway remains elusive, but there is evidence for degradation of GlcNAc-MurNAc by the *chb* operon, possibly involving an etherase. Also, the activity of an as yet unknown phosphatase was observed, which may serve a detoxification function in the presence of harmful accumulation products. For the purification of chitin and PGN oligomers, there is still no decisive breakthrough. Since the procedure with standard HPLC columns has

proven to be difficult, other techniques such as size exclusion chromatography and gel electrophoresis should be explored. Research on WTA recycling in Gram-positive bacteria is just beginning and offers potential for further discovery of WTA hydrolases and a clean purification of the linker disaccharide offers the possibility of elucidating its fate.

## 4 References

- Adams, David W et al. (2019). "DNA-uptake pili of *Vibrio cholerae* are required for chitin colonization and capable of kin recognition via sequence-specific self-interaction". In: *Nature microbiology* 4.9, pp. 1545–1557.
- Ali, Sabrina S et al. (2014). "Silencing by H-NS potentiated the evolution of Salmonella". In: *PLoS Pathog* 10.11, e1004500.
- Allison, Sarah E et al. (2011). "Studies of the genetics, function, and kinetic mechanism of TagE, the wall teichoic acid glycosyltransferase in *Bacillus subtilis* 168". In: *Journal of Biological Chemistry* 286.27, pp. 23708–23716.
- Archibald, AR et al. (1961). "Teichoic acids and the structure of bacterial walls". In: *Nature* 191.4788, pp. 570–572.
- Blokesch, Melanie (2012). "Chitin colonization, chitin degradation and chitin-induced natural competence of *Vibrio cholerae* are subject to catabolite repression". In: *Environmental microbiology* 14.8, pp. 1898–1912.
- Boothby, Derek et al. (1973). "Turnover of bacterial cell wall peptidoglycans". In: *Journal of Biological Chemistry* 248.6, pp. 2161–2169.
- Borisova, Marina et al. (2016). "Peptidoglycan recycling in Gram-positive bacteria is crucial for survival in stationary phase". In: *MBio* 7.5.
- Botella, Eric et al. (2011). "Cell envelope gene expression in phosphate-limited *Bacillus subtilis* cells". In: *Microbiology* 157.9, pp. 2470–2484.
- Brøndsted, Lone and Tove Atlung (1996). "Effect of growth conditions on expression of the acid phosphatase (cyx-appA) operon and the appY gene, which encodes a transcriptional activator of *Escherichia coli*." In: *Journal of bacteriology* 178.6, pp. 1556–1564.
- Brown, Stephanie, John P Santa Maria Jr, and Suzanne Walker (2013). "Wall teichoic acids of gram-positive bacteria". In: *Annual review of microbiology* 67, pp. 313–336.
- Brown, Stephanie et al. (2012). "Methicillin resistance in *Staphylococcus aureus* requires glycosylated wall teichoic acids". In: *Proceedings of the National Academy of Sciences* 109.46, pp. 18909–18914.
- Brun, Emmanuel et al. (1997). "Solution structure of the cellulose-binding domain of the endoglucanase Z secreted by *Erwinia chrysanthemi*". In: *Biochemistry* 36.51, pp. 16074–16086.

- CAZypedia (2017). *Glycoside hydrolases — CAZypedia, 1 2007-2017 The Authors and Curators of CAZypedia*. [Online; accessed 18-December-2020 ]. URL: [http://www.cazypedia.org/index.php?title=Glycoside\\_hydrolases&oldid=11575](http://www.cazypedia.org/index.php?title=Glycoside_hydrolases&oldid=11575).
- CAZypedia, Consortium (2018). “Ten years of CAZypedia: a living encyclopedia of carbohydrate-active enzymes”. In: *Glycobiology* 28.1, pp. 3–8.
- Chen, Lei et al. (2014). “Fully deacetylated chitooligosaccharides act as efficient glycoside hydrolase family 18 chitinase inhibitors”. In: *Journal of Biological Chemistry* 289.25, pp. 17932–17940.
- Cheng, Qiaomei and James T Park (2002). “Substrate specificity of the AmpG permease required for recycling of cell wall anhydro-muropeptides”. In: *Journal of bacteriology* 184.23, pp. 6434–6436.
- Cheng, Qiaomei et al. (2000). “Molecular Characterization of the  $\beta$ -N-Acetylglucosaminidase of *Escherichia coli* and Its Role in Cell Wall Recycling”. In: *Journal of bacteriology* 182.17, pp. 4836–4840.
- Connell, Terry D et al. (1998). “Endochitinase Is Transported to the Extracellular Milieu by the eps-Encoded General Secretory Pathway of *Vibrio cholerae*”. In: *Journal of bacteriology* 180.21, pp. 5591–5600.
- Crane, Jennine M and Linda L Randall (2017). “The Sec system: protein export in *Escherichia coli*”. In: *EcoSal Plus* 7.2.
- Dassa, Elie et al. (1982). “The acid phosphatase with optimum pH of 2.5 of *Escherichia coli*. Physiological and Biochemical study.” In: *Journal of Biological Chemistry* 257.12, pp. 6669–6676.
- Davis, Brian and Douglas E Eveleigh (1984). “Chitosanases: occurrence, production and immobilization”. In: *Chitin, chitosan and related enzymes*, pp. 161–179.
- Doyle, R Jennings, J Chaloupka, and V Vinter (1988). “Turnover of cell walls in microorganisms.” In: *Microbiological reviews* 52.4, p. 554.
- Ellwood, DC and DW Tempest (1969). “Control of teichoic acid and teichuronic acid biosynthesis in chemostat cultures of *Bacillus subtilis* var. niger”. In: *Biochemical Journal* 111.1, pp. 1–5.
- Figueroa-Bossi, Nara et al. (2009). “Caught at its own game: regulatory small RNA inactivated by an inducible transcript mimicking its target”. In: *Genes & development* 23.17, pp. 2004–2015.
- Fleming, Alexander and VD Allison (1922). “Observations on a bacteriolytic substance (lysozyme) found in secretions and tissues”. In: *British journal of experimental pathology* 3.5, p. 252.

- Formstone, Alex et al. (2008). "Localization and interactions of teichoic acid synthetic enzymes in *Bacillus subtilis*". In: *Journal of bacteriology* 190.5, pp. 1812–1821.
- Francetic, Olivera et al. (2000b). "Expression of the endogenous type II secretion pathway in *Escherichia coli* leads to chitinase secretion". In: *The EMBO Journal* 19.24, pp. 6697–6703.
- Francetic, Olivera et al. (2000a). "The ChiA (YheB) protein of *Escherichia coli* K-12 is an endochitinase whose gene is negatively controlled by the nucleoid-structuring protein H-NS". In: *Molecular microbiology* 35.6, pp. 1506–1517.
- Fritz, Georg and Thorsten Mascher (2014). "A balancing act times two: sensing and regulating cell envelope homeostasis in *Bacillus subtilis*". In: *Molecular microbiology* 94.6, pp. 1201–1207.
- Fukushima, Tatsuya, Toshihiko Kitajima, and Junichi Sekiguchi (2005). "A polysaccharide deacetylase homologue, PdaA, in *Bacillus subtilis* acts as an N-acetylmuramic acid deacetylase in vitro". In: *Journal of bacteriology* 187.4, pp. 1287–1292.
- Fukushima, Tatsuya et al. (2004). "Characterization of a polysaccharide deacetylase gene homologue (pdaB) on sporulation of *Bacillus subtilis*". In: *Journal of biochemistry* 136.3, pp. 283–291.
- Gisin, Jonathan et al. (2013). "A cell wall recycling shortcut that bypasses peptidoglycan de novo biosynthesis". In: *Nature chemical biology* 9.8, pp. 491–493.
- Glauner, Bernd (1988). "Separation and quantification of muropeptides with high-performance liquid chromatography". In: *Analytical biochemistry* 172.2, pp. 451–464.
- Gonçalves, Isabelle R et al. (2016). "Genome-wide analyses of chitin synthases identify horizontal gene transfers towards bacteria and allow a robust and unifying classification into fungi". In: *BMC evolutionary biology* 16.1, pp. 1–17.
- Gram, Christian (1884). "The differential staining of *Schizomycetes* in tissue sections and in dried preparations". In: *Fortschritte der Medicin* 2.6, pp. 185–189.
- Grant, WD (1979). "Cell wall teichoic acid as a reserve phosphate source in *Bacillus subtilis*." In: *Journal of Bacteriology* 137.1, pp. 35–43.
- Hamer, Stefanie Nicole et al. (2015). "Enzymatic production of defined chitosan oligomers with a specific pattern of acetylation using a combination of chitin oligosaccharide deacetylases". In: *Scientific reports* 5, p. 8716.
- Hamid, Rifat et al. (2013). "Chitinases: an update". In: *Journal of pharmacy & bioallied sciences* 5.1, p. 21.

- Hancock, Ian and Ian Poxton (1988). *Bacterial cell surface techniques*. Wiley & Sons.
- Harz, Hartmann, Knut Burgdorf, and Joachim-Volker Höltje (1990). "Isolation and separation of the glycan strands from murein of *Escherichia coli* by reversed-phase high-performance liquid chromatography". In: *Analytical biochemistry* 190.1, pp. 120–128.
- Henrissat, Bernard and Amos Bairoch (1996). "Updating the sequence-based classification of glycosyl hydrolases". In: *Biochemical Journal* 316.2, pp. 695–696.
- Henrissat, Bernard and Gideon Davies (1997). "Structural and sequence-based classification of glycoside hydrolases". In: *Current opinion in structural biology* 7.5, pp. 637–644.
- Hirano, Shigehiro, Yasuo Ohe, and Haruhiro Ono (1976). "Selective N-acylation of chitosan". In: *Carbohydrate Research* 47.2, pp. 315–320.
- Höltje, Joachim-Volker (1998). "Growth of the stress-bearing and shape-maintaining murein sacculus of *Escherichia coli*". In: *Microbiology and molecular biology reviews* 62.1, pp. 181–203.
- Jackson, Peter (1990). "The use of polyacrylamide-gel electrophoresis for the high-resolution separation of reducing saccharides labelled with the fluorophore 8-aminonaphthalene-1, 3, 6-trisulphonic acid. Detection of picomolar quantities by an imaging system based on a cooled charge-coupled device". In: *Biochemical Journal* 270.3, pp. 705–713.
- Jacobs, C et al. (1994). "Bacterial cell wall recycling provides cytosolic muropeptides as effectors for beta-lactamase induction." In: *The EMBO journal* 13.19, pp. 4684–4694.
- Jaeger, Tina, Momo Arsic, and Christoph Mayer (2005). "Scission of the lactyl ether bond of N-acetylmuramic acid by *Escherichia coli* etherase". In: *Journal of Biological Chemistry* 280.34, pp. 30100–30106.
- Jorge, Ana Maria et al. (2017). "Utilization of glycerophosphodiesterases by *S. taphylococcus aureus*". In: *Molecular microbiology* 103.2, pp. 229–241.
- Kazami, Nao et al. (2015). "A simple procedure for preparing chitin oligomers through acetone precipitation after hydrolysis in concentrated hydrochloric acid". In: *Carbohydrate polymers* 132, pp. 304–310.
- Keyhani, Nemat O, Kirsten Bacia, and Saul Roseman (2000a). "The Transport/Phosphorylation of N,N-Diacetylchitobiose in *Escherichia coli* characterization of phospho-IIBChb and of a potential transition state analogue in the phosphotransfer reaction between the proteins IIAChb and IIBChb". In: *Journal of Biological Chemistry* 275.42, pp. 33102–33109.
- Keyhani, Nemat O, Olga Boudker, and Saul Roseman (2000b). "Isolation and Characterization of IIAChb, a Soluble Protein of the Enzyme II Complex Required for the Trans-

- port/Phosphorylation of N, N-Diacetylchitobiose in *Escherichia coli*". In: *Journal of Biological Chemistry* 275.42, pp. 33091–33101.
- Keyhani, Nemat O and Saul Roseman (1997). "Wild-type *Escherichia coli* grows on the chitin disaccharide, N, N-diacetylchitobiose, by expressing the cel operon". In: *Proceedings of the National Academy of Sciences* 94.26, pp. 14367–14371.
- Keyhani, Nemat O et al. (2000c). "The Chitin Disaccharide, N, N-Diacetylchitobiose, Is Catabolized by *Escherichia coli* and Is Transported/Phosphorylated by the Phosphoenolpyruvate: Glycose Phosphotransferase System". In: *Journal of Biological Chemistry* 275.42, pp. 33084–33090.
- Kluj, Robert Maria et al. (2018). "Recovery of the Peptidoglycan Turnover Product released by the Autolysin Atl in *Staphylococcus aureus* involves the Phosphotransferase System Transporter MurP and the Novel 6-phospho-N-acetylmuramidase MupG". In: *Frontiers in microbiology* 9, p. 2725.
- Koshland Jr, DE (1953). "Stereochemistry and the mechanism of enzymatic reactions". In: *Biological reviews* 28.4, pp. 416–436.
- Kovács, Márta et al. (2006). "A functional dlt operon, encoding proteins required for incorporation of d-alanine in teichoic acids in gram-positive bacteria, confers resistance to cationic antimicrobial peptides in *Streptococcus pneumoniae*". In: *Journal of bacteriology* 188.16, pp. 5797–5805.
- Kubota, Naoji et al. (2000). "A simple preparation of half N-acetylated chitosan highly soluble in water and aqueous organic solvents". In: *Carbohydrate research* 324.4, pp. 268–274.
- Kuznetsova, Ekaterina et al. (2006). "Genome-wide analysis of substrate specificities of the *Escherichia coli* haloacid dehalogenase-like phosphatase family". In: *Journal of Biological Chemistry* 281.47, pp. 36149–36161.
- Larson, Timothy J and Ali T van Loo-Bhattacharya (1988). "Purification and characterization of glpQ-encoded glycerophosphodiester phosphodiesterase from *Escherichia coli* K-12". In: *Archives of biochemistry and biophysics* 260.2, pp. 577–584.
- Larson, TJ, M Ehrmann, and W Boos (1983). "Periplasmic glycerophosphodiester phosphodiesterase of *Escherichia coli*, a new enzyme of the glp regulon." In: *Journal of Biological Chemistry* 258.9, pp. 5428–5432.
- Li, Zhengzheng et al. (2013). "Preparation and characterization of glycol chitin as a new thermogelling polymer for biomedical applications". In: *Carbohydrate polymers* 92.2, pp. 2267–2275.



- Litzinger, Silke et al. (2010a). "Muropeptide rescue in *Bacillus subtilis* involves sequential hydrolysis by  $\beta$ -N-acetylglucosaminidase and N-acetylmuramyl-L-alanine amidase". In: *Journal of bacteriology* 192.12, pp. 3132–3143.
- Litzinger, Silke et al. (2010b). "Structural and kinetic analysis of *Bacillus subtilis* N-acetylglucosaminidase reveals a unique Asp-His dyad mechanism". In: *Journal of Biological Chemistry* 285.46, pp. 35675–35684.
- Lu, Shaojie et al. (2004). "Preparation of water-soluble chitosan". In: *Journal of Applied Polymer Science* 91.6, pp. 3497–3503.
- Lucchini, Sacha et al. (2006). "H-NS mediates the silencing of laterally acquired genes in bacteria". In: *PLoS Pathog* 2.8, e81.
- Mack, Dietrich et al. (1996). "The intercellular adhesin involved in biofilm accumulation of *Staphylococcus epidermidis* is a linear beta-1, 6-linked glucosaminoglycan: purification and structural analysis." In: *Journal of bacteriology* 178.1, pp. 175–183.
- Matias, Valério RF et al. (2003). "Cryo-transmission electron microscopy of frozen-hydrated sections of *Escherichia coli* and *Pseudomonas aeruginosa*". In: *Journal of bacteriology* 185.20, pp. 6112–6118.
- Mayer, Christoph et al. (2019). "Bacteria's different ways to recycle their own cell wall". In: *International Journal of Medical Microbiology* 309.7, p. 151326.
- Mesnage, Stéphane et al. (2014). "Molecular basis for bacterial peptidoglycan recognition by LysM domains". In: *Nature communications* 5.1, pp. 1–11.
- Mima, Seiichi et al. (1983). "Highly deacetylated chitosan and its properties". In: *Journal of Applied Polymer Science* 28.6, pp. 1909–1917.
- Montero-Morán, Gabriela M et al. (2001). "On the multiple functional roles of the active site histidine in catalysis and allosteric regulation of *Escherichia coli* glucosamine 6-phosphate deaminase". In: *Biochemistry* 40.34, pp. 10187–10196.
- Morath, Siegfried, Armin Geyer, and Thomas Hartung (2001). "Structure–function relationship of cytokine induction by lipoteichoic acid from *Staphylococcus aureus*". In: *The Journal of experimental medicine* 193.3, pp. 393–398.
- Myers, Cullen L et al. (2016). "Identification of two phosphate starvation-induced wall teichoic acid hydrolases provides first insights into the degradative pathway of a key bacterial cell wall component". In: *Journal of Biological Chemistry* 291.50, pp. 26066–26082.
- Nega, Mulugeta et al. (2020). "New insights in the coordinated amidase and glucosaminidase activity of the major autolysin (Atl) in *Staphylococcus aureus*". In: *Communications biology* 3.1, pp. 1–10.

- Neuhaus, Francis C and James Baddiley (2003). "A continuum of anionic charge: structures and functions of D-alanyl-teichoic acids in gram-positive bacteria". In: *Microbiology and molecular biology reviews* 67.4, pp. 686–723.
- No, Hong K and Samuel P Meyers (1995). "Preparation and characterization of chitin and chitosana review". In: *Journal of aquatic food product technology* 4.2, pp. 27–52.
- O'Brie, Patrick J and Daniel Herschlag (2001). "Functional interrelationships in the alkaline phosphatase superfamily: phosphodiesterase activity of *Escherichia coli* alkaline phosphatase". In: *Biochemistry* 40.19, pp. 5691–5699.
- Ohshima, Noriyasu et al. (2008). "*Escherichia coli* cytosolic glycerophosphodiester phosphodiesterase (UgpQ) requires Mg<sup>2+</sup>, Co<sup>2+</sup>, or Mn<sup>2+</sup> for its enzyme activity". In: *Journal of bacteriology* 190.4, pp. 1219–1223.
- Oshida, Tadahiro et al. (1995). "A *Staphylococcus aureus* autolysin that has an N-acetylmuramoyl-L-alanine amidase domain and an endo-beta-N-acetylglucosaminidase domain: cloning, sequence analysis, and characterization". In: *Proceedings of the National Academy of Sciences* 92.1, pp. 285–289.
- Park, James T and Tsuyoshi Uehara (2008). "How bacteria consume their own exoskeletons (turnover and recycling of cell wall peptidoglycan)". In: *Microbiology and Molecular Biology Reviews* 72.2, pp. 211–227.
- Park, Young Seo et al. (1993). "Expression, purification, and characterization of CTP: glycerol-3-phosphate cytidyltransferase from *Bacillus subtilis*." In: *Journal of Biological Chemistry* 268.22, pp. 16648–16654.
- Parker, Laura L and Barry G Hall (1990). "Mechanisms of activation of the cryptic cel operon of *Escherichia coli* K12." In: *Genetics* 124.3, pp. 473–482.
- Percy, Matthew G and Angelika Gründling (2014). "Lipoteichoic acid synthesis and function in gram-positive bacteria". In: *Annual review of microbiology* 68, pp. 81–100.
- Peri, Krishna G, Hughes Goldie, and E Bruce Waygood (1990). "Cloning and characterization of the N-acetylglucosamine operon of *Escherichia coli*". In: *Biochemistry and Cell Biology* 68.1, pp. 123–137.
- Plumbridge, JA (1991). "Repression and induction of the nag regulon of *Escherichia coli* K-12: the roles of nagC and nagA in maintenance of the uninduced state". In: *Molecular microbiology* 5.8, pp. 2053–2062.
- Plumbridge, Jacqueline (2009). "An alternative route for recycling of N-acetylglucosamine from peptidoglycan involves the N-acetylglucosamine phosphotransferase system in *Escherichia coli*". In: *Journal of bacteriology* 191.18, pp. 5641–5647.

- Plumbridge, Jacqueline and Olivier Pellegrini (2004). "Expression of the chitobiose operon of *Escherichia coli* is regulated by three transcription factors: NagC, ChbR and CAP". In: *Molecular microbiology* 52.2, pp. 437–449.
- Pon, Cynthia L, Raffaele A Calogero, and Claudio O Gualerzi (1988). "Identification, cloning, nucleotide sequence and chromosomal map location of hns, the structural gene for *Escherichia coli* DNA-binding protein H-NS". In: *Molecular and General Genetics MGG* 212.2, pp. 199–202.
- Pooley, HM, FX Abellan, and D Karamata (1992). "CDP-glycerol: poly (glycerophosphate) glycerophosphotransferase, which is involved in the synthesis of the major wall teichoic acid in *Bacillus subtilis* 168, is encoded by tagF (rodC)." In: *Journal of bacteriology* 174.2, pp. 646–649.
- Raasch, Carsten et al. (2000). "*Thermotoga maritima* AglA, an extremely thermostable NAD<sup>+</sup>, Mn 2<sup>+</sup>, and thiol-dependent  $\alpha$ -glucosidase". In: *Extremophiles* 4.4, pp. 189–200.
- Rasmussen, Anders Aamann et al. (2009). "A conserved small RNA promotes silencing of the outer membrane protein YbfM". In: *Molecular microbiology* 72.3, pp. 566–577.
- Reichmann, Nathalie T and Angelika Gründling (2011). "Location, synthesis and function of glycolipids and polyglycerolphosphate lipoteichoic acid in Gram-positive bacteria of the phylum Firmicutes". In: *FEMS microbiology letters* 319.2, pp. 97–105.
- Reith, Jan and Christoph Mayer (2011). "Peptidoglycan turnover and recycling in Gram-positive bacteria". In: *Applied microbiology and biotechnology* 92.1, p. 1.
- Reizer, Jonathan et al. (1988). "The phosphoenolpyruvate: sugar phosphotransferase system in gram-positive bacteria: properties, mechanism, and regulation". In: *CRC Critical reviews in microbiology* 15.4, pp. 297–338.
- Rinaudo, Marguerite (2006). "Chitin and chitosan: properties and applications". In: *Progress in polymer science* 31.7, pp. 603–632.
- Rismondo, Jeanine, Matthew G Percy, and Angelika Gründling (2018). "Discovery of genes required for lipoteichoic acid glycosylation predicts two distinct mechanisms for wall teichoic acid glycosylation". In: *Journal of Biological Chemistry* 293.9, pp. 3293–3306.
- Rismondo, Jeanine et al. (2019). "GtcA is required for LTA glycosylation in *Listeria monocytogenes* serovar 1/2a and *Bacillus subtilis*". In: *bioRxiv*.
- Rivas, Luis A et al. (2000). "The *Bacillus subtilis* 168 csn gene encodes a chitosanase with similar properties to a *Streptomyces* enzyme". In: *Microbiology* 146.11, pp. 2929–2936.
- Rogers, Howard J (1974). "Peptidoglycans (mucopeptides): structure, function, and variations". In: *Annals of the New York Academy of Sciences* 235.1, pp. 29–51.

- Romeis, Tina, Waldemar Vollmer, and Joachim-Volker Höltje (1993). "Characterization of three different lytic transglycosylases in *Escherichia coli*". In: *FEMS microbiology letters* 111.2-3, pp. 141–146.
- Schaub, Ryan E and Joseph P Dillard (2017). "Digestion of peptidoglycan and analysis of soluble fragments". In: *Bio-protocol* 7.15.
- Schertzer, Jeffrey W and Eric D Brown (2003). "Purified, recombinant TagF protein from *Bacillus subtilis* 168 catalyzes the polymerization of glycerol phosphate onto a membrane acceptor in vitro". In: *Journal of Biological Chemistry* 278.20, pp. 18002–18007.
- Scheurwater, Edie, Chris W Reid, and Anthony J Clarke (2008). "Lytic transglycosylases: bacterial space-making autolysins". In: *The international journal of biochemistry & cell biology* 40.4, pp. 586–591.
- Schirner, Kathrin et al. (2009). "Distinct and essential morphogenic functions for wall-and lipo-teichoic acids in *Bacillus subtilis*". In: *The EMBO journal* 28.7, pp. 830–842.
- Schleifer, Karl Heinz and Otto Kandler (1972). "Peptidoglycan types of bacterial cell walls and their taxonomic implications." In: *Bacteriological reviews* 36.4, p. 407.
- Schmitz, Christian et al. (2019). "Conversion of chitin to defined chitosan oligomers: Current status and future prospects". In: *Marine drugs* 17.8, p. 452.
- Seltmann, Guntram and Otto Holst (2002). "Periplasmic space and rigid layer". In: *The Bacterial Cell Wall*. Springer, pp. 103–132.
- Shi, Liang et al. (2008). "Crystal structure of glycerophosphodiester phosphodiesterase (GDPD) from *Thermoanaerobacter tengcongensis*, a metal ion-dependent enzyme: Insight into the catalytic mechanism". In: *Proteins: Structure, Function, and Bioinformatics* 72.1, pp. 280–288.
- Shida, Toshio et al. (2000). "Overexpression, purification, and characterization of *Bacillus subtilis* N-acetylmuramoyl-L-alanine amidase Cwlc". In: *Bioscience, biotechnology, and biochemistry* 64.7, pp. 1522–1525.
- Shimahara, Kenzo and Yasuyuki Takiguchi (1988). "Preparation of crustacean chitin". In: *Methods in enzymology*. Vol. 161. Elsevier, pp. 417–423.
- Shirvan, AR, M Shakeri, and A Bashari (2019). *The Impact and Prospects of Green Chemistry for Textile Technology: Recent Advances in Application of Chitosan and Its Derivatives in Functional Finishing of Textiles*.
- Silhavy, Thomas J, Daniel Kahne, and Suzanne Walker (2010). "The bacterial cell envelope". In: *Cold Spring Harbor perspectives in biology* 2.5, a000414.

- Simpson, Helen D and Frederic Barras (1999). "Functional analysis of the carbohydrate-binding domains of *Erwinia chrysanthemi* Cel5 (Endoglucanase Z) and an *Escherichia coli* putative chitinase". In: *Journal of bacteriology* 181.15, pp. 4611–4616.
- Smith, Thomas J, Steve A Blackman, and Simon J Foster (2000). "Autolysins of *Bacillus subtilis*: multiple enzymes with multiple functions". In: *Microbiology* 146.2, pp. 249–262.
- Soldo, Blazenska et al. (2002). "Characterization of a *Bacillus subtilis* thermosensitive teichoic acid-deficient mutant: gene *mnaA* (*yvyH*) encodes the UDP-N-acetylglucosamine 2-epimerase". In: *Journal of bacteriology* 184.15, pp. 4316–4320.
- Souza, José M, Jacqueline A Plumbridge, and Mario L Calcagno (1997). "N-Acetylglucosamine-6-phosphate Deacetylase from *Escherichia coli*: Purification and Molecular and Kinetic Characterization". In: *Archives of Biochemistry and Biophysics* 340.2, pp. 338–346.
- Soysa, H Sasimali M and Wipa Suginta (2016). "Identification and functional characterization of a novel OprD-like chitin uptake channel in non-chitinolytic bacteria". In: *Journal of Biological Chemistry* 291.26, pp. 13622–13633.
- Swoboda, Jonathan G et al. (2010). "Wall teichoic acid function, biosynthesis, and inhibition". In: *Chembiochem* 11.1, pp. 35–45.
- Tews, Ivo et al. (1997). "Substrate-assisted catalysis unifies two families of chitinolytic enzymes". In: *Journal of the American Chemical Society* 119.34, pp. 7954–7959.
- Thadathil, Nidheesh and Suresh Puthanveetil Velappan (2014). "Recent developments in chitosanase research and its biotechnological applications: a review". In: *Food chemistry* 150, pp. 392–399.
- Tharanathan, Rudrapatnam N and Farooqahmed S Kittur (2003). "Chitin the undisputed biomolecule of great potential". In:
- Thompson, John et al. (1998). "The Gene *glvA* of *Bacillus subtilis* 168 Encodes a Metal-requiring, NAD (H)-dependent 6-Phospho- $\alpha$ -glucosidase assignment to family 4 of the glycosylhydrolase superfamily". In: *Journal of Biological Chemistry* 273.42, pp. 27347–27356.
- Thompson, John et al. (1999). "Cellobiose-6-Phosphate Hydrolase (CelF) of *Escherichia coli*: Characterization and Assignment to the Unusual Family 4 of Glycosylhydrolases". In: *Journal of bacteriology* 181.23, pp. 7339–7345.
- Tremblay, Lee W, Debra Dunaway-Mariano, and Karen N Allen (2006). "Structure and activity analyses of *Escherichia coli* K-12 NagD provide insight into the evolution of biochemical function in the haloalkanoic acid dehalogenase superfamily". In: *Biochemistry* 45.4, pp. 1183–1193.

- Uehara, Tsuyoshi and James T Park (2004). "The N-acetyl-D-glucosamine kinase of *Escherichia coli* and its role in murein recycling". In: *Journal of bacteriology* 186.21, pp. 7273–7279.
- Uehara, Tsuyoshi et al. (2005). "Recycling of the anhydro-N-acetylmuramic acid derived from cell wall murein involves a two-step conversion to N-acetylglucosamine-phosphate". In: *Journal of bacteriology* 187.11, pp. 3643–3649.
- Uehara, Tsuyoshi et al. (2006). "MurQ etherase is required by *Escherichia coli* in order to metabolize anhydro-N-acetylmuramic acid obtained either from the environment or from its own cell wall". In: *Journal of bacteriology* 188.4, pp. 1660–1662.
- Varrot, Annabelle et al. (2005). "NAD<sup>+</sup> and metal-ion dependent hydrolysis by family 4 glycosidases: structural insight into specificity for phospho- $\beta$ -D-glucosides". In: *Journal of molecular biology* 346.2, pp. 423–435.
- Verma, Subhash Chandra and Subramony Mahadevan (2012). "The chbG gene of the chitobiose (chb) operon of *Escherichia coli* encodes a chitooligosaccharide deacetylase". In: *Journal of bacteriology* 194.18, pp. 4959–4971.
- Vollmer, Waldemar and Joachim-Volker Höltje (2004). "The architecture of the murein (peptidoglycan) in gram-negative bacteria: vertical scaffold or horizontal layer (s)?" In: *Journal of bacteriology* 186.18, pp. 5978–5987.
- Vuong, Cuong et al. (2004). "Polysaccharide intercellular adhesin (PIA) protects *Staphylococcus epidermidis* against major components of the human innate immune system". In: *Cellular microbiology* 6.3, pp. 269–275.
- Walter, Axel and Christoph Mayer (2019). "Peptidoglycan Structure, Biosynthesis, and Dynamics During Bacterial Growth". In: *Extracellular Sugar-Based Biopolymers Matrices*. Springer, pp. 237–299.
- Wang, San-Lang and Wen-Tsu Chang (1997). "Purification and characterization of two bifunctional chitinases/lysozymes extracellularly produced by *Pseudomonas aeruginosa* K-187 in a shrimp and crab shell powder medium." In: *Applied and environmental microbiology* 63.2, pp. 380–386.
- Weidel, W and H Pelzer (1964). "Bagshaped macromolecules—a new outlook on bacterial cell walls". In: *Adv Enzymol Relat Areas Mol Biol* 26, pp. 193–232.
- Weidel, Wolfhard, H Frank, and HH Martin (1960). "The rigid layer of the cell wall of *Escherichia coli* strain B". In: *Microbiology* 22.1, pp. 158–166.

- Weidenmaier, Christopher et al. (2004). "Role of teichoic acids in *Staphylococcus aureus* nasal colonization, a major risk factor in nosocomial infections". In: *Nature medicine* 10.3, pp. 243–245.
- White, RJ and CA Pasternak (1967). "The purification and properties of N-acetylglucosamine 6-phosphate deacetylase from *Escherichia coli*". In: *Biochemical Journal* 105.1, pp. 121–125.
- Will, W Ryan et al. (2014). "Evolutionary expansion of a regulatory network by counter-silencing". In: *Nature communications* 5.1, pp. 1–12.
- Yip, Vivian LY, John Thompson, and Stephen G Withers (2007). "Mechanism of GlvA from *Bacillus subtilis*: a detailed kinetic analysis of a 6-phospho- $\alpha$ -glucosidase from glycoside hydrolase family 4". In: *Biochemistry* 46.34, pp. 9840–9852.
- Yip, Vivian LY and Stephen G Withers (2006). "Mechanistic analysis of the unusual redox-elimination sequence employed by *Thermotoga maritima* BglT: a 6-phospho- $\beta$ -glucosidase from glycoside hydrolase family 4". In: *Biochemistry* 45.2, pp. 571–580.
- Yip, Vivian LY et al. (2004). "An unusual mechanism of glycoside hydrolysis involving redox and elimination steps by a family 4  $\beta$ -glycosidase from *Thermotoga maritima*". In: *Journal of the American Chemical Society* 126.27, pp. 8354–8355.
- Yokogawa, Kanae et al. (1974). "Mutanolysin, bacteriolytic agent for cariogenic streptococci: partial purification and properties". In: *Antimicrobial Agents and Chemotherapy* 6.2, pp. 156–165.

# Appendix

## Publication 1

**Walter, A.**, Friz, S., Mayer, C. (2021). Chitin and diacetylchitobiose metabolism of *Escherichia coli* revisited: adjustment of the roles of ChiA, ChbR, ChbF and ChbG. *Microbial Physiology*.



# Chitin, Chitin Oligosaccharide, and Chitin Disaccharide Metabolism of *Escherichia coli* Revisited: Reassignment of the Roles of ChiA, ChbR, ChbF, and ChbG

Axel Walter · Simon Friz · Christoph Mayer

Interfaculty Institute of Microbiology and Infection Medicine, Organismic Interactions/Glycobiology, Eberhard Karls Universität Tübingen, Tübingen, Germany

## Keywords

Chitin · Peptidoglycan · Chitobiose · *chb* operon · Diacetylchitobiose 6'-phosphate monodeacetylase · 6-Phospho- $\beta$ -glucosaminidase · Family 4 glycosidase

## Abstract

*Escherichia coli* is unable to grow on polymeric and oligomeric chitin, but grows on chitin disaccharide (GlcNAc-GlcNAc; *N,N'*-diacetylchitobiose) and chitin trisaccharide (GlcNAc-GlcNAc-GlcNAc; *N,N',N''*-triacetylchitotriose) via expression of the *chb* operon (*chbBCARFG*). The phosphotransferase system (PTS) transporter ChbBCA facilitates transport of both saccharides across the inner membrane and their concomitant phosphorylation at the non-reducing end, intracellularly yielding GlcNAc 6-phosphate-GlcNAc (GlcNAc6P-GlcNAc) and GlcNAc6P-GlcNAc-GlcNAc, respectively. We revisited the intracellular catabolism of the PTS products, thereby correcting the reported functions of the 6-phospho-glycosidase ChbF, the monodeacetylase ChbG, and the transcriptional regulator ChbR. Intracellular accumulation of glucosamine 6P-GlcNAc (GlcN6P-GlcNAc) and GlcN6P-GlcNAc-GlcNAc in a *chbF* mutant unraveled a role for ChbG as a monodeacetylase that removes the *N*-acetyl group at the non-reducing end. Consequently, GlcN6P- but not GlcNAc6P-containing saccharides likely function as co-

activators of ChbR. Furthermore, ChbF removed the GlcN6P from the non-reducing terminus of the former saccharides, thereby degrading the inducers of the *chb* operon and facilitating growth on the saccharides. Consequently, ChbF was unable to hydrolyze GlcNAc6P-residues from the non-reducing end, contrary to previous assumptions but in agreement with structural modeling data and with the unusual catalytic mechanism of the family 4 of glycosidases, to which ChbF belongs. We also refuted the assumption that ChiA is a bifunctional endochitinase/lysozyme ChiA, and show that it is unable to degrade peptidoglycans but acts as a bona fide chitinase in vitro and in vivo, enabling growth of *E. coli* on chitin oligosaccharides when ectopically expressed. Overall, this study revises our understanding of the chitin, chitin oligosaccharide, and chitin disaccharide metabolism of *E. coli*.

© 2021 The Author(s).  
Published by S. Karger AG, Basel

## Introduction

Chitin is a homopolymer composed of  $\beta$ -1,4 linked *N*-acetylglucosamine (GlcNAc) found in the cell walls of fungi, exoskeletons of crustaceans and insects, as well as the shells of molluscs. It is the most abundant nitrogen-

containing polysaccharide on earth, with an annual turnover rate of  $10^{11}$  tons, therefore playing a central role in the global nitrogen and carbon cycle [Tharanathan and Kittur, 2003]. Degradation of the recalcitrant chitin biopolymer is achieved by chitinolytic fungi as well as bacteria, e.g., gram-positive bacteria of the genus *Bacillus* or *Streptomyces*, and gram-negative bacteria of the genus *Serratia*, *Aeromonas*, or *Vibrio*, which play an important role in chitin recycling in soil and aquatic (marine) ecosystems [Blokesch, 2012; Hamid et al., 2013; Adams et al., 2019; Wucher et al., 2019]. These organisms secrete various forms of chitinases and *N*-acetylglucosaminidases that fragment polymeric chitin into shorter chitin oligosaccharides, *N,N',N''*-triacetylchitotriose (GlcNAc-GlcNAc-GlcNAc, triacetyl-chitotriose), *N,N'*-diacetylchitobiose (GlcNAc-GlcNAc, diacetyl-chitobiose), and GlcNAc [Itoh and Kimoto, 2019]. Furthermore, they possess uptake and catabolic systems to grow on chitin and chitin oligosaccharides [Hamid et al., 2013; Itoh and Kimoto, 2019].

*Escherichia coli* K12 is unable to grow on chitin and chitin oligosaccharides, despite possessing a functional chitinase (ChiA/YheB) and an outer membrane porin that facilitates chitin oligosaccharide uptake (ChiP) [Francetic et al., 2000a; Soysa and Suginta, 2016]. Under normal laboratory growth conditions, the expression of ChiA and its secretion via the type 2 secretion system is silenced, requiring a mutation in the *hns* gene for activation [Francetic et al., 2000a, b]. As ChiA contains a native signal sequence, in an *hns* background, the chitinase is expressed and partially secreted to the periplasm via the Sec system and to the extracellular space via the type 2 secretome [Francetic et al., 2000a, b]. We became interested in the cryptic ChiA, since it had been described as a bifunctional enzyme with endo-chitinase and lysozyme activity, an assumption that, however, solely relied on the enzyme's ability to cleave the artificial lysozyme substrate ethylene glycol-chitin [Francetic et al., 2000a]. We thus aimed to re-examine the function of ChiA and chitin metabolism in *E. coli*.

Growth of *E. coli* on diacetyl-chitobiose and triacetyl-chitotriose depends on the chitobiose operon *chb-BCARFG*. This operon was initially identified as the cryptic *cel* (cellobiose utilization) operon, which requires secondary mutations in order to metabolize  $\beta$ -glycosides such as cellobiose, arbutin, and salicin [Parker and Hall, 1990]. Later it was shown that the operon is not cryptic but induced by diacetyl-chitobiose, an end product of chitin degradation, and therefore renamed to *chb* [Keyhani and Roseman, 1997]. Encoded by the *chbBCARFG*

operon are components of a phosphotransferase system (PTS) transporter (ChbBCA; EIIB, EIIC, and EIIA) involved in both, the transport of diacetyl-chitobiose and triacetyl-chitotriose and their simultaneous phosphorylation at the 6-hydroxyl group of the GlcNAc at the non-reducing end [Keyhani et al., 2000a, b, c]. Further encoded by this operon is a transcriptional repressor/activator (ChbR), repressing *chb* transcription by default and acting as an activator upon effector binding [Plumbridge and Pellegrini, 2004]. The *chb* operon is also subject to catabolite repression and is repressed by NagC, the transcriptional regulator of the GlcNAc catabolism, which is derepressed upon GlcNAc6P binding [Plumbridge and Pellegrini, 2004]. The enzymes ChbG and ChbF are involved in the intracellular processing of the phosphorylated diacetyl-chitobiose (diacetyl-chitobiose-P) and triacetyl-chitotriose (triacetyl-chitotriose-P). ChbG was identified as a monodeacetylase that is essential for growth on diacetyl-chitobiose and triacetyl-chitotriose but is dispensable for growth on cellobiose and chitobiose (chitosan dimer; GlcN- $\beta$ -1,4-GlcN) [Verma and Mahadevan, 2012]. Verma and Mahadevan [2012] further showed that activation of the *chb* promoter by the regulatory protein ChbR is dependent on ChbG, suggesting that deacetylation of diacetyl-chitobiose-P and triacetyl-chitotriose-P is necessary for their function as co-activators of ChbR. The authors proposed that ChbG removes the *N*-acetyl group from the reducing end, yielding GlcNAc6P-GlcN and GlcNAc6P-GlcNAc-GlcN, which may act as the inducers of the *chb* operon upon ChbR binding [Verma and Mahadevan, 2012]. Subsequent cleavage of these saccharides would yield GlcNAc6P, which upon binding to NagC could relieve repression of the *chb* operon. We questioned these assumptions, because the ChbF protein, which is responsible for the hydrolysis of the ChbG products, monoacetyl-chitobiose-P and diacetyl-chitotriose-P, was initially characterized as cellobiose-6-phosphate (Glc6P-Glc) hydrolase (named CelF) [Parker and Hall, 1990; Thompson et al., 1999]. Since ChbF cleaves Glc6P-Glc and other 6-phosphoglycosides (e.g., arbutin-P and salicin-P) and as well as chitobiose-P (GlcN6P-GlcN), we suggest that ChbF likely cleaves GlcN6P-glycosides (GlcN6P-GlcNAc and GlcN6P-GlcNAc-GlcNAc), rather than GlcNAc6P-glycosides. ChbF is assigned to the family 4 of glycosidases (GH4). The proposed mechanism for this class of enzymes is very distinct from that of classical glycosidases, which operate via nucleophilic substitution-mechanisms. GH4 glycosidases instead depend on a divalent metal ion and  $\text{NAD}^+$  as cofactors and catalyze an oxidation/reduc-

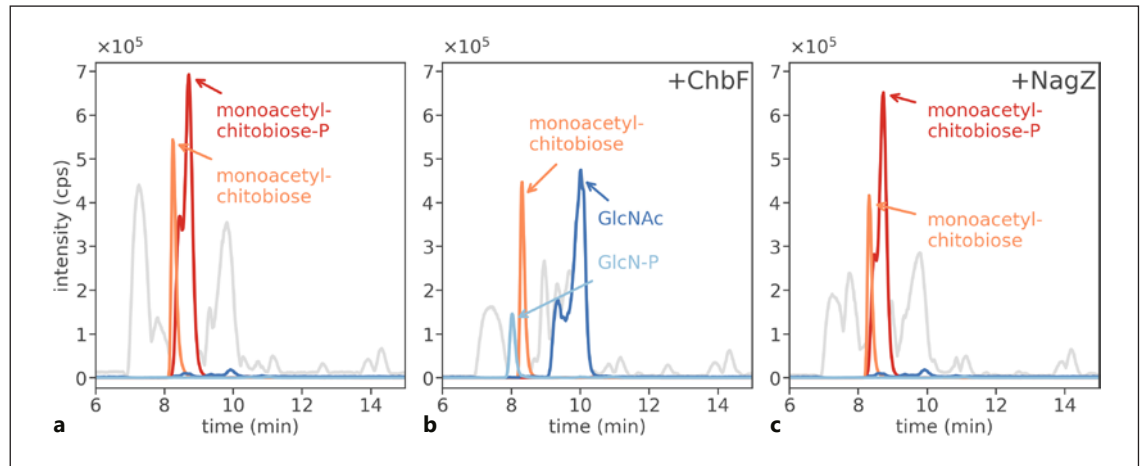


**Fig. 1.** Accumulation of monoacetyl-chitobiose-P and monoacetyl-chitobiose in  $\Delta chbF::kan$  cells and characterization of the ChbF and NagZ products. The cytosolic fraction of *E. coli*  $\Delta chbF::kan$  cells, grown in M9 CAA minimal medium supplemented with diacetyl-chitobiose, was extracted and analyzed by LC-MS. **a** Accumulation products with masses ( $m/z$ ) corresponding to monoacetyl-chitobiose-P ( $M+H$ )<sup>+</sup>  $m/z = 463.0976$  (red) and monoacetyl-chitobiose ( $M+H$ )<sup>+</sup>  $m/z = 383.1369$  (orange) were detected. **b** Upon treatment with ChbF (+ChbF), the monoacetyl-chitobiose-P ( $M+H$ )<sup>+</sup>  $m/z = 463.0976$  (red) completely disappeared, while

masses corresponding to GlcN-P ( $M+H$ )<sup>+</sup>  $m/z = 260.0362$  (light blue) and GlcNAc ( $M+H$ )<sup>+</sup>  $m/z = 222.0828$  (blue) appeared. The monoacetyl-chitobiose ( $M+H$ )<sup>+</sup>  $m/z = 383.1421$  (orange) instead remained intact. **c** Upon treatment with the exo-glucosaminidase NagZ (+NagZ), no GlcNAc was released from either of the accumulation products, indicating that GlcNAc is located at the reducing ends. Shown are the base peak chromatogram (BPC) mass range ( $M+H$ )<sup>+</sup>  $m/z = 120-800$  (gray) and the extracted ion chromatograms (EIC) based on the exact masses of displayed compounds (Table 1).

tion of the hydroxyl group at C3 of the sugar at the non-reducing end of a disaccharide. Formation of an intermediate carbonyl at C3 renders the C2 proton more acidic and thereby facilitates the elimination of the glycosidic oxygen, that is, the cleavage of the glycosidic bond [Rajan et al., 2004; Yip et al., 2004, 2007; Yip and Withers, 2006a, b]. Since ChbF operates by a mechanism that involves reactions at C3 and C2, the *N*-acetyl group at C2 likely interferes with this mechanism [Thompson et al., 1999]. Here we revised the function of ChbF as well as of ChbG and unraveled the nature of the effector molecules of the transcriptional regulator ChbR. Furthermore, we characterized ChiA as a bona fide chitinase that cleaves chitin but not chitosan and peptidoglycan, thus disproving its previously suggested role as a bifunctional endochitinase/lysozyme.

## Results and Discussion

### *Growth and Metabolite Accumulation Analyses of E. coli Wild Type, chbG and chbF Mutants*

To revisit the functions of ChbG and ChbF encoded by the *chb* operon, we first tested mutants deficient in either

*chbG* or *chbF* for growth on diacetyl-chitobiose and chitobiose as the sole carbon source in M9 minimal medium, compared to the parental *E. coli* strain (wild type; wt). *E. coli* wt grew overnight to a final OD<sub>600</sub> of 4.2 in M9 medium supplemented with 2 mM diacetyl-chitobiose, while it failed to grow with chitobiose (data not shown). It has previously been described that *E. coli* wt grows with diacetyl-chitobiose but poorly with chitobiose as the only carbon source, presumably due to the lack of induction of the *chb* operon [Verma and Mahadevan, 2012]. As expected, the  $\Delta chbG::kan$  and  $\Delta chbF::kan$  strains were unable to grow on either diacetyl-chitobiose and chitobiose (data not shown). To identify accumulation products in  $\Delta chbG::kan$  and  $\Delta chbF::kan$ , we grew the mutants overnight in M9 minimal medium with a mixture of amino acids (casamino acids; CAA) that was supplemented with 2 mM of either diacetyl-chitobiose or triacetyl-chitotriose, isolated the cytosolic fractions, and analyzed them via high-performance liquid chromatography-mass spectrometry (HPLC-MS). In the cytosolic fraction of  $\Delta chbF::kan$  cells, we detected large amounts of compounds with masses corresponding to monoacetyl-chitobiose-P ( $M+H$ )<sup>+</sup>  $m/z = 463.1324$   $m/z$ , which appears as a double peak due to separation of the  $\alpha$ - and  $\beta$ -anomeric

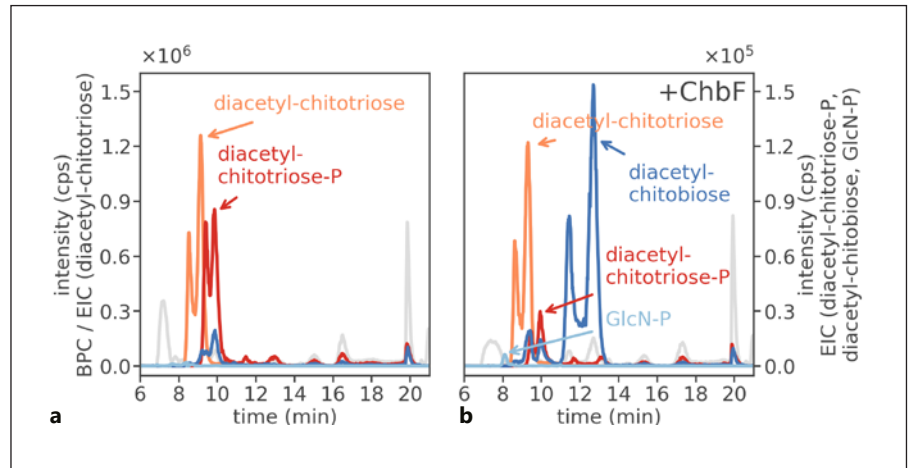


**Fig. 2.** Accumulation of diacetyl-chitotriose-P and diacetyl-chitotriose in  $\Delta chbF::kan$  cells and characterization of the ChbF products. The cytosolic fraction of *E. coli*  $\Delta chbF::kan$  cells, grown in M9 CAA minimal medium supplemented with triacetyl-chitotriose, was extracted and analyzed by LC-MS. **a** Accumulation products with masses ( $m/z$ ) corresponding to diacetyl-chitotriose-P ( $M+H$ )<sup>+</sup>  $m/z = 666.2133$  (red) and diacetyl-chitotriose ( $M+H$ )<sup>+</sup>  $m/z = 586.2453$  (orange) were detected. The latter appeared as the major accumulation product. **b** Upon treatment with ChbF (+ChbF), the diacetyl-chitotriose-P ( $M+H$ )<sup>+</sup>  $m/z = 666.2122$  (red) mostly disappeared, while masses corresponding to diacetyl-chitobiose ( $M+H$ )<sup>+</sup>

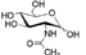
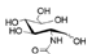
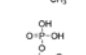
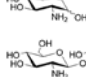
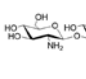
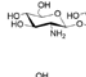
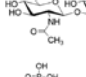
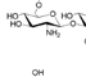
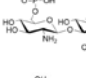
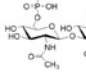
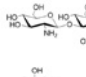
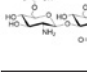
$m/z = 425.1790$  (blue) and GlcN-P ( $M+H$ )<sup>+</sup>  $m/z = 260.0543$  (light blue; a very small peak) appeared. The diacetyl-chitotriose ( $M+H$ )<sup>+</sup>  $m/z = 586.2445$  (orange) was not affected by ChbF. A compound appeared with a mass corresponding to diacetyl-chitobiose that elutes at the same retention time as the diacetyl-chitotriose-P (blue), and thus is not diacetyl-chitobiose but an unknown component with the same mass. Shown are the base peak chromatogram (BPC) mass range ( $M+H$ )<sup>+</sup>  $m/z = 180$ – $1,300$  (gray) and the extracted ion chromatograms (EIC) based on the exact masses of displayed compounds (Table 1).

forms, and to monoacetyl-chitobiose ( $M+H$ )<sup>+</sup> = 383.1660  $m/z$  (Fig. 1a; a list of compounds with their corresponding monoisotopic masses can be found in Table 1). These compounds are likely the products of the activity of the monodeacetylase ChbG, which accumulate due to the lack of ChbF. The additional appearance of a dephosphorylated product indicates that a phosphatase partially cleaves the accumulating monoacetyl-chitobiose-P. To test whether the dephosphorylation event is growth phase-dependent, cytosolic fractions were isolated also from exponential phase-cells ( $OD_{600} = 1$ ). However, no difference in the relative amount of the phosphorylated and non-phosphorylated accumulation products was found in comparison to the stationary phase cells, indicating the expression of the enigmatic phosphatase is not growth phase-dependent (data not shown). Similarly, when the  $\Delta chbF::kan$  strain was grown in CAA-M9 medium supplemented with 2 mM triacetyl-chitotriose, HPLC-MS analysis of cytosolic fractions revealed the presence of compounds with masses corresponding to diacetyl-chitotriose-P ( $M+H$ )<sup>+</sup> = 666.2117  $m/z$  (Fig. 2a) and diacetyl-chitotriose ( $M+H$ )<sup>+</sup> = 586.2454  $m/z$ , which both appear as double peaks due to separation of the  $\alpha$ - and  $\beta$ -anomeric forms. These compounds are the prod-

ucts of the activity of the monodeacetylase ChbG, which apparently deacetylates the trisaccharide-P and possibly also the non-phosphorylated trisaccharide. The appearance of large amounts of diacetyl-chitotriose indicates that the enigmatic phosphatase preferentially cleaves diacetyl-chitotriose-P as compared to monoacetyl-chitobiose-P (cf. Fig. 1a).

Conversely, in the  $\Delta chbG::kan$  cytosolic fractions, the expected accumulation products, diacetyl-chitobiose-P and triacetyl-chitotriose-P could not be detected (data not shown). One could speculate that these saccharides do not accumulate because they are metabolized by an unknown, ChbG-independent pathway. If diacetyl-chitobiose is metabolized via a different pathway and thus is used as a source of energy and carbon, growth on this saccharide would be expected. The  $\Delta chbG::kan$  mutant, however, failed to grow with diacetyl-chitobiose. It has previously been reported that ChbG is crucial for the generation of monoacetyl-chitobiose, which supposedly acts as the inducer of the *chb* operon [Verma and Mahadevan, 2012]. Thus, the more plausible explanation for the absence of an accumulation product is that no induction occurred and, consequently, the ChbBCA-transporter was not expressed and diacetyl-chitobiose was not taken up.

**Table 1.** Structures and exact monoisotopic masses of studied metabolites: overview of *chb* metabolites and their exact neutral masses and masses with proton adducts in positive ionization mode

Structure	Name	Formula	Exact monoisotopic mass [M]	Exact monoisotopic mass of the proton adduct [M+H] <sup>+</sup>
	GlcNAc	C <sub>8</sub> H <sub>15</sub> NO <sub>6</sub>	221.0899	222.0972
	reduced GlcNAc	C <sub>8</sub> H <sub>17</sub> NO <sub>6</sub>	223.1056	224.1129
	GlcN6P	C <sub>6</sub> H <sub>14</sub> NO <sub>8</sub> P	259.0457	260.0530
	chitobiose (GlcN-GlcN)	C <sub>12</sub> H <sub>24</sub> N <sub>2</sub> O <sub>9</sub>	340.1482	341.1555
	monoacetyl-chitobiose (GlcN-GlcNAc)	C <sub>14</sub> H <sub>26</sub> N <sub>2</sub> O <sub>10</sub>	382.1587	383.1660
	reduced monoacetyl-chitobiose	C <sub>14</sub> H <sub>28</sub> N <sub>2</sub> O <sub>10</sub>	384.1744	385.1817
	diacetyl-chitobiose (GlcNAc-GlcNAc)	C <sub>16</sub> H <sub>28</sub> N <sub>2</sub> O <sub>11</sub>	424.1693	425.1766
	monoacetyl-chitobiose-P (GlcN6P-GlcNAc)	C <sub>14</sub> H <sub>27</sub> N <sub>2</sub> O <sub>13</sub> P	462.1251	463.1324
	reduced monoacetyl-chitobiose-P	C <sub>14</sub> H <sub>29</sub> N <sub>2</sub> O <sub>13</sub> P	464.1407	465.1480
	diacetyl-chitobiose-P (GlcNAc6P-GlcNAc)	C <sub>16</sub> H <sub>29</sub> N <sub>2</sub> O <sub>14</sub> P	504.1356	505.1429
	diacetyl-chitotriose (GlcN-GlcNAc-GlcNAc)	C <sub>22</sub> H <sub>39</sub> N <sub>3</sub> O <sub>15</sub>	585.2381	586.2454
	diacetyl-chitotriose-P (GlcN6P-GlcNAc-GlcNAc)	C <sub>22</sub> H <sub>40</sub> N <sub>3</sub> O <sub>18</sub> P	665.2045	666.2117

### Deacetylation at the Non-Reducing End by ChbG Is Crucial for ChbF Function

To further characterize the accumulation products of the  $\Delta chbF::kan$  strain, the gene encoding the 6-phospho- $\beta$ -glycosidase ChbF (CelF) was cloned and recombinantly expressed. Recombinant ChbF completely degraded the phosphorylated accumulation product monoacetyl-chitobiose-P and yielded products with masses corresponding to GlcN-P (M+H)<sup>+</sup> m/z = 260.0530 and GlcNAc (M+H)<sup>+</sup> m/z = 222.0972, but was not able to cleave the non-phosphorylated accumulation product (Fig. 1b). It has previously been shown that diacetyl-chitobiose is phosphorylated at the non-reducing end during its transport into the cell by the ChbBCA-PTS system [Keyhani et

al., 2000a]. On this basis, the cleavage of the accumulation product of  $\Delta chbF::kan$  into GlcN-P and GlcNAc by ChbF suggests that ChbG deacetylates diacetyl-chitobiose-P at the non-reducing end, yielding GlcN6P-GlcNAc. To unequivocally exclude that the dephosphorylated accumulation product of  $\Delta chbF::kan$  is GlcNAc-GlcN, we treated it with *Bacillus subtilis* exo-N-acetylglucosaminidase NagZ. This enzyme plays a role in the recycling of peptidoglycan and specifically cleaves off GlcNAc residues from the non-reducing end [Litzinger et al., 2010a, b]. While GlcNAc is released from diacetyl-chitobiose with NagZ (data not shown), no product is observed during digestion of the accumulation products of  $\Delta chbF::kan$ , indicating the absence of GlcNAc entities at the non-reduc-

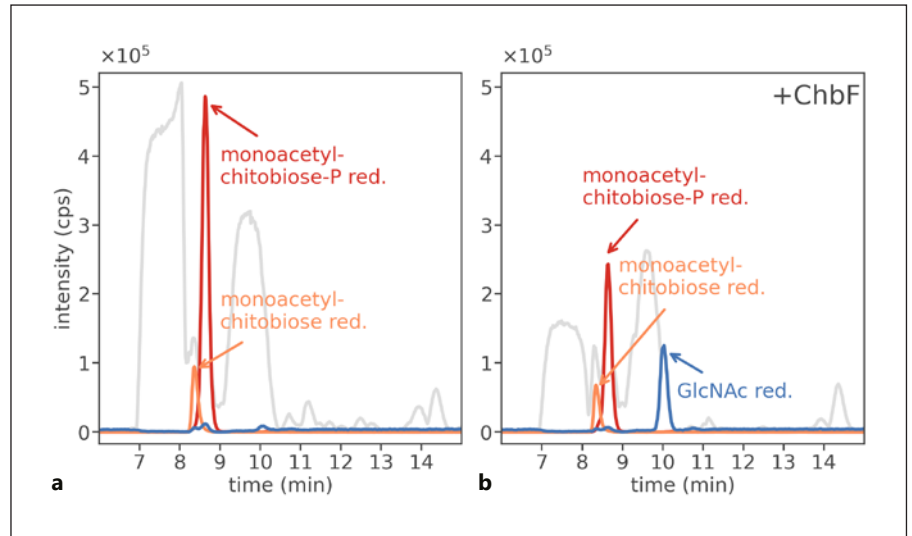


**Fig. 3.** Identification of the  $\Delta chbF::kan$  accumulation product as GlcNP-GlcNAc by reduction and LC-MS analysis of the reduced ChbF products. The cytosolic fraction of *E. coli*  $\Delta chbF::kan$  cells containing monoacetyl-chitobiose-P and monoacetyl-chitobiose (see Fig. 1) was reduced with sodium-borohydride, incubated with ChbF and analyzed by LC-MS. **a** Both, the reduced forms of monoacetyl-chitobiose-P ( $M+H$ )<sup>+</sup>  $m/z = 465.1157$  (red) and monoacetyl-chitobiose ( $M+H$ )<sup>+</sup>  $m/z = 385.1552$  (orange) were detected. They appear as single peaks, since  $\alpha$  and  $\beta$  anomers yield the same product after reduction. **b** Upon treatment with ChbF the peak of

reduced monoacetyl-chitobiose-P ( $M+H$ )<sup>+</sup>  $m/z = 465.1163$  (red) decreased significantly, but not the reduced monoacetyl-chitobiose ( $M+H$ )<sup>+</sup>  $m/z = 385.1555$  (orange), and reduced GlcNAc ( $M+H$ )<sup>+</sup>  $m/z = 224.0974$  (blue) appeared. Notably, the second breakdown product, glucosamine-phosphate (GlcN-P) could not be detected. Shown are the base peak chromatogram (BPC) mass range ( $M+H$ )<sup>+</sup>  $m/z = 120-800$  (gray) and the extracted ion chromatograms (EIC) based on the exact masses of displayed compounds (Table 1).

ing terminus (Fig. 1c). Similarly, it was shown that ChbF is able to cleave diacetyl-chitotriose-P, which accumulates in *E. coli*  $\Delta chbF::kan$  cells grown in the presence of triacetyl-chitotriose, yielding diacetyl-chitobiose and GlcN-P (Fig. 2b). This indicates that triacetyl-chitotriose is also phosphorylated and deacetylated at the non-reducing end by the ChbBCA-PTS and ChbG, respectively, yielding GlcN6P-GlcNAc-GlcNAc, from which GlcN6P at the non-reducing end is cleaved-off by ChbF.

A method to identify the sugar at the reducing end beyond doubt is the reduction with sodium borohydride followed by enzymatic cleavage and/or fragmentation by tandem MS (MS/MS). In these conditions, the reduction of the accumulation products of  $\Delta chbF::kan$  was complete and the two reduced products could be detected (Fig. 3a). When ChbF was added, the peak of the phosphorylated, reduced substrate became smaller and a distinct peak emerged, with a mass that corresponds to reduced GlcNAc ( $M+H$ )<sup>+</sup>  $m/z = 224.1129$  (Fig. 3b). A mass for GlcN-P, which would also be expected, was not detected. GlcN-P does not ionize very well in MS and its ionization could have been worsened in the samples that were reduced with sodium borohydride due to high salt

concentrations. These conditions are also suboptimal for ChbF and, accordingly, the substrate was not completely digested by ChbF. Nevertheless, the detection of reduced GlcNAc ( $[M+H]$ <sup>+</sup>  $m/z = 224.1129$ ) in significant abundance (83% relative to the reduced monoacetyl-chitobiose-P, which was set to 100%) indicates that there had been GlcNAc at the reducing end of the ChbF substrate (Fig. 4). Both compounds could also be detected in anhydrous forms with lower intensities. The mass difference between reduced monoacetyl-chitobiose-P and reduced GlcNAc corresponds exactly to uncharged GlcN-P -H<sub>2</sub>O ( $M$ ) = 241.0351 Da. Furthermore, the mass of GlcN-P -H<sub>2</sub>O itself could be detected, although in very low abundance of <0.5%. This indicates once more that GlcNAc ionizes readily in MS positive ion mode compared to GlcN-P.

In summary, our results indicate that ChbG deacetylates its substrate diacetyl-chitobiose-P at the non-reducing end. This finding fits well into the previous reports that *E. coli* is able to utilize the  $\beta$ -glucoside sugars cellobiose, arbutin and salicin by expressing the *chb* (formerly designated *cel*) operon [Parker and Hall, 1990]. In each of these sugars, the non-reducing end

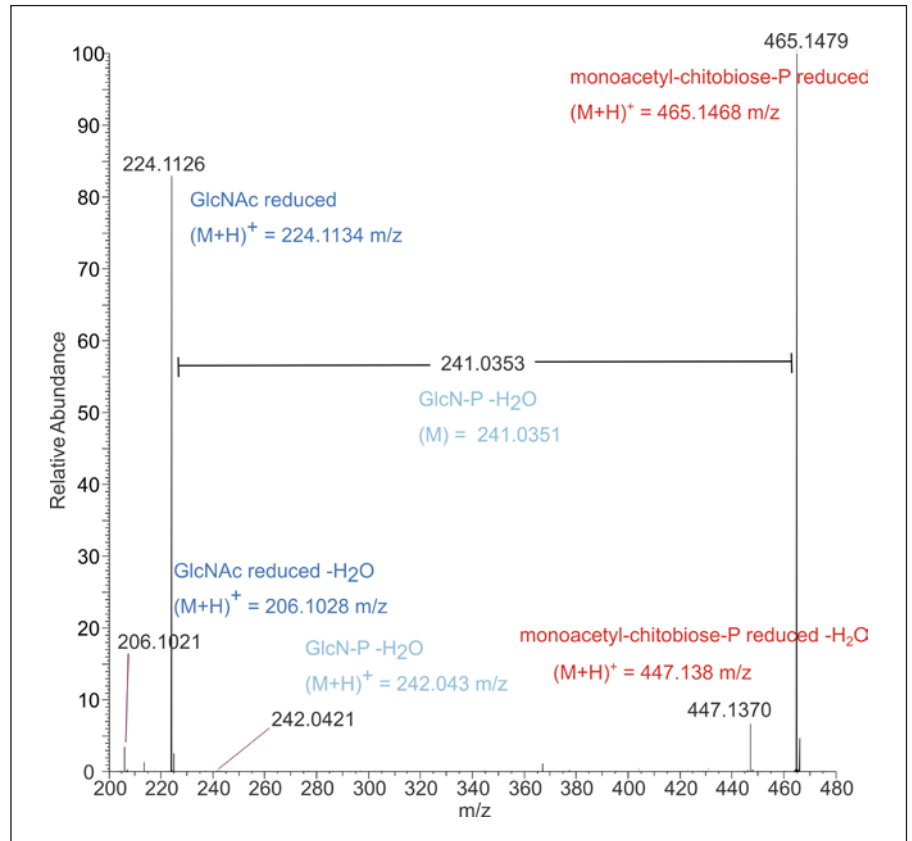


**Fig. 4.** MS-MS fragmentation analysis of the reduced  $\Delta chbF::kan$  accumulation product monoacetyl-chitobiose-P. In order to identify the position of deacetylation in the monoacetyl-chitobiose-P, the  $\Delta chbF::kan$  accumulation product was reduced with sodium borohydride (cf. Fig. 3) and analyzed by MS-MS. Reduced monoacetyl-chitobiose-P  $(M+H)^+ = 465.1480$  m/z (red) was set to 100% relative abundance. MS-MS fragmentation results in the formation of reduced GlcNAc  $(M+H)^+ m/z = 224.1129$  (blue), appearing

with a relative abundance of 83%, which results by loss of uncharged GlcN-P -H<sub>2</sub>O ( $M$ ) = 241.0351 Da (light blue). Detected were the mass of GlcN-P -H<sub>2</sub>O (light blue)  $(M+H)^+ m/z = 242.0424$  in very low abundance (<0.5%) and of anhydrous forms of reduced monoacetyl-chitobiose-P  $(M+H)^+ m/z = 447.1374$  (red) and reduced GlcNAc  $(M+H)^+ m/z = 206.1023$  in low relative abundances of 7 and 4.5%, respectively.

consists of glucose, while the residue at the reducing end is variable. These  $\beta$ -glucosides, after phosphorylation, were shown to be substrates for ChbF (previously named CelF) [Thompson et al., 1999]. Our data also fit well into the proposed enzymatic mechanism of GH4 members, which posits that the decisive reaction mechanism takes place at the carbohydrate at the non-reducing end. Indeed, oxidation/reduction of the hydroxyl group at C3 of the sugar at non-reducing end of a disaccharide to a carbonyl renders the C2 proton more acidic and thereby facilitates the elimination of the glycosidic oxygen, that is, the cleavage of the glycosidic bond [Rajan et al., 2004; Yip et al., 2004, 2007]. In the second step of the proposed mechanism, a proton gets released from the non-reducing end sugar's C2 hydrogen to a

catalytic base. This process is favored by a positive dipole on the C2, which is more pronounced with an amino instead of a *N*-acetyl functional group. The binding of  $Mn^{2+}$  to C2 and C3 functional groups would also be enhanced with the more negative dipole on the amino group. A well-studied member of GH4 is the 6-phospho- $\alpha$ -glucosidase GlvA from *B. subtilis* [Yip et al., 2007]. The crystal structure of GlvA bound to glucose 6-phosphate (Glc6P) revealed that at C2 there is relatively little space in the binding pocket and steric hindrance could occur with larger side chains. An amino acid sequence alignment among ChbF, GlvA, and other described GH4 enzymes revealed high similarities especially at the site next to the C2 functional group, where a cysteine residue is conserved across all queried enzymes. To

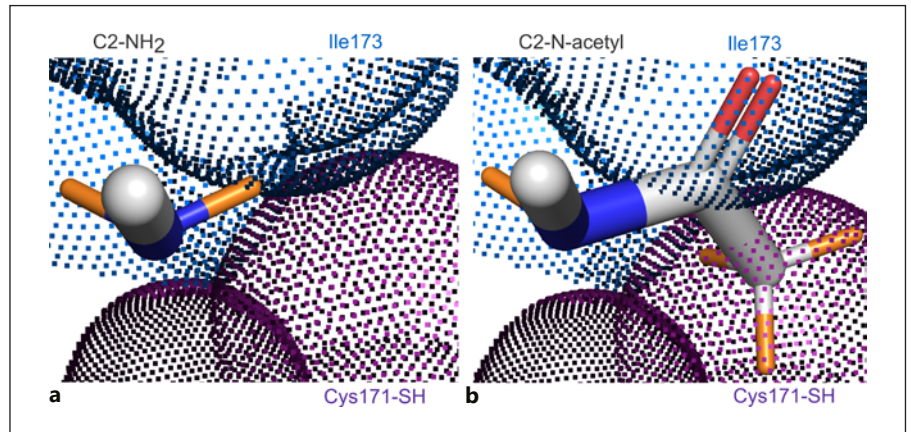


**Fig. 5.** Structural model of the binding pocket of ChbF in complex with substrates. Based on the crystal structure of the 6-phospho- $\alpha$ -glucosidase GlvA from *B. subtilis* in complex with its substrate glucose-6P (pdb code: 1U8X), the binding pocket of ChbF was modeled using Pymol, identifying steric constraints that discriminate binding of an *N*-acetyl group, but allow binding of an amino or hydroxyl group. **a, b** Shown is the C2 with the functional group shown as sticks (carbon = white, nitrogen = blue, oxygen = red, hydrogen = orange) and the amino acid residues isoleucine (blue) and cysteine (purple) in direct contact with this functional group at C2, shown as dotted spheres. Alignments between the amino

acid sequences of ChbF, GlvA, and other representatives of the GH4 family enzymes show a high degree of similarity and especially a conserved cysteine residue (ChbF Cys172, GlvA Cys171) close to the C2 functional group. Also close are Ile174 of ChbF and Met173 of GlvA. In this structure model, Met173 GlvA was exchanged with Ile to resemble the situation of ChbF. **a** The C2 functional group has been altered to an amino group like in GlcN, which fits well between the Ile and Cys residues. **b** The C2-functional group has been altered to *N*-acetyl group of GlcNAc, which, however, does not fit since the oxygen of the acetyl group collides with the Ile and the methyl group collides with the sulfur of Cys.

further clarify the difference between amino and *N*-acetyl groups at C2 for ChbF we modeled its structure using the GlvA-Glc6P cocrystal structure (pdb code: 1U8X) and exchanging the C2 hydroxyl group of the ligand with an amino or *N*-acetyl group. Two amino acids are in proximity of the functional group, the conserved cysteine and methionine in GlvA, the latter replaced with the isoleucine of ChbF. This modeling suggests that an amino group fits well between the residues (Fig. 5a), whereas the *N*-acetyl group on the other hand does not, as the oxygen collides with the isoleucine and the methyl group collides with the sulfur of cysteine (Fig. 5b).

To test *in vivo* the enzymatic activity of ChbF on diacetyl-chitobiose-P, *E. coli*  $\Delta$ *chbG::kan* was transformed with a plasmid that allows IPTG-inducible expression of the ChbBCA-PTS. Since under these conditions, due to the missing ChbR coactivator, the natural induction of the *chb* operon does not occur, we expected the accumulation of diacetyl-chitobiose-P, when grown overnight in M9 CAA minimal medium supplemented with diacetyl-chitobiose. Accordingly, diacetyl-chitobiose-P (M+H)<sup>+</sup>  $m/z = 505.1429$  accumulated in the cytosolic fraction (Fig. 6a). Intriguingly, ChbF is not able to digest this compound (Fig. 6b), which confirms the inability of ChbF to

take substrates with an *N*-acetyl group at the non-reducing end. Notably, as seen throughout in the accumulation studies, also here phosphorylated and non-phosphorylated saccharide represented the major accumulation product. This further suggests the action of a phosphatase that partially dephosphorylates the accumulation product GlcNAc6P-GlcNAc.

#### *ChiA Cleaves Chitin and Partially Acetylated Chitosan but Not Fully Deacetylated Chitosan*

*E. coli* ChiA was previously characterized as an endochitinase, since it cleaved the artificial chitinase substrate 4-methylumbelliferyl (4-MU)-(GlcNAc)<sub>3</sub> but not 4-MU-GlcNAc [Francetic et al., 2000a]. Furthermore, in the latter report, ChiA was described as a bifunctional chitinase/lysozyme, on the basis of its ability to cleave ethylene-glycol chitin (EGC), which is a common lysozyme substrate [Wang and Chang, 1997]. We aimed to re-evaluate the enzyme's specificity using natural substrates, chitin (-oligomers), chitosan (-oligomers), and peptidoglycan, and thus expressed and purified ChiA as a polyhistidine-tagged recombinant protein. Hydrolysis of 4-MU-(GlcNAc)<sub>3</sub> (Sigma-Aldrich) was confirmed with the recombinant protein (data not shown). A preferred substrate of chitinases is colloidal chitin, which was prepared



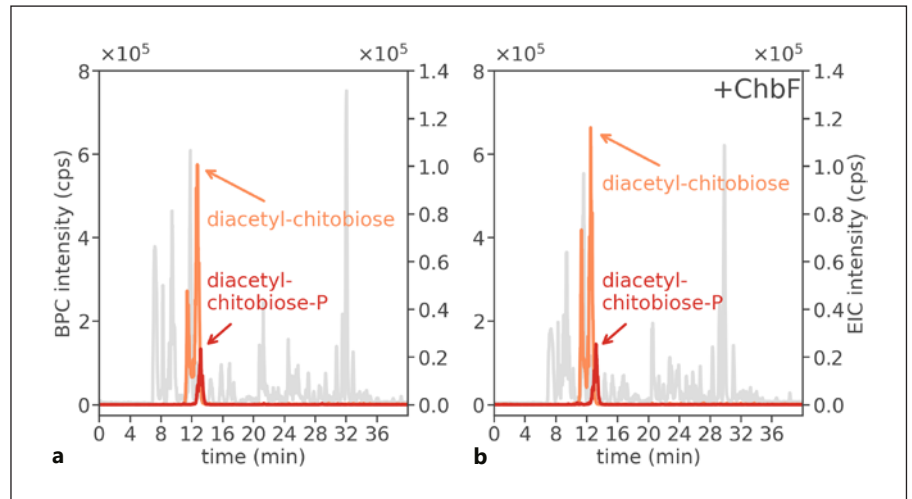


**Fig. 6.** ChbF is unable to cleave diacetyl-chitobiose-P. **a** Diacetyl-chitobiose ( $M+H$ )<sup>+</sup>  $m/z = 425.1776$  (orange) and diacetyl-chitobiose-P ( $M+H$ )<sup>+</sup>  $m/z = 505.1445$  (red) accumulate in cytosolic extracts of strain *E. coli*  $\Delta chbG::kan$  carrying pQE32-*chbBCA* and grown in M9 CAA medium in the presence of IPTG and diacetyl-chitobiose. **b** Incubation of the extract in **a** with recombinant ChbF

does not result in a decrease in the intensity of the mass peak of diacetyl-chitobiose ( $M+H$ )<sup>+</sup>  $m/z = 425.1780$  (orange) and diacetyl-chitobiose-P ( $M+H$ )<sup>+</sup>  $m/z = 505.1445$  (red). Shown are the base peak chromatogram (BPC) mass range ( $M+H$ )<sup>+</sup>  $m/z = 120-800$  (gray) and the extracted ion chromatograms (EIC) based on the exact masses of displayed compounds (Table 1).

by the acetylation of low molecular weight chitosan (<3 kDa in size; obtained from Carbosynth). ChiA was able to cleave colloidal chitin yielding diacetyl-chitotriose and triacetyl-chitotriose (Fig. 7b), whereas an endo-chitinase from *Streptomyces griseus*, in contrast, almost exclusively yielded diacetyl-chitobiose (Fig. 7c). That ChiA releases dimers and trimers in approximately equal amounts could be due to the fact that the enzyme features five chitin-binding type-3 domains which mediate binding to the glycan chains. To understand whether ChiA requires acetylated sugars, we incubated it with chitosan oligomers up to 3 kDa in size. The oligomer mix contained large amounts of chitotriose and chitotetraose and smaller amounts of chitobiose (Fig. 8a). Incubation with ChiA did not result in the release of small chitosan-oligosaccharides, but released significant amounts of diacetyl-chitotriose (Fig. 8b). As the diacetyl-chitotriose product of ChiA could not be further cleaved by the exo-*N*-acetylglucosaminidase NagZ from *B. subtilis*, we suggest the diacetyl-chitotriose product of ChiA is composed of GlcN-(GlcNAc)<sub>2</sub>. These data indicate that ChiA is able to cleave particular bonds within polymeric, acetylated chitosan releasing products that have GlcNAc at the reducing end. As a positive control, the chitosanase Csn from *B. subtilis* was cloned, expressed, and purified and the digestion was performed according to the conditions described [Rivas et al., 2000]. After incubation of the chito-

san oligomers with Csn an increased amount of chitobiose could be measured, while chitotetraose was completely digested (Fig. 8c).

#### *ChiA Has No Lysozyme Activity*

To investigate the lysozyme activity of ChiA, peptidoglycan was purified from *E. coli* and *B. subtilis*. Unlike the positive controls, Atl (Glc), the glucosaminidase domain of the bifunctional *N*-acetylmuramoyl-L-alanine amidase/endo- $\beta$ -*N*-acetylglucosaminidase Atl from *Staphylococcus aureus* [Oshida et al., 1995], and mutanolysin, the endo-*N*-acetylmuramidase from *Streptomyces* sp. [Rau et al., 2001], ChiA did not release products from the peptidoglycans of either source. From *E. coli* peptidoglycan, Atl (Glc) released MurNAc-GlcNAc in smaller and MurNAc-GlcNAc-tetrapeptide ([MurNAc-GlcNAc]-4P) in larger quantities (Fig. 9c). From *B. subtilis* peptidoglycan, Atl released disaccharides with and without peptides (online suppl. Fig. S1C; for all online suppl. material, see [www.karger.com/doi/10.1159/000515178](http://www.karger.com/doi/10.1159/000515178)). To test if ChiA possibly only cleaves denuded peptidoglycan, that is, poly-GlcNAc-MurNAc chains devoid of peptides, the *N*-acetylmuramoyl-L-alanine amidase Cw1C from *B. subtilis* [Shida et al., 2000] was used to remove the peptide stems from the peptidoglycan as reported elsewhere [Müller et al., 2021]. Cw1C quantitatively released tripeptides (3P) and tetrapeptides (4P) as well as crosslinked

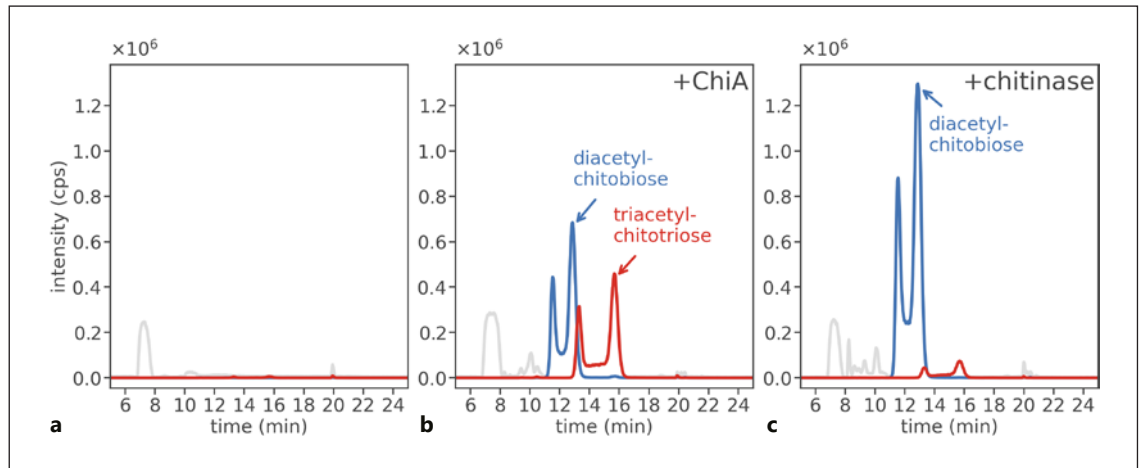


**Fig. 7.** ChiA cleaves colloidal chitin releasing diacetyl-chitobiose and triacetyl-chitotriose. Colloidal chitin was incubated with ChiA and a chitinase from *S. griseus* and the reaction products were analyzed by LC-MS. **a** Untreated colloidal chitin does not contain soluble chitoooligosaccharides, detectable by MS. **b** After a 2-hour digestion of colloidal chitin with ChiA diacetyl-chitobiose ( $M+H$ )<sup>+</sup>  $m/z$  = 425.1769 (blue) and triacetyl-chitotriose ( $M+H$ )<sup>+</sup>  $m/z$  =

628.2573 (red) are formed, but larger oligomers are not visible. **c** A chitinase from *S. griseus* (the positive control) almost exclusively released diacetyl-chitobiose ( $M+H$ )<sup>+</sup>  $m/z$  = 425.1765 (blue) from colloidal chitin. Shown are the base peak chromatogram (BPC) mass range ( $M+H$ )<sup>+</sup>  $m/z$  = 199–1,300 (gray) and the extracted ion chromatograms (EIC) based on the exact masses of displayed compounds (online suppl. Table S2).

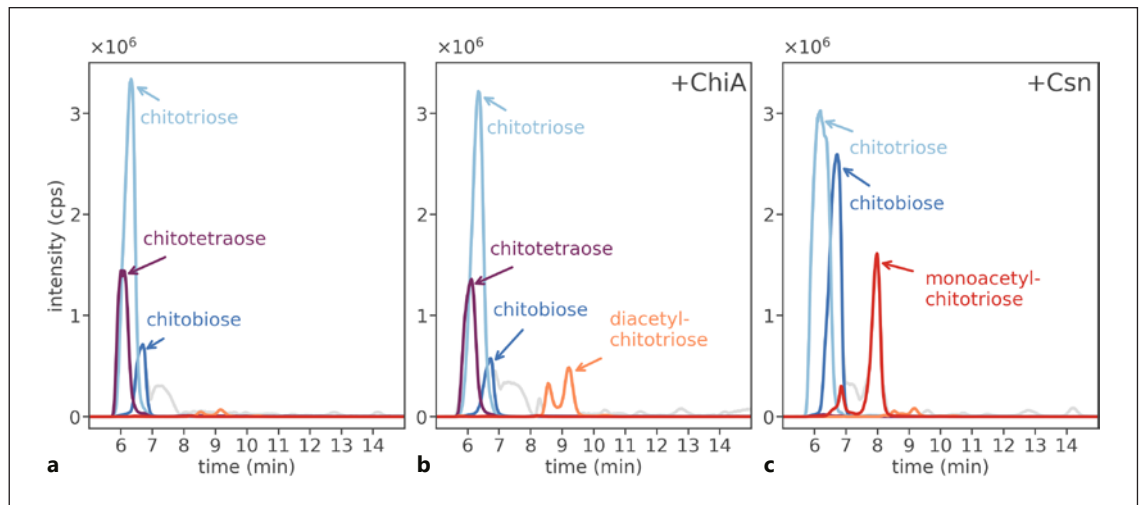
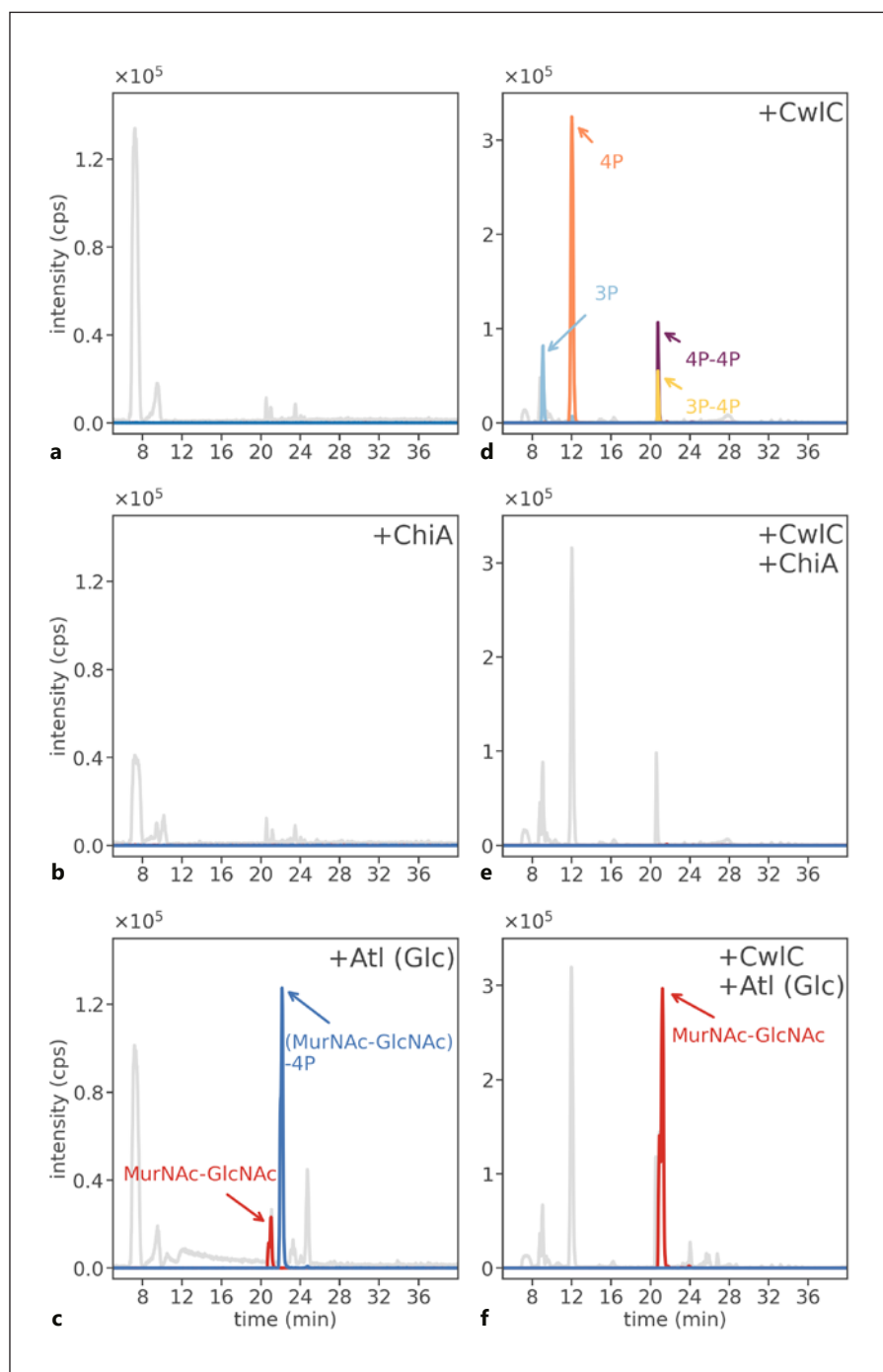


**Fig. 8.** ChiA cleaves partially acetylated chitosan yielding diacetyl-chitotriose. Chitosan (<3 kDa) was incubated with ChiA and a chitosanase from *B. subtilis* and the reaction products were analyzed by LC-MS. **a** Untreated chitosan (control) already contains small amounts of chitobiose ( $M+H$ )<sup>+</sup>  $m/z$  = 341.1576 (blue), chitotriose ( $M+H$ )<sup>+</sup>  $m/z$  = 502.2226 (light blue), and chitotetraose ( $M+H$ )<sup>+</sup>  $m/z$  = 663.2943 (purple). **b** Upon digestion of partially acetylated chitosan with ChiA (+ChiA), the amounts of deacetylated products were not increased, but the release of diacetyl-chitotriose

( $M+H$ )<sup>+</sup>  $m/z$  = 586.2508 (GlcN-GlcNAc-GlcNAc; orange) was detected. **c** Upon digestion of partially acetylated chitosan with *B. subtilis* chitosanase Csn the amount of chitobiose ( $M+H$ )<sup>+</sup>  $m/z$  = 341.1560 (blue) and also monoacetyl-chitotriose ( $M+H$ )<sup>+</sup>  $m/z$  = 544.2386 (red) were significantly increased, while the chitotetraose was completely digested. Shown are the base peak chromatogram (BPC) mass range ( $M+H$ )<sup>+</sup>  $m/z$  = 199–1,300 (gray) and the extracted ion chromatograms (EIC) based on the exact masses of displayed compounds (online suppl. Table S2).

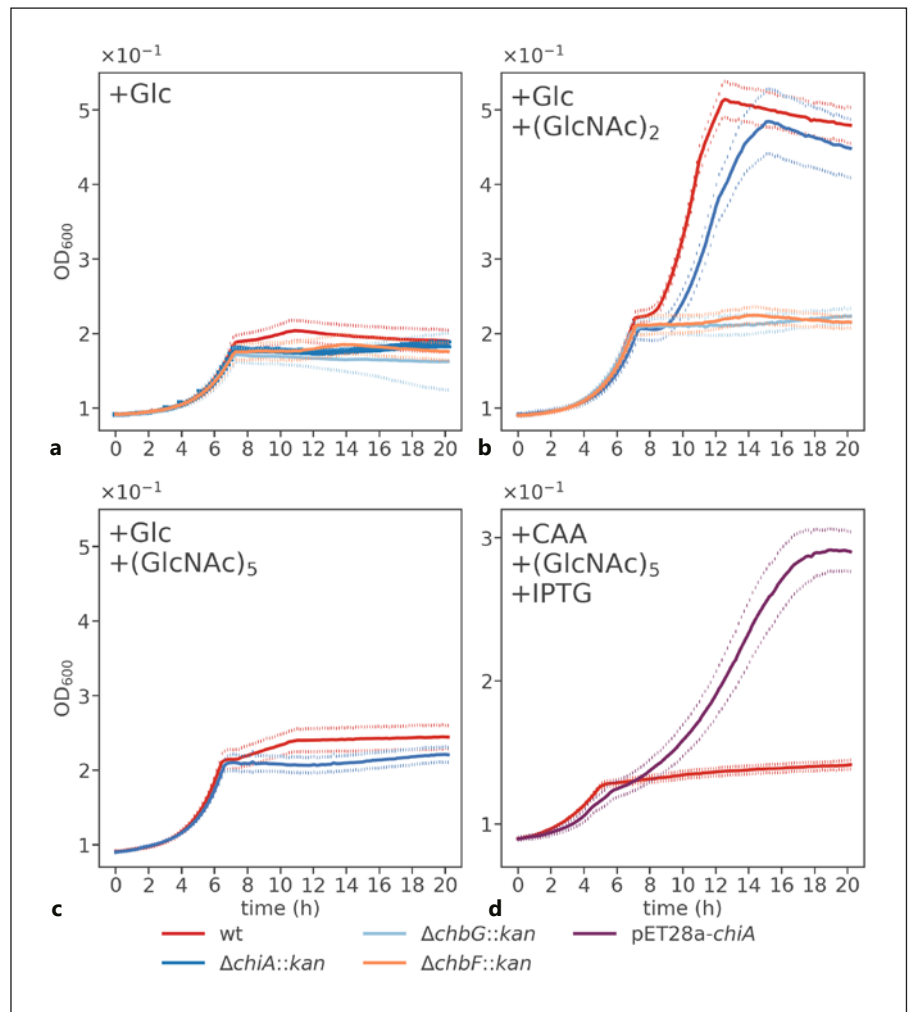
**Fig. 9.** ChiA does not cleave peptidoglycan. Intact peptidoglycan, derived from *E. coli* (left panels), and peptide-denuded peptidoglycan (right panels), that is, treated with amidase CwIC to remove the peptide stems, were incubated with ChiA or the endo-glucosaminidase Atl (Glc) of *S. aureus*. The formation of reaction products was analyzed by LC-MS. **a** Uncleaved *E. coli* peptidoglycan as a control. **b** Incubation of *E. coli* peptidoglycan with ChiA (+ChiA) does not release any soluble products. **c** Incubation of *E. coli* peptidoglycan with Atl (Glc) (+Atl (Glc)), releases large amounts of (MurNAc-GlcNAc)-tetra-peptide (M+H)<sup>+</sup>  $m/z = 940.3922$  ((MurNAc-GlcNAc)-4P; blue) and to a lesser extent also MurNAc-GlcNAc (M+H)<sup>+</sup>  $m/z = 497.1954$  (red). **d** CwIC (+CwIC) removes tri- (M+H)<sup>+</sup>  $m/z = 391.1650$  (3P, light blue), tetra- (M+H)<sup>+</sup>  $m/z = 462.2006$  (4P, orange), tri-tetra (M+H)<sup>+</sup>  $m/z = 834.3448$  (3P-4P, yellow), and tetra-tetra peptides (M+H)<sup>+</sup>  $m/z = 905.3808$  (4P-4P, purple) from *E. coli* peptidoglycan. **e** From **d**, ChiA (+CwIC+ChiA) is unable to cleave denuded peptidoglycan. **f** From **d**, Atl (Glc) (+CwIC+Atl (Glc)) is able to release large amounts of MurNAc-GlcNAc (M+H)<sup>+</sup>  $m/z = 497.1750$  (red). Intriguing, no MurNAc-GlcNAc-4P could be detected, indicating the complete removal of the stem peptides from the peptidoglycan by CwIC. Shown are the base peak chromatograms (BPC) mass range (M+H)<sup>+</sup>  $m/z = 200-2,000$  (gray) and the extracted ion chromatograms (EIC) based on the exact masses of displayed compounds (online suppl. Table S2).



4P-4P and 3P-4P peptides (Fig. 9d) from *E. coli* peptidoglycan. From *B. subtilis* peptidoglycan it released 3P\*, 3P\*-4P\*, and 3P-4P\*, in which the amino acid meso-diaminopimelic acid is amidated (assigned with \*) (online suppl. Fig. S1E). However, ChiA was not able to release any products from denuded peptidoglycan chains (Fig. 9e; online suppl. Fig. S1F). Atl (Glc), on the other hand, re-

leases significant amounts of MurNAc-GlcNAc as the only product in both cases. The fact that no disaccharide with peptides was released using Atl (Glc) indicates that CwIC has completely removed the peptides (Fig. 9f; online suppl. Fig. S1G). Mutanolysin, in contrast, cleaved native peptidoglycan, but was unable to degrade denuded peptidoglycan (online suppl. Fig. S1H). In summary, the

**Fig. 10.** ChiA is generally not expressed in *E. coli* wt, but periplasmic expression facilitates growth on penta-acetyl-chitopentaose (GlcNAc<sub>5</sub>). **a** *E. coli* wild-type (red),  $\Delta chiA::kan$  (blue),  $\Delta chbG::kan$  (light blue),  $\Delta chbF::kan$  (orange), and BL21 (DE3) pET28a-*chiA* (purple) strains were grown in minimal medium supplemented with 0.1% glucose (+Glc) as the only carbon source. wt,  $\Delta chbG::kan$ ,  $\Delta chbF::kan$ , and  $\Delta chiA::kan$  show a similar growth behavior reaching stationary phase after 7 h. **b** In minimal medium supplemented with 0.1% glucose and 0.2% diacetyl-chitobiose (+Glc+(GlcNAc)<sub>2</sub>), wt and  $\Delta chiA::kan$  showed biphasic growth, whereas  $\Delta chbG::kan$  and  $\Delta chbF::kan$  grew as in medium with sole glucose. **c** In minimal medium supplemented with 0.1% glucose and 0.2% penta-acetyl-chitopentaose (+Glc+(GlcNAc)<sub>5</sub>), wt and  $\Delta chiA::kan$  grew as in medium with sole glucose, indicating that penta-acetyl-chitopentaose is not utilized. **d** In minimal medium supplemented with 0.1% CAA and 0.2% penta-acetyl-chitopentaose (+CAA+(GlcNAc)<sub>5</sub>+IPTG), again, *E. coli* wt is not able to utilize the penta-acetyl-chitopentaose; however, periplasmic expression of ChiA from a plasmid facilitated growth on penta-acetyl-chitopentaose, resulting in a biphasic growth and a significantly higher final OD<sub>600</sub> of 0.3.



results show that ChiA can digest chitin but neither chitosan nor peptidoglycan polymers irrespectively of whether they are native or denuded.

#### *ChiA Expression Facilitates Growth on Penta-Acetyl-Chitopentaose*

With the sole role of ChiA as chitinase confirmed in vitro, the growth of *E. coli* wt and  $\Delta chiA::kan$  in M9 glucose minimal medium was compared in the presence of diacetyl-chitobiose or penta-acetyl-chitopentaose. As expected both strains were able to grow on glucose and diacetyl-chitobiose exhibiting a biphasic growth pattern due to carbon catabolite repression (Fig. 10b). With penta-acetyl-chitopentaose no biphasic growth was observed, as only glucose was utilized (Fig. 10c). However, the wt strain was expected to utilize penta-acetyl-chitopentaose if ChiP and ChiA were active. This was not the case, because *chiA* expression is usually si-

lenced by the nucleotide-structuring protein H-NS [Francetic et al., 2000a]. In contrast, ChiP expression is controlled by the small RNA ChiX but, expression of the *chb* transcript relieves *chiP* inhibition by functioning as trap-RNA [Figueroa-Bossi et al., 2009; Rasmussen et al., 2009]. Thus, expression of ChiA in the periplasm should allow growth on chitooligomers (e.g., penta-acetyl-chitopentaose), which are transported through ChiP into the periplasm. Cleavage by ChiA releases diacetyl-chitobiose and triacetyl-chitotriose, which can be taken up by the ChbCBA-PTS and metabolized by ChbG and ChbF. To test this, ChiA was artificially expressed in *E. coli* BL21 (DE3) from plasmid pET22b-*chiA* in an IPTG-inducible manner. Compared to *E. coli* K12 wt during growth in M9 CAA (to avoid carbon catabolite repression) minimal medium, the expression of ChiA clearly restored the availability to utilize penta-acetyl-chitopentaose (Fig. 10d). To exclude that *E. coli*

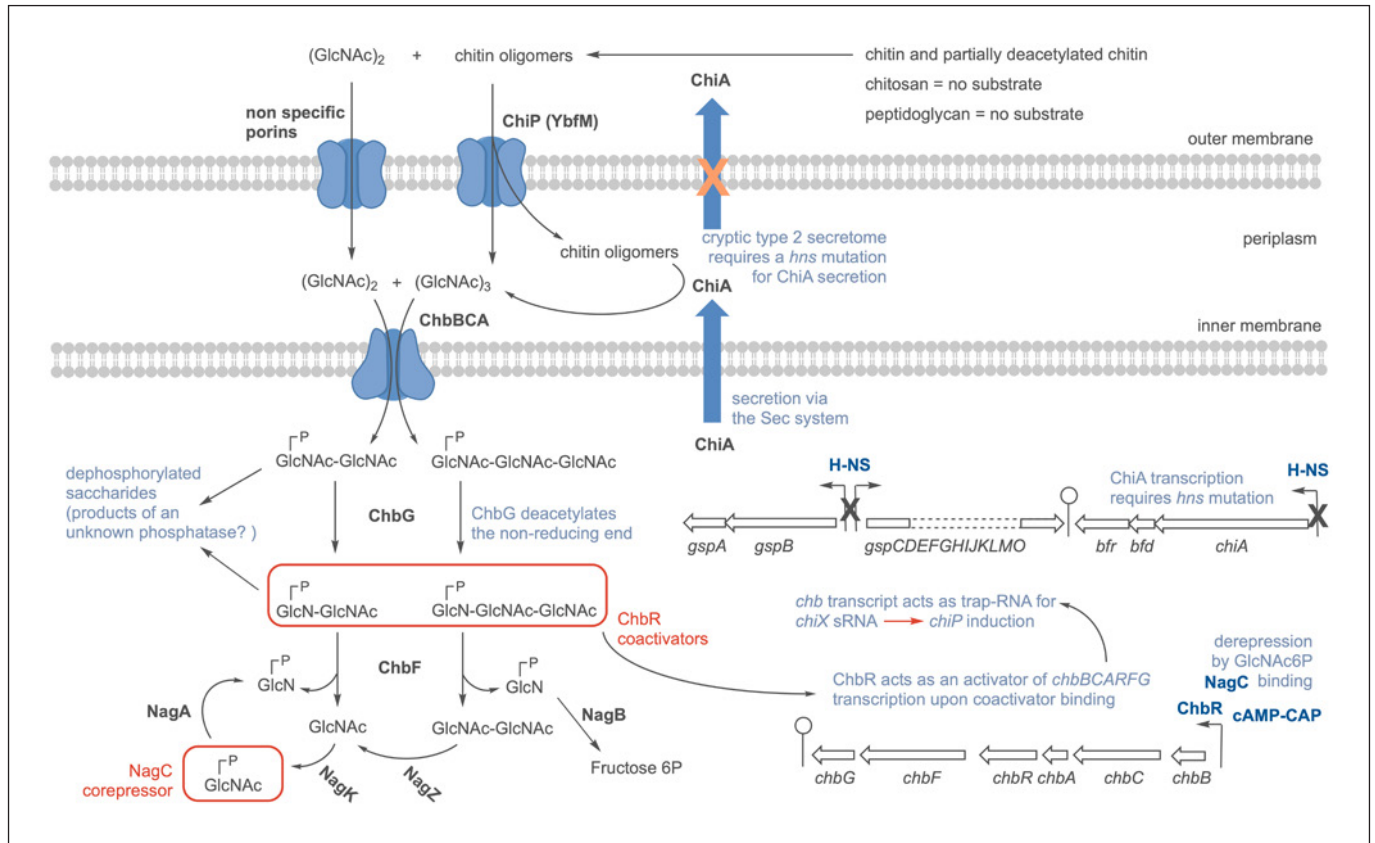


**Fig. 11.** Overview of the chitin, chitin oligomer, triacetyl-chitotriose, and diacetyl-chitobiose metabolism of *E. coli* and its regulation. Chitin and partially acetylated chitosan is cleaved by the chitinase ChiA, yielding transiently chitin oligomers and as final products triacetyl-chitotriose (GlcNAc<sub>3</sub>) and diacetyl-chitobiose (GlcNAc<sub>2</sub>). In *E. coli* K12, however, ChiA expression is repressed (silenced) by the nucleoid-structuring protein H-NS [Francetic et al., 2000a]. ChiA is exported into the periplasm via Sec secretion, provided it is expressed either artificially or in a *hns* mutant. In a *hns* strain, ChiA also gets partially secreted into the medium via activation of the cryptic type 2 secretome [Francetic et al., 2000b]. Diacetyl-chitobiose is taken up into the periplasm by nonspecific porins, whereas triacetyl-chitotriose and short-chain chitin oligomers pass through the membrane by a facilitated diffusion process mediated by the chitoporin ChiP [Soysa and Suginta, 2016]. If present in the periplasm, ChiA can cleave the chitin oligomers to diacetyl-chitobiose and triacetyl-chitotriose. *E. coli* grows on diacetyl-chitobiose and triacetyl-chitotriose via the expression of the *chb* operon (*chbBCARFG*). The phosphotransferase system (PTS)

transporter ChbBCA facilitates transport of both saccharides across the inner membrane and their concomitant phosphorylation at the non-reducing end. Subsequently, the phosphorylated saccharides are deacetylated at the non-reducing end by ChbG yielding monoacetyl-chitobiose-P (GlcN6P-GlcNAc) and diacetyl-chitotriose-P (GlcN6P-GlcNAc-GlcNAc). These two products also act as coactivators for ChbR (framed in red), resulting in increased transcription of the *chb* operon. They are cleaved by ChbF and further processed by the exo-glucosaminidase NagZ [Litzing et al., 2010a, b] and the *N*-acetyl-D-glucosamine kinase NagK [Uehara and Park, 2004]. The *N*-acetylglucosamine repressor NagC, which binds the *chb* promoter thereby inhibiting transcription, is released from the promoter by binding to GlcNAc6P (framed in red) [Plumbridge and Pellegrini, 2004]. Expression of the *chb* operon is also subject to catabolite repression (i.e., activated by cAMP-CAP). GlcNAc6P is degraded by the GlcNAc6P deacetylase NagA and GlcN-6P deaminase NagB to yield fructose 6P thereby entering glycolysis.

BL21 (DE3) expressed endogenous ChiA we monitored its growth on penta-acetyl-chitopentaose and observed the same growth pattern as that of *E. coli* K12 wt (data not shown). This clearly shows that *E. coli* has the potential to utilize chitin oligosaccharides in a ChiA-dependent manner. However, since *E. coli* ChiA expres-

sion and secretion is silenced, the bacterium either relies on scavenging chitinase end products from other organisms or, if there is enough evolutionary pressure, selection against H-NS repression of ChiA and the type 2 secretome might occur.

## Conclusion

In this study we refined the understanding of the catabolic pathways of diacetyl-chitobiose (GlcNAc-GlcNAc) and triacetyl-chitotriose (GlcNAc-GlcNAc-GlcNAc) in *E. coli*, as summarized in Figure 11. Catabolism of the saccharides involves phosphorylation via the ChbBCA PTS transporter, as shown previously [Keyhani et al., 2000a, b, c], and subsequent deacetylation via the monodeacetylase ChbG, which specifically removes the *N*-acetyl group from non-reducing end terminal GlcNAc6P entities, as shown in this study. Since activation of the *chb* promoter by the transcriptional regulator ChbR depends on the ChbG activity [Verma and Mahadevan, 2012], the correction of the function of ChbG indirectly identified GlcN6P-GlcNAc and GlcN6P-GlcNAc-GlcNAc as the inducers of the *chb* operon, which upon binding to ChbR activate *chbBCARFG* transcription. These saccharides were found to accumulate in a  $\Delta$ *chbF* strain, thus constituting the natural substrates of ChbF. Intriguingly, ChbF failed to cleave GlcNAc6P-GlcNAc, because the *N*-acetyl group of GlcNAc6P-glycosides sterically interferes with amino acids in the active site pocket and thus prevents binding to ChbF, as shown by structural modeling. Possibly, the unusual redox/elimination-type mechanism of ChbF, belonging to family 4 of Cazy glycosidases (URL: <http://www.cazy.org/GH4.html>) [Henrissat, 1991; Davies and Henrissat, 1995; Yip and Withers, 2012], excludes GlcNAc6P-glycosides as suitable substrates. Accumulation of non-phosphorylated saccharides in the *chbF* mutant indicates that an unidentified phosphatase is active intracellularly that cleaves the phosphorylated 6P-glycosides. We assume that the dephosphorylation occurs due to the accumulation of high concentrations of phosphorylated saccharides and, thus, likely constitutes a detoxification mechanism counteracting sugar phosphate stress. The identity of the phosphatase is so far unclear; however, it could be identical to the phosphatase YigL, which has been reported to relieve glucose-phosphate stress in *E. coli* [Kuznetsova et al., 2006; Sun and Vanderpool, 2013].

The reason for this particular catabolic pathway in *E. coli* is unclear, but may be linked to the function of the chitinase ChiA of *E. coli*. We showed that the chitinase ChiA specifically cleaves chitin as well as acetylated chitosan, yielding diacetyl-chitobiose/triacetyl-chitotriose and GlcN-GlcNAc-GlcNAc, respectively, but does not cleave intact or peptide-free, denuded peptidoglycan as well as chitosan. Chitin in nature barely occurs as a fully acetylated polymer. Since ChiA is able to cleave GlcNAc-beta-1,4-GlcN bonds, it thus generates saccharides that

upon uptake and phosphorylation by the ChbBCA PTS directly act as inducers of the *chb* operon. A still open question is why ChiA expression is silenced in *E. coli*. It is appealing to assume that *E. coli* laboratory strains have adapted to the use of LB- or similar media made up of yeast extract, which contains diacetyl-chitobiose and triacetyl-chitotriose but lacks chitooligomers; thus, ChiA is dispensable under these condition. It could be interesting to screen for undomesticated *E. coli* strains that lack a silent ChiA system and hence retain their ability to grow on polymeric chitin.

## Experimental Procedures

### Bacterial Strains and Growth Conditions

The bacterial strains used in this study are listed in online supplementary Table S1. *B. subtilis* 168 wild-type and *E. coli* K12 were used for the isolation of peptidoglycan. Bacteria were cultured at 37°C in lysogeny broth (LB broth Lennox, Carl Roth) with continuous shaking at 140 rpm. Overnight cultures (~16 h) were used to inoculate fresh LB medium. Cells were harvested by centrifugation (3,000 × *g*, 20 min, 4°C). *E. coli* BL21 (DE3) cells (New England Biolabs) used to heterologously express recombinant enzymes were grown in LB medium supplemented with 50 µg/mL kanamycin or 100 µg/mL ampicillin depending on the expression plasmid until OD<sub>600</sub> 0.7 was reached, followed by induction with 1 mM IPTG and further propagation for 3 h. Cells were harvested by centrifugation (3,000 × *g*, 20 min, 4°C) and used for the purification of recombinant proteins. For the extraction of accumulation products *E. coli*  $\Delta$ *chbG::kan*,  $\Delta$ *chbF::kan*, and *E. coli*  $\Delta$ *chbG::kan* pQE32-*chbBCA* were grown at 37°C o/n in 5 mL M9 minimal medium [Harwood and Cutting, 1990] with 6 g/L casamino acids (CAA) instead of glucose and 2 mM diacetyl-chitobiose. The growth curves were conducted in a Tecan plate reader at 37°C in 24-well plates filled with 400 µL M9 minimal medium [Harwood and Cutting, 1990] either with 0.1% glucose or 0.1% CAA and 0.1% of test substrate (diacetyl-chitobiose, triacetyl-chitotriose or penta-acetyl-chitopentaose; obtained from Carbosynth).

### Construction of Plasmids and Purification of Recombinant Enzymes

For the overexpression and purification of the enzymes used in this work, *E. coli* K12 ChbF (JW1723) and ChiA (JW3300), *B. subtilis* 168 Csn (BSU26890), NagZ (BSU01660), and CwlC (BSU17410), and *S. aureus* USA300 Atl (Glc) (ABD22514.1), the corresponding genes were amplified by PCR using the respective genomic DNA and primers listed in online supplementary Table S1. Prior to its insertion in pET28a, the *NcoI* site in *cwl* was deleted. The PCR products were purified (GeneJET purification kit and GeneRuler, 1-kb marker, Thermo Fisher Scientific). PCR product and vector (specified in primer name in online suppl. Table S1) were digested with restriction enzymes (specified in primer name in online suppl. Table S1; New England Biolabs) and ligated with T4 DNA ligase (Thermo Fisher Scientific). Chemically competent *E. coli* DH5α cells were transformed using the constructed plasmids and selected for growth on the respective

antibiotic. From positive clones plasmids were purified and checked by sequencing.

The positive plasmids were used to transform *E. coli* BL21 (DE3) cells, which were grown as described above and lysed in a French pressure cell. Recombinant His-tagged enzymes were purified by Ni<sup>2+</sup>-affinity chromatography using a 1-mL HisTrap column (GE Healthcare) followed by size exclusion chromatography on a HiLoad 16/60 Superdex 200 pg column (GE Healthcare) and purity was checked with a 12% SDS-PAGE. From a 1-L culture 3.6 mg ChbF, 1.75 mg CwlC, and 12.5 mg Csn were obtained. The enzymes were stored at -20°C in 20 mM Na<sub>2</sub>HPO<sub>4</sub> buffer (500 mM NaCl, pH 7.6). Gibson Assembly was used for the construction of a PTS transporter mutant in *E. coli*  $\Delta$ *chbG::kan*. The corresponding gene sections for *chbBCA* were amplified by PCR from *E. coli* K12 genomic DNA using the appropriate primers (online suppl. Table S1). The purified PCR product was cloned via Gibson Assembly into pQE32, which was linearized via digestion with *Bse*RI and *Hind*III. Chemically competent *E. coli*  $\Delta$ *chbG::kan* cells were transformed with pQE32-*chbBCA*. Positive clones selected by antibiotics were confirmed by sequencing.

#### Preparation of Peptidoglycan

For the preparation of *B. subtilis* 168 cell walls 2 L of culture (exponential growth phase, OD<sub>600</sub> = 1.0) were harvested and resuspended in 30 mL piperazine-acetate buffer (50 mM, pH 6) with 12 U proteinase K and boiled for 1 h. The cytosolic fractions were removed by centrifugation (3,000 × g, 15 min, 4°C). The pellet was resuspended in 6 mL buffer (10 mM Tris, 10 mM NaCl, 320 mM imidazole, adjusted to pH 7.0 with HCl) and 600 µg α-amylase, 250 U RNase A, 120 U DNase I, and 50 mM MgSO<sub>4</sub> were added. The sample was incubated at 37°C for 2 h while shaking, 12 U Proteinase K was added, and the incubation continued for 1 h. 4% SDS solution was added 1:1 and the mixture was boiled for 1 h. SDS was removed by repeated ultracentrifugation steps (20 times at 140,000 × g, 30 min, 40°C) and suspension in H<sub>2</sub>O<sub>bidistilled</sub> as well as dialysis against H<sub>2</sub>O<sub>bidistilled</sub>. The SDS content was controlled with the methylene blue assay described earlier [Hayashi, 1975]. The cell wall preparation was dried in a vacuum concentrator. Wall teichoic acids were removed by incubation with 1 M HCl for 4 h at 37°C.

For the preparation of *E. coli* K12 cell walls 2 L of culture (exponential growth phase, OD<sub>600</sub> = 1.0) were harvested and resuspended in 90 mL ice-cold H<sub>2</sub>O<sub>bidistilled</sub> (to prevent peptidoglycan autolysis activity). Boiling SDS solution (8%) was added dropwise until a final volume of 100 mL and boiled for 1 h further while stirring constantly. The SDS was removed as described for *B. subtilis* cell wall. After resuspending the pellet again in 20 mL H<sub>2</sub>O<sub>bidistilled</sub>, 300 µL α-amylase stock solution (12 mg α-amylase + 0.5 mL H<sub>2</sub>O<sub>bidistilled</sub> + 0.7 mL 10 mM Tris-HCl pH 7) were added and incubated at 37°C under constant shaking for 2 h. Pronase solution (100 mg pronase + 10 mL 10 mM Tris-HCl buffer pH 7) was pre-incubated at 60°C for 2 h. 500 µL pronase solution was added to the sample and incubation was continued for 2 h further. The sample was boiled for 1 h while stirring followed by one ultracentrifugation step. The cell wall preparation was dried in a vacuum concentrator.

#### Preparation of Colloidal Chitin

For the preparation of colloidal chitin chitosan (<3 kDa; obtained from Carbosynth) was acetylated with acetic anhydride. 20 mL 1 M sodium bicarbonate (freshly prepared) were added to 500

mg chitosan and mixed by swirling until a brown-colored foam developed. 0.5 mL of >99% acetic anhydride were added dropwise while mixing slowly, followed by incubation for 20 min at room temperature. The solution was precipitated by centrifugation (1,500 × g) and the pellet was resuspended again in 20 mL 1 M sodium bicarbonate with 0.5 mL acetic anhydride and further incubated for 20 min. The reaction was boiled for 10 min and washed with phosphate buffered saline until pH 7 was attained. The colloidal chitin was stored at 4°C.

#### Enzymatic Reactions

For the digestion of *E. coli* and *B. subtilis* peptidoglycan, colloidal chitin, and chitosan oligomers, 0.2 mg substrate were used. The following buffers were used for the enzymes: 0.1 M potassium phosphate pH 8 for Atl and CwlC; 0.1 M sodium phosphate pH 7.2 for ChiA, chitinase from *S. griseus*, NagZ and ChbF; 0.1 M potassium phosphate pH 6 for mutanolysin; 0.05 M sodium acetate pH 5.7 for Csn. In each case 5 µg of enzyme were used for one preparation and all reactions took place at 37°C. Peptidoglycan preparations were incubated for 1 h, colloidal chitin, chitosan, and cytosolic fractions for 2 h. The digestion volume was 50 µL total, except for the pre-digestion of peptidoglycan by CwlC, which had a volume of 25 µL. After CwlC pre-treatment the pH was adjusted to the corresponding pH value of the subsequent enzyme with 0.1 M potassium dihydrogen phosphate and the volume was adjusted to 50 µL. After each digestion the enzymes were heat-inactivated at 95°C for 10 min.

#### Generation of Cytosolic Fractions

A 5-mL culture was harvested by centrifugation at 16,000 × g for 10 min and was washed twice in 1 mL Tris-HCl (pH 7.6, 10 mM) buffer. The cells were resuspended in 200 µL buffer and incubated for 10 min at 95°C followed by a further centrifugation step. The supernatant was removed by pipetting and mixed with 800 µL acetone. After a further centrifugation step the supernatant was removed and dried under vacuum at 37°C. Samples were dissolved in 30 µL H<sub>2</sub>O<sub>bidistilled</sub> for LC-MS analysis [Gisin et al., 2013].

#### Reduction of Samples with NaBH<sub>4</sub>

Samples were reduced with sodium borohydride as described earlier [Schaub and Dillard, 2017; Kluj et al., 2018]. To prepare the reducing solution, 500 µL of 0.5 M borate buffer (pH 9) was added to 5 mg sodium borohydride. Samples dissolved in 30 µL H<sub>2</sub>O<sub>bidistilled</sub> were added to 30 µL reducing solution and incubated for 20 min at room temperature. By the addition of 10 µL 8.5% phosphoric acid the pH was adjusted to 3–4 before the samples were dried in a vacuum concentrator at 37°C and dissolved in 30 µL H<sub>2</sub>O<sub>bidistilled</sub> for LC-MS analysis.

#### Analysis of Reaction Products by LC-MS

Sample analysis was conducted using an electrospray ionization-time of flight (ESI-TOF) mass spectrometer (MicrOTOF II; Bruker Daltonics), operated in positive ion-mode that was connected to an UltiMate 3000 high-performance liquid chromatography (HPLC) system (Dionex). For HPLC-MS analysis 5 µL of the sample supernatant were injected into a Gemini C18 column (150 × 4.6 mm, 5 µm, 110 Å, Phenomenex). A 45-min program at a flow rate of 0.2 mL/min was used to separate the compounds as previously described [Gisin et al., 2013]. An Orbitrap Elite mass spectrometer (Thermo Scientific) was used to record higher energy collisional dissociation (HCD) MS/MS spectra.

## Acknowledgement

We acknowledge Marina Borisova, Tim Teufel, and Amanda Duckworth for providing plasmids and proteins as well as Johannes Madlung and Boris Macek for valuable expertise with MS/MS measurements.

## Statement of Ethics

Ethics approval was not required.

## Conflict of Interest Statement

The authors have no conflicts of interest to declare.

## References

- Adams DW, Stutzmann S, Stoudmann C, Blokesch M. DNA-uptake pili of *Vibrio cholerae* are required for chitin colonization and capable of kin recognition via sequence-specific self-interaction. *Nat Microbiol*. 2019 Sep; 4(9):1545–57.
- Blokesch M. Chitin colonization, chitin degradation and chitin-induced natural competence of *Vibrio cholerae* are subject to catabolite repression. *Environ Microbiol*. 2012 Aug;14(8): 1898–912.
- Davies G, Henrissat B. Structures and mechanisms of glycosyl hydrolases. *Structure*. 1995; 3(9):853–9.
- Figuerola-Bossi N, Valentini M, Malleret L, Fiorini F, Bossi L. Caught at its own game: regulatory small RNA inactivated by an inducible transcript mimicking its target. *Genes Dev*. 2009 Sep 1;23(17):2004–15.
- Francetic O, Badaut C, Rimsky S, Pugsley AP. The ChiA (YheB) protein of *Escherichia coli* K-12 is an endochitinase whose gene is negatively controlled by the nucleoid-structuring protein H-NS. *Mol Microbiol*. 2000a Mar;35(6): 1506–17.
- Francetic O, Belin D, Badaut C, Pugsley AP. Expression of the endogenous type II secretion pathway in *Escherichia coli* leads to chitinase secretion. *EMBO J*. 2000b Dec 15;19(24): 6697–703.
- Gisin J, Schneider A, Nägele B, Borisova M, Mayer C. A cell wall recycling shortcut that bypasses peptidoglycan de novo biosynthesis. *Nat Chem Biol*. 2013 Aug;9(8):491–3.
- Hamid R, Khan MA, Ahmad M, Ahmad MM, Abdin MZ, Musarrat J, et al. Chitinases: An update. *J Pharm Bioallied Sci*. 2013 Jan;5(1):21–9.
- Harwood CR, Cutting SM. Chemically defined growth media and supplements. Wiley, Chichester, UK; 1990.
- Hayashi K. A rapid determination of sodium dodecyl sulfate with methylene blue. *Anal Biochem*. 1975 Aug;67(2):503–6.
- Henrissat B. A classification of glycosyl hydrolases based on amino acid sequence similarities. *Biochem J*. 1991;280 ( Pt 2):309–16.
- Itoh T, Kimoto H. Bacterial chitinase system as a model of chitin biodegradation. *Adv Exp Med Biol*. 2019;1142:131–51.
- Keyhani NO, Bacia K, Roseman S. The transport/phosphorylation of N,N'-diacetylchitobiose in *Escherichia coli*. Characterization of phospho-IIChb and of a potential transition state analogue in the phosphotransfer reaction between the proteins IIChb and IIBChb. *J Biol Chem*. 2000a;275(42):33102–9.
- Keyhani NO, Boudker O, Roseman S. Isolation and characterization of IIChb, a soluble protein of the enzyme II complex required for the transport/phosphorylation of N, N'-diacetylchitobiose in *Escherichia coli*. *J Biol Chem*. 2000b;275(42):33091–101.
- Keyhani NO, Roseman S. Wild-type *Escherichia coli* grows on the chitin disaccharide, N,N'-diacetylchitobiose, by expressing the cel operon. *Proc Natl Acad Sci USA*. 1997;94(26): 14367–71.
- Keyhani NO, Wang LX, Lee YC, Roseman S. The chitin disaccharide, N,N'-diacetylchitobiose, is catabolized by *Escherichia coli* and is transported/phosphorylated by the phosphoenolpyruvate:glucose phosphotransferase system. *J Biol Chem*. 2000c;275(42):33084–90.
- Kluj RM, Ebner P, Adamek M, Ziemert N, Mayer C, Borisova M. Recovery of the peptidoglycan turnover product released by the autolysin Atl in *Staphylococcus aureus* involves the phosphotransferase system transporter MurP and the novel 6-phospho-N-acetylmuramidase MupG. *Front. Microbiol*. 2018 Nov 16; 9(2725).
- Kuznetsova E, Proudfoot M, Gonzalez CF, Brown G, Omelchenko MV, Borozan I, et al. Genome-wide analysis of substrate specificities of the *Escherichia coli* haloacid dehalogenase-like phosphatase family. *J Biol Chem*. 2006 Nov 24;281(47):36149–61.
- Litzinger S, Duckworth A, Nitzsche K, Risinger C, Wittmann V, Mayer C. Muropeptide rescue in *Bacillus subtilis* involves sequential hydrolysis by beta-N-acetylglucosaminidase and N-acetylmuramyl-L-alanine amidase. *J Bacteriol*. 2010a Jun;192(12):3132–43.
- Litzinger S, Fischer S, Polzer P, Diederichs K, Welte W, Mayer C. Structural and kinetic analysis of *Bacillus subtilis* N-acetylglucosaminidase reveals a unique Asp-His dyad mechanism. *J Biol Chem*. 2010b Nov 12; 285(46):35675–84.
- Müller M, Calvert M, Hottmann I, Kluj RM, Teufel T, Balbuchta K, et al. The exo- $\beta$ -N-acetylmuramidase NamZ from *Bacillus subtilis* is the founding member of a family of exolytic peptidoglycan hexosaminidases. *J Biol Chem*. 2021. <http://dx.doi.org/10.1016/j.jbc.2021.100519>. In press.
- Oshida T, Sugai M, Komatsuzawa H, Hong YM, Suganaka H, Tomasz A. A *Staphylococcus aureus* autolysin that has an N-acetylmuramoyl-L-alanine amidase domain and an endo- $\beta$ -N-acetylglucosaminidase domain: cloning, sequence analysis, and characterization. *Proc Natl Acad Sci USA*. 1995 Jan 3;92(1):285–9.
- Parker LL, Hall BG. Mechanisms of activation of the cryptic cel operon of *Escherichia coli* K12. *Genetics*. 1990;124(3):473–82.
- Plumbridge J, Pellegrini O. Expression of the chitobiose operon of *Escherichia coli* is regulated by three transcription factors: NagC, ChbR and CAP. *Mol Microbiol*. 2004 Apr;52(2): 437–49.

## Funding Sources

C.M. acknowledges funding by the ministry of science, research and art of the state Baden-Württemberg (program glycobiology and glycobiotechnology) and by the Deutsche Forschungsgemeinschaft (DFG, German Research Foundation), grants SFB766, Project-ID 398967434 – TRR 261 and Project-ID 174858087 – GRK1708. This work was further supported by the DFG-funded Cluster of Excellence EXC 2124 Controlling Microbes to Fight Infections.

## Author Contributions

A.W. conducted the experiments. S.F. provided the plasmid pQE32-ChbBCA. C.M. formulated the original problem and provided guidance throughout the study. C.M. and A.W. designed the experiments and developed the methodology. C.M., S.F., and A.W. wrote the manuscript.



- Rajan SS, Yang X, Collart F, Yip VLY, Withers SG, Varrot A, et al. Novel Catalytic Mechanism of Glycoside Hydrolysis Based on the Structure of an NAD<sup>+</sup>/Mn<sup>2+</sup>-Dependent Phospho- $\alpha$ -Glucosidase from *Bacillus subtilis*. *Structure*. 2004 Sep;12(9):1619–29.
- Rasmussen AA, Johansen J, Nielsen JS, Overgaard M, Kallipolitis B, Valentin-Hansen P. A conserved small RNA promotes silencing of the outer membrane protein YbfM. *Mol Microbiol*. 2009 May;72(3):566–77.
- Rau A, Hogg T, Marquardt R, Hilgenfeld R. A new lysozyme fold. Crystal structure of the muramidase from *Streptomyces coelicolor* at 1.65 Å resolution. *J Biol Chem*. 2001 Aug 24; 276(34):31994–9.
- Rivas LA, Parro V, Moreno-Paz M, Mellado RP. The *Bacillus subtilis* 168 *csn* gene encodes a chitosanase with similar properties to a *Streptomyces* enzyme. *Microbiology (Reading, Engl)*. 2000 Nov;146(Pt 11):2929–36.
- Schaub RE, Dillard JP. Digestion of peptidoglycan and analysis of soluble fragments. *Bio Protoc*. 2017 Aug 5;7(15).
- Shida T, Hattori H, Ise F, Sekiguchi J. Overexpression, purification, and characterization of *Bacillus subtilis* N-acetylmuramoyl-L-alanine amidase CwlC. *Biosci Biotechnol Biochem*. 2000 Jul;64(7):1522–5.
- Soysa HS, Suginta W. Identification and functional characterization of a novel OprD-like chitin uptake channel in non-chitinolytic bacteria. *J Biol Chem*. 2016 Jun 24;291(26):13622–33.
- Sun Y, Vanderpool CK. Physiological consequences of multiple-target regulation by the small RNA SgrS in *Escherichia coli*. *J Bacteriol*. 2013 Nov;195(21):4804–15.
- Tharanathan RN, Kittur FS. Chitin--the undisputed biomolecule of great potential. *Crit Rev Food Sci Nutr*. 2003;43(1):61–87.
- Thompson J, Ruvinov SB, Freedberg DI, Hall BG. Cellobiose-6-phosphate hydrolase (CelF) of *Escherichia coli*: characterization and assignment to the unusual family 4 of glycosylhydrolases. *J Bacteriol*. 1999;181(23):7339–45.
- Uehara T, Park JT. The N-acetyl-D-glucosamine kinase of *Escherichia coli* and its role in murein recycling. *J Bacteriol*. 2004 Nov;186(21):7273–9.
- Verma SC, Mahadevan S. The *chbG* gene of the chitobiose (*chb*) operon of *Escherichia coli* encodes a chitooligosaccharide deacetylase. *J Bacteriol*. 2012 Sep;194(18):4959–71.
- Wang SL, Chang WT. Purification and characterization of two bifunctional chitinases/lysozymes extracellularly produced by *Pseudomonas aeruginosa* K-187 in a shrimp and crab shell powder medium. *Appl Environ Microbiol*. 1997 Feb;63(2):380–6.
- Wucher BR, Bartlett TM, Hoyos M, Papenfort K, Persat A, Nadell CD. *Vibrio cholerae* filamentation promotes chitin surface attachment at the expense of competition in biofilms. *Proc Natl Acad Sci USA*. 2019 Jul 9;116(28):14216–21.
- Yip VL, Thompson J, Withers SG. Mechanism of GlvA from *Bacillus subtilis*: a detailed kinetic analysis of a 6-phospho- $\alpha$ -glucosidase from glycoside hydrolase family 4. *Biochemistry*. 2007 Aug 28;46(34):9840–52.
- Yip VL, Varrot A, Davies GJ, Rajan SS, Yang X, Thompson J, et al. An unusual mechanism of glycoside hydrolysis involving redox and elimination steps by a family 4 beta-glycosidase from *Thermotoga maritima*. *J Am Chem Soc*. 2004 Jul 14;126(27):8354–5.
- Yip VL, Withers SG. Breakdown of oligosaccharides by the process of elimination. *Curr Opin Chem Biol*. 2006a Apr;10(2):147–55.
- Yip VL, Withers SG. Mechanistic analysis of the unusual redox-elimination sequence employed by *Thermotoga maritima* BglT: a 6-phospho- $\beta$ -glucosidase from glycoside hydrolase family 4. *Biochemistry*. 2006b Jan 17; 45(2):571–80.
- Yip VL, Withers SG. Identification of Tyr241 as a key catalytic base in the family 4 glycoside hydrolase BglT from *Thermotoga maritima*. *Biochemistry*. 2012 Oct 23;51(42):8464–74.

## Supplemental Information

### Chitin, chitin oligosaccharide and chitin disaccharide metabolism of *Escherichia coli* revisited: reassignment of the roles of ChiA, ChbR, ChbF and ChbG

Axel Walter<sup>a</sup>, Simon Friz<sup>a</sup>, and Christoph Mayer<sup>a\*</sup>

<sup>a</sup>Microbiology/Glycobiology, Interfaculty Institute of Microbiology and Infection Medicine,  
University of Tübingen, Germany

Short title: chitin metabolism of *E. coli*

Supplemental Materials: 2 Tables, 1 Figure

#### Supplemental Tables

Table S1. Strains, plasmids and primers used in the study

Strain	Characteristics	References
<i>E. coli</i>		
K12, Strain BW25113 “wild-type” (wt)	$\Delta(\text{araD-araB})567$ , $\Delta\text{lacZ4787}(\text{:rrnB-3})$ ; $\lambda^-$ , <i>rph-1</i> , $\Delta(\text{rhaD-rhaB})568$ , <i>hsdR514</i>	Yale Genetic Stock Center
JW1723-1 $\Delta\text{chbF}::\text{kan}$	<i>F-</i> , $\Delta(\text{araD-araB})567$ , $\Delta\text{lacZ4787}(\text{:rrnB-3})$ , $\lambda^-$ , $\Delta\text{chbF733}::\text{kan}$ , <i>rph-1</i> , $\Delta(\text{rhaD-rhaB})568$ , <i>hsdR514</i>	Yale Coli Genetic Stock Center
JW1722-2 $\Delta\text{chbG}::\text{kan}$	<i>F-</i> , $\Delta(\text{araD-araB})567$ , $\Delta\text{lacZ4787}(\text{:rrnB-3})$ , $\lambda^-$ , $\Delta\text{chbG733}::\text{kan}$ , <i>rph-1</i> , $\Delta(\text{rhaD-rhaB})568$ , <i>hsdR514</i>	Yale Coli Genetic Stock Center
DH5 $\alpha$	<i>SupE44 hsdR17 recA1 endA1 gyrA96 thi-1 relA1</i>	[Hanahan, 1983]
BL21 (DE3)	<i>fhuA2 [lon] ompT gal (<math>\lambda</math> DE3) [dcm] <math>\Delta\text{hsdS } \lambda\text{DE3} = \lambda</math> <i>sBamHlo <math>\Delta\text{EcoRI-B int}::(\text{lacI}::\text{PlacUV5}::\text{T7 gene1}) i21</math> <math>\Delta\text{nin5}</math></i></i>	New England Biolabs
BL21(DE3) pET28a-ChbF	<i>fhuA2 [lon] ompT gal (<math>\lambda</math> DE3) [dcm] <math>\Delta\text{hsdS } \lambda\text{DE3} = \lambda</math> <i>sBamHlo <math>\Delta\text{EcoRI-B int}::(\text{lacI}::\text{PlacUV5}::\text{T7 gene1}) i21</math> <math>\Delta\text{nin5}</math>, pET28a-ChbF</i></i>	this work

BL21(DE3) pET22b-ChiA	<i>fhuA2 [lon] ompT gal (λ DE3) [dcm] ΔhsdS λDE3 = λ sBamHlo ΔEcoRI-B int::(lacI::PlacUV5::T7 gene1) i21 Δnin5</i> , pET22b-ChiA	this work
BL21(DE3) pET28a-Csn	<i>fhuA2 [lon] ompT gal (λ DE3) [dcm] ΔhsdS λDE3 = λ sBamHlo ΔEcoRI-B int::(lacI::PlacUV5::T7 gene1) i21 Δnin5</i> , pET28a-Csn	this work
Δ <i>chbG</i> :: <i>kan</i> pQE32-ChbBCA	<i>F-</i> , Δ( <i>araD-araB</i> )567, Δ <i>lacZ</i> 4787(:: <i>rrnB-3</i> ), λ <sup>-</sup> , Δ <i>chbG</i> 733:: <i>kan</i> , <i>rph-1</i> , Δ( <i>rhaD-rhaB</i> )568, <i>hsdR514</i> , pQE32- <i>chbBCA</i>	this work
BL21(DE3) pET28a-CwIC	<i>fhuA2 [lon] ompT gal (λ DE3) [dcm] ΔhsdS λDE3 = λ sBamHlo ΔEcoRI-B int::(lacI::PlacUV5::T7 gene1) i21 Δnin5</i> , pET28a-CwIC	[Müller et al., 2021]
BL21(DE3) pET16b-NagZ	<i>fhuA2 [lon] ompT gal (λ DE3) [dcm] ΔhsdS λDE3 = λ sBamHlo ΔEcoRI-B int::(lacI::PlacUV5::T7 gene1) i21 Δnin5</i> , pET16b-NagZ	[Litzinger et al., 2010a; Litzinger et al., 2010b]
BL21(DE3) pET28a-Atl(Glc)	<i>fhuA2 [lon] ompT gal (λ DE3) [dcm] ΔhsdS λDE3 = λ sBamHlo ΔEcoRI-B int::(lacI::PlacUV5::T7 gene1) i21 Δnin5</i> , pET28a-Atl(Glc)	[Müller et al., 2021]
<i>B. subtilis</i>		
strain 168 (wild-type)	<i>trpC2</i> ; genome sequenced <i>B. subtilis</i> type strain	Bacillus Genetic Stock Center
<b>plasmid</b>		
pET28a(+)	KanR, T7 promoter, ori pBR322, lacI, C/N-terminal His <sub>6</sub> -tag	Novagen
pET22b(+)	AmpR, T7 promoter, lacI, C-terminal His <sub>6</sub> -tag	Novagen
pQE32	AmpR, T5 promoter/lac operator, N-terminal His <sub>6</sub> -tag	Qiagen
pET28a-ChbF	KanR, T7 promoter, ori, pBR322, lacI, adds C-terminal His <sub>6</sub> -tag to <i>chbF</i>	this work
pET22b(+)-ChiA	AmpR, T7 promoter, lacI, adds C-terminal His <sub>6</sub> -tag to <i>chiA</i>	this work
pET28a-Csn	KanR, T7 promoter, ori, pBR322, lacI,	this work

	adds C-terminal His <sub>6</sub> -tag to <i>csn</i>	
pET28a-CwIC	KanR, T7 promoter, ori, pBR322, lacI, adds C-terminal His <sub>6</sub> -tag to <i>cwIC</i>	[Müller et al., 2021]
pET16b-NagZ	AmpR, T7 promotor, lacI, adds N-terminal His <sub>10</sub> -tag to <i>nagZ</i>	[Litzinger et al., 2010a;Litzinger et al., 2010b]
pET28a-Atl(Glc)	KanR, T7 promoter, ori, pBR322, lacI, adds C-terminal His <sub>6</sub> -tag to <i>atl(glc)</i>	[Müller et al., 2021]
pQE32-ChbBCA	AmpR, T5 promoter/lac operator, <i>chbBCA</i> without N-terminal His <sub>6</sub> -tag	this work
<b>primer</b>		
pET28a- <i>chbF</i> -NcoI-for	CACCATGGGAAGCCAGAAATTAAGTCGT	this work
pET28a- <i>chbF</i> -XhoI-rev	CACTCGAGATGTGCTTTTTAAGCTCTG	this work
pET22b- <i>chiA</i> -NdeI-for	GGCCCCATATGAAATTAATATATTTACTAAATC	this work
pET22b- <i>chiA</i> -HindIII-rev	CCAAGCTTTTGCTTAGTAAACGGCGCGA	this work
pET28a- <i>csn</i> -NcoI-for	CCACCATGGGAGCGGGACTGAATAAAGATCA	this work
pET28a- <i>csn</i> -XhoI-rev	CCACTCGAGTTTGATTACAAAATTACCGT	this work
pQE32- <i>chBCA</i> -GA-for	CAGAATTCATTAAGAGGAGAAATTAAGTAAAG AAACACATTTATCTGTTTTGT	this work
pQE32- <i>chBCA</i> -GA-rev	TCTATCAACAGGAGTCCAAGCTCAGCTAATTATGCCTTC AGTTTTTCATGAAGC	this work
pET28a- <i>cwIC</i> -NcoI-for	GCTCCATGGCGGTTAAAATTTTATTGATCCTGGACAT	[Müller et al., 2021]
pET28a- <i>cwIC</i> -XhoI-rev	GCTAGCTCGAGTGATTCTAGGATCACAATAGC	[Müller et al., 2021]
pET16b- <i>nagZ</i> -NdeI-for	AAAACCATGGGCCATATGTTTTTCGGGGCCAGACAGAC	[Litzinger et al., 2010a;Litzinger et al., 2010b]
pET16b- <i>nagZ</i> -XhoI-rev	TTTTCTCGAGTTAAAGCGGTCTTCCGTTTTG	[Litzinger et al., 2010a;Litzinger et al., 2010b]

pET28a- <i>atl(glc)</i> -Ncol- for	CAGCTCCATGGCTTATACTGTTACTAAACCAC	[Müller et al., 2021]
pET28a- <i>atl(glc)</i> -XhoI- rev	GCGCCTCGAGTTTATATTGTGGGATGTCGAAG	[Müller et al., 2021]

**Table S2. Exact monoisotopic masses of chitin, chitosan and PGN metabolites**

Overview of chitin, chitosan and PGN metabolites and their exact neutral masses and masses with proton adducts in positive ionization mode.

Name	Formula	exact monoisotopic mass [M]	exact monoisotopic mass of the proton adduct [M+H] <sup>+</sup>
chitobiose (GlcN-GlcN)	C <sub>12</sub> H <sub>24</sub> N <sub>2</sub> O <sub>9</sub>	340.1482	341.1555
chitotriose (GlcN-GlcN-GlcN)	C <sub>18</sub> H <sub>35</sub> N <sub>3</sub> O <sub>13</sub>	501.2170	502.2243
chitotetraose (GlcN-GlcN-GlcN-GlcN)	C <sub>24</sub> H <sub>46</sub> N <sub>4</sub> O <sub>17</sub>	662.2858	663.2931
diacetyl-chitobiose (GlcNAc-GlcNAc)	C <sub>16</sub> H <sub>28</sub> N <sub>2</sub> O <sub>11</sub>	424.1693	425.1766

triacetyl-chitotriose (GlcNAc-GlcNAc-GlcNAc)	C <sub>24</sub> H <sub>41</sub> N <sub>3</sub> O <sub>16</sub>	627.2487	628.2560
monoacetyl-chitotriose (GlcN-GlcNAc-GlcN)	C <sub>20</sub> H <sub>37</sub> N <sub>3</sub> O <sub>14</sub>	543.2276	544.2348
MurNAc-GlcNAc	C <sub>19</sub> H <sub>32</sub> N <sub>2</sub> O <sub>13</sub>	496.1904	497.1977
(MurNAc-GlcNAc)-4P	C <sub>37</sub> H <sub>61</sub> N <sub>7</sub> O <sub>21</sub>	939.3921	940.3993
(GlcNAc-MurNAc)-3P* (MurNAc-GlcNAc)-3P*	C <sub>34</sub> H <sub>57</sub> N <sub>7</sub> O <sub>19</sub>	867.3709	868.3782
3P* tri-peptide (1x amidation)	C <sub>15</sub> H <sub>27</sub> N <sub>5</sub> O <sub>7</sub>	389.1910	390.1983
3P tri-peptide	C <sub>15</sub> H <sub>26</sub> N <sub>4</sub> O <sub>8</sub>	390.1751	391.1823
4P tetra-peptide	C <sub>18</sub> H <sub>31</sub> N <sub>5</sub> O <sub>9</sub>	461.2122	462.2195

3P-4P tri-tetra-peptide	$C_{33}H_{55}N_9O_{16}$	833.3767	834.3840
4P-4P tetra-tetra-peptide	$C_{36}H_{60}N_{10}O_{17}$	904.4138	905.4211
3P*-4P* tri-tetra-peptide (2x amidations)	$C_{33}H_{57}N_{11}O_{14}$	831.4086	832.4159
3P-4P* tri-tetra-peptide (1x amidation)	$C_{33}H_{56}N_{10}O_{15}$	832.3927	833.3999

## Supplemental Figures

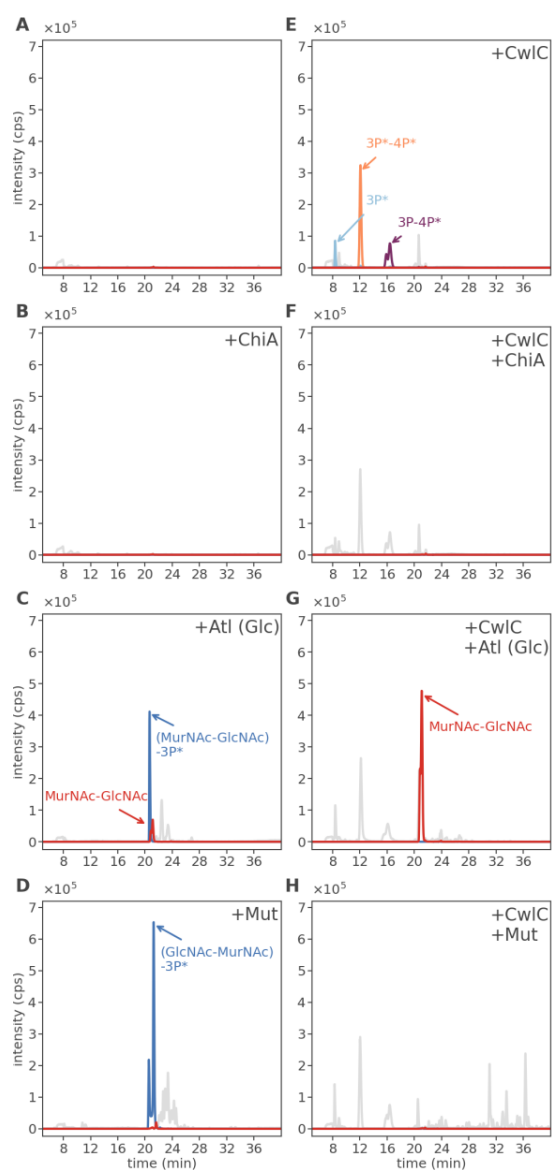


**Fig. S1. ChiA does not cleave *B. subtilis* peptidoglycan.**

Intact peptidoglycan, derived from *B. subtilis* (left panels), and denuded peptidoglycan (right panels), i.e. treated with the amidase CwIC to remove the peptide stems, were incubated with ChiA, the endo-glucosaminidase Atl (Glc) of *S. aureus* or Mutanolysin.

The formation of reaction products was analyzed by LC-MS. **(A)** Uncleaved *B. subtilis* peptidoglycan (control).

**(B)** Incubation of *B. subtilis* peptidoglycan with ChiA (+ChiA), which does not release any soluble products.

**(C)** Incubation of *B. subtilis* peptidoglycan with Atl (Glc) (-Atl (Glc)) releases large amounts of (MurNAc-GlcNAc)-tripeptide (amidated) (M+H)<sup>+</sup> m/z = 868.3701 (MurNAc-GlcNAc-3P\*; blue) and to a lesser extent MurNAc-GlcNAc (M+H)<sup>+</sup> m/z = 497.1902 (red).

**(D)** Mutanolysin (+Mut) exclusively releases (GlcNAc-MurNAc)-3P\* (M+H)<sup>+</sup> m/z = 868.3675 (blue). **(E)** CwIC (+CwIC) removes amidated tri- (M+H)<sup>+</sup> m/z = 390.1978 (3P\*, light blue), tri-tetra (M+H)<sup>+</sup> m/z = 833.3943 (3P-4P\*, purple) and double amidated tri-tetra peptides (M+H)<sup>+</sup> m/z = 832.4122 (3P\*-4P\*, orange) from *B. subtilis* peptidoglycan.

**(F)** From **(E)** ChiA (+CwIC+ChiA) is unable to cleave denuded peptidoglycan. **(G)** From **(E)**, Atl (Glc) (+CwIC+Atl (Glc)) is able to release large amounts of MurNAc-GlcNAc (M+H)<sup>+</sup> m/z = 497.1954 (red). Intriguing, no MurNAc-GlcNAc-4P could be detected, indicating the complete removal of the stem peptides from the peptidoglycan by CwIC. **(H)** From **(E)**, Mutanolysin (+CwIC+Mut), on the other hand, does not release disaccharides from the glycan chain, which indicates that this enzyme is not able to cleave denuded peptidoglycan. Shown are the base peak chromatogram (BPC) mass range (M+H)<sup>+</sup> m/z = 200 – 2000 (gray) and the extracted ion chromatograms (EIC) based on the exact masses of displayed compounds (Table S2).



## References

Hanahan D. Studies on transformation of *Escherichia coli* with plasmids. J Mol Biol. 1983 Jun 5;166(4):557-80.

Litzinger S, Duckworth A, Nitzsche K, Risinger C, Wittmann V, Mayer C. Muropeptide rescue in *Bacillus subtilis* involves sequential hydrolysis by  $\beta$ -*N*-acetylglucosaminidase and *N*-acetylmuramyl-L-alanine amidase. J Bacteriol. 2010a Jun;192(12):3132-43.

Litzinger S, Fischer S, Polzer P, Diederichs K, Welte W, Mayer C. Structural and kinetic analysis of *Bacillus subtilis* *N*-acetylglucosaminidase reveals a unique Asp-His dyad mechanism. J Biol Chem. 2010b Nov 12;285(46):35675-3584.

Müller M, Calvert M, Hottmann I, Kluj RM, Teufel T, Balbuchta K, et al. Exo- $\beta$ -*N*-acetylmuramidase NamZ of *Bacillus subtilis* is the founding member of a family of exo-lytic peptidoglycan hexosaminidases. bioRxiv 2021:2021.01.10.425899.

## **Publication 2**

**Walter, A.**, & Mayer, C. (2019). Peptidoglycan Structure, Biosynthesis, and Dynamics During Bacterial Growth. In *Extracellular Sugar-Based Biopolymers Matrices* (pp. 237-299). Springer, Cham.

# Chapter 6

## Peptidoglycan Structure, Biosynthesis, and Dynamics During Bacterial Growth



Axel Walter and Christoph Mayer

**Abstract** The peptidoglycan is the key structural component of the bacterial cell wall that rests outside the cytoplasmic membrane and provides bacterial cells with physical strength and shape. It constitutes a huge mesh-like macromolecule composed of linear glycans held together by short peptides: the glycans consist of alternating amino sugars, *N*-acetylglucosamine (GlcNAc), and *N*-acetylmuramic acid (MurNAc), connected by  $\beta$ -1,4-glycosidic linkages, and the peptides include noncanonical D-amino acids and cross-link the glycan chains via binding to MurNAc. The peptidoglycan macromolecule is ubiquitous in bacteria, regardless of whether displaying a Gram-positive, Gram-negative, or complex mycobacterial cell envelope structure, and it is also highly restricted to bacteria, thereby distinguishing bacteria from eukaryotic microorganisms and archaea. In all bacteria, the peptidoglycan is synthesized from a lipid-anchored precursor that is preformed in the cytoplasm, flipped outward through the plasma membrane by channeling proteins (flippases), and is finally polymerized by membrane-bound, outward-facing synthetic enzymes (glycosyltransferases and transpeptidases) building a net-shaped covering of the entire bacterial cell, called the peptidoglycan sacculus. The peptidoglycan sacculus allows bacteria to cope with osmotic and environmental challenges, and it secures cell integrity during all stages of bacterial growth. It has to be sufficiently strong and rigid but, at the same time, flexible and dynamic to assure integrity of the cell during enlargement, division, and differentiation processes. Thus, the synthesis and integrity of the peptidoglycan are major targets of antibacterial therapeutics. We are summarizing in this chapter present knowledge including recent discoveries of peptidoglycan structure, assembly, and dynamics during bacterial growth.

---

A. Walter · C. Mayer (✉)

IMIT – Microbiology and Biotechnology, University of Tübingen, Tübingen, Germany  
e-mail: [christoph.mayer@uni-tuebingen.de](mailto:christoph.mayer@uni-tuebingen.de)

© Springer Nature Switzerland AG 2019

E. Cohen, H. Merzendorfer (eds.), *Extracellular Sugar-Based Biopolymers Matrices*,  
Biologically-Inspired Systems 12, [https://doi.org/10.1007/978-3-030-12919-4\\_6](https://doi.org/10.1007/978-3-030-12919-4_6)

237

## 6.1 Introduction

The bacterial cell is encased in a rigid cell wall containing the macromolecule peptidoglycan (PGN; synonym murein) as the critical structural component, which protects the membrane-covered protoplast and forms a barrier toward the environment (Rogers 1974; Seltmann and Holst 2002). The PGN is ubiquitous within bacteria, with only few exceptions such as the members of the phylum *Tenericutes* (e.g., mycoplasma) or conditional cell wall-less bacteria, so-called L-forms, but absent beyond this domain of life (Litzinger and Mayer 2010). The elucidation of the PGN structure went along with the discovery of the biosynthesis precursors, the “Park nucleotides” by James Theodore “Ted” Park (1922–2014) (Park and Johnson 1949; Park 1952; Park and Strominger 1957), which at that time were the first examples of nucleotide activated sugar molecules, carrying unusual amino sugars and D-amino acids, also novel back then. These findings paved the path toward the identification of the chemical structure of the PGN and its biosynthesis. Early PGN research was also closely linked with the discovery of the function of two antibacterial agents targeting cell wall integrity and synthesis, lysozyme and penicillin, both discovered by Alexander Fleming (Fleming 1955; Geddes 2008). Lysozyme is an antibacterial enzyme that specifically cleaves the PGN backbone, and penicillin is an antibacterial drug that inhibits PGN synthesis, eventually both are causing lysis of bacterial cells. Ever since, PGN synthesis is one of the most important targets for antibiotics to treat bacterial infections, as the pathways and enzymes involved in PGN biosynthesis are usually essential for bacteria but do not exist in humans. With the advent of electron microscopy, the PGN cell wall could first be visualized (Mudd et al. 1941; Salton and Horne 1951; Chapman and Hillier 1953; Kellenberger and Ryter 1958). Later on, the bag-shaped PGN structure was recognized by Wolfhard Weidel and his group at the Max Planck Institute for Biology in Tübingen, who investigated how phages lyse bacterial cells to get themselves released (Weidel and Primosigh 1958). He observed that in this process bacteria lose their rodlike shape and identified characteristic sugar peptides (muropeptides) in the medium, produced by a lysozyme-like activity of the phage and very similar to the products released from bacteria treated with penicillin (see Braun 2015). In collaboration with his colleague Helmut Pelzer, he developed the concept of the “murein sacculus” (from Latin “sacculus” for the sack and “murus” wall) (Weidel et al. 1960; Weidel and Pelzer 1964). Accordingly, the murein or PGN sacculus constitutes a huge, net-shaped macromolecule that surrounds the bacterial cell and provides a backpressure against the intracellular turgor (Rogers 1974; Höltje 1998; Seltmann and Holst 2002). Some billion years ago, when the domain *Bacteria* arose from prokaryotic progenitors, this exoskeleton-like structural element was acquired to cope with an increase in the intracellular osmotic pressure (turgor) due to the accumulation of metabolites as the cellular metabolism became more and more complex (Litzinger and Mayer 2010). The PGN is also essential for cell morphogenesis, as it allows bacterial cells to maintain their characteristic shapes (Young 2003). Although these properties of the PGN imply rigidity, this molecule has at the

same time to be highly flexible and dynamic. The steady degradation and resynthesis of the PGN allows the bacterial cell wall to continuously adapt to environmental and physiological constraints in a highly dynamic process during growth and differentiation. Despite intense research for more than 60 years now, fundamental questions regarding the architecture, temporal and spatial assembly, and dynamic remodeling of PGN are still unsolved. Recently however, new technologies, in particular new visualization techniques as well as advances in the chemical and physical analysis of bacterial cell walls, have revived the field of PGN research and allowed a new view on this versatile and complex polymer. In the first parts of this chapter, we will describe the chemical nature and structure, including recent insights into the 3D architecture, as well as compositional modifications of the PGN within bacteria. In the further part, we will review the PGN biosynthesis and assembly, which includes new observations aided by advances in fluorescence microscopy, and finally, we will elaborate the PGN as a dynamic macromolecule that undergoes a permanent turnover.

## 6.2 The Peptidoglycan Cell Wall and Envelope Structures of Bacteria

As the name indicates, the PGN is a complex heteropolymer made of glycans that are cross-linked via short peptides (Fig. 6.1). The glycans of the PGN are linear sugar chains of variable length that are composed of alternating  $\beta$ -1,4-linked amino sugars *N*-acetylglucosamine (GlcNAc) and *N*-acetylmuramic acid (MurNAc) (Fig. 6.1). MurNAc is a characteristic acidic amino sugar exclusively found within bacteria. It is a derivative of GlcNAc, carrying a *D*-lactic acid substituent, ether-linked via the hydroxyl group at the 3-position of GlcNAc (i.e., 3-O-*D*-lactic acid-GlcNAc) (Fig. 6.1). To the free carboxylic acid of the lactic acid substituent of MurNAc, short-chain peptides are amide-bound, and they partially cross-link the glycans. Thereby, a netlike macromolecular fabric is formed that is unique to bacteria and also highly restricted to bacteria, thereby distinguishing bacteria from archaea and eukaryotic microorganisms, e.g., fungi which mainly contain chitin/chitosan (see Chapters 1 to 17 within this book). Although PGN is not present in archaea, some methanogenic archaea contain pseudopeptidoglycan (pseudoPGN or pseudomurein), which is a somewhat similar polymer that instead of MurNAc contains the amino sugar *N*-acetyltalosaminuronic acid (TalNAcUA),  $\beta$ -1,3-linked with GlcNAc (Fig. 6.1). Thus, while the repeating subunit of the PGN polymer of bacteria is a GlcNAc- $\beta$ -1,4-MurNAc-peptide, the repeating unit of the pseudoPGN is a GlcNAc- $\beta$ -1,3-TalNAcUA-peptide (Fig. 6.1). Information regarding the pseudoPGN is rather limited, and therefore we focus in this chapter on the PGN of bacteria. For more information about the pseudoPGN/pseudomurein, refer to Kandler and König (1978), König et al. (1983), Kandler and König (1993), Hartmann and König (1994), Shockman et al. (1996), and Kandler and König (1998).

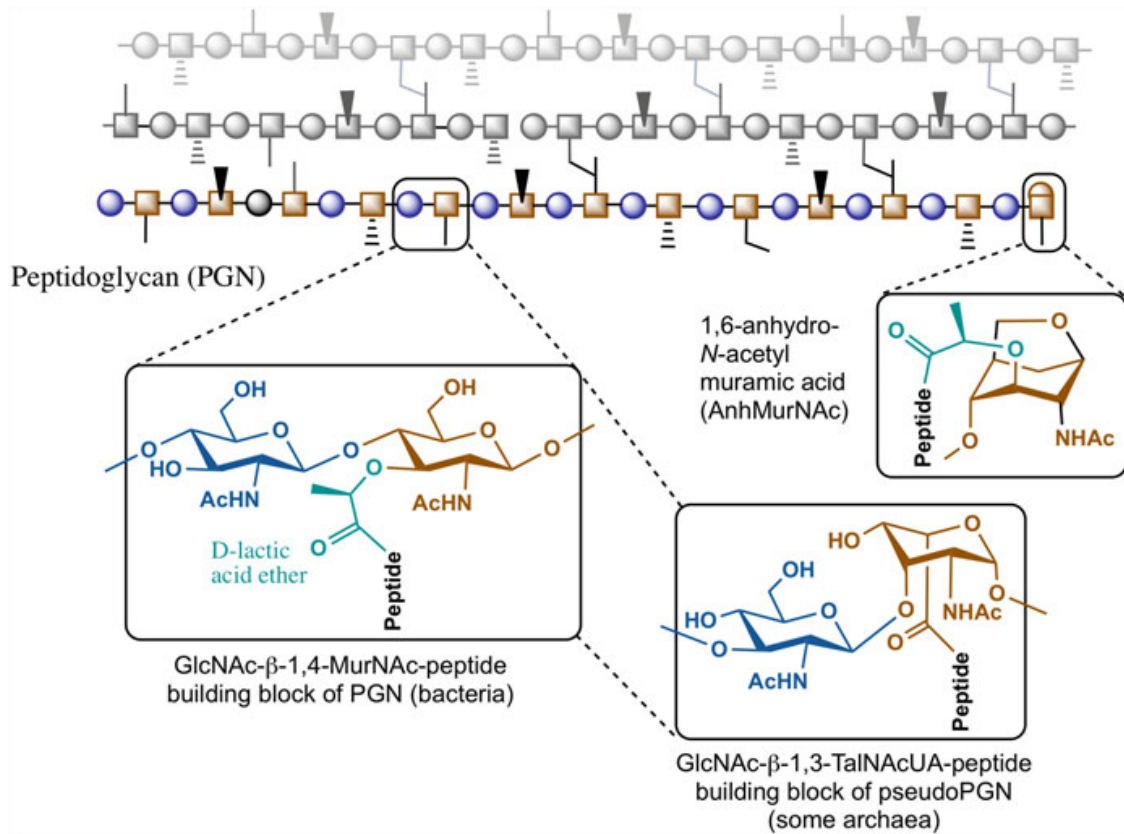


**Fig. 6.1 Peptidoglycans are heteropolymers made of disaccharide-peptides building a netlike macromolecular fabric.** They consist of linear glycan chains made of amino sugars and short-chain peptides that are partially interlinked. The PGN (murein) of bacteria is composed of alternating  $\beta$ -1,4-linked amino sugars *N*-acetyl-glucosamine (GlcNAc; blue, circles) and *N*-acetylmuramic acid (MurNAc; brown squares). Short-chain peptides (black lines), amide-linked to the *D*-lactic acid substituent (cyan structure) of MurNAc at C3, are used to cross-link the glycan chains yielding a 3D network. In most bacterial species, the glycan strands of the PGN terminate in 1,6-anhydro-*N*-acetylmuramic acid (AnhMurNAc) moieties, which are generated by the action of PGN-lytic transglycosylase enzymes. The pseudomurein (pseudoPGN) of some archaea is a polymer somewhat similar to PGN; however, it contains the  $\beta$ -1,3-linked amino sugars GlcNAc and *N*-acetyltalosaminuronic acid (TalNAcUA), which is substituted at the C6 carboxylic acid by peptides

Almost all bacteria contain PGN in their cell wall, yet they can have very distinct overall cell envelope structures (Silhavy et al. 2010). The traditional classification distinguishes Gram-positive bacteria and Gram-negative bacteria based on an ancient staining technique with the dye crystal violet developed by Hans Christian Gram in the 19th century (Gram 1884); see also Bartholomew and Mittwer (1952). The discrimination of bacteria by this technique relies, as we know now, on the retention of the dye in Gram-positive cells and the facile washing-out of the dye with organic solvents from the Gram-negative cell envelope (Popescu and Doyle 1996). Gram-positive bacteria (e.g., *Bacillus subtilis*, *Staphylococcus aureus*), which retain the dye, have a thick PGN layer that is covalently modified by secondary anionic glycopolymers (teichoic and teichuronic acid) and interweaved by lipoteichoic acids (Fig. 6.2a; see also heading 6.4.4; Chapman and Hillier 1953; Matias and Beveridge 2006). Moreover, they lack an outer membrane, which is characteristic for Gram-

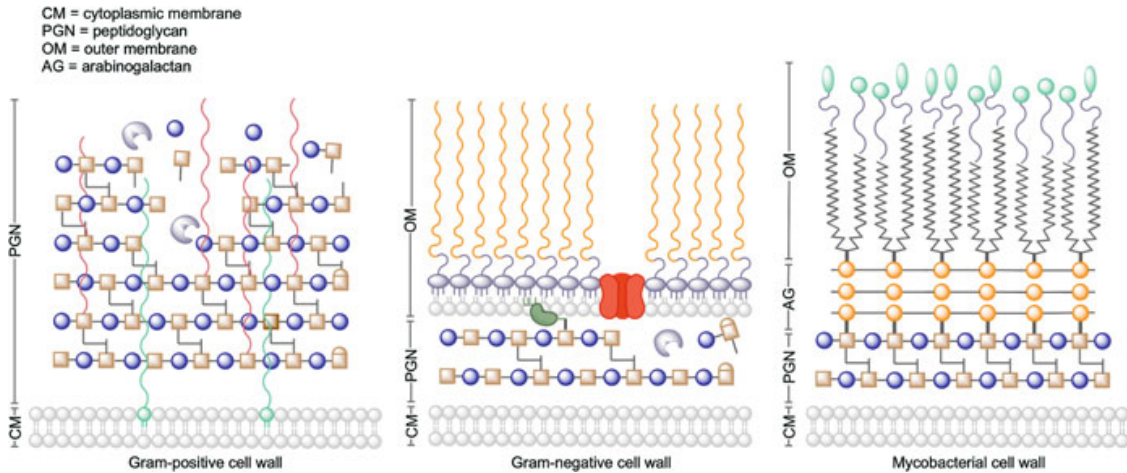


**Fig. 6.2 Cell envelope structures of Gram-positive, Gram-negative, and mycobacterial cell envelopes.** (a) The Gram-positive cell wall contains a thick layer of PGN adjacent to the cytoplasmic membrane (CM) with covalently bound secondary cell wall polymers, which include wall teichoic acids (WTA; red lines) and interweaved by lipoteichoic acids (LTA, green lines) that are membrane-bound. The PGN cell wall is rigid and at the same time flexible, to allow cell expansion: new PGN is deposited to the cell wall from below in a relaxed form, it is then stretched due to the turgor during cell expansion, and finally it is degraded in the outer regions by autolytic enzymes (violet symbols). (b) Gram-negative bacteria contain thin PGN connected to an additional outer membrane (OM) via lipoproteins (Braun's lipoprotein, green symbol, see heading 6.5.4). The OM includes lipopolysaccharides (LPS) (lipid part, violet; polysaccharide part, orange) in its outer leaflet, and cell wall-binding porins (red symbol). (c) The mycobacterial cell envelope is characterized by a PGN-arabinogalactan (AG; orange balls) complex and a lipid monolayer containing long-chain mycolic acids (MA) and glycolipids (green balloons). (This figure was modified after (Gerstmans et al. 2016))

negative bacteria (e.g., *Escherichia coli*, *Pseudomonas aeruginosa*) (Fig. 6.2b). Gram-negative bacteria are characterized (in most cases) by a thin PGN layer that is covered by an inner (the cytoplasmic membrane) and an additional outer membrane (Matias et al. 2003; Vollmer and Höltje 2004 and references cited within). The defined space between inner and outer membrane, in which the PGN layer is embedded, is called the periplasmic space. It is filled with a viscous gel, the periplasm, made of hydrated oligosaccharides, proteins, as well as the PGN (Hobot et al. 1984; Matias and Beveridge 2005; Silhavy et al. 2010).

The Gram classification, although generally useful, oversimplifies the variability of bacterial cell envelope structures. For example, the cyanobacteria, a large, diverse, and ancient group of bacteria, possess cell envelopes with combined features characteristic for both groups (Hoiczky and Hansel 2000). They mostly stain “Gram-positive” despite having an outer membrane and, thus, an overall Gram-negative envelope. However, the PGN layer of cyanobacteria is considerably thicker than that of most Gram-negative bacteria and complexed with anionic secondary cell wall polymers; thus the dye can be retained. An even more complex structure of the cell envelope is found in mycobacteria (e.g., *Mycobacterium tuberculosis*). Instead of a real outer membrane, they contain surface glycolipids bound to a lipid monolayer of long-chain fatty acids (mycolic acids), and instead of a PGN-wall teichoic

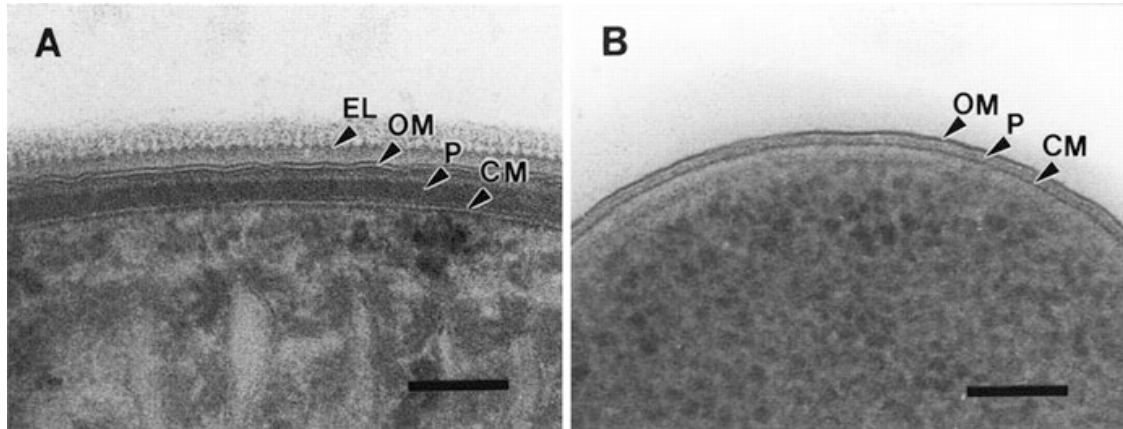


**Fig. 6.3** Electron microscopic comparison of Gram-negative cell envelopes of a cyanobacterium and *E. coli*. (a) The cell envelope of the cyanobacterium (*Phormidium uncinatum*) reveals a thick (35 nm) PGN layer (P) that is embedded between the cytoplasmic membrane (CM) and an outer membrane (OM). In addition, an external layer (EL) composed of an S-layer and oscillin fibrils is visible. (b) The cell envelope of *E. coli* shows typical Gram-negative features: a thin (3–6 nm) PGN layer (P) sandwiched between the cytoplasmic membrane (CM) and outer membrane (OM). Both bacteria were identically processed using cryo-substitution, bars 100 nm. (The figures were reproduced with permission from ASM (Hoiczky and Hansel 2000))

acid complex, they contain a PGN-arabinogalactan heteropolymeric cell wall (Fig. 6.2c; see also Sect. 6.5.5) (Brennan and Nikaido 1995; Jankute et al. 2015; Raghavendra et al. 2018). Mycobacteria and other bacteria (e.g., rickettsia and spirochetes) that do not respond to the Gram staining can be stained by the acid-fast technique (Ziehl-Neelsen stain) (Vilcheze and Kremer 2017); for a more detailed description of the mycobacterial PGN and cell envelope, refer to Sect. 6.5.5.

Classical light microscopy lacks high resolution and can barely assess the architectural differences of Gram-positive and Gram-negative cell envelopes. However, with the introduction of electron microscopy, particularly transmission electron microscopy (TEM) of thin sections in the mid-1950s, much better views on bacterial cell envelope structures were possible, and the multilayered architecture of Gram-negative cell walls was discovered (Kellenberger and Ryter 1958; Weidel et al. 1960; Murray et al. 1965; De Petris 1967). Conventional embedding and thin section techniques rely on harsh treatments, the removal of water, chemical fixation, and heavy metal staining for contrast, which may cause structural artifacts when sample preparation fails to preserve the native structural features. Recent advances in cryo-TEM avoided these difficulties and allowed to visualize the complex cell envelope structure of Gram-negative bacteria, including cyanobacteria, with a resolution as low as 1 nm (Hoiczky and Hansel 2000; Matias et al. 2003; Chen et al. 2010; Harris 2015) (Fig. 6.3). The gentle cryo-substitution technique enables the examination of native polymeric cell wall structures in sections of hydrated, frozen cells under cryogenic conditions. Ultrarapid freezing of bacteria immobilizes the samples in non-crystalline ice (i.e., vitrification) and allows to preserve close-to-native structures



(Matias et al. 2003; Chen et al. 2010; Wolf et al. 2014). Electron cryotomography (Cryo-ET) is a specialized application of cryo-TEM that allows to reconstruct 3D images (tomograms) of high (1–4 nm) resolution (Chen et al. 2010). Very recent developments replace the sectioning by the thinning of specimens via fast ion beam milling (FIB milling) of surfaces. It is expected that in the future this technique in combination with electron microscopy or electron tomography will provide more details about the native cell wall architectures (Villa et al. 2013).

With cryo-TEM as well as atomic force microscopy (AFM), the thickness of the PGN of Gram-negative bacteria was determined to be 1.5 to 3 nm in non-hydrated form (De Petris 1967; Yao et al. 1999;) and 3 to 6 nm ((Yao et al. 1999; Matias et al. 2003) or > 6 nm in hydrated form (Hobot et al. 1984; Leduc et al. 1989). This is in agreement with earlier measurements using small-angle neutron scattering that revealed a thickness of 2.5–3 nm, attributed to one single layer of PGN, which makes up 75–80% of the *E. coli* cell wall, and the remaining being triple-layered (Labischinski et al. 1991). AFM was also used to measure the thickness of collapsed PGN sacculi: air-dried sacculi from *E. coli* had a thickness of 3.0 nm, whereas those from *P. aeruginosa* were 1.5 nm thick (Yao et al. 1999). When rehydrated, the sacculi of both bacteria swelled to double their anhydrous thickness. Thus, the thickness of the PGN depends on its state of hydration. Also bacteria themselves can vary the thickness of their cell wall during growth and differentiation and even the thickness of the Gram-negative periplasm can vary significantly and largely depends on the osmolarity of the medium (Hobot et al. 1984). Recent work revealed that the intermembrane distance of the periplasm is critical in Gram-negative bacteria and controlled by periplasmic lipoproteins that anchor the outer membrane to the periplasmic PGN polymer (Miller and Salama 2018).

An about five- to tenfold thicker cell wall (20–55 nm) was visualized in Gram-positive bacteria using cryo-TEM. Surprisingly, this technique also revealed a periplasmic-like compartment in Gram-positive bacteria, classically attributed only to Gram-negative bacteria. Cryo-TEM of frozen-hydrated sections of *Bacillus subtilis* visualized a bipartite structure above the plasma membrane consisting of a low-density, 22-nm-thick inner wall zone (IWZ), above which a higher-density 33 nm region or outer wall zone (OWZ) resides (Matias and Beveridge 2005). Similarly, *Staphylococcus aureus* revealed a bipartite wall consisting of a 16 nm IWZ, followed by a 19 nm OWZ (Fig. 6.4a) (Matias and Beveridge 2006). Intriguingly, five different zones of alternating low and high densities are present in the septal regions (Fig. 6.4b). An overall thickness of approximately 32 nm was determined for *Corynebacterium* sp., with 8.5 nm corresponding to an outer layer, 6.5 nm to an electron translucent region, and 17 nm to the PGN (Marienfeld et al. 1997). The thickness of the PGN in cyanobacteria appears to be more in the range of Gram-positives, usually >10 nm (e.g., in *Synechococcus*), 15–35 nm in filamentous species (Fig. 6.3a), and in the extreme can reach 700 nm, although they possess a Gram-negative outer membrane (Hoiczky and Hansel 2000) (Fig. 6.3).

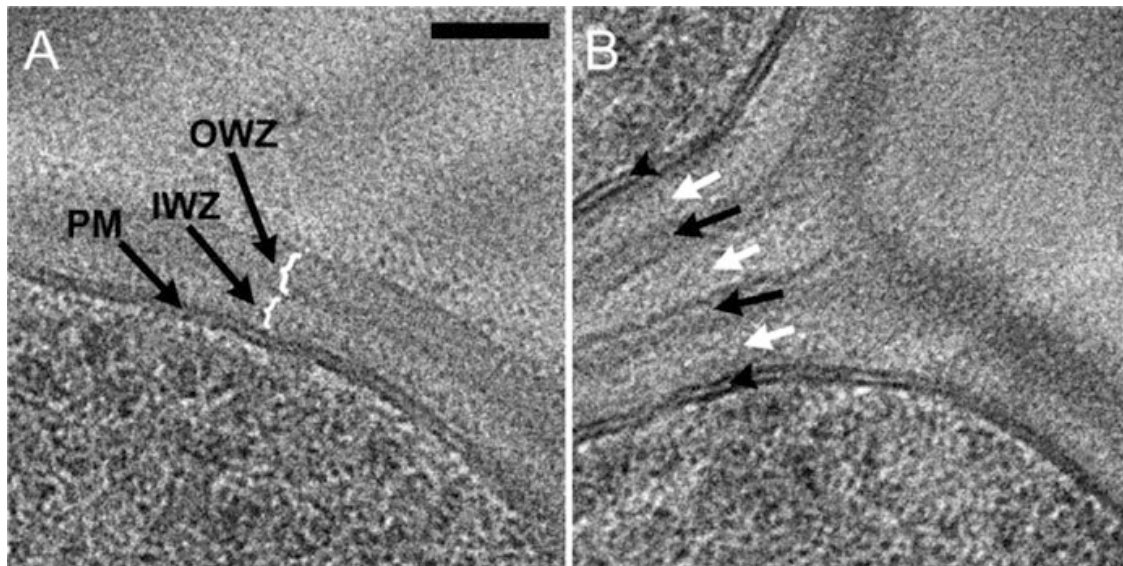


**Fig. 6.4** A bipartite cell wall structure revealed by cryo-TEM images of cross sections of frozen-hydrated *S. aureus* cells (Gram-positive). (a) High-magnification image detailing the dipartite cell wall at non-septal regions. A low-density inner wall zone (IWZ) and an adjacent high-density outer wall zone (OWZ) are visible adjacent to the plasma membrane (PM). (b) At the septum, five different zones of alternating low (white arrows) and high (black arrows) densities are distinguished between the two membranes of the septum (arrowheads). Both images are shown at the same magnification, bar 50 nm. (The figures were reproduced with permission from ASM (Matias and Beveridge 2006))

### 6.3 The Peptidoglycan Sacculus: A Protecting Shield and Determinant of Cell Shape

Bacteria come in a multitude of different shapes (Fig. 6.5a). This had become evident already when Antonie van Leeuwenhoek in the 1660s first observed bacteria and other microbes with his newly constructed microscope and described their morphology (Porter 1976). Remarkably, he already anticipated at that time that surface structures likely are responsible for the various shapes (Salton 1994). Considerably later, a cell wall surrounding bacterial cells was identified by staining techniques and connected with osmotic stability, cell division, and growth (reviewed in Vollmer and Höltje 2004). The invention of electron microscopy not only allowed to visualize bacterial cell walls but also to demonstrate that isolated bacterial cell walls retain the shape of the bacterium (Salton and Horne 1951) (Fig. 6.5b) and that lysozyme and penicillin affect bacteria shape by interference with PGN structure and biosynthesis, respectively (Strominger and Tipper, 1965). Electron microscopy also greatly facilitated the development of purification methods of cell walls (Salton and Horne 1951) and ultimately led to the discovery of the bag-shaped PGN structure the “murein sacculus” (Weidel et al. 1960; Weidel and Pelzer 1964). The murein or PGN sacculus constitutes a giant, single bag-shaped molecule of  $>3 \times 10^9$  Da (and approximately  $3.5 \times 10^6$  PGN building blocks, GlcNAc-MurNAc-peptides per *E. coli* cell). It is thus about the same size as the other huge macromolecule of the

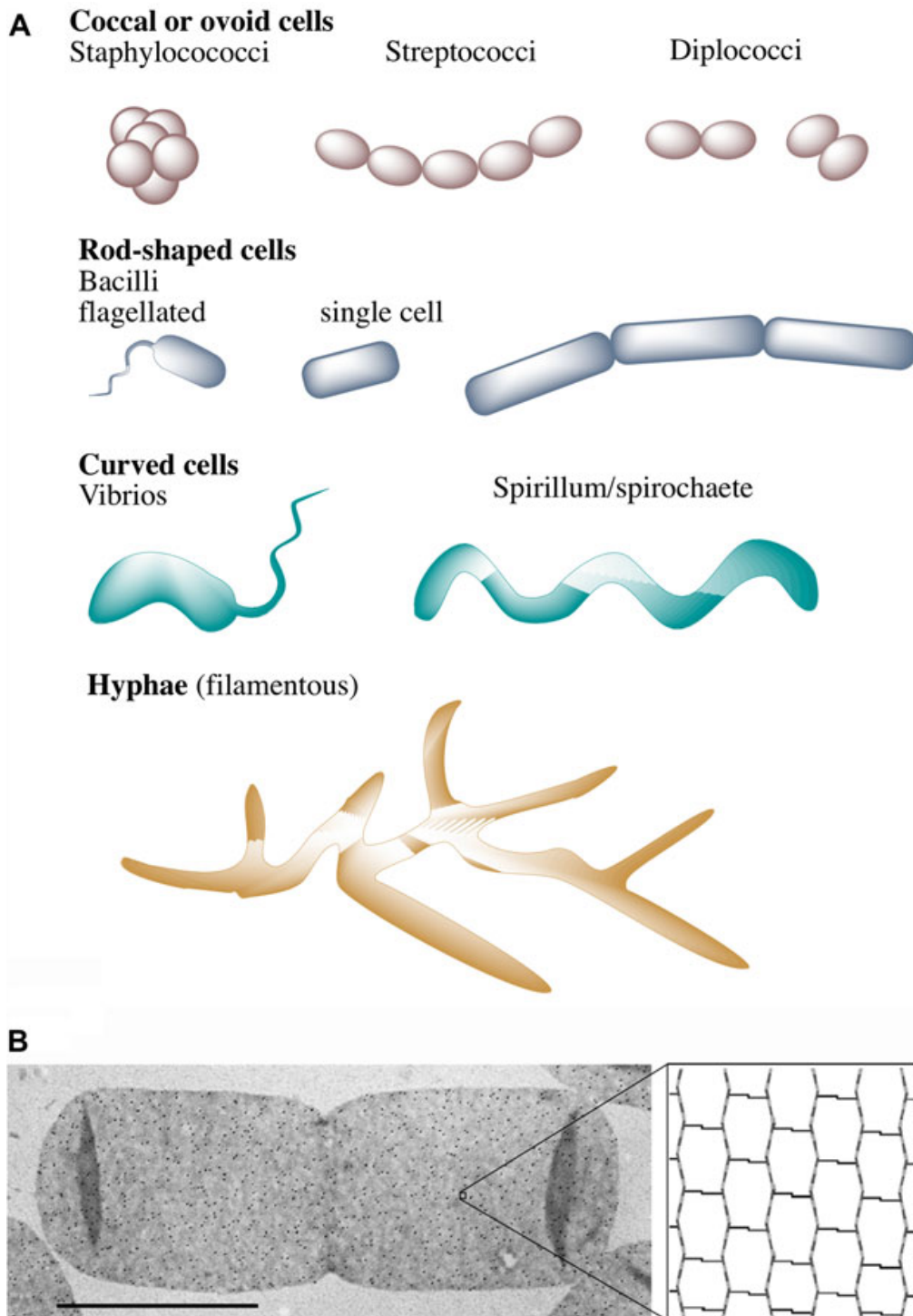


**Fig. 6.5** The cell shape-maintaining PGN or murein sacculus. (a) The PGN allows bacteria to adapt various shapes. (b) The PGN sacculus can be isolated and maintains the shape of the cell it was derived from. Electron micrograph (transmission electron microscopy, TEM) of a dividing *E. coli* cell (left side). The black dots are 6 nm gold particles used to visualize an anti-murein antibody bound to the sacculus. Bar, 1  $\mu\text{m}$ . The right side shows a model of the murein layer in a section of approximately  $30 \times 30$  nm. The glycan strands (zigzag lines) are running perpendicular to the long axis, and the peptides (thin lines) connect the glycans and run in the direction of the long axis of the sacculus. The smallest hexagonal unit is termed “tessera” and has a calculated mesh width of c. 1 nm. (Figure (b) was reproduced with permission from Elsevier (Vollmer and Bertsche 2008))

bacterial cell, the genomic DNA (Vollmer and Höltje 2004). Isolated sacculi retain the structure of the cell they were purified from, e.g., *E. coli* cells maintain the rod shape as visualized by electron microscopy (Fig. 6.5b), demonstrating the shape-controlling function of the PGN.

The PGN confers stability to the cell, allowing to withstand the high internal turgor pressure that can reach 5 atm in Gram-negative and up to 50 atm in Gram-positive bacteria (Archibald et al. 1993; Seltmann and Holst 2002). The absence or impairment of the PGN sacculus may cause cell disruption and lysis due to increased turgor in hypoosmotic medium or may interfere with cell growth and division due to reduced cell turgor causing plasmolysis in hyperosmotic medium (Witholt and Boekhout 1978; Morbach and Kramer 2002; Rojas et al. 2014). An exception from this rule are obligate intracellular bacteria, e.g., members of the genus *Mycoplasma*, and so-called L-forms, which are cell wall-deficient bacteria that have lost their PGN, e.g., upon treatment with cell wall-acting antibiotics or lytic substances (Errington et al. 2016; Kawai et al. 2018). These cell wall-deficient bacteria and L-forms lose their cell shape and become spheric but still are able to proliferate in osmo-protecting medium. As they are perfectly capable of growing and dividing, they distinguish from protoplasts and spheroplasts, which are viable but not propagating bacteria, Gram-positives or Gram-negatives, respectively, having their cell wall removed. Bacteria of the phylum *Tenericutes* (including *Mollicutes*, *Spiroplasma*, *Phytoplasma*) and L-forms are much more resistant to lysis by osmotic shock than were the bacterial protoplasts and spheroplasts, indicating that also other cell envelope structures participate in stabilization the cell envelope (Razin and Argaman 1963). Moreover, upregulation of lipid synthesis is associated with conversion of bacteria to stable L-forms (Strahl and Errington 2017). Notably, it was recently recognized that members of the phyla *Chlamydiae* and *Planctomycetes* do contain PGN in their cell wall, albeit only rudimentarily structured, which is not osmotically protecting and mainly synthesized during the cell division process (Liechti et al. 2014; Jeske et al. 2015; Liechti et al. 2016).

The current consensus is that the PGN sacculus maintains shape, which however is determined by the bacterial cytoskeleton directing PGN biosynthesis throughout cell expansion and division (Löwe et al. 2004; Cabeen and Jacobs-Wagner 2007; Young 2010; Fink et al. 2016) (see Sect. 6.5.4 for more details). The flexibility of PGN in the construction of different cell shapes was illustrated by an intriguing experiment described by Takeuchi et al. (2005). Single *E. coli* cells were grown in microchambers of agarose that forced the cells to adapt various shapes. The authors obtained viable *E. coli* cell that were round, spiral, or curved, as determined by the shape of the vessel they were grown in. Supposedly, the PGN synthesis can adapt different shapes and can be very flexibly adjusted in a bacterium to cope with environmental constraints. The process of biosynthesis of the PGN will be described in detail in Sect. 6.7. In the next chapter, we will first summarize still ongoing efforts to determine the structural organization of the PGN network that was boosted by recent advances in microscopic visualization techniques.

## 6.4 The Structural Organization of the Peptidoglycan Cell Wall

The small size of a bacterial cell and the insolubility, heterogeneity, and flexibility of the PGN network for a long time prevented the determination of its three-dimensional architecture by conventional low-resolution imaging or high-resolution structural techniques, such as X-ray crystallography and NMR spectroscopy. Thus, the topology of the PGN remained uncertain for a long time and therefore had been a subject of various theoretical considerations and speculations (Weidel and Pelzer 1964; Kelemen and Rogers 1971; Braun et al. 1973; Burge et al. 1977b; Burge et al. 1977a; Labischinski et al. 1979; Koch and Doyle 1985; Koch 1985; Koch 1995; Höltje 1998; Vollmer and Höltje 2001; Dmitriev et al. 2005). Until now, many structural views of the PGN cell wall depicted in textbooks are in part imaginations, as they are not experimentally supported. For example, the regular organization of the PGN, with twisted glycan strands oriented in parallel, forming hexagons (tessera) due to peptide cross-linkage, shown in Fig. 6.5b, clearly is an oversimplification (Vollmer and Bertsche 2008). Early X-ray diffraction studies revealed the lack of regular, semicrystalline structures within the PGN macromolecule but also recognized a not entirely disordered organisation (Formanek and Rauscher 1979; Labischinski et al. 1979). Moreover, the PGN sacculus was shown to be remarkably flexible: it can be stretched about three times the initial surface area as shown by low-angle light scattering (Koch and Woeste 1992).

In recent years, new techniques allowed to gain deeper insights into the structure and organization of the PGN, particularly cryo-TEM, Cryo-ET, and AFM, that provide structural information close to atomic resolution. These techniques helped to resolve the debate about the orientation of the glycan chains of the PGN. The “layered structural model,” in which the glycan strands of the PGN run mostly perpendicular to the long axis and parallel to the cell membrane, is the classical view of the cell wall PGN (Höltje 1998; Vollmer and Bertsche 2008). It is supported by theoretical considerations based on experimentally determined PGN thickness, amount of PGN material, glycan chain length, and degree of PGN cross-linkage (Vollmer and Höltje, 2004; Vollmer and Seligman 2010). However, based on computer modeling, an axial orientation, the so-called scaffold model had been suggested (Dmitriev et al. 1999; Dmitriev et al. 2000; Dmitriev et al. 2003; Dmitriev et al. 2004; Dmitriev et al. 2005). This model proposed that the glycan chain may extend perpendicular to the cell membrane. It had attracted attention, since this prediction fits well with the process of biosynthesis, the NMR structure of a synthetic PGN fragment, and the assembly of flagella and channel proteins within the cell wall (Meroueh et al. 2006). Vollmer and Höltje argued against this view, showing that at least for *E. coli* and other gram-negative bacteria the axial orientation of the PGN is not consistent with the data, but supports the layer structural model (Vollmer and Höltje 2004). Further support for the layered model originates from measurements of elasticity and stiffness of the cell wall PGN. With the development of AFM at the end of the 1990s, the elucidation of the mechanical properties of the PGN was possible (Yao et al. 1999; Arnoldi et al. 2000; Touhami et al. 2004; Scheuring and

Dufrene 2010; Loskill et al. 2014; Mularski et al. 2015). AFM can be used either to acquire topological images of the bacterial surface and isolated sacculi or to measure adhesion forces to quantify the cell surface elasticity. With the latter method, Yao et al. (1999) determined an anisotropy of elasticity of the *E. coli*-hydrated sacculi that are 1.8 times more stretchable in the longitudinal axis than in the perpendicular axis. This likely results from the flexible peptides being oriented more or less parallel to the cell longitudinal axis, while the glycan chains would be predominantly perpendicular to it. Similar measurements were performed in *S. aureus* (Loskill et al. 2014) and revealed that the stiffness of the PGN increased with elevated percentage of cross-linkage. As a result, the cell radius and cell wall stiffness are correlated to stress and pressure, thus offering a regulatory mechanism for cell shape changes under environmental conditions. Cryo-ET experiments conducted by Grant Jensen and coworkers (Gan et al. 2008) ultimately revealed that the PGN of *E. coli* is mostly arranged in a layer roughly parallel to the membrane strands and the glycan chains, encircling the cell in a disorganized hooplike fashion (Fig. 6.6). With Cryo-ET technique as well as with sensitive radioactive assays, it was shown recently that

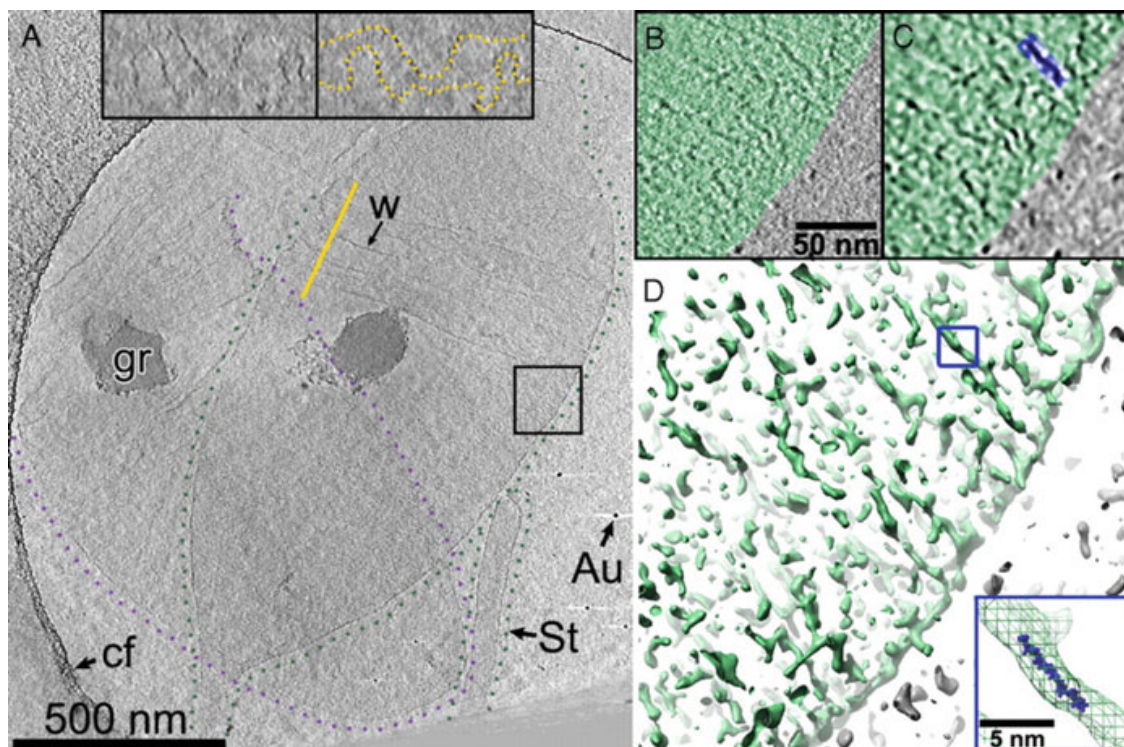


**Fig. 6.6** 3D-organization of *Caulobacter crescentus* (Gram-negative) PGN revealed by Cryo-ET. (a) Image showing the 30-nm-thick Z-slice of two overlapping *C. crescentus* cells, outlined by green and violet dotted lines. Inserts showing 30-nm-thick cross sections cut through the yellow line in the main panel. The yellow dotted line follows the “upper” and “lower” halves of the PGN. (b and c) Enlarged views (of a 4-nm-thick slice; boxed in a) after 3D median filtration (b) and image (c). The green-shaded region demarcates the PGN with one putative glycan strand highlighted in blue. (d) Iso-surface rendering; the putative glycan is boxed in blue. Blue box: Superposition of a PGN 9-mer atomic model. Abbreviations: W, wrinkle; gr, grain; St, stalk (part of the PGN-extension of *C. crescentus*); Au, gold particle; cf, carbon support film. The figure was from Gan et al. (2008), copyright (2008) National Academy of Sciences.

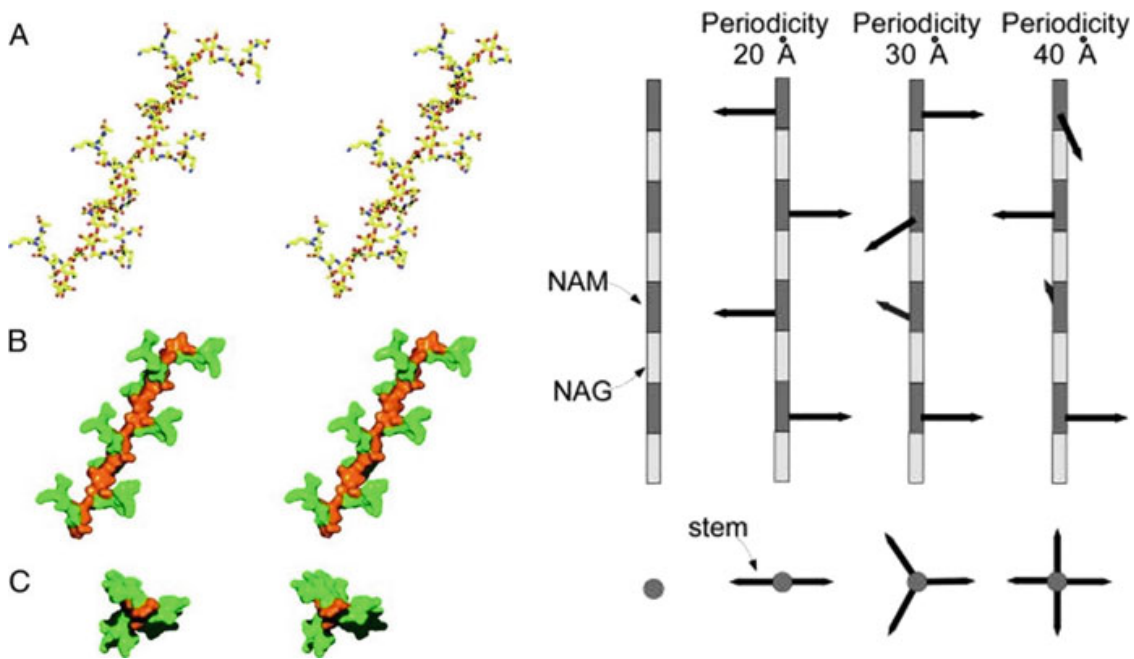


**Fig. 6.7 Architecture of glycan backbone of the PGN and orientation of the peptide stems.** (a) Stereoview of a (NAG-NAM-Peptide)<sub>8</sub> octamer construct with threefold symmetry (periodicity 30 Å) derived from the NMR structure of a synthetic fragment (Meroueh et al. 2006). The (NAG-NAM)<sub>8</sub> conformer, shown in capped-stick representation (O, N, and C are shown in red, blue, and yellow, respectively). (b) Solvent-accessible Connolly surface representation with the glycan backbone shown in orange and the peptide in green for the same perspective shown in a. (c) Stereoview of this construct seen from above (down the helical axis), shown as a solvent-accessible Connolly surface with the same color coding as in b. (d) Different possible glycan backbone conformations with twofold (periodicity 20 Å), threefold (30 Å), or fourfold (40 Å) symmetry (Kim et al. 2015). (The Figures a–c were from Meroueh et al. (2006), copyright (2006) National Academy of Sciences, and Figure d from Kim et al. (2015) reproduced with permission from Elsevier)

bacteria so far assumed to entirely lack a PGN wall, *Chlamydiales* and *Planctomycetales*, do contain PGN in the cell wall (Pilhofer et al. 2013; Liechti et al. 2014; Jeske et al. 2015; van Teeseling et al. 2015).

The glycan strands of the PGN were initially thought to adopt a chitin-like parallel (or antiparallel) orientation with a disaccharide periodicity of 20 Å and stem peptide rotated by 180° relative to the previous and next one (Vollmer and Höltje 2004; Kim et al. 2015) (Fig. 6.7). However, a solution structure of a synthetic tetrasaccharide-pentapeptide fragment was determined by NMR techniques, which revealed a right-handed helix with a periodicity of three subunits per turn and a 120° rotation symmetry (Fig. 6.7a–c) (Meroueh et al. 2006). Thus, cross-linkage of these glycans would make up a PGN network of hexagonal honeycomb-like structure with 70-Å diameter pores, since the peptide bridges could not be oriented in plane. In contrast, solid-state NMR studies using <sup>13</sup>C-labeled PGN indicated a fourfold axial symmetry (Fig. 6.7d) that would allow for a maximum of 50% cross-linkage in a single-layered PGN (Gram-negative) and up to 100% cross-linkage of densely packed glycan strands in thick Gram-positive PGN, as applied for *S. aureus* (Kim

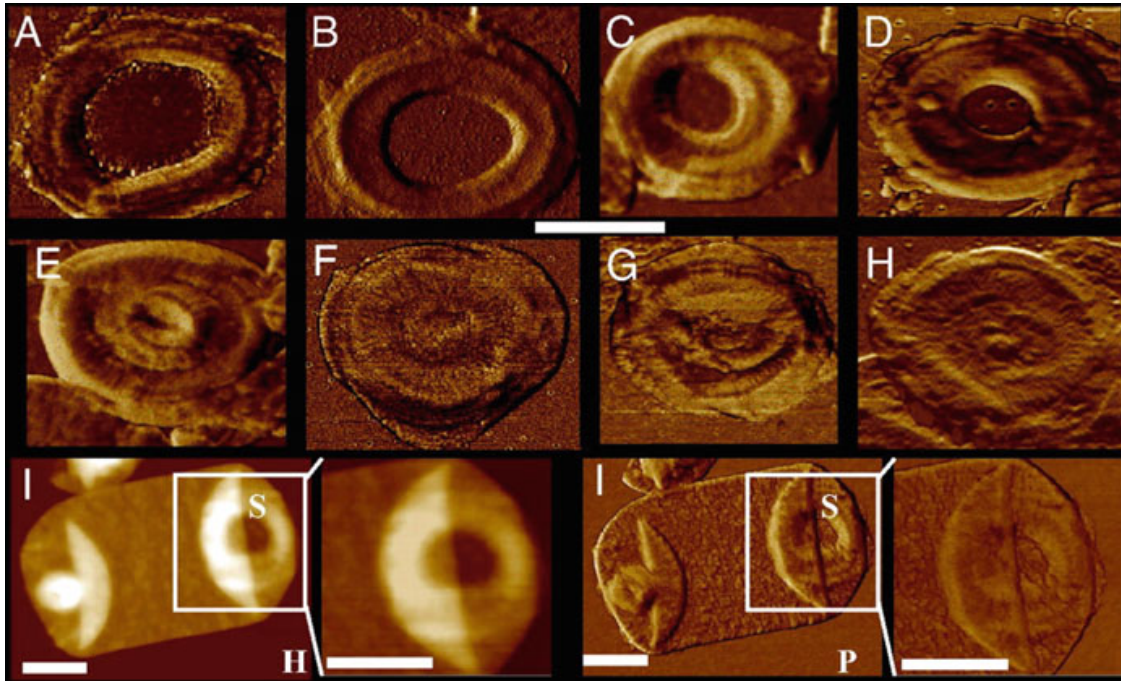


**Fig. 6.8 Atomic force microscopy (AFM) analysis of *B. subtilis* sacculi and the septal architecture.** The images (a–h) show the progression from early septum (a) to complete septum (h). Visible are large cables and cross-striations transversing the larger cables. All images are phase top view, scale bar, 500 nm. (I) Height (H) and phase (P) images of an entire cell with a partially completed septum (S) containing a hole and a completed septum at the other end of the sacculus that contains a small annular closing plug. (The figure was taken from Hayhurst et al. (2008), copyright (2008) National Academy of Sciences)

et al. 2015). The extent of cross-linkage however is variable in bacteria and, with the exception of *S. aureus*, usually less than 50% (see Sect. 6.5.1).

With AFM, besides assessing mechanical properties, the surface structures of bacteria, isolated cell walls, and even single chains of PGN can be mapped (Turner et al. 2016). AFM studies with *B. subtilis* sacculi resulted in surprising findings that the inner surface of cell walls has a regular macrostructure of thick, ca. 50-nm-wide cables running circumferential around the short axis of the rod-shaped cell (Hayhurst et al. 2008). If these structures, which are very different from the classical view of a layered cell wall, reveal intertwined PGN cables and how these may be synthesized is currently unknown. AFM can also visualize the PGN architecture at the septation sites (Hayhurst et al. 2008). Defined septa at all stages of septal closure can be seen in Fig. 6.8. The cable-like structures of in average 135 nm width form a spiral toward the center.

Combining AFM with size exclusion chromatography, Hayhurst et al. 2008 reported that the glycan chains in *B. subtilis* have an average length of 1.3  $\mu\text{m}$  and are up to 5  $\mu\text{m}$  long, which corresponds to a glycan composed of 5000 disaccharides. This finding contrasts earlier reports of glycans with an average length of 54–96 disaccharides in *B. subtilis* (Ward 1973), 25–40 disaccharides in *E. coli* (Glauner et al. 1988), and only 6–9 disaccharides in *S. aureus* (Tipper et al. 1967; Ward 1973; Boneca et al. 2000). However, the glycan chain length in these older reports is likely



an underestimation of the portion of longer chains. Harz and coauthors have already mentioned that ca. 30% of the PGN glycans that could not be separated by size exclusion have a size of >30 disaccharides (Harz et al. 1990). Although *S. aureus* has rather small-sized glycans, it was recently reported that only 30% of the glycans in this organism have a chain length of <50 disaccharides (Wheeler et al. 2015). Clearly, this long glycan chains are not consistent with the “scaffold model” of PGN architecture. Glycans in its normal rod shape are long and circumferentially oriented; however, when a spheroid shape is induced (chemically or genetically), glycans become short and disordered (Turner et al. 2018). Thus, altered cell shape is associated with substantial changes in PGN biophysical properties.

## 6.5 Variations of the Chemical Composition of the Peptidoglycan

Although the overall chemical composition of the PGN is very similar within bacteria, considerable variations from the general scheme exist in different species. Particularly, the chemical composition of the peptides, and whether the cross-linkage involves bridging peptides, varies significantly among different bacteria (Schleifer and Kandler 1972; Vollmer et al. 2008a; Litzinger and Mayer 2010). In their monumental work, Schleifer and Kandler distinguished over hundred different PGN chemotypes of bacteria according to their amino acid composition and mode of cross-linkage and used variations within the PGN for taxonomic classification (Schleifer and Kandler 1972). The glycan part of PGN is less variable, yet still a number of sugar modifications do occur, e.g., *O*-acetylation, *N*-deacetylation, or *N*-glycolylation (with mycobacteria), and also differences in the chain length of the glycans, as well as modification by secondary cell wall polymers (via MurNAc 6-phosphate, MurNAc 6P) and 1,6-anhydro-MurNAc end-capping (Vollmer 2008). It should be noted that bacteria are able to flexibly change their PGN structure depending on cell cycle, growth phase, and nutrient status. Moreover, they can retrieve PGN building blocks from the environment and incorporate them into their cell walls, e.g., different amino acid, including noncanonical and even nonnatural fluorogenic amino acids (see Sect. 6.7.3). Thus, the chemical composition of the bacterial PGN can be rather flexible. Nevertheless, differences between bacterial strains exist and are summarized in the following sections. The variation in the peptide part of the PGN will be addressed first, followed by the description of glycan modifications, and then three further sections will address (i) modifications that occur during spore cell wall biogenesis; (ii) attachment of proteins, secondary polysaccharides, and teichoic acids to the PGN; and (iii) special PGN modifications within mycobacteria.

### 6.5.1 Variation in the Stem Peptide and Modes of Cross-Linkage

Characteristic for the PGN peptides is that they contain noncanonical D-amino acids (D-Ala; D-Glu), besides L-amino acids (L-Ala; L-Lys; seldomly L-ornithine, L-Orn) and amino acids carrying two amino groups (diamino acids), that may thus contain both a D- and an L-stereochemical site, e.g., meso-diaminopimelic acid (m-DAP) (Fig. 6.9). These amino acids are connected in such a way that they generate peptides with alternating D,L- and L,D-peptide/amide linkages, beginning with the D-lactic acid

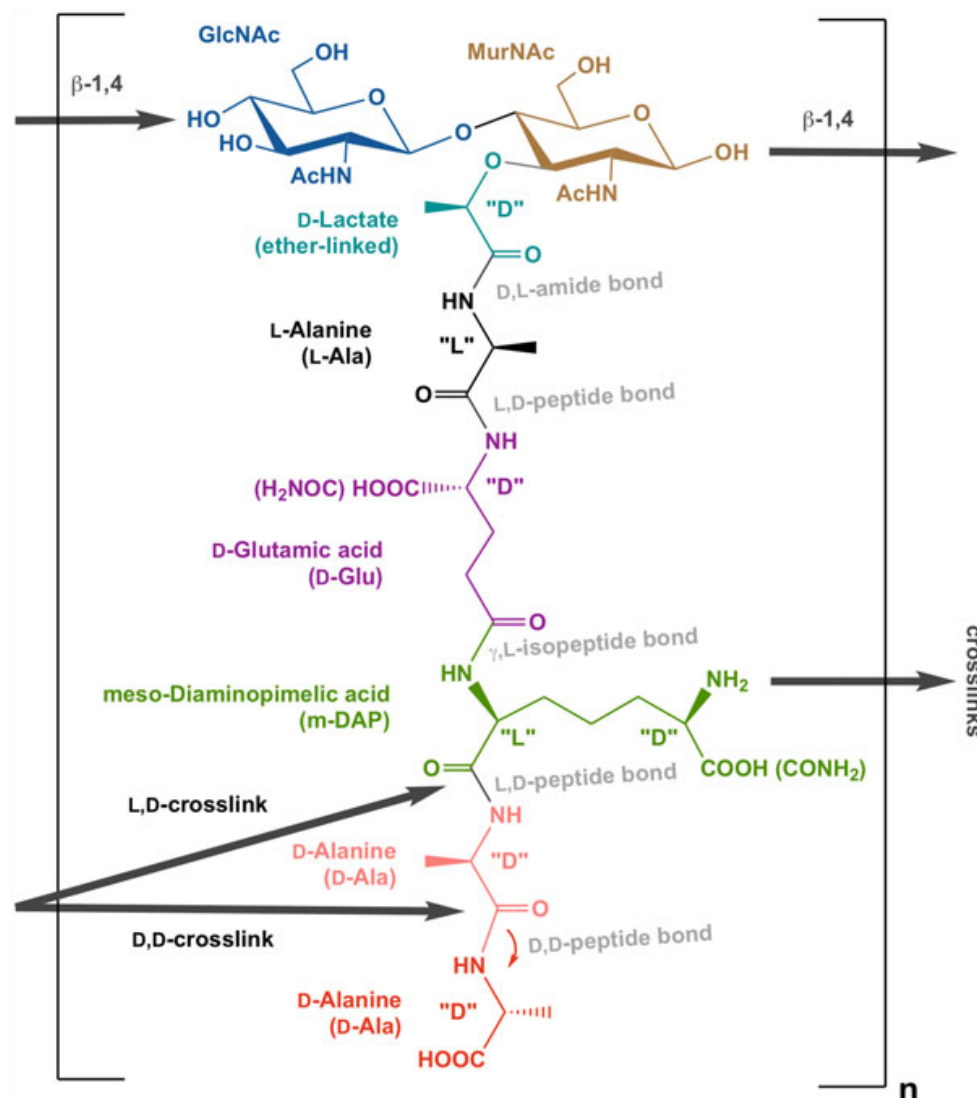


**Fig. 6.9 Chemical structure of the GlcNAc-MurNAc-pentapeptide building block of the PGN and modes of cross-linkage.** The stem peptide shown is the variant found in most Gram-negative bacteria and many bacilli and contains m-DAP at position 3 (green). The amino group at the stereochemical D-site of m-DAP is used to generate PGN cross-linkages with D-Ala residues of neighboring strands. These cross-linkages occur via transpeptidation reactions, energized by the cleavage of a terminal D-Ala residue (red), and yield either D,D-(4,3) or L,D-(3,3) peptide bonds. (This figure was adapted from Litzinger and Mayer (2010))

substituent of MurNAc. The last amino acids in the stem peptides, usually two D-Ala, are linked by a D,D-peptide bond. The resulting D,L,D,L,D,D-sequence of the peptides within the PGN makes them insensitive to cleavage by normal proteases/peptidases, which are specific for L,L-peptide bonds (Litzinger and Mayer 2010). In addition, it gives the peptides more flexibility by preventing the formation of alpha-helical structures and results in a compact disposition with the terminal D-Ala-D-Ala hidden in a curled peptide that can be stretched 2.5-fold from 10 Å to 25 Å (de Pedro and Cava 2015). Fig. 6.9 depicts the chemical structure of the general disaccharide-peptide building block of PGN as it is found within *E. coli* and *Bacillus subtilis* that contains a stem peptide with the general sequence L-Ala-iso-D-Glu-m-DAP-D-Ala-D-Ala (Fig. 6.9). Variations in this building block among bacteria involves primarily the presence of either meso-diaminopimelic acid (mDAP) at the third position within the stem peptide, which occurs in most Gram-negative as well as in some bacilli (e.g., *B. subtilis*), or L-Lys, which occurs in the majority of Gram-positive bacteria. However, some bacteria also contain L,L-DAP (e.g., *Actinobacteria*), L-ornithine (L-Orn), or, in some rare cases, L-2,4-diaminobutyric acid (Vollmer 2008; Litzinger and Mayer 2010). The diamino acids, mostly located at the third position in the stem peptide, contain a second amino group (diamino acids) that is used to cross-link the stem peptides in the PGN network (Fig. 6.9). Besides the free amino group of a diamino acid, the terminal D-Ala-D-Ala of the pentapeptide stem is critical for the cross-linkage of peptide via transpeptidases (penicillin-binding proteins, PBPs, involved in PGN biosynthesis; see Sect. 6.7.3). However, these enzymes that catalyze the cleavage of the D,D-peptide bond between the amino acids at the fourth and the fifth position, D-Ala(4)-D-Ala (5), do not catalyze an hydrolysis but a transpeptidation reaction. After release of D-Ala(5), the D-Ala(4) remains bound to the enzyme, and in a second reaction step, the free amino group of a diamino acid of a neighboring peptide strand attacks the D-alanyl-enzyme intermediate, thereby catalyzing the formation of a new peptide/amide bond (Fig. 6.9). Since these enzymes catalyze the cleavage as well as the reformation of a peptide/amide bond, they are called “transpeptidases.” These transpeptidases are very famous enzymes since they are the targets of penicillin and other  $\beta$ -lactam antibiotics. They were identified by their interaction with penicillin and thus were called penicillin-binding proteins (PBPs) (Sauvage et al. 2008). Of course, the physiological function of the PBPs is not binding of penicillin; rather this is a fatal reaction for the bacterium as it interferes with its capability to cross-link the PGN. To circumvent penicillin stress or to provide themselves with immunity toward antibiotics targeting the D-Ala-D-Ala part, bacteria can instead of D,D-transpeptidases use penicillin-insensitive L,D-transpeptidases to cross-link their PGN (Mainardi et al. 2008). These enzymes cleave the DAP(3)-D-Ala(4) or L-Lys-D-Ala(4) bonds to initiate the transpeptidation reaction forming L,D- instead of D,D-cross-linkages. Enterococci use this “alternative” cross-linkage to become insensitive to  $\beta$ -lactam and glycopeptide antibiotics which bind to the D-Ala-D-Ala structure (Cremniter et al. 2006; Magnet et al. 2007a). It should be noted that members of the L,D-transpeptidase family also links Braun’s lipoprotein with the PGN (Magnet et al. 2008) (see Sect. 6.5.4).

Amino acids at the other positions of the stem peptides are less frequently modified (Vollmer et al. 2008a). The fifth amino acid, i.e., the D-Ala(5) which is used for the transpeptidation reaction, can be substituted by glycine, D-serine, or D-lactate. These modifications are associated with vancomycin antibiotic resistance, which is a result of weaker binding of these antibiotics to the modified peptide (Boneca and Chiosis 2003). Bacteria are able to adjust stem-peptide composition (e.g., D-Ala-D-lactate instead of D-Ala-D-Ala) well as the linkage type (e.g., L,D- instead of L,D-cross-bridges) in response to treatment with vancomycin or  $\beta$ -lactam antibiotics, respectively (Magnet et al. 2008). However, also within the same bacterial strain, there are considerable variations in the PGN composition and structure. Bacteria generally are able to chemically adjust the PGN composition and the cross-linkage in dependence on growth condition, growth phase, or environmental and antibiotic constraints. Bacteria are also able to add unusual or even nonnatural amino acids within their cell wall. This had paved the route for fluorescent labeling of the PGN (see Fig. 6.17; Sect. 6.7.3).

The predominant cross-linkage type is the direct connection between mDAP and L-Lys at position 3 of one stem peptide with an D-Ala residue at position 4 of another peptide (direct 3–4 cross-linkage; A1 $\gamma$ - type; see Fig. 6.10; Schleifer and Kandler 1972). However, the cross-linkage within bacteria can vary and may involve amino acid or peptide bridges. The sizes of these bridges range from one to seven amino acids (Vollmer et al. 2008a). Most prominent is the penta-glycine (Gly<sub>5</sub>) bridge of *S. aureus* (Fig. 6.10). Worth mentioning is also the peptide bridge of *Micrococcus luteus*, in which the peptide stem is duplicated (Fig. 6.10). Presumably, the stem peptides become detached by an amidase and is cross-bridged by an unusual transpeptidase reaction (Vollmer et al. 2008a). Bridging can also involve charged amino acids, such as in *Lactobacillus* or *Enterococcus* sp. (Fig. 6.10). The three digit code established by Schleifer and Kandler to classify the types of cross-linkages within bacteria is explained in the legend to Fig. 6.10 (Schleifer and Kandler 1972).

## 6.5.2 Modifications of the Glycan Backbone

The glycan part of the PGN shows less variation among different bacteria, compared to the peptide part. Nevertheless, these few variations are of great importance, since they greatly alter the susceptibility of bacteria toward lysozyme and other cell wall hydrolases and affect the recognition by the innate immune system (Vollmer 2008). This holds in particular for *N*-deacetylation and *O*-acetylation of the sugars within the PGN. *O*-Acetylation is used by *Bacillus*, *Staphylococcus*, or *Neisseria* sp. to alter its susceptibility toward lysozyme and other muramidases. Lysozyme-resistant strains of *B. cereus* and *B. anthracis* are characterized by high proportion of glucosamine (77% or 88%, respectively) and muramic acid (50% or 34%, respectively) (Araki et al. 1971; Zipperle et al. 1984). Even the lysozyme-sensitive *B. subtilis* 168 contains a significant amount of glucosamine (19%) and muramic acid (33%) in its PGN; however, *B. subtilis* strain W23 contains only glucosamine

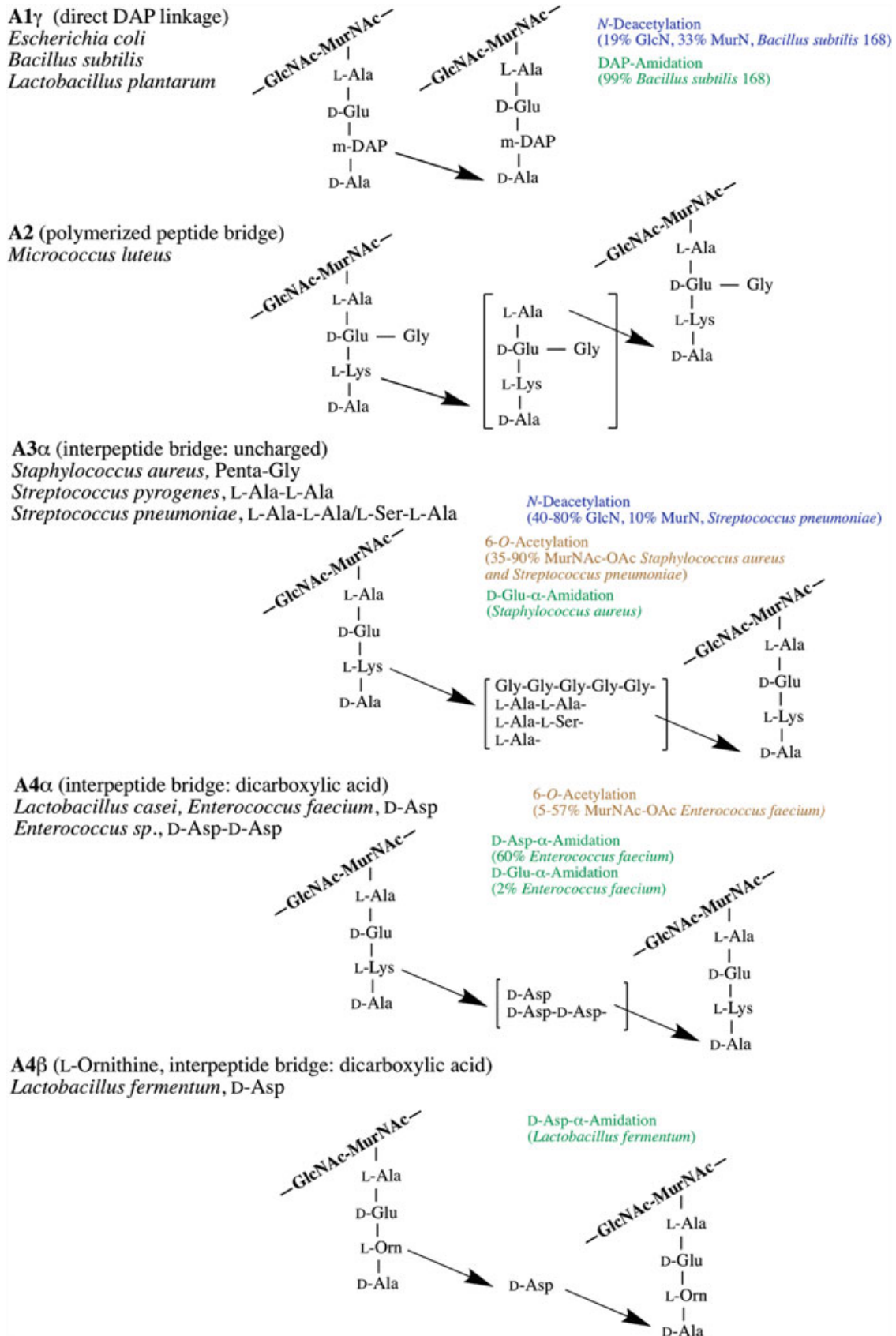


**Fig. 6.10 Primary structures and cross-linkage types of PGN in different bacteria.** According to Schleifer and Kandler 1972, 3–4 cross-linkages, which are the most common, are designated with the letter A. A1 $\gamma$ -type PGN is characterized by direct 3–4 cross-linkages involving meso-DAP and is present in *E. coli* and most other Gram-negative bacteria, as well as some bacilli (e.g., *Bacillus subtilis*, *Bacillus megaterium*, *Lactobacillus plantarum*), which however may comprise some

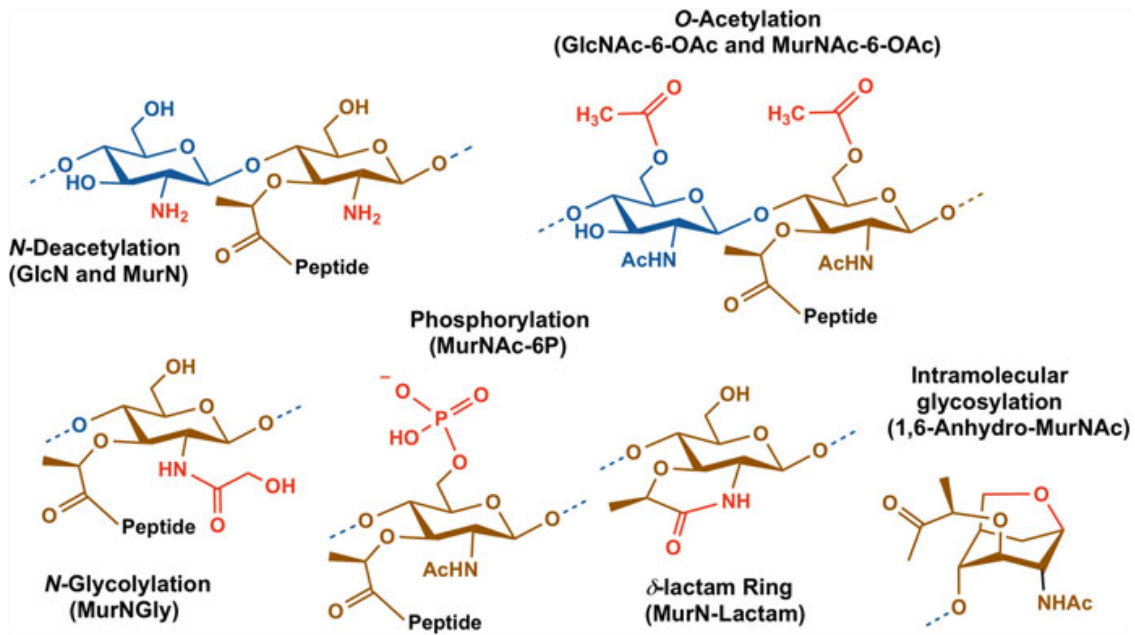


**Fig. 6.11 Modifications of the PGN glycan part.** The GlcNAc (blue) and/or the MurNAc (brown) within the PGN can be de-*N*-acetylated or *O*-acetylated and thereby renders resistant against PGN-glycosidases such as lysozyme. The MurNAc can be phosphorylated, which is used to covalently attach secondary cell wall polymers, such as teichoic acids. It can be *N*-glycolylated, e.g., in mycobacteria, or form a delta-lactam ring, e.g., in *Bacillus* spore PGN, or can have a 1,6-anhydro-bond, which is the product of PGN cleavage by lytic transglycosylases. Modifications are highlighted in red

(16%) and no *N*-deacetylated MurNAc (Zipperle et al. 1984; Atrih et al. 1999). *S. aureus* is characterized by a significant portion of MurNAc that is *O*-acetylated at the C-6 hydroxyl. *O*-acetylation of the GlcNAc is of only minor relevance. While all Gram-positive bacteria and most Gram-negative bacteria *O*-acetylate their PGN, the well-studied *E. coli* and *P. aeruginosa* are among the few exceptions where such modifications are absent (Moynihan et al. 2014). *N*-deacetylation and *O*-acetylation of the PGN have been implicated in PGN chain-length regulation and control of autolysins. A comprehensive survey of bacterial PGN glycan modifications can be found in Vollmer 2008 and Moynihan et al. (2014). These reviews also describe the different enzymes that catalyze these modifications. The glycan modification becomes particularly important during cell differentiations. Fig. 6.11 depicts the various observed modifications of the glycan part of the PGN. How these



**Fig. 6.10** (continued) modifications such as sugar *N*-deacetylation and mDAP amidation. Three to four cross-linkages that include an interpeptide bridge can be found primarily in Gram-positive bacteria. The A2-type PGN found in *M. luteus* is characterized by stem peptide duplications; it also contains a glycine modification at position 2. A3 $\alpha$ , A4 $\alpha$ , and A4b types of PGN contain neutral amino acid or peptide bridges, either pentaglycine bridges as found in *Staphylococcus aureus* or L-Ala-L-Ala bridge such as in *Enterococcus faecalis*, double-charged amino acid (Asn/Asp) bridges such as in *Lactobacillus* sp. or involve D-ornitin (D-Orn) at position 3. Other possible linkage types may involve 2–4 cross-linkages (not shown)

modifications occur during *Bacillus* spore PGN synthesis will be addressed in the following section.

### 6.5.3 PGN Alterations During Starvation: The *B. subtilis* Spore PGN

Major alterations of PGN structure in most bacteria occur during differentiation under nutrient starvation. One of the most radical processes of differentiation is endospore formation in some bacteria, e.g., *Bacillus* and *Clostridium* sp. (Foster and Popham 2002; Popham 2002). Rearrangement of the vegetative PGN cell wall starts with an asymmetric cell division event, and subsequent thinning of the thick PGN of the smaller cell (the prespore or forespore) by a process called prespore engulfment. In this process, three layers of the spore wall are formed simultaneously: (1) a thin inner PGN layer adjacent to the cell membrane, known as the primordial cell wall or germ cell wall, which has the same PGN composition as the vegetative wall but its thickness is reduced (Fig. 6.12); (2) an additional membrane, covering the newly formed cell wall; and (3) a new cell wall layer, called the cortex, which is a thick PGN with a very unique structure (Fig. 6.12). In the cortex PGN, the stem peptides and the *N*-acetyl groups are removed from c. 50% of the MurNAc residues, and a special delta-lactam ring is formed in the molecule between the free carboxylic acid of the *D*-lactate substituent and the free amino group of the muramic acid (Fig. 6.11). Furthermore, c. 24% of the MurNAc residues contain no stem peptide that can be cross-linked but only *L*-Ala substitutions (Fig. 6.12). Thus, the cross-linkage of the cortex PGN is very low (cross-linkage index = 3%). The outermost layer of the spore wall is composed of the proteinous spore coat, which is most responsible for the resistant properties of the spore. During spore germination the cortex is cleaved to allow outgrowth of the spore by specialized autolytic enzymes that target the cortex PGN but keep the primordial cell wall intact.

### 6.5.4 Covalent Attachments to the Peptidoglycan

Most Gram-positive bacteria but also some Gram-negatives (e.g., cyanobacteria) are characterized by a PGN cell wall that is modified by secondary cell wall polymers (e.g., teichoic acids and capsule polysaccharides). These polymers are attached via phosphodiester bonds to the PGN, particularly to the 6-hydroxyl group of MurNAc (Fig. 6.11). The enzymatic process of transfer of the polymers to the PGN had long been enigmatic. However recently, proteins of the LCP (LytR, CpsA, Psr) family were shown to be involved in the linkage of teichoic acid, mycobacterial arabinogalactans, and capsule polysaccharides to the PGN (Kawai et al. 2011; Eberhardt et al. 2012; Chan et al. 2014; Harrison et al. 2016). Mutants lacking the

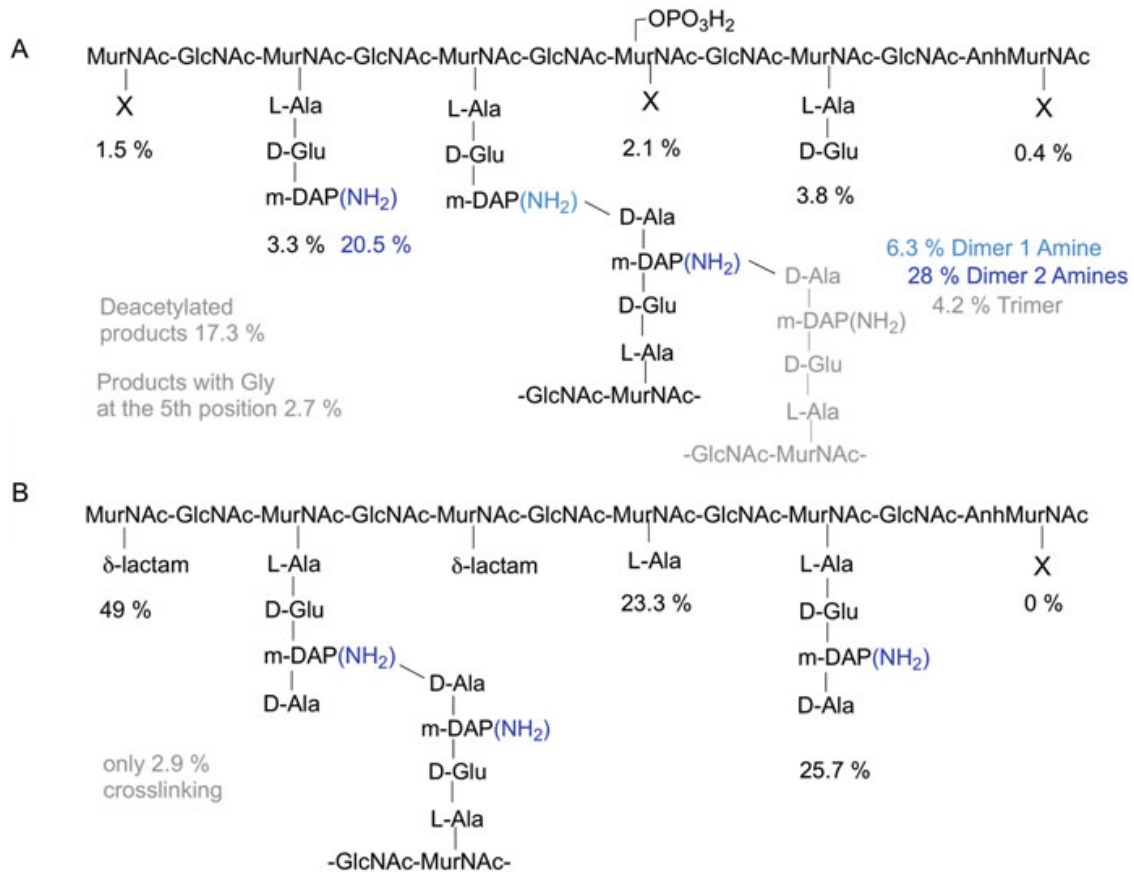


**Fig. 6.12 Comparison of the structures of the *B. subtilis* PGN in the vegetative wall/primordial spore wall and in the endospore cortex.** (a) The primordial or germ wall contains PGN that is identical to the vegetative PGN. The cross-linkage index is high (27–33%), and the main muuropeptides found in cell wall analyses are shown (Atrih et al. 1999; Atrih and Foster 1999). (b) Profound alterations within the PGN occur in the cortex layer. The cross-linkage index of spore cortex PGN is very low (c. 3%) (Atrih et al. 1996; Atrih and Foster 1999)

LCP family proteins release wall teichoic acids into the medium, as they are preformed but cannot be attached to the PGN (Chan et al. 2013). Moreover, PGN is the anchor point for surface proteins. The covalent attachment of proteins to the PGN occurs mostly in Gram-positive bacteria, where the PGN is the outermost layer that exposes proteins and enzymes to the cell surface. The signal peptide-directed localization of proteins to the PGN is called “cell wall sorting” (Schneewind and Missiakas 2012). Secreted proteins may carry a C-terminal amino acid motif, which is the sorting signal that is cleaved by the sortase and transfers the protein to the PGN. Specific sorting signals are recognized by dedicated sortase enzymes, e.g., pilus-specific sortases. However, all Gram-positive bacteria express sortase A, a membrane-anchored transpeptidase that cleaves the C-terminal LPXTG signal peptide of proteins destined for cell wall anchoring (Mazmanian et al. 1999; Ton-That et al. 1999). Somewhat similar to the protein sorting within Gram-positives is the process by which Gram-negative bacteria connect their PGN sacculus with the outer membrane. This is crucial for Gram-negative bacteria in order to avoid the loss of



outer membrane vesicles into the medium. They carry a great number of Braun's lipoprotein (Braun and Rehn 1969; Braun (1975)). In *E. coli* approximately  $10^5$  lipoprotein molecules are anchored to the inner leaflet of the outer membrane by an acylated N-terminal cysteine, which is a characteristic linkage of lipoproteins, and approximately one third of them are covalently connected via the amino group of the C-terminal lysine residue of the protein to the stem peptides of the PGN via an L,D-peptide bond. *E. coli* contains five L,D-transpeptidases, which are similar to the enzymes catalyzing the PGN cross-linkage in  $\beta$ -lactamase-resistant strains via L,D-transpeptidation (see Fig. 6.9). In *E. coli* three of these enzymes can individually anchor of the outer membrane-bound lipoprotein to the PGN. Two other enzymes of the same family are able to generate L,D-peptide cross-linkages, connecting two m-DAPs of distinct stem peptides in the PGN (Magnet et al. 2008). The biosynthesis and connection of the Braun lipoprotein is shown in Fig. 6.13.

### 6.5.5 *Special Mycobacterial Peptidoglycan*

A very complex cell envelope structure is found in mycobacteria (e.g., *M. tuberculosis*), which, instead of a real outer membrane, contain a lipid layer of long-chain fatty acids (mycolic acids) and glycolipids, which is connected to a PGN-arabinogalactan heteropolymeric cell wall (Fig. 6.2c) (Raghavendra et al. 2018). Mycobacteria and other bacteria that do not respond to the Gram staining (e.g., rickettsia and spirochetes) can be stained by the acid-fast technique (Ziehl-Neelsen stain) (Vilcheze and Kremer 2017). Mycobacteria, including *M. tuberculosis*, the etiological agent of tuberculosis, are a group of bacteria characterized by a very special cell envelope structure that is distinct from the cell envelope of both Gram-negative and Gram-positive (Jankute et al. 2015) (cf. Fig. 6.2). The mycolic acids within the mycobacterial cell envelope are connected to highly branched arabinogalactan polysaccharides, which themselves are covalently bound to the PGN (Jankute et al. 2015). Additional lipoglycans (lipoarabinomannan; LAM) connected with the inner membrane and the PGN-arabinogalactan heteropolymer functionally resemble the wall and lipoteichoic acids of Gram-positives (Raghavendra et al. 2018). Although the PGN of mycobacteria is classified as the common A1y-type (Schleifer and Kandler 1972), it contains some unique features: besides MurNAc, mycobacteria as well as related actinobacteria contain *N*-glycolylmuramic acid (MurNGly) (Holt et al. 1994; Vollmer, 2008). The modification is introduced in the cytoplasm by the monooxygenase NamH (UDP-MurNAc hydroxylase), which oxidizes the acetamido group in the soluble precursor using oxygen and NADPH (Raymond et al. 2005). This modification is believed to be involved in increasing the overall strength of PGN by providing sites for hydrogen bonding, as well as in decreasing susceptibility toward lysozyme (Raymond et al. 2005). The Mur ligases of mycobacteria have a broad substrate specificity allowing to accept the *N*-glycolyl form of UDP-MurNAc-peptides). The usual 3–4 cross-linkages between mDAP and L-Ala are predominant

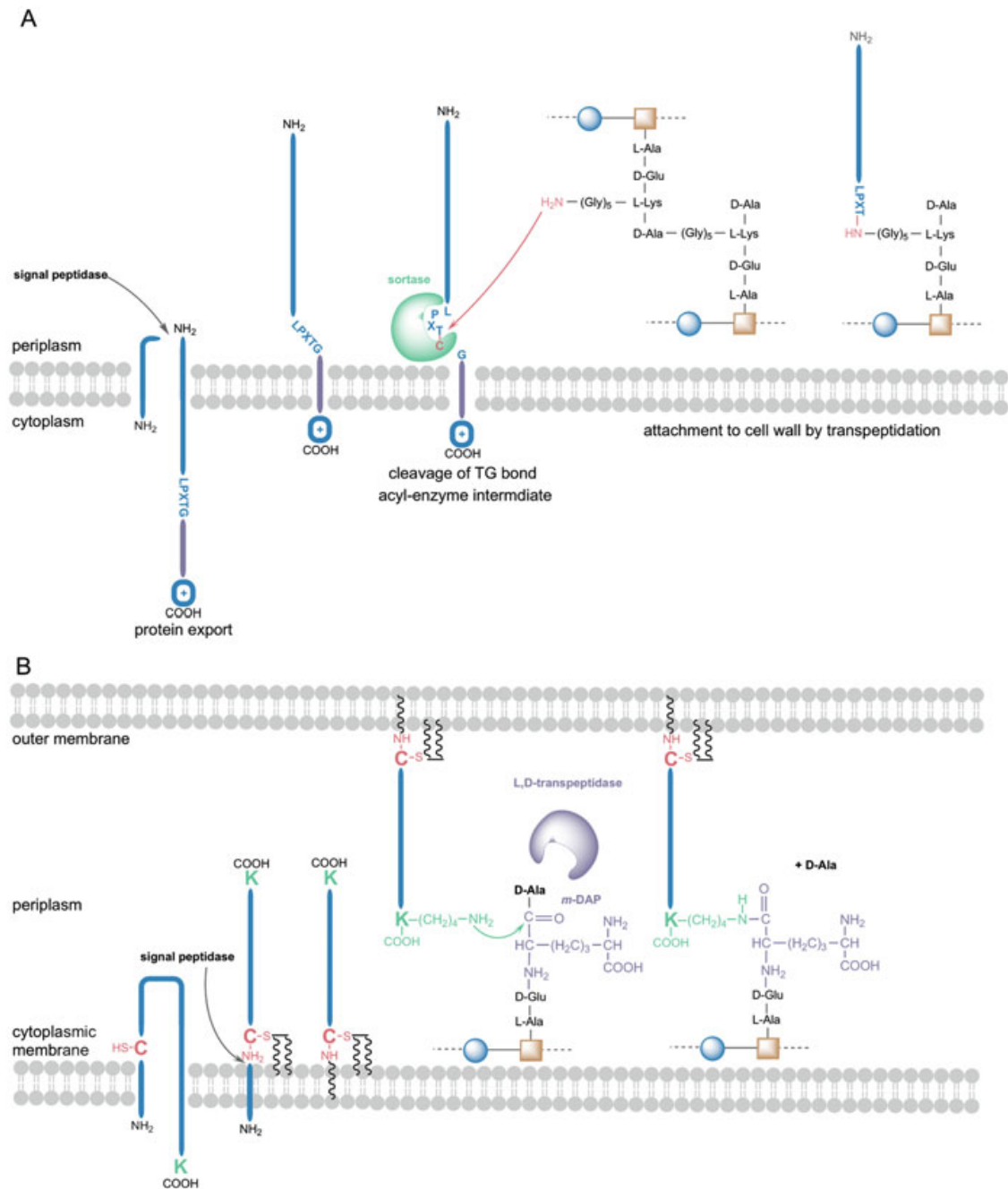


**Fig. 6.13 Covalent attachment of proteins to the PGN.** Linking of surface proteins by sortase enzymes (cell sorting) in Gram-positives (a) and attachment of Braun's lipoprotein to PGN in Gram-negatives (b). The proteins are synthesized in the cytoplasm as precursor polypeptides that carry an N-terminal signal sequence for the translocation through the cytoplasmic membrane via the secretion system (Sec). (a) Complete translocation of the polypeptide is blocked due to positively charged amino acids near the C-terminus adjacent to a hydrophobic domain (violet). Membrane-anchored sortase enzymes recognize the LPXTG amino acid motif, the sorting signal, located upstream of the hydrophobic domain of this stuck polypeptide, and cleave between the amino acids Thr and Gly. An acyl-enzyme is formed with the active site cysteine of the sortase and the threonine residue of the cleaved polypeptide. The peptidyl is then transferred from the sortase to a stem peptide within the lipid II or nascent PGN, e.g., to the pentaglycine (Gly<sub>5</sub>) in *S. aureus*. Thereby the cell wall-anchored protein is subsequently moved outward with progression of PGN synthesis. This figure was drawn based on published cartoons (Schneewind et al. 1995; Ton-That et al. 1999; Schneewind and Missiakas 2012). (b) The prolipoprotein is composed of 78 amino acids containing an N-terminal signal sequence and an adjacent lipobox (L,S/A,A/G,C). Signal cleavage of Braun's lipoprotein does not occur directly after secretion but only after a diacylglycerol from

in mycobacteria. However L-Ala is often substituted by Gly, and thus mDAP-Gly crosslinkages occur and further modifications include amidation of D-Glu and DAP (Botella et al. 2017; Squeglia et al. 2018).

## 6.6 Compositional Analytics of Peptidoglycans

Characterization of the PGN classically involves the compositional analysis (of amino acid and amino sugars) by thin layer chromatography or gas chromatography/mass spectrometry after total or partial hydrolysis of isolated PGN with hydrochloric acid. Further analysis involves glycan chain length distribution and cross-linkage types, as well as the amount of stem-peptides undergoing cross-links (degree of cross-linkage). Characterization of a novel bacterial species, for example, necessitates the classification of the PGN-type according to Schleifer and Kandler (1972) and classification of PGN types (Ghuysen 1968; Schleifer and Kandler 1972; Litzinger and Mayer 2010) (see Sect. 6.5.1). Before conducting a PGN analysis, the sacculi need to be purified. This process of purification of intact PGN sacculi involves the instant boiling in a solution of sodium dodecyl sulfate (SDS), which simultaneously inactivates endogenic autolytic enzymes and disrupts the cell by solubilizing the membranes. Further steps involve the extensive washing to remove the SDS, which would interfere with the following enzymatic digests, and the subsequent enzymatic degradation of protein linked to the PGN, glycogen, and DNA/RNA by proteases, amylase, and nucleases, respectively (Desmarais et al. 2013; Desmarais et al. 2014). PGN purified by this procedure has a good cleanliness and can be used for compositional analyses (muropeptide analysis), which relies on a controlled enzymatic digest, generally using a lysozyme from *Streptomyces* sp., called mutanolysin or cellosyl. High-performance liquid chromatography (HPLC) is generally used to separate the muropeptide building blocks generated by chemical or enzymatic digests of isolated sacculi (Glauner 1988; Glauner et al. 1988; de Jonge et al. 1992; Atrih et al. 1999). For *E. coli*, more than 80 distinct muropeptides can be resolved by HPLC analysis, indicating an intriguing complexity of PGN chemical structure. De Pedro and Cava (2015) stressed out that even minor components of a muropeptide analytes provide significant numbers in biological terms. Complete digestion of PGN with an amidase enables the isolation of glycan strand for chain length analysis (Harz et al. 1990). Apart from radiodetection, mainly UV-detection



**Fig. 6.13** (continued) phosphatidylglycerol is transferred to the SH group of the cysteine residue located within the lipobox of the protein. Thereafter, the N-terminus is cleaved, and an additional fatty acid residue is transferred to the free amino group of the cysteine. This modification is required for the recognition by the Lol system that transfers the lipoprotein to the outer membrane (Dramsi et al. 2008). After being inserted in the outer membrane, the C-terminal Lys reacts with the PGN stem peptide in a L,D-transpeptidase reaction, thereby connecting the lipoprotein with the PGN (Magnet et al. 2007b)

(200–210 nm), although not very sensitive, is generally applied for muropeptide analysis. Recently, a fast and sensitive LC-MS-based high-throughput muropeptide analysis method was reported (Kühner et al. 2014).

## 6.7 Peptidoglycan Biosynthesis

The synthesis of PGN in bacteria is a conserved process that can be divided into three stages occurring within different compartments. It starts in the cytoplasm with the formation of the soluble precursors, UDP-GlcNAc, UDP-MurNAc, and UDP-MurNAc-peptides (the so-called Park nucleotides). The PGN building block is then anchored to the cell membrane by transfer onto the lipid carrier, called undecaprenol-phosphate or bactoprenol-phosphate. First, MurNAc-pentapeptide from UDP-MurNAc-pentapeptide is transferred to undecaprenol-phosphate yielding lipid I (undecaprenyl-pyrophosphoryl-MurNAc-pentapeptide). Subsequently, GlcNAc is transferred from UDP-GlcNAc to lipid I to give the final substrate for PGN assembly, called lipid II (undecaprenyl-pyrophosphoryl-MurNAc-pentapeptide-GlcNAc). Lipid II is the general membrane-anchored precursor of PGN biosynthesis of bacteria that can be further modified (e.g., in *S. aureus* five glycine residues are added to the L-Lys to yield a lipid II with a pentapeptide-pentaglycine stem). The lipid II molecule is then flipped through the cell membrane, and the PGN precursors are polymerized outside of the cell by glycan synthases that are anchored within the outer leaflet of the cytoplasmic membrane. They polymerize the PGN by the action of glycosyltransferases and incorporate the newly formed PGN into the existing wall by cross-linking transpeptidases. The complete process is schematically depicted in Fig. 6.14. In the following section, the enzymatic steps of these three stages will be described in more detail. As the synthesis of PGN is unique to bacteria and mostly conserved across species but absent in humans, the pathway is an ideal target for antibiotics. Thus we will also discuss various antibiotics targeting individual steps of PGN synthesis.

### 6.7.1 Soluble Precursor Biosynthesis

The synthesis of the precursors UDP-GlcNAc and UDP-MurNAc, depicted in Fig. 6.15, starts in the cytoplasm of the bacterial cell. D-Fructose-6-phosphate (fructose-6P) derived from the glycolysis metabolic pathway is converted to D-glucosamine-6-phosphate (GlcN 6P) by the glutamine-fructose-6-phosphate-amidotransferase (GlmS) (Badet et al. 1988). The amino group originates from L-glutamine, which is hydrolyzed by the N-terminal glutaminase domain of GlmS into glutamate and ammonia; the latter is channeled to the C-terminal isomerase domain of GlmS, which conducts the isomerization and attachment of the amino group (Badet-Denisot and Badet 1992). GlmS is a critical enzyme controlling the amino

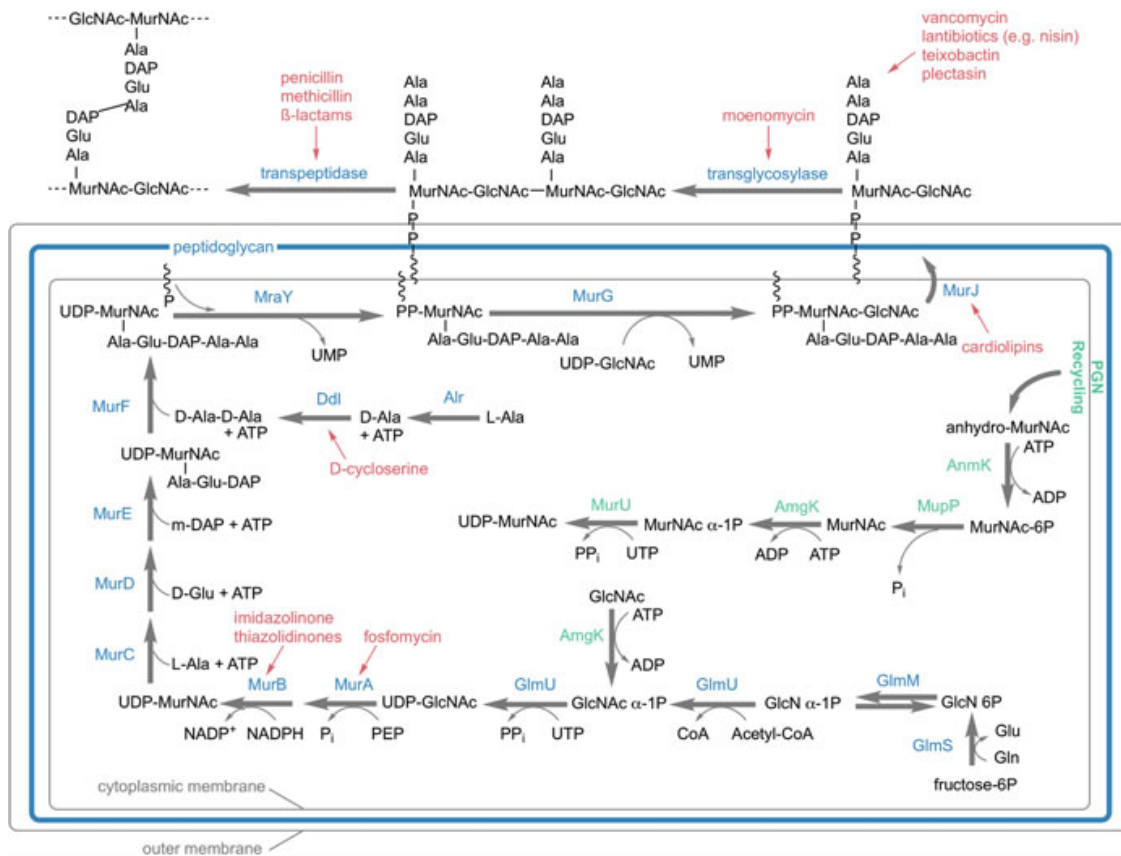


**Fig. 6.14 Overview of the PGN biosynthesis occurring in three stages, within the cytoplasm, the cell membrane, and the cell wall compartment.** Shown is the PGN biosynthesis pathway as it occurs in most Gram-negative bacteria and Gram-positive bacilli (blue enzymatic steps). With minor differences, the pathway also occurs in other Gram-positive bacteria or mycobacteria (for details see text). Furthermore, the recycling pathway (green enzymatic steps) as it occurs in *Pseudomonas* sp. and many other Gram-negative bacteria adds to the PGN precursor pool. Selected antibiotics inhibiting specific steps of these pathways are indicated (red). The standard pathway (blue): GlmSMU generate UDP-GlcNAc from fructose-6P; MurA (inhibited by fosfomycin) and MurB (inhibited by imidazolinone and thiazolidinones) in a further process yield UDP-GlcNAc and UDP-MurNac, respectively; MurCDEF successively add single amino acids forming the stem peptide; D-Ala-D-Ala is attached as a dipeptide, which is provided by Ddl (and inhibited by D-cycloserine); D-Ala is provided by the Alr racemase from L-Ala; MraY loads the MurNac-pentapeptide onto the undecaprenyl-phosphate (undecaprenyl-P) lipid carrier, forming lipid I; and lipid II is generated by the addition of GlcNAc from UDP-GlcNAc. This is carried out by MurG, which thereby forms the  $\beta$ -1,4-glycosidic bond between MurNac and GlcNAc; lipid II is subsequently flipped across the membrane by the flippase MurJ, for which cardiolipins have been found to be inhibitors; the further polymerization of lipid II in the periplasm can be inhibited by various antibiotics such as vancomycin and lantibiotics like nisin, teixobactin, and plectasin; moenomycin inhibits the transglycosylase step, whereas the transpeptidation, conducted by PBP transpeptidase domains, is inhibited by  $\beta$ -lactams such as methicillin and penicillin; some bacteria have developed alternative pathways for UDP-MurNac synthesis; *Pseudomonas* (green) uses anhydro-MurNac derived from cell wall turnover to generate UDP-MurNac via anhydro-MurNac kinase AnmK, MurNac-6P phosphatase MupP, anomeric MurNac/GlcNAc kinase AmgK, which can phosphorylate both MurNac and GlcNAc at C1 position, and the MurNac  $\alpha$ -1P uridylyltransferase MurU; MupP, AmgK, and MurU homologues have been identified in many Gram-negative bacteria suggesting a *Pseudomonas* like pathway (Gisin et al. 2013; Borisova et al. 2017)

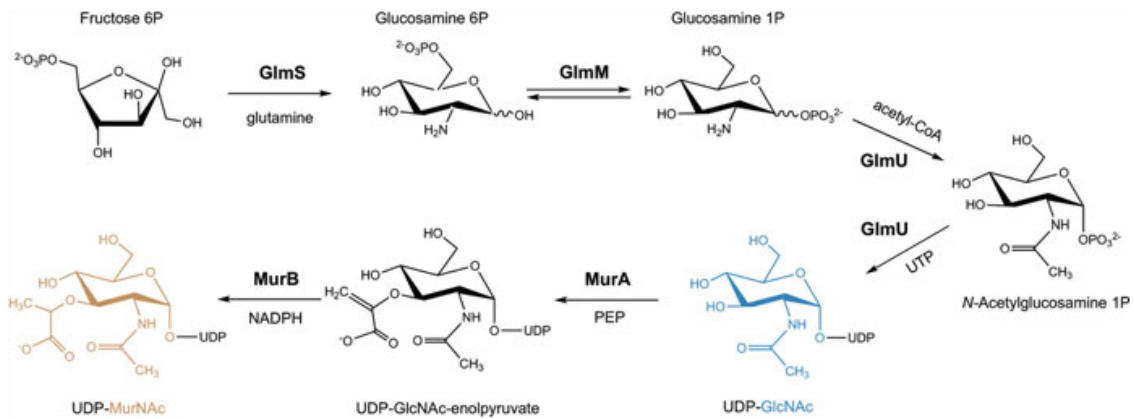


**Fig. 6.15** Enzymatic steps toward the synthesis of the PGN precursors UDP-GlcNAc and UDP-MurNAc. Shown is the biosynthesis of UDP-MurNAc from fructose-6P by GlmSMU, which generates UDP-GlcNAc with an amino group derived from L-glutamine, an acetyl group derived from acetyl-CoA and UTP, and MurAB, which converts UDP-GlcNAc to UDP-MurNAc with the addition of an enolpyruvate derived from PEP followed by a reduction to form the D-lactyl residue of UDP-MurNAc

sugar metabolism and is thus delicately regulated in bacteria. In Gram-positive bacteria, a ribozyme sensing rising glucosamine-6-P levels cleaves the *glmS* mRNA, thereby repressing transcription and expression of GlmS (Winkler et al. 2004). In *E. coli* posttranscriptional regulation of *glmS* in response to GlcN 6P levels involves small regulatory RNAs (Kalamorz et al. 2007). GlcN 6P is then isomerized to  $\alpha$ -glucosamine 1-P (GlcN  $\alpha$ -1P) by the hexose-phosphate mutase GlmM (Mengin-Lecreulx and van Heijenoort 1996). GlmM converts GlcN 6-P to GlcN  $\alpha$ -1P via a glucose-1,6-diphosphate intermediate. The reaction can proceed in reverse direction although at a reduced rate (Jolly et al. 1999). The next step involves the essential, bifunctional enzyme GlmU that converts GlcN  $\alpha$ -1P to UDP-GlcNAc in a two-step process. First, it transfers an acetyl group provided by acetyl-CoA to the amino group generating  $\alpha$ -N-acetylglucosamine 1-phosphate (GlcNAc  $\alpha$ -1P), which remains bound to the enzyme. In a second step, an uridyl group from UTP is transferred to GlcNAc  $\alpha$ -1P, while UMP and pyrophosphate (PPi) are released, and UDP-GlcNAc is generated. The first dedicated step of PGN synthesis is the formation of UDP-MurNAc from UDP-GlcNAc, and both are used directly for PGN synthesis (Gehring et al. 1996; Mengin-Lecreulx and van Heijenoort 1994). For the formation of UDP-MurNAc from UDP-GlcNAc, two steps are necessary, which are catalyzed by MurA and MurB. MurA transfers an enolpyruvyl group from phosphoenolpyruvate to the 3' hydroxyl group of UDP-GlcNAc (Du et al. 2000). The MurA reaction proceeds through a tetrahedral intermediate of substrates, UDP-GlcNAc and phosphoenolpyruvate, followed by elimination of the phosphate to yield the enolpyruvyl product from which phosphate is released generating UDP-GlcNAc-enolpyruvate (Brown et al. 1994; Eschenburg et al. 2003; Zhu et al. 2012). The final step toward UDP-MurNAc is catalyzed by the flavoprotein MurB. FAD serves as a redox intermediate since it gets reduced by NADPH to FADH<sub>2</sub>, which subsequently reduces the vinyl enol group of UDP-GlcNAc-enolpyruvate yielding

UDP-MurNAc (Benson et al. 1993; Benson et al. 1997). MurA can be inhibited by fosfomycin, an epoxide and structural analog of PEP, which covalently binds the MurA active site cysteine (Eschenburg et al. 2005). Thiazolidinones inhibit MurB by mimicking the diphosphate moiety of UDP-GlcNAc-enolpyruvate (Andres et al. 2000). Also some imidazolinone analogues that show antibacterial activity against *S. aureus* have been identified (Bronson et al. 2003). Because of their unfavorable physicochemical properties, these compounds were not further studied, and new inhibitors were not discovered for over a decade until, based on the MurB crystal structure (Chen et al. 2013), novel tetrazole inhibitors of MurB were discovered, although they do not possess in vitro antimicrobial activity against *S. aureus* or *E. coli* (Hrast et al. 2018).

To yield the final soluble PGN precursor UDP-MurNAc-pentapeptide, a pentapeptide chain needs to be attached at the lactyl residue of UDP-MurNAc. This occurs by stepwise addition of amino acids and is catalyzed by the ATP-dependent Mur ligases MurCDEF (van Heijenoort 2001; Vollmer and Bertsche 2008; Kouidmi et al. 2014). The reaction mechanism is common in all Mur ligases. The carboxyl group of UDP-MurNAc (or UDP-MurNAc-peptides) is activated by ATP resulting in an acyl phosphate intermediate and ADP. A nucleophilic attack on the amide group of the added amino acid results in an intermediate from which the phosphate group dissociates generating an amide or peptide bond (Bouhss et al. 2002). An ATP-binding consensus sequence and six invariant residues define the Mur ligases as a family of enzymes (Bouhss et al. 1997). The domain organization is similar in all Mur ligases with the UDP-precursor binding N-terminal domain, the central ATP binding domain, and the amino acid or dipeptide binding C-terminal domain (Smith 2006). L-Ala is the first amino acid added to UDP-MurNAc (Schleifer and Kandler 1972) with a stereo specificity for the L-amino acid, and D-Ala is not recognized as a substrate (Liger et al. 1995). D-Glu is the second amino acid of the peptide stem in most species (Schleifer and Kandler 1972). Although there are variations like amidation of the  $\alpha$ -carboxylic acid group, these modifications are introduced after incorporation of D-Glu, which is the substrate of MurD in all species (Vollmer et al. 2008a). D-Glu is provided by the glutamate racemase MurI from L-Glu in *E. coli* (Doublet et al. 1994). The third amino acid, incorporated by MurE, is in most cases either *meso*-diaminopimelic acid (*m*-DAP), such as in Gram-negatives and some bacilli, or L-Lys, such as in most Gram-positives (Schleifer and Kandler 1972; Ruane et al. 2013). MurE is highly specific for the correspondent amino acid, and false incorporation, for example, L-Lys in *E. coli*, leads to cell lysis (Mengin-Lecreulx et al. 1999). In *B. subtilis* *m*-DAP gets amidated by the amidotransferase AsnB. The  $\Delta$ *asnB* mutant exhibits increased sensitivity to cell wall targeting antibiotics and has a disturbed balance between PGN synthesis and hydrolysis ultimately leading to cell lysis (Dajkovic et al. 2017). In *Corynebacterium glutamicum*, a *m*-DAP amidase, LtsA, has been identified as well with similar effects in the mutant such as high lysozyme and  $\beta$ -lactam susceptibility (Levefaudes et al. 2015). Finally, the dipeptide D-Ala-D-Ala is added by MurF, which exclusively utilizes dipeptide substrates composed of D-amino acids (Bugg and Walsh 1992). MurF is more promiscuous regarding substrates than the other Mur ligases (Anderson et al. 1996) and can also

integrate noncanonical D-amino acids such as D-Met, D-cystein, or fluorescent derivatives (see Fig. 6.17) into the PGN. D-Ala-D-Ser or D-Ala-D-Lac are used in vancomycin-resistant strains (Healy et al. 2000), for example, in *Enterococcus faecalis* via a D-Ala-D-Ser ligase (Meziane-Cherif et al. 2012). D-Ala is provided by the alanine racemases Alr and DadX (Wild et al. 1985) and used by the D-Ala-D-Ala ligase DdlA yielding the dipeptide (Zawadzke et al. 1991). The Ddl ligase can be inhibited by D-cycloserine (Batson et al. 2017). *E. coli* Mpl is a nonessential murein ligase (Mengin-Lecreulx et al. 1996) that can ligate the L-Ala-iso-D-Glu-*m*-DAP tripeptide, derived from the cell wall turnover, directly with UDP-MurNAc (Park and Uehara 2008).

## 6.7.2 Membrane-Bound Precursors

Lipids I and II describe undecaprenyl-pyrophosphate (undecaprenyl-PP)-bound MurNAc-pentapeptide and GlcNAc-MurNAc-pentapeptide, respectively. The first membrane associated step starts with the de novo synthesis of the C<sub>55</sub>-P lipid carrier (undecaprenyl-P). UppS initially forms undecaprenyl-PP in the inner leaflet of the plasma membrane (Fujihashi et al. 2001), which is then dephosphorylated by the phosphatase UppP in the outer leaflet (Manat et al. 2014). Subsequently, the phospho-MurNAc-pentapeptide generated by the Mur ligases is loaded onto undecaprenyl-P by the membrane protein MraY, a prenyl sugar transferase (Al-Dabbagh et al. 2008) with the predicted active site in the cytoplasm and an extended hydrophobic groove which could be harboring the acyl lipid tail of the carrier (Chung et al. 2013). The antibiotic tunicamycin rearranges transmembrane helices and cytoplasmic loops of MraY thus preventing the substrate binding (Hakulinen et al. 2017). Lipid II is formed with the addition of GlcNAc by the membrane-tethered glycosyltransferase (GT) MurG (Anderson et al. 1965; Bouhss et al. 2004; van Heijenoort 2007). The MurG crystal structure revealed a common GT-B superfamily fold (Hu et al. 2003). In some Gram-positive bacteria like *S. aureus* lipid II is further modified, where five glycine residues are added to the amino group on position 3 of L-Lys (Navarre and Schneewind 1999). Also D-Glu can be amidated by the glutamine amidotransferase-like GatD and Mur ligase homologue MurT, which form a stable bi-enzyme complex. Mutants show an increased susceptibility to methicillin and are less viable (Münch et al. 2012). An antibiotic termed teixobactin was discovered by a screening of previously uncultured bacteria. It is able to bind a highly conserved motif of lipid II and even lipid III, which is the precursor for wall teichoic acids in Gram-positive bacteria. It is effective against important pathogens such as *S. aureus* and *M. tuberculosis* (Ling et al. 2015). Lipid II is also a target for the vancomycin group of glycopeptides and several lantibiotics such as nisin. The mode of action is complexation, which prevents cross-linking and incorporation into the cell wall (Bugg et al. 2011). The same mode of action has been demonstrated for the fungal defending plectasin (Schneider et al. 2010).



After synthesis in the cytoplasm, the lipid II must be translocated across the membrane in order to get incorporated into the PGN. The translocation does not occur spontaneously. In fact, a specialized protein machinery is required for this process (van Dam et al. 2007). A candidate was identified by a reductionist bioinformatics approach suggesting MurJ (MviN) as the PGN lipid II flippase in *E. coli* (Ruiz 2008). MurJ is part of the MATE (multi-antimicrobial extrusion)-like superfamily, from which members have been shown to function as drug and sodium antiporters. MurJ-deficient cells have been shown to swell and burst (Omote et al. 2006; Inoue et al. 2008). Furthermore, the integral membrane protein FtsW of the SEDS (shape, elongation, division, and sporulation) family, which is essential in the bacterial division machinery, is able to flip lipid-linked PGN precursors across model membranes in in vitro assays (Mohammadi et al. 2011). Another hint for FtsW is that all MurJ homologues could be deleted in *B. subtilis* (Fay and Dworkin 2009) although a flippase is supposed to be essential. However, an alternative flippase, Amj, was found in *B. subtilis*. It is upregulated in the absence of MurJ via an envelope stress-response pathway (Meeske et al. 2015) and has no sequence or structural homology to MurJ (Sham et al. 2014). Another recent discovery favors MurJ as the main flippase, since variants of WzxC, a flippase involved in *E. coli* capsule (colanic acid) synthesis, were able to rescue lethal MurJ deficiency (Sham et al. 2018). MurJ can be inhibited by exogenous cardiolipins that associate with MurJ and reduce lipid II binding (Bolla et al. 2018). Furthermore, MurJ inhibitors inspired from the human microbiome, synthesized on the basis of bioinformatics predictions, have been shown to potentiate  $\beta$ -lactams, making the combination effective even against the infamous methicillin-resistant *S. aureus* (MRSA) and vancomycin-resistant *E. faecalis* (VRE) (Lai et al. 2017).

### 6.7.3 Polymerization of the Peptidoglycan Network

After the lipid II is exported, it needs to be incorporated into the existing PGN. Therefore, two types of enzymes are essential. Glycosyltransferases (GT) attach the nonreducing end of the existing PGN strand via a  $\beta$ -1,4-glycosidic bond to the lipid II (Lovering et al. 2007), and transpeptidases (TP) assemble the peptide cross-links (Lovering et al. 2012); both reactions are demonstrated in Fig. 6.16. Penicillin-binding proteins (PBPs), named after their susceptibility for  $\beta$ -lactam antibiotics, are important enzymes in this process. They can be either bifunctional GT/TP (class A, aPBPs) or monofunctional TP (class B, bPBPs). Most species possess a variety of PBPs for different conditions like growth, division, stress, and antibiotic resistance, and they are spatially and temporally regulated by protein-protein interactions (Egan et al. 2015) with activator proteins like LpoA (Sathiyamoorthy et al. 2017) and LpoB, a regulator of PBP1B (Egan et al. 2014; King et al. 2014). Even though monofunctional GT like MtgA in *E. coli* (Di Berardino et al. 1996; Vollmer and Bertsche 2008) were found, the bifunctional aPBPs were presumed to be the major GT. However, aPBPs are not the only PGN GT. It has been shown that *B. subtilis*

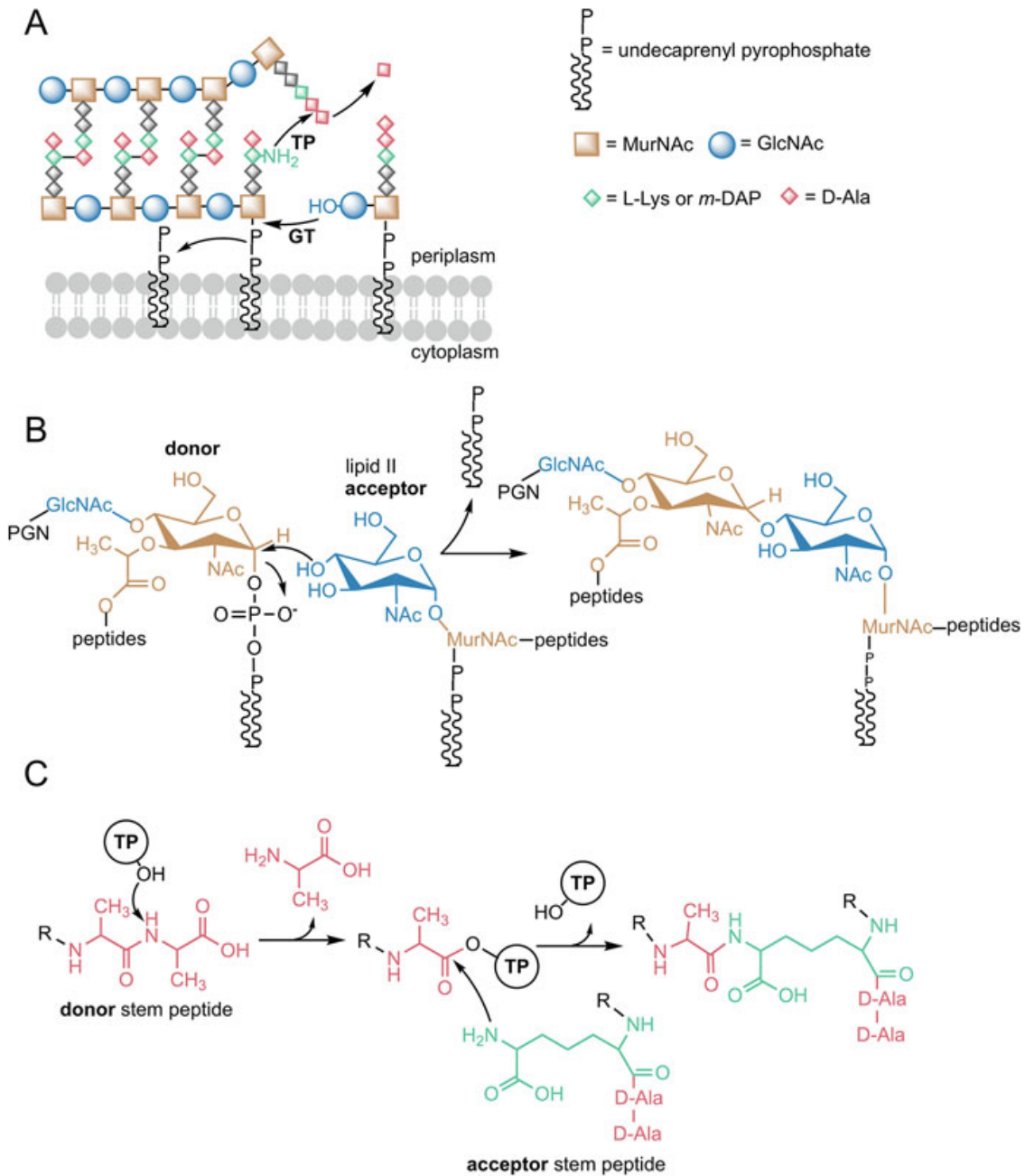


**Fig. 6.16 Glycosyltransferase (GT) and transpeptidase reaction (TP).** (a) The growing PGN chain gets transferred onto lipid II via a GT followed by peptide cross-linking between D-Ala on position 4 of the donor stem peptide L-Lys or *m*-DAP on position 3 of the acceptor stem peptide. (b) GT reaction in detail: the growing PGN strand is the donor for a new lipid II acceptor; the C4 hydroxyl group on the lipid II GlcNAc attacks the C1 on MurNAc of the donor releasing undecaprenyl-pyrophosphate, and a new  $\beta$ -1,4-glycosidic bond is formed. (c) TP reaction in detail: The hydroxyl group of serine in the transpeptidase attacks the peptide bond between the D-Ala-D-Ala on the donor stem peptide, releasing the terminal D-Ala and forming an enzyme substrate intermediate, which can be attacked by the free amino group of the diamino acid on position 3 of the acceptor stem peptide (in this example *m*-DAP) releasing the transpeptidase and covalently bonding the two stem peptides forming the cross-link

deficient in all aPBPs is still viable (McPherson and Popham 2003). The crucial role of SEDS (shape, elongation, division, and sporulation) family PGN polymerases has been demonstrated. The overexpression of RodA, a member of the Rod complex involved in cell elongation, can compensate aPBP deletion (Meeske et al. 2016). Also a screening with the known GT inhibitor moenomycin revealed the SEDS protein RodA as the missing GT in *B. subtilis* with a novel catalytic mechanism (van Heijenoort et al. 1987), since it was not inhibited by moenomycin (Emami et al. 2017). While RodA is necessary for cell elongation, the SEDS protein FtsW is suggested to be the GT of the divisome (Henrichfreise et al. 2016). RodA and FtsW form cognate enzyme pairs with the monofunctional PGN TP PBP2B and FtsI, making them specialized GT/TP pairs acting on their specific subcellular sites (Egan et al. 2015; van der Ploeg et al. 2015). They are also independent from the multifunctional aPBPs, which function outside of the elongasome and divisome independent from SEDS proteins (Cho et al. 2016). Instead of having one of the common GT folds (GT-A and GT-B), the murein GT of family G51 resemble lysozyme (Coutinho et al. 2003). The GT domain features an active site cleft between an  $\alpha$ -helical head subdomain and a membrane-fixed jaw domain. Same as lysozyme, the active site cleft is occupied by six sugar moieties. Inside the jaw domain, a hydrophobic channel binds the acyl chain of lipid II (Lovering et al. 2007). After polymerization, the glycan strands can be further modified. The *O*-acetyltransferase OatA, an integral membrane protein, acetylates MurNAc at the C6 hydroxyl group conveying lysozyme resistance (Bera et al. 2005). Additionally, the C6 *O*-acetylation of GlcNAc has been described in *Lactobacillus plantarum*, which protects the cells from autolysins in a similar manner as MurNAc *O*-acetylation (Bernard et al. 2011). Also GlcNAc *N*-deacetylation by PgdA in *Streptococcus pneumonia* (Vollmer and Tomasz 2000) and MurNAc *N*-glycosylation by NamH can be observed in mycobacteria (Raymond et al. 2005).

The glycan strands polymerized by GT are incorporated into the cell wall by TP, which catalyze the cross-linking of peptide stems between adjacent glycan strands (Archibald et al. 1993; Foster and Popham 2002). The active site of TP features a catalytic serine and a general base, lysine (Goffin and Ghuysen 1998). The donor stem peptide binds non-covalently to the TP, the serine attacks the *D*-Ala-*D*-Ala peptide bond forming an acyl intermediate, and the terminal *D*-Ala is released. The acyl intermediate can be cross-linked with the acceptor stem peptide (McDonough et al. 2002) by a nucleophilic attack of the non- $\alpha$ -amino group of the dibasic amino acid (Gram-negatives and bacilli) or the last amino acid of the cross-bridge peptides (most Gram-positives) on position 3 of the acceptor stem peptide toward the C-terminus of *D*-Ala on position 4 of the donor stem peptide (Lovering et al. 2012; Sobhanifar et al. 2013). Even though the amino acids differ, the mechanism is conserved across species (Lupoli et al. 2011). During the reaction, undecaprenyl-PP is released and de-phosphorylated, yielding the lipid carrier bactoprenol, which is flipped back to be reused for new lipid II assembly (El Ghachi et al. 2005; van Heijenoort 2007). The enzymes with *D*,*D*-TP activity are known as PBPs, since  $\beta$ -lactam antibiotics like penicillin mimic the *D*-Ala-*D*-Ala dipeptide substrate (Tipper and Strominger 1965) inducing a *D*,*D*-TP active-site serine attack on the  $\beta$ -lactam

ring resulting in a covalent complex and impaired TP activity (Lovering et al. 2012). Some PBPs have evolved to be resistant against  $\beta$ -lactam antibiotics like PBP2a, which functions as an alternative to PBP2 and can be found in MRSA. The TP domain of PBP2 is rendered inactive with the TP of PBP2a being used instead (Lim and Strynadka 2002).

The 4,3-D,D-cross-links formed by the majority of transpeptidases such as PBPs can be exchanged with 3,3-L,D-cross-links under stress conditions like  $\beta$ -lactam antibiotics, to which L,D-TP have a much lower affinity. In *Mycobacterium* the L,D-transpeptidation is abundant even during growth without  $\beta$ -lactam stress (Lavollay et al. 2008). The production of the *E. coli* L,D-TP YcbB in combination with elevated ppGpp alarmone levels bypasses all D,D-TP activity and leads to broad-spectrum  $\beta$ -lactam resistance. YcbB uses only a tetrapeptide stem as a substrate, not a classical pentapeptide stem. D,D-carboxypeptidases like DacA are essential for subsequent L,D-TP activity, since they cleave off the D-Ala of the pentapeptide stem, providing the tetrapeptide (Hugonnet et al. 2016). Interestingly, the L,D-TP Ldt<sub>Mt2</sub> of *M. tuberculosis* only cross-links stem peptides with amidated *m*-DAP, making the responsible amidotransferase AsnB an attractive target for anti-mycobacterial drugs (Ngadjjeua et al. 2018).

Recently, a nifty strategy for in situ labeling of PGN with fluorescent D-amino acids (FDAAs) in combination with fluorescence microscopy has been introduced, allowing to directly visualize PGN biosynthesis within cells and to study the location of enzymes involved in cell wall deposition (Kuru et al. 2015; Hsu et al. 2017). The labeling is based on the inherent promiscuity of bacterial PBPs and L,D-TP, which, instead of catalyzing cross-linkages of PGN, performs a transpeptidation reaction that incorporate FDAAs (Fig. 6.17) (Hsu et al. 2017). The synthesis of FDAAs with different emission wavelengths spanning the entire visible spectrum (Hsu et al. 2017) (see Figs. 6.17 and 6.18) allows to add different dyes at different times to obtain a virtual time lapse labeling zones of active PGN synthesis (Fig. 6.18). This technique has emerged using an important and effective tool for studies of PGN synthesis and dynamics.

#### 6.7.4 Peptidoglycan Deposition in Cell Walls

The different cell shapes of bacterial species require individual structural organization of the cell wall for cell growth and division. While coccoid bacteria like *S. aureus* can rely solely on PGN synthesis during cell division, rod-shaped bacteria like *E. coli* and *B. subtilis* need a synthesis machinery that is able to provide lateral cell wall growth for cell elongation. The insertion of cell wall in these rod-shaped bacteria is dispersed throughout the lateral body and mainly excludes the inert polar caps. This contrasts with the polar growth prevalent in Gram-positive *Actinomycetales*, including mycobacteria, and in Gram-negative  $\alpha$ -proteobacteria. In these bacteria the zone of cell wall growth resides at the polar tip region. In all cases, however, bacteria need to divide, and thus, the cell wall synthesis machinery at the division site, the divisome, is widespread across bacterial species and described in detail in the next section. It uses

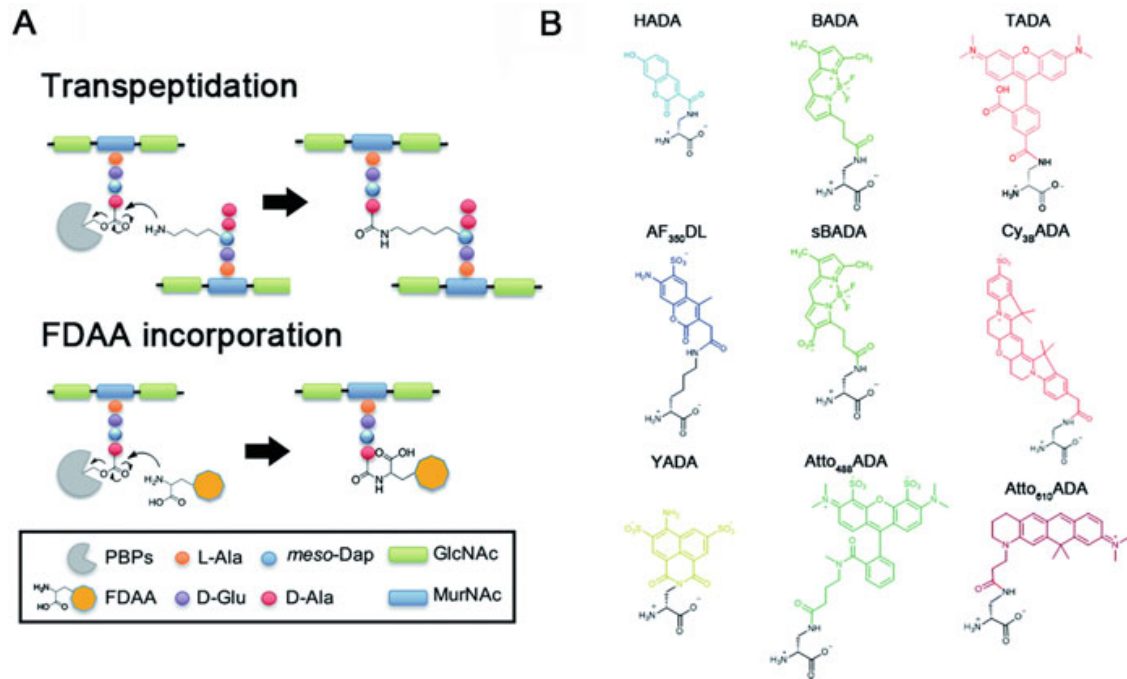


**Fig. 6.17 Cell wall synthesis and labeling with fluorescent D-amino acids.** (a) Comparison between transpeptidation (PGN cross-linking) and incorporation of FDAA, both reactions are performed by PBPs. The PBP peptide intermediate is attacked by a free amino group of *m*-DAP, resulting in cross-linking. The amino group of the fluorescently labeled lysin can attack the donor acyl group as well, resulting in FDAA incorporation. (b) Different fluorescence labels can enable the use of different fluorescent colors to illustrate growth dynamics. (This figure was taken from Hsu et al. (2017). Copyright (2008) National Academy of Sciences)

the protein FtsZ, a homologue to the eukaryotic tubulin, to form a contractile ring powered by its GTPase domain to constrict the cell, while new PGN is incorporated and the daughter cells are separated by hydrolases. Rod-shaped bacteria require lateral growth, for which they, among others, use a machinery named Rod complex, described in more detail in a following section. In principle the synthesis machinery circumferentially moves around the cell guided by the cytoskeleton consisting of a bacterial homologue to eukaryotic actin (such as MreB), where mature PGN is broken up by hydrolysis to incorporate a new cell wall in a “break before make”-like fashion (Zhao et al. 2017). Interestingly, some symbiotic rod-shaped bacteria, attached to their host on one cell pole, seem to divide across their longitudinal axis with their divisome spanning across the length of the cell (Pende et al. 2018). Some filamentous bacteria like *Streptomyces* grow by tip extension and initiation of new branches. The polar growth is directed by the cytoskeletal-like protein DivIVA, which acts as a polar recruitment factor to assemble the cell wall synthesis machinery named polarisome (Flärdh 2010). Recently discovered bacteria-specific factors are the bactofilins, which are polymer-forming proteins that shape elongated structures in the cell poles of *Myxococcus xanthus* and provide a scaffold for the chromosome segregation machinery (Lin et al. 2017). In the next two sections, the cell division and elongation will be discussed in more detail with a focus on the model organisms *E. coli* and *B. subtilis*.

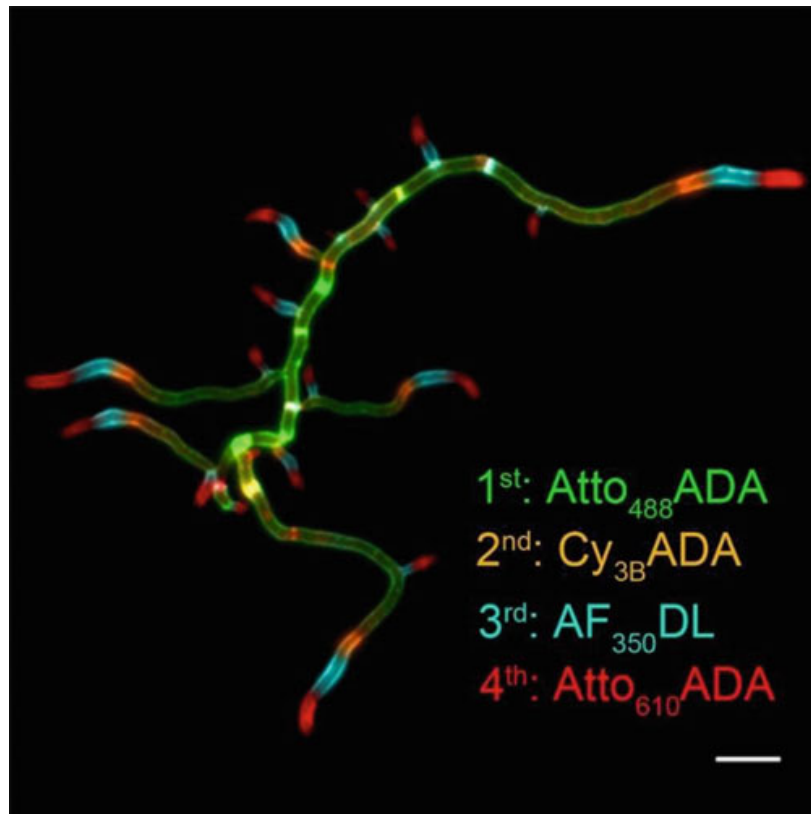


**Fig. 6.18** Successive FDAA labeling in polar growing bacteria, *Streptomyces venezuelae*. This labeling method is known as virtual time-lapse labeling (Hsu et al. 2017). Labeling with different FDAA visualizes apical growth of *Streptomyces* and the formation of new branches; first labeling 3 h with Atto<sub>488</sub>ADA (green), second labeling 15 min with Cy<sub>3B</sub>ADA (orange), third labeling 15 min with AF<sub>350</sub>DL (cyan), and fourth labeling 15 min with Atto<sub>610</sub>ADA (red); between every labeling step the previous FDAA were washed out. (This figure was taken from Hsu et al. (2017). Copyright (2008) National Academy of Sciences)

#### 6.7.4.1 Cell Division

The cell division machinery is best understood in the model organisms *E. coli* and *B. subtilis*. A simplified scheme with the essential divisome components is shown in Fig. 6.19. The cell division genes in *E. coli* were discovered using thermosensitive mutants that exhibited a filamentous phenotype with cells unable to divide. Therefore, the genes were named *fts* for their filamentous temperature-sensitive phenotype (Rowlett and Margolin 2015). One of the first components discovered by immunogold labeling was FtsZ, forming a structure that is called the Z ring at the site of mid-cell division of *E. coli* (Bi and Lutkenhaus 1991). Successively, it was shown that FtsA, FtsQ, FtsW, and FtsI also localize at the division site in a FtsZ-dependent manner (Addinall and Lutkenhaus 1996; Weiss et al. 1997; Wang et al. 1998; Buddelmeijer et al. 1998). FtsN localization depends on the prior localization of FtsZ and FtsA (Small and Addinall 2003). FtsZ, the initiator of division, polymerizes at the inner face of the cytoplasmic membrane forming filaments (Michie and Lowe 2006). The Z ring anchors a dynamic multiprotein complex with structural, cell wall synthesis, and turnover proteins (Egan and Vollmer 2013). The FtsZ

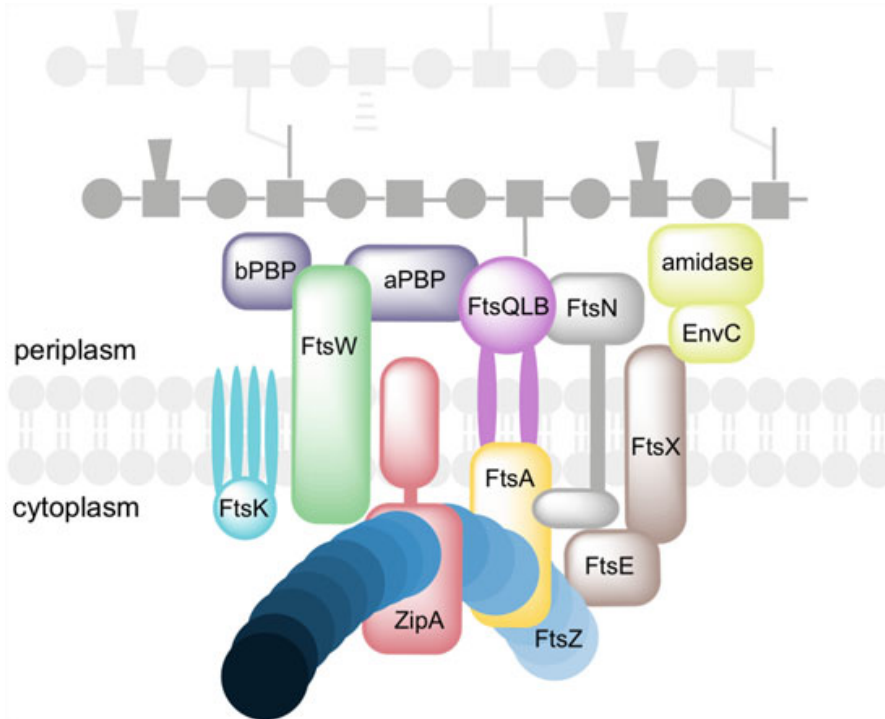


**Fig. 6.19 Scheme displaying the essential divisome components.** FtsZ (blue) filaments form the Z ring, which is able to contract by FtsZ GTPase activity. ZipA (red) and FtsA (yellow) anchor the Z ring to the cytoplasmic membrane. The FtsEX (brown) ATP transporter recruits EnvC (lime) to the septum, which in turn activates amidases (lime) that cleave PGN cross-links in order to separate the two daughter cells. FtsK (cyan) consists of a DNA translocase domain and four membrane-spanning segments, which might play a role in fusion of the invaginating membrane. The FtsQLB complex (purple) might function as a link between the Z ring and PGN synthesis enzymes. The role of FtsW (green) is not completely understood, being a RodA homologue TG activity is possible; however, flippase activity has been demonstrated as well. FtsW interacts with class aPBPs and bPBPs (violet). FtsN (gray) interacts with FtsQLB and FtsA initiating synthesis

filament displays a rotational, inward movement driven by its own GTPase activity. The movement coincides with the deposition of new cell wall material (Yang et al. 2017; Bisson-Filho et al. 2017). FtsZ generating its own motion, inducing cell wall synthesis in the process, might be necessary to apply enough force for cell division (Zhao et al. 2017). The two essential division proteins ZipA and FtsA interact directly with FtsZ and are required to recruit additional division proteins (Hale and de Boer 1997; Wang 1997; Pichoff 2002). ZipA possesses a N-terminal membrane-spanning domain and a C-terminal domain that binds FtsZ (Hale and de Boer 1997) and can bundle FtsZ protofilaments in vitro (Hale et al. 2000). Although FtsA, which is structurally related to eukaryotic actin, has no membrane-spanning domain, it has a conserved C-terminal amphipathic helix that targets FtsA to the membrane and to the Z ring. FtsA is much more conserved in bacteria than ZipA, suggesting it to be the main membrane anchor for the Z ring (Pichoff and Lutkenhaus 2005). After formation of the Z ring, at least nine additional proteins are recruited to this domain (Schmidt et al. 2004; Goehring and Beckwith 2005). FtsE and FtsX encode an ABC transporter homologue to the *lol* system in *E. coli* (Schmidt et al. 2004) with the transmembrane component FtsX and the ATPase FtsE. Interestingly, FtsEX is only

essential in low-salt media (Reddy 2007). FtsEX has been identified as a regulator of cell wall hydrolysis at the division site. Via a periplasmic loop of FtsX, EnvC is recruited to the septum. EnvC is activated by conformational changes of FtsEX, mediated by ATP hydrolysis in the cytoplasm. EnvC subsequently activates the amidase AmiB, which splits dividing cells (Yang et al. 2011). The FtsQLB enzyme complex activity is unknown; however, it seems to function as a link between the Z ring and PGN synthesis enzymes (Goehring and Beckwith 2005). FtsK consist of a DNA translocase domain and four membrane-spanning segments (Begg et al. 1995). The latter may play a role in fusing the invaginating membrane to complete cytokinesis (Fleming et al. 2010). FtsI and FtsW are orthologues of PBP2 and RodA, respectively (Typas et al. 2012), which are the major TP and TG during cell elongation as part of the Rod complex. However, FtsW has been reported to have flippase activity (Mohammadi et al. 2011), but the identification of RodA as a TG instead of a flippase suggests the same for FtsW. Moreover, both TG form cognate enzyme pairs with a TP (Henrichfreise et al. 2016). On the other hand, FtsW forms a complex with bPBP3 and aPBP1B, which as a bifunctional PBP possesses a TG domain. Intriguingly, FtsW negatively regulated aPBP1B in in vitro assay and did not exhibit TG activity in these experiments (Leclercq et al. 2017). The trigger for septation is the arrival of FtsN at the division complex (Goehring and Beckwith 2005; Gerding et al. 2009), which is a bitopic protein with a short cytoplasmic region and a large periplasmic region connected by a transmembrane domain (Dai et al. 1993). FtsN is suggested to act on both sides of the membrane inducing a conformational change in both FtsA and the FtsQLB complex de-repressing septal PGN synthesis and membrane invagination in *E. coli*. Thus, a premature start of synthesis is prevented, while the complex is not yet assembled completely (Liu et al. 2015). Cell separation is regulated differently in Gram-positive and Gram-negative bacteria (Yang et al. 2011). The septal PGN shared between the daughter cells needs to be split by hydrolases in order to complete the division (Vollmer et al. 2008b). These hydrolases need to be tightly regulated together with PGN synthesis since too much hydrolysis activity would bear the danger of cell lysis (Uehara and Bernhardt 2011). In *E. coli* the LytC-type amidases AmiA, AmiB, and AmiC are most important (Heidrich et al. 2001). The divisome-associated proteins EnvC and NlpD contain LytM domains, which usually possess endopeptidase activity against PGN cross-links (Firczuk and Bochtler 2007b). However, experiments have shown that rather than directly cleaving PGN, EnvC activates AmiA and AmiB and NlpD activates AmiC (Uehara et al. 2010). Since EnvC is activated by FtsEX, which interacts with FtsZ (Corbin et al. 2007), the amidase activation could be coupled directly with the contraction of the Z ring, enabling amidase activity only after the start of synthesis without the risk of cell lysis (Yang et al. 2011). In Gram-positive bacteria the expression of PGN hydrolase gene is controlled among others by the WalK/WalR regulon, a key player in the maintenance of cell wall homeostasis. The WalR response regulator, being phosphorylated by the WalK kinase, induces the expression of PGN hydrolases and represses the expression of their inhibitors (Dubrac et al. 2008). WalK seems to interact with components of the septal ring and needs an intact divisome in order to phosphorylate WalR (Fukushima et al. 2011). The localization



and activity of hydrolases seem to be controlled by teichoic acid distribution (Yamamoto et al. 2008; Schlag et al. 2010) as well as the acetylation status of the sugar backbone (Moynihan and Clarke 2011).

#### 6.7.4.2 Cell Elongation

Cell elongation is conducted by a multiprotein complex (Laddomada et al. 2016; Egan et al. 2017). The essential components are depicted in Fig. 6.20. The eukaryotic actin homologue MreB, which is localized on the lateral cell wall (Jones et al. 2001), directs the spatiotemporal elongation process (van den Ent et al. 2001). A loss of MreB, which is found in most rod-shaped bacteria, leads to a reduced lateral cell wall synthesis and eventually to a loss of the rod shape. MreB localizes in areas of negative Gaussian curvature where the cell shape is dented and therefore needs strengthening. Thereby, the rod shape is initiated and maintained (Ursell et al. 2014). Interestingly, MreB orthologues have not been found in coccoid bacteria (Zapun et al. 2008). The polymerization of MreB, which happens in the presence of ATP, results in antiparallel double filaments that form a patch-like structure bound to the membrane via a

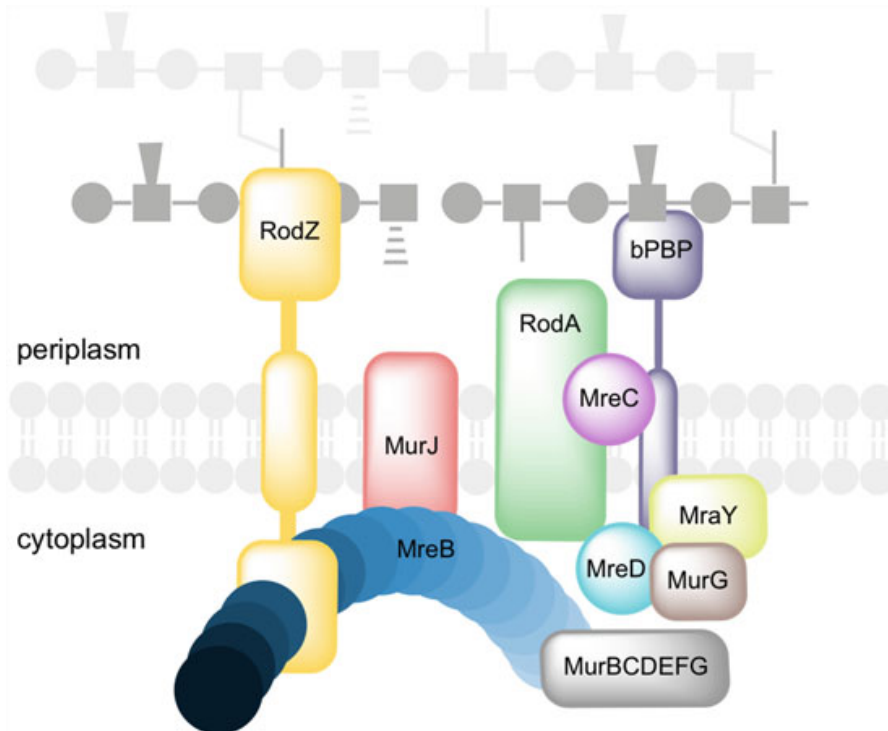


**Fig. 6.20 Essential components of the Rod complex.** The actin homologue MreB (blue) polymerizes in patches rotating circumferentially. RodZ (yellow) connects MreB filaments with PGN; that way PGN synthesis can drive the rotation of the Rod complex. The flippase MurJ (red) provides lipid II for the glycosyltransferase RodA (green); the peptide cross-linking is conducted by bPBPs (violet). MreC (purple) controls the spatial organization of PBPs in the periplasm. MreD (cyan) interacts with the precursor synthesis enzymes MraY (lime) and MurG (brown) as well as determining MreB location. MreB also recruits the MurBCDEF precursor synthesis enzymes (gray), providing a high amount of precursors at the Rod complex location

hydrophobic loop and N-terminal amphipathic helix (van den Ent et al. 2001; Salje et al. 2011; van den Ent et al. 2014; Errington 2015). RodZ, an integral transmembrane protein, assembles as a complex with MreB (van den Ent et al. 2010) and mediates MreB rotation by coupling MreB to the cell wall synthesis enzymes, RodA (TG) and PBP2 (TP). The rotation is required for the robustness of rod shape and growth under cell-wall stress conditions (Morgenstein et al. 2015). This complex (MreB-RodAZ-bPBP) will be referred to as the Rod complex. Instead of forming continuous filaments, MreB rotates circumferentially around the cell in patches, the motion driven by bPBP activity and the presence of RodA. Yet at least in *E. coli*, the activity of aPBPs is not necessary (Dominguez-Escobar et al. 2011; Garner et al. 2011). Hence, the MreB movement is not driven by its own polymerization, but the periplasmic cell wall synthesis machinery, acting like a motor, pulls the MreB patches in the cytoplasm and periplasmic and cytoplasmic components connected via RodZ across the membrane (van Teeffelen et al. 2011). The location of synthesis is also coordinated by MreC, controlling the spatial orientation of the penicillin-binding proteins in the periplasm, and MreD, interacting with the precursor synthesis enzymes MurG and MraY as well as determining MreB localization. Additionally, MreB cables are required for the organization of MurBCEF (White et al. 2010) and can even recruit DapI, the enzyme required for the synthesis of *m*-DAP (Rueff et al. 2014). All in all, this leads to a concentrated precursor availability near the Rod complex. In vivo cell wall polymerase assays in *E. coli* revealed that cell wall synthesis is mediated by two distinct polymerase systems, the Rod complex and the aPBPs, the latter being active outside of the Rod complexes (Cho et al. 2016). *B. subtilis* flippase Amj can replace the *E. coli* flippase MurJ. Since Amj and MurJ are no homologues, it is unlikely for Amj to interact with either synthesis complex, suggesting that flippases work independently from both Rod complex and aPBPs (Meeske et al. 2015). RodA TG activity contributes significantly to the lateral cell wall synthesis in *E. coli* (Cho et al. 2016), but unlike in Gram-positive bacteria, where RodA is sufficient to sustain growth, the Gram-negative bacterium *Vibrio cholerae* relies on the bifunctional PBP1A during transition into stationary phase (Dörr et al. 2014). A model for a flippase providing for both RodA/bPBP and aPBP independently is shown in Fig. 6.21. PGN is a rigid molecule that needs to be broken before the insertion of new material for cell elongation (Vollmer et al. 2008b). The *B. subtilis* hydrolases LytE and CwlO are essential for cell elongation, since their inactivation blocks the process (Bisicchia et al. 2007). Both LytE, localizing at the septa, poles and the cylindrical part of the cell, and CwlO, localizing at the cylindrical part, are essential for cell proliferation and the only D,L-endopeptidases acting on the lateral cell wall. Chimeric protein assays with LytF and CwlS, which localize to the septum and hydrolyze PGN during cell division (Fukushima et al. 2006), revealed that the N-terminal domain is responsible for the localization (Hashimoto et al. 2011). Furthermore, a deletion of LytE or CwlO severely impairs transformation efficiency in *B. subtilis*, which indicates a possible role in the natural competence of *B. subtilis* (Liu et al. 2018). Remarkably, FtsX, which is known to be involved in cell division in *E. coli*, has been shown to be required for CwlO hydrolase activity during cell wall elongation in *B. subtilis* (Meisner et al. 2013; Dominguez-Cuevas et al. 2013). Prior to the incorporation of new cell wall material,

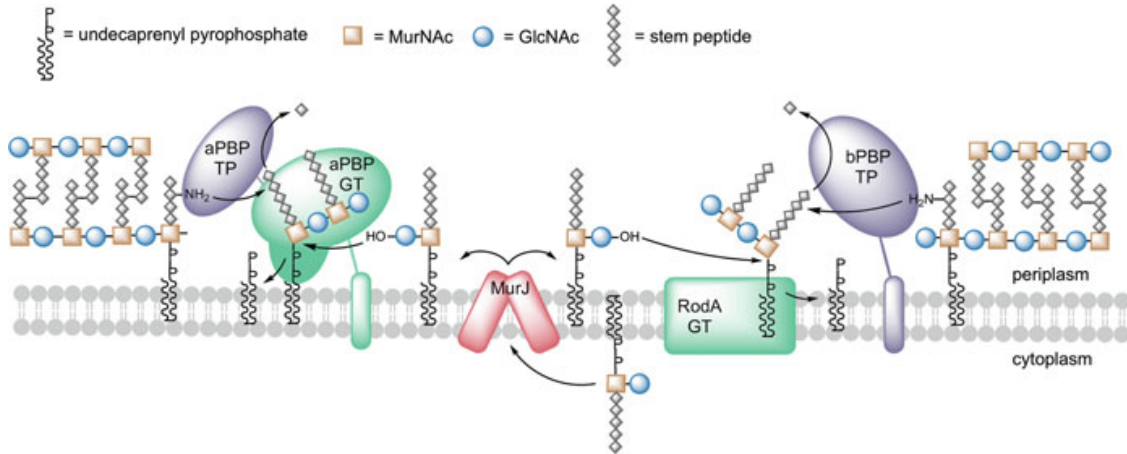


**Fig. 6.21 Model for lateral cell wall synthesis by aPBPs and RodA/bPBPs during cell elongation.** The MurJ flippase (red) provides lipid II for both synthesis machineries, which are either single-acting aPBPs with GT (green) and TP (violet) domains or a combination of the GT RodA (green) with bPBPs (violet) that work together as part of the Rod complex

the existing cell wall needs to be cleaved by endopeptidases (Vollmer 2012). Matching this hypothesis, MreB homologues in *B. subtilis* have been shown to direct LytE as well as CwIO (Dominguez-Cuevas et al. 2013). Based on these recent discoveries, Zhao et al. (2017) proposes a “break before make” mechanism, where endopeptidases cleave cross-links in mature PGN. Rod A then provides a template PGN strand, with the circumferentially moving Rod complex, which is attached to the sacculus by bPBPs. Subsequently, aPBPs, exhibiting a diffusive motion with prolonged persistence (Cho et al. 2016; Lee et al. 2016), generate additional strands along the template and connect them to the existing PGN (Zhao et al. 2017). However, it has also been shown in *E. coli* that endopeptidase activity increases cell wall attachment of aPBPs during bPBP2 inhibition, indicating Rod complex independent starting points of cell wall synthesis (Lai et al. 2017).

## 6.8 The Dynamic Cell Wall: Peptidoglycan Turnover and Recycling

The bacterial cell wall is not static but subject to constant degradation and resynthesis, in a process that is called cell wall or PGN turnover (Boothby et al. 1973; Doyle et al. 1988; Park and Uehara 2008; Reith and Mayer 2011). During cell growth (elongation), cell division, as well as various processes of adaptation, due to osmotic challenges, starvation, or exposure to antibiotics, the PGN is steadily remodeled and newly synthesized to adapt structure and shape. Thereby, the PGN is partially cleaved and renewed at a significant rate. It has been calculated that as much as 50% of cell wall material per generation is turned over (Park and Uehara 2008; Reith and Mayer 2011; Borisova et al. 2016). At the same time, old PGN is removed and degraded. Cell wall degradation and turnover are conducted by PGN hydrolases

and lytic transglycosylases (LTs), termed autolysins, as they have the potential to lyse its own cell wall (Smith et al. 2000). Thus, the PGN turnover must occur without compromising its stabilizing function in a delicately balanced manner. The tight connection between cell wall lysis and synthesis has been demonstrated by interaction of respective enzymes, stressing the significance of cell wall turnover for bacterial cell growth (Vollmer and Bertsche 2008; Egan et al. 2017). Considering the huge amounts of material, it seems reasonable that bacteria recover the released PGN fragments to save on resources. Only up to 8% of the cell wall material was found to be released to the medium in the Gram-negative bacterium *E. coli* (Goodell and Schwarz 1985); however, the major part of PGN is efficiently recycled (Goodell 1985). PGN fragments derived from the turnover process are taken up and intracellularly reused for energy metabolism or PGN de novo synthesis (Park and Uehara 2008; Johnson et al. 2013; Gisin et al. 2013). In many Gram-negative bacteria, a direct shortcut pathway exists that converts recycled amino sugars to UDP-activated PGN precursors and thus leads to intrinsic resistance to the antibiotic fosfomycin, shown in Fig. 6.15 (Gisin et al. 2013; Borisova et al. 2017). This pathway is absent in Gram-positive bacteria, but it was shown recently that *B. subtilis*, *S. aureus*, and *Streptomyces coelicolor* do recycle their PGN via a pathway that involves the use of MurNAc (Borisova et al. 2016). The following sections will briefly summarize current knowledge of the PGN turnover and recycling in the model organisms *E. coli*, *B. subtilis*, and *S. aureus*.

### 6.8.1 Cell Wall Hydrolases and Autolysins

Autolysins, lytic enzymes acting on the producers own cell wall, can be classified as glycosidases and amidases (Smith et al. 2000; van Heijenoort 2011). There is a specialized group of lytic enzymes for almost every bond within the bacterial cell wall (an overview is given in Fig. 6.22). The sugar backbone in general can be cleaved by exo- or endo-acting *N*-acetylglucosaminidases and *N*-acetylmuramidases (e.g., lysozyme), which target either of the two distinct glycosidic bonds within the PGN, GlcNAc- $\beta$ -1,4-MurNAc or MurNAc- $\beta$ -1,4-GlcNAc, respectively (Höltje 1995). A very distinct family of MurNAc- $\beta$ -1,4-GlcNAc-cleaving enzymes are the lytic transglycosylases (LTs), which, unlike lysozyme and other muramidases, do not hydrolyze this bond. Instead they cleave the glycosidic bond by an intramolecular attack of the 6-hydroxyl group, thereby generating an 1,6-anhydro bond at the MurNAc residue (Scheurwater et al. 2008). By the action of lytic transglycosylases, anhydro-muropeptides (GlcNAc-anhydro-MurNAc-peptides) are released. They are subsequently recovered by a specific transporter and further reused in a process called cell wall or PGN recycling (Park and Uehara 2008). *E. coli* has a soluble Slt70 LT as well as the membrane-bound MltA, B, C, D, E, and F LTs, which are anchored in the outer membrane facing the periplasm with their catalytic domains. MltA and MltB are exoenzymes that cut from the reducing end of the glycan chain (Vollmer and Bertsche 2008; Scheurwater et al. 2008). *B. subtilis* has the Slt70 homologues,

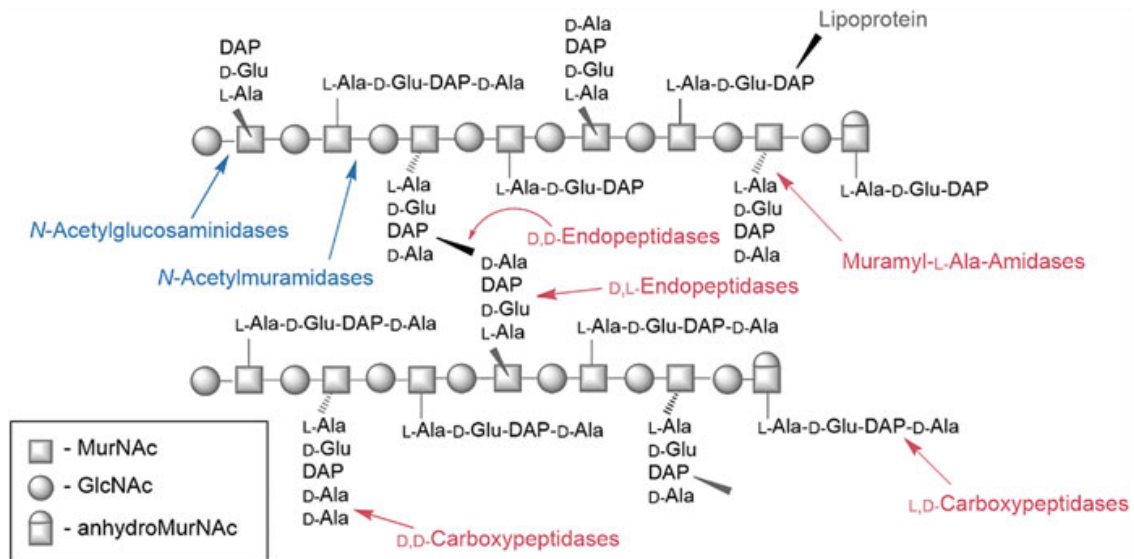


**Fig. 6.22 Cleavage sites within the PGN sugar backbone PGN hydrolases, potential autolysins.** *N*-acetylglucosaminidases and *N*-acetylmuramidases (blue) cleave the glycosidic bond between GlcNAc-MurNAc and MurNAc-GlcNAc, respectively. For every peptide bond within the cross-link, specialized enzymes can be found with often redundant function (red). In general, the cleavage of five different bonds is possible. The amide bond between the lactyl residue of MurNAc and L-Ala can be cleaved by muramyl-L-Ala-amidases. D,D-Endopeptidases cleave D,D-peptide bonds, e.g., between *m*-DAP and D-Ala and between cross-linked stem peptides, whereas D,L-endopeptidases cleave D,L-bonds like D-Glu-DAP. Carboxypeptidases cleave uncross-linked stem peptides between D-Ala-D-Ala (D,D-carboxypeptidases) or *m*-DAP-D-Ala (L,D-carboxypeptidases). This figure was modified after (Mayer 2012)

CwIP and CwIQ, the latter being a bifunctional enzyme with muramidase and lytic transglycosylase activity. The major autolysins during vegetative growth, however, are the *N*-acetylglucosaminidases LytD and LytG (Smith et al. 2000; Horsburgh et al. 2003; Sudiarta et al. 2010). PGN amidases are abundant and diverse with more than several enzymes for each amide linkage. This redundancy emphasizes their crucial function, since a bacterial cell cannot for instance afford their inhibition by antibiotics. Amidases can be classified by their mode of action into metallo-, serine- and cysteine-amidases and further discriminated into nine different fold groups (Firczuk and Bochtler 2007a). Metal-dependent amidases, the structurally most diverse group, represent five- out of the ninefolds. They all feature a single  $Zn^{2+}$  in their active site with the exception of the *B. subtilis* D,D-aminopeptidase DppA, which has two  $Zn^{2+}$  and cleaves the D-Ala-D-Ala peptide bond (Cheggour et al. 2000; Remaut et al. 2001). In *E. coli*, the penicillin-insensitive D,L-endopeptidase MepA (Marcyjaniak et al. 2004) and D,D-endopeptidase MpaA (Uehara and Park 2003) are examples of metallo amidases. Representative of the cysteine amidases are classified within the L,D-transpeptidases (Ldt) family, some of them acting as transpeptidases rather than amidases under physiological conditions (Magnet et al. 2007a). Serine amidases can be categorized into a L,D-carboxypeptidase and  $\beta$ -lactamase type (Firczuk and Bochtler 2007a). LdcA of *E. coli* belongs to the former type and is involved in PGN recycling in the cytoplasm (Templin et al. 1999).

Some  $\beta$ -lactamase-type members possess  $\beta$ -lactamase or transpeptidase rather than hydrolase activities (Scheffers and Pinho 2005). The *E. coli* PBP4 and PBP5 both have D-Ala-D-Ala carboxypeptidase activity, while PBP4 has an additional D-Ala-*m*-DAP-endopeptidase activity (Nicholas et al. 2003; Kishida et al. 2006). The membrane-associated PBP7 lacks carboxypeptidase activity and has D,D-endopeptidase activity instead that hydrolyzes the D-Ala-*m*-DAP cross-link (Romeis and Höltje 1994). The reaction mechanism of serine amidases is similar to the transpeptidation reaction with the hydroxyl group of serine attacking the amide bond and the formation of an acyl intermediate (Firczuk and Bochtler 2007a). The main four zinc-dependent Muramyl-L-Ala-amidases in *E. coli*, AmiABCD, are crucial for cell growth and separation. AmiA, B, and C deletion mutants grow in long chains unable to separate at the division site (Heidrich et al. 2001). While AmiA, B, and C are soluble enzymes in the periplasm, AmiD is an outer membrane-anchored lipoprotein (Pennartz et al. 2009). In *B. subtilis*, CwlB and CwlC possess muramyl-L-Ala-amidase function and are required for mother cell lysis during sporulation (Shida et al. 2000, 2001). The four D,L-endopeptidases LytE, LytF, CwlO, and CwlS are involved in cell morphology maintenance with varied roles in cell elongation and separation (Hashimoto et al. 2018).

### 6.8.2 Peptidoglycan Turnover, Scavenging, and Recycling

The turnover of PGN components in Gram-positive and Gram-negative bacteria, and the enzymes involved in this process, is summarized in Fig. 6.23. During PGN turnover in Gram-negative bacteria, the major fragments released by lytic transglycosylases and amidases are GlcNAc-anhydro-MurNAc-peptides (muropeptides) and small peptides. While the latter are small and may easily diffuse through the outer membrane, the former are mostly trapped within the periplasm, from which they have to be recovered for reutilization. In *E. coli*, the PGN-derived peptides (tri- and tetrapeptides) are taken up by the oligopeptide ABC-transporter Opp, which requires the periplasmic binding protein MppA to collect the peptides (Park 1993; Park et al. 1998). The muropeptides are almost exclusively taken up by the AmpG permease (Cheng and Park 2002; Park and Uehara 2008). Moreover, MurNAc and GlcNAc can be taken up by sugar-specific PTS transporters (Dahl et al. 2004). Muropeptides are processed intracellularly by the  $\beta$ -*N*-acetylglucosaminidase NagZ that cleaves off GlcNAc (Vötsch and Templin 2000; Cheng et al. 2000) and the anhydro-MurNAc-L-Ala amidase AmpD, which is highly specific for anhydro-muropeptides leaving the UDP-MurNAc-pentapeptide cell wall precursor intact (Jacobs et al. 1995). The L,D-carboxypeptidase LdcA cleaves the terminal D-Ala off the tetrapeptide, releasing the tripeptide L-Ala-D-Glu-*m*-DAP (Templin et al. 1999). The tripeptide is attached to UDP-MurNAc by the murein peptide ligase Mpl, thereby bypassing the de novo PGN biosynthesis enzymes MurCDE (Mengin-Lecreulx et al. 1996). Mpl is also able to transfer the “wrong” tetrapeptide, but this is a fatal reaction as it obviates the addition D-Ala-D-Ala by MurF (Templin et al.

1999). Anhydro-MurNAc can be further converted into MurNAc 6P by the AnmK kinase, and GlcNAc is phosphorylated by NagK (Uehara and Park 2004; Uehara et al. 2005). The etherase MurQ generates GlcNAc 6P from MurNAc 6P by cleavage of the lactyl residue. GlcNAc 6P can then be further degraded to fructose-6P by NagA and NagB and used in glycolysis or directed into PGN de

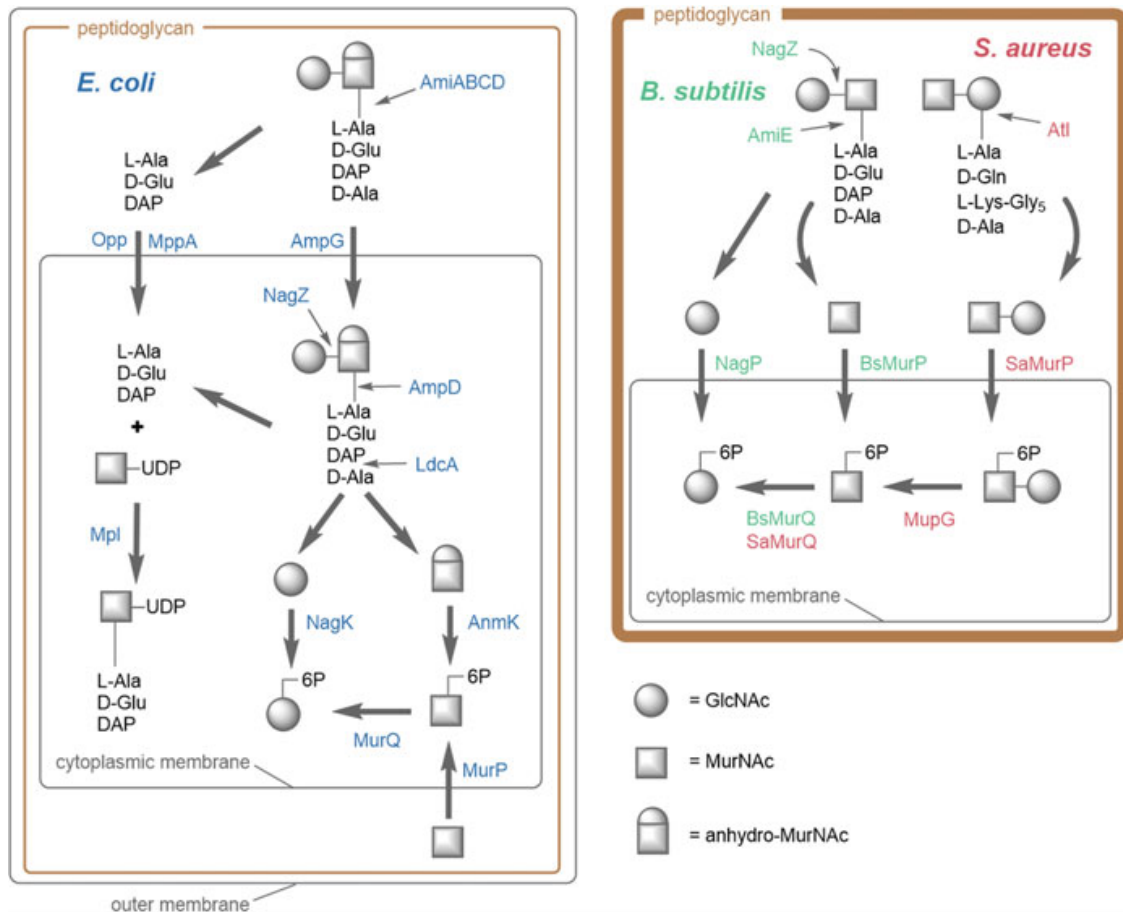


**Fig. 6.23 PGN recycling in *E. coli*, *B. subtilis*, and *S. aureus*.** *E. coli* PGN recycling metabolism (left panel; blue) involves the AmpG permease that transports anhydro-muropeptides derived from turnover into the cell; Opp transports tripeptides with the help of the periplasmic binding protein MppA; the anhydro-muropeptide is further processed intracellularly: NagZ cleaves off GlcNAc, which gets phosphorylated by NagK; AmpD cleaves off the stem peptide, from which D-Ala gets released by LdcA, and the tripeptide can be transferred onto UDP-MurNAc for new PGN synthesis; anhydro-MurNAc is phosphorylated by AnmK, and the lactyl residue is removed by MurQ yielding GlcNAc-6P, which can be channeled into either de novo PGN synthesis or catabolism; the phosphotransferase system PTS transporter MurP takes up and concomitantly phosphorylates MurNAc, generating MurNAc-6P. Both *B. subtilis* (right; green) and *S. aureus* (right; red) carry a MurQ orthologue (BsMurQ, SaMurQ, respectively). In *B. subtilis*, the major turnover products are processed outside of the cell by NagZ, which releases GlcNAc, and AmiE, which cuts off the peptide stem from MurNAc; MurNAc and GlcNAc are transported into the cell and phosphorylated by the individual PTS transporter MurP and NagP, respectively; intracellularly MurNAc-6P can be converted into GlcNAc-6P followed by de novo PGN synthesis or catabolism, similar to *E. coli*. In *S. aureus* the major autolysin Atl, a bifunctional amidase and *N*-acetylglucosaminidase, releases the disaccharide MurNAc-GlcNAc from the PGN. The PTS transporter SaMurP takes up this disaccharide and phosphorylates it yielding MurNAc-6P-GlcNAc, which is subsequently cleaved by a MurNAc-6P-glycosidase (MupG) and MurNAc-6P etherase (MurQ) (Kluj et al. 2018)

novo synthesis (Jaeger et al. 2005; Uehara et al. 2006). In *B. subtilis*, most of the recycling happens extracellularly followed by the uptake of the released products into the cell by specialized transporters. Most of the related genes are located in a putative MurNAc uptake and recovery pathway operon orthologous to *E. coli* (Reith and Mayer 2011). The *B. subtilis* NagZ, an orthologue to the *E. coli* *N*-acetylglucosaminidase, is secreted and acts on GlcNAc-MurNAc-peptide fragments, releasing GlcNAc and MurNAc-peptides, the substrate of AmiE, which cleaves the peptides from MurNAc (Litzinger et al. 2010). GlcNAc and MurNAc, released extracellularly, are taken up by the PTS transporters NagP and BsMurP, respectively, phosphorylating their substrates at C6 in the process (Reizer et al. 1988). The *B. subtilis* MurQ orthologue YbbI converts MurNAc 6P to GlcNAc 6P from which it can be utilized as a carbon source or redirected into de novo PGN biosynthesis similar to *E. coli* (Reith and Mayer 2011). Recently, a novel deviation of this pathway was recognized in *S. aureus*. The *S. aureus* PTS-transporter SaMurP, besides MurNAc, can transport and concomitantly phosphorylate MurNAc-GlcNAc, the product of PGN cleavage by Atl, the major autolysin of *S. aureus* (Kluj et al. 2018). Intracellularly, the MurNAc-6-phosphate-GlcNAc product is hydrolyzed by a novel 6-phosphomuramidase named MupG (Kluj et al. 2018).

## 6.9 Concluding Remarks

Research on PGN has attained a tremendous revival in the last years. It has long been considered as a completed field, yet actually nothing is farther from truth. New technologies have provided us with a surprisingly complex view of PGN structure, a stunning richness in variations of its composition, and intriguing new insights in its biosynthesis and assembly. As different as bacteria themselves, the PGN of each species has its own particularity. Thus, PGN has turned into a fascinating biological asset for advanced research, as well as for pharmaceutical strategies to develop antibacterial drugs,

**Acknowledgments** CM thanks Marina and Florian Alexander for their support to finish up this manuscript.

## References

- Addinall SG, Lutkenhaus J (1996) FtsA is localized to the septum in an FtsZ-dependent manner. *J Bacteriol* 178:7167–7172
- Al-Dabbagh B, Henry X, El Ghachi M, Auger G, Blanot D, Parquet C, Mengin-Lecreulx D, Bouhss A (2008) Active site mapping of MraY, a member of the polyprenyl-phosphate *N*-acetylhexosamine 1-phosphate transferase superfamily, catalyzing the first membrane step of peptidoglycan biosynthesis. *Biochemistry* 47:8919–8928



- Anderson JS, Matsuhashi M, Haskin MA, Strominger JL (1965) Lipid-phosphoacetylmuramyl-pentapeptide and lipid-phosphodisaccharide-pentapeptide: presumed membrane transport intermediates in cell wall synthesis. *Proc Natl Acad Sci USA* 53:881–889
- Anderson MS, Eveland SS, Onishi HR, Pompliano DL (1996) Kinetic mechanism of the *Escherichia coli* UDPMurNAc-tripeptide D-alanyl- D-alanine-adding enzyme: use of a glutathione S-transferase fusion. *Biochemistry* 35:16264–16269
- Andres CJ, Bronson JJ, D'Andrea SV, Deshpande MS, Falk PJ, Grant-Young KA, Harte WE, Ho HT, Misco PF, Robertson JG, Stock D, Sun Y, Walsh AW (2000) 4-Thiazolidinones: novel inhibitors of the bacterial enzyme MurB. *Bioorg Med Chem Lett* 10:715–717
- Araki Y, Nakatani T, Hayashi H, Ito E (1971) Occurrence of non-*N*-substituted glucosamine residues in lysozyme-resistant peptidoglycan from *Bacillus cereus* cell walls. *Biochem Biophys Res Commun* 42:691–697
- Archibald AR, Hancock IC, Harwood CR (1993) Cell wall structure, synthesis, and turnover. In: Sonenshein AL, Hoch JA, Losick R (eds) *Bacillus subtilis* and other Gram-positive bacteria: Biochemistry, physiology, and molecular genetics. ASM press, Washington, DC, pp 381–410
- Arnoldi M, Fritz M, Bauerlein E, Radmacher M, Sackmann E, Boulbitch A (2000) Bacterial turgor pressure can be measured by atomic force microscopy. *Phys Rev E Stat Phys Plasmas Fluids Relat Interdiscip Topics* 62:1034–1044
- Atrih A, Foster SJ (1999) The role of peptidoglycan structure and structural dynamics during endospore dormancy and germination. *Antonie Van Leeuwenhoek* 75:299–307
- Atrih A, Zöllner P, Allmaier G, Foster SJ (1996) Structural analysis of *Bacillus subtilis* 168 endospore peptidoglycan and its role during differentiation. *J Bacteriol* 178:6173–6183
- Atrih A, Bacher G, Allmaier G, Williamson MP, Foster SJ (1999) Analysis of peptidoglycan structure from vegetative cells of *Bacillus subtilis* 168 and role of PBP 5 in peptidoglycan maturation. *J Bacteriol* 181:3956–3966
- Badet B, Vermoote P, Le Goffic F (1988) Glucosamine synthetase from *Escherichia coli*: kinetic mechanism and inhibition by *N*3-fumaroyl-L-2,3-diaminopropionic derivatives. *Biochemistry* 27:2282–2287
- Badet-Denisot MA, Badet B (1992) Chemical modification of glucosamine-6-phosphate synthase by diethyl pyrocarbonate: evidence of histidine requirement for enzymatic activity. *Arch Biochem Biophys* 292:475–478
- Bartholomew JW, Mittwer T (1952) The Gram stain. *Bacteriol Rev* 16:1–29
- Batson S, de Chiara C, Majce V, Lloyd AJ, Gobec S, Rea D, Fulop V, Thoroughgood CW, Simmons KJ, Dowson CG, Fishwick CWG, de Carvalho LPS, Roper DI (2017) Inhibition of D-Ala:D-Ala ligase through a phosphorylated form of the antibiotic D-cycloserine. *Nat Commun* 8(1):1939. <https://doi.org/10.1038/s41467-017-02118-7>
- Begg KJ, Dewar SJ, Donachie WD (1995) A new *Escherichia coli* cell division gene, *ftsK*. *J Bacteriol* 177:6211–6222
- Benson TE, Marquardt JL, Marquardt AC, Etkorn FA, Walsh CT (1993) Overexpression, purification, and mechanistic study of UDP-N-acetylenolpyruvylglucosamine reductase. *Biochemistry* 32:2024–2030
- Benson TE, Walsh CT, Massey V (1997) Kinetic characterization of wild-type and S229A mutant MurB: evidence for the role of Ser 229 as a general acid. *Biochemistry* 36:796–805
- Bera A, Herbert S, Jakob A, Vollmer W, Götz F (2005) Why are pathogenic staphylococci so lysozyme resistant? The peptidoglycan *O*-acetyltransferase OatA is the major determinant for lysozyme resistance of *Staphylococcus aureus*. *Mol Microbiol* 55:778–787
- Bernard E, Rolain T, Courtin P, Guillot A, Langella P, Hols P, Chapot-Chartier MP (2011) Characterization of *O*-acetylation of *N*-acetylglucosamine: a novel structural variation of bacterial peptidoglycan. *J Biol Chem* 286:23950–23958
- Bi EF, Lutkenhaus J (1991) FtsZ ring structure associated with division in *Escherichia coli*. *Nature* 354:161–164

- Bisicchia P, Noone D, Lioliou E, Howell A, Quigley S, Jensen T, Jarmer H, Devine KM (2007) The essential YycFG two-component system controls cell wall metabolism in *Bacillus subtilis*. *Mol Microbiol* 65:180–200
- Bisson-Filho AW, Hsu YP, Squyres GR, Kuru E, Wu F, Jukes C, Sun Y, Dekker C, Holden S, VanNieuwenhze MS, Brun YV, Garner EC (2017) Treadmilling by FtsZ filaments drives peptidoglycan synthesis and bacterial cell division. *Science* 355:739–743
- Bolla JR, Sauer JB, Wu D, Mehmood S, Allison TM, Robinson CV (2018) Direct observation of the influence of cardiolipin and antibiotics on lipid II binding to MurJ. *Nat Chem* 10:363–371
- Boneca IG, Chiosis G (2003) Vancomycin resistance: occurrence, mechanisms and strategies to combat it. *Expert Opin Ther Targets* 7:311–328
- Boneca IG, Huang ZH, Gage DA, Tomasz A (2000) Characterization of *Staphylococcus aureus* cell wall glycan strands, evidence for a new  $\beta$ -N-acetylglucosaminidase activity. *J Biol Chem* 275:9910–9918
- Boothby D, Daneo-Moore L, Higgins ML, Coyette J, Shockman GD (1973) Turnover of bacterial cell wall peptidoglycans. *J Biol Chem* 248:2161–2169
- Borisova M, Gaupp R, Duckworth A, Schneider A, Dalugge D, Mühleck M, Deubel D, Unsleber S, Yu W, Muth G, Bischoff M, Götz F, Mayer C (2016) Peptidoglycan recycling in gram-positive bacteria is crucial for survival in stationary phase. *MBio* 7(5):e00923–e00916. <https://doi.org/10.1128/mBio.00923-16>
- Borisova M, Gisin J, Mayer C (2017) The N-acetylmuramic acid 6-phosphate phosphatase MupP completes the *Pseudomonas* peptidoglycan recycling pathway leading to intrinsic fosfomycin resistance. *MBio* 8(2). <https://doi.org/10.1128/mBio.00092-17>
- Botella H, Yang G, Ouerfelli O, Ehrt S, Nathan CF, Vaubourgeix J (2017) Distinct spatiotemporal dynamics of peptidoglycan synthesis between *Mycobacterium smegmatis* and *Mycobacterium tuberculosis*. *mBio*, 8(5). <https://doi.org/10.1128/mBio.01183-17>
- Bouhss A, Mengin-Lecreux D, Blanot D, van Heijenoort J, Parquet C (1997) Invariant amino acids in the Mur peptide synthetases of bacterial peptidoglycan synthesis and their modification by site-directed mutagenesis in the UDP-MurNAc:L-alanine ligase from *Escherichia coli*. *Biochemistry* 36:11556–11563
- Bouhss A, Dementin S, van Heijenoort J, Parquet C, Blanot D (2002) MurC and MurD synthetases of peptidoglycan biosynthesis: borohydride trapping of acyl-phosphate intermediates. *Methods Enzymol* 354:189–196
- Bouhss A, Crouvoisier M, Blanot D, Mengin-Lecreux D (2004) Purification and characterization of the bacterial MraY translocase catalyzing the first membrane step of peptidoglycan biosynthesis. *J Biol Chem* 279:29974–29980
- Braun V (1975) Covalent lipoprotein from the outer membrane of *Escherichia coli*. *Biochim Biophys Acta* 415:335–377
- Braun V (2015) Bacterial cell wall research in Tübingen: a brief historical account. *Int J Med Microbiol* 305:178–182
- Braun V, Rehn K (1969) Chemical characterization, spatial distribution and function of a lipoprotein (murein-lipoprotein) of the *E. coli* cell wall. The specific effect of trypsin on the membrane structure. *Eur J Biochem* 10:426–438
- Braun V, Gnirke H, Henning U, Rehn K (1973) Model for the structure of the shape-maintaining layer of the *Escherichia coli* cell envelope. *J Bacteriol* 114:1264–1270
- Brennan PJ, Nikaido H (1995) The envelope of mycobacteria. *Annu Rev Biochem* 64:29–63
- Bronson JJ, DenBleyker KL, Falk PJ, Mate RA, Ho HT, Pucci MJ, Snyder LB (2003) Discovery of the first antibacterial small molecule inhibitors of MurB. *Bioorg Med Chem Lett* 13:873–875
- Brown ED, Marquardt JL, Lee JP, Walsh CT, Anderson KS (1994) Detection and characterization of a phospholactoyl-enzyme adduct in the reaction catalyzed by UDP-N-acetylglucosamine enolpyruvoyl transferase, MurZ. *Biochemistry* 33:10638–10645
- Buddelmeijer N, Aarsman ME, Kolk AH, Vicente M, Nanninga N (1998) Localization of cell division protein FtsQ by immunofluorescence microscopy in dividing and nondividing cells of *Escherichia coli*. *J Bacteriol* 180:6107–6116

- Bugg TD, Walsh CT (1992) Intracellular steps of bacterial cell wall peptidoglycan biosynthesis: enzymology, antibiotics, and antibiotic resistance. *Nat Prod Rep* 9:199–215
- Bugg TD, Braddick D, Dowson CG, Roper DI (2011) Bacterial cell wall assembly: still an attractive antibacterial target. *Trends Biotechnol* 29:167–173
- Burge RE, Adams R, Balyuzi HH, Reaveley DA (1977a) Structure of the peptidoglycan of bacterial cell walls. II *J Mol Biol* 117:955–974
- Burge RE, Fowler AG, Reaveley DA (1977b) Structure of the peptidoglycan of bacterial cell walls. I *J Mol Biol* 117:927–953
- Cabeen MT, Jacobs-Wagner C (2007) Skin and bones: the bacterial cytoskeleton, cell wall, and cell morphogenesis. *J Cell Biol* 179:381–387
- Chan YG, Frankel MB, Dengler V, Schneewind O, Missiakas D (2013) *Staphylococcus aureus* mutants lacking the LytR-CpsA-Psr family of enzymes release cell wall teichoic acids into the extracellular medium. *J Bacteriol* 195:4650–4659
- Chan YG, Kim HK, Schneewind O, Missiakas D (2014) The capsular polysaccharide of *Staphylococcus aureus* is attached to peptidoglycan by the LytR-CpsA-Psr (LCP) family of enzymes. *J Biol Chem* 289:15680–15690
- Chapman GB, Hillier J (1953) Electron microscopy of ultra-thin sections of bacteria I. Cellular division in *Bacillus cereus*. *J Bacteriol* 66:362–373
- Cheggour A, Fanuel L, Duez C, Joris B, Bouillenne F, Devreese B, Van Driessche G, Van Beeumen J, Frere JM, Goffin C (2000) The *dppA* gene of *Bacillus subtilis* encodes a new D-aminopeptidase. *Mol Microbiol* 38:504–513
- Chen S, McDowall A, Dobro MJ, Briegel A, Ladinsky M, Shi J, Tocheva EI, Beeby M, Pilhofer M, Ding HJ, Li Z, Gan L, Morris DM, Jensen GJ (2010) Electron cryotomography of bacterial cells. *J Vis Exp: JoVE* 39. <https://doi.org/10.3791/1943>
- Chen MW, Lohkamp B, Schnell R, Lescar J, Schneider G (2013) Substrate channel flexibility in *Pseudomonas aeruginosa* MurB accommodates two distinct substrates. *PLoS One* 8(6):e66936
- Cheng Q, Park JT (2002) Substrate specificity of the AmpG permease required for recycling of cell wall anhydro-muropeptides. *J Bacteriol* 184:6434–6436
- Cheng Q, Li H, Merdek K, Park JT (2000) Molecular characterization of the  $\beta$ -N-acetylglucosaminidase of *Escherichia coli* and its role in cell wall recycling. *J Bacteriol* 182:4836–4840
- Cho H, Wivagg CN, Kapoor M, Barry Z, Rohs PD, Suh H, Marto JA, Garner EC, Bernhardt TG (2016) Bacterial cell wall biogenesis is mediated by SEDS and PBP polymerase families functioning semi-autonomously. *Nat Microbiol*:16172. <https://doi.org/10.1038/nmicrobiol.2016.172>
- Chung BC, Zhao J, Gillespie RA, Kwon DY, Guan Z, Hong J, Zhou P, Lee SY (2013) Crystal structure of MraY, an essential membrane enzyme for bacterial cell wall synthesis. *Science* 341:1012–1016
- Corbin BD, Wang Y, Beuria TK, Margolin W (2007) Interaction between cell division proteins FtsE and FtsZ. *J Bacteriol* 189:3026–3035
- Coutinho PM, Deleury E, Davies GJ, Henrissat B (2003) An evolving hierarchical family classification for glycosyltransferases. *J Mol Biol* 328:307–317
- Cremniter J, Mainardi JL, Josseaume N, Quincampoix JC, Dubost L, Hugonnet JE, Marie A, Gutmann L, Rice LB, Arthur M (2006) Novel mechanism of resistance to glycopeptide antibiotics in *Enterococcus faecium*. *J Biol Chem* 281:32254–32262
- Dahl U, Jaeger T, Nguyen BT, Sattler JM, Mayer C (2004) Identification of a phosphotransferase system of *Escherichia coli* required for growth on N-acetylmuramic acid. *J Bacteriol* 186:2385–2392
- Dai K, Xu Y, Lutkenhaus J (1993) Cloning and characterization of *ftsN*, an essential cell division gene in *Escherichia coli* isolated as a multicopy suppressor of *ftsA12*(Ts). *J Bacteriol* 175:3790–3797
- Dajkovic A, Tesson B, Chauhan S, Courtin P, Keary R, Flores P, Marliere C, Filipe SR, Chapot-Chartier MP, Carballido-Lopez R (2017) Hydrolysis of peptidoglycan is modulated by

- amidation of meso-diaminopimelic acid and Mg(2+) in *Bacillus subtilis*. *Mol Microbiol* 104:972–988
- de Jonge BL, Chang YS, Gage D, Tomasz A (1992) Peptidoglycan composition of a highly methicillin-resistant *Staphylococcus aureus* strain. The role of penicillin binding protein 2A. *J Biol Chem* 267:11248–11254
- de Pedro MA, Cava F (2015) Structural constraints and dynamics of bacterial cell wall architecture. *Front Microbiol* 6:449. <https://doi.org/10.3389/fmicb.2015.00449>
- De Petris S (1967) Ultrastructure of the cell wall of *Escherichia coli* and chemical nature of its constituent layers. *J Ultrastruct Res* 19:45–83
- Desmarais SM, De Pedro MA, Cava F, Huang KC (2013) Peptidoglycan at its peaks: how chromatographic analyses can reveal bacterial cell wall structure and assembly. *Mol Microbiol* 89:1–13
- Desmarais SM, Cava F, de Pedro MA, Huang KC (2014) Isolation and preparation of bacterial cell walls for compositional analysis by ultra performance liquid chromatography. *J Vis Exp: JoVE* 83:e51183. <https://doi.org/10.3791/51183>
- Di Berardino M, Dijkstra A, Stuber D, Keck W, Gubler M (1996) The monofunctional glycosyltransferase of *Escherichia coli* is a member of a new class of peptidoglycan-synthesising enzymes. *FEBS Lett* 392:184–188
- Dmitriev BA, Ehlers S, Rietschel ET (1999) Layered murein revisited: a fundamentally new concept of bacterial cell wall structure, biogenesis and function. *Med Microbiol Immunol* 187:173–181
- Dmitriev BA, Ehlers S, Rietschel ET, Brennan PJ (2000) Molecular mechanics of the mycobacterial cell wall: from horizontal layers to vertical scaffolds. *Int J Med Microbiol* 290:251–258
- Dmitriev BA, Toukach FV, Schaper K-J, Holst O, Rietschel ET, Ehlers S (2003) Tertiary structure of bacterial murein: the scaffold model. *J Bacteriol* 185:3458–3468
- Dmitriev BA, Toukach FV, Holst O, Rietschel ET, Ehlers S (2004) Tertiary structure of *Staphylococcus aureus* cell wall murein. *J Bacteriol* 186:7141–7148
- Dmitriev B, Toukach F, Ehlers S (2005) Towards a comprehensive view of the bacterial cell wall. *Trends Microbiol* 13:569–574
- Dominguez-Cuevas P, Porcelli I, Daniel RA, Errington J (2013) Differentiated roles for MreB-actin isologues and autolytic enzymes in *Bacillus subtilis* morphogenesis. *Mol Microbiol* 89:1084–1098
- Dominguez-Escobar J, Chastanet A, Crevenna AH, Fromion V, Wedlich-Soldner R, Carballido-Lopez R (2011) Processive movement of MreB-associated cell wall biosynthetic complexes in bacteria. *Science* 333:225–228
- Dörr T, Lam H, Alvarez L, Cava F, Davis BM, Waldor MK (2014) A novel peptidoglycan binding protein crucial for PBP1A-mediated cell wall biogenesis in *Vibrio cholerae*. *PLoS Genet* 10(6): e1004433
- Doublet P, van Heijenoort J, Mengin-Lecreulx D (1994) The glutamate racemase activity from *Escherichia coli* is regulated by peptidoglycan precursor UDP-N-acetylmuramoyl-L-alanine. *Biochemistry* 33:5285–5290
- Doyle RJ, Chaloupka J, Vinter V (1988) Turnover of cell walls in microorganisms. *Microbiol Rev* 52:554–567
- Dramsi S, Magnet S, Davison S, Arthur M (2008) Covalent attachment of proteins to peptidoglycan. *FEMS Microbiol Rev* 32:307–320
- Du W, Brown JR, Sylvester DR, Huang J, Chalker AF, So CY, Holmes DJ, Payne DJ, Wallis NG (2000) Two active forms of UDP-N-acetylglucosamine enolpyruvyl transferase in gram-positive bacteria. *J Bacteriol* 182:4146–4152
- Dubrac S, Bisicchia P, Devine KM, Msadek T (2008) A matter of life and death: cell wall homeostasis and the WalKR (YycGF) essential signal transduction pathway. *Mol Microbiol* 70:1307–1322

- Eberhardt A, Hoyland CN, Vollmer D, Bisle S, Cleverley RM, Johnsborg O, Havarstein LS, Lewis RJ, Vollmer W (2012) Attachment of capsular polysaccharide to the cell wall in *Streptococcus pneumoniae*. *Microb Drug Resist* 18:240–255
- Egan AJ, Vollmer W (2013) The physiology of bacterial cell division. *Ann N Y Acad Sci* 1277:8–28
- Egan AJ, Jean NL, Koumoutsis A, Bougault CM, Biboy J, Sassine J, Solovyova AS, Breukink E, Typas A, Vollmer W, Simorre JP (2014) Outer-membrane lipoprotein LpoB spans the periplasm to stimulate the peptidoglycan synthase PBP1B. *Proc Natl Acad Sci USA* 111:8197–8202
- Egan AJ, Biboy J, van't Veer I, Breukink E, Vollmer W (2015) Activities and regulation of peptidoglycan synthases. *Philos Trans R Soc Lond Ser B Biol Sci* 370(1679). <https://doi.org/10.1098/rstb.2015.0031>
- Egan AJ, Cleverley RM, Peters K, Lewis RJ, Vollmer W (2017) Regulation of bacterial cell wall growth. *FEBS J* 284:851–867
- El Ghachi M, Derbise A, Bouhss A, Mengin-Lecreulx D (2005) Identification of multiple genes encoding membrane proteins with undecaprenyl pyrophosphate phosphatase (UppP) activity in *Escherichia coli*. *J Biol Chem* 280:18689–18695
- Emami K, Guyet A, Kawai Y, Devi J, Wu LJ, Allenby N, Daniel RA, Errington J (2017) RodA as the missing glycosyltransferase in *Bacillus subtilis* and antibiotic discovery for the peptidoglycan polymerase pathway. *Nat Microbiol* 2:16253. <https://doi.org/10.1038/nmicrobiol.2016.253>
- Errington J (2015) Bacterial morphogenesis and the enigmatic MreB helix. *Nat Rev Microbiol* 13:241–248
- Errington J, Mickiewicz K, Kawai Y, Wu LJ (2016) L-form bacteria, chronic diseases and the origins of life. *Philos Trans R Soc Lond Ser B Biol Sci* 371(1707). <https://doi.org/10.1098/rstb.2015.0494>
- Eschenburg S, Kabsch W, Healy ML, Schönbrunn E (2003) A new view of the mechanisms of UDP-N-acetylglucosamine enolpyruvyl transferase (MurA) and 5-enolpyruvylshikimate-3-phosphate synthase (AroA) derived from X-ray structures of their tetrahedral reaction intermediate states. *J Biol Chem* 278:49215–49222
- Eschenburg S, Priestman M, Schönbrunn E (2005) Evidence that the fosfomycin target Cys115 in UDP-N-acetylglucosamine enolpyruvyl transferase (MurA) is essential for product release. *J Biol Chem* 280:3757–3763
- Fay A, Dworkin J (2009) *Bacillus subtilis* homologs of MviN (MurJ), the putative *Escherichia coli* lipid II flippase, are not essential for growth. *J Bacteriol* 191:6020–6028
- Fink G, Szewczak-Harris A, Löwe J (2016) SnapShot: The Bacterial Cytoskeleton. *Cell* 166:522–522. e521. <https://doi.org/10.1016/j.cell.2016.06.057>
- Firczuk M, Bochtler M (2007a) Folds and activities of peptidoglycan amidases. *FEMS Microbiol Rev* 31:676–691
- Firczuk M, Bochtler M (2007b) Mutational analysis of peptidoglycan amidase MepA. *Biochemistry* 46(1):120–128
- Flärdh K (2010) Cell polarity and the control of apical growth in *Streptomyces*. *Curr Opin Microbiol* 13:758–765
- Fleming A (1955) The story of penicillin. *Bull Georgetown Univ Med Cent* 8:128–132
- Fleming TC, Shin JY, Lee SH, Becker E, Huang KC, Bustamante C, Pogliano K (2010) Dynamic SpoIIIE assembly mediates septal membrane fission during *Bacillus subtilis* sporulation. *Genes Dev* 24:1160–1172
- Formanek H, Rauscher R (1979) Electron diffraction studies of the peptidoglycan of bacterial cell walls. *Ultramicroscopy* 3:337–342
- Foster SJ, Popham DL (2002) Structure and synthesis of cell wall, spore cortex, teichoic acids, S-layers, and capsules. In: Sonenshein AL, Hoch JA, Losick R (eds) *Bacillus subtilis* and its closest relatives: From genes to cells. ASM Press, Washington, DC, pp 21–41
- Fujihashi M, Zhang YW, Higuchi Y, Li XY, Koyama T, Miki K (2001) Crystal structure of cis-prenyl chain elongating enzyme, undecaprenyl diphosphate synthase. *Proc Natl Acad Sci USA* 98:4337–4342

- Fukushima T, Afkham A, Kurosawa S, Tanabe T, Yamamoto H, Sekiguchi J (2006) A new D, L-endopeptidase gene product, YojL (renamed CwlS), plays a role in cell separation with LytE and LytF in *Bacillus subtilis*. *J Bacteriol* 188:5541–5550
- Fukushima T, Furihata I, Emmins R, Daniel RA, Hoch JA, Szurmant H (2011) A role for the essential YycG sensor histidine kinase in sensing cell division. *Mol Microbiol* 79:503–522
- Gan L, Chen S, Jensen GJ (2008) Molecular organization of Gram-negative peptidoglycan. *Proc Natl Acad Sci USA* 105:18953–18957
- Garner EC, Bernard R, Wang W, Zhuang X, Rudner DZ, Mitchison T (2011) Coupled, circumferential motions of the cell wall synthesis machinery and MreB filaments in *B. subtilis*. *Science* 333:222–225
- Geddes A (2008) 80th Anniversary of the discovery of penicillin: An appreciation of Sir Alexander Fleming. *Int J Antimicrob Agents* 32(5):373. <https://doi.org/10.1016/j.ijantimicag.2008.06.001>
- Gehring AM, Lees WJ, Mendiola DJ, Walsh CT, Brown ED (1996) Acetyltransfer precedes uridylyltransfer in the formation of UDP-N-acetylglucosamine in separable active sites of the bifunctional GlmU protein of *Escherichia coli*. *Biochemistry* 35:579–585
- Gerding MA, Liu B, Bendezu FO, Hale CA, Bernhardt TG, de Boer PA (2009) Self-enhanced accumulation of FtsN at division sites and roles for other proteins with a SPOR domain (DamX, DedD, and RlpA) in *Escherichia coli* cell constriction. *J Bacteriol* 191:7383–7401
- Gerstmans H, Rodriguez-Rubio L, Lavigne R, Briens Y (2016) From endolysins to Artilysin(R): novel enzyme-based approaches to kill drug-resistant bacteria. *Biochem Soc Trans* 44:123–128
- Ghuysen JM (1968) Use of bacteriolytic enzymes in determination of wall structure and their role in cell metabolism. *Bacteriol Rev* 32:425–464
- Gisin J, Schneider A, Nägele B, Borisova M, Mayer C (2013) A cell wall recycling shortcut that bypasses peptidoglycan *de novo* biosynthesis. *Nat Chem Biol* 9:491–493
- Glauner B (1988) Separation and quantification of muropeptides with high-performance liquid chromatography. *Anal Biochem* 172:451–464
- Glauner B, Höltje JV, Schwarz U (1988) The composition of the murein of *Escherichia coli*. *J Biol Chem* 263:10088–10095
- Goehring NW, Beckwith J (2005) Diverse paths to midcell: assembly of the bacterial cell division machinery. *Curr Biol* 15:R514–R526
- Goffin C, Ghuysen JM (1998) Multimodular penicillin-binding proteins: an enigmatic family of orthologs and paralogs. *Microbiol Mol Biol Rev* 62:1079–1093
- Goodell EW (1985) Recycling of murein by *Escherichia coli*. *J Bacteriol* 163:305–310
- Goodell EW, Schwarz U (1985) Release of cell wall peptides into culture medium by exponentially growing *Escherichia coli*. *J Bacteriol* 162:391–397
- Gram H (1884) The differential staining of Schizomycetes in tissue sections and in dried preparations. *Fortschr Med* 2:185–189
- Hakulinen JK, Hering J, Branden G, Chen H, Snijder A, Ek M, Johansson P (2017) MraY-antibiotic complex reveals details of tunicamycin mode of action. *Nat Chem Biol* 13:265–267
- Hale CA, de Boer PA (1997) Direct binding of FtsZ to ZipA, an essential component of the septal ring structure that mediates cell division in *E. coli*. *Cell* 88:175–185
- Hale CA, Rhee AC, de Boer PA (2000) ZipA-induced bundling of FtsZ polymers mediated by an interaction between C-terminal domains. *J Bacteriol* 182:5153–5166
- Harris JR (2015) Transmission electron microscopy in molecular structural biology: a historical survey. *Arch Biochem Biophys* 581:3–18
- Harrison J, Lloyd G, Joe M, Lowary TL, Reynolds E, Walters-Morgan H, Bhatt A, Lovering A, Besra GS, Alderwick LJ (2016) Lcp1 Is a phosphotransferase responsible for ligating arabinogalactan to peptidoglycan in *Mycobacterium tuberculosis*. *mBio* 7(4). <https://doi.org/10.1128/mBio.00972-16>
- Hartmann E, König H (1994) A novel pathway of peptide biosynthesis found in methanogenic Archaea. *Arch Microbiol* 162:430–432

- Harz H, Burgdorf K, Höltje JV (1990) Isolation and separation of the glycan strands from murein of *Escherichia coli* by reversed-phase high-performance liquid chromatography. *Anal Biochem* 190:120–128
- Hashimoto M, Ooiwa S, Sekiguchi J (2011) Synthetic lethality of the *lytE cw10* genotype in *Bacillus subtilis* is caused by lack of D,L-endopeptidase activity at the lateral cell wall. *J Bacteriol* 194:796–803
- Hashimoto M, Matsushima H, Suparthana IP, Ogasawara H, Yamamoto H, Teng C, Sekiguchi J (2018) Digestion of peptidoglycan near the cross-link is necessary for the growth of *Bacillus subtilis*. *Microbiology* 164:299–307
- Hayhurst EJ, Kailas L, Hobbs JK, Foster SJ (2008) Cell wall peptidoglycan architecture in *Bacillus subtilis*. *Proc Natl Acad Sci USA* 105:14603–14608
- Healy VL, Lessard IA, Roper DI, Knox JR, Walsh CT (2000) Vancomycin resistance in enterococci: reprogramming of the D-ala-D-Ala ligases in bacterial peptidoglycan biosynthesis. *Chem Biol* 7:R109–R119
- Heidrich C, Templin MF, Ursinus A, Merdanovic M, Berger J, Schwarz H, de Pedro MA, Höltje JV (2001) Involvement of *N*-acetylmuramyl-L-alanine amidases in cell separation and antibiotic-induced autolysis of *Escherichia coli*. *Mol Microbiol* 41:167–178
- Henrichfreise B, Brunke M, Viollier PH (2016) Bacterial surfaces: the wall that SEDS built. *Curr Biol* 26:R1158–R1160
- Hobot JA, Carlemalm E, Villiger W, Kellenberger E (1984) Periplasmic gel: new concept resulting from the reinvestigation of bacterial cell envelope ultrastructure by new methods. *J Bacteriol* 160:143–152
- Hoiczek E, Hansel A (2000) Cyanobacterial cell walls: news from an unusual prokaryotic envelope. *J Bacteriol* 182:1191–1199
- Holt JG, Krieg NR, Sneath PHA, Staley JT, Williams ST (1994) *Bergey's manual of determinative bacteriology*, 9th edn. Williams and Wilkins, Philadelphia
- Höltje J-V (1995) From growth to autolysis: the murein hydrolases in *Escherichia coli*. *Arch Microbiol* 164:243–254
- Höltje JV (1998) Growth of the stress-bearing and shape-maintaining murein sacculus of *Escherichia coli*. *Microbiol Mol Biol Rev* 62:181–203
- Horsburgh GJ, Atrih A, Williamson MP, Foster SJ (2003) *LytG* of *Bacillus subtilis* is a novel peptidoglycan hydrolase: the major active glucosaminidase. *Biochemistry* 42:257–264
- Hrast M, Jukic M, Patin D, Tod J, Dowson CG, Roper DI, Barreteau H, Gobec S (2018) *In silico* identification, synthesis and biological evaluation of novel tetrazole inhibitors of MurB. *Chem Biol Drug Des* 91:1101–1112
- Hsu YP, Rittichier J, Kuru E, Yablonowski J, Pasciak E, Tekkam S, Hall E, Murphy B, Lee TK, Garner EC, Huang KC, Brun YV, VanNieuwenhze MS (2017) Full color palette of fluorescent D-amino acids for in situ labeling of bacterial cell walls. *Chem Sci* 8:6313–6321
- Hu Y, Chen L, Ha S, Gross B, Falcone B, Walker D, Mokhtarzadeh M, Walker S (2003) Crystal structure of the MurG:UDP-GlcNAc complex reveals common structural principles of a superfamily of glycosyltransferases. *Proc Natl Acad Sci USA* 100:845–849
- Hugonnet JE, Mengin-Lecreulx D, Monton A, den Blaauwen T, Carbonnelle E, Veckerle C, Brun YV, van Nieuwenhze M, Bouchier C, Tu K, Rice LB, Arthur M (2016) Factors essential for L, D-transpeptidase-mediated peptidoglycan cross-linking and  $\beta$ -lactam resistance in *Escherichia coli*. *Elife*:5. <https://doi.org/10.7554/eLife.19469>
- Inoue A, Murata Y, Takahashi H, Tsuji N, Fujisaki S, Kato JI (2008) Involvement of an essential gene, *mviN*, in murein synthesis in *Escherichia coli*. *J Bacteriol* 190:7298–7301
- Jacobs C, Joris B, Jamin M, Klarsov K, Van Beeumen J, Mengin-Lecreulx D, van Heijenoort J, Park JT, Normark S, Frere JM (1995) AmpD, essential for both  $\beta$ -lactamase regulation and cell wall recycling, is a novel cytosolic *N*-acetylmuramyl-L-alanine amidase. *Mol Microbiol* 15:553–559
- Jaeger T, Arsic M, Mayer C (2005) Scission of the lactyl ether bond of *N*-acetylmuramic acid by *Escherichia coli* “etherase”. *J Biol Chem* 280:30100–30106
- Jankute M, Cox JA, Harrison J, Besra GS (2015) Assembly of the mycobacterial cell wall. *Annu Rev Microbiol* 69:405–423

- Jeske O, Schüler M, Schumann P, Schneider A, Boedeker C, Jogler M, Bollschweiler D, Rohde M, Mayer C, Engelhardt H, Spring S, Jogler C (2015) Planctomycetes do possess a peptidoglycan cell wall. *Nat Commun* 6:7116. <https://doi.org/10.1038/ncomms8116>
- Johnson JW, Fisher JF, Mobashery S (2013) Bacterial cell-wall recycling. *Ann N Y Acad Sci* 1277:54–75
- Jolly L, Ferrari P, Blanot D, Van Heijenoort J, Fassy F, Mengin-Lecreulx D (1999) Reaction mechanism of phosphoglucosamine mutase from *Escherichia coli*. *Eur J Biochem* 262:202–210
- Jones LJ, Carballido-Lopez R, Errington J (2001) Control of cell shape in bacteria: helical, actin-like filaments in *Bacillus subtilis*. *Cell* 104:913–922
- Kalamorz F, Reichenbach B, Marz W, Rak B, Görke B (2007) Feedback control of glucosamine-6-phosphate synthase GlmS expression depends on the small RNA GlmZ and involves the novel protein YhbJ in *Escherichia coli*. *Mol Microbiol* 65:1518–1533
- Kandler O, König H (1978) Chemical composition of the peptidoglycan-free cell walls of methanogenic bacteria. *Arch Microbiol* 118:141–152
- Kandler O, König H (1993) Cell envelopes of archaea: Structure and chemistry. In: Mea K (ed) *The biochemistry of Archaea (Archaeobacteria)*. Elsevier Science Publishers B. H, Amsterdam, pp 223–259
- Kandler O, König H (1998) Cell wall polymers in Archaea (Archaeobacteria). *Cell Mol Life Sci* 54:305–308
- Kawai Y, Marles-Wright J, Cleverley RM, Emmins R, Ishikawa S, Kuwano M, Heinz N, Bui NK, Hoyland CN, Ogasawara N, Lewis RJ, Vollmer W, Daniel RA, Errington J (2011) A widespread family of bacterial cell wall assembly proteins. *EMBO J* 30:4931–4941
- Kawai Y, Mickiewicz K, Errington J (2018) Lysozyme counteracts  $\beta$ -lactam antibiotics by promoting the emergence of L-form bacteria. *Cell* 172:1038–1049
- Kelemen MV, Rogers HJ (1971) Three-dimensional molecular models of bacterial cell wall mucopolymers (peptidoglycans). *Proc Natl Acad Sci USA* 68:992–996
- Kellenberger E, Ryter A (1958) Cell wall and cytoplasmic membrane of *Escherichia coli*. *J Biophys Biochem Cytol* 4:323–326
- Kim SJ, Chang J, Singh M (2015) Peptidoglycan architecture of Gram-positive bacteria by solid-state NMR. *Biochim Biophys Acta* 1848(1 Pt B):350–362
- King DT, Lameignere E, Strynadka NC (2014) Structural insights into the lipoprotein outer membrane regulator of penicillin-binding protein 1B. *J Biol Chem* 289:19245–19253
- Kishida H, Unzai S, Roper DI, Lloyd A, Park SY, Tame JR (2006) Crystal structure of penicillin binding protein 4 (*dacB*) from *Escherichia coli*, both in the native form and covalently linked to various antibiotics. *Biochemistry* 45:783–792
- Kluj RM, Ebner P, Adamek M, Ziemert N, Mayer C, Borisova M (2018) Recovery of the peptidoglycan turnover product released by the Autolysin Atl in *Staphylococcus aureus* involves the phosphotransferase system transporter MurP and the Novel 6-phospho-N-acetylmuramidase MupG. *Front Microbiol* 9(2725). <https://doi.org/10.3389/fmicb.2018.02725>
- Koch AL (1985) How bacteria grow and divide in spite of internal hydrostatic pressure. *Can J Microbiol* 31:1071–1084
- Koch AL (1995) *Bacterial growth and form: Evolution and biophysics*. Chapman and Hall, New York
- Koch AL, Doyle RJ (1985) Inside-to-outside growth and turnover of the wall of Gram-positive rods. *J Theor Biol* 117:137–157
- Koch AL, Woeste S (1992) Elasticity of the sacculus of *Escherichia coli*. *J Bacteriol* 174:4811–4819
- König H, Kandler O, Jensen M, Rietschel ET (1983) The primary structure of the glycan moiety of pseudomurein from *Methanobacterium thermoautotrophicum*. *Hoppe Seylers Z Physiol Chem* 364:627–636
- Kouidmi I, Levesque RC, Paradis-Bleau C (2014) The biology of Mur ligases as an antibacterial target. *Mol Microbiol* 94:242–253
- Kühner D, Stahl M, Demircioglu DD, Bertsche U (2014) From cells to muropeptide structures in 24 h: peptidoglycan mapping by UPLC-MS. *Sci Rep* 4:7494. <https://doi.org/10.1038/srep07494>



- Kuru E, Tekkam S, Hall E, Brun YV, Van Nieuwenhze MS (2015) Synthesis of fluorescent D-amino acids and their use for probing peptidoglycan synthesis and bacterial growth in situ. *Nat Protoc* 10:33–52
- Labischinski H, Barnickel G, Bradaczek H, Giesbrecht P (1979) On the secondary and tertiary structure of murein. Low and medium-angle X-ray evidence against chitin-based conformations of bacterial peptidoglycan. *Eur J Biochem* 95:147–155
- Labischinski H, Goodell EW, Goodell A, Hochberg ML (1991) Direct proof of a “more-than-single-layered” peptidoglycan architecture of *Escherichia coli* W7: a neutron small-angle scattering study. *J Bacteriol* 173:751–756
- Laddomada F, Miyachiro MM, Dessen A (2016) Structural insights into protein-protein interactions involved in bacterial cell wall biogenesis. *Antibiotics (Basel)* 5(2):E14. <https://doi.org/10.3390/antibiotics5020014>
- Lai GC, Cho H, Bernhardt TG (2017) The mecillinam resistome reveals a role for peptidoglycan endopeptidases in stimulating cell wall synthesis in *Escherichia coli*. *PLoS Genet* 13(7): e1006934
- Lavollay M, Arthur M, Fourgeaud M, Dubost L, Marie A, Veziris N, Blanot D, Gutmann L, Mainardi JL (2008) The peptidoglycan of stationary-phase *Mycobacterium tuberculosis* predominantly contains cross-links generated by L,D-transpeptidation. *J Bacteriol* 190:4360–4366
- Leclercq S, Derouaux A, Olatunji S, Fraipont C, Egan AJ, Vollmer W, Breukink E, Terrak M (2017) Interplay between Penicillin-binding proteins and SEDS proteins promotes bacterial cell wall synthesis. *Sci Rep* 7:43306. <https://doi.org/10.1038/srep43306>
- Leduc M, Frehel C, Siegel E, Van Heijenoort J (1989) Multilayered distribution of peptidoglycan in the periplasmic space of *Escherichia coli*. *J Gen Microbiol* 135:1243–1254
- Lee TK, Meng K, Shi H, Huang KC (2016) Single-molecule imaging reveals modulation of cell wall synthesis dynamics in live bacterial cells. *Nat Commun* 7:13170. <https://doi.org/10.1038/ncomms13170>
- Levefaudes M, Patin D, de Sousa-d’Auria C, Chami M, Blanot D, Herve M, Arthur M, Houssin C, Mengin-Lecreux D (2015) Diaminopimelic acid amidation in Corynebacteriales: new insights into the role of LtsA in peptidoglycan modification. *J Biol Chem* 290:13079–13094
- Liechti GW, Kuru E, Hall E, Kalinda A, Brun YV, VanNieuwenhze M, Maurelli AT (2014) A new metabolic cell-wall labelling method reveals peptidoglycan in *Chlamydia trachomatis*. *Nature* 506:507–510
- Liechti G, Kuru E, Packiam M, Hsu YP, Tekkam S, Hall E, Rittichier JT, VanNieuwenhze M, Brun YV, Maurelli AT (2016) Pathogenic *Chlamydia* lack a classical sacculus but synthesize a narrow, mid-cell peptidoglycan ring, regulated by MreB, for cell division. *PLoS Pathog* 12(5): e1005590
- Liger D, Masson A, Blanot D, van Heijenoort J, Parquet C (1995) Over-production, purification and properties of the uridine-diphosphate-*N*-acetylmuramate:L-alanine ligase from *Escherichia coli*. *Eur J Biochem* 230:80–87
- Lim D, Strynadka NC (2002) Structural basis for the  $\beta$ -lactam resistance of PBP2a from methicillin-resistant *Staphylococcus aureus*. *Nat Struct Biol* 9:870–876
- Lin L, Osorio Valeriano M, Harms A, Sogaard-Andersen L, Thanbichler M (2017) Bactofilin-mediated organization of the ParABS chromosome segregation system in *Myxococcus xanthus*. *Nat Commun* 8(1):1817. <https://doi.org/10.1038/s41467-017-02015-z>
- Ling LL, Schneider T, Peoples AJ, Spoering AL, Engels I, Conlon BP, Mueller A, Schaberle TF, Hughes DE, Epstein S, Jones M, Lazarides L, Steadman VA, Cohen DR, Felix CR, Fetterman KA, Millett WP, Nitti AG, Zullo AM, Chen C, Lewis K (2015) A new antibiotic kills pathogens without detectable resistance. *Nature* 517:455–459
- Litzinger S, Mayer C (2010) Chapter 1: The murein sacculus. In: König H, Claus H, Varma A (eds) *Prokaryotic cell wall compounds – Structure and biochemistry*. Springer, Heidelberg/Berlin/New York, pp 3–52
- Litzinger S, Duckworth A, Nitzsche K, Risinger C, Wittmann V, Mayer C (2010) Muropeptide rescue in *Bacillus subtilis* involves sequential hydrolysis by  $\beta$ -*N*-acetylglucosaminidase and *N*-acetylmuramyl-L-alanine amidase. *J Bacteriol* 192:3132–3143

- Liu B, Persons L, Lee L, de Boer PA (2015) Roles for both FtsA and the FtsBLQ subcomplex in FtsN-stimulated cell constriction in *Escherichia coli*. *Mol Microbiol* 95:945–970
- Liu TY, Chu SH, Shaw GC (2018) Deletion of the cell wall peptidoglycan hydrolase gene *cwlO* or *lytE* severely impairs transformation efficiency in *Bacillus subtilis*. *J Gen Appl Microbiol* 64:139–144
- Loskill P, Pereira PM, Jung P, Bischoff M, Herrmann M, Pinho MG, Jacobs K (2014) Reduction of the peptidoglycan crosslinking causes a decrease in stiffness of the *Staphylococcus aureus* cell envelope. *Biophys J* 107:1082–1089
- Lovering AL, de Castro LH, Lim D, Strynadka NC (2007) Structural insight into the transglycosylation step of bacterial cell-wall biosynthesis. *Science* 315:1402–1405
- Lovering AL, Safadi SS, Strynadka NC (2012) Structural perspective of peptidoglycan biosynthesis and assembly. *Annu Rev Biochem* 81:451–478
- Löwe J, van den Ent F, Amos LA (2004) Molecules of the bacterial cytoskeleton. *Annu Rev Biophys Biomol Struct* 33:177–198
- Lupoli TJ, Tsukamoto H, Doud EH, Wang TS, Walker S, Kahne D (2011) Transpeptidase-mediated incorporation of D-amino acids into bacterial peptidoglycan. *J Am Chem Soc* 133:10748–10751
- Magnet S, Arbeloa A, Mainardi JL, Hugonnet JE, Fourgeaud M, Dubost L, Marie A, Delfosse V, Mayer C, Rice LB, Arthur M (2007a) Specificity of L,D-transpeptidases from gram-positive bacteria producing different peptidoglycan chemotypes. *J Biol Chem* 282:13151–13159
- Magnet S, Bellais S, Dubost L, Fourgeaud M, Mainardi JL, Petit-Frere S, Marie A, Mengin-Lecreulx D, Arthur M, Gutmann L (2007b) Identification of the L,D-transpeptidases responsible for attachment of the Braun lipoprotein to *Escherichia coli* peptidoglycan. *J Bacteriol* 189:3927–3931
- Magnet S, Dubost L, Marie A, Arthur M, Gutmann L (2008) Identification of the L, D-transpeptidases for peptidoglycan cross-linking in *Escherichia coli*. *J Bacteriol* 190:4782–4785
- Mainardi JL, Villet R, Bugg TD, Mayer C, Arthur M (2008) Evolution of peptidoglycan biosynthesis under the selective pressure of antibiotics in Gram-positive bacteria. *FEMS Microbiol Rev* 32:386–408
- Manat G, Roure S, Auger R, Bouhss A, Barreateau H, Mengin-Lecreulx D, Touze T (2014) Deciphering the metabolism of undecaprenyl-phosphate: the bacterial cell-wall unit carrier at the membrane frontier. *Microb Drug Resist* 20:199–214
- Marcyjaniak M, Odintsov SG, Sabala I, Bochtler M (2004) Peptidoglycan amidase MepA is a LAS metallopeptidase. *J Biol Chem* 279:43982–43989
- Marienfeld S, Uhlemann EM, Schmid R, Kramer R, Burkovski A (1997) Ultrastructure of the *Corynebacterium glutamicum* cell wall. *Antonie Van Leeuwenhoek* 72:291–297
- Matias VR, Beveridge TJ (2005) Cryo-electron microscopy reveals native polymeric cell wall structure in *Bacillus subtilis* 168 and the existence of a periplasmic space. *Mol Microbiol* 56:240–251
- Matias VR, Beveridge TJ (2006) Native cell wall organization shown by cryo-electron microscopy confirms the existence of a periplasmic space in *Staphylococcus aureus*. *J Bacteriol* 188:1011–1021
- Matias VR, Al-Amoudi A, Dubochet J, Beveridge TJ (2003) Cryo-transmission electron microscopy of frozen-hydrated sections of *Escherichia coli* and *Pseudomonas aeruginosa*. *J Bacteriol* 185:6112–6118
- Mayer C (2012) Bacterial cell wall recycling. eLS: <https://doi.org/10.1002/9780470015902.a0021974>
- Mazmanian SK, Liu G, Ton-That H, Schneewind O (1999) *Staphylococcus aureus* sortase, an enzyme that anchors surface proteins to the cell wall. *Science* 285:760–763
- McDonough MA, Anderson JW, Silvaggi NR, Pratt RF, Knox JR, Kelly JA (2002) Structures of two kinetic intermediates reveal species specificity of penicillin-binding proteins. *J Mol Biol* 322:111–122
- McPherson DC, Popham DL (2003) Peptidoglycan synthesis in the absence of class A penicillin-binding proteins in *Bacillus subtilis*. *J Bacteriol* 185:1423–1431

- Meeske AJ, Sham LT, Kimsey H, Koo BM, Gross CA, Bernhardt TG, Rudner DZ (2015) MurJ and a novel lipid II flippase are required for cell wall biogenesis in *Bacillus subtilis*. *Proc Natl Acad Sci USA* 112:6437–6442
- Meeske AJ, Riley EP, Robins WP, Uehara T, Mekalanos JJ, Kahne D, Walker S, Kruse AC, Bernhardt TG, Rudner DZ (2016) SEDS proteins are a widespread family of bacterial cell wall polymerases. *Nature* 537:634–638
- Meisner J, Montero Llopis P, Sham LT, Garner E, Bernhardt TG, Rudner DZ (2013) FtsEX is required for CwLO peptidoglycan hydrolase activity during cell wall elongation in *Bacillus subtilis*. *Mol Microbiol* 89:1069–1083
- Mengin-Lecreulx D, van Heijenoort J (1994) Copurification of glucosamine-1-phosphate acetyltransferase and *N*-acetylglucosamine-1-phosphate uridylyltransferase activities of *Escherichia coli*: characterization of the *glmU* gene product as a bifunctional enzyme catalyzing two subsequent steps in the pathway for UDP-*N*-acetylglucosamine synthesis. *J Bacteriol* 176:5788–5795
- Mengin-Lecreulx D, van Heijenoort J (1996) Characterization of the essential gene *glmM* encoding phosphoglucosamine mutase in *Escherichia coli*. *J Biol Chem* 271:32–39
- Mengin-Lecreulx D, van Heijenoort J, Park JT (1996) Identification of the *mpl* gene encoding UDP-*N*-acetylmuramate: L-alanyl- $\gamma$ -D-glutamyl-*meso*-diaminopimelate ligase in *Escherichia coli* and its role in recycling of cell wall peptidoglycan. *J Bacteriol* 178(18):5347–5352
- Mengin-Lecreulx D, Falla T, Blanot D, van Heijenoort J, Adams DJ, Chopra I (1999) Expression of the *Staphylococcus aureus* UDP-*N*-acetylmuramoyl-L-alanyl-D-glutamate:L-lysine ligase in *Escherichia coli* and effects on peptidoglycan biosynthesis and cell growth. *J Bacteriol* 181:5909–5914
- Meroueh SO, Bencze KZ, Heseck D, Lee M, Fisher JF, Stemmler TL, Mobashery S (2006) Three-dimensional structure of the bacterial cell wall peptidoglycan. *Proc Natl Acad Sci USA* 103:4404–4409
- Meziane-Cherif D, Saul FA, Haouz A, Courvalin P (2012) Structural and functional characterization of VanG D-Ala:D-Ser ligase associated with vancomycin resistance in *Enterococcus faecalis*. *J Biol Chem* 287:37583–37592
- Michie KA, Lowe J (2006) Dynamic filaments of the bacterial cytoskeleton. *Annu Rev Biochem* 75:467–492
- Miller SI, Salama NR (2018) The gram-negative bacterial periplasm: size matters. *PLoS Biol* 16(1): e2004935
- Mohammadi T, van Dam V, Sijbrandi R, Vernet T, Zapun A, Bouhss A, Diepeveen-de Bruin M, Nguyen-Disteche M, de Kruijff B, Breukink E (2011) Identification of FtsW as a transporter of lipid-linked cell wall precursors across the membrane. *EMBO J* 30:1425–1432
- Morbach S, Kramer R (2002) Body shaping under water stress: osmosensing and osmoregulation of solute transport in bacteria. *Chembiochem* 3:384–397
- Morgenstein RM, Bratton BP, Nguyen JP, Ouzounov N, Shaevitz JW, Gitai Z (2015) RodZ links MreB to cell wall synthesis to mediate MreB rotation and robust morphogenesis. *Proc Natl Acad Sci USA* 112:12510–12515
- Moynihan PJ, Clarke AJ (2011) O-Acetylated peptidoglycan: controlling the activity of bacterial autolysins and lytic enzymes of innate immune systems. *Int J Biochem Cell Biol* 43:1655–1659
- Moynihan PJ, Sychantha D, Clarke AJ (2014) Chemical biology of peptidoglycan acetylation and deacetylation. *Bioorg Chem* 54:44–50
- Mudd S, Polevitzky K, Anderson TF, Chambers LA (1941) Bacterial morphology as shown by the electron microscope: II. The bacterial cell-wall in the genus *Bacillus*. *J Bacteriol* 42:251–264
- Mularski A, Wilksch JJ, Wang H, Hossain MA, Wade JD, Separovic F, Strugnell RA, Gee ML (2015) Atomic force microscopy reveals the mechanobiology of lytic peptide action on bacteria. *Langmuir* 31:6164–6171
- Münch D, Roemer T, Lee SH, Engeser M, Sahl HG, Schneider T (2012) Identification and in vitro analysis of the GatD/MurT enzyme-complex catalyzing lipid II amidation in *Staphylococcus aureus*. *PLoS Pathog* 8(1):e1002509
- Murray RG, Steed P, Elson HE (1965) The location of the mucopeptide in sections of the cell wall of *Escherichia coli* and other Gram-negative bacteria. *Can J Microbiol* 11:547–560

- Navarre WW, Schneewind O (1999) Surface proteins of Gram-positive bacteria and mechanisms of their targeting to the cell wall envelope. *Microbiol Mol Biol Rev* 63:174–229
- Ngadjjeu F, Braud E, Saidjalolov S, Iannazzo L, Schnappinger D, Ehrt S, Hugonnet JE, Mengin-Lecreulx D, Patin D, Etheve-Quellejeu M, Fonvielle M, Arthur M (2018) Critical impact of peptidoglycan precursor amidation on the activity of L,D-transpeptidases from *Enterococcus faecium* and *Mycobacterium tuberculosis*. *Chemistry* 24:5743–5747
- Nicholas RA, Krings S, Tomberg J, Nicola G, Davies C (2003) Crystal structure of wild-type penicillin-binding protein 5 from *Escherichia coli*: implications for deacylation of the acyl-enzyme complex. *J Biol Chem* 278:52826–52833
- Omote H, Hiasa M, Matsumoto T, Otsuka M, Moriyama Y (2006) The MATE proteins as fundamental transporters of metabolic and xenobiotic organic cations. *Trends Pharmacol Sci* 27:587–593
- Park JT (1952) Uridine-5'-pyrophosphate derivatives. I Isolation from *Staphylococcus aureus*. *J Biol Chem* 194:877–884
- Park JT (1993) Turnover and recycling of the murein sacculus in oligopeptide permease-negative strains of *Escherichia coli*: indirect evidence for an alternative permease system and for a monolayered sacculus. *J Bacteriol* 175:7–11
- Park JT, Johnson MJ (1949) Accumulation of labile phosphate in *Staphylococcus aureus* grown in the presence of penicillin. *J Biol Chem* 179:585–592
- Park JT, Strominger JL (1957) Mode of action of penicillin. *Science* 125:99–101
- Park JT, Uehara T (2008) How bacteria consume their own exoskeletons (turnover and recycling of cell wall peptidoglycan). *Microbiol Mol Biol Rev* 72:211–227
- Park JT, Raychaudhuri D, Li H, Normark S, Mengin-Lecreulx D (1998) MppA, a periplasmic binding protein essential for import of the bacterial cell wall peptide L-alanyl-gamma-D-glutamyl-meso-diaminopimelate. *J Bacteriol* 180:1215–1223
- Pende N, Wang J, Weber PM, Verheul J, Kuru E, Rittmann SKR, Leisch N, VanNieuwenhze MS, Brun YV, den Blaauwen T, Bulgheresi S (2018) Host-polarized cell growth in animal symbionts. *Curr Biol* 28:1039–1051
- Pennartz A, Genereux C, Parquet C, Mengin-Lecreulx D, Joris B (2009) Substrate-induced inactivation of the *Escherichia coli* AmiD N-acetylmuramoyl-L-alanine amidase highlights a new strategy to inhibit this class of enzyme. *Antimicrob Agents Chemother* 53:2991–2997
- Pichoff S, Shen B, Sullivan B, Lutkenhaus J (2002) FtsA mutants impaired for self-interaction bypass ZipA suggesting a model in which FtsA's self-interaction competes with its ability to recruit downstream division proteins. *Microbiology* 83:151–167. <https://doi.org/10.1111/j.1365-2958.2011.07923.x>. Epub
- Pichoff S, Lutkenhaus J (2005) Tethering the Z ring to the membrane through a conserved membrane targeting sequence in FtsA. *Mol Microbiol* 55:1722–1734
- Pilhofer M, Aistleitner K, Biboy J, Gray J, Kuru E, Hall E, Brun YV, VanNieuwenhze MS, Vollmer W, Horn M, Jensen GJ (2013) Discovery of chlamydial peptidoglycan reveals bacteria with murein sacculi but without FtsZ. *Nat Commun* 4:2856. <https://doi.org/10.1038/ncomms3856>
- Popescu A, Doyle RJ (1996) The Gram stain after more than a century. *Biotech Histochem* 71:145–151
- Popham DL (2002) Specialized peptidoglycan of the bacterial endospore: the inner wall of the lockbox. *Cell Mol Life Sci* 59:426–433
- Porter JR (1976) Antony van Leeuwenhoek: tercentenary of his discovery of bacteria. *Bacteriol Rev* 40:260–269
- Raghavendra T, Patil S, Mukherjee R (2018) Peptidoglycan in Mycobacteria: chemistry, biology and intervention. *Glycoconj J* 35:421–432
- Raymond JB, Mahapatra S, Crick DC, Pavelka MS Jr (2005) Identification of the *namH* gene, encoding the hydroxylase responsible for the N-glycolylation of the mycobacterial peptidoglycan. *J Biol Chem* 280:326–333
- Razin S, Argaman M (1963) Lysis of Mycoplasma, bacterial protoplasts, spheroplasts and L-forms by various agents. *J Gen Microbiol* 30:155–172

- Reddy M (2007) Role of FtsEX in cell division of *Escherichia coli*: viability of *ftsEX* mutants is dependent on functional SufI or high osmotic strength. *J Bacteriol* 189:98–108
- Reith J, Mayer C (2011) Peptidoglycan turnover and recycling in Gram-positive bacteria. *Appl Microbiol Biotechnol* 92:1–11
- Reizer J, Saier MH Jr, Deutscher J, Grenier F, Thompson J, Hengstenberg W (1988) The phosphoenolpyruvate:sugar phosphotransferase system in gram-positive bacteria: properties, mechanism, and regulation. *Crit Rev Microbiol* 15:297–338
- Remaut H, Bompard-Gilles C, Goffin C, Frere JM, Van Beeumen J (2001) Structure of the *Bacillus subtilis* D-aminopeptidase DppA reveals a novel self-compartmentalizing protease. *Nat Struct Biol* 8:674–678
- Rogers HJ (1974) Peptidoglycans (mucopeptides): structure, function, and variations. *Ann N Y Acad Sci* 235:29–51
- Rojas E, Theriot JA, Huang KC (2014) Response of *Escherichia coli* growth rate to osmotic shock. *Proc Natl Acad Sci USA* 111:7807–7812
- Romeis T, Höltje JV (1994) Penicillin-binding protein 7/8 of *Escherichia coli* is a DD-endopeptidase. *Eur J Biochem* 224:597–604
- Rowlett VW, Margolin W (2015) The bacterial divisome: ready for its close-up. *Philos Trans R Soc Lond Ser B Biol Sci* 370(1679). <https://doi.org/10.1098/rstb.2015.0028>
- Ruane KM, Lloyd AJ, Fulop V, Dowson CG, Barreateau H, Boniface A, Dementin S, Blanot D, Mengin-Lecreulx D, Gobec S, Dessen A, Roper DI (2013) Specificity determinants for lysine incorporation in *Staphylococcus aureus* peptidoglycan as revealed by the structure of a MurE enzyme ternary complex. *J Biol Chem* 288:33439–33448
- Rueff AS, Chastanet A, Dominguez-Escobar J, Yao Z, Yates J, Prejean MV, Delumeau O, Noirot P, Wedlich-Soldner R, Filipe SR, Carballido-Lopez R (2014) An early cytoplasmic step of peptidoglycan synthesis is associated to MreB in *Bacillus subtilis*. *Mol Microbiol* 91:348–362
- Ruiz N (2008) Bioinformatics identification of MurJ (MviN) as the peptidoglycan lipid II flippase in *Escherichia coli*. *Proc Natl Acad Sci USA* 105:15553–15557
- Salje J, van den Ent F, de Boer P, Lowe J (2011) Direct membrane binding by bacterial actin MreB. *Mol Cell* 43:478–487
- Salton MR (1994) The bacterial cell envelope – a historical perspective. In: Ghuysen J-M, Hakenbeck R (eds) *Bacterial cell wall*, vol 29. Elsevier, Amsterdam, pp 1–22
- Salton MR, Horne RW (1951) Studies of the bacterial cell wall. II Methods of preparation and some properties of cell walls. *Biochim Biophys Acta* 7:177–197
- Sathiyamoorthy K, Vijayalakshmi J, Tirupati B, Fan L, Saper MA (2017) Structural analyses of the *Haemophilus influenzae* peptidoglycan synthase activator LpoA suggest multiple conformations in solution. *J Biol Chem* 292:17626–17642
- Sauvage E, Kerff F, Terrak M, Ayala JA, Charlier P (2008) The penicillin-binding proteins: structure and role in peptidoglycan biosynthesis. *FEMS Microbiol Rev* 32:234–258
- Scheffers DJ, Pinho MG (2005) Bacterial cell wall synthesis: new insights from localization studies. *Microbiol Mol Biol Rev* 69:585–607
- Scheuring S, Dufrene YF (2010) Atomic force microscopy: probing the spatial organization, interactions and elasticity of microbial cell envelopes at molecular resolution. *Mol Microbiol* 75:1327–1336
- Scheurwater E, Reid CW, Clarke AJ (2008) Lytic transglycosylases: bacterial space-making autolysins. *Int J Biochem Cell Biol* 40:586–591
- Schlag M, Biswas R, Krismer B, Kohler T, Zoll S, Yu W, Schwarz H, Peschel A, Gotz F (2010) Role of staphylococcal wall teichoic acid in targeting the major autolysin Atl. *Mol Microbiol* 75:864–873
- Schleifer KH, Kandler O (1972) Peptidoglycan types of bacterial cell walls and their taxonomic implications. *Bacteriol Rev* 36:407–777
- Schmidt KL, Peterson ND, Kustusich RJ, Wissel MC, Graham B, Phillips GJ, Weiss DS (2004) A predicted ABC transporter, FtsEX, is needed for cell division in *Escherichia coli*. *J Bacteriol* 186:785–793
- Schneewind O, Missiakas DM (2012) Protein secretion and surface display in Gram-positive bacteria. *Philos Trans R Soc Lond Ser B Biol Sci* 367:1123–1139

- Schneewind O, Fowler A, Faull KF (1995) Structure of the cell wall anchor of surface proteins in *Staphylococcus aureus*. *Science* 268:103–106
- Schneider T, Kruse T, Wimmer R, Wiedemann I, Sass V, Pag U, Jansen A, Nielsen AK, Mygind PH, Raventos DS, Neve S, Ravn B, Bonvin AM, De Maria L, Andersen AS, Gammelgaard LK, Sahl HG, Kristensen HH (2010) Plectasin, a fungal defensin, targets the bacterial cell wall precursor Lipid II. *Science* 328:1168–1172
- Seltmann G, Holst O (2002) Periplasmic space and rigid layer. In: Seltmann G, Holst O (eds) *The bacterial cell wall*. Springer-Verlag, Berlin, pp 103–132
- Sham LT, Butler EK, Lebar MD, Kahne D, Bernhardt TG, Ruiz N (2014) Bacterial cell wall. MurJ is the flippase of lipid-linked precursors for peptidoglycan biogenesis. *Science* 345:220–222
- Sham LT, Zheng S, Yakhnina AA, Kruse AC, Bernhardt TG (2018) Loss of specificity variants of WzxC suggest that substrate recognition is coupled with transporter opening in MOP-family flippases. *Mol Microbiol* 109:633–641
- Shida T, Hattori H, Ise F, Sekiguchi J (2000) Overexpression, purification, and characterization of *Bacillus subtilis* N-acetylmuramoyl-L-alanine amidase CwlC. *Biosci Biotech Bioch* 64:1522–1525
- Shida T, Hattori H, Ise F, Sekiguchi J (2001) Mutational analysis of catalytic sites of the cell wall lytic N-acetylmuramoyl-L-alanine amidases CwlC and CwlV. *J Biol Chem* 276:28140–28146
- Shockman GD, Daneo-Moore L, Kariyama R, Massidda O (1996) Bacterial walls, peptidoglycan hydrolases, autolysins, and autolysis. *Microb Drug Resist* 2:95–98
- Silhavy TJ, Kahne D, Walker S (2010) The bacterial cell envelope. *Cold Spring Harb Perspect Biol* 2(5):a000414. <https://doi.org/10.1101/cshperspect.a000414>
- Small E, Addinall SG (2003) Dynamic FtsZ polymerization is sensitive to the GTP to GDP ratio and can be maintained at steady state using a GTP-regeneration system. *Microbiology* 149:2235–2242
- Smith CA (2006) Structure, function and dynamics in the mur family of bacterial cell wall ligases. *J Mol Biol* 362:640–655
- Smith TJ, Blackman SA, Foster SJ (2000) Autolysins of *Bacillus subtilis*: multiple enzymes with multiple functions. *Microbiology* 146:249–262
- Sobhanifar S, King DT, Strynadka NC (2013) Fortifying the wall: synthesis, regulation and degradation of bacterial peptidoglycan. *Curr Opin Struct Biol* 23:695–703
- Squeglia F, Ruggiero A, Berisio R (2018) Chemistry of peptidoglycan in *Mycobacterium tuberculosis* life cycle: an off-the-wall balance of synthesis and degradation. *Chemistry* 24:2533–2546
- Strahl H, Errington J (2017) Bacterial membranes: structure, domains, and function. *Annu Rev Microbiol* 71:519–538
- Strominger JL, Tipper DJ (1965) Bacterial cell wall synthesis and structure in relation to the mechanism of action of penicillins and other antibacterial agents. *Am J Med* 39:708–721
- Sudiarta IP, Fukushima T, Sekiguchi J (2010) *Bacillus subtilis* CwlQ (previous YjbJ) is a bifunctional enzyme exhibiting muramidase and soluble-lytic transglycosylase activities. *Biochem Biophys Res Commun* 398:606–612
- Takeuchi S, DiLuzio WR, Weibel DB, Whitesides GM (2005) Controlling the shape of filamentous cells of *Escherichia coli*. *Nano Lett* 5:1819–1823
- Templin MF, Ursinus A, Höltje JV (1999) A defect in cell wall recycling triggers autolysis during the stationary growth phase of *Escherichia coli*. *EMBO J* 18:4108–4117
- Tipper DJ, Strominger JL (1965) Mechanism of action of penicillins: a proposal based on their structural similarity to acyl-D-alanyl-D-alanine. *Proc Natl Acad Sci USA* 54:1133–1141
- Tipper DJ, Strominger JL, Ensign JC (1967) Structure of the cell wall of *Staphylococcus aureus*, strain Copenhagen. VII Mode of action of the bacteriolytic peptidase from *Myxobacter* and the isolation of intact cell wall polysaccharides. *Biochemistry* 6:906–920
- Ton-That H, Liu G, Mazmanian SK, Faull KF, Schneewind O (1999) Purification and characterization of sortase, the transpeptidase that cleaves surface proteins of *Staphylococcus aureus* at the LPXTG motif. *Proc Natl Acad Sci USA* 96:12424–12429

- Touhami A, Jericho MH, Beveridge TJ (2004) Atomic force microscopy of cell growth and division in *Staphylococcus aureus*. *J Bacteriol* 186:3286–3295
- Turner RD, Hobbs JK, Foster SJ (2016) Atomic force microscopy analysis of bacterial cell wall peptidoglycan architecture. *Methods Mol Biol* 1440:3–9
- Turner RD, Mesnage S, Hobbs JK, Foster SJ (2018) Molecular imaging of glycan chains couples cell-wall polysaccharide architecture to bacterial cell morphology. *Nat Commun* 9(1):1263. <https://doi.org/10.1038/s41467-018-03551-y>
- Typas A, Banzhaf M, Gross CA, Vollmer W (2012) From the regulation of peptidoglycan synthesis to bacterial growth and morphology. *Nat Rev Microbiol* 10:123–136
- Uehara T, Bernhardt TG (2011) More than just lysins: peptidoglycan hydrolases tailor the cell wall. *Curr Opin Microbiol* 14:698–703
- Uehara T, Park JT (2003) Identification of MpaA, an amidase in *Escherichia coli* that hydrolyzes the gamma-D-glutamyl-meso-diaminopimelate bond in murein peptides. *J Bacteriol* 185:679–682
- Uehara T, Park JT (2004) The *N*-acetyl-D-glucosamine kinase of *Escherichia coli* and its role in murein recycling. *J Bacteriol* 186:7273–7279
- Uehara T, Suefujii K, Valbuena N, Meehan B, Donegan M, Park JT (2005) Recycling of the anhydro-*N*-acetylmuramic acid derived from cell wall murein involves a two-step conversion to *N*-acetylglucosamine-phosphate. *J Bacteriol* 187:3643–3649
- Uehara T, Suefujii K, Jaeger T, Mayer C, Park JT (2006) MurQ etherase is required by *Escherichia coli* in order to metabolize anhydro-*N*-acetylmuramic acid obtained either from the environment or from its own cell wall. *J Bacteriol* 188:1660–1662
- Uehara T, Parzych KR, Dinh T, Bernhardt TG (2010) Daughter cell separation is controlled by cytokinetic ring-activated cell wall hydrolysis. *EMBO J* 29:1412–1422
- Ursell TS, Nguyen J, Monds RD, Colavin A, Billings G, Ouzounov N, Gitai Z, Shaevitz JW, Huang KC (2014) Rod-like bacterial shape is maintained by feedback between cell curvature and cytoskeletal localization. *Proc Natl Acad Sci USA* 111:E1025–E1034
- van Dam V, Sijbrandi R, Kol M, Swiezewska E, de Kruijff B, Breukink E (2007) Transmembrane transport of peptidoglycan precursors across model and bacterial membranes. *Mol Microbiol* 64:1105–1114
- van den Ent F, Amos LA, Lowe J (2001) Prokaryotic origin of the actin cytoskeleton. *Nature* 413:39–44
- van den Ent F, Johnson CM, Persons L, de Boer P, Lowe J (2010) Bacterial actin MreB assembles in complex with cell shape protein RodZ. *EMBO J* 29:1081–1090
- van den Ent F, Izore T, Bharat TA, Johnson CM, Lowe J (2014) Bacterial actin MreB forms antiparallel double filaments. *elife* 3:e02634. <https://doi.org/10.7554/eLife.02634>
- van der Ploeg R, Goudelis ST, den Blaauwen T (2015) Validation of FRET assay for the screening of growth inhibitors of *Escherichia coli* reveals elongasome assembly dynamics. *Int J Mol Sci* 16:17637–17654
- van Heijenoort J (2001) Recent advances in the formation of the bacterial peptidoglycan monomer unit. *Nat Prod Rep* 18:503–519
- van Heijenoort J (2007) Lipid intermediates in the biosynthesis of bacterial peptidoglycan. *Microbiol Mol Biol Rev* 71:620–635
- van Heijenoort J (2011) Peptidoglycan hydrolases of *Escherichia coli*. *Microbiol Mol Biol Rev* 75:636–663
- van Heijenoort Y, Leduc M, Singer H, van Heijenoort J (1987) Effects of moenomycin on *Escherichia coli*. *J Gen Microbiol* 133:667–674
- van Teeffelen S, Wang S, Furchtgott L, Huang KC, Wingreen NS, Shaevitz JW, Gitai Z (2011) The bacterial actin MreB rotates, and rotation depends on cell-wall assembly. *Proc Natl Acad Sci USA* 108:15822–15827
- van Teeseling MC, Mesman RJ, Kuru E, Espaillet A, Cava F, Brun YV, VanNieuwenhze MS, Kartal B, van Niftrik L (2015) Anammox Planctomycetes have a peptidoglycan cell wall. *Nat Commun* 6:6878. <https://doi.org/10.1038/ncomms7878>

- Vilcheze C, Kremer L (2017) Acid-fast positive and acid-fast negative *Mycobacterium tuberculosis*: the Koch paradox. *Microbiol Spectr* 5(2). <https://doi.org/10.1128/microbiolspec.TBTB2-0003-2015>
- Villa E, Schaffer M, Plitzko JM, Baumeister W (2013) Opening windows into the cell: focused-ion-beam milling for cryo-electron tomography. *Curr Opin Struct Biol* 23:771–777
- Vollmer W (2008) Structural variation in the glycan strands of bacterial peptidoglycan. *FEMS Microbiol Rev* 32:287–306
- Vollmer W (2012) Bacterial growth does require peptidoglycan hydrolases. *Mol Microbiol* 86:1031–1035
- Vollmer W, Bertsche U (2008) Murein (peptidoglycan) structure, architecture and biosynthesis in *Escherichia coli*. *Biochim Biophys Acta* 1778:1714–1734
- Vollmer W, Höltje JV (2001) Morphogenesis of *Escherichia coli*. *Curr Opin Microbiol* 4:625–633
- Vollmer W, Höltje JV (2004) The architecture of the murein (peptidoglycan) in Gram-negative bacteria: vertical scaffold or horizontal layer(s)? *J Bacteriol* 186:5978–5987
- Vollmer W, Seligman SJ (2010) Architecture of peptidoglycan: more data and more models. *Trends Microbiol* 18:59–66
- Vollmer W, Tomasz A (2000) The *pgdA* gene encodes for a peptidoglycan *N*-acetylglucosamine deacetylase in *Streptococcus pneumoniae*. *J Biol Chem* 275:20496–20501
- Vollmer W, Blanot D, de Pedro MA (2008a) Peptidoglycan structure and architecture. *FEMS Microbiol Rev* 32:149–167
- Vollmer W, Joris B, Charlier P, Foster S (2008b) Bacterial peptidoglycan (murein) hydrolases. *FEMS Microbiol Rev* 32:259–286
- Vötsch W, Templin MF (2000) Characterization of a  $\beta$ -*N*-acetylglucosaminidase of *Escherichia coli* and elucidation of its role in muropeptide recycling and  $\beta$ -lactamase induction. *J Biol Chem* 275:39032–39038
- Wang X, Huang J, Mukherjee A, Cao C, Lutkenhaus J (1997) Analysis of the interaction of FtsZ with itself, GTP, and FtsA. *J Bacteriol* 179:5551–5559
- Wang L, Khattar MK, Donachie WD, Lutkenhaus J (1998) FtsI and FtsW are localized to the septum in *Escherichia coli*. *J Bacteriol* 180:2810–2816
- Ward JB (1973) The chain length of the glycans in bacterial cell walls. *Biochem J* 133:395–398
- Weidel W, Pelzer H (1964) Bagshaped macromolecules – a new outlook on bacterial cell walls. *Adv Enzymol* 26:193–232
- Weidel W, Primosigh J (1958) Biochemical parallels between lysis by virulent phage and lysis by penicillin. *J Gen Microbiol* 18:513–517
- Weidel W, Frank H, Martin HH (1960) The rigid layer of the cell wall of *Escherichia coli* strain B. *J Gen Microbiol* 22:158–166
- Weiss DS, Pogliano K, Carson M, Guzman L-M, Fraipont C, Nguyen-Distèche M, Losick R, Beckwith J (1997) Localization of the *Escherichia coli* cell division protein FtsI (PBP3) to the division site and cell pole. *Mol Microbiol* 25:671–681
- Wheeler R, Turner RD, Bailey RG, Salamaga B, Mesnage S, Mohamad SA, Hayhurst EJ, Horsburgh M, Hobbs JK, Foster SJ (2015) Bacterial cell enlargement requires control of cell wall stiffness mediated by peptidoglycan hydrolases. *mBio* 6(4):e00660. <https://doi.org/10.1128/mBio.00660-15>
- White CL, Kitich A, Gober JW (2010) Positioning cell wall synthetic complexes by the bacterial morphogenetic proteins MreB and MreD. *Mol Microbiol* 76:616–633
- Wild J, Hennig J, Lobočka M, Walczak W, Kłopotowski T (1985) Identification of the *dadX* gene coding for the predominant isozyme of alanine racemase in *Escherichia coli* K12. *Mol Gen Genet* 198:315–322
- Winkler WC, Nahvi A, Roth A, Collins JA, Breaker RR (2004) Control of gene expression by a natural metabolite-responsive ribozyme. *Nature* 428:281–286
- Witholt B, Boekhout M (1978) The effect of osmotic shock on the accessibility of the murein layer of exponentially growing *Escherichia coli* to lysozyme. *Biochim Biophys Acta* 508:296–305



- Wolf SG, Houben L, Elbaum M (2014) Cryo-scanning transmission electron tomography of vitrified cells. *Nat Methods* 11:423–428
- Yamamoto H, Miyake Y, Hisaoka M, Kurosawa S, Sekiguchi J (2008) The major and minor wall teichoic acids prevent the sidewall localization of vegetative DL-endopeptidase LytF in *Bacillus subtilis*. *Mol Microbiol* 70:297–310
- Yang DC, Peters NT, Parzych KR, Uehara T, Markovski M, Bernhardt TG (2011) An ATP-binding cassette transporter-like complex governs cell-wall hydrolysis at the bacterial cytokinetic ring. *Proc Natl Acad Sci USA* 108:E1052–E1060
- Yang X, Lyu Z, Miguel A, McQuillen R, Huang KC, Xiao J (2017) GTPase activity-coupled treadmilling of the bacterial tubulin FtsZ organizes septal cell wall synthesis. *Science* 355:744–747
- Yao X, Jericho M, Pink D, Beveridge T (1999) Thickness and elasticity of gram-negative murein sacculi measured by atomic force microscopy. *J Bacteriol* 181:6865–6875
- Young KD (2003) Bacterial shape. *Mol Microbiol* 49:571–580
- Young KD (2010) Bacterial shape: two-dimensional questions and possibilities. *Annu Rev Microbiol* 64:223–240
- Zapun A, Vernet T, Pinho MG (2008) The different shapes of cocci. *FEMS Microbiol Rev* 32:345–360
- Zawadzke LE, Bugg TD, Walsh CT (1991) Existence of two D-alanine:D-alanine ligases in *Escherichia coli*: cloning and sequencing of the *ddlA* gene and purification and characterization of the DdlA and DdlB enzymes. *Biochemistry* 30:1673–1682
- Zhao H, Patel V, Helmann JD, Dörr T (2017) Don't let sleeping dogmas lie: new views of peptidoglycan synthesis and its regulation. *Mol Microbiol* 106:847–860
- Zhu JY, Yang Y, Han H, Betzi S, Olesen SH, Marsilio F, Schönbrunn E (2012) Functional consequence of covalent reaction of phosphoenolpyruvate with UDP-N-acetylglucosamine 1-carboxyvinyltransferase (MurA). *J Biol Chem* 287:12657–12667
- Zipperle GF Jr, Ezzell JW Jr, Doyle RJ (1984) Glucosamine substitution and muramidase susceptibility in *Bacillus anthracis*. *Can J Microbiol* 30:553–559

### **Publication 3**

Mayer, C., Kluj, R. M., Mühleck, M., **Walter, A.**, Unsleber, S., Hottmann, I., & Borisova, M. (2019). Bacteria's different ways to recycle their own cell wall. *International Journal of Medical Microbiology*, 309(7), 151326.



Contents lists available at ScienceDirect

## International Journal of Medical Microbiology

journal homepage: [www.elsevier.com/locate/ijmm](http://www.elsevier.com/locate/ijmm)

## Bacteria's different ways to recycle their own cell wall

Christoph Mayer\*, Robert Maria Kluj, Maraike Mühleck, Axel Walter, Sandra Unsleber, Isabel Hottmann, Marina Borisova

Mikrobiologie/Biotechnologie, Interfakultäres Institut für Mikrobiologie und Infektionsmedizin Tübingen (IMIT), Eberhard Karls Universität Tübingen, Auf der Morgenstelle 28, 72076, Tübingen, Germany

## ARTICLE INFO

## Keywords:

Peptidoglycan turnover  
Cell wall recycling  
Autolysis  
N-Acetylmuramic acid  
MurQ etherase  
Anabolic recycling pathway  
*Escherichia coli*  
*Pseudomonas aeruginosa*  
*Tannerella forsythia*  
*Bacillus subtilis*  
*Staphylococcus aureus*

## ABSTRACT

The ability to recover components of their own cell wall is a common feature of bacteria. This was initially recognized in the Gram-negative bacterium *Escherichia coli*, which recycles about half of the peptidoglycan of its cell wall during one cell doubling. Moreover, *E. coli* was shown to grow on peptidoglycan components provided as nutrients. A distinguished recycling enzyme of *E. coli* required for both, recovery of the cell wall sugar N-acetylmuramic acid (MurNAc) of the own cell wall and for growth on external MurNAc, is the MurNAc 6-phosphate (MurNAc 6P) lactyl ether hydrolase MurQ. We revealed however, that most Gram-negative bacteria lack a *murQ* ortholog and instead harbor a pathway, absent in *E. coli*, that channels MurNAc directly to peptidoglycan biosynthesis. This “anabolic recycling pathway” bypasses the initial steps of peptidoglycan *de novo* synthesis, including the target of the antibiotic fosfomicin, thus providing intrinsic resistance to the antibiotic. The Gram-negative oral pathogen *Tannerella forsythia* is auxotrophic for MurNAc and apparently depends on the anabolic recycling pathway to synthesize its own cell wall by scavenging cell wall debris of other bacteria. In contrast, Gram-positive bacteria lack the anabolic recycling genes, but mostly contain one or two *murQ* orthologs. Quantification of MurNAc 6P accumulation in *murQ* mutant cells by mass spectrometry allowed us to demonstrate for the first time that Gram-positive bacteria do recycle their own peptidoglycan. This had been questioned earlier, since peptidoglycan turnover products accumulate in the spent media of Gram-positives. We showed, that these fragments are recovered during nutrient limitation, which prolongs starvation survival of *Bacillus subtilis* and *Staphylococcus aureus*. Peptidoglycan recycling in these bacteria however differs, as the cell wall is either cleaved exhaustively and monosaccharide building blocks are taken up (*B. subtilis*) or disaccharides are released and recycled involving a novel phosphomuramidase (MupG; *S. aureus*). In *B. subtilis* also the teichoic acids, covalently bound to the peptidoglycan (wall teichoic acids; WTAs), are recycled. During phosphate limitation, the sn-glycerol-3-phosphate phosphodiesterase GlpQ specifically degrades WTAs of *B. subtilis*. In *S. aureus*, in contrast, GlpQ is used to scavenge external teichoic acid sources. Thus, although bacteria generally recover their own cell wall, they apparently apply distinct strategies for breakdown and reutilization of cell wall fragments. This review summarizes our work on this topic funded between 2011 and 2019 by the DFG within the collaborative research center SFB766.

## 1. Introduction: the dynamic bacterial cell wall

The cell wall of bacteria rests outside the cytoplasmic membrane and covers the entire cell. It contains the peptidoglycan (PGN), a cell-stabilizing and shape-maintaining macromolecule, building a sack-like structure, the murein or PGN sacculus. The sacculus structure of the bacterial PGN was first recognized in the 1960s in Tübingen by Wolfhard Weidel and his group (Weidel and Pelzer, 1964). They isolated pure PGN cell walls from *Escherichia coli* cells and demonstrated

by electron microscopy that these maintain the size and rod-shape of the cells they were derived from (for an historical account see (Braun, 2015)). They also provided a first structural model of the PGN macromolecule, which is a mesh-like heteropolymer composed of long glycan strands of alternating N-acetylglucosamine (GlcNAc) and N-acetylmuramic acid (MurNAc) sugars cross-linked by short peptides ((Weidel and Pelzer, 1964); for recent reviews see (Litzinger and Mayer, 2010; Walter and Mayer, 2019)). The PGN sacculus is essential to protect bacteria from cell disruption and lysis due to high intracellular

Abbreviations: PGN, peptidoglycan; WTA, wall teichoic acids; LTA, lipoteichoic acids; MurNAc, N-acetylmuramic acid; GlcNAc, N-acetylglucosamine

\* Corresponding author.

E-mail address: [christoph.mayer@uni-tuebingen.de](mailto:christoph.mayer@uni-tuebingen.de) (C. Mayer).

<https://doi.org/10.1016/j.ijmm.2019.06.006>

Received 27 April 2019; Received in revised form 28 May 2019; Accepted 30 June 2019

1438-4221/ © 2019 Elsevier GmbH. All rights reserved.

osmotic pressure (turgor), which can reach up to 5 atm in Gram-negative bacteria (containing a mostly single-layered PGN that is sandwiched between an inner and an outer membrane), and up to 50 atm in Gram-positive bacteria (containing a thick peptidoglycan wall but lacking an outer membrane) (Seltmann and Holst, 2002). In Gram-negative bacteria the PGN is connected to the outer membrane via Braun's lipoprotein, which is covalently linked with the PGN (Hantke and Braun, 1973). In Gram-positive bacteria, polyol-phosphate polymers are covalently attached to the PGN (wall teichoic acids; WTA) or are non-covalently enmeshed in the PGN network (lipoteichoic acids; LTA) (Brown et al., 2013; Percy and Gründling, 2014; Weidenmeier and Peschel, 2008).

The cell wall protects bacteria from adverse impacts of the environment and from disruption due to osmotic shock, thus it has to be sufficiently rigid. At the same time, it needs to be highly flexible, allowing bacteria to steadily adjust shape and mechanical properties of their cell wall during growth and differentiation. Thus, the PGN is constantly remodeled and degraded, involving large sets of potentially autolytic enzymes (autolysins), produced by the bacteria themselves, which potentially target every covalent bond connecting the building blocks within the PGN network (Vermassen et al., 2019). The peptide part of the PGN is cleaved by various amidases and peptidases, whereas the glycan part of the PGN is targeted by lytic transglycosylases, *N*-acetylmuramidases (or *N*-acetylmuraminidases) and *N*-acetylglucosaminidases (Fig. 1). As these cell wall-lytic enzymes are capable of destroying the own PGN mesh, the action of these enzymes must be delicately balanced in bacteria. Indeed, the action of autolysin is controlled by various mechanisms, including structural modifications within the PGN network, which is a distinctive process in bacteria. The Gram-positive pathogen *Staphylococcus aureus*, for example, protects itself from the action of lysozyme-like *N*-acetylmuramidases, cleaving the MurNac- $\beta$ -1,4-GlcNac bond within the glycan backbone of the PGN, by *O*-acetylation of the MurNac residues within the PGN (Bera et al., 2005). The bacterium therefore applies endogenous *N*-acetylglucosaminidases to degrade its own PGN during cell growth (Biswas et al., 2006; Oshida et al., 1995). *Bacillus subtilis* and many other

bacteria in turn control cell wall cleavage via the action of *N*-acetylmuramidases and *N*-acetylglucosaminidases by partial de-*N*-acetylation of the amino sugar part of the PGN (Araki et al., 1980; Benachour et al., 2012; Kobayashi et al., 2012; Psylinakis et al., 2005). Control of PGN autolysis is also achieved by activation mechanisms that restrict the enzyme activity to certain regions, e.g. the inter septal region during cell separation (Meisner et al., 2013; Yang et al., 2011). This allows cell wall degradation within regions prone to decay and leaves portions intact that are required for cell wall stability.

Cleavage of the PGN by endogenous autolytic enzymes releases cell wall-derived fragments (cell wall turnover). In Gram-positive bacteria large amounts of these fragments are found in the growth medium, as these lack an outer membrane as permeability barrier (Reith and Mayer, 2011). This had been the reason why the capability of Gram-positive bacteria to recycle their cell wall had been questioned earlier (Reith and Mayer, 2011). In Gram-negative bacteria, the outer membrane restricts diffusion of larger molecules and cell wall-derived fragments are mostly trapped within the periplasm, from which they are efficiently recovered (cell wall recycling). Cell wall recycling was initially recognized in *E. coli* (Goodell, 1985). This organism releases only small amounts of cell wall-derived peptides into the medium, the major part of the PGN turnover products however are recovered (Goodell, 1985; Goodell and Schwarz, 1985). In *E. coli* and other Gram-negative bacteria, the continuous cleavage of the PGN within the periplasm involves lytic transglycosylases, which generate 1,6-anhydro-MurNac (anhMurNac)-containing PGN fragments (Dik et al., 2017b) (Fig. 1). These anhydromuropeptides (GlcNac-anhMurNac-peptides) are the major PGN recycling products of Gram-negative bacteria (Park and Uehara, 2008). It was estimated that as much as half of the PGN is recycled during one cell doubling in *E. coli*, thus PGN recycling represents a major salvage pathway of bacteria. Recycling of anhydromuropeptides had attracted particular attention due to the connection with  $\beta$ -lactam resistance in Enterobacteriales and Pseudomonales (Bertsche et al., 2015; Dik et al., 2018; Fisher and Mobashery, 2014; Jacobs et al., 1997; Mark et al., 2011). These bacteria are able to sense the relative amounts of the PGN precursor UDP-MurNac-pentapeptide

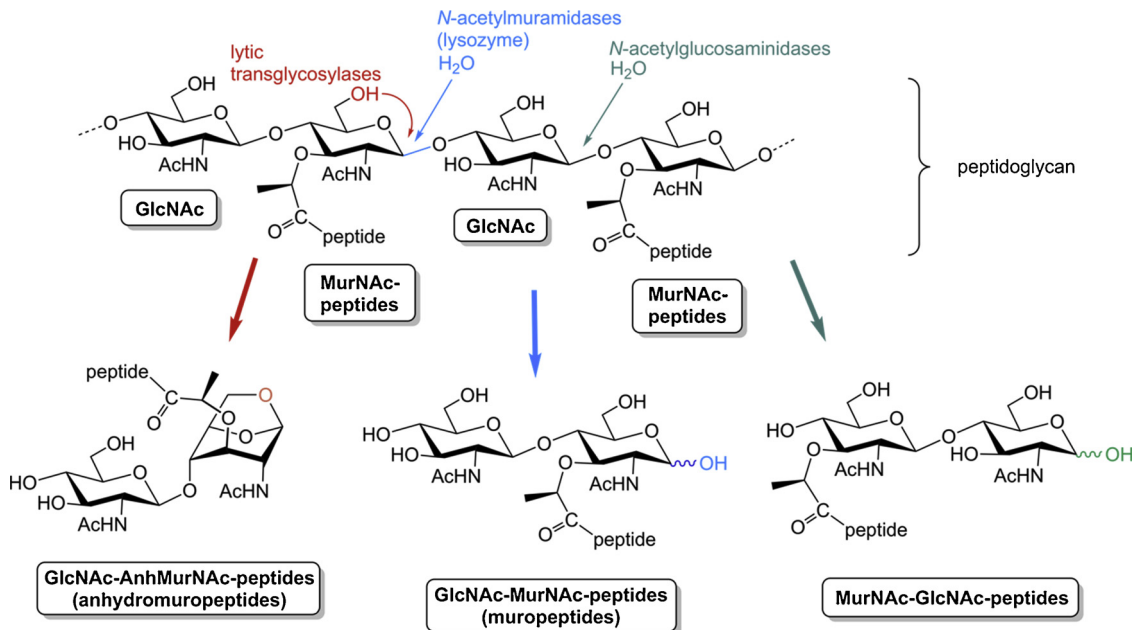


**Fig. 1.** The glycan backbone of the PGN can be cleaved by lytic transglycosylases (LTs), *N*-acetylmuramidases, and *N*-acetylglucosaminidases. LTs and *N*-acetylmuramidases catalyze cleavage of the same glycosidic bond (MurNac- $\beta$ -1,4-GlcNac). However, only the *N*-acetyl-muramidases catalyze hydrolysis this bond, generating GlcNac-MurNac-peptides (muropeptides), whereas the LTs catalyzes non-hydrolytic cleavage, generating 1,6-anhydroMurNac (AnhMurNac)-containing fragments (anhydromuropeptides). Endo-acting *N*-acetylglucosaminidases catalyze the hydrolysis of the other glycosidic bond (GlcNac- $\beta$ -1,4-MurNac), thus generating distinct MurNac-GlcNac-peptides. It should be noted here that recently LTs have been identified, which are also able to generate 1,6-anhydro-GlcNac-containing fragments (Williams et al., 2018).

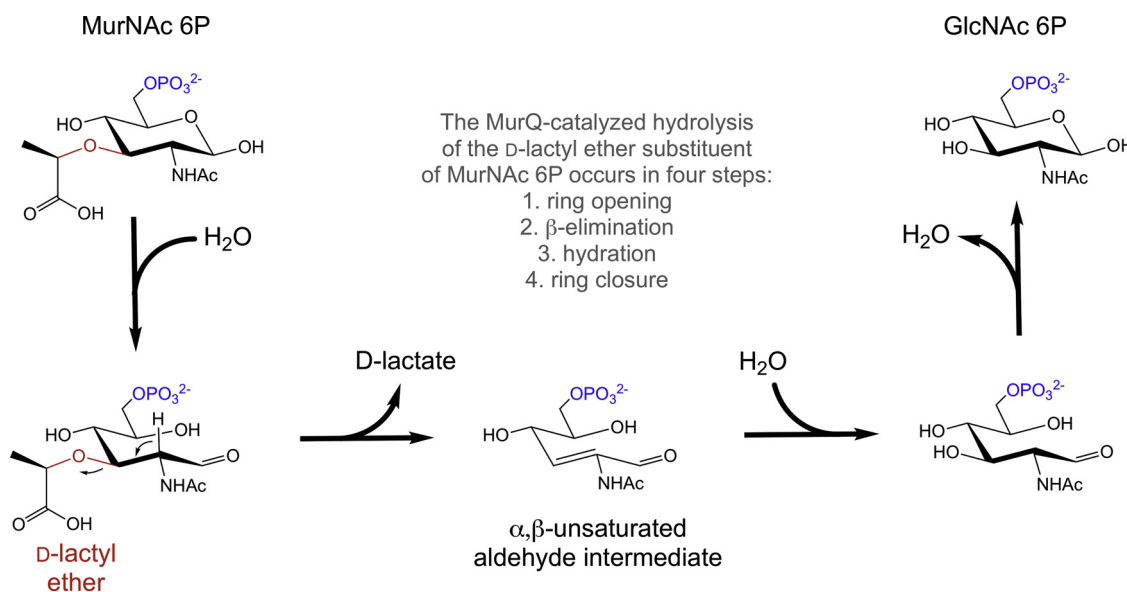


**Fig. 2.** The etherase MurQ is a distinguished cell wall recycling enzyme, first identified in *E. coli*. It catalyzed the hydrolysis of the D-lactyl ether substituent of MurNAc 6P by an  $\beta$ -elimination/hydration mechanism and via formation of an  $\alpha,\beta$ -unsaturated aldehyde intermediate, finally yielding GlcNAc 6P.

and the cell wall turnover product anhydroMurNAc-pentapeptide, thereby monitoring the status of the cell wall and eventually inducing the expression of chromosomally encoded AmpC-type  $\beta$ -lactamase (Dik et al., 2017a; Vadlamani et al., 2015).

## 2. The etherase MurQ and PGN recycling in *E. coli*

A dedicated PGN recycling enzyme had been identified earlier in our group, which converts MurNAc 6-phosphate (MurNAc 6P) to GlcNAc 6-phosphate (GlcNAc 6P) (Jaeger et al., 2005). The enzyme acts as a unique MurNAc 6P lactyl ether hydrolase (named etherase MurQ) that cleaves off the D-lactic acid side chain from MurNAc 6P by a  $\beta$ -elimination/hydration mechanism (Hadi et al., 2008; Jaeger et al., 2005; Jaeger and Mayer, 2008a) (Fig. 2). MurQ had been initially characterized as an enzyme required for growth of *E. coli* on MurNAc as the sole source of carbon and energy, together with the MurNAc-PTS transporter MurP (Dahl et al., 2004; Jaeger et al., 2005; Jaeger and Mayer, 2008b). Later on, it was shown that MurQ is also necessary for the recycling of anhydroMurNAc (Uehara et al., 2006). Anhydromuropeptides, generated by lytic transglycosylases, are imported into the cell via AmpG permease and AnhydroMurNAc is released together with GlcNAc and cell wall-peptides by the concerted action of dedicated PGN recycling enzymes: the *N*-acetylglucosaminidase NagZ, the AnhydroMurNAc-L-alanine amidase AmpD, and the L,D-carboxypeptidase LdcA (Park and Uehara, 2008) (Fig. 3). AnhydroMurNAc is further phosphorylated by a specific AnhydroMurNAc kinase (AnmK) yielding MurNAc 6P (Uehara et al., 2005), GlcNAc is converted to GlcNAc 6P by the GlcNAc kinase NagK (Park and Uehara, 2008) and MurQ converts MurNAc 6P to GlcNAc 6P (Jaeger et al., 2005). Finally, GlcNAc 6P enters the known catabolic pathway of GlcNAc or is used for PGN re-synthesis (Park and Uehara, 2008; White, 1968). The peptide portion of the PGN can be catabolized after cleavage by amidases/peptidases (during amino acid starvation), but normally the intact murein tripeptide L-Ala-iso-D-Glu-mDAP is added to UDP-MurNAc by the Mpl ligase, yielding UDP-MurNAc-tripeptide, thereby substituting three amino acid ligase enzymes (MurCDE) of the PGN *de novo* biosynthesis (Park and Uehara, 2008). Notably, the L,D-carboxypeptidase LdcA is required to trim cell wall-derived tetra- and pentapeptides to tripeptides. If this enzyme is missing, *E. coli* cell lyse in the onset of stationary phase (Templin et al., 1999), presumably because accumulation of tetrapeptides leads to the formation of "wrong" UDP-MurNAc-tetrapeptide precursors that do not

allow the PGN to get normally crosslinked by D,D-transpeptidation.

## 3. An anabolic recycling route identified in *Pseudomonas* sp

We recognized that the MurNAc 6P etherase (MurQ) unexpectedly is absent in many Gram-negative bacteria (Jaeger and Mayer, 2008a). Most *Pseudomonas* sp. for example, lack MurQ despite possessing all upstream recycling enzymes, e.g. AmpG, AmpD, NagZ, and AnmK. They also contain the recycling route that channels murein tripeptide to PGN biosynthesis (LdcA, Mpl). In *Pseudomonas putida*, all enzymes required for the catabolism of cell wall-derived amino sugars are missing, including MurP, MurQ, NagK and also NagA and NagB. We hypothesized that in organisms that lack MurQ the amino sugars of the PGN cell wall might be channeled directly to PGN biosynthesis, by a so far unknown route, analogous to the tripeptide recycling via Mpl. We further argued that a hypothetical PGN recycling bypass to UDP-MurNAc should affect fosfomycin resistance in these organisms (Gisin et al., 2013). Fosfomycin is a broad spectrum antibiotic that targets the enzyme MurA catalyzing first step of PGN synthesis towards the formation of uridine diphosphate *N*-acetylmuramic acid (UDP-MurNAc) (Fig. 4). Since about half of the PGN is recycled in one generation, this should massively contribute to the UDP-MurNAc pool, and should thus affect fosfomycin susceptibility. Indeed, when we tested known *Pseudomonas* recycling mutants (*ampG*, *nagZ*, *ampD*), they were severely affected in fosfomycin susceptibility (Borisova et al., 2014; Gisin et al., 2013). We used this test, to screen putative candidate genes involved in an UDP-MurNAc biosynthetic (anabolic) recycling metabolism. A nucleotidyl transferase similar to transferase domain of GlmS (the enzyme converting glucosamine 6P to UDP-MurNAc) was identified as MurNAc  $\alpha$ -1-phosphate uridylyltransferase (MurU) and the preceding enzyme was found to be an anomeric kinase that phosphorylates MurNAc as well as GlcNAc at the  $\alpha$ -1-position (AmgK, for anomeric MurNAc/GlcNAc kinase) (Gisin et al., 2013; Renner-Schneek et al., 2015). Simultaneously, in the group of Tom Bernhardt and in our group the last enzyme of the anomeric recycling route was identified, a specific MurNAc 6P phosphatase named MupP (Borisova et al., 2017; Fumeaux and Bernhardt, 2017). Thus, the complete "anabolic PGN recycling pathway" of *Pseudomonas* sp. includes the phosphorylation of anhydroMurNAc by AnmK, dephosphorylation by MupP, re-phosphorylation at the anomeric position with AmgK and the uridylyl transfer reaction catalyzed by MurU, yielding UDP-MurNAc (Fig. 4). The anomeric kinase AmgK is also able

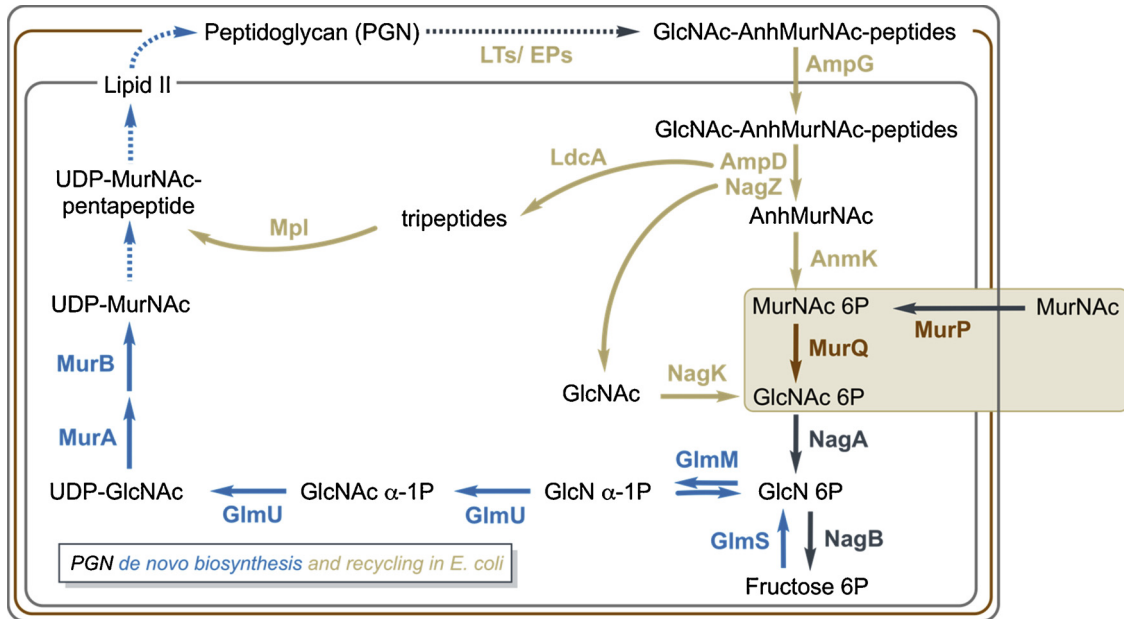


**Fig. 3.** Overview of the PGN recycling and MurNAc catabolic pathways of *E. coli*. PGN turnover in *E. coli* involves lytic transglycosylases (LTs) and endopeptidases (EPs) which generate GlcNAc-AnhMurNAc-peptides (anhydromuropeptides) in the periplasm. These are taken up by the AmpG permease and are then processed in the cytoplasm by dedicated recycling enzymes: the *N*-acetyl-glucosaminidase NagZ, the AnhMurNAc-L-alanine amidase AmpD and the L,D-carboxypeptidase LdcA. Tripeptides are channelled into the PGN biosynthesis or are catabolized and the amino sugars AnhMurNAc and GlcNAc are phosphorylated by specific kinases (AnmK, NagK) and further catabolized via NagA/NagB or used for PGN resynthesis. The MurQ etherase is required for both, recycling of anhydromuropeptides as well as for growth on external MurNAc, which is imported and concomitantly phosphorylated via MurP.

to phosphorylate GlcNAc, yielding GlcNAc α-1-phosphate, and this product is accepted as a substrate by GlmU (bifunctional *N*-acetylglucosamine 1-phosphate uridylyltransferase). Thus both amino sugars of the PGN are recycled and channelled into the PGN biosynthesis.

The fosfomycin sensitivity phenotype of recycling mutants could be rescued, not only by complementation with the respective recycling genes from *Pseudomonas* sp., but also by expressing distantly related orthologs from *Neisseria meningitidis* (β-Proteobacterium), *Caulobacter*

*crescentus* (α-Proteobacterium), or *Tannerella forsythia* (Bacteroidetes) (Gisin et al., 2013); Hottmann, unpublished). This revealed that distantly related recycling genes are functional and, thus, the anabolic recycling route constitutes a common pathway within Gram-negative bacteria. The distribution of the different recycling enzymes within the bacterial phylogeny is shown in Fig. 5. The major conclusions drawn from this tree are: i) Gram-negative bacteria mostly contain the anabolic recycling route except for *E. coli* and related Enterobacteriales,

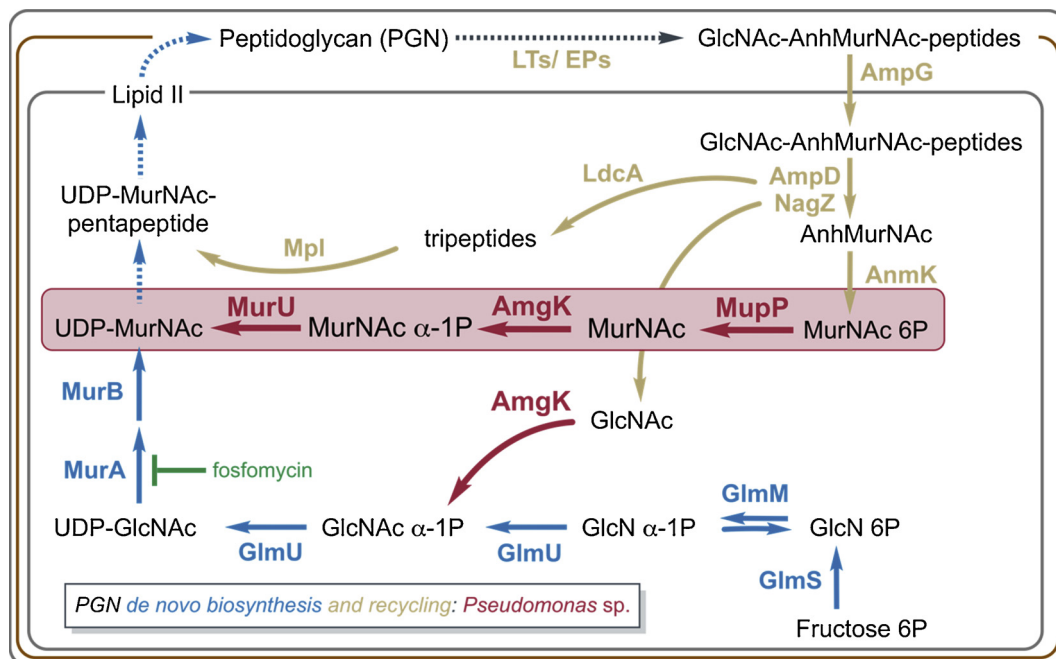


**Fig. 4.** Overview of the PGN recycling in *Pseudomonas putida*. The MurQ enzyme and most other enzymes involved in amino sugar recycling and catabolism are missing in *Pseudomonas* sp. Instead these bacteria harbor an "anabolic recycling pathway" (MupP, AmgK, MurU) that channels MurNAc 6P into the PGN biosynthesis pathway on the level of UDP-MurNAc, and GlcNAc to UDP-GlcNAc (AmgK, GlmU).

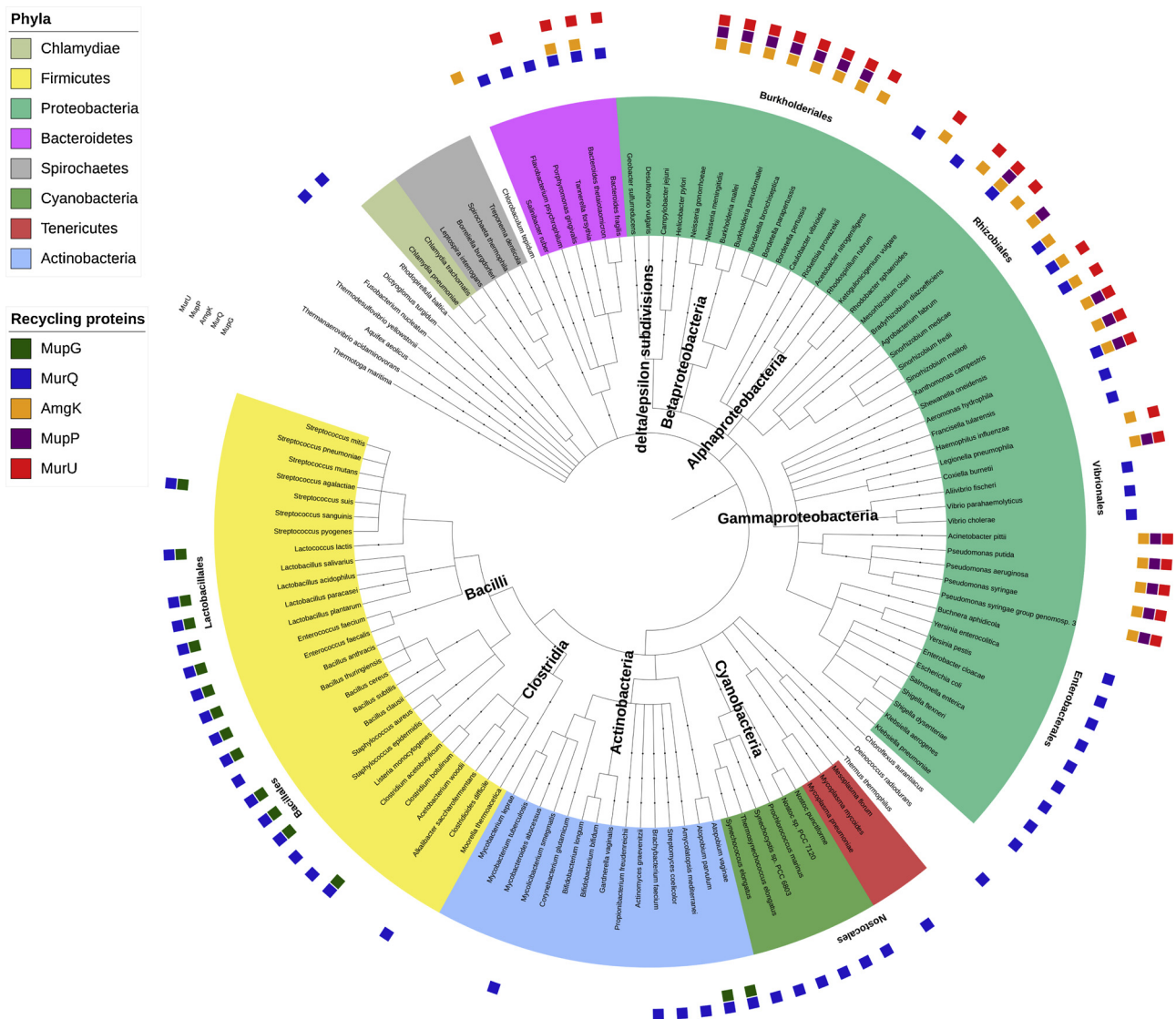


**Fig. 5.** Phylogenetic tree of representative bacterial species showing the distribution of PGN recycling-associated proteins in bacterial taxa. MurQ (blue; represents the MurQ pathway known from *E. coli* and *B. subtilis*) and MupG (green; see chapter entitled "Peptidoglycan recycling in *Staphylococcus aureus*" for description of MupG function); AmgK (orange), MupP (purple) and MurU (red), constituting the anabolic recycling pathway known from *Pseudomonas* sp. The tree was built on the taxonomy according to NCBI and BLAST searches for proteins identified in (Fumeau and Bernhardt, 2017; Gisin et al., 2013). (For interpretation of the references to colour in this figure legend, the reader is referred to the web version of this article).

Vibrionales and some others. Only few bacteria, mostly Bacteroidetes and Rhizobiales sp., contain both the catabolic recycling pathway (MurQ) and the anabolic recycling pathway (MupP/AmgK/MurU). The latter pathway, however, is absent in Cyanobacteria and in all Gram-positives, which generally contain one or two MurQ orthologs (Fig. 5). Intriguingly, some bacterial sp. (e.g. *Streptococcus* sp., as well as  $\delta$ - and  $\epsilon$ -Proteobacteria) apparently lack both pathways and it remains to be investigated, whether these are not able to recycle their cell wall (as had been suggested (Boersma et al., 2015)) or they apply different strategies to recover their cell wall components.

#### 4. MurNac recycling and scavenging in *Tannerella forsythia*, a MurNac auxotrophic bacterium

Only few bacteria, e.g. some Bacteroidetes species, contain both the MurQ and the AmgK/MurU pathway. One such example is the oral pathogen *Tannerella forsythia*. This bacterium is phylogenetically related to *Bacteroides* species, but was classified based on 16S rRNA-analyses into its own genus *Tannerella* within the *Porphyromonadacea*

(Sakamoto et al., 2002) (cf. Fig. 5). We are currently exploring the PGN metabolism in *T. forsythia*. Its natural habitat is the oral cavity where it lives as in a consortium together with *P. gingivalis* and *T. denticola*, called the "red complex consortium". This complex is known to cause severe forms of periodontitis (Holt and Ebersole, 2005). The most intriguing observation regarding *T. forsythia* is that this organism has a demand for MurNac if grown in axenic culture (Wyss, 1989). The observed MurNac auxotrophy of *T. forsythia* appeared consequential after genome analysis (Friedrich et al., 2015): *T. forsythia* lacks *murA/murB* and *gmsS/gmU* orthologs (see Fig. 6), which are generally essential for PGN *de novo* biosynthesis in other bacteria. As *T. forsythia* apparently is unable to synthesize MurNac on its own, it has to acquire this amino sugar from the environment. Indeed *T. forsythia* was shown to grow in co-culture with different bacteria (Sharma et al., 2005). Many bacteria use a phosphotransferase system (PTS) transporter (MurP in *E. coli*) for the uptake of MurNac (Dahl et al., 2004). These transporters phosphorylate MurNac by the means of a phosphorylation cascade concomitant with the uptake (Deutscher et al., 2006). Thorough examination revealed that *T. forsythia* entirely lacks PTS transporters.

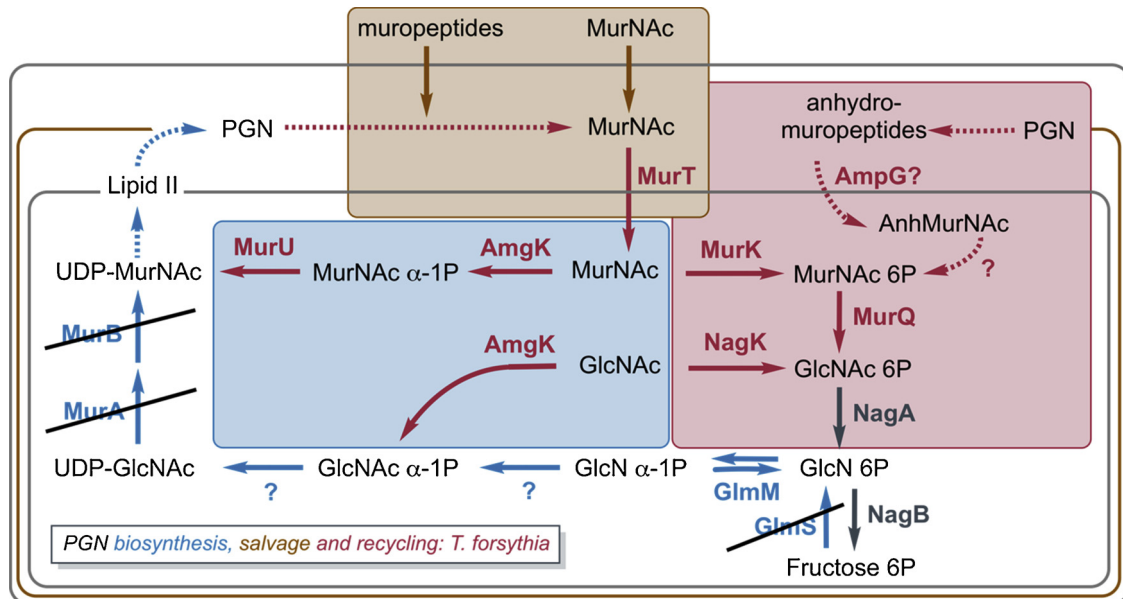


**Fig. 6.** Overview of the PGN recycling pathways of the oral pathogen *Tannerella forsythia*, which harbors both, the *E. coli* MurQ and the *Pseudomonas* AmgK-MurU pathways. *T. forsythia* lacks generally essential enzymes of the PGN *de-novo* biosynthesis pathway (blue), thus is auxotrophic for MurNAc. MurNAc uptake is mediated by a non-PTS transporter (MurT) and the sugar is then either phosphorylated at the C6 hydroxyl group (MurK), thereby is prone for energy metabolism, or phosphorylated at the anomeric position (AmgK), leading to UDP-MurNAc. (For interpretation of the references to colour in this figure legend, the reader is referred to the web version of this article).

However, this organism carries a putative *murQ* orthologue (*Tanf\_08385*) on its chromosome, which encodes a functional MurNAc 6P lactyl ether hydrolase named Tf\_MurQ (Ruscitto et al., 2016). Two other genes are located upstream of *murQ* on the *T. forsythia* genome: a membrane protein (*Tanf\_08375*) and a putative kinase (*Tanf\_08380*). The membrane protein was identified as a PTS-independent MurNAc transporter named Tf\_MurT, constituting a novel transporter family conserved within the Bacteroidetes (Ruscitto et al., 2016). The gene upstream of *murQ* subsequently was identified as a gene encoding an amino sugar kinase (Tf\_MurK) that specifically phosphorylates MurNAc at the position C6, thereby generating MurNAc 6P, the substrate for Tf\_MurQ (Hottmann et al., 2018). Biochemical characterization revealed that the Tf\_MurK kinase exhibits exclusive specificity for MurNAc, thereby distinguishes from the GlcNAc/MurNAc-kinase of *Clostridium acetobutylicum* (Reith et al., 2011). In *T. forsythia* the Tf\_MurT/MurK/MurQ pathway displays a MurNAc catabolic route generating GlcNAc 6P, which is further shuttled into glycolysis (Hottmann et al., 2018). Surprisingly, however, the *Tf.murK* deletion mutant was found to accumulate the PGN precursor molecule UDP-MurNAc-pentapeptide in stationary growth phase and cells showed a growth advantage in MurNAc-limited medium (Hottmann et al., 2018). These results indicate that in this organism, MurNAc may be shuttled into PGN biosynthesis via an anabolic pathway. Genome analysis revealed that orthologues of *amgK* and *murU* are indeed present in *T. forsythia*. Likely the AmgK/MurU pathway replaces the MurA/B pathway and represents the principle route for PGN synthesis in this organism (Fig. 6).

## 5. Peptidoglycan recycling in *Bacillus subtilis*

As mentioned above, an ortholog encoding the recycling enzyme MurQ is found on the genome of *B. subtilis* (48% amino acid sequence identity with *E. coli* MurQ). It is organized in an operon together with orthologs of *murR*, encoding a transcriptional MurNAc 6P-sensitive repressor, and *murP*, encoding a phosphotransferase system (PTS) transporter for MurNAc (amino acid sequence identities of 27% and 38%, respectively) (Dahl et al., 2004; Jaeger and Mayer, 2008b). Using high performance liquid chromatography/mass spectrometry (HPLC-MS),

we could show that MurNAc 6P accumulates in *B. subtilis*  $\Delta$ *murQ* cells grown in nutrient-rich medium (Borisova et al., 2016; Borisova and Mayer, 2017). The corresponding wild-type strain revealed no accumulation of MurNAc 6P, and also no accumulation was observed in a mutant lacking the whole operon, *murQ-murR-murP* (Borisova et al., 2016). This led to the conclusion that recycling of the MurNAc portion of the PGN takes place in Gram-positives and relies on a functional MurQ etherase. In addition, we showed that uptake and concomitant phosphorylation of MurNAc occurs via MurP (Borisova et al., 2016). The absence of MurNAc 6P accumulation in the operon mutant further indicates that MurP is the only transporter for MurNAc in *B. subtilis*. MurNAc 6P accumulated only in small amounts during exponential growth phase, but increased significantly in transition phase, and reached a maximum in stationary phase (Borisova et al., 2016; Unsleber et al., 2017). Thus, apparently PGN recycling in *B. subtilis* proceeds differently from *E. coli*, where recycling occurs continuously during exponential growth phase (Borisova et al., 2016; Jaeger and Mayer, 2008b). MurNAc 6P accumulation strongly increased when the growth medium was supplemented with MurNAc. Addition of MurNAc however did not sustain growth neither of wild-type nor of  $\Delta$ *murQ* mutant cells. However, in late stationary phase, cultures of *B. subtilis* wild-type cells remained higher optical density when grown in a medium supplemented with MurNAc as compared to cultures of mutant cells or cultures of cells grown without MurNAc. This led to the assumption that MurNAc might have an impact on cell survival (Borisova et al., 2016). Indeed, higher numbers of colony forming units were observed in late stationary phase in wild-type cells grown with MurNAc, whereas  $\Delta$ *murQ* cells showed a dramatic decrease in viability (Borisova et al., 2016). A survival benefit, albeit much weaker, was also observed when wild-type versus mutant cells were grown in nutrient rich-medium without MurNAc (Borisova et al., 2016). The lower viability of  $\Delta$ *murQ* cells is likely due to increased cell lysis in the stationary phase. *B. subtilis* is known to lyse under nutrient-depletion conditions involving autolytic enzymes by mechanisms not completely understood (Jolliffe et al., 1981; Lewis, 2000; Smith et al., 2000). Usually autolysins are strictly regulated, however during nutrient limitation they apparently become deregulated. There is evidence that the collapse of the proton motive force (PMF) is responsible for the activation of autolysins, which



involves the proton buffering capacity of teichoic acids (Calamita and Doyle, 2002; Calamita et al., 2001; Jolliffe et al., 1981). In the onset of sporulation, *B. subtilis* undergoes cell lysis by a mechanism named cannibalism, which is the feeding of a starving subpopulation on sibling cells (Gonzalez-Pastor et al., 2003). In a heterogeneous cell population, some cells recognize nutrient limitation earlier than others. These cells activate the global regulator Spo0A by phosphorylation (Spo0A-P) (Chastanet et al., 2010; Chung et al., 1994). Spo0A-P is responsible for the expression of cannibalism toxins, sporulation delay factor (SDP) and sporulation killing factor (SKF), as well as their cognate immunity proteins (Ellermeier et al., 2006; Gonzalez-Pastor, 2011). Cannibalistic cells attack prey cells which have not sensed nutrient limitation, and hence have not activated Spo0A. Activity of the toxins SDP and SKF on prey cells leads to a collapse of the PMF and in a second consequence leads to the activation of autolysins, and thereby cell lysis (Lamsa et al., 2012). Lysed cells release nutrients including peptidoglycan fragments due to autolysin action, on which cannibalistic cells can feed on. *B. subtilis* cleaves peptidoglycan by endo-acting (Smith et al., 2000) as well as exo-acting hydrolases (*N*-acetylglucosaminidase NagZ and MurNac-L-alanine amidase AmiE) (Litzinger et al., 2010). Thereby released cell wall sugars, MurNac and GlcNac, are taken up into the cytoplasm and are concomitantly phosphorylated by PTS transporters (Fig. 7). The MurQ etherase converts MurNac 6P to GlcNac 6P, which is deacetylated by NagA, and the product glucosamine 6P (GlcN 6P) either enters glycolysis or is used for PGN re-synthesis. Also the peptide portion of the PGN is recovered, which is however less well investigated (Amoroso et al., 2012). Thus, recovery of prey cell peptidoglycan might help cannibalistic cells to enhance survival during nutrient limitation and to delay sporulation (Lamsa et al., 2012).

## 6. Peptidoglycan recycling in *Staphylococcus aureus*

*Staphylococcus aureus* is a spherical non-sporulating Gram-positive bacterium, belonging to the phylum Firmicutes. It is usually part of the human microbiota, but methicillin-resistant *S. aureus* (MRSA) can also cause life-threatening infections due to multiple drug resistance (Hiramatsu et al., 2014; Tong et al., 2015). *S. aureus* protects itself from the action of lysozyme-like *N*-acetyl muramidases by *O*-acetylation of the C6 hydroxyl group of MurNac residues within the PGN (Bera et al., 2005; Moynihan et al., 2014). In consequence, the bacterium cleaves its

own PGN network using endo-acting *N*-acetylglucosaminidases, instead of *N*-acetylmuramidases, which are not affected by MurNac *O*-acetylation. *S. aureus* processes, besides other *N*-acetylglucosaminidases, the enzyme Atl, which is the major autolysin of the organism (Bose et al., 2012; Oshida et al., 1995; Wheeler et al., 2015; Yamada et al., 1996). Atl is a bifunctional *N*-acetylmuramyl-L-alanine amidase/endo-*N*-acetylglucosaminidase, that is affected by binding to cell wall structures and releases MurNac-GlcNac disaccharide and peptides from the cell wall (Biswas et al., 2006; Götz et al., 2014; Oshida et al., 1995; Schlag et al., 2010). Atl is proteolytically processed and occurs in a cell surface-bound as well as a soluble form in the culture supernatant (Komatsuzawa et al., 1997; Yamada et al., 1996).

Alike *E. coli* and *B. subtilis*, *S. aureus* is able to recover extracellular MurNac via the MurQ pathway (Borisova et al., 2016). However, the Atl autolysin as well as other *N*-acetylglucosaminidases of *S. aureus* generate MurNac-GlcNac disaccharides instead of MurNac. The *S. aureus* recycling operon, encodes genes for the MurQ etherase, the PTS transporter MurP (SaMurP) and the MurR-like transcriptional regulator SaMurR. In addition, the operon contains a gene of unknown function downstream of *murQ*. We recently showed that this gene (SAUSA300\_0192) encodes a 6-phospho-*N*-acetylmuramidase (named MupG), which cleaves the phosphorylated disaccharide MurNac 6P-GlcNac yielding MurNac 6P and GlcNac (Kluj et al., 2018). Accordingly, MurNac 6P-GlcNac accumulates in the *S. aureus* USA300  $\Delta$ mupG mutant. As the disaccharide MurNac-GlcNac accumulates in the culture supernatant of a *S. aureus*  $\Delta$ murP mutant, which is the main turnover product in *S. aureus* generated by Atl, the natural substrate of the PTS transporter is the disaccharide MurNac-GlcNac and not MurNac. SaMurP is able to transport and phosphorylate both the disaccharide as well as MurNac, however, MurNac is a fortuitous substrate and not a natural product of PGN degradation in this organism. By fragmentation MS, the product of phosphorylation by SaMurP and the respective substrate for MupG was identified as a disaccharide carrying a phosphorylation at the C6 hydroxyl group of the non-reducing terminal MurNac. The action of MupG produces MurNac 6P, which is converted into GlcNac 6P by the etherase MurQ, as well as GlcNac. The fate of the second product remains so far unknown. Thus, the reaction catalyzed by MupG represents an additional step in the MurQ pathway compared to *E. coli* and *B. subtilis*, which is necessary in *S. aureus* to recycle the turnover product MurNac-GlcNac. The enzyme MupG

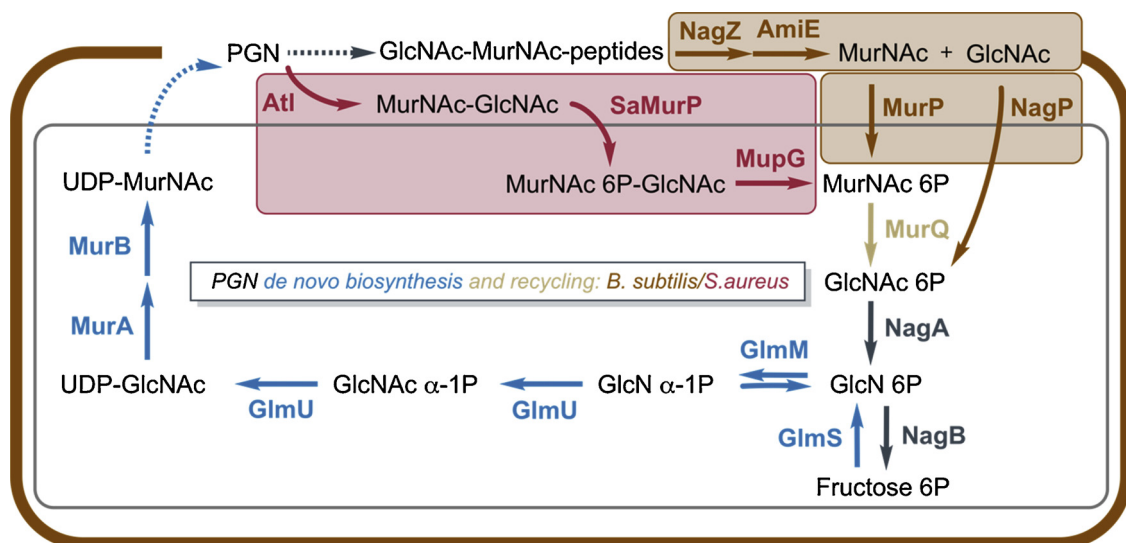
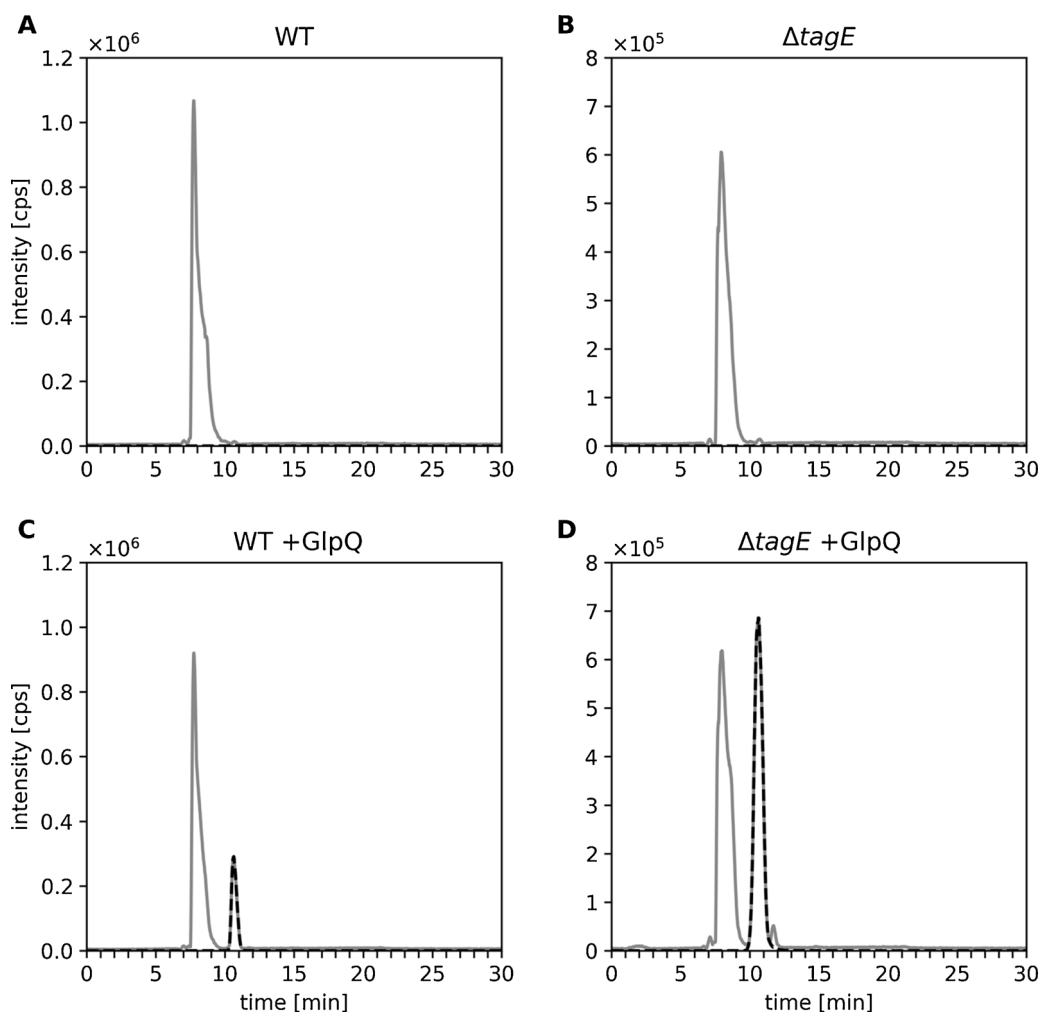


Fig. 7. Overview of the PGN recycling pathways of *B. subtilis* (brown) and *S. aureus* (red). Both Gram-positive bacteria recycle the MurNac portion of their PGN via MurQ. In *B. subtilis*, the PGN is cleaved exhaustively outside the cell, yielding the sugars MurNac and GlcNac, which are taken up and phosphorylated by PTS transporters MurP and NagP, respectively. In *S. aureus* a unique turnover product, the disaccharide MurNac-GlcNac is generated by the action of the major autolysin Atl, which is taken up and concomitantly phosphorylated by SaMurP and the product is cleaved in the cytoplasm by a novel MurNac 6P hydrolase (MupG). (For interpretation of the references to colour in this figure legend, the reader is referred to the web version of this article).



**Fig. 8.** GlpQ preferentially releases sn-glycerol 3P from WTA isolated from  $\Delta tagE$  mutant cells over WTA from wild-type (WT) cells. Purified *B. subtilis* cell wall (100  $\mu$ g, containing PGN and covalently bound WTAs) was incubated with GlpQ (1  $\mu$ g) and the formation of reaction products was analyzed by HPLC-MS. Shown are the base peak chromatograms (BPC; mass range  $[M + H]^+ = 100\text{--}1500\text{ m/z}$ ; gray) and the extracted ion chromatograms (EIC  $\times 10^5$  cps) of glycerol-phosphate (GroP) ( $[M + H]^+ = 173.022 \pm 0.02\text{ m/z}$ ; blue). (A and C) wild type WTA (= partially glycosylated WTA) without GlpQ (control) and incubated with GlpQ incubated for 30 min. The peak area (area under the curve; AUC) of released Gly-3P was  $AUC = 7.8 \times 10^6$ . (B and D) non-glycosylated  $\Delta tagE$  WTA without GlpQ (control) and with GlpQ incubated for 30 min. The obtained  $AUC = 29.8 \times 10^6$  was 3.8 times as much compared to the release of Gly-3P from WT WTA.

belongs to a so far unexplored protein family containing domain of unknown function 871 (DUF871) (Kluj et al., 2018) (Fig. 5). This protein family is narrowly distributed mostly among the Firmicutes, including Bacilli, but a MupG ortholog is absent in *B. subtilis*. Intriguingly, some bacteria contain multiple versions of MupG protein. The protein family divides in two distinct phylogenetic clades, one representing MupG and close homologs, and a second clade, with more distantly related orthologs (MupG-like proteins), may contain enzymes with different substrate specificities and functions (Kluj et al., 2018).

## 7. Degradation of wall teichoic acids and the role of the teichoicase GlpQ

Since recycling of the PGN in Gram-positive bacteria has been demonstrated, we questioned whether the wall teichoic acids (WTAs), which are covalently linked to the PGN, are also recovered. WTAs and PGN make up roughly equal amounts in the cell wall of Gram-positive bacteria. It has been shown that phosphate deficiency can be compensated by scavenging the phosphate stored within the WTA chain polymers (Grant, 1979). The reduction in WTA is accompanied by synthesis of phosphate-free teichuronic acids (TUA), consisting of poly-*N*-acetylglucosamine-glucuronic acid. About 70% of WTA are exchanged with TUA during phosphate starvation (Bhavsar et al., 2004; Ellwood and Tempest, 1969; Lang et al., 1982; Soldo et al., 1999). This WTA-to-TUA-shift is mediated by the two-component system PhoPR. The sensor kinase PhoR is inhibited by WTA biosynthesis intermediates, which are abundant during phosphate excess. When phosphate gets limiting, these intermediates are reduced and PhoR is able to phosphorylate the

response regulator PhoP (Devine, 2018). The phosphorylated response regulator PhoR subsequently inhibits the transcription of WTA biosynthesis genes and activates transcription of TUA biosynthesis genes (Botella et al., 2014, 2011; Götz et al., 2014). Although it is long known that WTAs are degraded during phosphate starvation, the process is so far not completely understood. Proteome studies with *B. subtilis* have shed some light on that question. Cells were grown under phosphate limitation supplemented with purified WTA fragments and the proteome was compared with cells grown in phosphate excess (Unsleber, Franz-Wachtel, Macek, Mayer, unpublished results). Amongst other proteins, e.g. the alkaline phosphatase PhoB, the phosphodiesterases GlpQ and PhoD, were found to be highly upregulated (Unsleber, 2017). GlpQ and PhoD are controlled by the PhoPR regulon and preferentially degrade non-glycosylated WTAs (Myers et al., 2016; Unsleber, 2017). While GlpQ cleaves in an exo-acting manner releasing sn-glycerol 3-phosphate (Fig. 8), PhoD apparently catalyzes endo-hydrolysis at non-specific sites throughout the polymer (Myers et al., 2016). It has also been demonstrated that  $\Delta glpQ$  or  $\Delta phoD$  mutants retained WTA and ceased growth upon phosphate limitation, suggesting that they are key enzymes in WTA degradation (Myers et al., 2016). Interestingly, GlpQ is not able to use LTA as a substrate. The crystal structure of GlpQ reveals a binding cleft that specifically accommodates sn-glycerol 3-phosphate, which explains the stereochemical differentiation between WTA and LTA (Unsleber, 2017) (Walter & Mayer, unpublished). However, GlpQ is not only involved in WTA degradation. In *S. aureus* GlpQ permits growth within the host, where nutrient levels like glucose fluctuate. GlpQ is responsible for extracellular phosphodiesterase activity, by which *S. aureus* can scavenge glycerophosphodiester (GPD)

within body fluids. The released glycerol-3-phosphate serves as a carbon and phosphate source (Jorge et al., 2017, 2018). GlpQ is also involved in the general glycerol metabolism as part of the *glp* regulon, induced by glycerol-phosphate (Nilsson et al., 1994).

## 8. Conclusion

All bacteria - Gram-negative bacteria and Gram-positives - degrade their own cell wall by specific sets of autolytic enzymes, which is a prerequisite for bacterial growth and differentiation. As different as the sets of autolytic enzymes, are the released turnover fragments: diverse disaccharides, disaccharide-peptides (anhydromuropeptides, GlcNAc-MurNAc-peptides and MurNAc-GlcNAc-peptides), or after further extracellular cleavage, monosaccharides and peptides/amino acids. Bacteria generally are also able to recycle their cell wall turnover products using different strain-specific routes. They use specific sets of transporters, which may or may not phosphorylate the incoming fragments. Intracellularly, the fragments may be further degraded (catabolic recycling; MurQ) or channeled into the biosynthesis pathways (anabolic recycling; AmgK/MurU). This distinguishes Gram-negative bacteria, including the model organisms *E. coli* and *Pseudomonas* sp., whereas *T. forsythia* harbors both pathways. Gram-positive bacteria (*B. subtilis* and *S. aureus*) lack the anabolic recycling route but mostly contain a MurQ etherase. *B. subtilis* is distinguished by the ability to cleave the cell wall to monosaccharides and use specific transporters for these, whereas many other firmicutes bacteria, including *S. aureus*, apply the novel phospho-muramidase MupG enzymes to intracellularly degrade phosphorylated MurNAc-GlcNAc. Thus, although the ability to recycle their own cell wall is a general feature of bacteria, different recovery and reutilization strategies are applied.

## Acknowledgements

This work was supported by the Deutsche Forschungsgemeinschaft (DFG) within the Sonderforschungsbereich SFB766 - project A15. We thank Prof. Wolfgang Wohlleben for his commitment to the SFB over all the years.

## References

- Amoroso, A., Boudet, J., Berzigotti, S., Duval, V., Teller, N., Mengin-Lecreux, D., Luxen, A., Simorre, J.P., Joris, B., 2012. A peptidoglycan fragment triggers  $\beta$ -lactam resistance in *Bacillus licheniformis*. *PLoS Pathog.* 8, e1002571.
- Araki, Y., Oba, S., Araki, S., Ito, E., 1980. Enzymatic deacetylation of *N*-acetylglucosamine residues in cell wall peptidoglycan. *J. Biochem. (Tokyo)* 88, 469–479.
- Benachour, A., Ladjouzi, R., Le Jeune, A., Hebert, L., Thorpe, S., Courtin, P., Chaptier-Chartier, M.P., Prajsnar, T.K., Foster, S.J., Mesnage, S., 2012. The lysozyme-induced peptidoglycan *N*-acetylglucosamine deacetylase PgdA (EF1843) is required for *Enterococcus faecalis* virulence. *J. Bacteriol.* 194, 6066–6073.
- Bera, A., Herbert, S., Jakob, A., Vollmer, W., Götz, F., 2005. Why are pathogenic staphylococci so lysozyme resistant? The peptidoglycan O-acetyltransferase OatA is the major determinant for lysozyme resistance of *Staphylococcus aureus*. *Mol. Microbiol.* 55, 778–787.
- Bertsche, U., Mayer, C., Götz, F., Gust, A.A., 2015. Peptidoglycan perception — sensing bacteria by their common envelope structure. *Int. J. Med. Microbiol.* 305, 217–223.
- Bhavsar, A.P., Erdman, L.K., Schertzer, J.W., Brown, E.D., 2004. Teichoic acid is an essential polymer in *Bacillus subtilis* that is functionally distinct from teichuronic acid. *J. Bacteriol.* 186, 7865–7873.
- Biswas, R., Voggu, L., Simon, U.K., Hentschel, P., Thumm, G., Götz, F., 2006. Activity of the major staphylococcal autolysin Atl. *FEMS Microbiol. Lett.* 259, 260–268.
- Boersma, M.J., Kuru, E., Rittichier, J.T., VanNieuwenhze, M.S., Brun, Y.V., Winkler, M.E., 2015. Minimal peptidoglycan (PG) turnover in wild-type and PG hydrolase and cell division mutants of *Streptococcus pneumoniae* D39 growing planktonically and in host-relevant biofilms. *J. Bacteriol.* 197, 3472–3485.
- Borisova, M., Gaupp, R., Duckworth, A., Schneider, A., Dalugge, D., Mühleck, M., Deubel, D., Unsleber, S., Yu, W., Muth, G., Bischoff, M., Götz, F., Mayer, C., 2016. Peptidoglycan recycling in gram-positive bacteria is crucial for survival in stationary phase. *mBio* 7, e00923–00916.
- Borisova, M., Gisin, J., Mayer, C., 2014. Blocking peptidoglycan recycling in *Pseudomonas aeruginosa* attenuates intrinsic resistance to fosfomycin. *Microb. Drug Resist.* 20, 231–237.
- Borisova, M., Gisin, J., Mayer, C., 2017. The *N*-acetylmuramic acid 6-phosphate phosphatase MupP completes the *Pseudomonas* peptidoglycan recycling pathway leading to intrinsic fosfomycin resistance. *mBio* 8, e00092–00017.
- Borisova, M., Mayer, C., 2017. Analysis of *N*-acetylmuramic acid-6-phosphate (MurNAc-6P) accumulation by HPLC-MS. *BioProtocol* 7, e2420.
- Bose, J.L., Lehman, M.K., Fey, P.D., Bayles, K.W., 2012. Contribution of the *Staphylococcus aureus* Atl AM and Gl murein hydrolase activities in cell division, autolysis, and biofilm formation. *PLoS One* 7, e24244.
- Botella, E., Devine, S.K., Hübner, S., Salzberg, L.L., Gale, R.T., Brown, E.D., Link, H., Sauer, U., Codee, J.D., Noone, D., Devine, K.M., 2014. PhoR autokinase activity is controlled by an intermediate in wall teichoic acid metabolism that is sensed by the intracellular PAS domain during the PhoPR-mediated phosphate limitation response of *Bacillus subtilis*. *Mol. Microbiol.* 94, 1242–1259.
- Botella, E., Hübner, S., Hokamp, K., Hansen, A., Bisicchia, P., Noone, D., Powell, L., Salzberg, L.L., Devine, K.M., 2011. Cell envelope gene expression in phosphate-limited *Bacillus subtilis* cells. *Microbiology* 157, 2470–2484.
- Braun, V., 2015. Bacterial cell wall research in Tübingen: a brief historical account. *Int. J. Med. Microbiol.* 305, 178–182.
- Brown, S., Santa Maria Jr., J.P., Walker, S., 2013. Wall teichoic acids of gram-positive bacteria. *Annu. Rev. Microbiol.* 67, 313–336.
- Calamita, H.G., Doyle, R.J., 2002. Regulation of autolysins in teichuronic acid-containing *Bacillus subtilis* cells. *Mol. Microbiol.* 44, 601–606.
- Calamita, H.G., Ehringer, W.D., Koch, A.L., Doyle, R.J., 2001. Evidence that the cell wall of *Bacillus subtilis* is protonated during respiration. *Proc. Natl. Acad. Sci. U. S. A.* 98, 15260–15263.
- Chastanet, A., Vitkup, D., Yuan, G.C., Norman, T.M., Liu, J.S., Losick, R.M., 2010. Broadly heterogeneous activation of the master regulator for sporulation in *Bacillus subtilis*. *Proc. Natl. Acad. Sci. U. S. A.* 107, 8486–8491.
- Chung, J.D., Stephanopoulos, G., Ireton, K., Grossman, A.D., 1994. Gene expression in single cells of *Bacillus subtilis*: evidence that a threshold mechanism controls the initiation of sporulation. *J. Bacteriol.* 176, 1977–1984.
- Dahl, U., Jaeger, T., Nguyen, B.T., Sattler, J.M., Mayer, C., 2004. Identification of a phosphotransferase system of *Escherichia coli* required for growth on *N*-acetylmuramic acid. *J. Bacteriol.* 186, 2385–2392.
- Deutscher, J., Francke, C., Postma, P.W., 2006. How phosphotransferase system-related protein phosphorylation regulates carbohydrate metabolism in bacteria. *Microbiol. Mol. Biol. Rev.* 70, 939–1031.
- Devine, K.M., 2018. Activation of the PhoPR-Mediated response to phosphate limitation is regulated by wall teichoic acid metabolism in *Bacillus subtilis*. *Front. Microbiol.* 9, 2678.
- Dik, D.A., Dominguez-Gil, T., Lee, M., Heseck, D., Byun, B., Fishovitz, J., Boggess, B., Hellman, L.M., Fisher, J.F., Hermoso, J.A., Mobashery, S., 2017a. Muropeptide binding and the X-ray structure of the effector domain of the transcriptional regulator AmpR of *Pseudomonas aeruginosa*. *J. Am. Chem. Soc.* 139, 1448–1451.
- Dik, D.A., Fisher, J.F., Mobashery, S., 2018. Cell-wall recycling of the gram-negative bacteria and the nexus to antibiotic resistance. *Chem. Rev.* 118, 5952–5984.
- Dik, D.A., Marous, D.R., Fisher, J.F., Mobashery, S., 2017b. Lytic transglycosylases: concinnity in concision of the bacterial cell wall. *Crit. Rev. Biochem. Mol. Biol.* 52, 503–542.
- Ellermeier, C.D., Hobbs, E.C., Gonzalez-Pastor, J.E., Losick, R., 2006. A three-protein signaling pathway governing immunity to a bacterial cannibalism toxin. *Cell* 124, 549–559.
- Ellwood, D.C., Tempest, D.W., 1969. Control of teichoic acid and teichuronic acid biosyntheses in chemostat cultures of *Bacillus subtilis* var. *Niger*. *Biochem. J.* 111, 1–5.
- Fisher, J.F., Mobashery, S., 2014. The sentinel role of peptidoglycan recycling in the  $\beta$ -lactam resistance of the Gram-negative Enterobacteriaceae and *Pseudomonas aeruginosa*. *Bioorg. Chem.* 56, 41–48.
- Friedrich, V., Pabinger, S., Chen, T., Messner, P., Dewhirst, F.E., Schäffer, C., 2015. Draft genome sequence of *Tannerella forsythia* type strain ATCC 43037. *Genome Announc.* 3, e00660–00615.
- Fumeaux, C., Bernhardt, T.G., 2017. Identification of MupP as a new peptidoglycan recycling factor and antibiotic resistance determinant in *Pseudomonas aeruginosa*. *mBio* 8, e00102–00117.
- Gisin, J., Schneider, A., Nägele, B., Borisova, M., Mayer, C., 2013. A cell wall recycling shortcut that bypasses peptidoglycan *de novo* biosynthesis. *Nat. Chem. Biol.* 9, 491–493.
- Gonzalez-Pastor, J.E., 2011. Cannibalism: a social behavior in sporulating *Bacillus subtilis*. *FEMS Microbiol. Rev.* 35, 415–424.
- Gonzalez-Pastor, J.E., Hobbs, E.C., Losick, R., 2003. Cannibalism by sporulating bacteria. *Science* 301, 510–513.
- Goodell, E.W., 1985. Recycling of murein by *Escherichia coli*. *J. Bacteriol.* 163, 305–310.
- Goodell, E.W., Schwarz, U., 1985. Release of cell wall peptides into culture medium by exponentially growing *Escherichia coli*. *J. Bacteriol.* 162, 391–397.
- Götz, F., Heilmann, C., Stehle, T., 2014. Functional and structural analysis of the major amidase (Atl) in *Staphylococcus*. *Int. J. Med. Microbiol.* 304, 156–163.
- Grant, W.D., 1979. Cell wall teichoic acid as a reserve phosphate source in *Bacillus subtilis*. *J. Bacteriol.* 137, 35–43.
- Hadi, T., Dahl, U., Mayer, C., Tanner, M.E., 2008. Mechanistic studies on *N*-acetylmuramic acid 6-phosphate hydrolase (MurQ): an etherase involved in peptidoglycan recycling. *Biochemistry* 47, 11547–11558.
- Hantke, K., Braun, V., 1973. Covalent binding of lipid to protein. Diglyceride and amide-linked fatty acid at the *N*-terminal end of the murein-lipoprotein of the *Escherichia coli* outer membrane. *Eur. J. Biochem.* 34, 284–296.
- Hiramatsu, K., Katayama, Y., Matsuo, M., Sasaki, T., Morimoto, Y., Sekiguchi, A., Baba, T., 2014. Multi-drug-resistant *Staphylococcus aureus* and future chemotherapy. *J. Infect. Chemother.* 20, 593–601.
- Holt, S.C., Ebersole, J.L., 2005. *Porphyromonas gingivalis*, *Treponema denticola*, and *Tannerella forsythia*: the “red complex”, a prototype polybacterial pathogenic

- consortium in periodontitis. *Periodontology* 2000 (38), 72–122.
- Hottmann, I., Mayer, V.M.T., Tomek, M.B., Friedrich, V., Calvert, M.B., Titz, A., Schäffer, C., Mayer, C., 2018. *N*-Acetylmuramic acid (MurNAc) auxotrophy of the oral pathogen *Tannerella forsythia*: characterization of a MurNAc kinase and analysis of its role in cell wall metabolism. *Front. Microbiol.* 9, 19.
- Jacobs, C., Frere, J.M., Normark, S., 1997. Cytosolic intermediates for cell wall biosynthesis and degradation control inducible  $\beta$ -lactam resistance in gram-negative bacteria. *Cell* 88, 823–832.
- Jaeger, T., Arsic, M., Mayer, C., 2005. Scission of the lactyl ether bond of *N*-acetylmuramic acid by *Escherichia coli* "etherase". *J. Biol. Chem.* 280, 30100–30106.
- Jaeger, T., Mayer, C., 2008a. *N*-acetylmuramic acid 6-phosphate lyases (MurNAc etherases): role in cell wall metabolism, distribution, structure, and mechanism. *Cell Mol. Life Sci.* 65, 928–939.
- Jaeger, T., Mayer, C., 2008b. The transcriptional factors MurR and catabolite activator protein regulate *N*-acetylmuramic acid catabolism in *Escherichia coli*. *J. Bacteriol.* 190, 6598–6608.
- Jolliffe, L.K., Doyle, R.J., Streips, U.N., 1981. The energized membrane and cellular autolysis in *Bacillus subtilis*. *Cell* 25, 753–763.
- Jorge, A.M., Schneider, J., Unsleber, S., Gohring, N., Mayer, C., Peschel, A., 2017. Utilization of glycerophosphodiester by *Staphylococcus aureus*. *Mol. Microbiol.* 103, 229–241.
- Jorge, A.M., Schneider, J., Unsleber, S., Xia, G., Mayer, C., Peschel, A., 2018. *Staphylococcus aureus* counters phosphate limitation by scavenging wall teichoic acids from other staphylococci via the teichoicase GlpQ. *J. Biol. Chem.* 293, 14916–14924.
- Kluj, R.M., Ebner, P., Adamek, N., Ziemert, N., Mayer, C., Borisova, M., 2018. Recovery of the peptidoglycan turnover product released by the autolysin Atl in *Staphylococcus aureus* involves the phosphotransferase system transporter MurP and the novel 6-phospho-*N*-acetylmuramidase MupG. *Front. Microbiol.* 9, 2725.
- Kobayashi, K., Sudiarta, I.P., Kodama, T., Fukushima, T., Ara, K., Ozaki, K., Sekiguchi, J., 2012. Identification and characterization of a novel polysaccharide deacetylase C (PdaC) from *Bacillus subtilis*. *J. Biol. Chem.* 287, 9765–9776.
- Komatsuzawa, H., Sugai, M., Nakashima, S., Yamada, S., Matsumoto, A., Oshida, T., Suginaka, H., 1997. Subcellular localization of the major autolysin, ATL and its processed proteins in *Staphylococcus aureus*. *Microbiol. Immunol.* 41, 469–479.
- Lamsa, A., Liu, W.T., Dorrestein, P.C., Pogliano, K., 2012. The *Bacillus subtilis* cannibalism toxin SDP collapses the proton motive force and induces autolysis. *Mol. Microbiol.* 84, 486–500.
- Lang, W.K., Glassey, K., Archibald, A.R., 1982. Influence of phosphate supply on teichoic acid and teichuronic acid content of *Bacillus subtilis* cell walls. *J. Bacteriol.* 151, 367–375.
- Lewis, K., 2000. Programmed death in bacteria. *Microbiol. Mol. Biol. Rev.* 64, 503–514.
- Litzinger, S., Duckworth, A., Nitzsche, K., Risinger, C., Wittmann, V., Mayer, C., 2010. Muropeptide rescue in *Bacillus subtilis* involves sequential hydrolysis by  $\beta$ -*N*-acetylglucosaminidase and *N*-acetylmuramyl-L-alanine amidase. *J. Bacteriol.* 192, 3132–3143.
- Litzinger, S., Mayer, C., 2010. Chapter 1: The murein sacculus. In: König, H., Claus, H., Varma, A. (Eds.), *Prokaryotic Cell Wall Compounds - Structure and Biochemistry*. Springer, Heidelberg, Berlin, New York, pp. 3–52.
- Mark, B.L., Vocadlo, D.J., Oliver, A., 2011. Providing  $\beta$ -lactams a helping hand: targeting the AmpC  $\beta$ -lactamase induction pathway. *Future Microbiol.* 6, 1415–1427.
- Meisner, J., Montero Llopis, P., Sham, L.T., Garner, E., Bernhardt, T.G., Rudner, D.Z., 2013. FtsEX is required for CwlO peptidoglycan hydrolase activity during cell wall elongation in *Bacillus subtilis*. *Mol. Microbiol.* 89, 1069–1083.
- Moynihan, P.J., Sychantha, D., Clarke, A.J., 2014. Chemical biology of peptidoglycan acetylation and deacetylation. *Bioorg. Chem.* 54, 44–50.
- Myers, C.L., Li, F.K., Koo, B.M., El-Halfawy, O.M., French, S., Gross, C.A., Strynadka, N.C., Brown, E.D., 2016. Identification of two phosphate starvation-induced wall teichoic acid hydrolases provides first insights into the degradative pathway of a key bacterial cell wall component. *J. Biol. Chem.* 291, 26066–26082.
- Nilsson, R.P., Beijer, L., Rutberg, B., 1994. The *glpT* and *glpQ* genes of the glycerol regulon in *Bacillus subtilis*. *Microbiology-UK* 140, 723–730.
- Oshida, T., Sugai, M., Komatsuzawa, H., Hong, Y.M., Suginaka, H., Tomasz, A., 1995. A *Staphylococcus aureus* autolysin that has an *N*-acetylmuramoyl-L-alanine amidase domain and an endo- $\beta$ -*N*-acetylglucosaminidase domain: cloning, sequence analysis, and characterization. *Proc. Natl. Acad. Sci. U. S. A.* 92, 285–289.
- Park, J.T., Uehara, T., 2008. How bacteria consume their own exoskeletons (turnover and recycling of cell wall peptidoglycan). *Microbiol. Mol. Biol. Rev.* 72, 211–227.
- Percy, M.G., Gründling, A., 2014. Lipoteichoic acid synthesis and function in gram-positive bacteria. *Annu. Rev. Microbiol.* 68, 81–100.
- Psylinakis, E., Boneca, I.G., Mavromatis, K., Deli, A., Hayhurst, E., Foster, S.J., Varum, K.M., Bouriotis, V., 2005. Peptidoglycan *N*-acetylglucosamine deacetylases from *Bacillus cereus*, highly conserved proteins in *Bacillus anthracis*. *J. Biol. Chem.* 280, 30856–30863.
- Reith, J., Berking, A., Mayer, C., 2011. Characterization of an *N*-acetylmuramic acid/*N*-acetylglucosamine kinase of *Clostridium acetobutylicum*. *J. Bacteriol.* 193, 5386–5392.
- Reith, J., Mayer, C., 2011. Peptidoglycan turnover and recycling in Gram-positive bacteria. *Appl. Microbiol. Biotechnol.* 92, 1–11.
- Renner-Schneck, M., Hinderberger, I., Gisin, J., Exner, T., Mayer, C., Stehle, T., 2015. Crystal structure of the *N*-acetylmuramic acid  $\alpha$ -1-phosphate (MurNAc- $\alpha$ -1-P) uridylyltransferase MurU, a minimal sugar nucleotidyltransferase and potential drug target enzyme in Gram-negative pathogens. *J. Biol. Chem.* 290, 10804–10813.
- Ruscitto, A., Hottmann, I., Stafford, G.P., Schaffer, C., Mayer, C., Sharma, A., 2016. Identification of a novel *N*-acetylmuramic acid transporter in *Tannerella forsythia*. *J. Bacteriol.* 198, 3119–3125.
- Sakamoto, M., Suzuki, M., Umeda, M., Ishikawa, I., Benno, Y., 2002. Reclassification of *Bacteroides forsythus* (Tanner et al. 1986) as *Tannerella forsythensis* corrig., gen. nov., comb. Nov. *Int. J. Syst. Evol. Microbiol.* 52, 841–849.
- Schlag, M., Biswas, R., Krismer, B., Kohler, T., Zoll, S., Yu, W., Schwarz, H., Peschel, A., Götz, F., 2010. Role of staphylococcal wall teichoic acid in targeting the major autolysin Atl. *Mol. Microbiol.* 75, 864–873.
- Seltmann, G., Holst, O., 2002. Periplasmic space and rigid layer. In: Seltmann, G., Holst, O. (Eds.), *The Bacterial Cell Wall*. Springer-Verlag, Berlin, pp. 103–132.
- Sharma, A., Inagaki, S., Sigurdson, W., Kuramitsu, H.K., 2005. Synergy between *Tannerella forsythia* and *Fusobacterium nucleatum* in biofilm formation. *Oral Microbiol. Immunol.* 20, 39–42.
- Smith, T.J., Blackman, S.A., Foster, S.J., 2000. Autolysins of *Bacillus subtilis*: multiple enzymes with multiple functions. *Microbiology* 146 (Pt 2), 249–262.
- Soldo, B., Lazarevic, V., Pagni, M., Karamata, D., 1999. Teichuronic acid operon of *Bacillus subtilis* 168. *Mol. Microbiol.* 31, 795–805.
- Templin, M.F., Ursinus, A., Höltje, J.V., 1999. A defect in cell wall recycling triggers autolysis during the stationary growth phase of *Escherichia coli*. *EMBO J.* 18, 4108–4117.
- Tong, S.Y., Davis, J.S., Eichenberger, E., Holland, T.L., Fowler Jr., V.G., 2015. *Staphylococcus aureus* infections: epidemiology, pathophysiology, clinical manifestations, and management. *Clin. Microbiol. Rev.* 28, 603–661.
- Uehara, T., Suefujii, K., Jaeger, T., Mayer, C., Park, J.T., 2006. MurQ etherase is required by *Escherichia coli* in order to metabolize anhydro-*N*-acetylmuramic acid obtained either from the environment or from its own cell wall. *J. Bacteriol.* 188, 1660–1662.
- Uehara, T., Suefujii, K., Valbuena, N., Meehan, B., Donegan, M., Park, J.T., 2005. Recycling of the anhydro-*N*-acetylmuramic acid derived from cell wall murein involves a two-step conversion to *N*-acetylglucosamine-phosphate. *J. Bacteriol.* 187, 3643–3649.
- Unsleber, S., 2017. Degradation and Recovery of the Peptidoglycan-wall Teichoic Acid-complex in *Bacillus subtilis*, Mathematisch-naturwissenschaftliche Fakultät University of Tübingen, PhD Thesis.
- Unsleber, S., Borisova, M., Mayer, C., 2017. Enzymatic synthesis and semi-preparative isolation of *N*-acetylmuramic acid 6-phosphate. *Carbohydr. Res.* 445, 98–103.
- Vadlamani, G., Thomas, M.D., Patel, T.R., Donald, L.J., Reeve, T.M., Stetefeld, J., Standing, K.G., Vocadlo, D.J., Mark, B.L., 2015. The  $\beta$ -lactamase gene regulator AmpR is a tetramer that recognizes and binds the D-Ala-D-Ala motif of its repressor UDP-*N*-acetylmuramic acid (MurNAc)-pentapeptide. *J. Biol. Chem.* 290, 2630–2643.
- Vermassen, A., Leroy, S., Talon, R., Provot, C., Popowska, M., Desvaux, M., 2019. Cell wall hydrolases in bacteria: insight on the diversity of cell wall amidases, glycosidases and peptidases toward peptidoglycan. *Front. Microbiol.* 10, 331.
- Walter, A., Mayer, C., 2019. Chapter 6: peptidoglycan structure, biosynthesis, and dynamics during bacterial growth. In: Cohen, E., Merzendorfer, H. (Eds.), *Extracellular Sugar-Based Biopolymere Matrices*. Elsevier, pp. 237–299. <https://link.springer.com/chapter/10.1007%2F978-3-030-12919-4-6>.
- Weidel, W., Pelzer, H., 1964. Bagshaped macromolecules – a new outlook on bacterial cell walls. *Adv. Enzymol.* 26, 193–232.
- Weidenmeier, C., Peschel, A., 2008. Teichoic acids and related cell-wall glycopolymers in Gram-positive physiology and host interactions. *Nature Microb. Rev.* 6, 276–287.
- Wheeler, R., Turner, R.D., Bailey, R.G., Salamaga, B., Mesnage, S., Mohamad, S.A., Hayhurst, E.J., Horsburgh, M., Hobbs, J.K., Foster, S.J., 2015. Bacterial cell enlargement requires control of cell wall stiffness mediated by peptidoglycan hydrolases. *mBio* 6, e00660.
- White, R.J., 1968. Control of amino sugar metabolism in *Escherichia coli* and isolation of mutants unable to degrade amino sugars. *Biochem. J.* 106, 847–858.
- Williams, A.H., Wheeler, R., Rateau, L., Malosse, C., Chamot-Rooke, J., Haouz, A., Taha, M.K., Boneca, I.G., 2018. A step-by-step in crystallo guide to bond cleavage and 1,6-anhydro-sugar product synthesis by a peptidoglycan-degrading lytic transglycosylase. *J. Biol. Chem.* 293, 6000–6010.
- Wyss, C., 1989. Dependence of proliferation of *Bacteroides forsythus* on exogenous *N*-acetylmuramic acid. *Infect. Immun.* 57, 1757–1759.
- Yamada, S., Sugai, M., Komatsuzawa, H., Nakashima, S., Oshida, T., Matsumoto, A., Suginaka, H., 1996. An autolysin ring associated with cell separation of *Staphylococcus aureus*. *J. Bacteriol.* 178, 1565–1571.
- Yang, D.C., Peters, N.T., Parzych, K.R., Uehara, T., Markovski, M., Bernhardt, T.G., 2011. An ATP-binding cassette transporter-like complex governs cell-wall hydrolysis at the bacterial cytotkinetic ring. *Proc. Natl. Acad. Sci. U. S. A.* 108, e1052–1060.

## Publication 4

**Walter, A.**, Unsleber, S., Rismondo, J., Jorge, A. M., Peschel, A., Gründling, A., & Mayer, C. (2020). Phosphoglycerol-type wall and lipoteichoic acids are enantiomeric polymers differentiated by the stereospecific glycerophosphodiesterase GlpQ. *Journal of Biological Chemistry*, 295(12), 4024-4034.



# Phosphoglycerol-type wall and lipoteichoic acids are enantiomeric polymers differentiated by the stereospecific glycerophosphodiesterase GlpQ

Received for publication, January 7, 2020, and in revised form, February 11, 2020. Published, Papers in Press, February 11, 2020, DOI 10.1074/jbc.RA120.012566

✉ Axel Walter<sup>†</sup>, Sandra Unsleber<sup>†</sup>, Jeanine Rismondo<sup>S1</sup>, ✉ Ana Maria Jorge<sup>¶</sup>, Andreas Peschel<sup>¶2</sup>,  
✉ Angelika Gründling<sup>S3</sup>, and ✉ Christoph Mayer<sup>†4</sup>

From <sup>†</sup>Microbiology/Glycobiology and <sup>¶</sup>Infection Biology, Interfaculty Institute of Microbiology and Infection Medicine Tübingen, University of Tübingen, 72076 Tübingen, Germany and the <sup>S3</sup>Section of Molecular Microbiology and Medical Research Council Centre for Molecular Bacteriology and Infection, Imperial College London, London SW7 2AZ, United Kingdom

Edited by Chris Whitfield

The cell envelope of Gram-positive bacteria generally comprises two types of polyanionic polymers linked to either peptidoglycan (wall teichoic acids; WTA) or to membrane glycolipids (lipoteichoic acids; LTA). In some bacteria, including *Bacillus subtilis* strain 168, both WTA and LTA are glycerolphosphate polymers yet are synthesized through different pathways and have distinct but incompletely understood morphogenetic functions during cell elongation and division. We show here that the exolytic *sn*-glycerol-3-phosphodiesterase GlpQ can discriminate between *B. subtilis* WTA and LTA. GlpQ completely degraded unsubstituted WTA, which lacks substituents at the glycerol residues, by sequentially removing glycerolphosphates from the free end of the polymer up to the peptidoglycan linker. In contrast, GlpQ could not degrade unsubstituted LTA unless it was partially precleaved, allowing access of GlpQ to the other end of the polymer, which, in the intact molecule, is protected by a connection to the lipid anchor. Differences in stereochemistry between WTA and LTA have been suggested previously on the basis of differences in their biosynthetic precursors and chemical degradation products. The differential cleavage of WTA and LTA by GlpQ reported here represents the first direct evidence that they are enantiomeric polymers: WTA is made of *sn*-glycerol-3-phosphate, and LTA is made of *sn*-glycerol-1-phosphate. Their distinct stereochemistries reflect the dissimilar physiological and immunogenic properties of WTA and LTA. It also

enables differential degradation of the two polymers within the same envelope compartment *in vivo*, particularly under phosphate-limiting conditions, when *B. subtilis* specifically degrades WTA and replaces it with phosphate-free teichuronic acids.

The cell membrane of bacteria is covered by a complex multilayered cell envelope that protects the susceptible protoplast from lysis and from detrimental effects of the environment (1). Based on the composition of the cell envelope, bacteria are classified into two major groups: Gram-negative and Gram-positive. Gram-negative bacteria are encased in a thin peptidoglycan (PGN)<sup>5</sup> layer that is covered by an external outer membrane, carrying negatively charged lipopolysaccharide in the outer leaflet. In contrast, Gram-positive bacteria lack an outer membrane but possess a thick PGN layer that is interwoven by polyanionic glycopolymers, teichoic acids, which were discovered by Baddiley and co-workers 60 years ago (2–4). Teichoic acids can be very variable in composition and structure, although they mostly feature glycerolphosphate, ribitol-phosphate, or sugar phosphate repeating units connected through phosphodiester bonds (5–8). These phosphodiester polymers are either covalently bound to the PGN and called wall teichoic acids (WTA) or linked to glycolipids in the cell membrane and named lipoteichoic acids (LTA) (4, 9, 10). WTA are characteristic constituents of the Gram-positive cell walls (PGN–WTA complex), comprising chains of 30–50 polyolphosphate repeats anchored via a linker disaccharide (*N*-acetylmannosamine- $\beta$ -1,4-GlcNAc (ManNAc- $\beta$ -1,4-GlcNAc)) to about every ninth *N*-acetylmuramic acid residue of the PGN (9). They make up about half of the cell wall dry weight (11, 12) and are responsible for the generally high phosphate content of Gram-positive cell walls (4, 13). It has been shown that WTA can serve as phosphate storage, allowing *Bacillus subtilis* to continue growth under phosphate-depleted conditions (13–15). To cope with this stress, teichoic acids are

This work was supported by the Deutsche Forschungsgemeinschaft under Germany's Excellence Strategy (EXC 2124 Controlling Microbes to Fight Infections). The authors declare that they have no conflicts of interest with the contents of this article.

✂ Author's Choice—Final version open access under the terms of the Creative Commons CC-BY license.

This article contains Figs. S1–S5, Table S1, and references.

<sup>1</sup> Present address: Dept. of General Microbiology, GZMB, Georg-August-Universität Göttingen, 37077 Göttingen, Germany. Supported by Deutsche Forschungsgemeinschaft Grant RI 2920/1-1.

<sup>2</sup> Supported by Deutsche Forschungsgemeinschaft Grants SFB766, TRR 34, and TRR 156.

<sup>3</sup> Supported by Wellcome Trust Grant 210671/Z/18/Z and Medical Research Council Grant MR/P011071/1.

<sup>4</sup> Supported by Deutsche Forschungsgemeinschaft Grants SFB766, Project ID 398967434-TRR 261, and Project ID 174858087-GRK1708. To whom correspondence should be addressed: Interfaculty Institute of Microbiology and Infection Medicine Tübingen, Microbiology/Glycobiology, University of Tübingen, Auf der Morgenstelle 28, 72076 Tübingen, Germany. Tel.: 49-7071-29-74645; E-mail: christoph.mayer@uni-tuebingen.de.

<sup>5</sup> The abbreviations used are: PGN, peptidoglycan; ManNAc, *N*-acetylmannosamine; PG, phosphatidylglycerol; DAG, diacylglycerol; PGP, phosphatidylglycerol phosphate; Gro3P, *sn*-glycerol-3-phosphate; Gro1P, *sn*-glycerol-1-phosphate; GPC, *sn*-glycerol-3-phosphocholine; AUC, area under the curve; LB, lysogeny broth; BPC, base peak chromatogram; EIC, extracted ion chromatogram.

exchanged with phosphate-free teichuronic acids in an adaptation process known as the “teichoic acid–to–teichuronic acid switch.” LTA are more widespread in bacteria than WTAs, and their composition is less dependent on growth conditions (16). Commonly, LTA contain polyol-phosphate chains (type I LTA) that are anchored to the cytoplasmic membrane via glycolipids; in the case of *B. subtilis*, a gentibiosyl disaccharide (glucose- $\beta$ -1,6-glucose)  $\beta$ -glycosidically bound to diacylglycerol (10). WTA and LTA differ in chemical composition, cellular compartmentation and route of biosynthesis, yet their distinguishable physiological roles are insufficiently understood (4, 17–19). Although inactivation of both LTA and WTA is lethal in *B. subtilis*, indicating partially redundant functions, comparison of the individual mutants suggests differential roles during cell elongation (WTA) and division (LTA) (18). Further proposed functions of teichoic acids include control of cell wall-targeting enzymes during envelope homeostasis and divalent cation binding (3, 20), interaction with host and bacteriophage receptors (18, 21), as well as pathogenicity (22–24). Recently, LTA have been suggested to functionally resemble the osmo-regulated periplasmic glycans of Gram-negative bacteria (10, 25, 26).

In some Gram-positive bacteria, including *B. subtilis* 168, *Staphylococcus epidermidis*, and *Staphylococcus lugdunensis*, both LTA and WTA are glycerophosphate polymers (17, 18, 27, 28). Nevertheless, they are synthesized through distinct routes (9, 10, 29). WTA are synthesized from CDP-glycerol in the cytoplasm, and the polymers are then flipped outward (Fig. 1A). In contrast, LTA are synthesized from the precursor phosphatidylglycerol (PG), generated via diacylglycerol (DAG) CDP and PG phosphate (PGP). The PG precursor is subsequently translocated across the cell membrane and then polymerized on the outside of the cell (Fig. 1B). Intriguingly, the glycerophosphate in the precursors of WTA and LTA has different stereochemistry (17). The prochirality of glycerol leads to two 3-phosphate products; by convention, L-glycerol is the configuration that determines the stereochemical numbering (*sn* nomenclature) of glycerolphosphates (Fig. 2). CDP-glycerol has a *sn*-3 configuration, whereas the free glycerolphosphate of PG has a *sn*-1 configuration. The use of different precursors and the compartmentalization of their synthesis allow differential regulation of production of WTA and LTA, which is important for their specific roles in cell envelope integrity and morphogenesis (18). However, how WTA and LTA execute these distinct functions in the same cell envelope compartment is still unclear.

Modification of polyols by alanylation and glycosylation is an important means to alter the physiological properties of WTA and LTA and also affect recognition by the innate immune system (6, 30, 31). D-alanylation adds a positive charge (free amino groups) to the polyolphosphate polymers, conferring the anionic character and, as a consequence, the binding properties (10, 32). The multienzyme complex DltABCD is responsible for adding D-Ala modifications onto LTA on the outer leaflet of the cell membrane and indirectly also onto WTA (Fig. 1) (32–35). LTA and WTA can also be  $\alpha$ - or  $\beta$ -glycosylated, modifications that strongly increase the stability of these polymers against alkaline hydrolysis (9, 10). In *B. subtilis*, the enzyme TagE trans-

fers  $\alpha$ -glucosyl residues from UDP-glucose onto preformed WTA within the cytoplasm and represents the only WTA glycosylating enzyme in this bacterium (Fig. 1A) (36, 37). Although WTA glycosylation usually occurs prior to translocation of the polymer across the cell membrane, it was recently proposed to also occur after translocation in *Listeria monocytogenes* (37, 38). Like alanylation, glycosylation of LTA generally occurs, along with synthesis, outside of the cell, and membrane-associated, three-component LTA glycosylation systems have recently been characterized in *B. subtilis* and *Staphylococcus aureus* (CsbB/GtcA/YfhO) as well as in *L. monocytogenes* (GtlA/GtlB) (Fig. 1B) (38–40).

Besides synthesis, turnover of WTA and LTA also needs to be differentially regulated, but so far this process has been poorly investigated. Recently, the exo-acting *sn*-glycerol-3-phosphate phosphodiesterase GlpQ, along with an endo-acting phosphodiesterase, PhoD, has been implicated in degradation of WTA during phosphate starvation (41). However, apart from WTA degradation during adaptation to phosphate starvation, turnover of WTA likely occurs along with turnover of PGN of the cell wall in *B. subtilis* and other Gram-positive bacteria (42–44). Because strains of *B. subtilis* lacking both WTA and LTA are not viable, simultaneous degradation of both polymers would be detrimental (18). We thus wondered how differential degradation of WTA and LTA by hydrolases (“teichoicases”) is regulated. Previous studies with the glycerophosphodiesterase GlpQ of *B. subtilis* as well as orthologous enzymes from *Escherichia coli* and *S. aureus* (amino acid sequence identities of 29% and 54%, respectively) have revealed strict stereospecificity for glycerophosphodiesterases harboring *sn*-glycerol-3-phosphoryl groups, e.g. produced by phospholipases from membrane phospholipids (41, 45–47). Accordingly, phosphatidylglycerol or lysophosphatidylglycerol, which harbor only free *sn*-glycerol-1-phosphoryl ends, are not hydrolyzed by GlpQ, and bis(*p*-nitrophenyl) phosphate, a chromogenic substrate for other phosphodiesterases, is also not cleaved by GlpQ (45, 46). Intriguingly, GlpQ is also unable to hydrolyze LTA of *S. aureus*, but this could be due to the presence of modifications on the phosphoglycerol backbone (47). In contrast, the enzyme shows broad substrate specificity with respect to the alcohol moiety and can hydrolyze a variety of different phospholipid headgroups, such as glycerophosphocholine, glycerophosphoethanolamine, glycerophosphoglycerol, and bis(glycerophosphoglycerol) (41, 45, 47).

So far, differential cleavage of WTA and LTA polymers by GlpQ has not been examined in detail. In this work, we show that the stereospecific *sn*-glycerol-3P phosphodiesterase GlpQ acts as an exolytic hydrolase that sequentially cleaves off *sn*-glycerol-3-phosphate (Gro3P) entities from the exposed end of WTA but is unable to hydrolyze intact LTA. Thereby, we provide biochemical evidence that these polymers have opposite stereochemistry: WTA constitute phosphodiester-polymers made of Gro3P and LTA polymers of *sn*-glycerol-1-phosphate (Gro1P). This stereochemical difference likely determines many of the polymers’ distinct properties, such as interactions with hydrolases and binding of proteins throughout the cell cycle, bacterial growth, and differentiation.

## Stereochemistry of Teichoic Acids

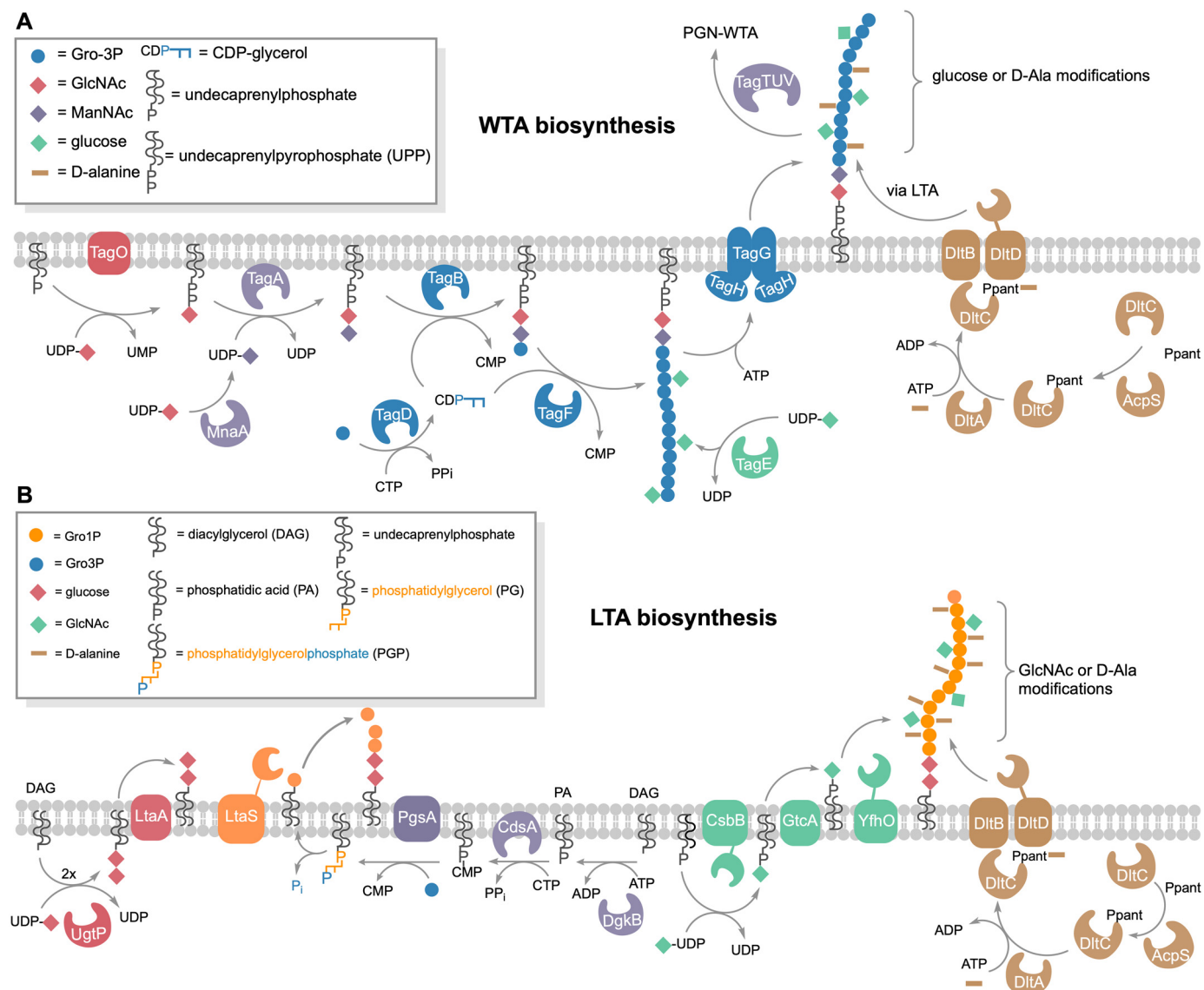


**Figure 1. Comparison of the biosynthetic pathways of WTA and LTA.** *A*, overview of WTA biosynthesis. TagO initiates WTA biosynthesis by transferring GlcNAc (red diamonds) from UDP-GlcNAc onto the lipid carrier undecaprenyl phosphate while releasing UMP. MnaA converts UDP-GlcNAc to UDP-ManNAc, which, in turn, is used to transfer ManNAc (purple diamonds) to the TagO product, forming the WTA linker disaccharide bound to undecaprenyl pyrophosphate (UPP). The TagB protein catalyzes a priming step of WTA synthesis in *B. subtilis*, completing the linkage unit (GlcNAc-ManNAc-Gro3P); a single Gro3P (blue circles) is added from CDP-glycerol (generated by TagD from Gro3P and CTP) to the membrane-anchored linker disaccharide while releasing CMP. TagF further elongates the WTA chain polymer by repeatedly transferring Gro3P from CDP-glycerol. The Gro3P units of the WTA polymer are partially glycosylated in the cytoplasm. The enzyme TagE utilizes UDP-glucose to attach glucose (green diamonds) onto the C2 hydroxyl group of Gro3P of the chain polymer. The degree of glycosylation strongly depends on growth conditions and growth phase. The WTA polymer is translocated across the cell membrane via the ABC transporter TagGH. Finally, the membrane-anchored TagTUV ligases transfer WTA polymers to PGN and the DltABCD system attaches D-alanyl esters to nonglycosylated parts of WTA in an LTA-dependent process (34). DltA transfers D-alanine in an ATP-dependent two-step reaction to DltC, which has been modified with 4'-phosphopantetheine (Ppant) at Ser-35 by acyl carrier protein synthase (AcpS) (56). DltB interacts with DltC-Ppant and together with DltD transfers the D-alanyl onto the C2 hydroxyl group of Gro3P of teichoic acid chains (10, 57). *B*, overview of LTA biosynthesis. The LTA precursor PGP is generated by a series of reactions within the cytoplasm. Synthesis starts by phosphorylation of DAG, yielding DAG phosphate (phosphatidic acid (PA)). The enzyme CdsA then transfers a CMP moiety from CTP onto phosphatidic acid, yielding DAG-CMP, while releasing pyrophosphate (PP<sub>i</sub>). The CMP moiety of the latter is exchanged with Gro3P by PgsA, forming PGP. Notably, PG is formed by releasing the *sn*-3-phosphoryl group from PGP, retaining a Gro1P entity. It is unclear whether this reaction is catalyzed by a dedicated but uncharacterized phosphatase or by the LTA synthase (LtaS) to energize polymerization of Gro1P entities onto the DAG-anchored linker disaccharide in the outer leaflet of the plasma membrane. The linker disaccharide (red diamonds) is synthesized by UgtP by addition of two glucose from UDP-glucose onto DAG, which is then flipped across the membrane by LtaA (58). LTA polymers may be modified by D-alanylation (brown) and glycosylation (green). As described above, alanylation is catalyzed by the Dlt alanylation system; DltA transfers D-alanine to DltC-Ppant, and subsequently DltB together with DltD transfers D-alanyl onto C2 of Gro1P (10, 57). Glycosylation of LTA is catalyzed by the glycosyltransferase CsbB, which adds GlcNAc onto undecaprenyl phosphate (C<sub>55</sub>-P) using UDP-GlcNAc. As this modification occurs outside of the cell in *B. subtilis*, C<sub>55</sub>-P-GlcNAc is first flipped across the membrane by the flippase GtcA, and then the glycosyltransferase YfhO modifies C2 of Gro1P with GlcNAc (38, 40).



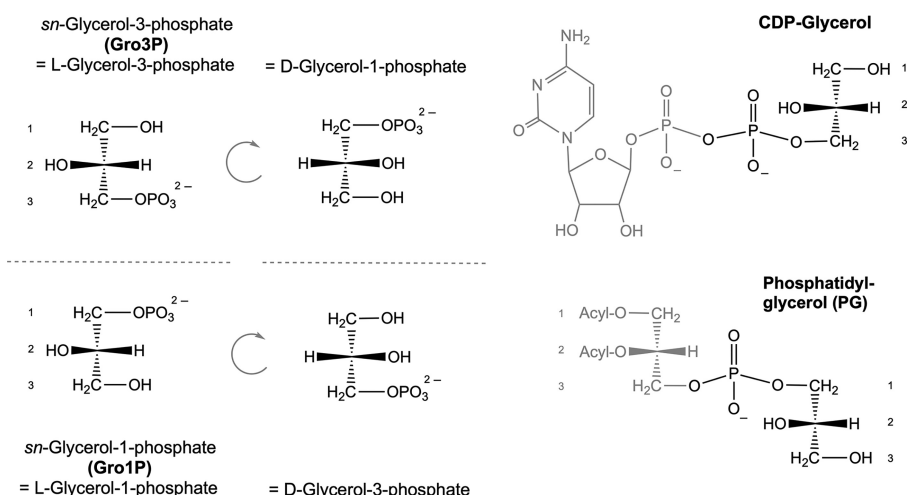


**Figure 2. Stereochemistry of glycerolphosphates and teichoic acid precursors.** The precursors of WTA and LTA synthesis carry enantiomeric glycerolphosphates: *sn*-glycerol-3-phosphoryl (CDP-glycerol) and *sn*-glycerol-1-phosphoryl (PG), respectively. Glycerolphosphate enantiomers are defined by convention according to stereochemical numbering (*sn* nomenclature) as *sn*-glycerol-3-phosphate (Gro3P = L-glycerol-3-phosphate = D-glycerol-1-phosphate) and *sn*-glycerol-1-phosphate (Gro1P = L-glycerol-1-phosphate = D-glycerol-3-phosphate).

## Results and discussion

### GlpQ is a stereospecific *sn*-glycerol-3-phosphoryl phosphodiesterase

GlpQ of *B. subtilis* and orthologs from other bacteria have been shown previously to specifically release Gro3P from *sn*-glycero-3-phosphocholine (GPC), glycerophosphoethanol amine, glycerophosphoglycerol, and bis(glycero-phospho)glycerol. For the latter two substrates,  $K_m$  and  $k_{cat}$  values of 1.0 mM and 1275 min<sup>-1</sup> and, respectively, 1.4 mM and 1517 min<sup>-1</sup> were determined for *B. subtilis* GlpQ (41, 45, 47). We confirmed the stereospecificity of recombinant *B. subtilis* GlpQ for *sn*-glycero-3-phosphoryl substrates and determined the enzyme's stability and catalytic optima using GPC as substrate (Fig. S1). Our analysis revealed that GlpQ is rather temperature-sensitive. It readily loses stability at temperatures above 30 °C; more than 50% of its activity was lost within 30 min at 37 °C. At the same time, however, enzymatic turnover steadily increased with temperature up to an optimum at 55 °C with about half-maximum activity at 30 °C. Furthermore, the enzyme was shown to be stable over a remarkably wide pH range, between 2 and 10, but had a very narrow optimum at pH 8.0 (Fig. S1B). We thus conducted all experiments with the enzyme GlpQ in this study at 30 °C and pH 8.0.

Although the detailed mechanism of phosphodiester cleavage by GlpQ is currently unknown, Ca<sup>2+</sup> ions were recognized as crucial for catalytic activity (but they can be substituted with Cd<sup>2+</sup> and partially with Mn<sup>2+</sup> and Cu<sup>2+</sup>) (45, 48). Accordingly, the catalytic reaction was inhibited with EDTA. Nevertheless, addition of Ca<sup>2+</sup> ions was not required when using the recombinant GlpQ that was purified from the cytosolic extracts of *E. coli*. The recently solved crystal structure of *B. subtilis* GlpQ with Gro3P bound to the active site (PDB codes 5T9B and 5T9C) confirmed the importance of a Ca<sup>2+</sup> ion for catalysis as well as for the stereospecific coordination of the substrate (41, 48). The active site of GlpQ includes a residue (His-85) that is located on a small additional, so-called glycerophosphodiester phosphodiesterase domain that is inserted between the

$\beta$ -strand and  $\alpha$ -helix of the second  $\beta/\alpha$  motif of a classical triose phosphate isomerase barrel structure (41, 49). As shown in Fig. 3, the substrate binding cleft can be divided into a hydrophilic side, including the active-site Ca<sup>2+</sup> ion, and a hydrophobic side consisting of hydrophobic amino acids, including phenylalanine and tyrosine (Phe-190, Tyr-259, and Phe-279). The active site Ca<sup>2+</sup> ion adopts a pentagonal bipyramidal coordination; it is held in place by glutamic and aspartic acid residues (Glu-70, Glu-152, and Asp-72) and is also coordinated by the two hydroxyl groups of Gro3P (Fig. 3). The phosphate as well as the hydroxyl groups at C2 and C3 of Gro3P are drawn toward the Ca<sup>2+</sup> ion in the active site and moved away from the hydrophobic side of the binding cleft. Coordination of the Ca<sup>2+</sup> ion by amino acids with charged side chains and the hydroxyl and phosphate groups of the substrate as well as the orientation of the hydrophobic C-H groups of the substrate toward the hydrophobic side of the binding cleft restrict productive binding to the unsubstituted *sn*-glycero-3-phosphoryl stereoisomer, only allowing hydrolysis of *sn*-glycerol-3-phosphoryl groups. Instead, the C2 hydroxyl group of *sn*-glycerol-1-phosphoryl would face toward the hydrophobic side, precluding productive binding. The hydrophilic side of the binding cleft also coordinates the phosphate group of the substrate involving the basic side chains of His-43, Arg-44, and His-85 (Fig. 3). His-43 and His-85 presumably function as general acid and base residues in the mechanism of phosphodiester hydrolysis (48). The proposed catalytic mechanism of GlpQ involves anchimeric assistance of the C2 hydroxyl group, requiring this group to be unmodified, *i.e.* not glycosylated or alanylated at the C2 hydroxyl group of GroP (41).

### GlpQ sequentially cleaves unmodified WTA by an exolytic mechanism

The glycerophosphodiesterase GlpQ of *B. subtilis* has recently been identified as a teichoicase that preferentially digests polyGroP-type WTA that lack modifications on the glycerol subunits (41). However, in this study, the product of

## Stereochemistry of Teichoic Acids

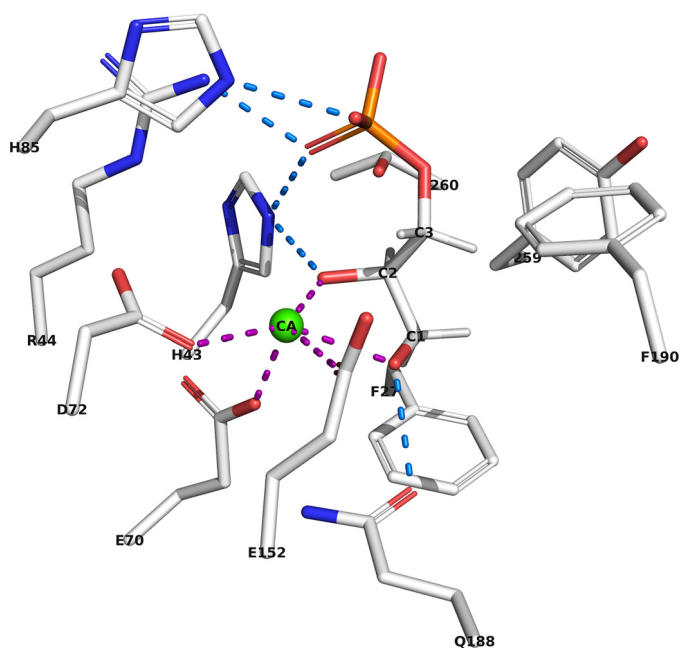


**Figure 3. The cocrystal structure of GlpQ in complex with Gro3P rationalizes the strict stereospecificity of GlpQ for *sn*-glycero-3-phosphoryl groups.** In the cocrystal structure of Myers *et al.* (PDB code 5T9B (41)), the active site of GlpQ features a hydrophilic side with His-85, His-43, Arg-44, Asp-72, Gln-188, Glu-152, and Glu-70 (left of Gro3P; carbon chains, gray; oxygens, red; phosphorus, orange; nitrogens, blue). The other side of the binding cleft (right of Gro3P) consists of hydrophobic amino acids like phenylalanine, tyrosine, and leucine (Phe-190, Tyr-259, and Phe-279). The  $\text{Ca}^{2+}$  ion adopts a pentagonal bipyramidal coordination and is coordinated by Glu-70, Glu-152, and Asp-72 as well as by the two hydroxyl groups of Gro3P. The phosphate of the Gro3P substrate makes hydrogen bond interactions with Arg-44, His-43, and His-85. The C2 hydroxyl group of Gro3P interacts with  $\text{Ca}^{2+}$  and His-43. Further, the C3 hydroxyl group of the substrate binds to  $\text{Ca}^{2+}$  and Gln-188.

digestion of polymeric teichoic acids by GlpQ was not monitored. Hence, neither the strict specificity for unmodified WTA nor the exolytic mechanism have been shown unequivocally. We thus aimed to directly monitor product release by GlpQ from cell wall (PGN–WTA complex) preparations using HPLC-MS. We first applied cell wall preparations containing modified (glycosylated) WTA extracted from *B. subtilis* 168 WT cells and cell wall preparations containing unmodified (nonglycosylated) WTA extracted from  $\Delta tagE::erm$  cells that lack the WTA  $\alpha$ -glucosyl transferase TagE (*cf.* Fig. 1A). These samples were digested with GlpQ, and product formation was followed by HPLC-MS. In both cell wall preparations, GroP was detected in the presence but not in the absence of GlpQ (Fig. 4). However, GlpQ released large amounts of GroP from  $\Delta tagE::erm$  cell wall samples and very little GroP from WT cell wall samples (Fig. 4). The amounts of GroP, determined by calculating the area under the curve (AUC), were about 22 times higher when applying cell walls containing nonglycosylated WTA ( $\text{AUC} = 5.9 \times 10^6$ ) compared with cell walls containing glycosylated WTA prepared from WT cells ( $\text{AUC} = 2.7 \times 10^5$ ), which is in agreement with the proposed chain length of the WTA polymers of 30–50 polyolphosphate repeats. The identity of the GroP reaction product was confirmed by MS via the exact mass and typical adduct pattern and isotope profiles for GroP (Fig. S2A). It should be noted that it is not possible with the HPLC-MS method to discriminate between the two stereoisomers of GroP (*cf.* Fig. 2); however,

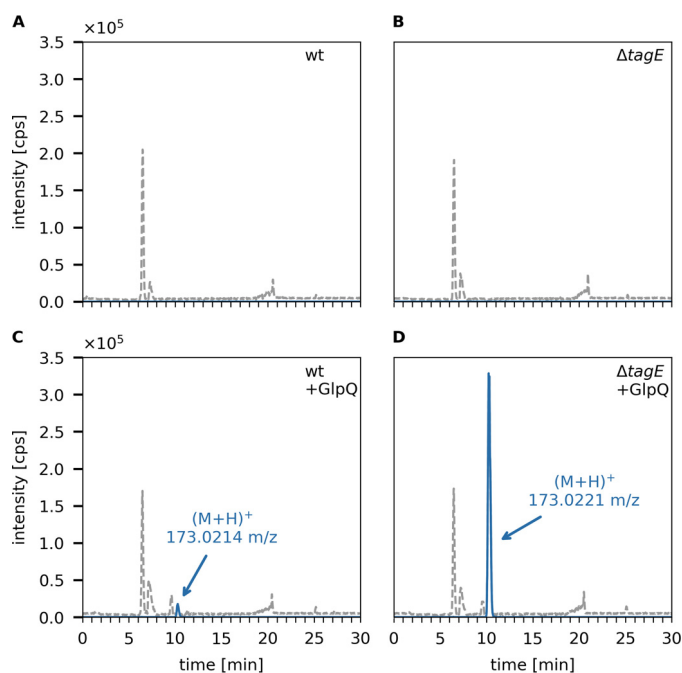


**Figure 4. GlpQ predominantly releases Gro3P from the cell walls of  $\Delta tagE$  *B. subtilis* 168.** The purified cell wall of *B. subtilis* (containing peptidoglycan and covalently bound WTA (PGN–WTA complex)) was incubated with GlpQ, and the formation of reaction products was analyzed by LC-MS. Shown are the BPC for mass range  $(M+H)^+ = 120\text{--}800$  (gray dashed lines) and the EICs of glycerolphosphate  $(M+H)^+ m/z = 173.022 \pm 0.02$  (blue solid lines). A and B, analysis of the WT containing partially glycosylated WTA and  $\Delta tagE$  containing nonglycosylated WTA cell walls in the absence of GlpQ (control). C and D, analysis of processing of WT and  $\Delta tagE$  cell walls after 30-min incubation with GlpQ. The peak areas (AUC) of released GroP were  $2.7 \times 10^5$  and  $5.9 \times 10^6$ , respectively. No glycosylated or alanylated GroP products were detected.

given the strict stereospecificity of GlpQ, the product of WTA cleavage has to be *sn*-glycerol-3-phosphate. The little amount of GroP detected in WT cell wall samples is presumably the result of the activity of GlpQ on nonglycosylated GroP at the free ends of the substrate. As GlpQ encounters a glycosylated (or alanylated) GroP in the chain polymer, the hydrolysis reaction and, consequently, GroP release stop. This hypothesis is corroborated by the finding that neither glycosylated GroP-Glc or alanylated GroP-Ala nor larger polymeric products but only unmodified GroP could be detected by HPLC-MS. Thus, GlpQ can be classified as a teichoicase that specifically hydrolyzes unmodified *sn*-glycero-3-phosphoryl–WTA.

In further support of this model, D-Ala substitutions were removed from the teichoic acid samples by pretreatment as well as by applying the GlpQ reaction at pH 8. It has been reported earlier that alanyl esters are rather labile at pH levels of 7 or higher, with a half-time of hydrolysis at pH 8 and 37 °C of 3.9 h (32, 50). Accordingly, no difference in release of GroP was observed between nontreated and pH 8–pretreated WTA samples (data not shown). Furthermore, in a time course experiment, we observed that the majority of the product in both glycosylated (WT cell–extracted) and nonglycosylated ( $\Delta tagE$  cell–extracted) samples was released by GlpQ already after a few seconds (Fig. S3). Moreover, the amount of GroP released from nonglycosylated substrate did not increase over time (over 2 h of incubation) and remained 22-fold higher than the product released from the WT substrate. These data indicate that

GlpQ has only exo- but no endolytic activity and stops when glycosylated (or alanylated) GroP appears at the free end of the polymer, protecting the rest of the chain from further digestion.

Complete digestion of WTA by GlpQ should remove all GroP residues up to the linker disaccharide ManNAc-GlcNAc. To show that this is indeed the case, cell wall preparations (PGN-WTA complex) were thoroughly digested by GlpQ. As the enzyme is rather unstable, GlpQ was added repeatedly; after each round of enzymatic digestion for 10 min at 30 °C, the supernatant was checked for GroP release by HPLC-MS and fresh GlpQ was enzyme added until only very minor additional amounts of GroP were detected. These exhaustively digested cell wall samples were then treated with 5% TCA for 2 h at 60 °C to enable cleavage of the glycosidic phosphodiester bond connecting the WTA linker with the PGN. The release of the linker disaccharide was analyzed by HPLC-MS after neutralization of the sample. The identity of the linker disaccharide was confirmed by a mass spectrum that revealed the exact mass and presence of typical fragmentations (loss of water), sodium and potassium ion adducts, and a  $^{13}\text{C}$  isotope pattern (Fig. S2B). As control, complete chemical digestion of the PGN-WTA complex was performed by treatment with 0.5 M NaOH for 2 h at 60 °C to completely remove the GroP chain polymer. Subsequently, the linker disaccharide was released from the latter samples by TCA treatment and analyzed by HPLC-MS. The linker disaccharide was obtained from both WT and nonglycosylated PGN-WTA complexes by chemical digestion in equal amounts, as shown in Fig. 5, A and B. The amount of linker disaccharide released by chemical digestion was set as to 100% of linker disaccharide in the substrate. As a further control, the PGN-WTA complex was treated with TCA alone to determine the amounts of linker disaccharide TCA can release in absence of NaOH pretreatment. Very small amounts of linker disaccharide (approximately 3.6% of the total) were released from both PGN-WTA variants under these conditions (Fig. 5, C and D). The difference, however, became significant when the substrate was predigested with GlpQ. Although GlpQ treatment released no more linker than TCA treatment alone from WT PGN-WTA, GlpQ was able to digest about 60% of WTA up to the linker in the cell wall sample derived from *tagE* mutant cells (Fig. 5, E and F).

#### GlpQ cleaves unmodified LTA only after predigestion

Because GlpQ specifically cleaves nonglycosylated WTA, we next assessed whether nonglycosylated LTA can also act as a substrate of the enzyme. Recently, the glycosyltransferase CsbB has been shown to be required for glycosylation of LTA in *B. subtilis* (38). Hence, LTA was purified from *B. subtilis* WT and  $\Delta\text{csbB}::\text{kan}$  cells according to established protocols (51, 52). Because LTA has been reported to be extensively modified by D-alanyl esters, we set out to also remove these modifications prior to GlpQ treatment. Although incubation of LTA at pH 8.5 for 24 h at room temperature leads to almost complete removal of D-alanyl esters, it may also induce limited degradation of LTA according to data reported previously (22). Hence, to absolutely avoid any degradation of LTA, we decided to apply slightly milder conditions and preincubated the LTA preparations in borate buffer at pH 8 for 24 h. The removal of alanine

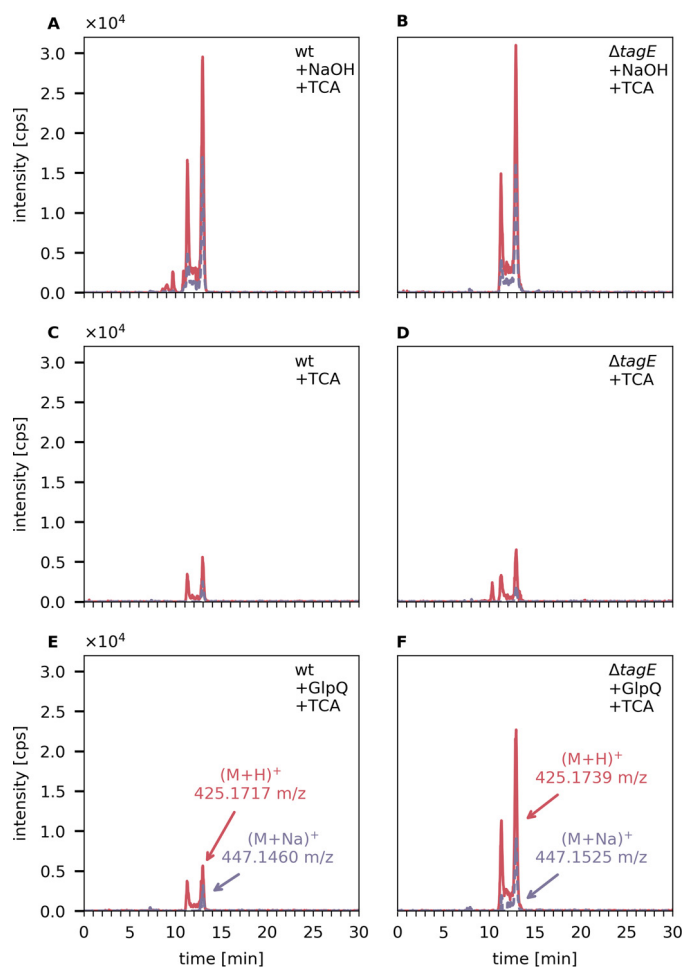


**Figure 5. GlpQ completely digests nonglycosylated WTA up to the linker disaccharide ManNAc-GlcNAc.** Purified cell walls (PGN-WTA complex, 0.1 mg each) of *B. subtilis* 168 WT and  $\Delta\text{tagE}$  were repeatedly incubated with GlpQ (seven times for 10 min at 30 °C) and then treated with 5% TCA for 2 h at 60 °C to release the linker disaccharide. The release of ManNAc-GlcNAc was analyzed by LC-MS. As a control, the cell wall was treated with 0.5 M NaOH for 2 h at 60 °C to release all GroP from the WTA chain polymers, followed by TCA treatment to release the linker disaccharide. Shown are the EICs of ManNAc-GlcNAc  $(\text{M}+\text{H})^+$   $m/z = 425.177 \pm 0.02$  (red solid lines) and  $(\text{M}+\text{Na})^+$   $m/z = 447.159 \pm 0.02$  (purple dashed lines). A and B, complete release of the linker disaccharide after NaOH and TCA treatment from WT cell walls (AUC =  $15.1 \times 10^5$ ) and from  $\Delta\text{tagE}$  cell walls containing nonglycosylated WTA (AUC =  $14.8 \times 10^5$ ). C and D, linker disaccharide released by TCA treatment alone from WT cell walls (AUC =  $2.38 \times 10^5$ ) and  $\Delta\text{tagE}$  cell walls (AUC =  $3.2 \times 10^5$ ). E and F, linker disaccharide released by TCA treatment after predigestion with GlpQ from WT cell walls (AUC =  $2.84 \times 10^5$ , i.e. 3.6% of the total linker disaccharide) and  $\Delta\text{tagE}$  cell wall (AUC =  $1.0 \times 10^6$ , i.e. 59% of the totally present linker disaccharide).

modifications was monitored by NMR (Fig. S5). The  $^1\text{H}$  NMR spectra of LTA showed characteristic resonances corresponding to D-alanyl ester modifications; the signal at  $\delta = 5.35, 4.20, 1.64,$  and  $4.2$  ppm could be assigned to resonances of Gro-2-CH (D-Ala), D-Ala- $\beta\text{H}$ , and D-Ala- $\alpha\text{H}$ , respectively. These resonances decreased significantly and shifted, indicating release of D-Ala from the GroP polymer. According to the NMR results, about 70% of the D-alanyl esters were removed by treatment of *B. subtilis* 168 LTA in borate buffer at pH 8 for 24 h at room temperature.

Only very small amounts of GroP were released by GlpQ from LTA extracted from WT or  $\Delta\text{csbB}$  mutant cells, with AUC values of  $1.0 \times 10^5$  and  $1.8 \times 10^5$ , respectively (Fig. 6). In the

## Stereochemistry of Teichoic Acids

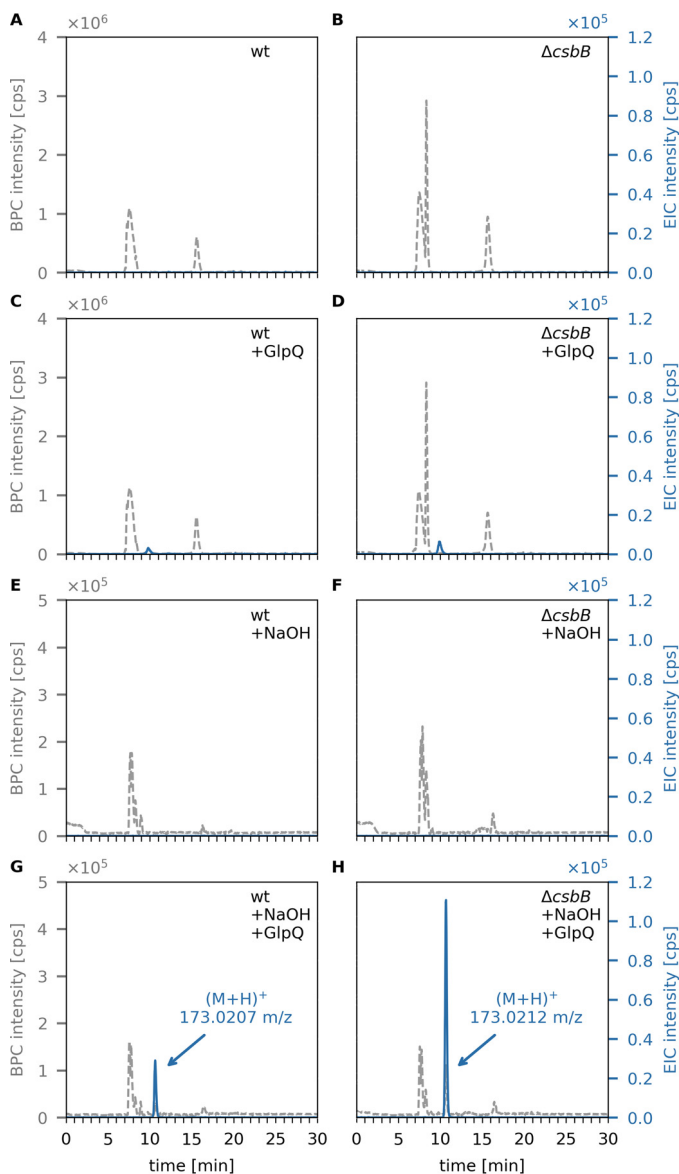


**Figure 6.** GlpQ releases *sn*-glycerol-3P from NaOH-pretreated LTA of *B. subtilis* WT and  $\Delta csbB$  mutant cells. Purified *B. subtilis* LTA was incubated for 24 h at room temperature and pH 8, followed by incubation with GlpQ. The formation of reaction products was analyzed by LC-MS. Shown are the BPC mass range  $(M+H)^+ = 120-800$  (gray dashed lines) and EICs of glycerol phosphate  $(M+H)^+ m/z = 173.022 \pm 0.02$  (blue solid lines). A and C, WT LTA (partially glycosylated LTA) incubated without GlpQ (control) and with GlpQ. The peak area of released GroP was AUC =  $1 \times 10^5$ . B and D, nonglycosylated  $\Delta csbB$  LTA incubated without GlpQ (control) and with GlpQ. The peak area of released GroP was AUC =  $1.8 \times 10^5$ . E and G, WT LTA pretreated with NaOH incubated without GlpQ (+NaOH) and with GlpQ. The peak area of released GroP was AUC =  $4.6 \times 10^5$ . F and H, nonglycosylated  $\Delta csbB$  LTA pretreated with NaOH incubated without GlpQ (+NaOH) and with GlpQ. The peak area of released GroP was AUC =  $1.69 \times 10^6$ .

absence of preincubation under mildly alkaline conditions (borate buffer (pH 8), 24 h), the amount of GroP released by GlpQ did not change (Fig. S4). When LTA extracts were incubated under alkaline conditions (0.1 M NaOH, 60 °C, 30 min) in the absence of GlpQ to partially hydrolyze phosphodiester bonds within the polymer, no GroP could be detected, indicating little degradation of LTA (Fig. 6, E and F). Subsequent addition of GlpQ, however, released substantial amounts of GroP, particularly from nonglycosylated LTA preparations (Fig. 6, G

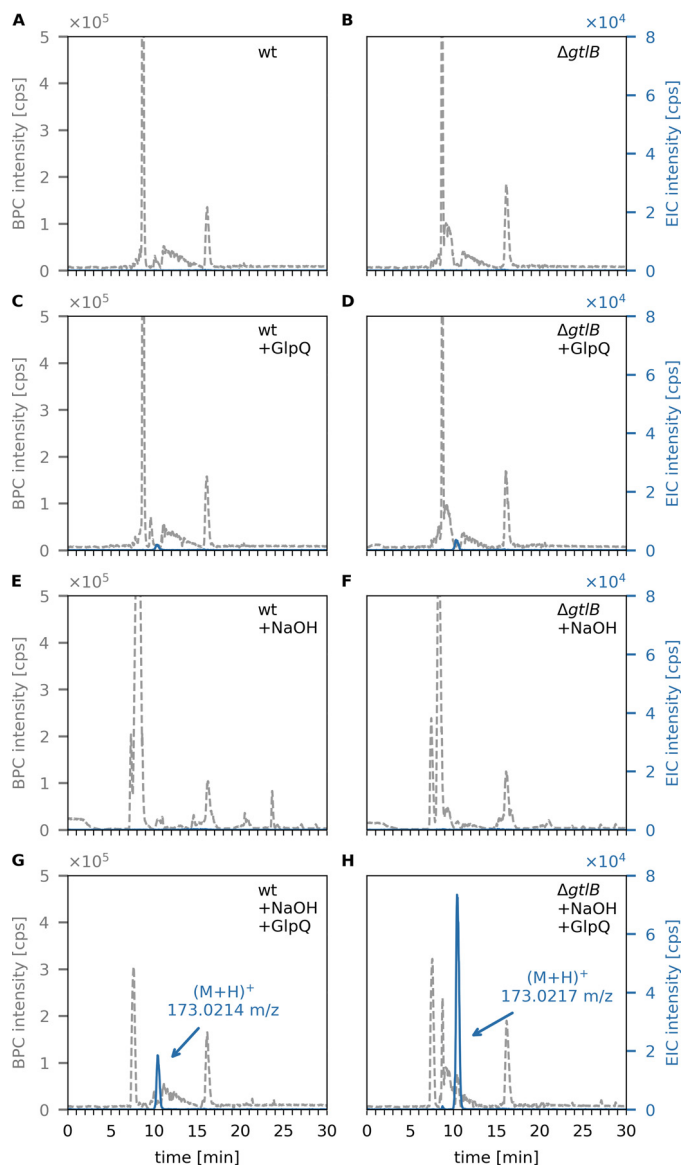


**Figure 7.** GlpQ releases *sn*-glycerol-3P from NaOH-pretreated LTA of *L. monocytogenes* WT and  $\Delta gtlB$  mutant cells. Purified *L. monocytogenes* LTA was incubated with GlpQ, and the formation of reaction products was analyzed by LC-MS. Shown are the BPC mass range  $(M+H)^+ = 120-800$  (gray dashed lines) and EICs of glycerol phosphate  $(M+H)^+ m/z = 173.022 \pm 0.02$  (blue solid lines). A and C, WT LTA (partially glycosylated LTA) incubated without GlpQ (control) and with GlpQ. The peak area of released GroP was AUC =  $6 \times 10^4$ . B and D, nonglycosylated  $\Delta gtlB$  LTA incubated without GlpQ (control) and with GlpQ. The peak area of released GroP was AUC =  $1.2 \times 10^5$ . E and G, WT LTA pretreated with NaOH incubated without GlpQ (+NaOH) and with GlpQ. The peak area of released GroP was AUC =  $4.5 \times 10^5$ . F and H, nonglycosylated  $\Delta gtlB$  LTA pretreated with NaOH incubated without GlpQ (+NaOH) and with GlpQ. The peak area of released GroP was AUC =  $1.87 \times 10^6$ .

and H). The amount of GroP released by GlpQ was about 3.7 times higher with nonglycosylated LTA (AUC =  $1.69 \times 10^6$ ) compared with WT glycosylated LTA (AUC =  $4.6 \times 10^5$ ). The same pattern could be observed for LTA obtained from *L. monocytogenes* WT and LTA glycosylation-deficient ( $\Delta gtlB$ ) strains. Although GlpQ released only small amounts of GroP from WT (AUC =  $6 \times 10^4$ ) and nonglycosylated ( $\Delta gtlB$ ) (AUC =  $1.2 \times 10^5$ ) LTA (Figs. 7, C and D), the amount increased significantly after NaOH pretreatment (Fig. 7, G and

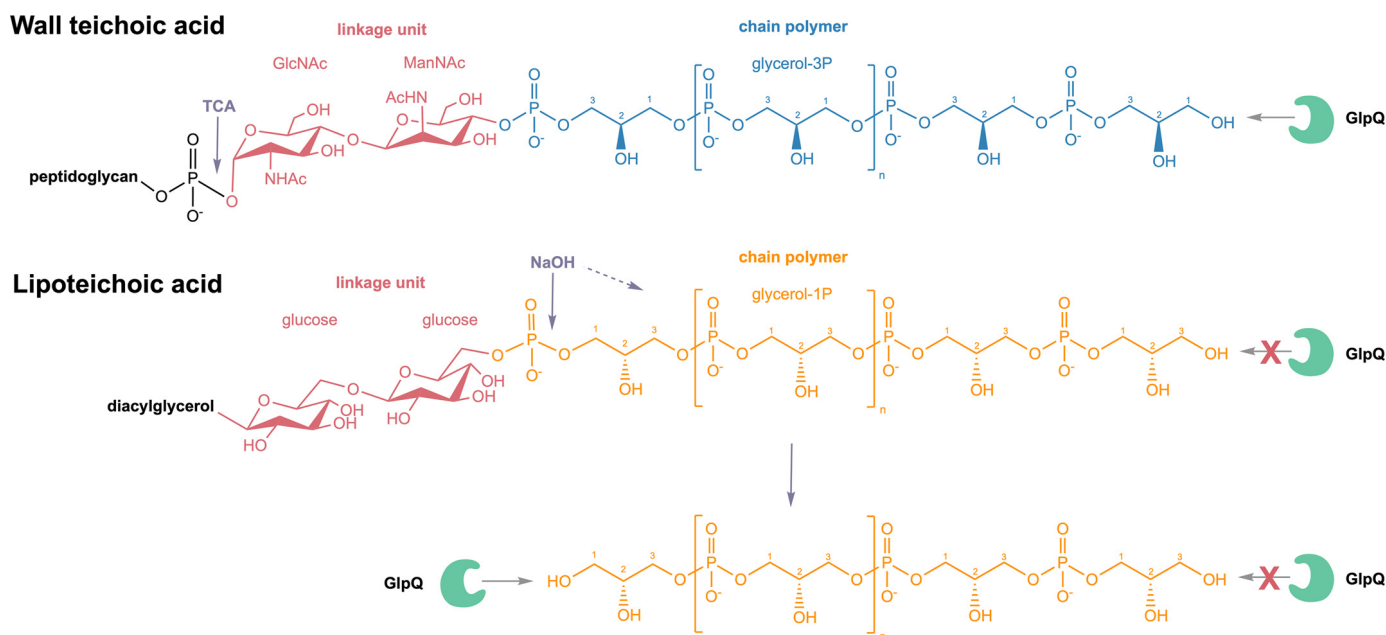


**Figure 8. Differential digestion of WTA and LTA by the stereospecific *sn*-glycerol-3P phosphodiesterase GlpQ.** WTA of *B. subtilis* 168 are phosphodiester polymers made of Gro3P subunits that are generally substituted at the hydroxyl group at the C2 position to a certain degree with D-alanine or alpha-glucose. Via a linkage unit (red) consisting of a disaccharide, ManNAc- $\beta$ (1-4)-GlcNAc, and an unsubstituted Gro3P, WTA are linked to the C6 of N-acetylmuramic acid of the peptidoglycan via a phosphodiester bond. Trichloroacetic acid (TCA) treatment enables cleavage of the glycosidic phosphodiester bond that connects the WTA linker with the PGN. LTA of *B. subtilis* 168 is a phosphodiester polymer made of Gro1P subunits; hence, it represents an enantiomer of the WTA polymer. It can be modified at the C2 position with D-alanine or GlcNAc and linked to a diacylglycerol via a glucose- $\beta$ -1,6-glucose linker disaccharide. GlpQ is able to cleave off Gro3P from the terminal ends of WTA. Conversely, GlpQ is not able to chip off Gro1P from the terminal ends of LTA. The stereospecific enzyme GlpQ is able to discriminate the orientation of the hydroxyl group on the C2. Treatment with NaOH enables precleavage of phosphodiester bonds within the LTA chain polymer, resulting in fragments that contain Gro3P terminal ends. From these ends, GlpQ is able to cleave off Gro3P moieties. The differential cleavage of WTA and LTA by GlpQ unravels the different stereochemistry of the polymers.

H) with 4.2 times more GroP released from nonglycosylated LTA (AUC =  $1.87 \times 10^6$ ) than from the WT (AUC =  $4.5 \times 10^5$ ). These results indicate that GlpQ is only able to release significant amounts of GroP from LTA when the polymer is precleaved with NaOH, which generates LTA fragments that expose *sn*-glycero-3-phosphoryl groups at the free ends (Fig. 8). The low amounts of GroP that are released by GlpQ from LTA preparations under mildly alkaline conditions may be the result of partial phosphodiester cleavage of the polymer at pH 8.0. However, phosphodiester cleavage under these conditions is unlikely, and, consistently, we were unable to detect LTA degradation by  $^1\text{H}$  NMR analysis. The most likely explanation is that low amounts of GroP are released by GlpQ from the free *sn*-glycero-3-phosphoryl ends of lipid II-bound WTA precursors, which are copurified with LTA on a hydrophobic interaction column during sample preparation. It could be argued that GlpQ may not be able to degrade LTA because of limited accessibility to the membrane-bound substrate and that the enzyme only works well when LTA is predigested, which removes the membrane anchor. However, LTA is water-soluble, and there is no reason to doubt that GlpQ can have access to the hydrophilic free ends of the polymer. Moreover, it was shown that membrane-anchored precursor molecules of WTA are readily cleaved by GlpQ (41). Clearly, substitutions at GroP by glycosylation or alanylation impede the action of GlpQ, leaving the question of how substituted WTA (and LTA) may be processed. Presumably, the cells have additional enzymes that can act on substituted teichoic acids. PhoD of *B. subtilis*, recently

identified as an endolytic teichoicase, is able to cleave glycosylated WTA (41).

In summary, GlpQ releases GroP in significant amounts from WTA (Fig. 4) but only very small amounts from LTA preparations (Figs. 6C and 7C). These findings experimentally confirm differences in the stereochemistry of the two polyglycerolphosphate polymers. In agreement with the described stereospecificity of GlpQ, WTA consist of Gro3P- and LTA of Gro1P-repeating units. The origin of this difference can be found in the early stages of biosynthesis. WTA biosynthesis starts with Gro3P, which is transferred to CTP by TagD with simultaneous release of pyrophosphate, generating CDP-glycerol. The chain polymer is elongated in the cytoplasm with addition of Gro3P to the growing chain, and CMP is released (Fig. 1A) (53). In contrast, LTA biosynthesis starts with phosphatidylglycerol-CMP, onto which PgsA transfers Gro3P while releasing CMP. The 3P group of Gro3P is released, and the product PG is translocated across the membrane and polymerized. The glycerolphosphate group of PG carries a 1-phosphate group, incorporating Gro1P in the growing LTA chains (Fig. 1B) (10).

### Conclusions

Our work reveals the distinct stereoisomerism of the glycerolphosphate polymers WTA and LTA of *B. subtilis* by differential digestion with the stereospecific phosphodiesterase GlpQ. First, we were able to show that the stereospecific *sn*-glycerol-3P phosphodiesterase GlpQ is an exolytic hydrolase that

## Stereochemistry of Teichoic Acids

sequentially cleaves off GroP entities from unmodified WTA, which lack any modification in form of D-alanylation or  $\alpha$ -glucosylation, up to the linker unit that connects WTA with the PGN. Second, GlpQ is unable to cleave intact, unmodified LTA. Thus, WTA and LTA polymers of *B. subtilis* 168 constitute enantiomers consisting of Gro3P (WTA) and Gro1P (LTA) building blocks, respectively. Accordingly, limited hydrolysis of LTA with NaOH, which leads to random cleavage of phosphodiester bonds within the polymer, yields fragments that contain Gro3P terminal ends from which GlpQ is able to cleave off Gro3P entities. The difference in stereochemistry between WTA and LTA has critical consequences for the differential physiological functions, regulation, and turnover of both polymers. The results of this study rationalize the specific interaction of WTA and LTA with stereospecific enzymes and protection against simultaneous degradation with possibly fatal effects for cell viability.

### Experimental procedures

#### Bacterial strains and growth conditions

The bacterial strains, plasmids, and oligonucleotides used in this study are listed in Table S1. The *B. subtilis* 168 WT and  $\Delta tagE::erm$  strains were obtained from the Bacillus Genetic Stock Center (Columbus, OH). *B. subtilis*  $\Delta csbB::kan$ , *L. monocytogenes* WT strain 10403S, and the  $\Delta gtlB::strep$  mutant were obtained from the Gründling laboratory (38). These bacteria were used for isolation of whole cell wall (peptidoglycan–WTA complex) and teichoic acid preparations. They were cultured at 37 °C in lysogeny broth (LB; Lennox, Carl Roth) with continuous shaking at 140 rpm or on solid LB supplemented with 1.5% agar. Overnight cultures (~16 h) were used to inoculate fresh LB medium and grown to yield an  $A_{600}$  of 1. Cells were harvested by centrifugation (3000  $\times$  g, 20 min, 4 °C). *E. coli* BL21 (DE3) cells (New England Biolabs) were used to heterologously express recombinant GlpQ phosphodiesterase from *B. subtilis*. These cells, transformed with pET28a-*glpQ*, were grown in LB medium supplemented with 50  $\mu$ g/ml kanamycin until  $A_{600}$  0.7 was reached, followed by induction with 1 mM isopropyl 1-thio- $\beta$ -D-galactopyranoside and further propagation for 3 h. Cells were harvested by centrifugation (3000  $\times$  g, 20 min, 4 °C) and used for purification of recombinant GlpQ.

#### Construction of plasmids and purification of recombinant GlpQ

*B. subtilis* 168 *glpQ* was amplified by PCR with the primers pET28a-*glpQ*-for and pET28a-*glpQ*-rv (MWG Eurofins, Ebersberg, Germany). Oligonucleotide primers are listed in Table S1. The PCR products were purified (GeneJET Purification Kit and Gene Ruler, 1-kb marker, Thermo Fisher Scientific), digested with the appropriate restriction enzymes (New England Biolabs), and ligated with T4 DNA ligase (Thermo Fisher Scientific) into the expression vector pET28a (Novagen), allowing them to overproduce a C-terminal His<sub>6</sub> tag fusion protein. *E. coli* BL21 (DE3) cells carrying pET28a-*glpQ* were grown as described above and lysed in a French pressure cell. The His-tagged GlpQ protein was purified by Ni<sup>2+</sup> affinity chromatography using a 1-ml HisTrap column (GE Healthcare), followed by size exclusion chromatography on a HiLoad 16/60 Superdex

200  $\mu$ g column (GE Healthcare), and purity was checked with 12% SDS-PAGE. The purity of the enzyme was confirmed via SDS-PAGE (Fig. 2A). From a 1-liter culture, 3.6 mg of GlpQ was obtained. The enzyme was stored at a concentration of 0.23 mg/ml at –20 °C in 0.1 M Tris-HCl buffer (pH 8).

#### Biochemical characterization of GlpQ

To determine the enzymatic properties of GlpQ, 1 pmol of pure recombinant enzyme was incubated with 10 mM GPC. The reaction was stopped by adding 200  $\mu$ l of pH 3.3 buffer (0.1% formic acid and 0.05% ammonium formate), and the released glycerolphosphate was measured by HPLC-MS. For pH stability, GlpQ was preincubated in buffers at different pH values (pH 2, HCl; pH 3–6, acetic acid; pH 6–7, MES; pH 7–9, Tris; pH 10, NaHCO<sub>3</sub>) for 30 min at 30 °C before adding 5  $\mu$ l of each to a 45- $\mu$ l mixture with 0.1 M Tris (pH 8) buffer and substrate for 5 min. The pH optimum was tested by incubating GlpQ with 10 mM GPC for 5 min in buffers with different pH values. For temperature stability, GlpQ was preincubated in 0.1 M Tris-HCl (pH 8) at different temperatures ranging from 4 °C to 75 °C for 30 min, followed by 5-min incubation with GPC at 30 °C and pH 8.0. The optimum temperature was tested by incubating GlpQ for 5 min at different temperatures with GPC at pH 8.

#### Preparation of cell walls, WTA, and LTA

For the preparation of cell walls (peptidoglycan–WTA complex), 2 liters of *B. subtilis* 168 WT or  $\Delta tagE::erm$  cultures (exponential growth phase,  $A_{600}$  = 0.9) were harvested and resuspended in 30 ml of piperazine acetate buffer (50 mM (pH 6)) with 12 units of proteinase K and boiled for 1 h. The cytosolic fractions were removed by centrifugation (3000  $\times$  g, 15 min, 4 °C). The pellet was resuspended in 6 ml of buffer (10 mM Tris, 10 mM NaCl, and 320 mM imidazole, adjusted to pH 7.0 with HCl), and 600  $\mu$ g of  $\alpha$ -amylase, 250 units of RNase A, 120 units of DNase I, and 50 mM of MgSO<sub>4</sub> were added. The sample was incubated at 37 °C for 2 h while shaking, and then 12 units of proteinase K was added, and the incubation continued for 1 h. 4% SDS solution was added 1:1, and the mixture was boiled for 1 h. SDS was removed by repeated ultracentrifugation steps (20 times at 140,000  $\times$  g, 30 min, 40 °C), suspension in double-distilled H<sub>2</sub>O, as well as dialysis against double-distilled H<sub>2</sub>O. The SDS content was controlled with a methylene blue assay described earlier (54). The cell wall preparation was dried in a vacuum concentrator. LTA from *B. subtilis* 168 (WT and  $\Delta csbB$ ) and *L. monocytogenes* 10403S (WT and  $\Delta gtlB$ ) was prepared by butanol extraction and purification by hydrophobic interaction chromatography using a 24  $\times$  1.6-cm octyl–Sepharose column, according to published protocols (51, 52).

#### Teichoic acid digestion with GlpQ and analysis of glycerolphosphate release

WTA assays were conducted in 0.1 M Tris-HCl buffer (pH 8, supplemented with 1 mM CaCl<sub>2</sub>) with 0.1 mg cell wall preparation (peptidoglycan with attached WTA from *B. subtilis* 168 WT and  $\Delta tagE::erm$ ) as a substrate and 0.7  $\mu$ M GlpQ. The samples were incubated for 30 min at 30 °C.

LTA assays occurred in 0.1 M Tris-HCl buffer (pH 8, supplemented with 1 mM CaCl<sub>2</sub>) with 0.2 mg LTA extract (*B. subtilis* 168 WT and  $\Delta$ *csbB::erm*) and 0.7  $\mu$ M GlpQ in a total volume of 50  $\mu$ l. The samples were incubated for 1 h at 30 °C. LTA was predigested by incubation with 0.1 M NaOH for 30 min at 60 °C, followed by neutralization with HCl and drying in a vacuum concentrator.

Sample analysis was conducted using an electrospray ionization–TOF mass spectrometer (MicroTOF II, Bruker Daltonics) operated in positive ion mode and connected to an UltiMate 3000 HPLC system (Dionex). For HPLC-MS analysis, 7  $\mu$ l of the sample supernatant was injected into a Gemini C18 column (150 by 4.6 mm, 5  $\mu$ m, 110 Å, Phenomenex). A 45-min program at a flow rate of 0.2 ml/min was used to separate the compounds as described previously (55). The mass spectra of the investigated samples were presented as base peak chromatograms (BPCs) and extracted ion chromatograms (EIC) in the DataAnalysis program and presented by generating diagrams using Python 3.6 with the Matplotlib (version 2.2.2) library.

**Author contributions**—A. W. and C. M. conceptualization; A. W., J. R., and A. G. resources; A. W. data curation; A. W. and S. U. formal analysis; A. W. validation; A. W. and S. U. investigation; A. W. visualization; A. W., S. U., J. R., and A. M. J. methodology; A. W. writing—original draft; A. P., A. G., and C. M. supervision; A. P., A. G., and C. M. funding acquisition; A. P., A. G., and C. M. writing—review and editing; C. M. project administration.

**Acknowledgment**—We thank Dr. Libera Lo Presti for linguistic editing and proofreading.

## References

- Silhavy, T. J., Kahne, D., and Walker, S. (2010) The bacterial cell envelope. *Cold Spring Harb. Perspect. Biol.* **2**, a000414 [Medline](#)
- Armstrong, J. J., Baddiley, J., Buchanan, J. G., Davison, A. L., Kelemen, M. V., and Neuhaus, F. C. (1959) Composition of teichoic acids from a number of bacterial walls. *Nature* **184**, 247–248 [CrossRef Medline](#)
- Archibald, A. R., Armstrong, J. J., Baddiley, J., and Hay, J. B. (1961) Teichoic acids and the structure of bacterial walls. *Nature* **191**, 570–572 [CrossRef Medline](#)
- Baddiley, J. (1989) Bacterial cell walls and membranes: discovery of the teichoic acids. *Bioessays* **10**, 207–210 [CrossRef Medline](#)
- Schäffer, C., and Messner, P. (2005) The structure of secondary cell wall polymers: how Gram-positive bacteria stick their cell walls together. *Microbiology* **151**, 643–651 [CrossRef Medline](#)
- Weidenmaier, C., and Peschel, A. (2008) Teichoic acids and related cell-wall glycopolymers in Gram-positive physiology and host interactions. *Nat. Rev. Microbiol.* **6**, 276–287 [CrossRef Medline](#)
- Kohler, T., Xia, G., Kulauzovic, E., and Peschel, A. (2010) In *Microbial Glycobiology: Structures, Relevance and Applications* (Moran, A., Holst, O., Brennan, P., and von Itzstein, M., eds.) pp. 75–91, Academic Press, London, UK
- Potekhina, N. V., Streshinskaya, G. M., Tul'skaya, E. M., Kozlova, Y. I., Senchenkova, S. N., and Shashkov, A. S. (2011) Phosphate-containing cell wall polymers of bacilli. *Biochemistry* **76**, 745–754
- Brown, S., Santa Maria, J. P., Jr, and Walker, S. (2013) Wall teichoic acids of gram-positive bacteria. *Annu. Rev. Microbiol.* **67**, 313–336 [CrossRef Medline](#)
- Percy, M. G., and Gründling, A. (2014) Lipoteichoic acid synthesis and function in Gram-positive bacteria. *Annu. Rev. Microbiol.* **68**, 81–100 [CrossRef Medline](#)
- De Boer, W. R., Kruyssen, F. J., and Wouters, J. T. (1976) The structure of teichoic acid from *Bacillus subtilis* var. *niger* WM as determined by C nuclear-magnetic-resonance spectroscopy. *Eur. J. Biochem.* **62**, 1–6 [CrossRef Medline](#)
- Romaniuk, J. A. H., and Cegelski, L. (2018) Peptidoglycan and teichoic acid levels and alterations in *S. aureus* by cell-wall and whole-cell NMR. *Biochemistry* **57**, 3966–3975 [CrossRef Medline](#)
- Grant, W. D. (1979) Cell wall teichoic acid as a reserve phosphate source in *Bacillus subtilis*. *J. Bacteriol.* **137**, 35–43 [CrossRef Medline](#)
- Ellwood, D. C., and Tempest, D. W. (1969) Control of teichoic acid and teichuronic acid biosyntheses in chemostat cultures of *Bacillus subtilis* var. *niger*. *Biochem. J.* **111**, 1–5 [Medline](#)
- Bhavsar, A. P., Erdman, L. K., Schertzer, J. W., and Brown, E. D. (2004) Teichoic acid is an essential polymer in *Bacillus subtilis* that is functionally distinct from teichuronic acid. *J. Bacteriol.* **186**, 7865–7873 [CrossRef Medline](#)
- Ellwood, D. C., and Tempest, D. W. (1972) in *Advances in Microbial Physiology* (Rose, A. H. and Tempest, D. W., eds.) pp. 82–117, Academic Press, London, UK
- Fischer, W. (1990) in *Handbook of Lipid Research: Glycolipids, Phosphoglycolipids, and Sulfoglycolipids* (Kates, M., ed.) pp. 123–234, Springer, New York, NY
- Schirner, K., Marles-Wright, J., Lewis, R. J., and Errington, J. (2009) Distinct and essential morphogenic functions for wall- and lipo-teichoic acids in *Bacillus subtilis*. *EMBO J.* **28**, 830–842 [CrossRef Medline](#)
- Xia, G., Kohler, T., and Peschel, A. (2010) The wall teichoic acid and lipoteichoic acid polymers of *Staphylococcus aureus*. *Int. J. Med. Microbiol.* **300**, 148–154 [CrossRef Medline](#)
- Heptinstall, S., Archibald, A. R., and Baddiley, J. (1970) Teichoic acids and membrane function in bacteria. *Nature* **225**, 519–521 [CrossRef Medline](#)
- Biswas, R., Martinez, R. E., Göhring, N., Schlag, M., Josten, M., Xia, G., Hegler, F., Gekeler, C., Gleske, A. K., Götz, F., Sahl, H. G., Kappler, A., and Peschel, A. (2012) Proton-binding capacity of *Staphylococcus aureus* wall teichoic acid and its role in controlling autolysin activity. *PLoS ONE* **7**, e41415 [CrossRef Medline](#)
- Morath, S., Geyer, A., and Hartung, T. (2001) Structure-function relationship of cytokine induction by lipoteichoic acid from *Staphylococcus aureus*. *J. Exp. Med.* **193**, 393–397 [CrossRef Medline](#)
- Morath, S., Stadelmaier, A., Geyer, A., Schmidt, R. R., and Hartung, T. (2002) Synthetic lipoteichoic acid from *Staphylococcus aureus* is a potent stimulus of cytokine release. *J. Exp. Med.* **195**, 1635–1640 [CrossRef Medline](#)
- Weidenmaier, C., Kokai-Kun, J. F., Kristian, S. A., Chanturiya, T., Kalbacher, H., Gross, M., Nicholson, G., Neumeister, B., Mond, J. J., and Peschel, A. (2004) Role of teichoic acids in *Staphylococcus aureus* nasal colonization, a major risk factor in nosocomial infections. *Nat. Med.* **10**, 243–245 [CrossRef Medline](#)
- Matias, V. R., and Beveridge, T. J. (2008) Lipoteichoic acid is a major component of the *Bacillus subtilis* periplasm. *J. Bacteriol.* **190**, 7414–7418 [CrossRef Medline](#)
- Bontemps-Gallo, S., Bohin, J. P., and Lacroix, J. M. (2017) Osmoregulated periplasmic glucans. *EcoSal Plus* [CrossRef Medline](#)
- Pooley, H. M., and Karamata, D. (2000) Incorporation of [2-<sup>3</sup>H]glycerol into cell surface components of *Bacillus subtilis* 168 and thermosensitive mutants affected in wall teichoic acid synthesis: effect of tunicamycin. *Microbiology* **146**, 797–805 [CrossRef Medline](#)
- Jorge, A. M., Schneider, J., Unsleber, S., Xia, G., Mayer, C., and Peschel, A. (2018) *Staphylococcus aureus* counters phosphate limitation by scavenging wall teichoic acids from other staphylococci via the teichoicase GlpQ. *J. Biol. Chem.* **293**, 14916–14924 [CrossRef Medline](#)
- van der Es, D., Hogendorf, W. F., Overkleef, H. S., van der Marel, G. A., and Codée, J. D. (2017) Teichoic acids: synthesis and applications. *Chem. Soc. Rev.* **46**, 1464–1482 [CrossRef Medline](#)
- Gerlach, D., Guo, Y., De Castro, C., Kim, S. H., Schlatterer, K., Xu, F. F., Pereira, C., Seeberger, P. H., Ali, S., Codee, J., Sirisarn, W., Schulte, B., Wolz, C., Larsen, J., Molinaro, A., et al. (2018) Methicillin-resistant *Staphylococcus aureus* alters cell wall glycosylation to evade immunity. *Nature* **563**, 705–709 [CrossRef Medline](#)

## Stereochemistry of Teichoic Acids

31. van Dalen, R., De La Cruz Diaz, J. S., Rumpret, M., Fuchsberger, F. F., van Teijlingen, N. H., Hanske, J., Rademacher, C., Geijtenbeek, T. B. H., van Strijp, J. A. G., Weidenmaier, C., Peschel, A., Kaplan, D. H., and van Sorge, N. M. (2019) Langerhans cells sense *Staphylococcus aureus* wall teichoic acid through Langerin to induce inflammatory responses. *mBio* **10**, e00330-19 [Medline](#)
32. Neuhaus, F. C., and Baddiley, J. (2003) A continuum of anionic charge: structures and functions of D-alanyl-teichoic acids in Gram-positive bacteria. *Microbiol. Mol. Biol. Rev.* **67**, 686–723 [CrossRef Medline](#)
33. Perego, M., Glaser, P., Minutello, A., Strauch, M. A., Leopold, K., and Fischer, W. (1995) Incorporation of D-alanine into lipoteichoic acid and wall teichoic acid in *Bacillus subtilis*: identification of genes and regulation. *J. Biol. Chem.* **270**, 15598–15606 [CrossRef Medline](#)
34. Reichmann, N. T., Cassona, C. P., and Gründling, A. (2013) Revised mechanism of D-alanine incorporation into cell wall polymers in Gram-positive bacteria. *Microbiology* **159**, 1868–1877 [CrossRef Medline](#)
35. Wood, B. M., Santa Maria, J. P., Jr, Matano, L. M., Vickery, C. R., and Walker, S. (2018) A partial reconstitution implicates DltD in catalyzing lipoteichoic acid D-alanylation. *J. Biol. Chem.* **293**, 17985–17996 [CrossRef Medline](#)
36. Brooks, D., Mays, L. L., Hatefi, Y., and Young, F. E. (1971) Glucosylation of teichoic acid: solubilization and partial characterization of the uridine diphosphoglucose: polyglycerolteichoic acid glucosyl transferase from membranes of *Bacillus subtilis*. *J. Bacteriol.* **107**, 223–229 [CrossRef Medline](#)
37. Allison, S. E., D'Elia, M. A., Arar, S., Monteiro, M. A., and Brown, E. D. (2011) Studies of the genetics, function, and kinetic mechanism of TagE, the wall teichoic acid glycosyltransferase in *Bacillus subtilis* 168. *J. Biol. Chem.* **286**, 23708–23716 [CrossRef Medline](#)
38. Rismondo, J., Percy, M. G., and Gründling, A. (2018) Discovery of genes required for lipoteichoic acid glycosylation predicts two distinct mechanisms for wall teichoic acid glycosylation. *J. Biol. Chem.* **293**, 3293–3306 [CrossRef Medline](#)
39. Kho, K., and Meredith, T. C. (2018) Salt-induced stress stimulates a lipoteichoic acid-specific three component glycosylation system in *Staphylococcus aureus*. *J. Bacteriol.* **200**, e00017-18 [Medline](#)
40. Rismondo, J., Haddad, T. F. M., Shen, Y., Loessner, M. J., and Gründling, A. (2019) GtcA is required for LTA glycosylation in *Listeria monocytogenes* serovar 1/2a and *Bacillus subtilis*. *bioRxiv* [CrossRef](#)
41. Myers, C. L., Li, F. K., Koo, B. M., El-Halfawy, O. M., French, S., Gross, C. A., Strynadka, N. C., and Brown, E. D. (2016) Identification of two phosphate starvation-induced wall teichoic acid hydrolases provides first insights into the degradative pathway of a key bacterial cell wall component. *J. Biol. Chem.* **291**, 26066–26082 [CrossRef Medline](#)
42. Borisova, M., Gaupp, R., Duckworth, A., Schneider, A., Dalügge, D., Mühleck, M., Deubel, D., Unsleber, S., Yu, W., Muth, G., Bischoff, M., Götz, F., and Mayer, C. (2016) Peptidoglycan recycling in Gram-positive bacteria is crucial for survival in stationary phase. *mBio* **7**, e00923-16 [Medline](#)
43. Kluj, R. M., Ebner, P., Adamek, M., Ziemert, N., Mayer, C., and Borisova, M. (2018) Recovery of the peptidoglycan turnover product released by the autolysin Atl in *Staphylococcus aureus* involves the phosphotransferase system transporter MurP and the novel 6-phospho-N-acetylmuramidase MupG. *Front. Microbiology* **9**, 2725 [CrossRef Medline](#)
44. Mayer, C., Kluj, R. M., Mühleck, M., Walter, A., Unsleber, S., Hottmann, I., and Borisova, M. (2019) Bacteria's different ways to recycle their own cell wall. *Int. J. Med. Microbiol.* **309**, 151326 [CrossRef Medline](#)
45. Larson, T. J., Ehrmann, M., and Boos, W. (1983) Periplasmic glycerophosphodiester phosphodiesterase of *Escherichia coli*, a new enzyme of the *glp* regulon. *J. Biol. Chem.* **258**, 5428–5432 [Medline](#)
46. Larson, T. J., and van Loo-Bhattacharya, A. T. (1988) Purification and characterization of *glpQ*-encoded glycerophosphodiester phosphodiesterase from *Escherichia coli* K-12. *Arch. Biochem. Biophys.* **260**, 577–584 [CrossRef Medline](#)
47. Jorge, A. M., Schneider, J., Unsleber, S., Göhring, N., Mayer, C., and Peschel, A. (2017) Utilization of glycerophosphodiesters by *Staphylococcus aureus*. *Mol. Microbiol.* **103**, 229–241 [CrossRef Medline](#)
48. Shi, L., Liu, J. F., An, X. M., and Liang, D. C. (2008) Crystal structure of glycerophosphodiester phosphodiesterase (GDPE) from *Thermoanaerobacter tengcongensis*, a metal ion-dependent enzyme: insight into the catalytic mechanism. *Proteins* **72**, 280–288 [CrossRef Medline](#)
49. Santelli, E., Schwarzenbacher, R., McMullan, D., Biorac, T., Brinen, L. S., Canaves, J. M., Cambell, J., Dai, X., Deacon, A. M., Elsliger, M. A., Eshagi, S., Floyd, R., Godzik, A., Grittini, C., Grzechnik, S. K., et al. (2004) Crystal structure of a glycerophosphodiester phosphodiesterase (GDPE) from *Thermotoga maritima* (TM1621) at 1.60 Å resolution. *Proteins* **56**, 167–170 [CrossRef Medline](#)
50. Childs, W. C., 3rd, and Neuhaus, F. C. (1980) Biosynthesis of D-alanyl-lipoteichoic acid: characterization of ester-linked D-alanine in the *in vitro*-synthesized product. *J. Bacteriol.* **143**, 293–301 [CrossRef Medline](#)
51. Gründling, A., and Schneewind, O. (2007) Synthesis of glycerol phosphate lipoteichoic acid in *Staphylococcus aureus*. *Proc. Natl. Acad. Sci. U.S.A.* **104**, 8478–8483 [CrossRef Medline](#)
52. Percy, M. G., Karinou, E., Webb, A. J., and Gründling, A. (2016) Identification of a lipoteichoic acid glycosyltransferase enzyme reveals that GW-domain-containing proteins can be retained in the cell wall of *Listeria monocytogenes* in the absence of lipoteichoic acid or its modifications. *J. Bacteriol.* **198**, 2029–2042 [CrossRef Medline](#)
53. Formstone, A., Carballido-López, R., Noirot, P., Errington, J., and Schefers, D. J. (2008) Localization and interactions of teichoic acid synthetic enzymes in *Bacillus subtilis*. *J. Bacteriol.* **190**, 1812–1821 [CrossRef Medline](#)
54. Hayashi, K. (1975) A rapid determination of sodium dodecyl sulfate with methylene blue. *Anal. Biochem.* **67**, 503–506 [CrossRef Medline](#)
55. Gisin, J., Schneider, A., Nägele, B., Borisova, M., and Mayer, C. (2013) A cell wall recycling shortcut that bypasses peptidoglycan *de novo* biosynthesis. *Nat. Chem. Biol.* **9**, 491–493 [CrossRef Medline](#)
56. Mootz, H. D., Finking, R., and Marahiel, M. A. (2001) 4'-phosphopantetheine transfer in primary and secondary metabolism of *Bacillus subtilis*. *J. Biol. Chem.* **276**, 37289–37298 [CrossRef Medline](#)
57. Ma, D., Wang, Z., Merrikh, C. N., Lang, K. S., Lu, P., Li, X., Merrikh, H., Rao, Z., and Xu, W. (2018) Crystal structure of a membrane-bound O-acyltransferase. *Nature* **562**, 286–290 [CrossRef Medline](#)
58. Reichmann, N. T., and Gründling, A. (2011) Location, synthesis and function of glycolipids and polyglycerolphosphate lipoteichoic acid in Gram-positive bacteria of the phylum Firmicutes. *FEMS Microbiol. Lett.* **319**, 97–105 [CrossRef Medline](#)



**Phosphoglycerol-type wall and lipoteichoic acids are enantiomeric polymers differentiated by the stereospecific glycerophosphodiesterase GlpQ**  
Axel Walter, Sandra Unsleber, Jeanine Rismondo, Ana Maria Jorge, Andreas Peschel, Angelika Gründling and Christoph Mayer

*J. Biol. Chem.* 2020, 295:4024-4034.

doi: 10.1074/jbc.RA120.012566 originally published online February 11, 2020

---

Access the most updated version of this article at doi: [10.1074/jbc.RA120.012566](https://doi.org/10.1074/jbc.RA120.012566)

Alerts:

- [When this article is cited](#)
- [When a correction for this article is posted](#)

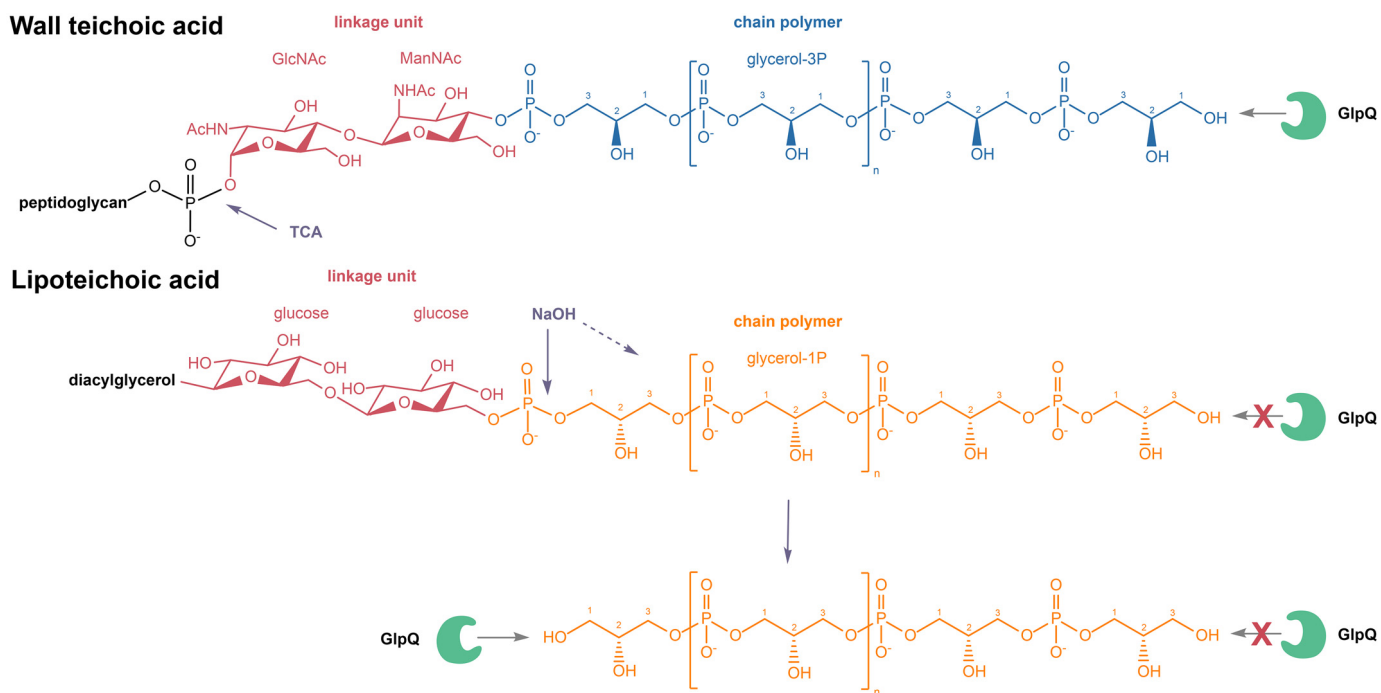
[Click here](#) to choose from all of JBC's e-mail alerts

This article cites 55 references, 23 of which can be accessed free at <http://www.jbc.org/content/295/12/4024.full.html#ref-list-1>

**Correction: Phosphoglycerol-type wall and lipoteichoic acids are enantiomeric polymers differentiated by the stereospecific glycerophosphodiesterase GlpQ**

Axel Walter, Sandra Unsleber, Jeanine Rismondo, Ana Maria Jorge, Andreas Peschel, Angelika Gründling, and Christoph Mayer

In Fig. 8, the structures of the linker disaccharides of wall and lipoteichoic acids (*red partial structures*) were erroneously shown in the wrong configuration. These structures have now been corrected. These errors do not affect the results and conclusions of this work.



## Supporting Information to

### Phosphoglycerol-type wall- and lipoteichoic acids are enantiomeric polymers differentiated by the stereospecific glycerophosphodiesterase GlpQ

Axel Walter<sup>#</sup>, Sandra Unsleber<sup>#</sup>, Jeanine Rismondo<sup>§</sup>, Ana Maria Jorge<sup>¶</sup>, Andreas Peschel<sup>¶</sup>,  
Angelika Gründling<sup>§</sup>, Christoph Mayer<sup>#</sup>

From <sup>#</sup>Microbiology/Glycobiology and <sup>¶</sup>Infection Biology, Interfaculty Institute of Microbiology and Infection Medicine Tübingen (IMIT), University of Tübingen, 72076 Tübingen, Germany and the <sup>§</sup>Section of Molecular Microbiology and Medical Research Council Centre for Molecular Bacteriology and Infection, Imperial College London, London SW7 2AZ, United Kingdom

#### Supporting Figures

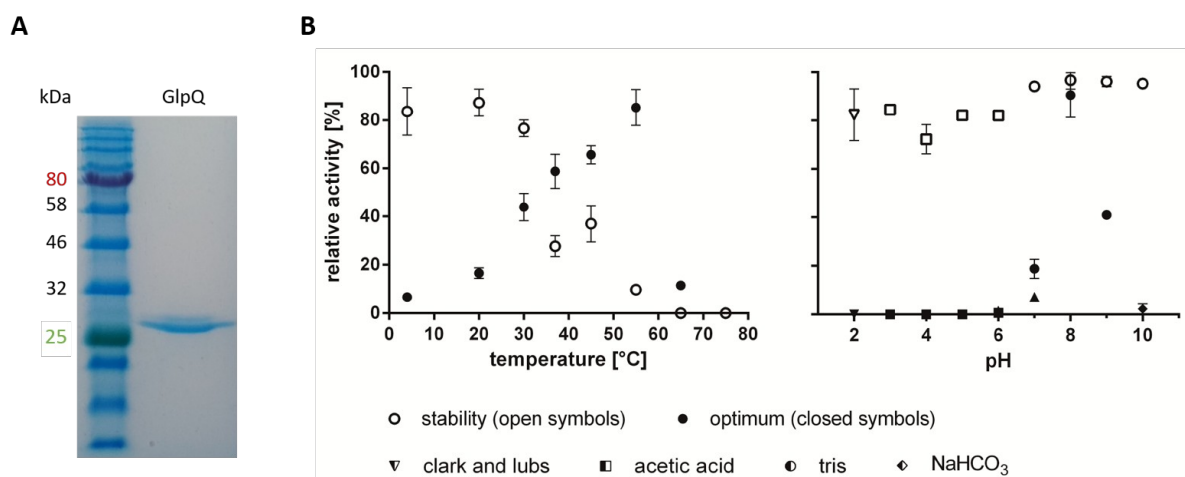


**Figure S1. Enzyme purity, stability and optima of recombinant GlpQ.** A, SDS-PAGE of heterologously expressed recombinant GlpQ-His<sub>6</sub> fusion protein (GlpQ) after purification of the enzyme by Ni<sup>2+</sup> affinity chromatography and size exclusion chromatography (1 µg protein was loaded on a 12% polyacrylamide gel). A protein band is visible that migrates similar to the 25 kDa marker protein, in agreement with the calculated molecular weight of GlpQ of 29.6 kDa. B, Temperature and pH characteristics of GlpQ. The enzyme is stable for 30 min at temperatures up to 30°C, but stability rapidly decreases at temperatures above 30°C within this time frame. Activity of GlpQ increases with temperature up to 55°C with half maximum activity at 30°C. GlpQ is stable within a broad range between pH 2-10 in the indicated buffers and has a very sharp pH-optimum at 8.0. In all assays, 1 pmol GlpQ was incubated with 10 mM GPC and the reaction product was analysed by LC-MS, after 30 min of incubation at 30°C. For temperature stability and optimum, 100% relative activity reflect area under the curve (AUC)-values of 2240 and 4088, respectively. For pH stability and pH optimum 100% AUC were 28571 and 31903, respectively.

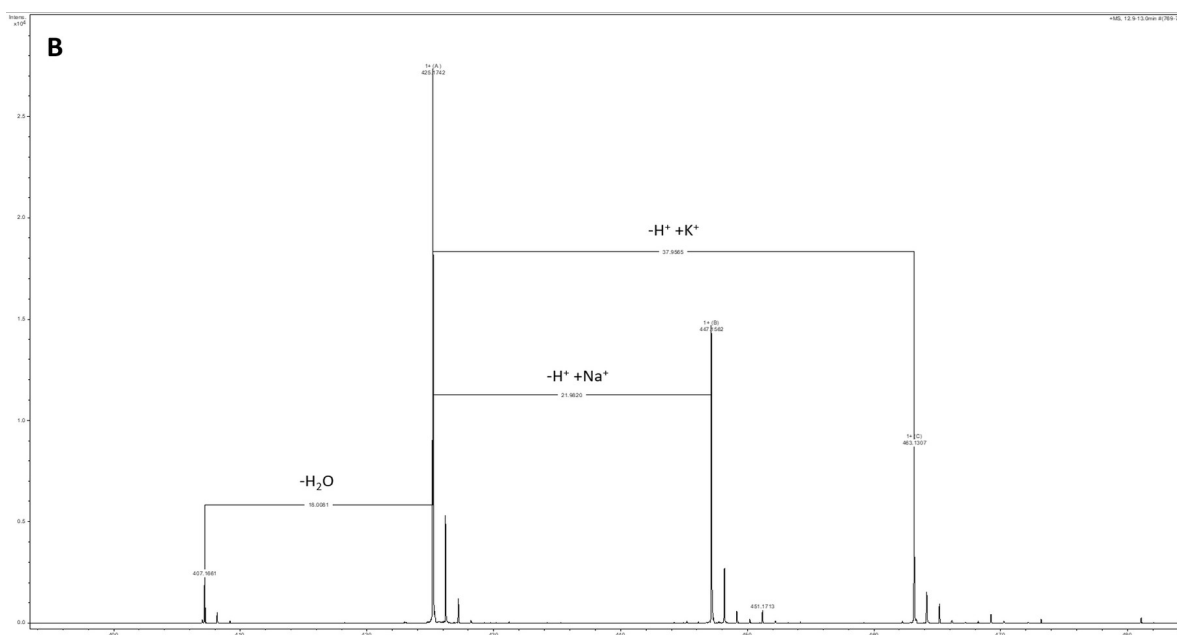
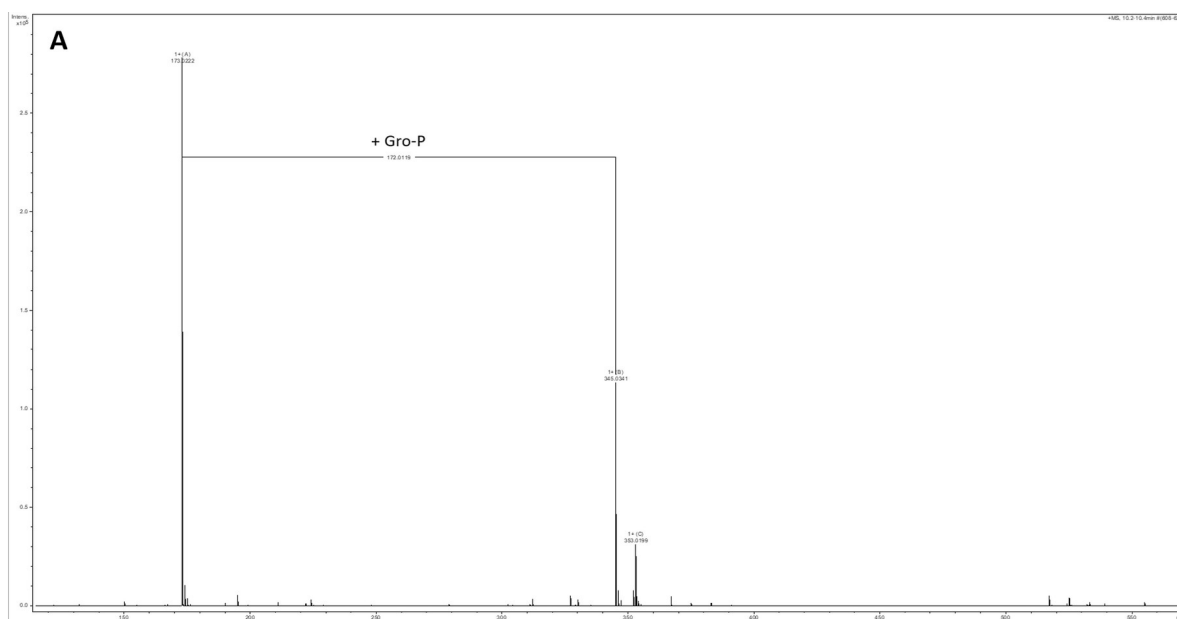


**Figure S2. Mass spectra of glycerolphosphate (GroP) and the WTA linker disaccharide ManNAc- $\beta$ -1,4-GlcNAc.** A, Mass spectrum of GroP analysed in positive ion mode  $[\text{M}+\text{H}]^+$  (experimental 173.0222; theoretical monoisotopic mass 173.0210), also revealing a non-covalently bound GroP dimer,  $[2\text{M}+\text{H}]^+$  (experimental 345.0341; theoretical 345.0346). B, Mass spectrum of the WTA linker disaccharide, ManNAc-GlcNAc, analysed in positive ion mode  $[\text{M}+\text{H}]^+$  (experimental 425.1742; theoretical monoisotopic mass 425.1766), also revealing the sodium adduct  $[\text{M}+\text{Na}]^+$  (experimental 447.1562; theoretical 447.1585), the potassium adduct  $[\text{M}+\text{K}]^+$  (experimental 461.1207; theoretical 461.1233), as well as a product of neutral water loss,  $[\text{M}-(\text{H}_2\text{O})+\text{H}]^+$  (experimental 407.1661; theoretical 407.1660).

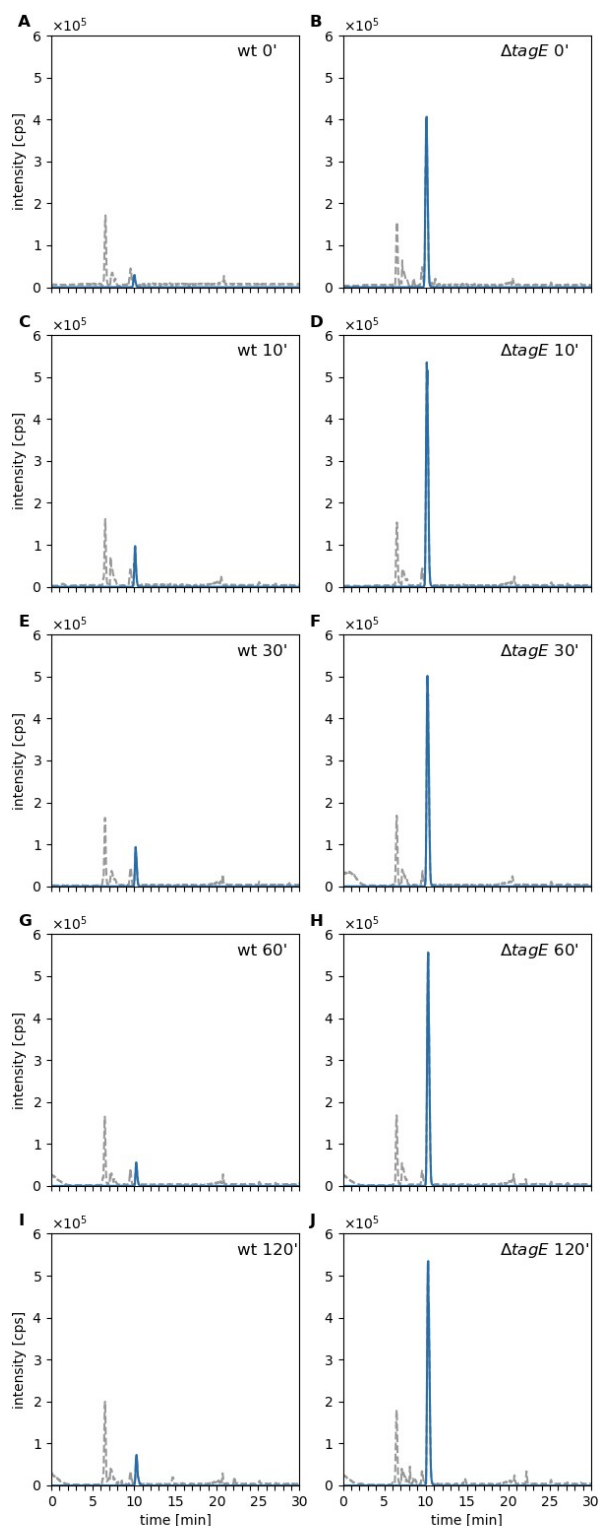


**Figure S3. Time course of WTA digestion by GlpQ.**

The vast amount of product (GroP; blue lines) is released by GlpQ within the first seconds of incubation of cell walls purified from wild-type cells (wt; A,C,E,G,I; incubation time in min) and non-glycosylated cell wall (from  $\Delta tagE$  cells; B,D,F,H,J; incubation time in min). GlpQ releases significantly more product from non-glycosylated (from  $\Delta tagE$  cells) than from the glycosylated wild-type substrate. Even over a long period of time no more GroP is released from wild-type cell wall, indicating that GlpQ has only exo- and no endo-lytic activity. 0.25 mg purified cell wall of *B. subtilis* (containing PGN and covalently bound WTA) was incubated with 0.7  $\mu\text{mol}$  GlpQ and the formation of reaction products was analysed by LC-MS. Shown are the base peak chromatograms (BPC) mass range  $(M+H)^+ = 120 - 800$  (gray dashed) and the extracted ion chromatograms (EIC) of GroP  $(M+H)^+ m/z = 173.022 \pm 0.02$  (blue solid). The reaction was stopped by incubation at 95°C followed by LC-MS analysis.

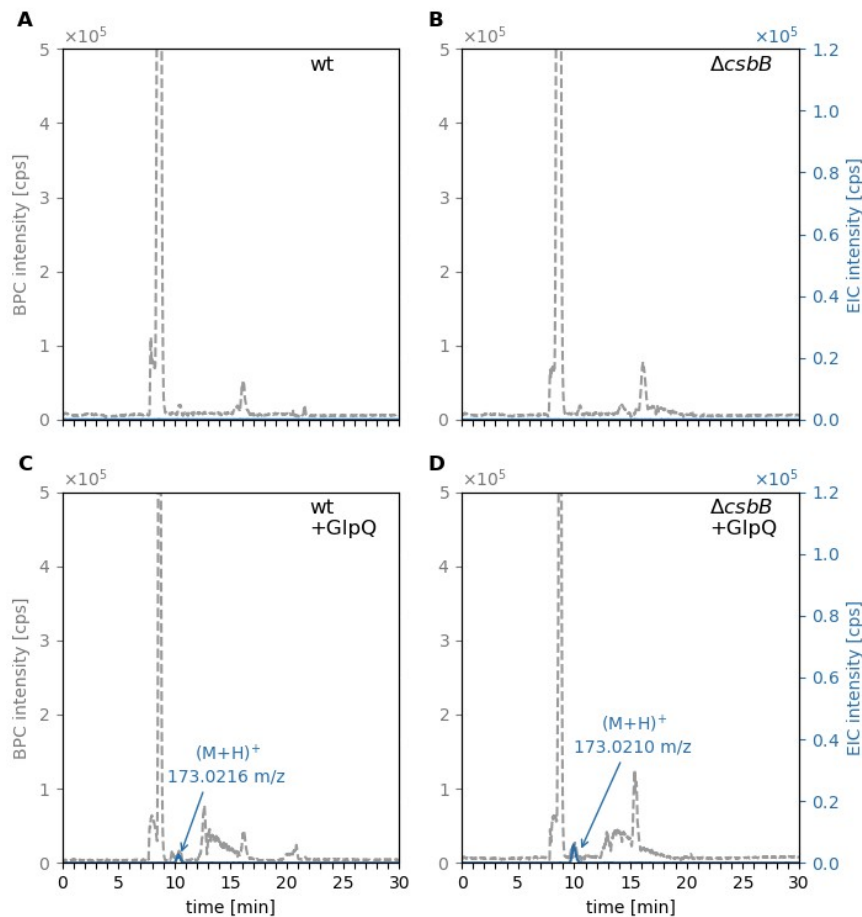


**Figure S4. *B. subtilis* 168 LTA not preincubated at pH 8 for 24 h cannot be cleaved by GlpQ.** Purified *B. subtilis* LTA was incubated with GlpQ and the formation of reaction products was analysed by LC-MS. Very little amounts of GroP were released by GlpQ. *A* and *C*, wild-type (wt) LTA (= partially glycosylated LTA) incubated without GlpQ (control) with GlpQ. The peak area of released GroP was  $AUC = 6 \times 10^4$ . *B* and *D*, non-glycosylated  $\Delta csbB$  LTA incubated without GlpQ (control) and with GlpQ. The peak area of released GroP was  $AUC = 1.4 \times 10^5$ . Shown are the base peak chromatograms (BPC) mass range  $(M+H)^+ = 120 - 800$  (gray dashed) and the extracted ion chromatograms (EIC) of glycerol-phosphate  $(M+H)^+ m/z = 173.022 \pm 0.02$  (blue solid).

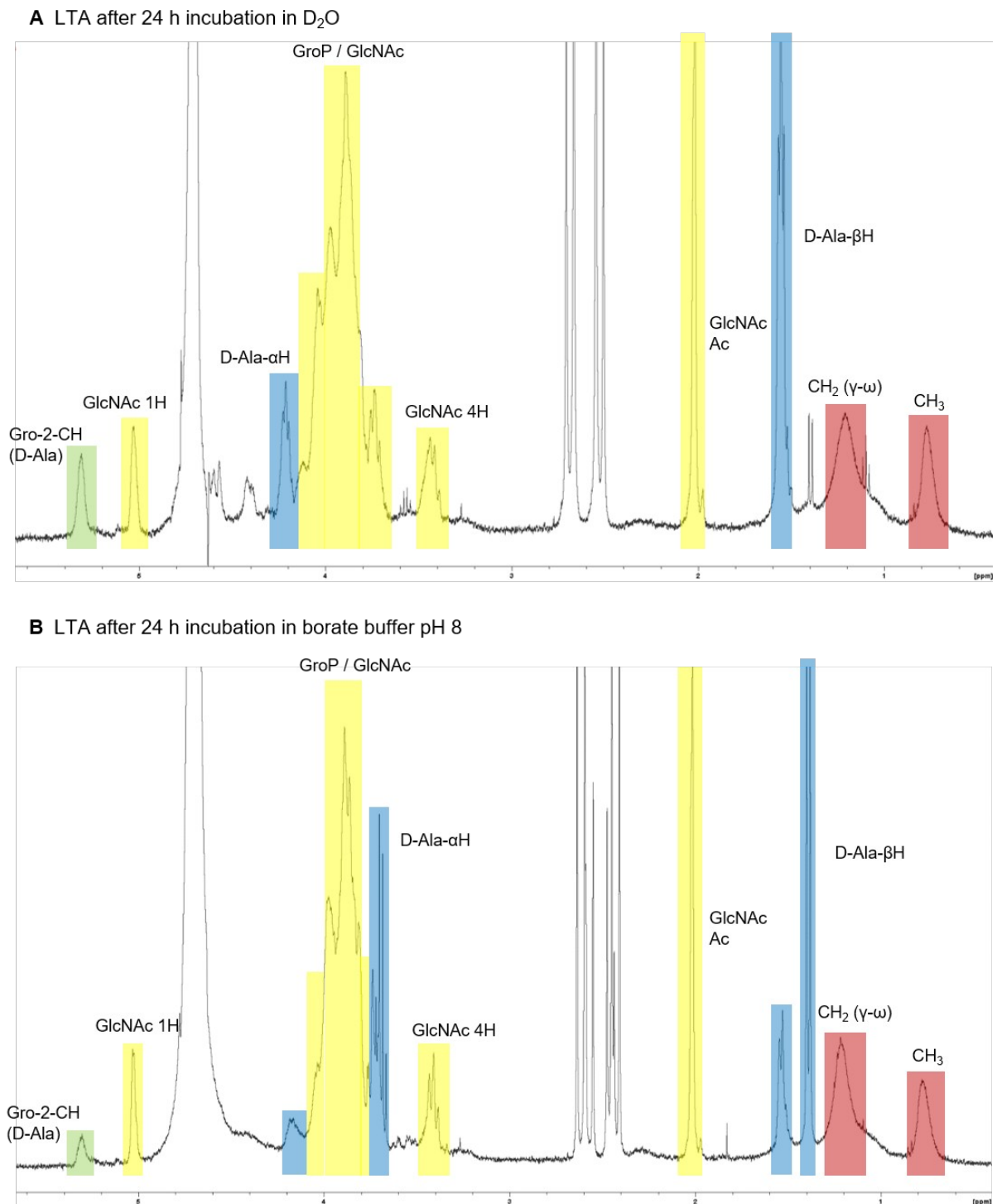


**Figure S5. <sup>1</sup>H-NMR analysis of LTA following incubation at pH 8 for 24 h.** Shown are the <sup>1</sup>H-NMR spectra (400 MHz, 303K) of LTA isolated from *B. subtilis* 168 wt (2 mg) either incubated for 24 h at room temperature in *A*, distilled water (D<sub>2</sub>O), pH 7.0, or in *B*, D<sub>2</sub>O containing 0.1 M borate buffer pH 8.0. Color coding identifies signals indicating removal of D-alanyl residue from the GroP polymer

(green): the resonance of the methine group of *sn*-glycerol (Gro-2-CH) containing an D-alanyl ester (D-Ala) is reduced and partially shifted from 5.3 ppm to 3.9 ppm and the D-Ala- $\alpha$ H and D-Ala- $\beta$ H resonances (blue) are significantly reduced and partially shifted in the LTA sample incubated at pH 8 compared to LTA in D<sub>2</sub>O. Other resonances assigned to GlcNAc substitution and the GroP polymer (yellow) and to the fatty acids of LTA (red) are not influenced by incubation in borate buffer at pH 8.0. From the signal integral estimation, about two-thirds of the D-Ala substituents are removed in the LTA sample by incubation at pH 8 for 24 h. NMR analysis was performed on a 400-MHz Bruker Advance III spectrometer at 303 K with a TCl cryoprobe. NMR spectra were interpreted according to (1).

## Supporting Table

**Table S1. Strains, plasmids and primer used in the study**

Strain or plasmid	Characteristics	References
<i>E. coli</i>		
BL21 (DE3)	<i>fhuA2 [lon] ompT gal (<math>\lambda</math> DE3) [dcm] <math>\Delta</math>hsdS <math>\lambda</math>DE3 = <math>\lambda</math> sBamHI <math>\Delta</math>EcoRI-B int::(<i>lacI</i>::<i>PlacUV5</i>::<i>T7 gene1</i>) i21 <math>\Delta</math>in5</i>	New England Biolabs
<i>B. subtilis</i>		
strain 168 (wild-type)	<i>trpC2</i> ; genome sequenced <i>B. subtilis</i> type strain	<i>Bacillus</i> Genetic Stock Center
$\Delta$ <i>tagE</i> :: <i>erm</i>	168; <i>trpC2</i> , <i>tagE</i> exchanged by <i>erm</i> <sup>R</sup> with flanking <i>loxP</i> sites	<i>Bacillus</i> Genetic Stock Center
$\Delta$ <i>csbB</i> :: <i>kan</i>	168; $\Delta$ <i>csbB</i> :: <i>kan</i>	(2)
<i>L. monocytogenes</i>		
strain 10403S (wild-type)	10403S; StrepR	(3)
$\Delta$ <i>gtlB</i> :: <i>strep</i>	10403S; $\Delta$ <i>gtlB</i> ; StrepR	(2)
<b>plasmids</b>		
pET28a	KanR, T7 promoter, ori pBR322, lacI	Novagen
pET28a- <i>glpQ</i>	KanR, T7 promoter, ori, pBR322, lacI, adds C-terminal His <sub>6</sub> -tag to <i>glpQ</i>	this work
<b>primer</b>		
pET28a- <i>glpQ</i> -for	GATATACCATGGTGGCGTCAAAAGGAAACCTGC	this work
pET28a- <i>glpQ</i> -rv	GTGGTGCTCGAGATAACCCTTTTTTACTTTGTGGA	this work



## References

1. Morath, S., Geyer, A., and Hartung, T. (2001) Structure-function relationship of cytokine induction by lipoteichoic acid from *Staphylococcus aureus*. *J Exp Med* **193**, 393-397
2. Rismondo, J., Percy, M. G., and Gründling, A. (2018) Discovery of genes required for lipoteichoic acid glycosylation predicts two distinct mechanisms for wall teichoic acid glycosylation. *J Biol Chem* **293**, 3293-3306
3. Webb, A. J., Karatsa-Dodgson, M., and Gründling, A. (2009) Two-enzyme systems for glycolipid and polyglycerolphosphate lipoteichoic acid synthesis in *Listeria monocytogenes*. *Mol Microbiol* **74**, 299-314

## Publication 5

Du, X., Larsen, J., Li, M., **Walter, A.**, Slavetinsky, C., Both, A., Sanchez Carballo, P. M., Stegger, M., Lehmann, E., Liu, Y., Liu, J., Slavetinsky, J., Duda, K. A., Krismer, B., Heilbronner, S., Weidenmaier, C., Mayer, C., Rohde, H., Winstel, V., & Peschel, A (2021). Emerging *Staphylococcus epidermidis* clones express *Staphylococcus aureus*-type wall teichoic acid to shift from a commensal to pathogen lifestyle. Accepted in Nature Microbiology.



# *Staphylococcus epidermidis* clones express *Staphylococcus aureus*-type wall teichoic acid to shift from a commensal to pathogen lifestyle

Xin Du<sup>1,2,3</sup>, Jesper Larsen<sup>4</sup>, Min Li<sup>5</sup>, Axel Walter<sup>1,3</sup>, Christoph Slavetinsky<sup>1,2,3,6</sup>, Anna Both<sup>7</sup>, Patricia M. Sanchez Carballo<sup>8,9</sup>, Marc Stegger<sup>4</sup>, Esther Lehmann<sup>1,2,3</sup>, Yao Liu<sup>5</sup>, Junlan Liu<sup>5</sup>, Jessica Slavetinsky<sup>1,2,3</sup>, Katarzyna A. Duda<sup>10</sup>, Bernhard Krismer<sup>1,2,3</sup>, Simon Heilbronner<sup>1,2,3</sup>, Christopher Weidenmaier<sup>1,2,11</sup>, Christoph Mayer<sup>1,3</sup>, Holger Rohde<sup>7</sup>, Volker Winstel<sup>1,2,12,13</sup> and Andreas Peschel<sup>1,2,3</sup> ✉

**Most clonal lineages of *Staphylococcus epidermidis* are commensals present on human skin and in the nose. However, some globally spreading healthcare-associated and methicillin-resistant *S. epidermidis* (HA-MRSE) clones are major causes of difficult-to-treat implant or bloodstream infections. The molecular determinants that alter the lifestyle of *S. epidermidis* have remained elusive, and their identification might provide therapeutic targets. We reasoned that changes in surface-exposed wall teichoic acid (WTA) polymers of *S. epidermidis*, which potentially shape host interactions, may be linked to differences between colonization and infection abilities of different clones. We used a combined epidemiological and functional approach to show that while commensal clones express poly-glycerolphosphate WTA, *S. epidermidis* multilocus sequence type 23, which emerged in the past 15 years and is one of the main infection-causing HA-MRSE clones, contains an accessory genetic element, *tarIJLM*, that leads to the production of a second, *Staphylococcus aureus*-type WTA (poly-ribitolphosphate (RboP)). Production of RboP-WTA by *S. epidermidis* impaired *in vivo* colonization but augmented endothelial attachment and host mortality in a mouse sepsis model. *tarIJLM* was absent from commensal human sequence types but was found in several other HA-MRSE clones. Moreover, RboP-WTA enabled *S. epidermidis* to exchange DNA with *S. aureus* via siphovirus bacteriophages, thereby creating a possible route for the inter-species exchange of methicillin resistance, virulence and colonization factors. We conclude that *tarIJLM* alters the lifestyle of *S. epidermidis* from commensal to pathogenic and propose that RboP-WTA might be a robust target for preventive and therapeutic interventions against MRSE infections.**

The major opportunistic pathogen *Staphylococcus epidermidis* is a core member of human skin and upper airway microbiomes and, at the same time, causes difficult-to-treat healthcare-associated (HA) infections, including bloodstream and implant-associated infections<sup>1,2</sup>. A major percentage of the invasive *S. epidermidis* clones are resistant to methicillin (MRSE) and other antibiotics<sup>3,4</sup>. The species *S. epidermidis* comprises a large number of clonal lineages that differ with regard to the human body parts they colonize and the ability to invade and persist in sterile tissues<sup>2,5,6</sup>. The molecular basis of the different habitat preferences and corresponding capacities to bind to specific host surfaces have remained largely unknown. The evolution of staphylococcal species and strains is shaped by the susceptibility to individual groups of bacteriophages, which use the species- or strain-specific structure of wall teichoic acid (WTA) to detect and bind to appropriate

bacterial host cells<sup>7,8</sup>. Phages are also the major vehicles for horizontal gene transfer (HGT) in staphylococci, governing the evolution of new clonal lineages<sup>9</sup>. Phages facilitate, for instance, the exchange of staphylococcal cassette chromosome *mec* (SCC*mec*) elements conferring methicillin resistance<sup>10,11</sup>, *Staphylococcus aureus* pathogenicity islands (SaPIs)<sup>12,13</sup> or accessory adhesion factor genes such as *sasX*<sup>14</sup>. While mechanisms of intra-species phage-mediated HGT are well documented<sup>15</sup>, it has remained elusive how the exchange of genetic material between *S. aureus* and *S. epidermidis* or other coagulase-negative staphylococci (CoNS) is accomplished. It has remained particularly enigmatic how such transducing phages can traverse the WTA-specific HGT boundaries between individual staphylococcal species, which produce either poly-ribitolphosphate (RboP)-WTA (most *S. aureus*) or poly-glycerolphosphate (GroP)-WTA (*S. epidermidis* and many other CoNS).

<sup>1</sup>Interfaculty Institute of Microbiology and Infection Medicine, University of Tübingen, Tübingen, Germany. <sup>2</sup>German Center for Infection Research (DZIF), partner site Tübingen, Tübingen, Germany. <sup>3</sup>Cluster of Excellence EXC2124 Controlling Microbes to Fight Infection, Tübingen, Germany. <sup>4</sup>Statens Serum Institut, København, Denmark. <sup>5</sup>Renji Hospital, School of Medicine, Shanghai Jiaotong University, Shanghai, China. <sup>6</sup>Pediatric Gastroenterology and Hepatology, University Children's Hospital Tübingen, Eberhard Karls University Tübingen, Tübingen, Germany. <sup>7</sup>Institute of Medical Microbiology, Virology and Hygiene, University Medical Center Hamburg-Eppendorf, Hamburg, Germany. <sup>8</sup>Division of Clinical Infectious Diseases, Research Center Borstel, Leibniz Lung Center, Borstel, Germany. <sup>9</sup>German Center for Infection Research (DZIF), Borstel, Germany. <sup>10</sup>Junior Research Group of Allergobiochemistry, Research Center Borstel, Leibniz Lung Center, Airway Research Center North (ARCN), German Center for Lung Research (DZL), Borstel, Germany. <sup>11</sup>Present address: Finch Therapeutics, Boston, MA, USA. <sup>12</sup>Present address: Research Group Pathogenesis of Bacterial Infections, TWINCORE, Centre for Experimental and Clinical Infection Research, a Joint Venture between the Hannover Medical School and the Helmholtz Centre for Infection Research, Hannover, Germany. <sup>13</sup>Present address: Institute of Medical Microbiology and Hospital Epidemiology, Hannover Medical School, Hannover, Germany. ✉e-mail: [andreas.peschel@uni-tuebingen.de](mailto:andreas.peschel@uni-tuebingen.de)

We have previously shown that certain WTA biosynthesis genes reside on genomic elements that seem to move between different *Staphylococcus* species. The rare *S. aureus* lineage sequence type 395 (ST395), for instance, has acquired the *tagNDF* genes to produce GroP-WTA and it shares susceptibility to specific transducing phages with GroP-WTA-containing CoNS<sup>15</sup>. Along this line, we hypothesized that some *S. epidermidis* strains may have gained the capacity to exchange DNA via typical *S. aureus* phages. We found that the production of RboP-WTA is not restricted to *S. aureus* but that several prominent HA-MRSE clones produce RboP-WTA in addition to GroP-WTA. In contrast, the RboP-WTA-specific *tarI-JLM* genes were absent from human nasal and skin isolates, which had critical consequences for *S. epidermidis* differential phage binding, nasal colonization and bloodstream infection.

## Results

**Some *S. epidermidis* isolates can be transduced by  $\Phi$ 11 and contain an accessory *tarI-JLM* gene cluster.** A collection of *S. epidermidis* isolates was screened for their capacity to take up a SaPI via the archetypical *S. aureus* siphophage  $\Phi$ 11, which binds to RboP-WTA<sup>15</sup>. SaPIbov1, a SaPI isolated from a bovine *S. aureus* isolate<sup>16</sup>, has previously been reported to integrate into *S. aureus* and *S. epidermidis* genomes at the same genomic position in the guanosine monophosphate synthase (*gmpS*) gene<sup>17</sup>. The vast majority of the tested isolates could not be transduced by  $\Phi$ 11 with SaPIbov1, which is in agreement with the absence of the RboP-WTA receptor structure at the *S. epidermidis* surface. However, some isolates could be transduced (Table 1 and Fig. 1a). These isolates were also distinguished from other *S. epidermidis* clones by their capacity to bind  $\Phi$ 11 in addition to the GroP-WTA-specific  $\Phi$ 187 (ref. <sup>15</sup>) (Extended Data Fig. 1a,b), which suggests that they express the  $\Phi$ 11 receptor.

The genome of one of the  $\Phi$ 11-transducible *S. epidermidis*, E73, was sequenced and found to belong to ST23, which has emerged in recent years as one of the frequent HA-MRSE clones<sup>3,4</sup>. It contained the genes for the synthesis of the WTA linkage unit (*tagOADB*) and the GroP-WTA polymerase gene *tagF*<sup>18</sup>, which are present in virtually all *S. epidermidis* genomes. Surprisingly, E73 and all other available *S. epidermidis* genomes also contained a gene cluster (*tarI-JL1*; Fig. 1b) encoding homologues of *S. aureus* proteins responsible for RboP synthesis (TarI and TarJ) and polymerization (TarL)<sup>18,19</sup>. Since RboP-WTA has never been documented to be produced by *S. epidermidis*, we assumed that these genes may be non-functional or silent. Indeed, expression of *tarL1* was very low or undetectable in the *S. epidermidis* laboratory strains RP62A, 1457 and ATCC12228, as well as in our clinical *S. epidermidis* isolates E6, E45 and E73. *tarL1* expression was at the detection limit at various growth conditions, including broth, synthetic nasal medium<sup>20</sup> and human serum (Fig. 1c and Extended Data Fig. 2), which suggests that *tarI-JL1* is non-functional or cannot be expressed. Notably, E73 contained a second putative RboP-WTA gene cluster (*tarI-JLM2*), which also encodes a homologue of the *S. aureus* RboP-WTA glycosyl transferase TarM<sup>21</sup>. *tarL2* was efficiently expressed in isolates E6, E45 and E73 at all tested growth conditions (Fig. 1c and Extended Data Fig. 2). All  $\Phi$ 11-transducible isolates contained *tarI-JLM2* except for one clone, which carried another *tarI-JLM2*-related accessory gene cluster (Table 1), which indicates that the rare capacity to acquire foreign DNA from *S. aureus* may depend on the presence of *tarI-JLM*.

***tarI-JLM*-encoding *S. epidermidis* strains produce both GroP- and RboP-WTA.** WTA was isolated from the *tarI-JLM2*-negative *S. epidermidis* laboratory strains RP62A, ATCC12228 and 1457 and was found to contain only GroP-WTA, as expected, which confirms that *tarI-JL1* is probably non-functional. In contrast, WTA of E73 contained two types of WTA: GroP-WTA and RboP-WTA (Fig. 2a and Extended Data Fig. 3). Strain 1457 transformed with a *tarI-JLM2*-expressing plasmid produced both GroP- and RboP-WTA

**Table 1 | Presence of *tarL2* and susceptibility to  $\Phi$ 11-mediated SaPIbov1 transduction in infection-derived isolates from *S. epidermidis* strain collections**

Strain collection	Number of strains			<i>tarL2</i> -positive sequence types (number)
	Total	<i>tarL2</i> -positive	SaPIbov1 transduction by $\Phi$ 11	
<b>Tübingen</b>				ST5 (2), ST10 (1), ST23 (4), ST87 (3)
Nose	155	0	0	
Skin	144	0	0	
Infection	72	10 (13.9%)	7 (9.7%) <sup>a</sup>	
<b>Hamburg</b>				ST10 (1), ST23 (3), ST87 (2)
Nose	37	0	0	
Infection	75	6 (8.0%)	3 (4.0%) <sup>a</sup>	
<b>Shanghai</b>				ST2 (5) <sup>b</sup> , ST23 (1), single-locus ST23 variant (3)
Nose	206	0	0	
Skin	138	0	0	
Infection	130	9 (6.9%)	6 (4.6%) <sup>a</sup>	
<b>Total</b>	<b>957</b>	<b>25 (2.6%)</b>	<b>16 (1.7%)<sup>a</sup></b>	

<sup>a</sup>Even isolates that were negative in the SaPIbov1 transduction assay bound to phage  $\Phi$ 11 (Extended Data Fig. 1a). Potential reasons for the lack of detectable SaPIbov1 transduction include a specific restriction barrier or CRISPR-Cas systems. <sup>b</sup>One of these ST2 isolates was positive for *tarI-JLM3* and  $\Phi$ 11 transduction.

(Fig. 2b and Extended Data Fig. 3) and could be transduced by  $\Phi$ 11 (Fig. 2c and Extended Data Fig. 1c), thereby confirming that *tarI-JLM2* confers the capacity to produce RboP-WTA and enables *S. epidermidis* to exchange DNA with *S. aureus* via RboP-WTA-binding phages. Moreover, deletion of *tarI-JLM2* in strain E73 (ST23) or E1 (ST87) abolished RboP-WTA production and transduction by  $\Phi$ 11 as well as binding by  $\Phi$ 11. These phenotypes were restored by complementation with a plasmid-encoded *tarI-JLM2* copy (Fig. 2b,c and Extended Data Figs. 1d,e and 3c). The E73  $\Delta$ *tarI-JLM2* mutant (E73 $\Delta$ *tarI-JLM2*) showed the same growth behaviour and microscopic appearance as the parental strain (Extended Data Fig. 4b,c), which indicates that the genes have no essential roles in basic cellular processes.

E73 $\Delta$ *tarI-JLM2* had a similar phosphate amount in its cell wall as the parental strain, which indicates that the mutant cells probably replaced RboP-WTA by increasing the level of GroP-WTA (Extended Data Fig. 4a). The impact of *tarI-JLM* on interactions with GroP-WTA-specific phages was studied using the previously described phages  $\Phi$ PH15 (ref. <sup>22</sup>) and  $\Phi$ 187 (ref. <sup>15</sup>), plus a previously uncharacterized bacteriophage  $\Phi$ E72 that was isolated from *S. epidermidis* E72. E73 $\Delta$ *tarI-JLM2* had an increased capacity to bind the three phages compared with the E73 wild type and the complemented mutant (Fig. 2d), which supports our finding that E73 still produces GroP-WTA, albeit at reduced amounts as a consequence of simultaneous RboP-WTA production.

***tarI-JLM* is found exclusively in HA-MRSE isolates.** To assess the prevalence and distribution of *tarI-JLM2* among *S. epidermidis* clones, three large collections of *S. epidermidis* isolates from human arm skin (282 isolates) and nasal cavity (398 isolates) of healthy humans or from clinically relevant infections (277 isolates) from Tübingen, from Hamburg and from Shanghai were screened for the presence of *tarL2* by PCR (Table 1). Only isolates that were identical in more than two samples from sterile tissues of the same participant on different days were included in the infection isolate collection to exclude contaminating skin strains. Twenty-four

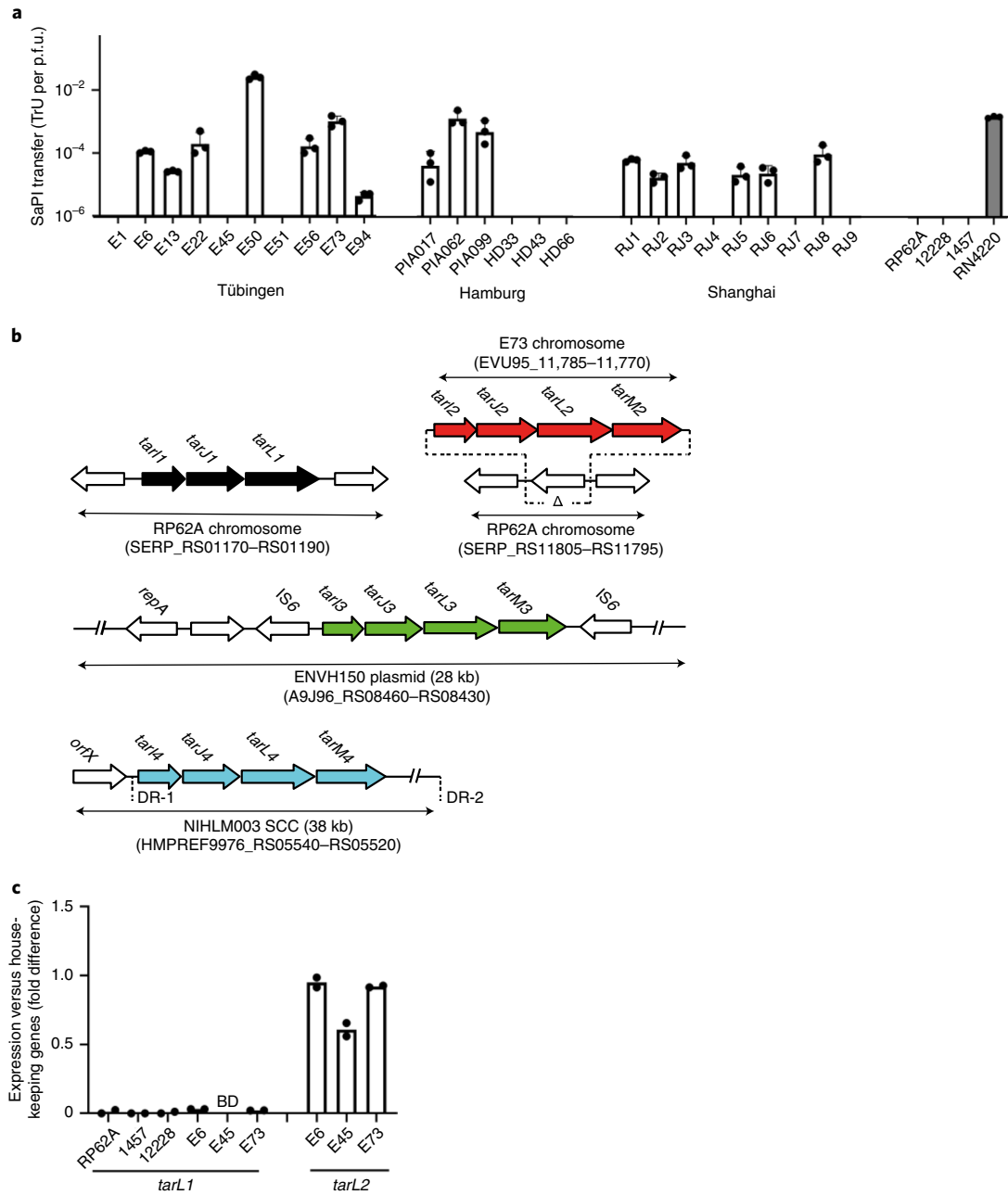


**Fig. 1 | Some *S. epidermidis* genomes encode *tarJLM* gene clusters, permitting transduction by *S. aureus* phage  $\Phi$ 11. **a**, Some infection-derived *S. epidermidis* isolates from Tübingen, from Hamburg and from Shanghai can be transduced with SaPIbov1 by  $\Phi$ 11. TrU per p.f.u. values indicate the ratio of transduction units (TrU, the number of transductants in 1 ml phage lysate) to p.f.u. (the number of phage plaques formed on RboP-WTA-producing *S. aureus* laboratory strain RN4220) given as the mean  $\pm$  s.d. of three independent experiments. Strains without a bar had not yielded any transductant. The origin and properties of the isolates are described in Supplementary Table 1. RP62A, ATCC12228 (12228) and 1457 are *S. epidermidis* laboratory strains and only produce GroP-WTA. **b**, Potential RboP-WTA biosynthesis gene clusters found in the genomes of all (*tarJL1*) or certain *S. epidermidis* STs (*tarJLM2-4*). The genetic location is shown in representative strains RP62A (ST10), E73 (ST23), ENVH150 (ST2) and NIHLM003 (ST218). The direct repeat sequences (DR-1 and DR-2) flanking the SCC element in NIHLM003 are indicated. The genomic location of *tarJLM5* genes in isolate SNUC\_2569 could not be determined due to their presence on two short contigs with no flanking sequences. The figure is not drawn to scale. **c**, While *tarL2* is efficiently transcribed in the *tarJLM2*-positive isolates E6, E45 and E73, *tarJL1* is not or only very weakly expressed in all tested *S. epidermidis* strains during growth in TSB after 6 h of growth as analysed by qPCR. The control strains RP62A, 1457 and 12228 lack *tarJLM2* and were negative in the PCR assay. Values represent means of two independent experiments. They were normalized for strongly and constitutively expressed housekeeping genes *gyrB*, *rho* and *tpiA*. BD, below detection limit.**

isolates, exclusively derived from infections, were *tarL2*-positive. They belonged to the HA clones ST2, ST5, ST10, ST23 and ST87 (refs. <sup>3,4,23-28</sup>), and three previously unknown single-locus variants of ST23. *tarJLM2* was found in all 11 ST23 and all 5 ST87 isolates,

and in 2 out of 4 ST10 isolates (Table 2). Moreover, the cluster was present in 10% and 6% of the ST2 and ST5 isolates, respectively, which represent the two most common HA-MRSE clones<sup>3,4,25,26,28</sup>. In contrast, none of the nasal or skin *S. epidermidis* isolates from

any of the collections was *tarL2*-positive, which indicates that the additional gene cluster may be associated with poor arm skin and nose colonization but strong invasion capacities. The only minor deviation from this rule was that we detected *tarIJLM2* in an additional ST10 isolate from Tübingen (E42), which was found only in a single blood culture and therefore did not meet our definition of a clinical isolate (Supplementary Table 1). It was therefore excluded from further functional analyses.

The identification of *tarIJLM2* in clinical isolates belonging to well-known hospital-adapted lineages but not in commensal isolates prompted us to determine the distribution of homologous genes in an international collection from two sources. An analysis of a previously described global collection of 227 *S. epidermidis* isolates from 96 hospitals in 24 countries<sup>3</sup> showed that *tarIJLM2* was present in all 50 ST23 isolates, 1 out of 131 ST2 isolates and both ST87 isolates from the ST5/ST87 clade (Fig. 2e and Table 2). In addition, *tarIJLM2* was identified in four of the 497 *S. epidermidis* genomes present in the NCBI Reference Sequence Database, including three ST23 isolates and one ST87 isolate (Fig. 2e and Table 2). *tarIJLM2* was not detected in any of the genomes from other, predominantly commensal, STs, which provides support that it occurs exclusively in HA ST2, ST5, ST10, ST23 and ST87 isolates (Fig. 2e and Table 2).

The *tarIJLM2* cluster replaced a chromosomal gene of unknown function found in most *S. epidermidis* genomes (Fig. 1b). It was integrated into the same chromosomal region between two conserved genes in all *tarIJLM2*-positive *S. epidermidis* isolates from our strain collections and the international collection (Fig. 1b). The genes flanking *tarIJLM2* in these isolates were also present in the chromosome of the *tarIJLM2*-negative *S. epidermidis* laboratory strain RP62A, but here they flanked another gene with no homology to *tarIJLM* (Fig. 1b). Analysis of the *tarIJLM2*-negative *S. epidermidis* isolates from the global collection (174 out of 227 isolates) showed that the region in RP62A was conserved in 82% (143 out of 174) of the genomes. The absence of mobile genetic elements (for example, insertion sequences (ISs)) between *tarIJLM2* and the flanking genes indicates that the missing gene might have been replaced by *tarIJLM2* in a process called homology-facilitated illegitimate recombination<sup>29</sup>.

**Three other *tarIJLM2*-related gene clusters are found in HA-MRSE clones.** Analysis of our strain collections and the international strain collection revealed the existence of three other *tarIJLM2*-related gene clusters, which were designated *tarIJLM3* to *tarIJLM5* (Figs. 1b and 2e, Table 2, Extended Data Fig. 5 and Supplementary Table 1).

*tarIJLM3* was detected in a clinical ST2 isolate from Shanghai and in three isolates from the international collection, including two clinical ST2 isolates from Germany and the United States and a *tarIJLM2*-positive ST23 isolate. *tarIJLM4* was detected in three isolates from the international collection, including a ST2 isolate and two clinical isolates from the United States belonging to ST5 and ST218. Finally, *tarIJLM5* was found in a bovine ST100 isolate from Canada. Isolates RJ8 and DAR1907 (both ST2) bearing *tarIJLM3*, and US06 (ST5) bearing *tarIJLM4*, were analysed and found to express both, RboP- and GroP-WTA (Extended Data Fig. 6). Moreover, RJ8 and US06 bound and acquired SaPIbov1 from phage  $\Phi$ 11, thereby confirming that the gene clusters are functional and have similar roles as *tarIJLM2*.

The *tarIJLM* genes from the different clusters shared 66–89% nucleotide sequence identities, and the corresponding *tarL2*, *tarL3*, *tarL4* and *tarL5* genes were more similar to the *S. aureus tarL* than the *S. epidermidis tarL1* gene (Extended Data Fig. 5a). These findings suggest that the *tarIJLM* gene clusters in *S. epidermidis* originated through HGT from an unknown donor rather than by gene duplication and diversification of the *S. epidermidis tarIJL1* cluster. This hypothesis is further supported by the patchy distribution of *tarIJLM* variants in the *S. epidermidis* phylogenetic tree (Fig. 2e and Extended Data Fig. 5b) and by our finding that both *tarIJLM3* and *tarIJLM4* are located on mobile genetic elements (Fig. 1b).

The *tarIJLM3* gene cluster was located on a 29-kb unannotated plasmid in the ST2 isolate DAR1907, and on 23- and 28-kb annotated contigs of unknown genomic origin in the other isolates. These contigs contained the *repA* plasmid replication gene and shared 100% nucleotide sequence identities with the plasmid sequence from DAR1907, which indicates that they are probably of plasmid origin (Fig. 1b). Of note, the *tarIJLM3* gene cluster was flanked by two pseudogenes homologous to IS elements belonging to the IS6 family (Fig. 1b).

Analysis of the contig containing the *tarIJLM4* gene cluster in the ST218 isolate NIHLM003 showed that it was carried on a 38-kb SCC element, which was integrated at a unique site at the 3'-end of *orfX* (referred to as integration site sequence (ISS)). It contained the *ccrA2B2* genes encoding site-specific recombinases<sup>30</sup>, and was flanked by direct repeat sequences containing the ISS. The contigs containing *orfX* and the *tarIJLM4* gene cluster from isolate VCU013 (ST2) and US06 (ST5) shared 100% nucleotide sequence identities with the first 12 and 8 kb of the SCC element from NIHLM003, respectively. Apart from the SCC*mec* element, the ST2 and ST5 isolates each contained a *mec* and *ccr* gene complex characteristic

**Fig. 2 | *tarIJLM* genes are responsible for RboP-WTA synthesis in *S. epidermidis* and are found in HA-MRSE clones.** **a**, All tested *S. epidermidis* strains contain GroP (blue lines, [M + H]<sup>+</sup> = 173.022), but only the *tarIJLM2*-positive E73 has also RboP (red line, [M + H]<sup>+</sup> = 233.042) as WTA constituents. Counts per second (c.p.s.) measured by LC-MS are shown. **b**, Disruption of *tarIJLM2* abolishes RboP-WTA production in strain E73, while transformation of strain 1457 with the *tarIJLM2*-expressing plasmid pRB-*IJLM2* confers RboP-WTA production. **c**, Expression of *tarIJLM2* enables *S. epidermidis* to accept SaPIbov1 from transducing *S. aureus* phage  $\Phi$ 11. Data are expressed as the mean  $\pm$  s.d. Significant differences of E73 wild type (WT) versus E73  $\Delta$ *IJLM2* ( $P < 0.0001$ ) and E73  $\Delta$ *IJLM2* (pRB-*IJLM2*) versus E73  $\Delta$ *IJLM2* ( $P < 0.0001$ ) were calculated by one-way analysis of variance (ANOVA) with Dunnett's post-test (two-sided). Significant difference of 1457 (pRB-*IJLM2*) versus 1457 WT ( $P = 0.000000024$ ) was calculated by unpaired t-test. Strains without a bar had not yielded any transductant. **d**, Inactivation of *tarIJLM2* in *S. epidermidis* E73 leads to increased binding of the GroP-WTA-specific phages  $\Phi$ 187,  $\Phi$ PH15 and  $\Phi$ E72. Values represent the mean  $\pm$  s.d. of three independent experiments in **c** and **d**. Significant differences versus E73 WT ( $P \leq 0.05$ ) were calculated by one-way ANOVA with Dunnett's post-test (two-sided). **e**, *tarIJLM2*-5 are almost exclusively found in *S. epidermidis* clones that are predominantly HA (red) or livestock-associated (blue)<sup>25</sup> and have probably been repeatedly imported by HGT. Since the definition of *S. epidermidis* healthcare-association is ambiguous, only clones implicated with the healthcare system in at least three independent studies<sup>3,4,18,20,21,23,24</sup> were labelled red. ST218 has also sporadically been found to cause infections<sup>23</sup>. Maximum-likelihood phylogeny of 71 *S. epidermidis* isolates representing major STs was inferred from an alignment of 87,048 core genome SNPs. The isolates represent different multilocus STs among 497 *S. epidermidis* genomes present in the NCBI Reference Sequence Database (accessed 3 July 2018), a global collection of 227 *S. epidermidis* isolates originating from 96 institutions across 24 countries<sup>3</sup> and 25 *tarIJLM*-positive clinical *S. epidermidis* isolates collected in this study (Supplementary Table 2). The number of isolates carrying different variants of *tarIJLM* (Supplementary Table 1) together with the total number of genomes within each ST are indicated. ST23, which includes three previously unknown single-locus variants, is marked with an asterisk. Phylogenetic reconstruction was carried out using the maximum-likelihood program PhyML with a GTR model of nucleotide substitution, and support for the nodes was assessed using aBayes (Methods). The length of the broken branch was reduced by fivefold. The tree was midpoint rooted. The scale bar denotes substitutions per variable sites.

of a type-III (3A) and type-IV (2B) SCCmec element, respectively, but they were present on different contigs and it was therefore not possible to determine their location in relation to the SCC element. We were also unable to determine the genomic location of the *tarI-JLM5* gene cluster in the bovine ST100 isolate SNUC\_2569 due to its presence on two short contigs with no flanking sequences. We have currently no indications for frequent mobility of any of the *tarI-JLM* clusters, which suggests that they might have evolved a long time ago, potentially originating from the core-genome-encoded *tar* genes of *S. aureus*.

***tarI-JLM* gene clusters are found in the genomes of other CoNS species.** The different *tarI-JLM* gene variants (Fig. 1b) were used as

queries in BLASTN searches against non-*S. epidermidis* genomes present in the NCBI Reference Sequence Database. The contigs containing the *S. epidermidis tarI-JLM3* gene cluster shared 98% identity with a 7-kb region on a 33-kb contig from a bovine *Staphylococcus warneri* isolate SNUC\_194 (accession number [NZ\\_PZFE000000000](#)) (Supplementary Table 1), including the *tarI-JLM3* gene cluster and flanking IS6-like pseudogenes. The presence of the *repA* gene on the *S. warneri* contig indicated a plasmid origin. The remaining part of the *S. warneri* contig showed little homology to the *tarI-JLM3*-carrying plasmid-like contigs from *S. epidermidis*, which provides support for mobilization of the *tarI-JLM3* cluster between plasmids from different *Staphylococcus* species. Analysis of the contigs containing the *tarI-JLM4* gene cluster showed that the

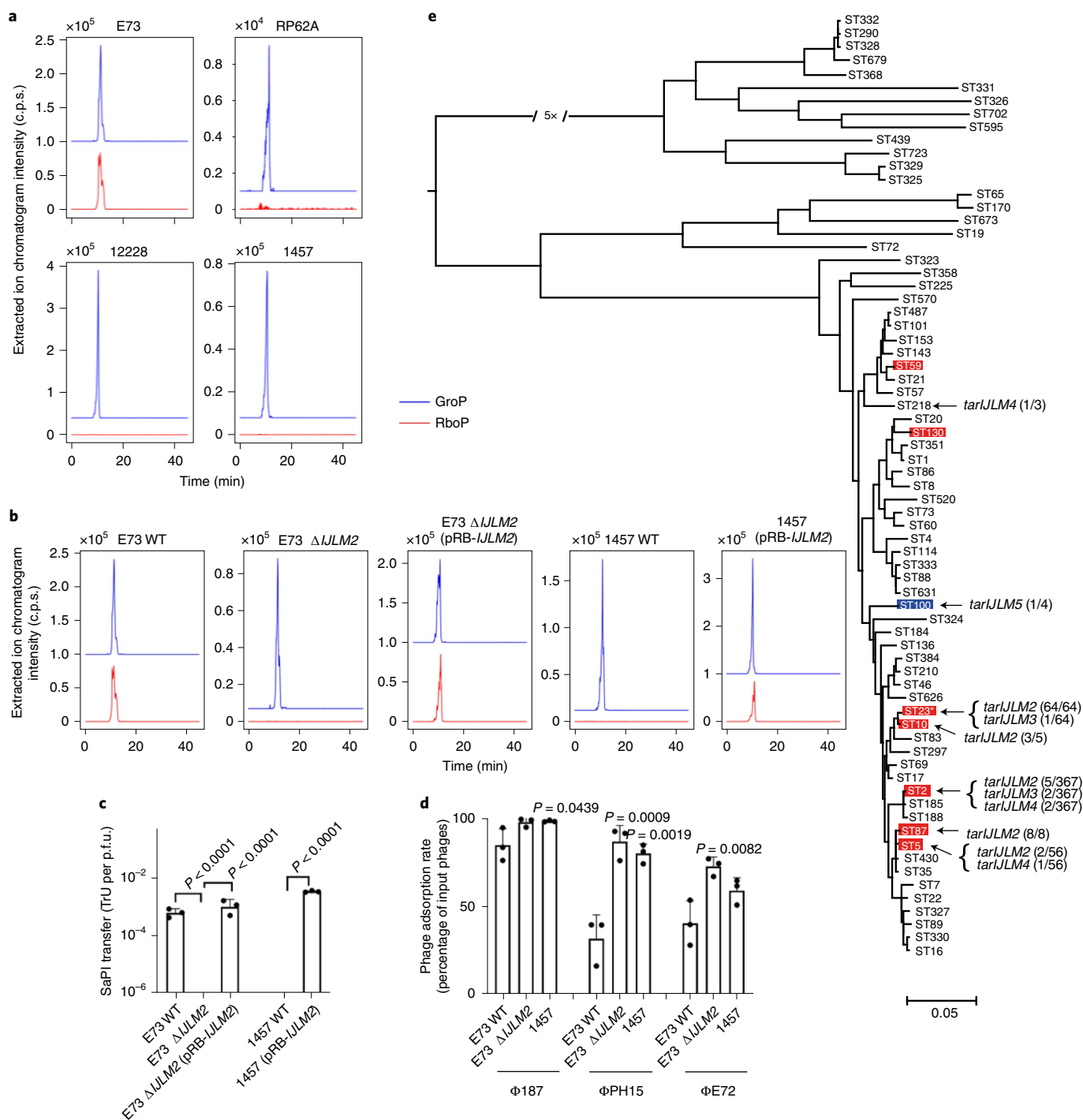


**Table 2 | Presence of *tarIJLM* in major HA-MRSE clones isolated from infections**

Clone	Hamburg	Shanghai	Tübingen	International collection <sup>f</sup>	All
	Number of clones with <i>tarIJLM</i> /total number				Percentage with <i>tarIJLM</i>
ST2	0/18	5/22 <sup>a</sup>	0/10	4/362 <sup>a</sup>	2.18
ST5	0/12	0/9	2/13	1/54 <sup>b</sup>	3.41
ST10	1/1	0/2	1/1	0/2	33.3
ST23	3/3	4/4 <sup>e</sup>	4/4	53/53 <sup>c</sup>	100
ST87	2/2	0/0	3/3	3/3	100
Several sporadic STs	0/39 (21 different STs)	0/93 (23 different STs)	0/41 (24 different STs)	2/250 <sup>d</sup>	1.01

Positive isolates contained *tarIJLM2* unless otherwise noted. <sup>a</sup>One ST2 isolate from Shanghai and two ST2 isolates from the international collection contained *tarIJLM3*, while one ST2 isolate from the international collection contained *tarIJLM4*. <sup>b</sup>One ST5 isolate from the international collection contained *tarIJLM4*. <sup>c</sup>One ST23 isolate from the international collection contained both *tarIJLM2* and *tarIJLM3*. <sup>d</sup>In the international collection, one ST218 isolate contained *tarIJLM4* while one ST100 isolate contained *tarIJLM5*. <sup>e</sup>One ST23 isolate and three single-locus ST23 variants. <sup>f</sup>The international collection included 497 *S. epidermidis* genomes present in the NCBI Reference Sequence Database (accessed 3 July 2018), a global collection of 227 *S. epidermidis* isolates originating from 96 institutions across 24 countries<sup>5</sup>. For some of these isolates, it is not clear whether they are from infections.

left extremity of the SCC element shared 98% identity with a 5-kb region at the right extremity of a contig from an isolate belonging to an as yet uncharacterized *Staphylococcus* species, HMSC069E07 (accession number NZ\_LTPB01000000) (Supplementary Table 1). The contig contained the left ISS and the *tarIJL4* gene cluster. Of note, *tarM* was not present in any of the contigs from this isolate. The *ccrA2B2* genes were located on a separate contig. The *tarIJLM5* gene cluster present in the bovine ST100 isolate, SNUC\_2569, was identified on a 14-kb SCC element in an isolate belonging to another uncharacterized *Staphylococcus* species, HMSC061F01 (accession number NZ\_LTNM01000000) (Supplementary Table 1). The SCC element contained the *ccrA4B4* genes and was preceded by a 23-kb SCC element, which was integrated into the 3'-end of *orfX* and contained the *ccrA1B1* genes. Besides the *tarIJLM5* gene cluster, the two SCC elements showed little homology to other contigs from SNUC\_2569. The *tarIJL5* genes, but not *tarM*, were also present in SCC elements in three bovine *Staphylococcus hominis* isolates: SNUC\_3404, SNUC\_5746 and SNUC\_5748 (accession numbers NZ\_PZHY00000000, NZ\_PZHW00000000 and NZ\_QXVQ00000000, respectively) (Supplementary Table 1).

In contrast to the other *tarIJLM* gene clusters, we did not find evidence of the presence of *tarIJLM2* homologues outside *S. epidermidis*. Nonetheless, our data support the hypothesis that the *tarIJLM* gene clusters were derived from other *Staphylococcus* species through exchange of genetic material. Furthermore, the identification of the *tarIJLM3* and *tarIJLM5* gene clusters in bovine *S. warneri* and *S. epidermidis* isolates, respectively, suggests the existence of an animal reservoir.

**RboP-WTA impairs *S. epidermidis* epithelial binding and colonization.** The absence of *tarIJLM2*-positive *S. epidermidis* from human arm skin and nose raised the question of whether RboP-WTA may impair the capacity of *S. epidermidis* to bind epithelial surfaces. E73 wild type and E73Δ*tarIJLM2* did not differ in their capacity to bind to the matrix protein fibronectin (Fig. 3a), which indicates that RboP-WTA did not change the general adhesive properties of E73. However, E73Δ*tarIJLM2* bound twofold better to the human airway epithelial A549 cell line and to primary human nasal epithelial cells (HNEpCs) than the parental strain (Fig. 4a,b). This interaction was blocked by the scavenger-receptor-specific ligand polyinositol<sup>31,32</sup> (Extended Data Fig. 7a), which suggests that GroP-WTA may promote the binding to epithelial receptors better than RboP-WTA. Similarly, the GroP-WTA-expressing *S. epidermidis* 1457 bound significantly better to A549 cells than the same strain expressing *tarIJLM2* (Extended Data Fig. 7b). These data reflect previous findings on the crucial role of the WTA structure for *S. aureus* to bind scavenger receptors on nasal epithelia<sup>32</sup>. E73Δ*tarIJLM2* also

exhibited a 2.1-fold increased nasal colonization capacity compared with the parental strain in a mouse model when inoculated alone or in competition with the parental strain (Fig. 4c,d). This result provides support for the capacity of *tarIJLM2* to interfere with nasal epithelial binding and may explain the absence of *tarIJLM*-positive isolates from the human nose.

#### RboP-WTA production increases the virulence of *S. epidermidis*.

The exclusive association of *tarIJLM2* with *S. epidermidis* isolates from infections raised the question of whether the altered WTA may increase HA-MRSE virulence. E73 and E73Δ*tarIJLM2* had the same low degree of cytotoxicity for human cells (Fig. 3b). ST2 clones are known for their particular capacity to form biofilms on plastic surfaces, which is believed to contribute to their invasiveness<sup>33–35</sup>. Several ST2 isolates from our collection indeed formed biofilms on polystyrene plates (Fig. 3c). However, none of the *tarIJLM2*-positive ST10, ST23 or ST87 isolates produced a notable biofilm compared with the biofilm-negative and -positive model strains ATCC12228 (ref. <sup>36</sup>) and 1457 (ref. <sup>37</sup>), respectively, although some of them contained the *icaADBC* locus that is required for synthesis of the biofilm-promoting intercellular adhesin glycopolymer<sup>38</sup>. Moreover, the biofilm-forming capacity of E73 (ST23) and E1 (ST87) was not altered by deletion of *tarIJLM2* (Fig. 3d). Thus, the altered WTA of *tarIJLM*-bearing isolates does not seem to affect the intrinsically low capacity of *S. epidermidis* ST10, ST23 and ST87 to form biofilms, which suggests that there may be another reason for the increased invasiveness of RboP-WTA-expressing clones. Since WTA composition has been found to shape the ability of *S. aureus* to adhere to endothelial cells<sup>39</sup>, it was tempting to assume that RboP-WTA is overrepresented among invasive *S. epidermidis* to promote endothelial cell interactions. In contrast to airway epithelial cells, human endothelial cells were significantly less effectively bound by E73Δ*tarIJLM2* compared with the parental and complemented mutant strains (Fig. 4e). Conversely, the exclusively GroP-WTA-expressing strain 1457 bound 1.7-fold better to endothelial cells following ectopic expression of *tarIJLM2* (Extended Data Fig. 7c).

Together, these findings suggest that RboP-WTA promotes the ability of *S. epidermidis* to persist in the bloodstream. In line with this assumption, significantly lower numbers of E73Δ*tarIJLM2* cells were found in the bloodstream of intravenously infected mice compared with the parental strain, and this ratio was similar when mutant and parental strains were simultaneously injected into the same animals (Fig. 4f,g). Following binding to endothelial cells, *S. epidermidis* can leave the vasculature to form abscesses in peripheral organ tissues. In agreement with their stronger ability to bind endothelial cells, E73 wild-type cells were more abundant in the



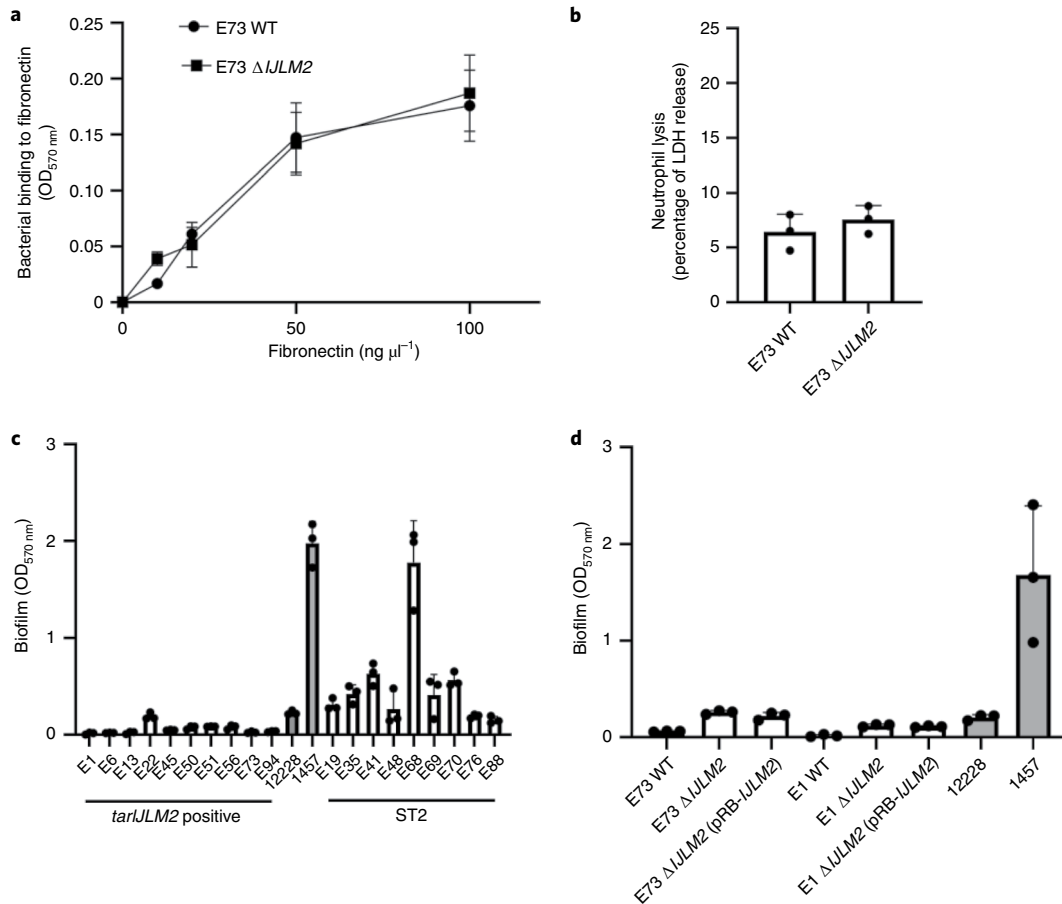


**Fig. 3 | RboP-WTA production does not affect the fibronectin binding, cytotoxic or biofilm-forming capacity of *S. epidermidis*.** **a**, Dose-dependent binding of E73 WT and E73  $\Delta$ IJLM2 to microtitre plates coated with the indicated fibronectin concentrations. **b**, *S. epidermidis* E73 and E73  $\Delta$ IJLM2 culture filtrates do not differ in their ability to lyse human neutrophils, as measured by the release of lactate dehydrogenase (LDH). **c**, In contrast to typical ST2 strains, *tarIJLM*-positive ST5 (E51 and E56), ST10 (E22), ST23 (E6, E13, E50 and E73) and ST87 (E1, E45 and E94) isolates do not produce a notable biofilm on polystyrene microtitre plates, although some of them contained the *icaADBC* locus (E6, E13, E50 and E73) required for synthesis of the biofilm-promoting intercellular adhesion glycopolymer<sup>38</sup>. **d**, Knockout of *tarIJLM2* does not alter biofilm formation by *S. epidermidis* E73 (ST23) or E1 (ST87). The laboratory *S. epidermidis* strains ATCC12228 (biofilm negative) and 1457 (biofilm positive) were included as control strains. The mean  $\pm$  s.d. of three independent experiments are shown (**a–d**).

kidneys of intravenously infected mice compared with E73 $\Delta$ *tarIJLM2* cells (Fig. 4h). Moreover, mice infected with the mutant exhibited strongly reduced mortality compared with the wild-type strain (Fig. 4i). Thus, RboP-WTA renders *S. epidermidis* more virulent in invasive infections, presumably by increasing its capacity to interact with blood vessel walls.

## Discussion

WTA is essential for efficient attachment to epithelial cells and for nasal colonization by *S. aureus*<sup>40</sup> since it facilitates binding to scavenger receptors that interact with zwitterionic bacterial polymers such as WTA<sup>32,41</sup>. However, the diversity and specificity of scavenger receptors on nasal epithelial and potentially on endothelial cells have remained elusive<sup>41</sup>. Our study indicated that the type of WTA is crucial for *S. epidermidis* interactions with human epithelial and endothelial cells and that RboP- and GroP-WTA differ in their impact on the adhesive properties for different human cell types, thereby shaping the colonization and invasion capacities of several HA-MRSE clones. WTA is essential for *S. aureus* nasal colonization in addition to several surface-anchored proteins<sup>40,42,43</sup>. Our study suggests that GroP-WTA may promote nasal colonization even more efficiently than RboP-WTA, which is reflected by the higher

prevalence of commensal *S. epidermidis* in the human nose (almost 100%) compared to *S. aureus* (~30% of the population)<sup>44,45</sup>. The fact that RboP-WTA-producing HA-MRSE strains do not seem to colonize human noses and skin of the arms raises the question of which niches they may use as their major reservoirs. An in-depth characterization of potential habitats on other human body sites or in specific HA environments may help find such niches, whose colonization may not be impaired or may even be promoted by the production of RboP-WTA.

The various HA-MRSE clones seem to use different virulence strategies. While ST2 isolates usually are strong biofilm formers but contain only rarely *tarIJLM* gene clusters, all known ST23 and ST87 isolates bear *tarIJLM* but appear to be poor biofilm formers. Future studies will show if these differences in bacterial properties may be reflected by different courses of infection. Future infection-control regimes will rely on biomarkers in pathogen genomes that will enable the stratification of risks associated with colonization or infection by a specific pathogen clone<sup>46</sup>. The *tarIJLM* cluster represents one of the few *S. epidermidis* determinants with a strong link to invasiveness and virulence, although it is used only by a subfraction of the invasive HA-MRSE clones. Nevertheless, it may be included as an indicator in surveillance programmes of this

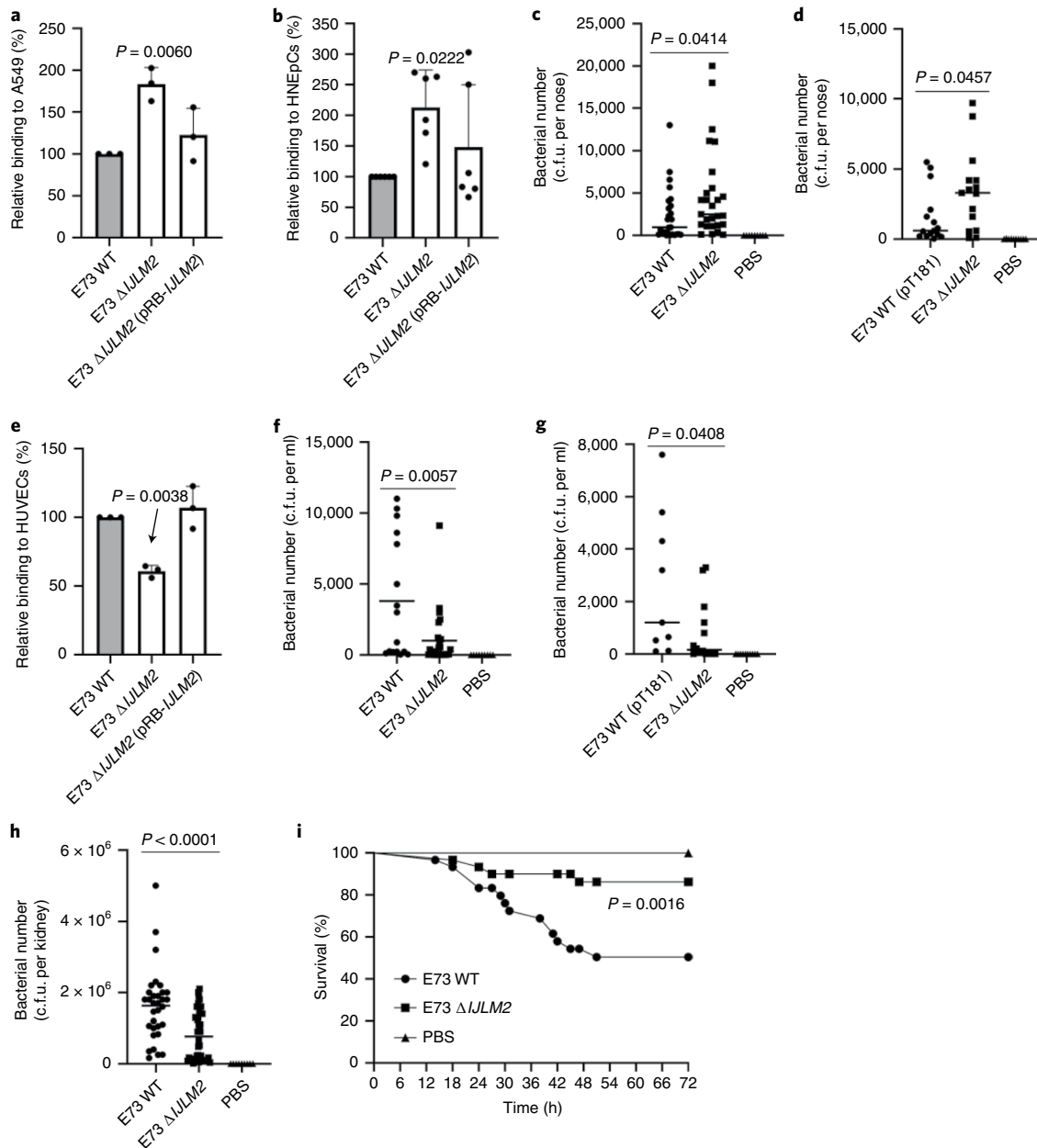


**Fig. 4 | RboP-WTA impairs colonization but increases infection capacities of *S. epidermidis*.** **a–d**, RboP-WTA production decreases *S. epidermidis* binding to the human airway epithelial cell line A549 (**a**) and to primary HNEpCs (**b**). The E73 $\Delta tarIJLM2$  mutant colonized mouse noses significantly better than the WT when the two strains were used to inoculate separate animals (**c**) or the same animals as a 1:1 mixture (**d**). **e**, RboP-WTA production promotes *S. epidermidis* binding to HUVECs. **f, g**, Blood of E73 $\Delta tarIJLM2$ -infected mice contained lower c.f.u. compared with WT-infected mice at 72 h post-infection in a bacteraemia model when the two strains were used to infect separate animals (**f**) or the same animals as a 1:1 mixture (**g**). **h**, RboP-WTA production leads to significantly increased numbers of bacteria in the kidneys of intravenously infected mice ( $P = 0.000022$ ). **i**, Strain E73 is attenuated for virulence after deletion of *tarIJLM2*, as shown in survival curves from a mouse bacteraemia model using individual bacterial strains. The mean  $\pm$  s.d. of three independent experiments are shown in **a, b** and **e**. Dot plots with medians are shown in **c, d** and **f–h**, with each dot representing one sample from each mouse. Significant differences ( $P \leq 0.05$ ) were calculated by one-way ANOVA with Dunnett’s post-test (two-sided) in **a, b** and **e** (versus WT), by unpaired *t*-test in **c, d** and **f–h** or log-rank (Mantel–Cox) test in **i**.

globally important pathogen. It is worth noting that a *tarIJL* cluster is also found in an epidemic lineage of the opportunistic pathogen *Staphylococcus capitis*, which causes severe infection outbreaks among newborns<sup>47</sup>. Protein-conjugated RboP-WTA represents a promising antigen for future preventive or therapeutic vaccines against *S. aureus*<sup>48</sup>. Our study suggests that such vaccines could also protect against RboP-WTA-producing HA-MRSE and other CoNS

clones. Development of an anti-*Staphylococcus* vaccine remains a major challenge though. A detailed understanding of the structure and variability of surface antigens will be essential for success<sup>48</sup>.

## Methods

**Bacterial strains and growth conditions.** *S. epidermidis* laboratory strains RP62A, ATCC12228 and 1457 were used as controls for WTA analytical and phenotypic

experiments. *S. aureus* strains RN4220 and PS187 were used as phage propagation and as test strains for phage binding and transduction experiments. *S. aureus* JP1794 (ref. 49) and PS187-H VW1 (ref. 15) were used as donor strains for SaPI particle propagation as described below. *Escherichia coli* DC10B was used as the cloning host. RN4220 and PS187 $\Delta$ sauUSI $\Delta$ hdsR<sup>50</sup> were used as donor strains for plasmid transduction. *S. epidermidis* and *S. aureus* strains were cultivated in tryptic soy broth (TSB) medium or Mueller–Hinton broth (MHB), unless otherwise noted, and incubated at 37 °C on an orbital shaker. *E. coli* strains were cultivated in lysogeny broth (LB). Media were supplemented with appropriate antibiotics (tetracycline (5  $\mu$ g ml<sup>-1</sup>), chloramphenicol (10  $\mu$ g ml<sup>-1</sup>) or ampicillin (100  $\mu$ g ml<sup>-1</sup>)). *S. epidermidis* isolates were obtained from clinical specimens or from nasal (anterior nasal mucosa of both nostrils) or skin (elbow pit of both arms) swabs from healthy volunteers. Bacteria were plated on blood agar plates immediately after swabbing. Colonies were analysed by matrix-assisted laser desorption–ionization time-of-flight (MALDI–TOF) mass spectrometry (MS) for species determination. Because many *S. epidermidis* isolates from clinical samples are known to result from contaminating skin bacteria, strict criteria were used for the definition of true clinical isolates. These included the repeated isolation of the same strain at two different days and the origin from a typical infection site such as a blood culture or infected implant.

**SaPI transfer and phage-adsorption assays.** SaPI-transfer experiments were performed according to standard procedures<sup>15</sup>. Briefly, approximately  $8.0 \times 10^7$  cells of a recipient strain grown overnight were mixed with 100  $\mu$ l of lysates obtained from *S. aureus* strain JP1794 or PS187-H VW1 bearing the tetracycline-resistance marker-labelled SaPIbov1 (~ $1.0 \times 10^6$  p.f.u. ml<sup>-1</sup>), incubated for 15 min at 37 °C, diluted and plated on tetracycline-containing TSB agar to count transducing colonies.

The adsorption efficiency of  $\Phi$ 11,  $\Phi$ 187,  $\Phi$ PH15 and  $\Phi$ E72 was determined as previously described with minor modifications<sup>15</sup>. Briefly, adsorption rates were analysed using a multiplicity of infection (m.o.i.) of 0.1. The adsorption rate was elucidated by determining the number of unbound phages in the supernatant and dividing the number of bound phages by the number of input phages.

The *S. epidermidis* phage phiE72 was isolated by incubating the clinical *S. epidermidis* isolate E72 with 5  $\mu$ g ml<sup>-1</sup> mitomycin C overnight at 30 °C, adding the culture supernatant to agar plates with lawns of the laboratory strain *S. epidermidis* 1457. Phage plaques were isolated and used to infect strain 1457 again to generate phage lysates. The genome of  $\Phi$ E72 was sequenced, which showed that  $\Phi$ E72 is a previously unknown member of the siphovirus phage family. The ability of  $\Phi$ E72 to infect *S. epidermidis* strain 1457, which produces only GroP-WTA, showed that  $\Phi$ E72 recognizes GroP-WTA.

**Whole-genome sequencing.** Whole-genome sequences were generated for the 25 *tarIJLM*-positive *S. epidermidis* isolates collected in this study (Table 1 and Supplementary Table 1). Bacterial DNA was extracted from mechanically or lysostaphine-lysed bacterial cells and quantified using a DNeasy Blood and Tissue kit (Qiagen) and a Qubit 3.0 Fluorometer (Invitrogen), respectively. Libraries were prepared with a Nextera XT DNA library prep kit (Illumina) or a NEBNext Ultra library prep kit (New England Biolabs) after shearing the DNA to fragments of 300 bp on a Bioruptor Pico instrument (Diagenode), and then sequenced on a MiSeq platform (Illumina) with 2  $\times$  251 bp using a MiSeq Reagent kit v2 or on a NextSeq platform with 2  $\times$  150 bp using a NextSeq 500/550 v2 kit. Velvet (v.1.2.10)<sup>51</sup> or SPAdes (v.3.11.1)<sup>52</sup> was used to generate de novo assemblies. *S. epidermidis* E73 was also sequenced using the PacBio Sequel platform. DNA was sheared to 10-kb fragments using g-TUBEs (Covaris). SMRTbell libraries were constructed using standard procedures (Pacific Biosciences). The genome was de novo assembled using the Hierarchical Genome Assembly Process (HGAP4) workflow in SMRT Link (v.5.1.0.26411; Pacific Biosciences). A second de novo assembly was made based on Illumina sequencing, and the combination of the sequence contigs resulted in the final genome, which was confirmed by mapping the Illumina reads to the final assembly. The circular chromosome was annotated using the NCBI Prokaryotic Genome Annotation Pipeline.

**Sequence analyses.** The *tarIJLM2* genes in E73 (Fig. 1b) were used as queries in BLASTN searches against 497 *S. epidermidis* genomes present in the NCBI Reference Sequence Database (accessed 3 July 2018), a global collection of 227 *S. epidermidis* isolates originating from 96 healthcare institutions across 24 countries<sup>1</sup>, and the 25 *S. epidermidis* isolates collected in this study (Table 1). Multilocus sequence typing (MLST) was performed by comparing contigs with the *S. epidermidis* MLST database<sup>53</sup>. SCCmec typing was carried out with SCCmecFinder (v.1.2)<sup>54</sup>. IS elements were classified according to transposase gene similarity by using BLAST analysis with the ISfinder database<sup>55</sup>.

**Phylogenetic analyses.** Mapping of sequence reads and single-nucleotide polymorphism (SNP) calling were carried out using the Northern Arizona SNP pipeline (v.1.0.0)<sup>56</sup>. In brief, sequence reads were mapped against the *S. epidermidis* ST2 reference isolate BPH0662 (GenBank accession number NC\_017673) using the Burrows–Wheeler Alignment tool<sup>57</sup>. SNP calling was achieved using the GATK Unified Genotyper<sup>58,59</sup> with the following parameters:  $\geq 10\times$  mapping coverage;

$\geq 90\%$  unambiguously base calls; and insertions and deletions were ignored. SNPs contained in repeats, as determined by NUCmer<sup>60,61</sup>, were excluded. Next, phages in BPH0662 were identified with PHASTER<sup>62</sup>, and SNPs residing within these were manually removed from the alignment, whereafter Gubbins (v.2.3.4)<sup>63</sup> was used to remove recombination tracts. The MUSCLE algorithm<sup>64</sup> was used to construct multiple sequence alignments for each of the *tarIJLM* genes and to calculate pairwise nucleotide identities. A subset of *tarIJLM* genes (Fig. 1b) representing the diversity observed within *S. epidermidis* was used as queries in BLASTN searches against non-*S. epidermidis* genomes present in the NCBI Reference Sequence Database (accessed 29 October 2018). Phylogenetic reconstruction was carried out using the maximum-likelihood program PhyML (v.3.0) with a GTR model of nucleotide substitution<sup>65,66</sup>. Support for the nodes was assessed using aBayes<sup>67</sup>.

**Specific PCR screening for different types of *tarL* genes.** Isolates were screened for different variants of *tarL* genes by PCR amplification using the primers listed in Supplementary Table 3. The following thermocycler conditions for amplification were used: 98 °C for 2 min, 98 °C for 30 s, 55 °C for 30 s, 72 °C for 1 min, 72 °C for 10 min, 32 cycles. The PCR products were confirmed by sequencing (Eurofins).

**Cell wall and WTA isolation.** Cell walls and WTA were isolated as previously described<sup>40</sup>. Briefly, bacteria were grown overnight in TSB supplemented with 0.25% glucose. Bacterial cells were disintegrated with a FastPrep-24 instrument (MP Biomedicals). Lysates were incubated overnight with DNase I (40 units per ml; Roche) and RNase A (80 units per ml; Sigma) at 37 °C, sonicated and washed with sodium dodecyl sulfate. WTA was then released from cell walls by treatment with 5% trichloroacetic acid dialysed against pyrogen-free water (Ambion), and quantified by phosphate assay as previously described<sup>40</sup>. To quantify the WTA amount per cell, 300  $\mu$ l cell wall suspension was mixed with 300  $\mu$ l 1 M NaOH and incubated at 60 °C with constant shaking at 600 r.p.m. After 2 h, the phosphate content in supernatants of this mixture was measured as described above. The same amount of 300  $\mu$ l cell wall was dried in a Speedvac concentrator and weighted to determine the phosphate amount per cell wall dry mass.

**WTA chromatography and MS analysis.** The composition of pure WTA samples was determined by methanolysis of the samples with 0.5 M HCl/MeOH at 85 °C for 45 min followed by peracetylation twice using acetic anhydride and pyridine (1:1, v/v) at 85 °C for 10 min and detection by gas–liquid chromatography (GLC) and GLC–MS. The systems used were an Agilent Technologies 7890A instrument equipped with a HP-5MS capillary column (30 m  $\times$  0.25 mm, film thickness 0.25  $\mu$ m) and applying a temperature gradient of 150 °C (kept for 3 min) to 250 °C at 3 °C min<sup>-1</sup> for GLC or an Agilent Technologies 7890A instrument equipped with a dimethylpolysiloxane column (Agilent, HP Ultra 1, 12 m  $\times$  0.2 mm, film thickness 0.33  $\mu$ m) and 5975C series MSD detector with electron impact ionization (EI) mode under autotuned condition at 70 eV applying a temperature gradient of 70 °C (kept for 1.5 min) to 110 °C at 60 °C min<sup>-1</sup> and then to 320 °C at 5 °C min<sup>-1</sup>. For the WTA sample of E73 wild type, the absolute configuration was determined by GLC by comparison with authentic standards of the acetylated (S)-2-butanol glycoside derivative after butanolysis (2 M HCl, (S)-2-butanol at 85 °C for 2 h) and acetylation as previously described<sup>48</sup>. The same system was used for detection, applying a temperature gradient of 120 °C (kept for 3 min) to 320 °C at 3 °C min<sup>-1</sup>.

Identification of the WTA polymer type was performed using an Ultimate 3000RS HPLC system (Dionex) coupled to a microTOFII electrospray-ionization (ESI) TOF mass spectrometer (Bruker). For HPLC, a Gemini C18 column (150  $\times$  4.6 mm, 110 Å, 5  $\mu$ M, Phenomenex) was used at 37 °C with a flow rate of 0.2 ml min<sup>-1</sup>. A 5-min equilibration step with 100% buffer A (0.1% formic acid, 0.05% ammonium formate) was applied, followed by a linear gradient of 0 to 40% buffer B (acetonitrile) for 30 min. A final washing step with 40% buffer B for 5 min and a re-equilibration step (100% buffer A) for 5 min completed the method. Samples were ionized via ESI in positive-ion mode. Exact masses in positive-ion mode for GroP [M + H]<sup>+</sup> = 173.022 m/z and RboP [M + H]<sup>+</sup> = 233.042 m/z were presented as extracted ion chromatograms with Data Analysis (Bruker). Base peak chromatograms were used for sample normalization.

**Nuclear magnetic resonance microscopy.** Experiments were carried out in D<sub>2</sub>O at 300 K. All one-dimensional (<sup>1</sup>H and <sup>13</sup>C) and two-dimensional homonuclear (COSY, TOCSY and ROESY) and heteronuclear (HSQC–DEPT and HMBC) experiments were recorded with a Bruker AvanceII 700 MHz spectrometer (operating frequencies of 700.43 MHz for <sup>1</sup>H nuclear magnetic resonance (NMR), and 176.13 MHz for <sup>13</sup>C NMR) using standard Bruker software. COSY, TOCSY and ROESY were recorded using datasets (t1 by t2) of 4,096 by 512 points, and four scans (E73 wild type, 1457 wild type and 1457 (pRB-IJLM2)), two scans (E73  $\Delta$ tarIJLM2) or one scan (E73  $\Delta$ tarIJLM2 (pRB-IJLM2)) were acquired for each t1 value in the case of COSY, eight scans (E73 wild type, E73  $\Delta$ tarIJLM2, E73  $\Delta$ tarIJLM2 (pRB-IJLM2) and 1457 (pRB-IJLM2)) or 16 scans (1457 wild type) in the case of TOCSY and eight scans in the case of ROESY. The TOCSY experiment was carried out in the phase-sensitive mode with mixing times of 120 ms. The <sup>1</sup>H–<sup>13</sup>C correlations were measured in the <sup>1</sup>H-detected mode via HSQC–DEPT with proton decoupling in the <sup>13</sup>C domain acquired using datasets of either 4,096 by 512 points (16 scans for each t1 value in the case of E73  $\Delta$ tarIJLM2 and E73

*ΔtarI/JLM2* (pRB-IJLM2); 48 scans for each t1 in the case of 1457 wild type and 1457 (pRB-IJLM2) or 4,096 by 1,024 points (32 scans for each t1 in the case of E73 wild type). The HMBC spectra were acquired using datasets of 4,096 by 512 points and either 32 scans (E73 *ΔtarI/JLM2* and 1457 wild type), 36 scans (E73 *ΔI/JLM2*(pRB-IJLM2)), 104 scans (E73 wild type) or 128 (1457(pRB-IJLM2)) for each t1 value. Chemical shifts are reported relative to external acetone (<sup>1</sup>H, 2.225; <sup>13</sup>C, 31.50).

**Molecular genetic methods.** For the construction of the *ΔtarI/JLM2* mutant in *S. epidermidis* E73, the pBASE6-erm/lox1 shuttle vector was used according to standard procedures<sup>69</sup>. For mutant complementation experiments, plasmid pRB474 was used<sup>70</sup>. The primers for knockout and complementation plasmid construction are listed in Supplementary Table 3. Plasmid transduction to *S. epidermidis* strains was performed using Φ11 with *S. aureus* RN4220 as the donor strain or Φ187 as the transduction phage with *S. aureus* PS187 as the donor strain according to the method by Winstel et al.<sup>50</sup>.

**RNA isolation and qRT-PCR.** Bacterial cultures grown overnight in TSB were diluted in fresh TSB, PBS with 50% pooled heat-inactivated human serum from healthy donors, or synthetic nasal medium (SNM3, containing 0.2 mM bipyridine)<sup>20</sup> and grown at 37 °C and 180 r.p.m. Bacteria were collected after 6 h (exponential growth phase) and immersed in RNAprotect bacteria reagent (Qiagen), and washed and resuspended in RLT lysis buffer, followed by mechanical lysis with a bead-beating homogenizer (Precellys). RNA was extracted from the lysate with a RNeasy Mini kit (Qiagen), transcribed into complementary DNA with iScript reverse transcriptase (Bio-Rad), and quantitative PCR with reverse transcription (RT-qPCR) was performed on a LightCycler480 instrument (Roche). Transcription levels of *tarL1* and *tarL2* were normalized against the expression of the constitutively transcribed *gyrB*, *rho* and *tpiA* housekeeping genes. PCR set-up, cycling conditions and assays for housekeeping genes were as previously described<sup>29</sup>. Each experiment was performed in biological and technical duplicates. qPCR results were analysed in LightCycler 480 SW 1.5.1. and GenEx software (multiD).

**Semi-quantitative biofilm assay.** *S. epidermidis* biofilm formation was analysed using 96-well Nunc delta microtitre plates as previously described<sup>71</sup> with the following modifications. After incubation at 37 °C for 24 h, the cells were washed gently three times in PBS and then stained with 0.1% crystal violet solution. The stain was washed off gently under slowly running water and plates were dried. Finally, 5% acetic acid was added to the wells to dissolve the stain. The absorbance was measured at 570 nm using a MicroELISA autoreader (Bio-Rad).

**Adherence of *S. epidermidis* to immobilized fibronectin.** Nunc delta microtitre plates were coated with fibronectin (Sigma) in carbonate-coating buffer (15 mM Na<sub>2</sub>CO<sub>3</sub>, 35 mM NaHCO<sub>3</sub>, pH 9.6), and incubated overnight at 4 °C. BSA (5 mg ml<sup>-1</sup> in PBS) was added and incubated for 2 h at 37 °C. The plates were then washed three times with PBS. A bacterial cell suspension ( $A_{600\text{nm}} = 1.0$  in PBS) was added and incubated for 1.5 h at 37 °C. Plates were washed three times with PBS and bound cells were fixed with formaldehyde (25% v/v) for 30 min followed by staining with crystal violet (0.5% v/v, 100 μl per well) for 1 min. After three washes with PBS, acetic acid (5% v/v) was added (100 μl per well) for 10 min at room temperature. The absorbance was measured at 570 nm.

**Fluorescein isothiocyanate labelling of *S. epidermidis* cells.** Overnight-grown *S. epidermidis* cultures were diluted in fresh MHB and grown at 37 °C to logarithmic growth phase ( $OD_{600\text{nm}} = 1.0$ ). Bacteria were then collected, washed three times with PBS labelled with fluorescein isothiocyanate (FITC; 0.1 mg ml<sup>-1</sup>) for 1 h at 37 °C and washed three times with PBS, resuspended in RPMI medium (Sigma) and stored at -80 °C. The concentration of FITC-labelled bacteria was determined using a Neubauer chamber.

**Cell culture.** A549 human bronchial epithelial cells (American Type Culture Collection (ATCC) CCL-185) were grown in DMEM (Gibco-BRL) supplemented with 100 μg ml<sup>-1</sup> streptomycin, 100 U ml<sup>-1</sup> penicillin, 10% heat-inactivated fetal bovine serum and 2 mM glutamine. Human umbilical vein endothelial cells (HUVECs) cryopreserved from pooled donors were purchased from PromoCell (C-12203) and grown in endothelial cell growth medium (PromoCell). Primary human nasal epithelial cells (HNEpCs) cryopreserved from normal human nasal mucosa of pooled donors were purchased from PromoCell (C-12620) and grown in airway epithelial cell growth medium. All cells used here were grown at 37 °C under 5% CO<sub>2</sub>. A549, HUVECs and HNEpCs were used until passage nine, seven and five, respectively.

**Lysis of human neutrophils.** Lysis of human neutrophils by culture filtrates of *S. epidermidis* was analysed as previously described<sup>72</sup>. Briefly, *S. epidermidis* strains were cultivated for 18 h in TSB medium. The culture supernatant was sterilized by filtration. After 1:5 dilution with RPMI, 100 μl culture filtrate was mixed with 100 μl human neutrophil suspension containing 10<sup>8</sup> cells, isolated by standard procedure<sup>73</sup>, and incubated for 1 h at 37 °C. The ability of bacteria to cause cell

lysis was quantified by measuring the release of cytoplasmic lactate dehydrogenase (LDH) (Cytotoxicity Detection kit, Roche Diagnostics).

**Interaction of *S. epidermidis* with epithelial or endothelial cells.** The capacity of *S. epidermidis* to adhere to epithelial or endothelial cells was analysed as previously described<sup>40</sup>. Briefly, approximately 1 × 10<sup>6</sup> A549 cells, HNEpCs or HUVECs were seeded onto ibiTreat slides (Ibidi) to form confluent cell monolayers. Cells were grown at 37 °C under 5% CO<sub>2</sub> in appropriate cell culture media. The cells were washed twice with DMEM (A549) or DMEM-F12 (HUVECs and HNEpCs) and inoculated with FITC-labelled bacteria at a m.o.i. of 100 for 1 h at 37 °C under 5% CO<sub>2</sub>. To mimic the liquid flow in nose and bloodstream, peristaltic pumps (Amersham) were used during infection (30 min) with FITC-labelled bacteria at a flow rate of 1 ml h<sup>-1</sup> at 0.3 dynes cm<sup>-2</sup>. The nuclei and cytoskeletons of the cells were stained with 4',6-diamidino-2-phenylindole and phalloidin tetramethylrhodamine B isothiocyanate, respectively. Bacteria were fixed using 3.5% paraformaldehyde (PFA) in PBS at room temperature. PFA was removed and wells were coated with 1 ml PBS. No morphological changes of bacterial or human cells were observed after this procedure. Bacteria adhering to epithelial or endothelial cells were counted using a confocal microscope. To assess whether scavenger receptors are involved in the cell binding process, A549 cells were pre-incubated for 30 min with different concentrations of the polyanionic scavenger receptor ligand poly I (Sigma). After washing with DMEM, cells were used in binding assays with FITC-labelled bacteria as described above.

**Mouse experiments.** Female 4–6-week-old BALB/c mice, kept at a temperature of 20–25 °C, relative humidity of 40–70% and light-dark alternation times of 12–14/12–10 h, and bacterial cells grown in TSB to mid-exponential growth phase ( $OD_{600\text{nm}} = 1.0$ ), washed, and resuspended in sterile PBS, were used for all animal experiments.

For the nasal colonization model, 27 mice per bacterial strain were given water containing kanamycin (25 μg ml<sup>-1</sup>) for 3 days before infection. The inoculum, which contained 10<sup>10</sup> colony forming units (c.f.u.) in 10 μl PBS or PBS alone, was pipetted slowly onto the nares of anaesthetized mice without touching the skin with the pipette tip. Three days after inoculation, mice were euthanized, nasal regions were wiped externally with 70% ethanol and the nasal tissues were homogenized in 0.5 ml of TSB. The total number of *S. epidermidis* c.f.u. per nose was assessed by plating 100 μl diluted nasal suspensions on TSA with 5% sheep blood and enumerating colonies after overnight growth at 37 °C.

To study the capacity of strain E73 and its mutant E73 $\Delta$ IJLM2 to compete with each other during nasal colonization, E73 was transformed with plasmid pT181 rendering the strain resistant to tetracycline to allow its discrimination from the tetracycline-susceptible E73 $\Delta$ IJLM2. The two strains grew equally well in TSB medium and the plasmid was almost 100% maintained in E73 over 72 h even without antibiotic selection (equal c.f.u. on antibiotic-selective and nonselective plates) (Extended Data Fig. 8). The two strains were mixed 1:1 in PBS. A total of 10 μl of the suspension containing 10<sup>10</sup> c.f.u. of or 10 μl PBS alone were used to colonize the mouse nares as described above. Homogenized tissue samples were plated on TSA with 5% sheep blood with or without tetracycline (25 μg ml<sup>-1</sup>) for strain distinction and determination of c.f.u.

For the bacteraemia model, 30 anaesthetized mice per bacterial strain received 10<sup>11</sup> c.f.u. of E73 wild type or mutant in 0.1 ml PBS or PBS alone by retro-orbital injection via the right eye. After inoculation, general animal health condition and disease advancement were regularly monitored for up to 72 h. Evaluation of animal morbidity was based on the following criteria: hunched posture, activity levels, ruffled fur and laboured breathing. All surviving mice were euthanized at 72 h post-infection. The blood and kidney samples were plated on TSA with 5% sheep blood to measure c.f.u. of *S. epidermidis* in blood.

To study the capacity of strain E73 wild type (pT181) and its mutant E73 $\Delta$ IJLM2 to compete with each other during systemic infection, 1:1 mixture of the two strains with 10<sup>11</sup> c.f.u. in 100 μl PBS or 100 μl PBS alone were used to infect mice by retro-orbital injection as described above. The mortality was monitored, and blood samples were obtained after 72 h and plated on TSA with 5% sheep blood with or without tetracycline (25 μg ml<sup>-1</sup>) for strain distinction and determination of c.f.u. in blood.

**Statistical analysis.** Statistical analysis was performed using the Prism 8.0 package (GraphPad Software). *P* values of ≤0.05 were considered significant.

**Ethics statement.** Bacterial samples from human volunteers were collected after written informed consent and approval by the institutional review boards of the Universities of Tübingen (577/2015A) and Shanghai Jiaotong University (protocol 2017001). Isolates from Hamburg were obtained in accordance with Section 12 of the Hamburg Hospital Law (HmbKHG). All mouse work was performed in China, which was approved by the Ethics Committee of Renji Hospital, School of Medicine, Shanghai Jiaotong University.

**Reporting Summary.** Further information on research design is available in the Nature Research Reporting Summary linked to this article.

## Data availability

The whole-genome sequence data from this study were deposited in the NCBI Sequence Read Archive; the accession numbers can be found in Supplementary Table 1. Source data are provided with this paper. Additional information can be obtained from the corresponding author upon reasonable request.

Received: 9 November 2020; Accepted: 20 April 2021;  
Published online: 24 May 2021

## References

- Becker, K., Heilmann, C. & Peters, G. Coagulase-negative staphylococci. *Clin. Microbiol. Rev.* **27**, 870–926 (2014).
- Byrd, A. L., Belkaid, Y. & Segre, J. A. The human skin microbiome. *Nat. Rev. Microbiol.* **16**, 143–155 (2018).
- Lee, J. Y. H. et al. Global spread of three multidrug-resistant lineages of *Staphylococcus epidermidis*. *Nat. Microbiol.* **3**, 1175–1185 (2018).
- Li, M., Wang, X., Gao, Q. & Lu, Y. Molecular characterization of *Staphylococcus epidermidis* strains isolated from a teaching hospital in Shanghai, China. *J. Med. Microbiol.* **58**, 456–461 (2009).
- Meric, G. et al. Disease-associated genotypes of the commensal skin bacterium *Staphylococcus epidermidis*. *Nat. Commun.* **9**, 5034 (2018).
- Heilmann, C., Ziebuhr, W. & Becker, K. Are coagulase-negative staphylococci virulent?. *Clin. Microbiol. Infect.* **25**, 1071–1080 (2019).
- Weidenmaier, C. & Peschel, A. Teichoic acids and related cell-wall glycopolymers in Gram-positive physiology and host interactions. *Nat. Rev. Microbiol.* **6**, 276–287 (2008).
- Moller, A. G., Lindsay, J. A. & Read, T. D. Determinants of phage host range in *Staphylococcus* species. *Appl. Environ. Microbiol.* **85**, e00209-19 (2019).
- Chen, J. et al. Genome hypermobility by lateral transduction. *Science* **362**, 207–212 (2018).
- Haaber, J., Penades, J. R. & Ingmer, H. Transfer of antibiotic resistance in *Staphylococcus aureus*. *Trends Microbiol.* **25**, 893–905 (2017).
- Lee, A. S. et al. Methicillin-resistant *Staphylococcus aureus*. *Nat. Rev. Dis. Primers* **4**, 18033 (2018).
- Penades, J. R. & Christie, G. E. The phage-inducible chromosomal islands: a family of highly evolved molecular parasites. *Annu. Rev. Virol.* **2**, 181–201 (2015).
- Meric, G. et al. Ecological overlap and horizontal gene transfer in *Staphylococcus aureus* and *Staphylococcus epidermidis*. *Genome Biol. Evol.* **7**, 1313–1328 (2015).
- Li, M. et al. MRSA epidemic linked to a quickly spreading colonization and virulence determinant. *Nat. Med.* **18**, 816–819 (2012).
- Winstel, V. et al. Wall teichoic acid structure governs horizontal gene transfer between major bacterial pathogens. *Nat. Commun.* **4**, 2345 (2013).
- Fitzgerald, J. R. et al. Characterization of a putative pathogenicity island from bovine *Staphylococcus aureus* encoding multiple superantigens. *J. Bacteriol.* **183**, 63–70 (2001).
- Maiques, E. et al. Role of staphylococcal phage and SaPI integrase in intra- and interspecies SaPI transfer. *J. Bacteriol.* **189**, 5608–5616 (2007).
- Brown, S., Santa Maria, J. P. Jr. & Walker, S. Wall teichoic acids of Gram-positive bacteria. *Annu. Rev. Microbiol.* **67**, 313–336 (2013).
- Winstel, V., Xia, G. & Peschel, A. Pathways and roles of wall teichoic acid glycosylation in *Staphylococcus aureus*. *Int. J. Med. Microbiol.* **304**, 215–221 (2014).
- Krismer, B. et al. Nutrient limitation governs *Staphylococcus aureus* metabolism and niche adaptation in the human nose. *PLoS Pathog.* **10**, e1003862 (2014).
- Xia, G. et al. Glycosylation of wall teichoic acid in *Staphylococcus aureus* by TarM. *J. Biol. Chem.* **285**, 13405–13415 (2010).
- Dean, B. A., Williams, R. E., Hall, F. & Corse, J. Phage typing of coagulase-negative staphylococci and micrococci. *J. Hyg. (Lond.)* **71**, 261–270 (1973).
- Miragaia, M. et al. Comparison of molecular typing methods for characterization of *Staphylococcus epidermidis*: proposal for clone definition. *J. Clin. Microbiol.* **46**, 118–129 (2008).
- Sivadon, V. et al. Partial *atlE* sequencing of *Staphylococcus epidermidis* strains from prosthetic joint infections. *J. Clin. Microbiol.* **47**, 2321–2324 (2009).
- Mertens, A. & Ghebremedhin, B. Genetic determinants and biofilm formation of clinical *Staphylococcus epidermidis* isolates from blood cultures and indwelling devices. *Eur. J. Microbiol. Immunol.* **3**, 111–119 (2013).
- Sharma, P. et al. Multilocus sequence typing for interpreting blood isolates of *Staphylococcus epidermidis*. *Interdiscip. Perspect. Infect. Dis.* **2014**, 787458 (2014).
- Post, V. et al. Comparative genomics study of *Staphylococcus epidermidis* isolates from orthopedic-device-related infections correlated with patient outcome. *J. Clin. Microbiol.* **55**, 3089–3103 (2017).
- Both, A. et al. Distinct clonal lineages and within-host diversification shape invasive *Staphylococcus epidermidis* populations. *PLoS Pathog.* **17**, e1009304 (2021).
- Weiser, J. et al. Sub-inhibitory tigecycline concentrations induce extracellular matrix binding protein Embp dependent *Staphylococcus epidermidis* biofilm formation and immune evasion. *Int. J. Med. Microbiol.* **306**, 471–478 (2016).
- Wang, L. & Archer, G. L. Roles of CcrA and CcrB in excision and integration of staphylococcal cassette chromosome *mec*, a *Staphylococcus aureus* genomic island. *J. Bacteriol.* **192**, 3204–3212 (2010).
- Jiang, Y., Oliver, P., Davies, K. E. & Platt, N. Identification and characterization of murine SCARA5, a novel class A scavenger receptor that is expressed by populations of epithelial cells. *J. Biol. Chem.* **281**, 11834–11845 (2006).
- Baur, S. et al. A nasal epithelial receptor for *Staphylococcus aureus* WTA governs adhesion to epithelial cells and modulates nasal colonization. *PLoS Pathog.* **10**, e1004089 (2014).
- Widerstrom, M., McCullough, C. A., Coombs, G. W., Monsen, T. & Christiansen, K. J. A multidrug-resistant *Staphylococcus epidermidis* clone (ST2) is an ongoing cause of hospital-acquired infection in a Western Australian hospital. *J. Clin. Microbiol.* **50**, 2147–2151 (2012).
- Ziebuhr, W. et al. Nosocomial infections by *Staphylococcus epidermidis*: how a commensal bacterium turns into a pathogen. *Int. J. Antimicrob. Agents* **28**, S14–S20 (2006).
- Du, X. et al. Molecular analysis of *Staphylococcus epidermidis* strains isolated from community and hospital environments in China. *PLoS ONE* **8**, e62742 (2013).
- Zhang, Y. Q. et al. Genome-based analysis of virulence genes in a non-biofilm-forming *Staphylococcus epidermidis* strain (ATCC 12228). *Mol. Microbiol.* **49**, 1577–1593 (2003).
- Mack, D., Siemssen, N. & Laufs, R. Parallel induction by glucose of adherence and a polysaccharide antigen specific for plastic-adherent *Staphylococcus epidermidis*: evidence for functional relation to intercellular adhesion. *Infect. Immun.* **60**, 2048–2057 (1992).
- Otto, M. Staphylococcal biofilms. *Microbiol. Spectr.* <https://doi.org/10.1128/microbiolspec.GPP3-0023-2018> (2018).
- Weidenmaier, C. et al. Lack of wall teichoic acids in *Staphylococcus aureus* leads to reduced interactions with endothelial cells and to attenuated virulence in a rabbit model of endocarditis. *J. Infect. Dis.* **191**, 1771–1777 (2005).
- Weidenmaier, C. et al. Role of teichoic acids in *Staphylococcus aureus* nasal colonization, a major risk factor in nosocomial infections. *Nat. Med.* **10**, 243–245 (2004).
- Schade, J. & Weidenmaier, C. Cell wall glycopolymers of Firmicutes and their role as nonprotein adhesins. *FEBS Lett.* **590**, 3758–3771 (2016).
- Weidenmaier, C. et al. Differential roles of sortase-anchored surface proteins and wall teichoic acid in *Staphylococcus aureus* nasal colonization. *Int. J. Med. Microbiol.* **298**, 505–513 (2008).
- Foster, T. J. Surface proteins of *Staphylococcus epidermidis*. *Front. Microbiol.* **11**, 1829 (2020).
- Zipperer, A. et al. Human commensals producing a novel antibiotic impair pathogen colonization. *Nature* **535**, 511–516 (2016).
- Iwase, T. et al. *Staphylococcus epidermidis* Esp inhibits *Staphylococcus aureus* biofilm formation and nasal colonization. *Nature* **465**, 346–349 (2010).
- Ladner, J. T., Grubaugh, N. D., Pybus, O. G. & Andersen, K. G. Precision epidemiology for infectious disease control. *Nat. Med.* **25**, 206–211 (2019).
- Wirth, T. et al. Niche specialization and spread of *Staphylococcus capitis* involved in neonatal sepsis. *Nat. Microbiol.* **5**, 735–745 (2020).
- van Dalen, R. et al. Do not discard *Staphylococcus aureus* WTA as a vaccine antigen. *Nature* **572**, E1–E2 (2019).
- Tormo, M. A. et al. *Staphylococcus aureus* pathogenicity island DNA is packaged in particles composed of phage proteins. *J. Bacteriol.* **190**, 2434–2440 (2008).
- Winstel, V., Kuhner, P., Rohde, H. & Peschel, A. Genetic engineering of untransformable coagulase-negative staphylococcal pathogens. *Nat. Protoc.* **11**, 949–959 (2016).
- Zerbino, D. R. & Birney, E. Velvet: algorithms for de novo short read assembly using de Bruijn graphs. *Genome Res.* **18**, 821–829 (2008).
- Bankevich, A. et al. SPAdes: a new genome assembly algorithm and its applications to single-cell sequencing. *J. Comput. Biol.* **19**, 455–477 (2012).
- Thomas, J. C. et al. Improved multilocus sequence typing scheme for *Staphylococcus epidermidis*. *J. Clin. Microbiol.* **45**, 616–619 (2007).
- Kaya, H. et al. SCC *mec*Finder, a web-based tool for typing of staphylococcal cassette chromosome *mec* in *Staphylococcus aureus* using whole-genome sequence data. *mSphere* <https://doi.org/10.1128/mSphere.00612-17> (2018).
- Siguier, P., Perochon, J., Lestrade, L., Mahillon, J. & Chandler, M. ISfinder: the reference centre for bacterial insertion sequences. *Nucleic Acids Res.* **34**, D32–D36 (2006).
- Sahl, J. W. et al. NASP: an accurate, rapid method for the identification of SNPs in WGS datasets that supports flexible input and output formats. *Micro. Genom.* **2**, e000074 (2016).
- Li, H. & Durbin, R. Fast and accurate long-read alignment with Burrows–Wheeler transform. *Bioinformatics* **26**, 589–595 (2010).

58. McKenna, A. et al. The Genome Analysis Toolkit: a MapReduce framework for analyzing next-generation DNA sequencing data. *Genome Res.* **20**, 1297–1303 (2010).
59. DePristo, M. A. et al. A framework for variation discovery and genotyping using next-generation DNA sequencing data. *Nat. Genet.* **43**, 491–498 (2011).
60. Delcher, A. L., Phillippy, A., Carlton, J. & Salzberg, S. L. Fast algorithms for large-scale genome alignment and comparison. *Nucleic Acids Res.* **30**, 2478–2483 (2002).
61. Kurtz, S. et al. Versatile and open software for comparing large genomes. *Genome Biol.* **5**, R12 (2004).
62. Arndt, D. et al. PHASTER: a better, faster version of the PHAST phage search tool. *Nucleic Acids Res.* **44**, W16–W21 (2016).
63. Croucher, N. J. et al. Rapid phylogenetic analysis of large samples of recombinant bacterial whole genome sequences using Gubbins. *Nucleic Acids Res.* **43**, e15 (2015).
64. Edgar, R. C. MUSCLE: multiple sequence alignment with high accuracy and high throughput. *Nucleic Acids Res.* **32**, 1792–1797 (2004).
65. Guindon, S. & Gascuel, O. A simple, fast, and accurate algorithm to estimate large phylogenies by maximum likelihood. *Syst. Biol.* **52**, 696–704 (2003).
66. Guindon, S. et al. New algorithms and methods to estimate maximum-likelihood phylogenies: assessing the performance of PhyML 3.0. *Syst. Biol.* **59**, 307–321 (2010).
67. Anisimova, M., Gil, M., Dufayard, J. F., Dessimoz, C. & Gascuel, O. Survey of branch support methods demonstrates accuracy, power, and robustness of fast likelihood-based approximation schemes. *Syst. Biol.* **60**, 685–699 (2011).
68. Gerwig, G. J., Kamerling, J. P. & Vliegthart, J. F. Determination of the absolute configuration of mono-saccharides in complex carbohydrates by capillary G.L.C. *Carbohydr. Res.* **77**, 10–17 (1979).
69. Geiger, T. et al. The stringent response of *Staphylococcus aureus* and its impact on survival after phagocytosis through the induction of intracellular PSMs expression. *PLoS Pathog.* **8**, e1003016 (2012).
70. Bruckner, R. A series of shuttle vectors for *Bacillus subtilis* and *Escherichia coli*. *Gene* **122**, 187–192 (1992).
71. Wang, L. et al. SarZ is a key regulator of biofilm formation and virulence in *Staphylococcus epidermidis*. *J. Infect. Dis.* **197**, 1254–1262 (2008).
72. Kretschmer, D., Rautenberg, M., Linke, D. & Peschel, A. Peptide length and folding state govern the capacity of staphylococcal beta-type phenol-soluble modulins to activate human formyl-peptide receptors 1 or 2. *J. Leukoc. Biol.* **97**, 689–697 (2015).

## Acknowledgements

We thank M. Marschal for clinical *S. epidermidis* strains and strain information; F. Oesterhelt for the help with microscopy; R. Stemmler, P. Kühner and L. Li for phage

propagation and WTA isolation; K. Jakob and H. Käßner for technical support with NMR spectroscopy and chemical composition analysis; R. Rosenstein and D. Gerlach for helpful discussions; A. Tooming-Klunderud for PacBio sequencing of strain E73; A. Schneider for help with LC–MS analysis of strain E73 WTA; J. Y. H. Lee for sending us the strain US06; D. A. Robinson for sending us the strain DAR1907; and J. Doškař for sending us the phage  $\Phi$ PH15. This work was financed by grants from the Deutsche Forschungsgemeinschaft (DFG) SFB766 to C.W., C.M. and A.P.; TRR34 to C.W. and A.P.; TRR156 (project ID 246807620) to A.P.; PE 805/7-1 to A.P.; the German Center of Infection Research to B.K., S.H., C.W. and A.P.; the National Natural Science Foundation of China 81861138043 to M.L.; and the Damp Foundation (HAPDICS project 2013-19) to H.R. B.K., S.H., C.M. and A.P. were supported by infrastructural funding from the Cluster of Excellence EXC 2124 ‘Controlling Microbes to Fight Infections’ (project ID 390838134) from the DFG.

## Author contributions

X.D. conceived the study and performed and analysed most of the bacteriological, molecular and cell culture experiments. J. Larsen performed most of the bioinformatics experiments (with support from M.S.). M.L., A.B. and H.R. collected and typed the *S. epidermidis* strains. M.L. provided important intellectual support and performed the animal experiments with the help of Y.L. and J. Liu. The WTA structure was analysed via MS by A.W. and C.M. and via NMR microscopy by P.M.S.C. and K.A.D. C.S., E.L., J.S. and C.W. contributed to the cell culture experiments. B.K. and S.H. helped with the design of the cloning experiments. V.W. and A.P. conceived and supervised the study.

## Competing interests

The authors declare no competing interests.

## Additional information

**Extended data** is available for this paper at <https://doi.org/10.1038/s41564-021-00913-z>.

**Supplementary information** The online version contains supplementary material available at <https://doi.org/10.1038/s41564-021-00913-z>.

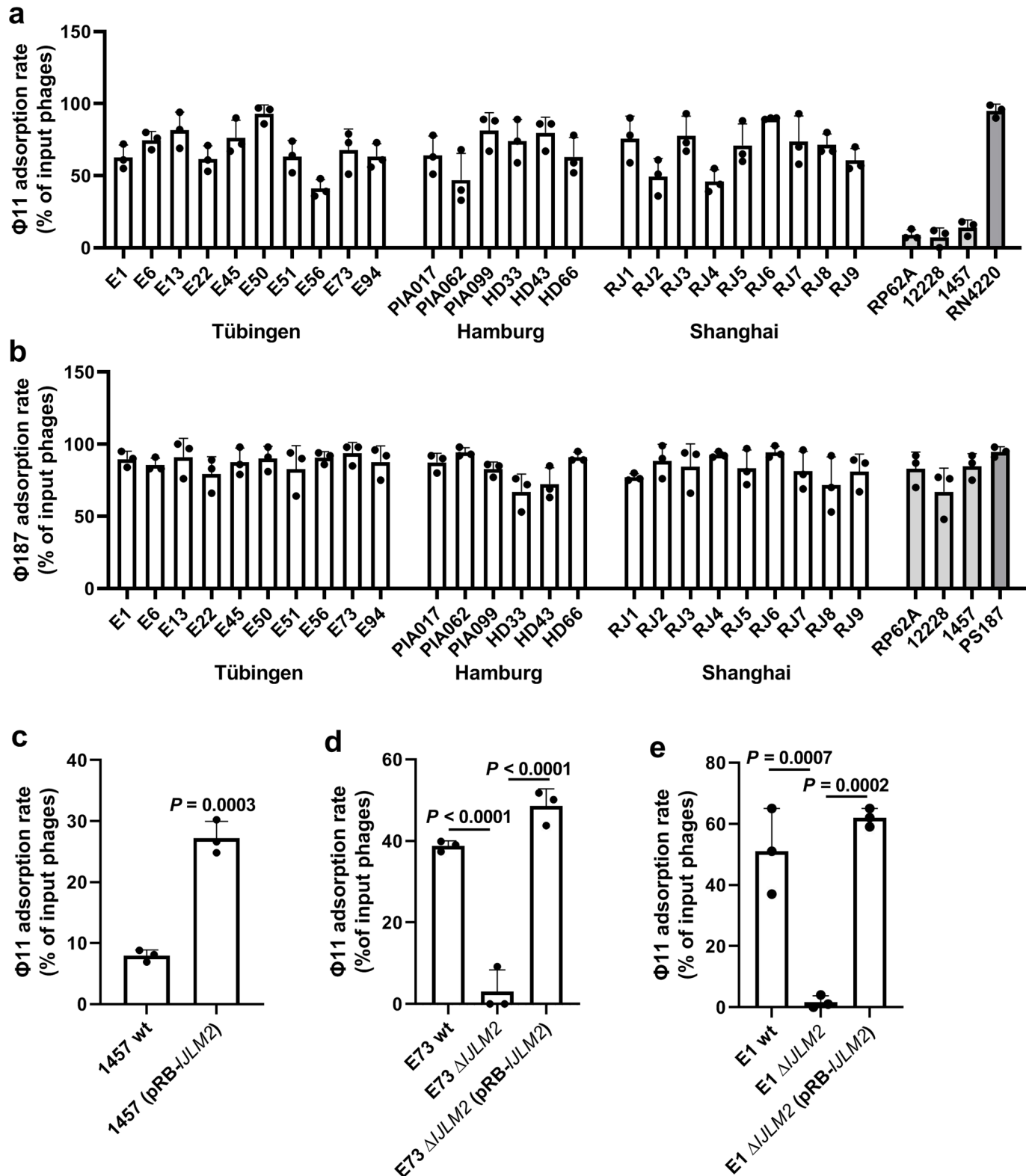
**Correspondence and requests for materials** should be addressed to A.P.

**Peer review information** *Nature Microbiology* thanks Victor Torres, Wilma Ziebuhr and the other, anonymous, reviewer(s) for their contribution to the peer review of this work. Peer reviewer reports are available.

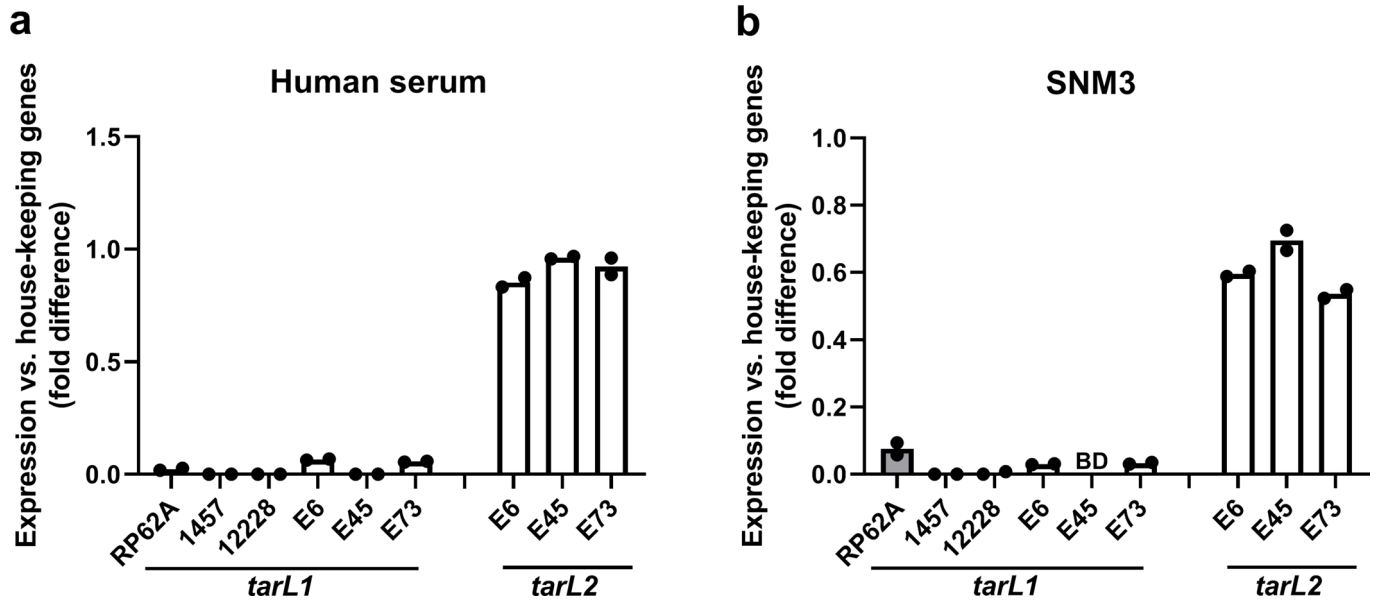
**Reprints and permissions information** is available at [www.nature.com/reprints](http://www.nature.com/reprints).

**Publisher's note** Springer Nature remains neutral with regard to jurisdictional claims in published maps and institutional affiliations.

© The Author(s), under exclusive licence to Springer Nature Limited 2021

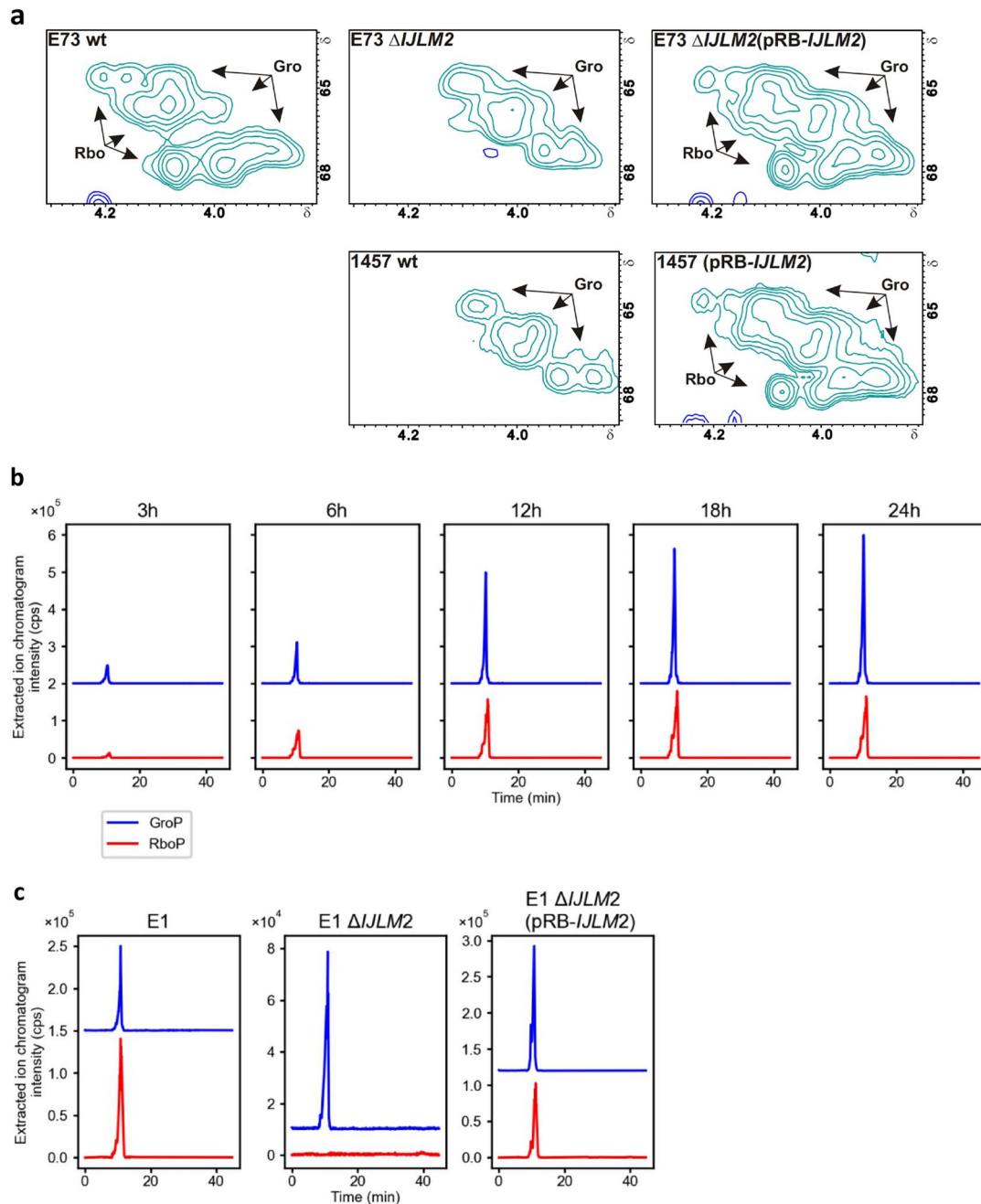


**Extended Data Fig. 1 |** Phage adsorption assay confirms presence of the RboP-WTA phage receptor on *tarJLM2*-positive *S. epidermidis* isolates. The binding rate of RboP-WTA specific phage Φ11 (**a**, **c**, **d**, **e**) and of GroP-WTA specific Φ187 (**b**) to the indicated strains is shown. RP62A, ATCC12228, and 1457 are *S. epidermidis* laboratory strains (light gray), only expressing GroP-WTA. *S. aureus* strains RN4220 or PS187 (dark gray) express RboP-WTA or GroP-WTA, respectively. Means ± s.d. of three independent experiments are shown. One-way ANOVA with Dunnett's post-test (two-sided) was used to analyze significant differences vs. mutant in (**d**) and (**e**). Unpaired *t*-test was used to analyze significant differences between wt and the hybrid strain in (**c**).

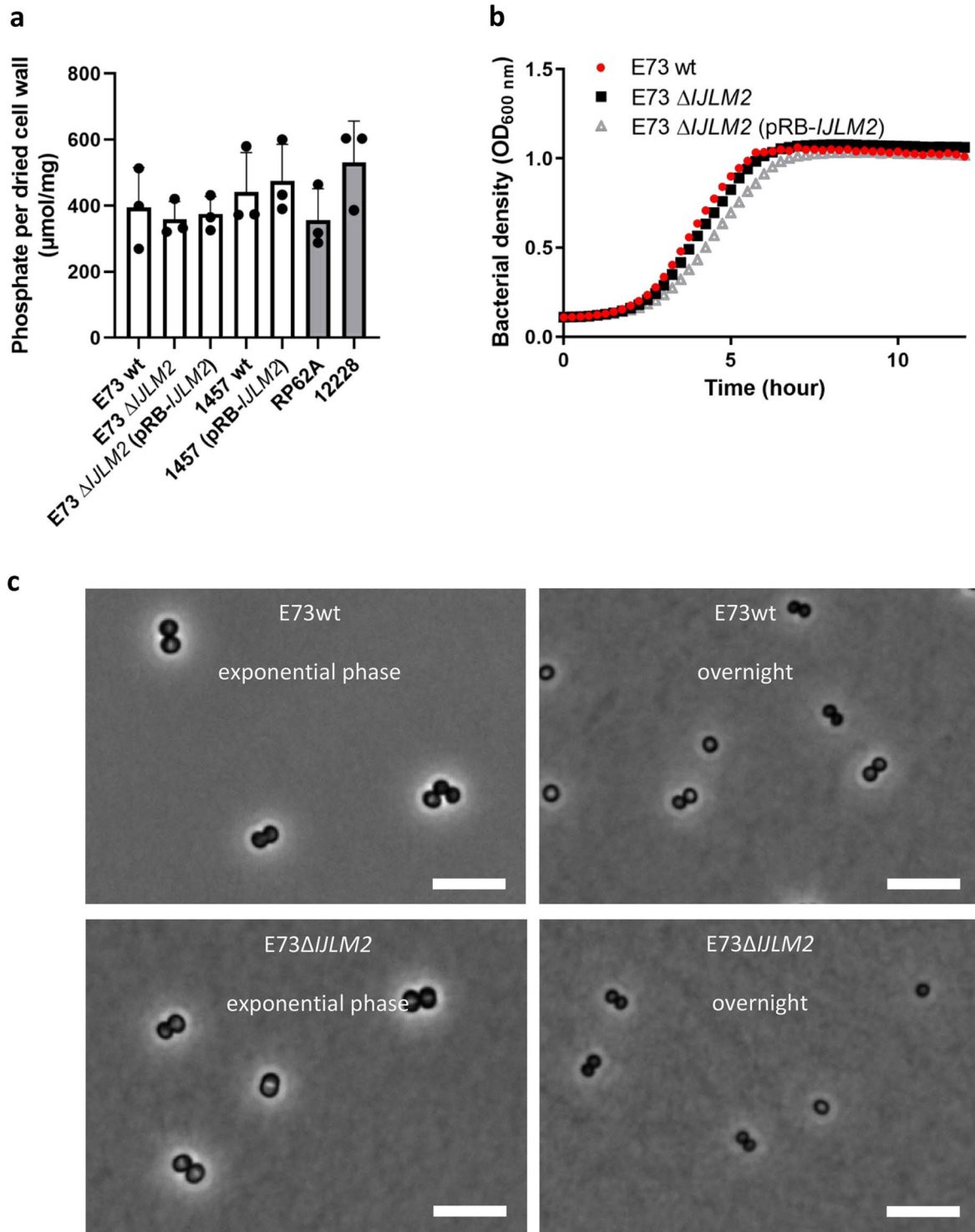


**Extended Data Fig. 2 |** While *tarL2* is efficiently transcribed in the *tarJLM2*-positive isolates E6, E45, and E73, *tarL1* is not or only very weakly expressed in all tested *S. epidermidis* strains during growth in human serum (a) or synthetic nasal medium 3 (SNM3) (b). The control strains RP62A, 1457, and 12228 lack *tarJLM2* and were negative in the PCR reaction. Values represent means of two independent experiments. They were normalized for strongly and constitutively expressed housekeeping genes *gyrB*, *rho*, and *tpiA*. BD, below detection limit.

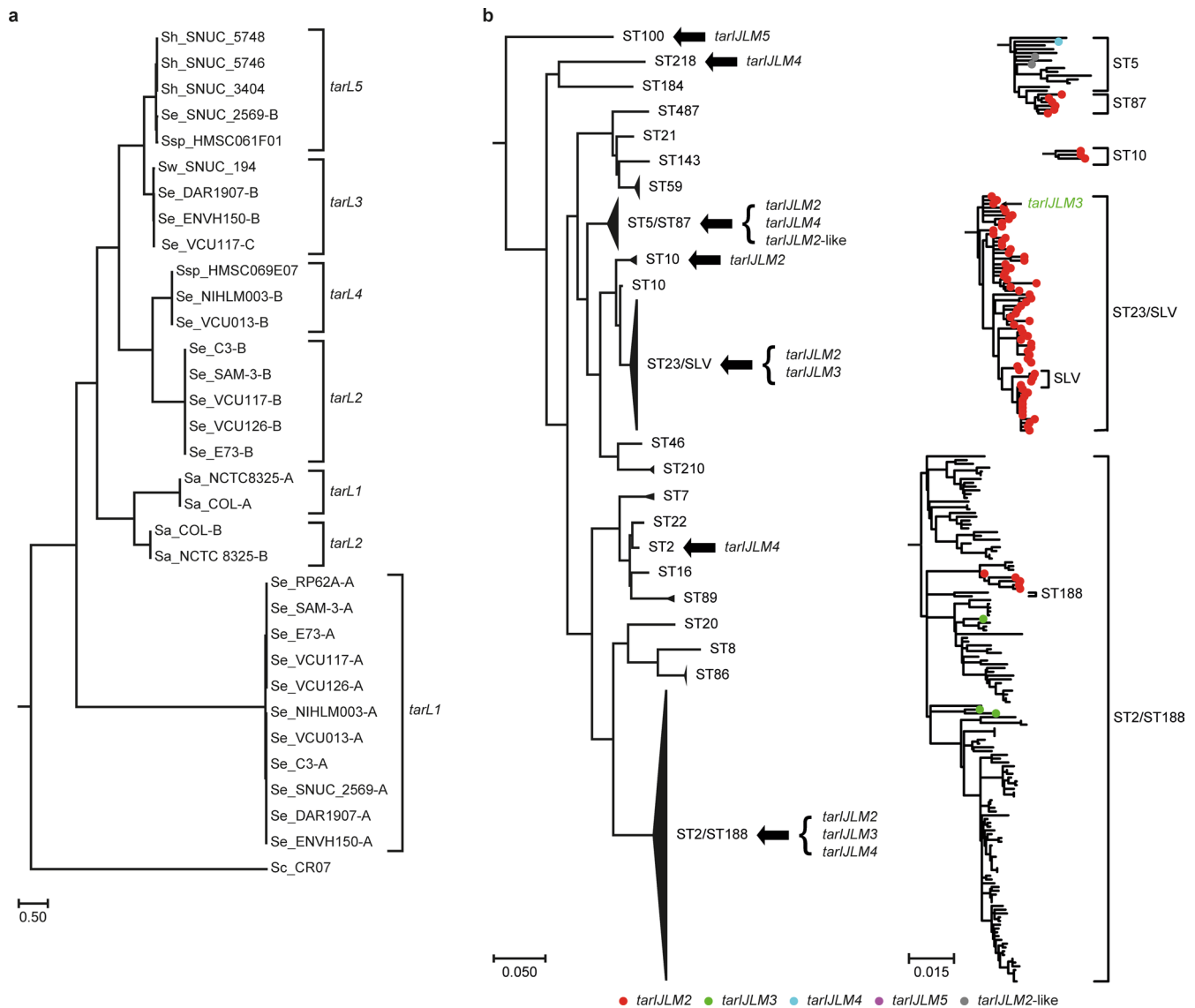




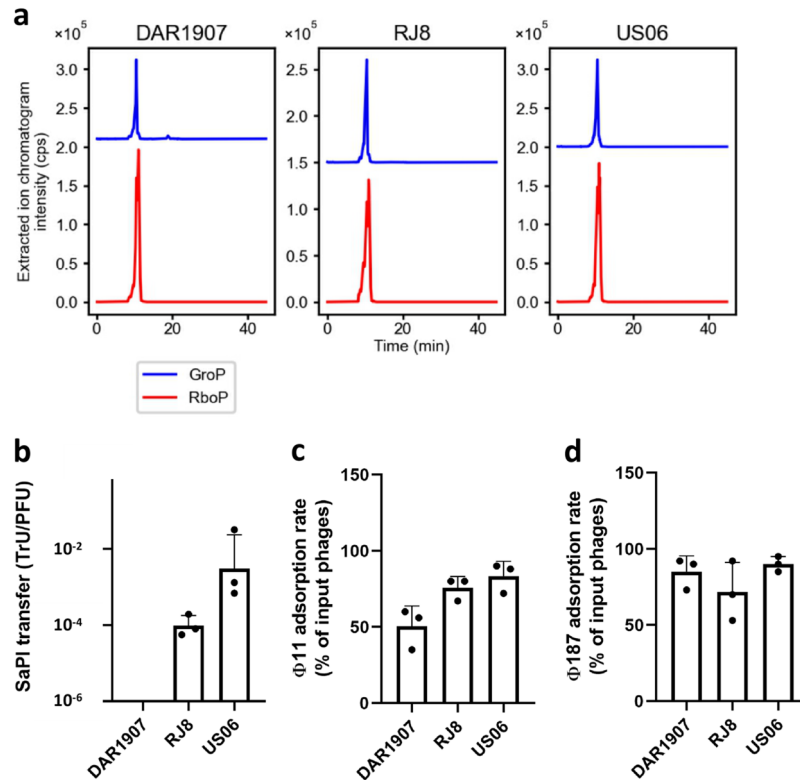
**Extended Data Fig. 3 | NMR and MS spectroscopy confirm that WTA from *tarIJM2*-positive *S. epidermidis* strains contains both, glycerol (Gro) and ribitol (Rbo), while WTA of *tarIJM2*-lacking strains contains only Gro. **a**, Part of the HSQC-DEPT spectra of the methylene region of Rbo/Gro in the poly-RboP/GroP of the indicated WTA samples are shown. Signals corresponding to different substitutions of the polymers are shifted depending on the substitution. The presence of poly-RboP is clearly seen in the case of the WTA samples E73 wild type (wt), E73 $\Delta$ IJLM2 (pRB-IJLM2), and 1457 (pRB-IJLM2) with signals at d 4.13;4.09/65.7, 4.07;3.98/67.8 and 4.20;4.16/64.7 (H/C), which are absent in the case of the other WTA samples. **b**, *S. epidermidis* E73 produces both, GroP (blue lines,  $[M + H]^+ = 173.022$  m/z) and RboP (red line,  $[M + H]^+ = 233.042$  m/z) in different growth phase as shown by LC-MS. **c**, another *tarIJM2*-positive *S. epidermidis* E1 also produces both, GroP (blue lines,  $[M + H]^+ = 173.022$  m/z) and RboP (red line,  $[M + H]^+ = 233.042$  m/z) as shown by LC-MS.**



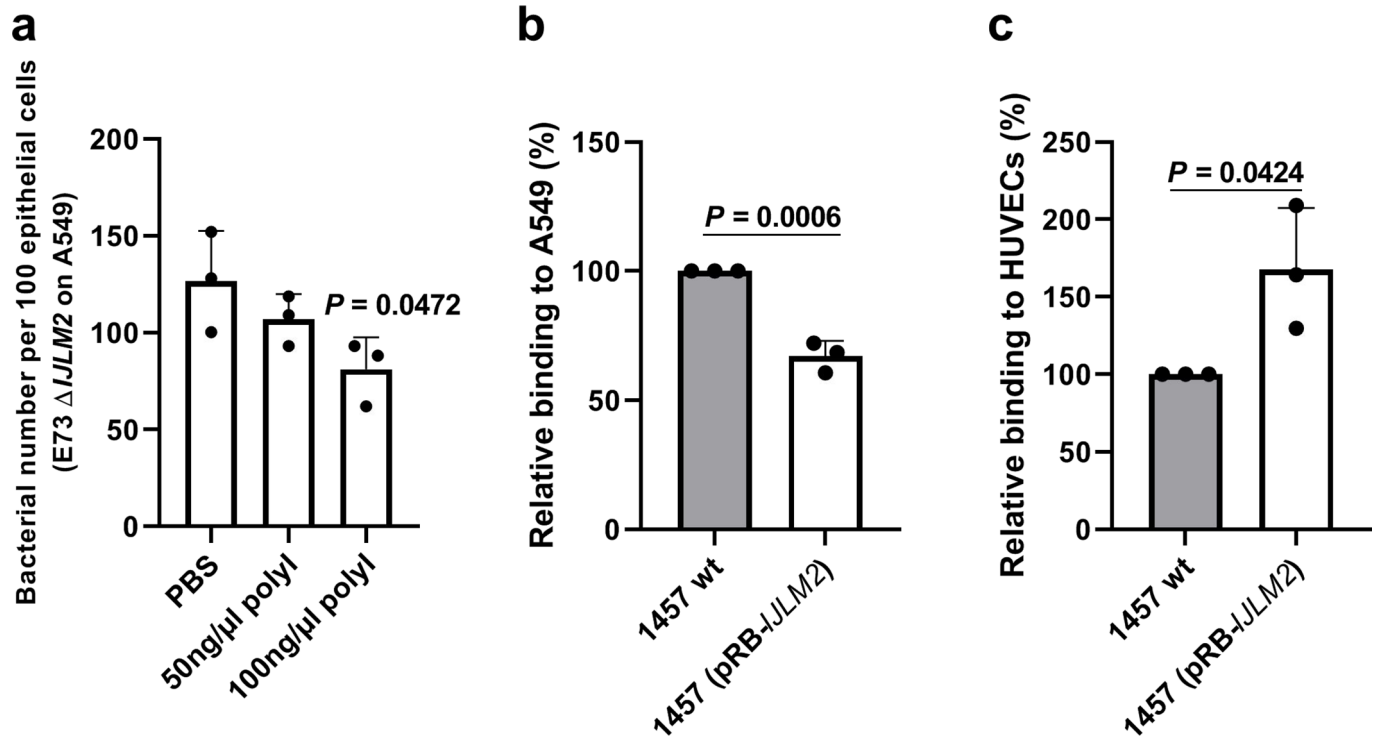
**Extended Data Fig. 4 | RboP-WTA production does not increase the overall WTA amounts and does not affect *S. epidermidis* growth behavior or microscopic appearance.** **a**, Total WTA phosphate amount per cell wall dry weight of the indicated *S. epidermidis* strains. Means  $\pm$  s.d. of three independent experiments are shown. None of the minor differences is significant. **b**, Growth curves of *S. epidermidis* E73 with or without *tarIJLM2* in TSB. Means of three independent experiments are shown. **c**, Microscopic images of E73 with or without *tarIJLM2*. Scale bars: 5  $\mu$ m.



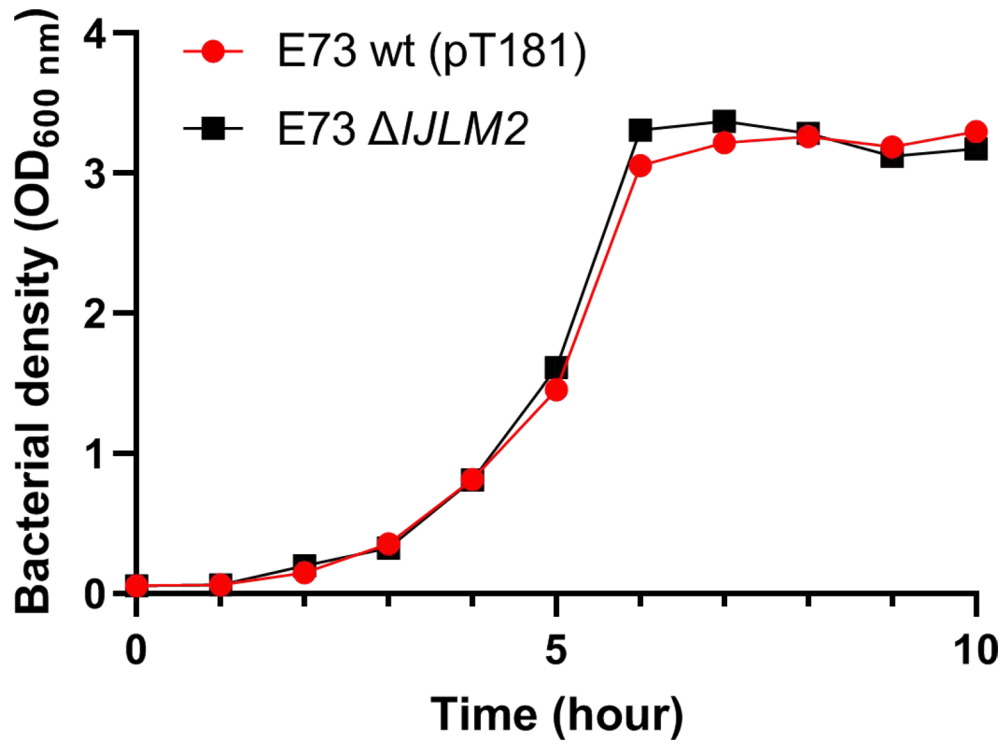
**Extended Data Fig. 5 | Detailed phylogenetic distribution of *tarJLM2-5* among selected *S. epidermidis* clones and evolutionary relation of *tarL* from different gene clusters. **a**, Maximum-likelihood phylogeny of 33 *tarL* genes from representative *S. epidermidis* (Se) and *S. aureus* (Sa) isolates and other *Staphylococcus* spp. isolates that carried *tarJL* with or without *tarM*, including *S. warneri* (Sw), *S. hominis* (Sh), *S. capitis* (Sc), and uncharacterised *Staphylococcus* species (Ssp) (Source Data). The *tarL2* gene found in *S. epidermidis* is more closely related to the two *tarL* genes in *S. aureus* than to *S. epidermidis tarL1*. The *S. epidermidis tarL3*, *tarL4*, and *tarL5* genes, but not *tarL2*, were also found in other *Staphylococcus* species. Phylogenetic reconstruction was carried out using the maximum-likelihood program PhyML with a GTR model of nucleotide substitution, and support for the nodes was assessed using aBayes (see Methods). The tree was midpoint rooted. The scale bar denotes substitutions per variable sites. **b**, Maximum-likelihood phylogeny of 261 *S. epidermidis* isolates, comprising 25 *tarJLM*-positive *S. epidermidis* isolates collected in this study, nine *tarJLM*-positive *S. epidermidis* genomes from in the NCBI Reference Sequence Database (accessed July 3 2018), and a global collection of 227 *S. epidermidis* isolates originating from 96 healthcare institutions across 24 countries<sup>3</sup> was inferred from an alignment of 39,298 single-nucleotide polymorphisms (Supplementary Table 2). Four *tarJLM*-negative isolates (BPH0677, BPH0704, BPH0737, and SEI) were manually removed from the phylogeny due to their extreme divergence, and clades containing isolates with the same or closely related STs were collapsed to reduce complexity. The *tarJLM2* genes in E73 (Fig. 1b) were used as queries in BLASTN searches. The multilocus sequence types (STs) are indicated. Phylogenetic reconstruction was carried out using the maximum-likelihood program PhyML with a GTR model of nucleotide substitution, and support for the nodes was assessed using aBayes (see Methods). The tree was rooted according to work of Lee *et al.*<sup>3</sup> The scale bar denotes substitutions per variable sites. Expanded subtrees illustrate the phylogenetic relationships of isolates belonging to ST5/ST87, ST10, ST23/single-locus variant (SLV), and ST2/ST188. The presence of *tarJLM2-5* is indicated in colors. A single ST23 isolate, VCU117, carried both, *tarJLM2* and *tarJLM3*.**



**Extended Data Fig. 6 | The gene cluster *tarJLM3* and *tarJLM4* lead to RboP-WTA synthesis in HA-MRSE ST2 and ST5 strains.** **a**, The tested *tarJLM3*-positive (DAR1907 and RJ8, both ST2) and *tarJLM4*-positive *S. epidermidis* strains (US06, ST5) contain both, GroP (blue lines,  $[M + H]^+ = 173.022$ ) and RboP (red line,  $[M + H]^+ = 233.042$ ) as WTA constituents; counts per second (CPS) measured by LC-MS are shown. **b**, Transduction with SaPI<sub>bov1</sub> via  $\Phi 11$ . **c**, The binding rate of RboP-WTA-specific phage  $\Phi 11$ . **d**, The binding rate of GroP-WTA-specific phage  $\Phi 187$ . Means  $\pm$  s.d. of three independent experiments are shown in (b-d).



**Extended Data Fig. 7 | RboP-WTA impairs *S. epidermidis* 1457 binding to A549 but promotes its binding to HUVECs. a**, The scavenger receptor inhibitor polyinosinic acid (poly-I) inhibits the increased binding of *S. epidermidis* E73 $\Delta$ JLM2 to A549. **b**, RboP-WTA production in the GroP-WTA *S. epidermidis* 1457 decreases its binding to the human airway epithelial cell line A549 but promotes its binding to HUVECs (**c**). Means  $\pm$  s.d. of three independent experiments are shown in (**a-c**). One-way ANOVA with Dunnett's post-test (two-sided) was used to analyze significant differences vs. PBS condition in (**a**). Significant differences ( $P \leq 0.05$ ) were calculated by unpaired t-test between wt and the hybrid strain in (**b**) and (**c**).



**Extended Data Fig. 8** | The presence of plasmid pT181 does not affect the growth behavior of *S. epidermidis* E73 wild type (wt) compared to E73 $\Delta$ I/LM2. The indicated bacterial strains were grown in TSB medium. Means of two independent experiments are shown.

## Publication 6

Vollmer, B., Steblau, N., Ladwig, N., Mayer, C., Macek, B., Mitousis, L., Sigle, S., **Walter, A.**, Wohlleben, W., & Muth, G. (2019). Role of the *Streptomyces* spore wall synthesizing complex SSSC in differentiation of *Streptomyces coelicolor* A3 (2). *International Journal of Medical Microbiology*, 309(6), 151327.



## Role of the *Streptomyces* spore wall synthesizing complex SSSC in differentiation of *Streptomyces coelicolor* A3(2)

B. Vollmer<sup>a</sup>, N. Steblau<sup>a</sup>, N. Ladwig<sup>a</sup>, C. Mayer<sup>a</sup>, B. Macek<sup>b</sup>, L. Mitousis<sup>a</sup>, S. Sigle<sup>a</sup>, A. Walter<sup>a</sup>, W. Wohlleben<sup>a</sup>, G. Muth<sup>a,\*</sup>

<sup>a</sup> Interfakultäres Institut für Mikrobiologie und Infektionsmedizin Tuebingen IMIT, Mikrobiologie/Biotechnologie, Eberhard Karls Universität Tuebingen, Auf der Morgenstelle 28, 72076, Tuebingen, Germany

<sup>b</sup> Proteome Center Tuebingen, Interfakultäres Institut für Zellbiologie, Eberhard Karls Universität Tuebingen, Auf der Morgenstelle 15, 72076 Tübingen, Germany



### ARTICLE INFO

#### Keywords:

Sporulation  
Cell envelope  
eSTPK  
Phosphorylation  
Cell wall glycopolymers

### ABSTRACT

A crucial stage of the *Streptomyces* life cycle is the sporulation septation, a process where dozens of cross walls are synchronously formed in the aerial hyphae in a highly coordinated manner. This process includes the remodeling of the spore envelopes to make *Streptomyces* spores resistant to detrimental environmental conditions. Sporulation septation and the synthesis of the thickened spore envelope in *S. coelicolor* A3(2) involves the *Streptomyces* spore wall synthesizing complex SSSC. The SSSC is a multi-protein complex including proteins directing peptidoglycan synthesis (MreBCD, PBP2, Sfr, RodZ) and cell wall glycopolymer synthesis (PdtA). It also includes two eukaryotic like serin/threonine protein kinases (eSTPK), PkaI and PkaH, which were shown to phosphorylate MreC. Since unbalancing phosphorylation activity by either deleting eSTPK genes or by expressing a second copy of an eSTPK gene affected proper sporulation, a model was developed, in which the activity of the SSSC is controlled by protein phosphorylation.

### 1. Introduction

*Streptomyces* are Gram-positive soil dwelling bacteria that are distinguished from most other bacteria by their mode of growth and their complex life cycle. A germinating spore develops one or two germ tubes which elongate by apical tip extension. Under optimal conditions the tips grow at a rate of  $20 \mu\text{m h}^{-1}$  (Jyothikumar et al., 2008). Peptidoglycan (PG) incorporation at the tips is directed by the polarisome composed of the cytoskeletal proteins DivIVA, Scy and FilP (Fuchino et al., 2013). In a distance of 10–40  $\mu\text{m}$  to the tip new branching points are established by small DivIVA clusters that splitted off from the tip assemblies. As the multiply branched mycelium develops, vegetative septal cross walls are built at irregular distances, often close to branching points (Flardh, 2003; Flardh et al., 2012; Richards et al., 2012).

Upon partial nutrient limitation, *Streptomyces* enters the next stage of its life cycle. Controlled by multiple *bld* genes (for bald, unable to form aerial hyphae), so-called aerial hyphae are formed on the surface (Flardh and Buttner, 2009; Salerno et al., 2013). The aerial hyphae are

unbranched and usually evade from the vegetative mycelium by growing into the air, although some species, like *S. venezuelae* and *S. griseus* are able to differentiate in liquid culture (Schlimpert et al., 2016). The membranes of aerial hyphae are equipped with bacterial sterols, the hopanoids, unlike those of vegetative hyphae, probably to resist oxygen stress (Poralla et al., 2000). To lower the surface tension, the aerial mycelium is covered by an amyloid layer of hydrophobic proteins consisting of rodlin and chaplins, which self-aggregate to characteristic rodlet structures (Claessen et al., 2004; Elliot et al., 2003). A hierarchic cascade of *whi* genes, encoding several transcriptional regulators control initiation of multiple cell division events and conversion of aerial hyphae into spore chains (Kelemen and Buttner, 1998; Bush et al., 2015). Replication of the chromosome is upregulated, generating multi-genomic aerial hyphae (Ruban-Ośmiałowska et al., 2006). Then, positioned by SsgB, the bacterial tubulin homolog FtsZ assembles to cytokinetic Z-rings at regular intervals (Willemse et al., 2011). FtsZ rings are stabilized by two dynamin-like proteins, DynA and DynB, and the stabilization of the newly formed Z-rings is crucial for completion of septum synthesis (Schlimpert et al., 2017). Proper

**Abbreviations:** PG, Peptidoglycan; CWG, Cell Wall Glycopolymer; PDP, Polydiglycosylphosphate; Kdn, 2-keto-3-deoxy-D-glycero-D-galacto-nononic acid; Gal, Galactose; MurNAc, N-acetylmuramic acid; GlcNAc, N-acetylglucosamine; BACTH, Bacterial Adenylate Cyclase based Two-Hybrid system; eSTPK, eukaryotic like serin/threonine protein kinase

\* Corresponding author.

E-mail address: [gmuth@biotech.uni-tuebingen.de](mailto:gmuth@biotech.uni-tuebingen.de) (G. Muth).

<https://doi.org/10.1016/j.ijmm.2019.07.001>

Received 28 December 2018; Received in revised form 2 July 2019; Accepted 7 July 2019

1438-4221/© 2019 Elsevier GmbH. All rights reserved.



synthesis of the sporulation septa and the spore envelope involves in addition further cytoskeletal proteins, the actin homologues MreB and Mbl (Heichlinger et al., 2011). With the help of ParAB, FtsK, the FtsK-like SffA and SmeA, which localizes SffA to the sporulation septa, the multiple chromosome copies segregate into the spore compartments (Wang et al., 2007; Ausmees et al., 2007; Jakimowicz et al., 2005). After thickening of the spore envelope uninucleoid spores are released, giving rise to a new life cycle.

## 2. Identification of genes involved in sporulation of *S. coelicolor* A3(2)

Like other streptomycetes, *S. coelicolor* A3(2) contains an *mre* gene cluster, encoding the key components of the lateral wall synthesizing complex for elongation growth of rod-shaped bacteria (Divakaruni et al., 2007): MreB, MreC, MreD, PBP2, and the FtsW-like SEDS (*shape, elongation, division, and sporulation*) family protein Sfr (Kleinschnitz et al., 2011a; Mazza et al., 2006). FtsW was recently shown to act as a PG-polymerase, thereby forming a complex with its partner PBP to polymerize lipid II into PG (Meeske et al., 2016; Taguchi et al., 2019). The actin-like MreB forms discrete small structures along the bacterial cell membrane that move independently around the cell circumference (Dominguez-Escobar et al., 2011; Garner et al., 2011). These MreB patches coordinate location of extracytoplasmic cell wall synthesis via interaction with the transmembrane linker RodZ (Morgenstein et al., 2015). Although the depletion phenotype of *mreC* and *mreD* is similar to that of *mreB*, the molecular function of MreC and MreD in elongation growth is still mysterious (Kruse et al., 2005).

The “rod-shape-determining” *mre* genes of *S. coelicolor* A3(2) have a specific role in proper sporulation, but are dispensable for vegetative growth (Kleinschnitz et al., 2011a; Mazza et al., 2006, Burger et al., 2000). Spores of single mutants were sensitive to detrimental environmental conditions, like heat, desiccation, high osmolarity, or cell wall damage by lysozyme or vancomycin, indicating that the integrity of the spore envelope was impaired. Moreover, fusion proteins of MreB and the MreB-like protein Mbl of *S. coelicolor* A3(2) were localized to sites of spore wall synthesis during the conversion of aerial hyphae into spore chains (Heichlinger et al., 2011). These data suggested that the Mre proteins, which direct PG incorporation at the lateral wall during elongation growth of rod-shaped bacteria have a different role in *Streptomyces* than in other bacteria and are involved in the synthesis of the thickened spore envelope. Since the *Streptomyces* MreBCD, PBP2, and Sfr proteins show a similar protein-protein interaction pattern as their homologues from rod-shaped bacteria, the term “*Streptomyces* spore wall synthesizing complex (SSSC) was coined in analogy to the “lateral wall synthesizing complex” of rod-shaped bacteria (Kleinschnitz et al., 2011a).

To identify additional genes involved in the morphological differentiation of *S. coelicolor* A3(2), two distinct strategies were applied: i. Identification of interaction partners of SSSC proteins by bacterial two-hybrid analyses and ii. transposon mutagenesis.

## 3. Identification of additional SSSC proteins by bacterial two-hybrid analyses

Genomic libraries of *S. coelicolor* A3(2), generated either by enzymatic digest (Kleinschnitz et al., 2011a) or nebulization (Mehari and Muth, unpublished) of M145 DNA were screened with the Bacterial Adenylate Cyclase based Two-Hybrid system (BACTH, Karimova et al., 1998) for interaction partners of MreB, MreC, MreD, PBP2, Sfr, and RodZ (Kleinschnitz et al., 2011a, Mitousis and Muth, unpublished). Only for MreB, known to be poorly interacting in BACTH analyses (Formstone et al., 2008), no interaction partner was found. However, screening of the library with the other SSSC proteins delivered multiple interaction partners. Some of the interacting protein fragments were even fished with different bait proteins (Table 1). Many of these Mre-

interaction partners have a role in proper sporulation, as it was demonstrated by gene inactivation studies. Deletion of *SCO1403*, *SCO2097*, *SCO2584*, *SCO6494*, or *SCO2578* (*pdta*), originally annotated as hypothetical protein encoding genes and *SCO4778*, encoding the eukaryotic type serine/threonine kinase (eSTPK) PkaI, interfered with proper sporulation. In all mutants, spore chains were formed that contained irregular sized spores and spores with impaired integrity of the spore envelope (Muth, unpublished, Sigle et al., 2016a; Kleinschnitz et al., 2011a, b; Ladwig et al., 2015). Thus, the mutant phenotype validated the strategy to identify novel differentiation proteins via protein-protein-interactions with already known differentiation proteins and expanded the composition of the SSSC and its activities (see below).

Since the C-terminal end (PkaI<sub>257-357</sub>) of the eSTPK PkaI was one of the most frequently fished prey polypeptides and was caught with MreC (8x), MreD (5x), PBP2 (1x), Sfr (6x), and RodZ (2x), a prominent role of PkaI in sporulation was suggested. A BACTH search for binding partners of the PkaI<sub>257-357</sub> interaction domain again revealed multiple proteins (Fig. 1, Table 1). The PkaI<sub>257-357</sub> interaction partners included BldB, AfsQ1, CrgA, or FtsH, which have a well-documented role in differentiation (Del Sol et al., 2003; Eccleston et al., 2002; Shu et al., 2009). Also, proteins were identified that were previously fished with one of the Mre proteins (e.g. *SCO2097*, *SCO1403*, *SCO3110*, *SCO6494*, *SCO3754*) (Ladwig et al., 2015). Moreover, the eSTPKs PkaD (*SCO4777*), encoded immediately next to *pkaI*, PkaI, and PkaA (*SCO2974*) were detected among the PkaI<sub>257-357</sub> interacting proteins.

In total, the BACTH screen identified several classes of interaction partners, revealing novel aspects of *Streptomyces* differentiation:

### 3.1. ABC-transporters

Strikingly, the SSSC seems to contain multiple (sugar) transporter proteins, in particular binding-protein-dependent transporters containing a Pfam BPD\_transp\_1 domain (*SCO1057* (UgbA), *SCO1064*, *SCO4141* (PstA), *SCO5119*, *SCO5322* (DasB), and *SCO5774* (GluD)). The ability to metabolize different sugars was already shown to influence differentiation and involvement of ABC transporters in proper sporulation of *Streptomyces* is well-documented (Colson et al., 2008; Nothhaft et al., 2010; Seo et al., 2002; Ma and Kendall, 1994). Most interestingly were *SCO3110* and *SCO3754*, which both were detected by their interaction with MreC and PkaI. *SCO3110* contains doubled MacB\_PCD (MacB-like periplasmic core domain) and FtsX domains, while *SCO3754* contains a single MacB\_PCD and two FtsX domains (Fig. 2). MacB is an antibiotic exporter that is distinguished from other ABC transporters in its transmission mechanism (Crow et al., 2017). MacB does not possess a central pore through which substrates might be passed, but operates through extracytoplasmic conformational change driven by cytoplasmic ATP hydrolysis. FtsEX was shown to be crucial for divisome assembly by forming a substrate-less ABC transporter involved in transmembrane signaling between cytoplasmic and periplasmic components of the cell division machinery in Gram-negative bacteria (Du et al., 2016).

### 3.2. Novel morphogenic proteins

*SCO2097* was isolated from the genomic library with RodZ, MreC, MreD, and with Sfr (Kleinschnitz et al., 2011a). Additionally, *SCO2097* interacted with the penicillin binding proteins PBP2, *SCO3580*, *SCO3901* and FtsI. *SCO2097* encodes a signature protein, only occurring in actinomycetes and is located in the *ftsI* and *ftsZ* containing *division and cell wall cluster* (*dcw*). Although the exact function of the 135 aa membrane protein *SCO2097* still has to be elucidated, the mutant phenotype indicating an impaired spore wall supported a role of *SCO2097* in proper sporulation (Kleinschnitz et al., 2011a). *SCO1403*, interacting with RodZ, MreC and PkaI and *SCO6494*, interacting with MreD and PkaI encode membrane proteins of unknown function. Both genes were deleted from the chromosome of M145. The respective

**Table 1**Interaction partners of SSSC proteins identified by BACTH screening of *S. coelicolor* A3(2) genomic libraries\*.

tag (protein) <sup>§</sup>	region (aa)	putative function	bait protein (isolation frequency)
<b>ABC- transporter</b>			
SCO1057 (UgpA)	24-108	ABC sugar permease,	MreC
SCO1058 (UgpE)	1-70	ABC transporter subunit	PkaI <sub>257-357</sub>
SCO1064	113-149	sugar transporter subunit	PBP2
SCO3110	431-473	ABC-transporter subunit	MreC, PkaI <sub>257-357</sub>
SCO3110	1-96	ABC transport system	MreC (2)
SCO3754	1-197	ABC transporter subunit	MreC, MreD (5),
SCO3754	1-184	ABC transporter subunit	PkaI <sub>257-357</sub>
SCO4141 (PstA)	255-336	phosphate ABC transport permease	PkaI <sub>257-357</sub>
SCO5119	8-94	ABC oligopeptide transporter	MreC
<b>SCO5233 (DasB)</b>	73-99	ABC Transporter	MreC
SCO5774 (GluD)	1-102	glutamate permease	MreC
<b>Protein phosphorylation</b>			
SCO2974 (PkaA)	474-523	eSTPK	MreC, PkaI <sub>257-357</sub> (2)
SCO3860	98-116	eSTPK	MreC
<b>SCO4777 (PkaD)</b>	400-548	serine/threonine protein kinase	PkaI <sub>257-357</sub> (2)
<b>SCO4778 (PkaI)</b>	257-357	eSTPK	Sfr (6), RodZ (2), PBP2, MreD (5), MreC (8), PkaI <sub>257-357</sub>
SCO7326 (RsbU)	772-824	serine/threonine phosphatase	PkaI <sub>257-357</sub>
<b>Cell wall synthesis / differentiation</b>			
<b>SCO2097</b>	21-120	membrane protein	MreD (6), RodZ (3), Sfr (29), PkaI <sub>257-357</sub> (35)
<b>SCO1403</b>	33-143	integral membrane protein	RodZ, MreC, PkaI <sub>257-357</sub> (5)
<b>SCO2578 (PdtA)</b>	176-246	LCP-CWG transferase	MreC (3), MreD (2)
<b>SCO2584</b>	145-228	membrane protein	MreC (3), Sfr
SCO2897	20-116	probable secreted PBP	PkaI <sub>257-357</sub>
<b>SCO3854 (CrgA)</b>	1-84	septation inhibitor protein	PkaI <sub>257-357</sub>
<b>SCO4129 (CmdD)</b>	51-108	sporulation	MreC
SCO4641	141-398	efflux protein, close to <i>murB</i>	PkaI <sub>257-357</sub>
<b>SCO4907 (AfsQ1)</b>	122-225	pleiotropic transcriptional regulator	PkaI <sub>257-357</sub>
SCO5039	608-716	bifunctional penicillin binding protein	MreC
<b>SCO5587 (FtsH)</b>	12-91	cell division protein	PkaI <sub>257-357</sub>
<b>SCO5723 (BldB)</b>	1-98	pleiotropic regulator of differentiation	PkaI <sub>257-357</sub>
SCO6374	215-257	bactoprenyl sugar transferase	MreC
SCO6374	298-478	bactoprenyl sugar transferase	PkaI <sub>257-357</sub>
<b>SCO6494</b>	27-205	membrane protein	MreD, PkaI <sub>257-357</sub> (2)
<b>Others</b>			
SCO3218	20-71	<i>mbtH</i> -like, Cda cluster	PkaI <sub>257-357</sub>
SCO3598	1-254	CPBP family metalloprotease	MreC
SCO4155	36-156	two component sensor protein	PBP2 (2), RodZ
SCO4597	1-249	two component sensor protein	MreC, MreD
SCO7048	13-306	delta fatty acid desaturase	MreD (5), PBP2
<b>Hypothetical proteins</b>			
SCO1385	1-246	hypothetical protein	Sfr
SCO1465	1-252	putative secreted protein	PkaI <sub>257-357</sub>
SCO1610	129-176	hypothetical membrane protein	MreC
SCO1994	32-110	integral membrane protein	PBP2
SCO1829	27-96	putative membrane protein	PkaI <sub>257-357</sub> (2)
SCO2124	139-202	membrane protein	MreC (2), Sfr
SCO2169	61-212	putative integral membrane protein	PkaI <sub>257-357</sub> (2)
SCO2187	29-213	conserved hypothetical protein	MreD
SCO2255	13-178	putative membrane protein	PkaI <sub>257-357</sub>
SCO2520	1-219	hypothetical protein	PBP2
SCO3146	9-58	putative secreted protein	PkaI <sub>257-357</sub>
SCO3513	1-169	secreted protein	RodZ (2), Sfr, PBP2 (3)
SCO3927	19-199	membrane protein	MreD
SCO3940	1-238	putative transmembrane protein	PkaI <sub>257-357</sub>
SCO4369	1-168	hypothetical protein	MreC
SCO4431	1-169	putative integral membrane protein	PkaI <sub>257-357</sub> (3)
SCO4732	13-286	membrane protein	MreC
SCO4811	390-438	hypothetical membrane protein	MreC
SCO4825	33-178	integral membrane protein	MreC, PBP2 (2)
SCO4846	236-307	putative integral membrane protein	PkaI <sub>257-357</sub>
SCO5013	1-129	putative secreted protein	PkaI <sub>257-357</sub> (3)
SCO5142	1-119	secreted protein	MreC, RodZ, Sfr
SCO5148	114-306	putative membrane protein	PkaI <sub>257-357</sub>
SCO5485	1-91	small hydrophobic membrane protein	PkaI <sub>257-357</sub>
SCO5935	41-278	putative membrane protein	PkaI <sub>257-357</sub>
SCO5993	49-144	putative membrane protein	PkaI <sub>257-357</sub>
SCO6002	44-142	hypothetical membrane protein	MreC
SCO6074	4-203	putative integral membrane protein	PkaI <sub>257-357</sub>
SCO6614	1-206	putative membrane protein	PkaI <sub>257-357</sub>
SCO6771	1-39	small hydrophobic secreted protein	RodZ, Sfr
SCO6899	1-251	membrane protein	RodZ, Sfr, PBP2, PkaI <sub>257-357</sub>
SCO7090	324-472	hypothetical membrane protein	MreC (2)
SCO7199	36-131	hypothetical membrane protein	MreC

(continued on next page)

Table 1 (continued)

tag (protein) <sup>§</sup>	region (aa)	putative function	bait protein (isolation frequency)
SCO7454	1-261	membrane protein	MreC
SCO7482	1-133	putative integral membrane protein	PkaI <sub>257-357</sub>

\* black letters indicate library generated by a partial Sau3A digest, grey letters mark a library containing nebulized DNA fragments.

§ bold letters indicate that the role in morphological differentiation is supported by experimental data.

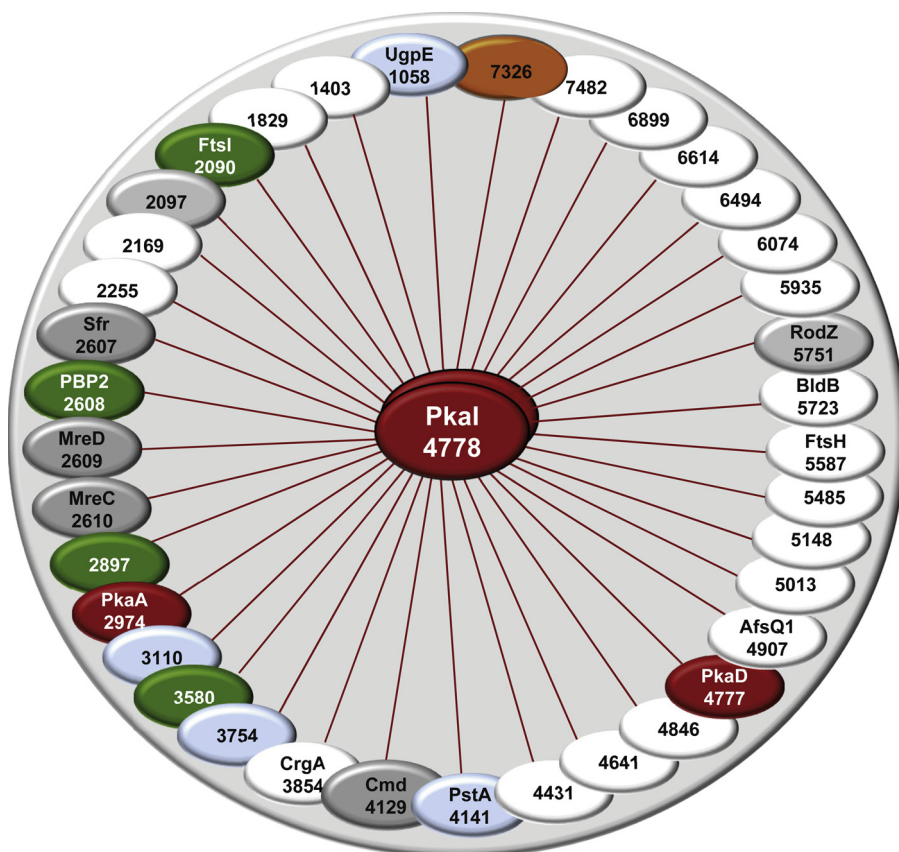


Fig. 1. Interaction pattern of PkaI. Interaction partners of the PkaI<sub>257-357</sub> interaction domain were identified by the screening of a genomic library with the bacterial two-hybrid system. SSSC proteins are shown in grey, ABC transporters in light blue, penicillin binding proteins in green, Ser/Thr protein kinases in red, and the putative Ser/Thr phosphatase SCO7326 in orange. The numbers refer to the SCO-numbers of the proteins. Self-interactions are indicated by double ellipses.

mutants were impaired in proper differentiation and formed aberrant spore chains containing non-viable spores, a phenotype characteristic for SSSC mutants (Muth et al., unpublished results).

### 3.3. Proteins involved in cell wall glycopolymer synthesis

Two of the proteins, SCO2578 and SCO2584 were predicted to be involved in the synthesis of cell wall glycopolymers (CWG), due to the location of the respective genes next to putative CWG genes. While SCO2584 represents an uncharacterized membrane protein, SCO2578 contains a LytR\_cpsA\_psr domain and is a predicted TagV homologous

transferase, which anchors CWGs to the PG layer (see below). Inactivation of both genes resulted in the formation of aberrant spores with impaired spore envelopes (Kleinschnitz et al., 2011b; Sigle et al., 2016a).

### 4. Identification of novel differentiation genes by random transposon mutagenesis of *S. coelicolor* A3(2)

Most of the previously isolated differentiation mutants had quite severe defects causing white (*whi*) and bald (*bld*) phenotypes (Kelemen and Buttner, 1998; Bush et al., 2015). The mutants affected in SSSC

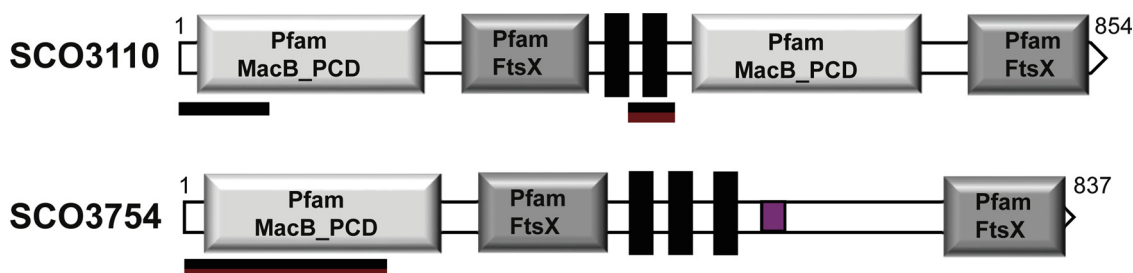


Fig. 2. Domain architecture of two uncommon ABC transporter components identified by their protein-protein interaction with MreC and PkaI. Domain architecture was determined with SMART (<http://smart.embl-heidelberg.de/>). The interacting regions with MreC (black) and PkaI (red) are indicated by horizontal bars. Regions of low compositional complexity are indicated in pink.

genes had been overseen in these previous screens, since their minor defect, aberrant spores with an impaired spore envelope, has no dramatic consequences for the colony morphology (Kleinschnitz et al., 2011, Ladwig et al., 2015).

To identify additional genes involved in morphological differentiation of *S. coelicolor* A3(2), transposon mutagenesis was performed (Muth et al., unpublished results). The transposon delivery vector pHL734 (Xu et al., 2017) was introduced into M145 protoplasts, yielding about 25.000 apramycin resistant transformants, where the mini-transposon consisting of the *E. coli* ori<sub>pMB1</sub>, the apramycin resistance gene *aac(3)IV*, and the recognition sites of the hyperactive Tn5 transposase has been inserted in the M145 genome. Transformants with altered colony morphology were directly picked from the transformation plates. Moreover, spores from the transformation plates were harvested and plated to single colonies on MS agar supplemented with 10.3% sucrose. Supplementation with 10.3% sucrose causes osmotic stress, which increases possible morphological defects. Colonies with aberrant morphology (e.g. retarded sporulation) were picked after 4 days of growth. To determine the transposon insertion sites, total DNA was isolated from ~ 120 colonies and digested with the restriction endonuclease SalI, which does not cut within the mini transposon. After religation and transformation of *E. coli*, the plasmids isolated from apramycin resistant transformants were sequenced with primers corresponding to the ends of the transposon (Thoma and Muth, unpublished). Surprisingly, about 10% of the transposon mutants were cointegrates, where the whole pHL734 plasmid had been inserted. This was unexpected, since Tn5 is known to “jump” via a cut-and-paste mechanism, not involving the formation of cointegrates (Reznikoff, 2008). Since in these mutants, the present transposase could cause secondary mutations by subsequent transposition events, these mutants were excluded from further analyses. The other mutants (Table 2) revealed interesting aspects of *Streptomyces* sporulation.

Several mutants were obtained which had a transposon insertion in genes already reported to be involved in sporulation, e.g. the regulatory *wblA*, *devA*, *adpA*, or *abrA1* genes. Quite unexpectedly and not detected in previous screenings for differentiation mutants, many mutants had insertions in nucleotide biosynthesis genes, e.g. *SCO1483* (*pyrA*) or *SCO1485*. Independent transposon insertions at three distinct positions were found in *SCO1486* (*pyrC*). Also purine biosynthesis was frequently a target, and transposon insertions affecting proper sporulation were observed at two positions in *purL* (*SCO4079*), in *purM* (*SCO4087*), and in *purH* (*SCO4814*). Since chromosome replication is highly upregulated during the outgrowth of the aerial hyphae (Ruban-Osmiałowska et al., 2006), it is conceivable that defects in nucleotide metabolism affect differentiation.

Interestingly, one of the transposon mutants affected in proper sporulation had an insertion in *SCO3110*, a gene previously identified in the BACTH screens (Table 1). The interaction with MreC and PkaI, the isolation from two independent BACTH libraries, as well as the impaired sporulation efficiency of the transposon insertion suggests a prominent role of *SCO3110* in differentiation. The *SCO3110/3111* transporter seems to be redundant in *S. coelicolor* A3(2), since *SCO3089/3090* and *SCO1031/1032* encode highly similar transporters. *SCO3110* was also identified by Hesketh et al., in a screen for *S. coelicolor* A3(2) genes becoming upregulated by antibiotics targeting cell wall synthesis (Hesketh et al., 2011). In this study, *SCO3110/3111* was 30-fold upregulated (together with *SCO3089/3090*). Whereas single mutants of these transporters showed a weak effect on bacitracin resistance, the double mutant strain exhibited markedly increased susceptibility to bacitracin, indicating a redundant function of these transporters in proper cell wall synthesis (Hesketh et al., 2011).

Three transposon insertions affecting sporulation were found in genes encoding putative exopolysaccharide phosphotransferases (*SCO2592*, *SCO2594*, and *SCO6022*), which show extensive sequence similarity to each other. These proteins probably function as hexose-1-phosphoryltransferases and might be involved in the biosynthesis of

Table 2

Transposon insertions affecting proper sporulation of *S. coelicolor* A3(2).

Tag <sup>a</sup>	Position of insertion	Predicted function
<b>Nucleotide synthesis</b>		
SCO1483	1587028	<i>pyrA</i> , carbamoylphosphate synthetase
SCO1485	1588592	membrane protein
SCO1486	1590157	dihydrorotase, pyrimidin synthesis
SCO1486	1589655	dihydrorotase, pyrimidin synthesis
SCO1486	1589379	dihydrorotase, pyrimidin synthesis
SCO4079	4472336	<i>purL</i> , phosphoribosyl formylglycinamide synthase II
SCO4079	4473251	<i>purL</i> , phosphoribosyl formylglycinamide synthase II
SCO4987	4481572	<i>purM</i> , phosphoribosylformylglycinamide cycloligase
SCO4091_	4485600	<i>bldC</i> region
SCO4814	5243085	<i>purH</i> , phosphoribosyl aminoimidazole carboxamide formyl transf.
<b>Transcriptional regulation</b>		
SCO1504	1608709	putative regulator
SCO1744	1864166	<i>abrA1</i> , two-component sensor histidine kinase
SCO2730	2976597	possible regulator
SCO2792	3047470	<i>adpA</i> regulator, $\gamma$ -butyrolactone-responsive
SCO3361	3720344	<i>lrpA</i> , probable AsnC-family transcriptional regulator
SCO3579	3957624	WblA, WhiB family Regulator
SCO4190	4599321	<i>devA</i> , transcriptional regulator
SCO4197	4606699	possible MarR-family regulator
SCO4215	4623777	<i>xlrR</i> , GntR-regulator
SCO4895	5329300	possible ECF sigma factor
SCO4965	5400159	<i>greA</i> , transcription elongation factor
SCO5085	5528534	ActII-Orf4 Regulator
SCO5357	5826787	<i>rho</i> , transcriptional termination factor
SCO5511	6002908	phosphodiesterase, diGMP metabolizing
SCO5621	6121475	<i>whiG</i> , RNA polymerase sigma factor
SCO5704	6215605	<i>nusA</i> transcriptional termination/ antitermination factor
SCO5755	6293132	<i>clgR</i> , transcriptional regulator
SCO6268	6893643	possible histidine kinase
SCO6609_	7330209	<i>lrpA</i> , probable AsnC-family transcriptional regulator
SCO7297	8104527	possible two-component sensor histidine kinase
<b>Antibiotic biosynthesis</b>		
SCO3232	3578691	<i>cdaPS3</i> , CDA peptide synthetase III
SCO5088	5531744	actinorhodin polyketide beta-ketoacyl synthase beta subunit
SCO7682	8511758	non-ribosomal peptide synthase
<b>Capsular polysaccharide biosynthesis</b>		
SCO2592	2806241	capsular polysaccharide phosphotransferases, PhoP dependent
SCO2594	2809040	capsular polysaccharide phosphotransferases, PhoP dependent
SCO6022	6605756	exopolysaccharide phosphotransferase
<b>Other function</b>		
SCO0764	809009	(1- > 3)-beta-glucan endohydrolase
SCO0764	809610	(1- > 3)-beta-glucan endohydrolase
SCO0917	962398	luciferase family oxidoreductase
SCO1357	1435022	hypothetical protein
SCO1469	1569116	serine protease
SCO1663	1784136	probable cysteinyl-tRNA synthetase
SCO1751	1871449	sugar transporter
SCO1851	1984186	<i>cobO</i> , cob(I)alamin adenosyltransferase
SCO1857	1990631	probable bifunctional protein (CbiGH), cobalamin biosynthesis
SCO1867	2001360	possible ectoine hydroxylase
SCO1899	2034522	ABC sugar transporter (sorbitol)
SCO1965	2104421	possible export associated protein
SCO2153	2315587	possible secreted protein
SCO2512_	2709448	operon with <i>uppS</i> (undecaprenyl phosphate synthetase)
SCO2672	2910036	possible membrane protein
SCO2758	3005654	<i>nagA</i> , beta-N-acetylglucosaminidase
SCO3104	3400775	type II restriction endonuclease subunit
SCO3110	3408997	ABC-Transporter
SCO3285	3631169	large glycine/alanine rich protein
SCO3550	3925868	possible helicase
SCO3820	4199037	<i>pksC</i> , probable serine/threonine protein kinase

(continued on next page)

Table 2 (continued)

Tag*	Position of insertion	Predicted function
SCO4240	4645919	<i>msiK</i> sn-glycerol-3-phosphate transport ATP-binding protein
SCO4248	4655746	hypothetical protein, BldD controlled
SCO4253	4661476	phage tail protein, BldD dependent
SCO4293	4708983	<i>thrC</i> , threonine synthase
SCO4293	4708934	<i>thrC</i> , threonine synthase
SCO4498	4917165	probable proton transport protein
SCO4540	4957556	multispecies protein
SCO4606	5029605	NADH dehydrogenase subunit NuoL2
SCO4700	5126942	hypothetical protein
SCO5354	5823283	<i>thrA</i> , homoserine dehydrogenase
SCO6383	7049339	integral membrane protein
SCO6392	7059795	probable transposase
SCO6640	7376046	probable ATP-dependent helicase

\* indicates Tn insertion upstream of the coding sequence.

exopolysaccharides. Such proteins are also called stealth proteins, since they help pathogenic bacteria to elude the host innate immune system. From six similar putative exopolysaccharide phosphotransferase genes of *S. coelicolor* A3(2) (*SCO2592*, *SCO2594*, *SCO6021*, *SCO6022*, *SCO6023*, *SCO6024*) three genes were inactivated by a transposon insertion (Table 2). Among these, the transposon insertion in *SCO6022* had the most severe phenotype resulting in very poor sporulation. The localization of *SCO2594* and *SCO2592* next to two TagF-like glycerophosphotransferase genes (*SCO2589*, *SCO2590*), the *tagTUV*-like *SCO2578* and the SSSC gene *SCO2584* supports a role of *SCO2592* and *SCO2594* in the synthesis of CWGs. Also, the predicted *SCO6021-6025* operon is preceded by the *tagTUV*-like *SCO6020*, suggesting that the polysaccharide synthesized by these enzymes is linked to the muramic acid of the PG by the *SCO6020* transferase.

### 5. Cell Wall Glycopolymers (CWGs) and the composition of the spore envelope of *S. coelicolor* A3(2)

Van der Aart and coworkers compared the PG compositions of spores and vegetative mycelia of *S. coelicolor* A3(2) by LC-MS analyses of muropeptides (van der Aart et al., 2018). Spore walls contained an increased amount (44%) of tetrapeptides, compared to 23%–25% tetrapeptides in PG of vegetative mycelium (Table 3). The increase in tetrapeptides correlates with the formation of 3-3 cross-links, which require tetrapeptides, rather than pentapeptides, as a substrate. In agreement, 35% of the dimers from spore PG were 3-3 cross-linked. Conversely, only 5% of the spore muropeptide monomers were

Table 3

Composition of cell envelopes of vegetative mycelium and spores.

Component	Vegetative mycelium	Spores	Reference
PG-crosslinking			
Tetrapeptides in PG	23-25%	44%	van der Aart et al., 2018
Pentapeptides in PG	10-22%	5%	
Cell wall glycopolymer composition			
CWG content	36%	22%	Sigle et al., 2016b
Kdn content	95 nmol/mg	80 nmol/mg	
Phosphate content	172 nmol/mg	88 nmol/mg	
PAGE of partially hydrolyzed CWGs			
Band pattern	Widely spaced (Fig. 3., left lane)	Narrow spaced (Fig. 3., right lane)	Stebblau et al., unpublished
HPLC-MS analysis of hydrolyzed CWGs*			
GalKdn-R (teichulosonic acid)R = H (431.14 [M + H] <sup>+</sup> )R = CH <sub>3</sub> (445.16 [M + H] <sup>+</sup> )R = GlcNAc (634.22 [M + H] <sup>+</sup> )	+	+	Stebblau et al., unpublished
GalGlcNAcP (PDP) 464.12 [M + H] <sup>+</sup>	+	+/-	

\* Hydrolyzed CWG fragments were separated by reversed-phase HPLC on a Gemini C18 column (Phenomenex) with a 0–40% acetonitrile gradient. Masses were detected by ESI-MS, micro-TOF (Bruker Daltonics) in the positive mode (range 200–2000 m/z), as described in Borisova et al. (2016). (+) indicates prominent peaks, (+/-) indicates peak detected only in minute amounts.

pentapeptides, while vegetative PG contained 10%–22% pentapeptides. Moreover, a tripeptide which lacks GlcNAc and contains a deacetylated MurNAc (MurN-Tri) made up 3.5% of the muropeptide monomers of spore PG (van der Aart et al., 2018). N-deacetylation of PG strands is widespread among bacteria and is commonly linked to lysozyme resistance (Meyrand et al., 2007). Taken together, these structural modifications of the spore PG probably contribute to the structural stability of *S. coelicolor* A3(2) spores.

To compare their CWG composition, cell envelopes from *S. coelicolor* A3(2) vegetative mycelium and spores were isolated according to Schäberle et al. (2011). Subsequently, the attached CWGs were separated from the PG by acidic hydrolysis. These analyses revealed that spore walls contained reduced amounts of CWGs: whereas cell walls of vegetative mycelium consisted of 64% PG and 36% CWGs, spore walls consisted of 78% PG and only 22% CWGs (Sigle et al., 2016b). This demonstrates that *S. coelicolor* A3(2) remodels its cell wall during differentiation, either by increasing the amount of PG or by removing CWGs (or both).

CWGs are synthesized on a sugar linker unit, which is attached to the muramic acid of PG via a phosphoester bond. Shashkov et al. characterized the CWGs of vegetatively grown *S. coelicolor* A3(2) (Shashkov et al., 2012). In their analyses, Shashkov and coworkers did not observe classical glycerol- or ribitolphosphate containing wall teichoic acids, but identified a phosphate free teichulosonic acid as a major CWG. The teichulosonic acid consists of up to seven repeating units of galactose (Gal) linked to the sialinic acid sugar 2-keto-3-deoxy-D-glycero-D-galacto-nononic acid (Kdn), often substituted with N-acetylglucosamine (GlcNAc) or a methyl group. They also found a diglycosylphosphate polymer (PDP) of Gal and GlcNAc-phosphate as a minor component (Shashkov et al., 2012). Genes (*SCO4879-SCO4882*) directing the synthesis of the Kdn sugar have been identified in the genomic sequence of *S. coelicolor* A3(2) and inactivated. The respective mutant did no longer produce teichulosonic acid, but accumulated the minor CWG component PDP (Ostash et al., 2014).

To distinguish the two CWGs, teichulosonic acid and PDP, photometric assays to determine specific CWG components were developed. PDP was quantified by the determination of the phosphate content of the CWG fraction, the amount of teichulosonic acid was calculated by determining the amount of Kdn. In addition, the amount of hexosamines, present in PDP, teichulosonic acid, and probably in the not yet known linker unit was quantified (Sigle et al., 2016b). Whereas the Kdn content of spore walls (80 nmol/mg) was only slightly lower than that of vegetative mycelium (95 nmol/mg), the phosphate content of spore wall glycopolymers (88 nmol/mg) showed a reduction of 49% compared to that of vegetative cell walls (172 nmol/mg). Therefore it

was suggested that spore walls contain significantly lower amounts of PDP (Sigle et al., 2016b).

HPLC-MS analysis (Gemini C18 column, Phenomenex) of hydrolyzed CWGs (50 mM HCl, 5–15 min, 90 °C) detected peaks corresponding to Kdn monomers substituted with either H (431.14 [M + H]<sup>+</sup>), CH<sub>3</sub> (445.16 [M + H]<sup>+</sup>), or GlcNAc (634.22 [M + H]<sup>+</sup>) in CWG samples of vegetative mycelium and of spores (Table 3, Steblau and Walter, unpublished). Thus, teichulosonic acid is not only present in the cell walls of vegetative mycelium, but is also a component of spore envelopes. Moreover, a prominent peak of the mass of the PDP monomer (464.12 [M + H]<sup>+</sup>) was detected in the CWGs of vegetative mycelium. Also, a second peak corresponding to the PDP dimer (909.22 [M + H]<sup>+</sup>) was present in the same intensity as the monomer peak at short hydrolysis conditions (5 min). During prolonged hydrolysis (> 10 min) the PDP dimer peak disappeared and the PDP monomer peak increased in intensity. In contrast, only a very small PDP monomer peak was found in hydrolyzed CWGs of spore envelopes (Stebblau and Walter, unpublished). These findings confirmed the analyses of Shskov et al. and revealed the existence of both polymers, teichulosonic acid and PDP in vegetative mycelium. In spores only teichulosonic acid was reliably detected. The small PDP peak in the spore wall hydrolysate could also result from a possible contamination of spore walls with remains of aerial hyphae.

Chain length of the CWGs of vegetative mycelium and spores were analyzed and compared by high resolution PAGE analyses. CWGs were partially hydrolyzed by mild acidic conditions (Sigle et al., 2016b), expected to selectively hydrolyze phosphoester bonds, and the resulting CWG fragments of increasing length were separated on a 40 cm acrylamide (20%) gel. A combined alcian blue/silver staining visualized ladder-like fragment patterns (Fig. 3). The non-uniform distances within the fragment patterns in the lower and upper parts of the gel indicates that the CWGs of vegetative mycelium are a mixture of two different polymers, hindering an exact calculation of the CWG chain length. Comparing the fragment pattern of mycelial CWGs with that of spore CWGs in the lower part of the gel showed clear differences (N. Steblau, unpublished results). Whereas, the spore CWG fragments were narrow spaced, the distance of the mycelial CWG bands was much larger (Fig. 3). This implies that the mycelial CWG and the spore CWG contain different subunits and that the CWG from vegetative mycelium is composed of larger subunits compared to the spore CWG. The differences in the envelope compositions of vegetative mycelium and spore envelopes are summarized in Table 3.

## 6. Distinct role of PdtA (SCO2578) in the life cycle of *S. coelicolor* A3(2)

The LytR-CpsA-Psr (LCP) protein SCO2578 (PdtA), which was identified as a SSSC protein and which is predicted to anchor exopolysaccharides or CWGs to the muramic acid of PG was deleted (Sigle et al., 2016a). Despite the presence of 10 additional LCP-homologues in *S. coelicolor* A3(2), the resulting  $\Delta pdtA$  mutant showed severe defects. First, integrity of the spore envelope was affected and 34% nonviable spores were produced. This defect coincided with a reduced phosphate content in the spore envelope, leading to the conclusion that the amount of PDP (or an unknown CWG) was reduced (Sigle et al., 2016a). Second, apical tip extension and normal branching of vegetative mycelium was impaired and staggered extensions with a bulbous morphology were formed. The defect was more dramatic under osmotic stress, when the  $\Delta pdtA$  mutant was grown on LB agar supplemented with 6% NaCl. Instead of normal branches occurring in a distance of more than 20–30  $\mu$ m to the tip, all hyphal tips of the  $\Delta pdtA$  mutant showed hyperbranching directly at the tips without further extension growth, resulting in a bulky and dented mycelium (Sigle et al., 2016a). Localization of the sites of peptidoglycan synthesis by BODIPY FL Vancomycin (Van-fl) staining, revealed an aberrant PG-incorporation pattern. The mislocalization of PG-synthesis and the morphology of the

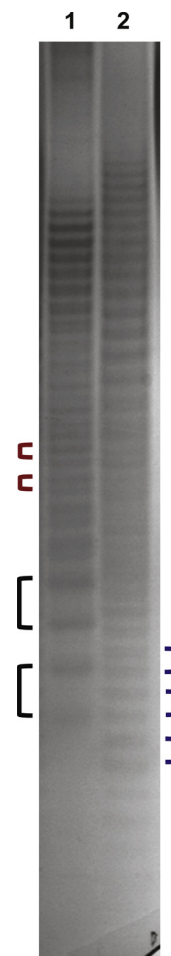


**Fig. 3.** PAGE analysis of *S. coelicolor* cell wall glycopolymers (CWGs). CWGs from vegetative mycelium (1) and spore envelopes (2) were hydrolyzed under mild acidic conditions (15 min 50 mM HCl). The resulting CWG fragments were separated on a 40 cm polyacrylamide gel (20%) at 18 mA for 7 h and stained with alcian blue/silver. The shown images are representative results of biological replicate experiments. Black and red brackets mark distinct fragment patterns in the CWGs of vegetative mycelium, indicating a mixture of two polymers. Blue brackets mark the distance of the spore CWG fragments.

aberrant hyphae suggested a defect in the tip localized PG-synthesis apparatus. As a consequence of the blocked tip extension, new tips are established close by, which also fail to elongate into normal hyphae. Therefore, PdtA itself or the CWG attached to the PG by the glycopolymer transferase PdtA is not only required for proper sporulation, but also has a crucial function in apical tip extension of vegetative hyphae under stress conditions (Fig. 4).

## 7. Control of differentiation by protein-phosphorylation

A crucial step in *Streptomyces* differentiation is the simultaneous formation of dozens of cross walls in the aerial hyphae. During sporulation septation the membrane- and PG-synthesizing machineries, including the SSSC, have to be provided in sufficient quantities and positioned properly. Moreover, the activities of the complexes have to be controlled to prevent aberrant sporulation by sporadic formation of single cross walls in a non-coordinated manner.

Controlling activity of proteins involved in cell division and cell wall synthesis by phosphorylation is a well-documented regulatory mechanism in many bacteria (Molle and Kremer, 2010; Hempel et al., 2012; Jarick et al., 2018; Sharma et al., 2016). However, phosphorylation of one of the Mre proteins has not been reported yet in any

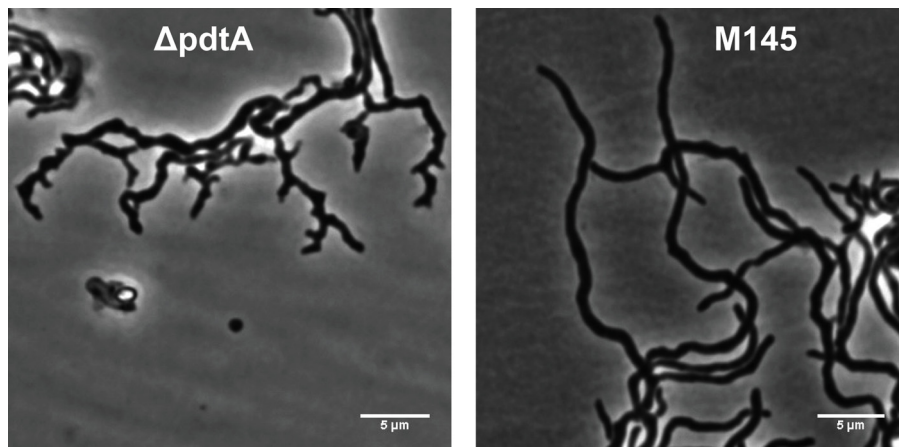


**Fig. 4.** Aberrant branching of the  $\Delta pdtA$  mutant under osmotic stress.  $\Delta pdtA$  (left) and M145 (right) were grown for 72 h on LB-agar, supplemented with 6% NaCl. In contrast to the wild type M145, the  $\Delta pdtA$  mutant shows hyperbranching and blocked elongation of the hyphae. The shown images are representative results of biological replicate experiments.

bacterium. The discovery that the eSTPK PkaI, which is encoded in a cluster of five consecutive eSTPK genes (*SCO4775 (pkaH)*, *SCO4776*, *SCO4777 (pkaD)*, *SCO4778 (pkaI)*, and *SCO4779 (pkaJ)*), had a central position in the SSSC interaction network (Kleinschnitz et al., 2011a), provided first evidence that the activity of the SSSC might be regulated by protein phosphorylation. Next it was shown that depletion of phosphorylation activity by inactivating *pkaI* or by deleting all five eSTPK genes affected sporulation. But also expressing a second copy of any one of the five eSTPK genes under control of its native promoter caused an even more severe phenotype. Aberrant spore chains were formed, containing irregular sized spore, dead spores, or spores without DNA. Moreover, the germinating spores were sensitive to osmotic stress and cell wall damage by lysozyme or vancomycin (Ladwig et al., 2015). Thus it was concluded that the balanced phosphorylation activity is crucial for proper sporulation.

To study whether PkaI or one of the other eSTPKs phosphorylate SSSC proteins, all five eSTPK genes were cloned into pCDF-Duet, fused to an N-terminal his-tag encoding sequence, and coexpressed with *mreC* fused to a C-terminal S-tag encoding sequence (Vollmer, unpublished results). Following induction of gene expression, the phosphorylation status of eSTPK-His and MreC-S-tag was studied by phosphostaining with ProQ diamond. Whereas MreC-S-tag was non-phosphorylated, when purified in the absence of one of the eSTPKs, it was phosphorylated, when it was coexpressed with either *pkaI* or *pkaH* (Ladwig et al., 2015, Vollmer, unpublished results).

The phosphosites of PkaI and MreC were identified using purified proteins, subjected to proteolytic digestion and analyses of the resulting peptide masses by LC-MS/MS (Ladwig et al., 2015). Two phosphorylated peptides, PkaI<sub>111-124</sub> (VLpTRGPVDAVEAAR) and PkaI<sub>164-177</sub> (FGVAQVAGAp[TT]LTE) were identified for PkaI. PkaI<sub>164-177</sub> corresponds to the so-called activation loop of eSTPKs, involved in determining substrate specificity (Pereira et al., 2011).

For MreC, a single peptide (MreC<sub>219-251</sub>, LVTFGSQADKPFVPGV-PVGp[TIT]RVDPNGGDLTR), derived from the Pfam\_MreC domain

(MreC<sub>121-273</sub>), was detected 100-fold more abundant in the phosphorylated form compared to the non-phosphorylated one. The fragmentation spectrum did not allow an unambiguous assignment of the phosphorylation to one of the two threonine (T<sub>238</sub>, T<sub>240</sub>) residues. T<sub>238</sub>/T<sub>240</sub> of MreC was only phosphorylated with low efficiency by PkaH, whereas T<sub>250</sub> was identified as its major phosphosite within MreC (Vollmer, unpublished results).

When *pbp2* was coexpressed with *pkaI*, PBP2 was only detected in the presence of PkaI, indicating that expression of *pbp2* was detrimental to the cell and only tolerated, when *pkaI* was coexpressed, resulting in phosphorylated PBP2. Four phosphorylated peptides were detected by LC-MS/MS: PBP2<sub>272-81</sub> (GVALADNEpTR), PBP2<sub>82-93</sub> (LVVp[SASRT]DLLK), PBP2<sub>210-220</sub> (SDQVGRpSGLER), and PBP2<sub>550-560</sub> (AVVSP-DGKpTVR). Presence of three phosphosites in the N-terminal dimerization domain (PBP2<sub>60-250</sub>) indicates that PBP2 phosphorylation affects its dimerization (Ladwig et al., 2015).

The effect of eSTPK expression/deletion on proper sporulation, the protein-protein interaction pattern of PkaI, as well as the specific phosphorylation of MreC by PkaI and PkaH suggest that all eSTPKs of the cluster are involved in the regulatory network controlling SSSC activity (Fig.5).

Based on these findings a model was developed, in which coordinated sporulation septation and synthesis of the spore envelope is triggered by the phosphorylation status of SSSC proteins (Fig. 6). In this model, some of the SSSC proteins are phosphorylated in the early phases of aerial hyphae development by the different eSTPKs to keep them inactive and to prevent the premature assembly of SSSC complexes. After the outgrowth of the aerial hyphae is completed and sufficient amounts of SSSC proteins have been synthesized and positioned, the SSSC proteins become activated by dephosphorylation (involving phosphatases). As a consequence they can form functional SSSC complexes for the coordinated synthesis of sporulation septa and spore envelopes.

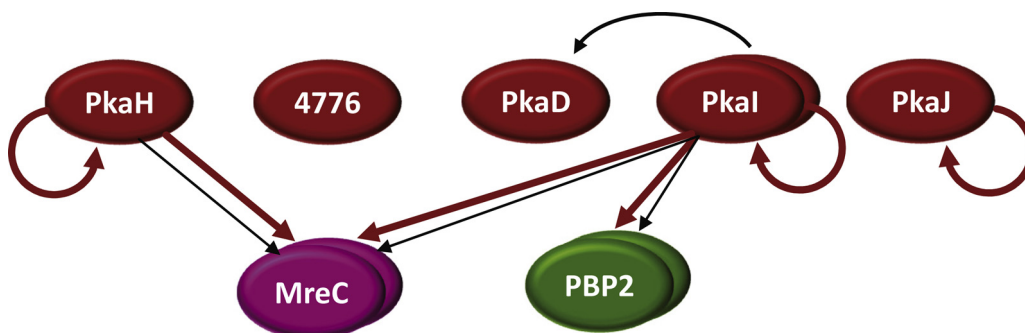


**Fig. 5.** Phosphorylation of the SSSC proteins MreC and PBP2 by multiple eSTPKs. eSTPKs, which were shown to affect proper sporulation are drawn as red ellipses. Red arrows indicate phosphorylation detected by ProQ diamond staining or LC-MS/MS, while a black arrow marks protein-protein interaction shown by co-purification or BACTH analyses (Ladwig et al., 2015, Vollmer et al., unpublished results). Self-interactions are indicated by double ellipses.

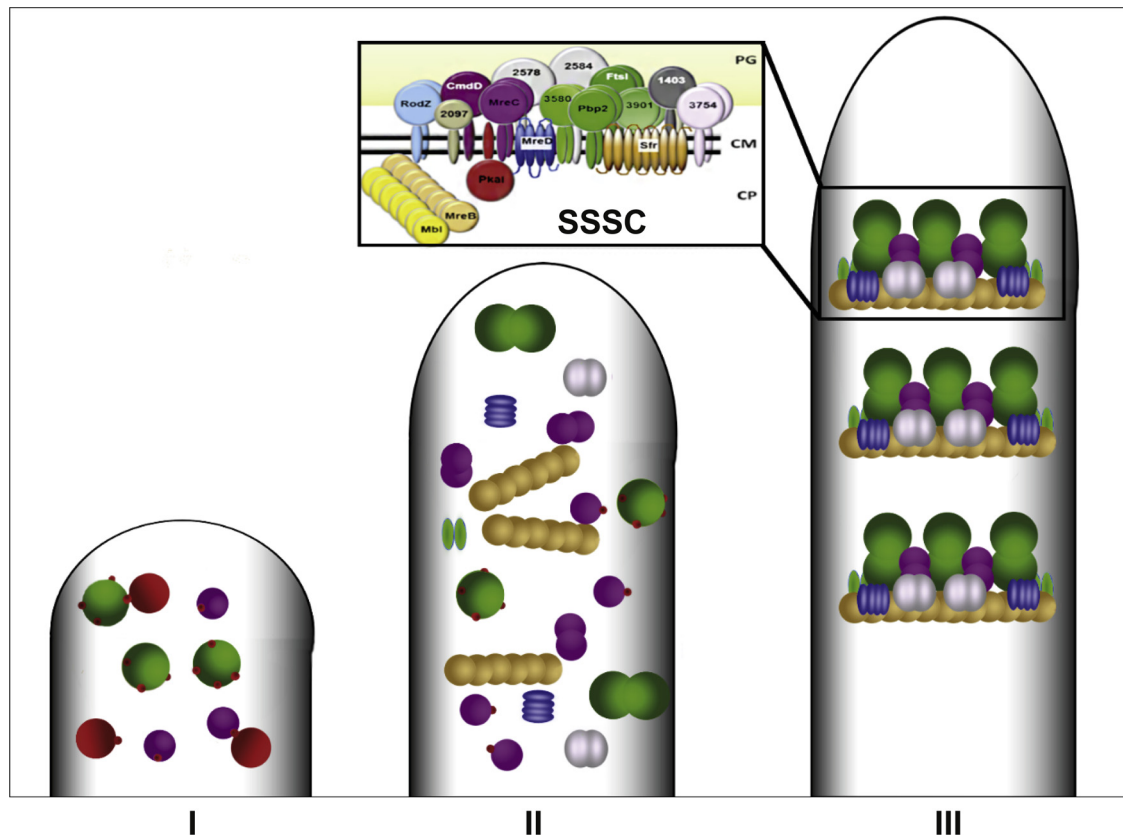


**Fig. 6.** Coordination of synchronized sporulation septation and synthesis of the thickened spore envelope by the phosphorylation of SSSC proteins. In this model, eSTPKs phosphorylate untimely expressed SSSC proteins (I-II) to prevent their premature assembly, which would result in non-coordinated septum synthesis. After completion of aerial hyphae growth (III), the phosphorylated SSSC proteins become dephosphorylated by phosphatases and functional SSSC complexes can assemble to build sporulation septa in a synchronized manner.

## Acknowledgements

This work was supported by the Deutsche Forschungsgemeinschaft: SFB766

## References

- Ausmees, N., Wahlstedt, H., Bagchi, S., Elliot, M.A., Buttner, M.J., Flardh, K., 2007. SmeA, a small membrane protein with multiple functions in *Streptomyces* sporulation including targeting of a SpoIII $\Phi$ /FtsK-like protein to cell division septa. *Mol. Microbiol.* 65, 1458–1473.
- Borisova, M., Gaupp, R., Duckworth, A., Schneider, A., Dalügge, D., Mühleck, M., Deubel, D., Unsleber, S., Yu, W., Muth, G., Bischoff, M., Götz, F., Mayer, C., 2016. Peptidoglycan recycling in Gram-positive bacteria is crucial for survival in stationary phase. *MBio* 7, e00923–16.
- Bush, M.J., Tschowri, N., Schlimpert, S., Flärdh, K., Buttner, M.J., 2015. c-di-GMP signalling and the regulation of developmental transitions in streptomycetes. *Nat. Rev. Microbiol.* 13, 749–760.
- Burger, A., Sichler, K., Kelemen, G., Buttner, M., Wohlleben, W., 2000. Identification and characterization of the *mre* gene region of *Streptomyces coelicolor* A3(2). *Mol. Gen. Genet.* 263, 1053–1060.
- Claessen, D., Stokroos, I., Deelstra, H.J., Penninga, N.A., Bormann, C., Salas, J.A., Dijkhuizen, L., Wosten, H.A., 2004. The formation of the rodlet layer of streptomycetes is the result of the interplay between rodlines and chaplins. *Mol. Microbiol.* 53, 433–443.
- Colson, S., van Wezel, G.P., Craig, M., Noens, E.E., Nothaft, H., Mommaas, A.M., Titgemeyer, F., Joris, B., Rigali, S., 2008. The chitinase-binding protein, DasA, acts as a link between chitin utilization and morphogenesis in *Streptomyces coelicolor*. *Microbiology* 154, 373–382.
- Crow, A., Greene, N.P., Kaplan, E., Koronakis, V., 2017. Structure and mechanism of the MacB ABC transporter superfamily. *Proc. Natl. Acad. Sci. U.S.A.* 114, 12572–12577.
- Del Sol, R., Pitman, A., Herron, P., Dyson, P., 2003. The product of a developmental gene, *crgA*, that coordinates reproductive growth in *Streptomyces* belongs to a novel family of small actinomycete-specific proteins. *J. Bacteriol.* 185, 6678–6685.
- Dominguez-Escobar, J., Chastanet, A., Crevenna, A.H., Fromion, V., Wedlich-Soldner, R., Carballido-Lopez, R., 2011. Processive movement of MreB-associated cell wall biosynthetic complexes in bacteria. *Science* 333, 225–228.
- Divakaruni, A.V., Baida, C., White, C.L., Gober, J.W., 2007. The cell shape proteins MreB and MreC control cell morphogenesis by positioning cell wall synthetic complexes. *Mol. Microbiol.* 66, 174–188.
- Du, S., Pichoff, S., Lutkenhaus, J., 2016. FtsEX acts on FtsA to regulate divisome assembly and activity. *Proc. Natl. Acad. Sci. U.S.A.* 113, 5052–5061.
- Eccleston, M., Ali, R.A., Seyler, R., Westpheling, J., Nodwell, J., 2002. Structural and genetic analysis of the BldB protein of *Streptomyces coelicolor*. *J. Bacteriol.* 184, 4270–4276.
- Elliot, M.A., Karounthaisiri, N., Huang, J., Bibb, M.J., Cohen, S.N., Kao, C.M., Buttner, M.J., 2003. The chaplins: a family of hydrophobic cell-surface proteins involved in aerial mycelium formation in *Streptomyces coelicolor*. *Genes Develop* 17, 1727–1740.
- Flardh, K., 2003. Growth polarity and cell division in *Streptomyces*. *Curr. Op. Microbiol.* 6, 564–571.
- Flardh, K., Buttner, M.J., 2009. *Streptomyces* morphogenetics: dissecting differentiation in a filamentous bacterium. *Nat. Rev. Microbiol.* 7, 36–49.
- Flardh, K., Richards, D.M., Hempel, A.M., Howard, M., Buttner, M.J., 2012. Regulation of apical growth and hyphal branching in *Streptomyces*. *Curr. Op. Microbiol.* 15, 737–743.
- Formstone, A., Carballido-Lopez, R., Noirot, P., Errington, J., Scheffers, D.J., 2008. Localization and interactions of teichoic acid synthetic enzymes in *Bacillus subtilis*. *J. Bacteriol.* 190, 1812–1821.
- Garner, E.C., Bernard, R., Wang, W., Zhuang, X., Rudner, D.Z., Mitchison, T., 2011. Coupled, circumferential motions of the cell wall synthesis machinery and MreB filaments in *B. Subtilis*. *Science*. 333, 222–225.
- Heichlinger, A., Ammelburg, M., Kleinschnitz, E.M., Latus, A., Maldener, I., Flardh, K., Wohlleben, W., Muth, G., 2011. The MreB-like protein Mbl of *Streptomyces coelicolor* A3(2) depends on MreB for proper localization and contributes to spore wall synthesis. *J. Bacteriol.* 193, 1533–1542.
- Hempel, A.M., Cantlay, S., Molle, V., Wang, S.B., Naldrett, M.J., Parker, J.L., Richards, D.M., Jung, Y.G., Buttner, M.J., Flardh, K., 2012. The Ser/Thr protein kinase AfsK regulates polar growth and hyphal branching in the filamentous bacteria *Streptomyces*. *Proc. Natl. Acad. Sci. U.S.A.* 109, 2371–2379.
- Hesketh, A., Hill, C., Mokhtar, J., Novotna, G., Tran, N., Bibb, M., Hong, H.J., 2011. Genome-wide dynamics of a bacterial response to antibiotics that target the cell envelope. *BMC Genomics* 12, 226.
- Jakimowicz, D., Gust, B., Zakrzewska-Czerwinska, J., Chater, K.F., 2005. Developmental-stage-specific assembly of ParB complexes in *Streptomyces coelicolor* hyphae. *J. Bacteriol.* 187, 3572–3580.
- Jarick, M., Bertsche, U., Stahl, M., Schultz, D., Methling, K., Lalk, M., Stigloher, C., Steger,



- M., Schlosser, A., Ohlsen, K., 2018. The serine/threonine kinase Stk and the phosphatase Stp regulate cell wall synthesis in *Staphylococcus aureus*. *Sci. Rep.* 8, 13693. <https://doi.org/10.1038/s41598-018-32109-7>.
- Jyothikumar, V., Tilley, E.J., Wali, R., Herron, P.R., 2008. Time-lapse microscopy of *Streptomyces coelicolor* growth and sporulation. *Appl. Environ. Microbiol.* 74, 6774–6781.
- Karimova, G., Pidoux, J., Ullmann, A., Ladant, D., 1998. A bacterial two-hybrid system based on a reconstituted signal transduction pathway. *Proc. Natl. Acad. Sci. U.S.A.* 95, 5752–5756.
- Kelemen, G.H., Buttner, M.J., 1998. Initiation of aerial mycelium formation in *Streptomyces*. *Curr. Op. Microbiol.* 1, 656–662.
- Kleinschnitz, E.M., Heichlinger, A., Schirmer, K., Winkler, J., Latus, A., Maldener, I., Wohlleben, W., Muth, G., 2011a. Proteins encoded by the *mre* gene cluster in *Streptomyces coelicolor* A3(2) cooperate in spore wall synthesis. *Mol. Microbiol.* 79, 1367–1379.
- Kleinschnitz, E.M., Latus, A., Sigle, S., Maldener, I., Wohlleben, W., Muth, G., 2011b. Genetic analysis of SCO2997, encoding a TagF homologue, indicates a role for wall teichoic acids in sporulation of *Streptomyces coelicolor* A3(2). *J. Bacteriol.* 193, 6080–6085.
- Kruse, T., Bork-Jensen, J., Gerdes, K., 2005. The morphogenetic MreBCD proteins of *Escherichia coli* form an essential membrane-bound complex. *Mol. Microbiol.* 55, 78–89.
- Ladwig, N., Franz-Wachtel, M., Hezel, F., Soufi, B., Macek, B., Wohlleben, W., Muth, G., 2015. Control of morphological differentiation of *Streptomyces coelicolor* A3(2) by phosphorylation of MreC and PBP2. *PLoS One* 10, e0125425.
- Ma, H., Kendall, K., 1994. Cloning and analysis of a gene cluster from *Streptomyces coelicolor* that causes accelerated aerial mycelium formation in *Streptomyces lividans*. *J. Bacteriol.* 176, 3800–3811.
- Meeske, A.J., Riley, E.P., Robins, W.P., Uehara, T., Mekalanos, J.J., Kahnm, D., Walker, S., Kruse, A.C., Bernhardt, T.G., Rudner, D.Z., 2016. SEDS proteins are a widespread family of bacterial cell wall polymerases. *Nature* 537, 634–638.
- Meyrand, M., Boughammoura, A., Courtin, P., Mezange, C., Guillot, A., Chapot-Chartier, M.P., 2007. Peptidoglycan N-acetylglucosamine deacetylation decreases autolysis in *Lactococcus lactis*. *Microbiology* 153, 3275–3285.
- Mazza, P., Noens, E.E., Schirmer, K., Grantcharova, N., Mommaas, A.M., Koerten, H.K., Muth, G., Flardh, K., van Wezel, G.P., Wohlleben, W., 2006. MreB of *Streptomyces coelicolor* is not essential for vegetative growth but is required for the integrity of aerial hyphae and spores. *Mol. Microbiol.* 60, 838–852.
- Molle, V., Kremer, L., 2010. Division and cell envelope regulation by Ser/Thr phosphorylation: *mycobacterium* shows the way. *Mol. Microbiol.* 75, 1064–1077.
- Morgenstein, R.M., Bratton, B.P., Nguyen, J.P., Ouzounov, N., Shaevitz, J.W., Gitai, Z., 2015. RodZ links MreB to cell wall synthesis to mediate MreB rotation and robust morphogenesis. *Proc Natl Acad Sci U S A.* 112, 12510–12515.
- Nothaft, H., Rigali, S., Boomsma, B., Swiatek, M., McDowall, K.J., van Wezel, G.P., Titgemeyer, F., 2010. The permease gene nagE2 is the key to N-acetylglucosamine sensing and utilization in *Streptomyces coelicolor* and is subject to multi-level control. *Mol. Microbiol.* 75, 1133–1144.
- Ostash, B., Shashkov, A., Streshinskaya, G., Tul'skaya, E., Baryshnikova, L., Dmitrenok, A., Dacyuk, Y., Fedorenko, V., 2014. Identification of *Streptomyces coelicolor* M145 genomic region involved in biosynthesis of teichulosonic acid-cell wall glycopolymer. *Folia Microbiol. (Praha)* 59, 355–360.
- Pereira, S.F., Goss, L., Dworkin, J., 2011. Eukaryote-like serine/threonine kinases and phosphatases in bacteria. *Microbiol. Mol. Biol. Rev.* 75, 192–212.
- Poralla, K., Muth, G., Hartner, T., 2000. Hopanoids are formed during transition from substrate to aerial hyphae in *Streptomyces coelicolor* A3(2). *FEMS Microbiol. Lett.* 189, 93–95.
- Reznikoff, W.S., 2008. Transposon Tn5. *Annu. Rev. Genet.* 42, 269–286.
- Richards, D.M., Hempel, A.M., Flardh, K., Buttner, M.J., Howard, M., 2012. Mechanistic basis of branch-site selection in filamentous bacteria. *PLoS Comput. Biol.* 8, e1002423.
- Ruban-Ośmiałowska, B., Jakimowicz, D., Smulczyk-Krawczynszyn, A., Chater, K.F., Zakrzewska-Czerwińska, J., 2006. Replisome localization in vegetative and aerial hyphae of *Streptomyces coelicolor*. *J. Bacteriol.* 188, 7311–7316.
- Salerno, P., Persson, J., Bucca, G., Laing, E., Ausmees, N., Smith, C.P., Flardh, K., 2013. Identification of new developmentally regulated genes involved in *Streptomyces coelicolor* sporulation. *BMC Microbiol.* 13, 281.
- Schäberle, T.F., Vollmer, W., Frasch, H.J., Huttel, S., Kulik, A., Rottgen, M., von Thaler, A.K., Wohlleben, W., Stegmann, E., 2011. Self-resistance and cell wall composition in the glycopeptide producer *Amycolatopsis balhimycina*. *Antimicrob. Agents Chemother.* 55, 4283–4289.
- Schlimpert, S., Flardh, K., Buttner, J., 2016. Fluorescence time-lapse imaging of the complete *S. venezuelae* life cycle using a microfluidic device. *J. Vis. Exp.* 108, E53863.
- Schlimpert, S., Wasserstrom, S., Chandra, G., Bibb, M.J., Findlay, K.C., Flardh, K., Buttner, M.J., 2017. Two dynamin-like proteins stabilize FtsZ rings during *Streptomyces* sporulation. *Proc. Natl. Acad. Sci. U.S.A.* 114, 6176–6183.
- Seo, J.W., Ohnishi, Y., Hirata, A., Horinouchi, S., 2002. ATP-binding cassette transport system involved in regulation of morphological differentiation in response to glucose in *Streptomyces griseus*. *J. Bacteriol.* 184, 91–103.
- Sharma, A.K., Arora, D., Singh, L.K., Gangwal, A., Sajid, A., Molle, V., Singh, Y., Nandicoori, V.K., 2016. Serine/Threonine protein phosphatase PstP of *Mycobacterium tuberculosis* is necessary for accurate cell division and survival of pathogen. *J. Biol. Chem.* 291, 24215–24230.
- Shashkov, A.S., Ostash, B.E., Fedorenko, V.A., Streshinskaya, G.M., Tul'skaya, E.M., Senchenkova, S.N., Baryshnikova, L.M., Evtushenko, L.I., 2012. Novel teichulosonic acid from cell wall of *Streptomyces coelicolor* M145. *Carbohydr. Res.* 359, 70–75.
- Shu, D., Chen, L., Wang, W., Yu, Z., Ren, C., Zhang, W., Yang, S., Lu, Y., Jiang, W., 2009. afsQ1-Q2-sigQ is a pleiotropic but conditionally required signal transduction system for both secondary metabolism and morphological development in *Streptomyces coelicolor*. *Appl. Microbiol. Biotechnol.* 81, 1149–1160.
- Sigle, S., Steblau, N., Wohlleben, W., Muth, G., 2016a. Polydiglycosylphosphate transferase PdtA (SCO2578) of *Streptomyces coelicolor* A3(2) is crucial for proper sporulation and apical tip extension under stress conditions. *Appl. Environ. Microbiol.* 82, 5661–5672.
- Sigle, S., Steblau, N., Wohlleben, W., Muth, G., 2016b. A toolbox to measure changes in the cell wall glycopolymer composition during differentiation of *Streptomyces coelicolor* A3(2). *J. Microbiol. Methods* 128, 52–57.
- Taguchi, A., Welsh, M.A., Marmont, L.S., Lee, W., Sjodt, M., Kruse, A.C., Kahne, D., Bernhardt, T.G., Walker, S., 2019. FtsW is a peptidoglycan polymerase that is functional only in complex with its cognate penicillin-binding protein. *Nat. Microbiol.* 4, 587–594.
- van der Aart, L.T., Spijksma, G.K., Harms, A., Vollmer, W., Hankemeier, T., van Wezel, G.P., 2018. High-resolution analysis of the peptidoglycan composition in *Streptomyces coelicolor*. *J. Bacteriol.* 200, e00290–18. <https://doi.org/10.1128/JB.00290-18>.
- Wang, L., Yu, Y., He, X., Zhou, X., Deng, Z., Chater, K.F., Tao, M., 2007. Role of an FtsK-like protein in genetic stability in *Streptomyces coelicolor* A3(2). *J. Bacteriol.* 189, 2310–2318.
- Willemsse, J., Borst, J.W., de Waal, E., Bisseling, T., van Wezel, G.P., 2011. Positive control of cell division: FtsZ is recruited by SsgB during sporulation of *Streptomyces*. *Genes Dev.* 25, 89–99.
- Xu, Z., Wang, Y., Chater, K.F., Ou, H.Y., Xu, H.H., Deng, Z., Tao, M., 2017. Large-scale transposition mutagenesis of *Streptomyces coelicolor* identifies hundreds of genes influencing antibiotic biosynthesis. *Appl. Environ. Microbiol.* 83, e02889–16.

## Acknowledgement

Ich möchte mich bei Prof. Dr. Christoph Mayer für die Möglichkeit zur Doktorarbeit und die hervorragende Betreuung bedanken. Er stand mir mit Ideen, konstruktiver Kritik und einem unermüdlichen, wissenschaftlichen Enthusiasmus zur Seite.

Besten Dank an Prof. Dr. Hannes Link für das Zweitgutachten dieser Arbeit sowie Prof. Dr. Andreas Peschel und Prof. Dr. Klaus Hantke für die Teilnahme an der mündlichen Prüfung.

Für die gute Zusammenarbeit in Kooperationsprojekten danke ich Xin Du der AG Peschel und Nadja Steblau der AG Muth.

Ein besonderer Dank gilt Marina für ihre Unterstützung. Die Zusammenarbeit war eine Freude, besonders wenn es komplexe Probleme zu lösen galt.

Ein ebenso großes Dankeschön an Isa, Robert, Simon, Martina und alle anderen Mitarbeiter der AG Mayer für die gute Zeit.

Danke an meine Freunde Chris, Martin, Vlad und Julian, die schon seit Beginn des Studiums mit dabei sind.

Lieben Dank an meine Familie für die super Unterstützung während des gesamten Studiums und danke an Martina für den Rückhalt vor allem während den schwierigen Phasen dieser Arbeit.